

RESEARCH ON HORIZONTALLY CURVED STEEL BOX GIRDERS

Chai H. Yoo

Kyungsik Kim

Byung H. Choi

Highway Research Center

Auburn University

Auburn University, Alabama

December 2005

Acknowledgements

The investigation which led to the results presented herein was supported by Alabama Department of Transportation Project Number 930-563. The authors gratefully acknowledge the financial support and the guidance provided by the advising council.

Disclaimer

The opinions and conclusions expressed or implied in the report are those of the authors. They are not necessarily those of the funding agency.

TABLE OF CONTENTS

TABLE OF CONTENTS	i
LIST OF TABLES	vi
LIST OF FIGURES	viii
EXECUTIVE SUMMARY	xix
CHAPTER 1. INTRODUCTION	1
1.1 Objectives and Scope	8
1.2 Methodolgy	11
CHAPTER 2. LITERATURE REVIEW	13
CHAPTER 3. LATERAL BRACING SYSTEMS	20
3.1 Introduction	20
3.2 Background	23
3.3 Finite Element Modeling	27
3.4 Bracing Member Forces due to Torsional Loads	29
3.5 Bracing Member Forces due to Vertical Bending	38
3.6 Equations for Brace Forces	41
3.7 Comparison of Lateral Bracing Forces	42
3.8 Summary and Concluding Remarks	51
CHAPTER 4. CROSS-FRAMES IN STEEL BOX GIRDERS	53
4.1 Introduction	53
4.2 Background	55
4.3 Limitation on Distortional Stresses	58
4.4 Pure Torsional and Distortional Loads	60
4.5 Brace Forces in Cross-Frames	62
4.5.1 X-Frames	63
4.5.2 K-Frames	64
4.6 Finite Element Modeling	65
4.7 Comparison of Results from Equations and Finite Element Analysis	66
4.8 Effect of Number of Cross-Frames on Distortion and Cross-Frame Forces ...	77
4.9 Summary and Concluding Remarks	88

CHAPTER 5. COUPLING ACTION OF LATERAL BRACING AND CROSS-FRAMES	94
5.1 Introduction.....	94
5.2 Background.....	96
5.3 Brace Forces in Box Girder with K-Frames	103
5.4 Brace Forces in Box Girder with Internal X-Frames.....	111
5.5 Forces in Bracing Members near Interior Supports.....	118
5.6 Comparison of Bracing Forces	121
5.7 Summary and Concluding Remarks	128
CHAPTER 6. EXTERNAL CROSS-FRAMES	130
6.1 Introduction.....	130
6.2 Definition of Deck Unevenness Ratio	133
6.3 Finite Element Modeling	136
6.4 Simple-Span Box Girder Bridges	138
6.5 Three-Span Continuous Box Girder Bridges.....	143
6.6 Concluding Remarks.....	154
CHAPTER 7. ELASTOMERIC BEARINGS	155
7.1 Introduction.....	155
7.2 General Behaviors of Elastomeric Bearing.....	158
7.3 Review of AASHTO LRFD Design Requirements	161
7.3.1 Compressive Stress	161
7.3.2 Compressive Deflection.....	162
7.3.3 Shear Deformation.....	162
7.3.4 Combined Compression and Rotation	162
7.3.5 Stability of Elastomeric Bearings	164
7.3.6 Reinforcement.....	165
7.4 Design Examples	166
7.4.1. Loading Combinations.....	166
7.4.2 Design of Elastomeric Bearings.....	167
7.5 Hyperelastic Material Model	175
7.6 Numerical Examples	178
7.7 Summary and Concluding Remarks	180
CHAPTER 8. ULTIMATE STRENGTH INTERACTION OF COMPOSITE BOX GIRDERS	186
8.1 Introduction.....	186
8.2 Numerical Investigation.....	188
8.2.1 Constitutive Modeling for Concrete and Verification	189
8.2.2 Ultimate Strength Interaction of Composite Box Girders	195
8.3 Analytical Investigation.....	204
8.4 Ultimate Strength Interaction Equation	211
8.5 Summary and Concluding Remarks	215

CHAPTER 9. REQUIREMENTS FOR LONGITUDINAL STIFFENERS	217
9.1. Introduction.....	217
9.1.1. Problem Statement	219
9.1.2. Objective	221
9.1.3. Organization.....	221
9.2. Literature Review.....	222
9.2.1. Stiffened Flanges and Webs.....	222
9.2.1.1. Elastic Buckling Method.....	223
9.2.1.2. Ultimate Strength Method – Strut Approach vs. Plate	227
Approach	
9.2.1.3. Ultimate Strength Method Based on Elastic Buckling with a Factor of Safety	231
9.2.1.4. Modern Ultimate Strength Analysis	233
9.2.2. Stress Evaluation in Horizontally Curved Box Girders.....	233
9.3. Theory on Stiffened Plates.....	237
9.3.1. Introduction.....	237
9.3.2. Timoshenko and Gere’s Theory.....	238
9.3.3. Mattock’s Work	242
9.3.4. Current AASHTO Provision.....	244
9.3.4.1. Errors in Mattock’s Work	244
9.3.4.2. Limitation in Available Timoshenko and Gere’s Equation	247
9.3.5. Theoretical Formulation of Design Equation	249
9.4. Buckling of Straight Stiffened Plates.....	250
9.4.1. Introduction.....	250
9.4.2. Exploratory Modeling.....	251
9.4.3. Modeling of Compression Flange.....	254
9.4.4. Minimum Required Stiffener Rigidity.....	255
9.4.5. Parametric Study.....	259
9.4.5.1. Number of Longitudinal Stiffeners	259
9.4.5.2. Aspect Ratio	259
9.4.5.3. Flange Thickness.....	260
9.4.5.4. Flange Width Between Stiffeners	260
9.4.5.5. Torsional Rigidity of Stiffeners	261
9.4.5.6. Area of Stiffeners	261
9.4.6. Regression Analysis.....	262
9.5. Induced Stresses in Horizontally Curved Box Girder Flanges	267
9.5.1. Introduction.....	267
9.5.2. Static Behaviors of a Horizontally Curved Box Girder	267
9.5.3. Distortional Stresses	268
9.5.4. Effects of Internal Diaphragm on Distortional Stress.....	279
9.5.5. Design Requirements for Distortional Stresses	282
9.5.6. Analytical Studies	283
9.5.6.1. Model Description.....	284
9.5.6.2. Loading Combination	287

9.5.7. Modeling for Finite Element Analysis.....	288
9.5.7.1. Internal Cross Frames	289
9.5.7.2. Bracing of Tub Flanges.....	290
9.5.8. Analysis Results.....	290
9.5.8.1. Effect of Top Flange Lateral Bracing	291
9.5.8.2. Effect of Stiffness of Cross-Frames on Distortional Stress	291
9.5.8.3. Effect of Spacing of Cross-Frames on Distortional Stress	292
9.5.9. Stress Distribution in a Well-Designed Box Flange	300
9.5.10. Longitudinal Stiffeners for the Flanges of a Horizontally Curved Box Girder	300
9.6. Stability of Horizontally Curved Stiffened Flanges.....	303
9.6.1. Introduction.....	303
9.6.2. Model Description	304
9.6.3. Analysis Results.....	305
9.6.3.1. Linear Static Analysis	305
9.6.3.2. Elastic Buckling Analysis	308
9.7. Moment of Inertia of Longitudinal Stiffeners Attached to Curved Box Girder Flanges.....	318
9.7.1. Introduction.....	318
9.7.2. Parameters for Data Collection.....	318
9.7.3. Regression Analysis.....	319
9.7.4. Conservatisms of the Proposed Design Equation	323
9.7.4.1. Effect of Boundary Condition.....	323
9.7.4.2. Effect of Continuous Boundary on Flange Edges.....	324
9.7.4.3. Effect of Stiffener Edge Boundary Condition.....	325
9.7.4.4. Effect of Moment Gradient	327
9.8. Inelastic Buckling Strength	331
9.8.1. Introduction.....	331
9.8.2. Background.....	331
9.8.2.1. Inelastic Buckling Strength of Stiffened Flanges.....	331
9.8.2.2. AASHTO Inelastic Transition Curve.....	332
9.8.2.3. Plate Inelastic Buckling Strength Prediction.....	333
9.8.3. Initial Geometric Imperfections	335
9.8.4. Effects of Various Geometric Imperfections on Ultimate Strengths	342
9.8.5. Minimum Required Rigidity for Subpanels in Inelastic Buckling Range	345
9.8.6. Further Validation of Eq. (9.27)	354
9.8.7. Comparative Design.....	357
9.9 Summary and Concluding Remarks	366
CHAPTER 10. SUMMARY AND CONCLUSIONS.....	370
REFERENCES.....	377

APPENDICES	395
APPENDIX 3.A. Lateral Stiffness Contribution of Webs to Top Flanges.....	397
APPENDIX 4.A. Condensation and Verification of Transfer Matrices	405
APPENDIX 9.A. Compression Straight Flange Geometric Parameters and Data for the Anti-Symmetric Buckling Modes	413
APPENDIX 9.B. Horizontally Curved Box Girder Flange Parameters and Data for the Anti-Symmetric Buckling Modes	421
APPENDIX 9.C. Typical NASTRAN Input Files for Eigenvalue Buckling Analysis of Hypothetical Horizontally Box Girder Model....	425
APPENDIX 9.D. Typical NASTRAN Input File for Incremental Nonlinear Analysis of Hypothetical Horizontally Box Girder Model	439
APPENDIX 9.E. Ultimate Strength Curves	455

LIST OF TABLES

Table 3.1. Equivalent thickness of top lateral bracing systems (adopted from Kollbrunner and Basler 1969)	24
Table 3.2. Diagonal forces, three-span continuous horizontally curved girder (kips)	48
Table 3.3. Strut forces, three-span continuous horizontally curved girder (kips)	49
Table 4.1. Ratio of distortional warping stress to bending stress (σ_w/σ_b) at bottom flange (internal K-frames).....	80
Table 4.2. Ratio of warping stress to bending stress (σ_w/σ_b) at bottom flange at midspan (internal X-frames).....	81
Table 6.1. Effects of cross-frame stiffness on member forces	142
Table 6.2. Strength and stiffness of partially stiffened concrete with aging	149
Table 7.1. Maximum vertical reactions and horizontal movements	168
Table 8.1. Ultimate bending and torsional strengths of composite box girders	200
Table 9.1. Buckling Coefficient, k , according to the AASHTO Design Equation.....	243
Table 9.2. Variation of α_{cr} with n and k	246
Table 9.3. Comparison of F_{cr} (ksi) from FEM Analysis and Eq. (9.14)	248
Table 9.4. Minimum Required Moment of Inertia (in^4).....	266
Table 9.5. Elastic Buckling Stress of Curved Stiffened Flanges	317
Table 9.6. Critical Stress, F_{cr} (ksi) for Test Flange with Continuous Boundaries	326
Table 9.7. Effect of Different Stiffener Edge Boundary Conditions	327
Table 9.8. Critical Stress, F_{cr} (ksi) for Test Flange under Linear Moment Gradient	328
Table 9.9. Critical Stresses versus Initial Imperfection Types.....	346

Table 9.10. Comparison of Ultimate Strength of Straight Flange, F_{cr} (ksi)	358
Table 9.11. Comparison of Ultimate Strength of Curved Flange, F_{cr} (ksi).....	360
Table 9.12. Section Properties	363
Table 9.13. Stress Results (ksi)	363
Table 3.A.1. Lateral stiffness contribution of top flange and web (top flange width = 18 in.)	403
Table 3.A.2 Lateral stiffness contribution of top flange and web (top flange width = 16 in.)	404

LIST OF FIGURES

Fig. 1.1. Steel box girders: (a) Enclosed box girder; (b) Tub girder with lateral bracing (quasi-closed box girder)	2
Fig. 1.2. Steel/concrete composite box girders: (a) Single box; (b) Multi-box (twin-box); (c) Multi-cellular box	3
Fig. 3.1. Superstructure of box girder bridge.....	21
Fig. 3.2. Lateral bracing systems: (a) Single diagonal type (SD type); (b) Crossed diagonal type (XD type).....	22
Fig. 3.3. Forces affecting bracing members: (a) Longitudinal deformation; (b) Lateral force components due to inclined webs	26
Fig. 3.4. Lateral bracing systems: (a) SD type A; (b) SD type B; (c) XD type; (d) Cross-sectional properties; (e) Applied torque; (f) Applied vertical load.....	28
Fig. 3.5. Strut forces in simple span girder due to torsion.....	30
Fig. 3.6. Torsion and distortion components (adopted from Fan and Helwig, 2002)	30
Fig. 3.7. Differential lateral displacements of top flanges due to torsion and distortion...32	
Fig. 3.8. Lateral force resultants balanced from diagonal forces.....	32
Fig. 3.9. Lateral forces from diagonals: (a) Lateral forces; (b) Lateral force affecting lateral bending; (c) Lateral force affecting struts; (d) Deformation of two repeating adjacent panels	33
Fig. 3.10. Lateral forces from cross-frames: (a) Lateral forces; (b) Lateral force affecting lateral bending; (c) Lateral force affecting bracing members; (d) Deformation of two repeating adjacent panels; (e) Interface forces.....	35
Fig. 3.11. Elongation components of a diagonal member	36
Fig. 3.12. Interface forces between the top flange and lateral bracing members due to lateral force components (w_{lat}).....	40
Fig. 3.13. Lateral displacements of top flanges due to lateral force components (w_{lat})	40

Fig. 3.14. Comparison of diagonal forces in straight girder due to torsion.....	43
Fig. 3.15. Comparison of strut forces in straight girder due to torsion.....	43
Fig. 3.16. Forces in bracing members in straight girder due to vertical bending	44
Fig. 3.17. Three-span continuous horizontally curved tub girder.....	45
Fig. 3.18. Bending and torsional moment diagrams of three-span continuous horizontally curved girder	47
Fig. 3.19. Diagonal forces in lateral bracing system of three-span continuous horizontally curved girder	50
Fig. 3.20. Strut forces in lateral bracing system of three-span continuous horizontally curved girder	50
Fig. 4.1. Internal cross-frames for box girders: (a) Internal K-frame; (b) Internal X-frame	54
Fig. 4.2. External torsional loads on box girder: (a) Opposing two vertical loads; (b) Opposing two horizontal loads	56
Fig. 4.3. Lateral force component on a horizontally curved flange element	57
Fig. 4.4. Torsional and distortional components: (a) Due to opposing vertical loads; (b) Due to opposing horizontal loads; (c) Combined from opposing vertical and horizontal loads	61
Fig. 4.5. Internal X-frame under distortional load components	63
Fig. 4.6. Top lateral bracing systems: (a) SD type A; (b) SD type B; (c) XD type; (d) Cross-sectional properties; (e) Applied torque	67
Fig. 4.7. Member forces in X-frame diagonal due to torsion (straight box girder)	69
Fig. 4.8. Distortional warping stress gradients along the girder length.....	69
Fig. 4.9. Forces induced in diagonal members of internal K-frames	70
Fig. 4.10. Forces induced in strut members of internal K-frames	70
Fig. 4.11. Member forces in internal K-frames versus number of K-frames per span.....	71

Fig. 4.12. Planar dimensions of three-span continuous horizontally curved girder and vertical loading.....	73
Fig. 4.13. Dimensions of three cross sections and bracing members	73
Fig. 4.14. Diagonal forces of X-frames in three-span curved girder	74
Fig. 4.15. Plan view of the simply supported curved box girders with different arrangements of top lateral bracing systems: (a) SD type A; (b) SD type B; (c) XD type	75
Fig. 4.16. Internal K-frame diagonal member forces of simply supported curved girders subjected to uniformly distributed vertical loads.....	76
Fig. 4.17. Internal X-frame diagonal member forces of simply supported curved girders subjected to uniformly distributed vertical loads.....	76
Fig. 4.18. Horizontally curved box girders with SD type lateral bracings and internal K-frames: (a) One-panel spacing; (b) Two-panel spacing.....	78
Fig. 4.19. Two different cross sections of box girders with internal K-frames	80
Fig. 4.20. Two different cross sections of box girders with internal X-frames.....	81
Fig. 4.21. Distortional warping stress distribution in girders of shallow cross section with K-frames ($L=160$ ft, $R=700$ ft).....	82
Fig. 4.22. Distortional warping stress distribution in girders of deep cross section with K-frames ($L=160$ ft, $R=700$ ft).....	82
Fig. 4.23. Effect of aspect ratio of horizontally curved trapezoidal box girder with internal K-frames and XD type lateral bracing.....	84
Fig. 4.24. Effect of aspect ratio of horizontally curved trapezoidal box girder with internal X-frames and XD type lateral bracing.....	85
Fig. 4.25. Effect of aspect ratio of horizontally curved trapezoidal box girder with internal K-frames and SD type lateral bracing	86
Fig. 4.26. Effect of aspect ratio of horizontally curved trapezoidal box girder with internal X-frames and SD type lateral bracing	87
Fig. 4.27. Effect of spacing on cross-frame member forces (K-frame with SD type A)...	89
Fig. 4.28. Effect of spacing on cross-frame member forces (K-frame with SD type B)...	90

Fig. 4.29. Effect of spacing on cross-frame member forces (X-frame with SD type A)...	91
Fig. 4.30. Effect of spacing on cross-frame member forces (X-frame with SD type B)...	92
Fig. 5.1. Simple span box girders: (a) SD type; (b) XD type; (c) Cross-sectional properties; (d) Applied vertical load; (e) Notation K-frame members; (f) Notation for X-frame members.....	98
Fig. 5.2. Effects of internal cross-frame spacing on diagonal forces in lateral bracing	99
Fig. 5.3 Effects of internal cross-frame spacing on strut forces in lateral bracing	99
Fig. 5.4. Diagonal forces in K-frames provided at one-panel spacing	100
Fig. 5.5. Lateral displacement of top flanges due to vertical bending.....	101
Fig. 5.6. Differential lateral displacement between top flanges due to vertical bending	101
Fig. 5.7. Average lateral displacement at the bottom flange	102
Fig. 5.8. Interactive forces between top flanges and lateral bracing members (internal K-frames)	104
Fig. 5.9. Assumed lateral displacements (internal K-frames): (a) Top flanges and lateral bracing members; (b) Lateral deflection of top flange	106
Fig. 5.10. Interactive forces between top flanges and lateral bracing (internal X-frames)	112
Fig. 5.11. Assumed lateral displacements (internal X-frames): (a) Top flanges and lateral bracing members; (b) Lateral deflection of top flange; (c) Cross section with X-frame	114
Fig. 5.12. Lateral displacements of top flanges and lateral bracing near interior supports	120
Fig. 5.13. Forces in lateral bracing of simple span box girder with internal K-frames ..	122
Fig. 5.14. Diagonal forces in internal K-frames of simple span girder	122
Fig. 5.15. Three-span continuous straight girder with various cross sections subjected to vertical loads	123

Fig. 5.16. Diagonal forces in lateral bracing of three-span continuous box girder with internal K-frames	124
Fig. 5.17. Strut forces in three-span continuous box girder with internal K-frames	124
Fig. 5.18. K-diagonal forces three-span continuous box girder	125
Fig. 5.19. Forces in lateral bracing in simple span box girder with internal X-frames ...	126
Fig. 5.20. X-diagonal forces in simple span box girder.....	126
Fig. 5.21. Diagonal forces in lateral bracing of three-span continuous box girder with internal X-frames	127
Fig. 5.22. Strut forces in three-span continuous box girder with internal X-frames	127
Fig. 5.23. X-diagonal forces in three-span continuous box girder	128
Fig. 6.1. Twin-box girder bridge: (a) Completed stage; (b) Cross section of steel tub girder during construction.....	131
Fig. 6.2. Notation for twin-box girder bridge cross-section: (a) Deck width; (b) Deformed shape	134
Fig. 6.3. Cross-sectional dimensions of the hypothetical twin-box girder bridge in simple-span	139
Fig. 6.4. Effect of the number of external cross-frames on the unevenness ratio (subtended angle = 1.0 rad.).....	140
Fig. 6.5. Effect of the stiffness of bracing members on the unevenness ratio (Members, I, II, and III are as given in Table 6.1)	141
Fig. 6.6. Planar dimensions of a three-span continuous twin-girder and dimensions of three different cross sections.....	144
Fig. 6.7. Two different deck pouring sequences considered for three-span continuous bridges.....	145
Fig. 6.8. Analysis steps for staged deck pouring with partially stiffened deck concrete	147
Fig. 6.9. Relative gain in strength with time of concretes with different water/cement (w/c) ratios (adopted from Mindess et al. 2003).....	148

Fig. 6.10. Effect of external cross-frames and radius of curvature on the unevenness ratio of a three-span continuous bridge with one-step pouring	150
Fig. 6.11. Comparison of unevenness ratio during deck pouring sequence after the first stage completed.....	150
Fig. 6.12. Comparison of unevenness ratio during deck pouring sequence after the second stage completed.....	151
Fig. 6.13. Comparison of unevenness ratio during deck pouring sequence after the final stage completed.....	151
Fig. 6.14. Effect of the time lag between the first and second stage on the unevenness ratio (with external cross-frames)	153
Fig. 7.1. Deformed shapes of plain elastomeric bearings (without reinforcing shims) under applied loads: (a) compression; (b) shear force; and (c) applied moment.....	159
Fig. 7.2. Effects of reinforcing shims and frictions between elastomer and solid plates: (a) Elastomer on the support; (b) deformed shape between solid plates without frictions; (c) deformed shape with friction; (d) deformed shape with friction and reinforced shims...	159
Fig. 7.3. Positive vertical temperature gradient in concrete and steel superstructures	169
Fig. 7.4. Notation used for rectangular elastomeric bearings	170
Fig. 7.5. Possible thickness range of interior elastomeric layer versus number of layers (Type I, $G = 100$ psi)	171
Fig. 7.6. Possible total thickness of elastomeric bearing (Type I, $G = 100$ psi)	171
Fig. 7.7. Possible thickness range of interior elastomeric layer versus number of layers (Type I, $G = 200$ psi)	172
Fig. 7.8. Possible total thickness of elastomeric bearing (Type I, $G = 200$ psi)	172
Fig. 7.9. Possible thickness range of interior elastomeric layer versus number of layers (Type II, $G = 100$ psi)	173
Fig. 7.10. Possible total thickness of elastomeric bearing (Type II, $G = 100$ psi)	173
Fig. 7.11. Possible thickness range of interior elastomeric layer versus number of layers (Type II, $G = 200$ psi)	174
Fig. 7.12. Possible total thickness of elastomeric bearing (Type II, $G = 100$ psi)	174

Fig. 7.13. Pure homogeneous deformation diagram: (a) undeformed state; (b) deformed state	175
Fig. 7.14. Finite element model for an elastomeric bearing with reinforced shims	182
Fig. 7.15. Deformed shape under compressive forces.....	182
Fig. 7.16. Deformed shape under shearing force.....	183
Fig. 7.17. Deformed shape under the combination of compressive force and moment ..	183
Fig. 7.18. Compressive strain-strain curves with various shape factors ($G = 100$ psi) ..	184
Fig. 7.19. Compressive stress-strain curves with various shape factors ($G = 200$ psi) ..	184
Fig. 7.20. Effect of frictional coefficients between elastomer and rigid plates on compressive stress-strain curve.....	185
Fig. 8.1. Idealized uniaxial stress-strain relationship: (a) concrete; and (b) steel	190
Fig. 8.2. Alternative stress-strain diagrams for concrete in tension	192
Fig. 8.3. Dimension of corner supported reinforced flat plate.....	193
Fig. 8.4. Load-deflection response of the corner supported reinforced flat plate (1 in. = 25.3 mm, 1 kips = 4.45 N)	194
Fig. 8.5. Typical finite element mesh used in incremental nonlinear analysis	196
Fig. 8.6. Steel/concrete composite box section: (a) Cross-sectional properties; and (b) Element types used in FEA.....	197
Fig. 8.7. Schematics for analysis of simply supported composite box girder in combined bending and torsion.....	198
Fig. 8.8. Applied bending moment versus deflection curve for composite box specimen (1 in. = 25.4 mm)	201
Fig. 8.9. Applied torsional moment versus rotation curve for composite box specimen	202
Fig. 8.10. Ultimate strength interaction between bending and torsion of the composite box girder in positive moment region.....	203

Fig. 8.11. Concrete deck element subjected to shear and normal stresses: (a) Shear flow in composite section; (b) Stress state in positive moment region; and (c) Corresponding principal state	205
Fig. 8.12. Crack detection curve: (a) Yield surface for stress in concrete; and (b) Simplified crack detection curve in the plane of positive σ_1 and negative σ_2	207
Fig. 8.13. Relationship between τ and σ from Eq. (8.4)	209
Fig. 8.14. Relationship between composite girder moment and longitudinal stress in deck concrete.	212
Fig. 8.15. Comparison of ultimate strength interaction curve from EFA and theory for a composite box girder in positive moment zone	213
Fig. 8.16. Proposed ultimate strength interaction curve for composite box girders in positive moment zone	214
Fig. 9.1. Longitudinally Stiffened Plate.....	239
Fig. 9.2. Buckling Mode Shapes from F.E.M Analysis.....	248
Fig. 9.3. Compression Flange Showing Rectangular and T-section Stiffeners	252
Fig. 9.4. Undeformed Shape of Typical Compression Flange	256
Fig. 9.5. Deformed Shape of Typical Compression Flange	256
Fig. 9.6. Critical Stress versus Moment of Inertia of Longitudinal Stiffeners	258
Fig. 9.7. Required I_s versus Number of Stiffeners.....	263
Fig. 9.8. Required I_s versus Aspect Ratio, a/w	263
Fig. 9.9. Required I_s versus Flange Thickness.....	264
Fig. 9.10. Required I_s versus Flange Subpanel Width.....	264
Fig. 9.11. Required I_s versus Torsional Rigidity of Stiffener	265
Fig. 9.12. Required I_s versus Cross-Sectional Area Ratio, A_s/A_f	265
Fig. 9.13. Normal Stress Components in Bottom Flange	269

Fig. 9.14. Distortional Force on a Box Girder	270
Fig. 9.15. Lateral Force Component on a Horizontally Curved Flange	271
Fig. 9.16. Distortional Force in the Horizontally Curved Box Girder.....	273
Fig. 9.17. Distortional Force Direction in Horizontally Curved Girder	274
Fig. 9.18. Angular Change, γ , in a Box Girder due to Distortion.....	277
Fig. 9.19. Distortional Normal Stress Distribution on a Box Girder	278
Fig. 9.20. Internal Diaphragms and Corresponding Support Type In BEF Analogy	280
Fig. 9.21. BEF Analogy for Horizontally Curved Box Girder	281
Fig. 9.22. Cross-sections of Curved Box Girder Model	285
Fig. 9.23. Finite Element Model Description	286
Fig. 9.24. Non-Uniform Normal Stress Distribution in the Bottom Flange (Under DL1)	293
Fig. 9.25. Non-Uniform Normal Stress Distribution in the Bottom Flange (Under DL2)	294
Fig. 9.26. Non-Uniform Normal Stress Distribution in the Bottom Flange (Under LL+I)	295
Fig. 9.27. Non-Uniform Normal Stress Distribution In the Bottom Flange (Under the Load Combination Group (I))	296
Fig. 9.28. Effect of Top Flange Bracing on Distortional Stress	297
Fig. 9.29. Effect of Sectional Area of Cross-Frames Distortional Stress	298
Fig. 9.30. Variation of Maximum Distortional Stress Ratio vs Number of Cross-Frames	299
Fig. 9.31. Typical Connection of Transverse Bracing of Cross-Frames and Longitudinal Stiffener in Box Girder	302
Fig. 9.32. Loading Scheme and Approximate Moment Diagram.....	306

Fig. 9.33. Finite Element Mesh of Box Girder Model.....	307
Fig. 9.34. Distortional Normal Stress Variation in Curved Bottom Flange Model ($n=1$, $a=5$, $w=80$ in., $t_f=1.0$ in., $R=800$ ft.)	309
Fig. 9.35. Maximum Distortional Stress versus Subtended Angle ($n=1$, $a=3$, $w=60$ in., $t_f=1.0$ in.)	310
Fig. 9.36. Typical Buckling Mode Shapes of Curved Stiffened Flanges ($n=1$, $a=5$)	313
Fig. 9.37. Buckling Mode Shape in a Hypothetical Box Girder Model	314
Fig. 9.38. Elastic Critical Stresses of Curved Stiffened Flange ($n=2$, $a=5$, $w=60$ in., $t_f=1.0$ in., $R=300$ ft.)	315
Fig. 9.39. Required Stiffener Rigidity along with Subtended Angle ($n=2$, $a=5$, $w=60$ in., $t_f=1.0$ in.)	322
Fig. 9.40. Typical Buckling Mode Shape of Test Flange with Continuous Boundary....	326
Fig. 9.41. Bending Moment Gradient and Applied Compressive Stress Gradient.....	329
Fig. 9.42. Typical Buckling Mode Shape of Test Flange under Linear Moment Gradient	330
Fig. 9.43. Out-of-Plane Deviations.....	337
Fig. 9.44. Cross-Sectional Shapes of Geometric Imperfections	343
Fig. 9.45. Failure Mode Shape for Imperfection Type a	347
Fig. 9.46. Failure Mode Shape for Imperfection Type b	347
Fig. 9.47. Failure Mode Shape for Imperfection Type c	348
Fig. 9.48. Failure Mode Shape for Imperfection Type d	348
Fig. 9.49. Failure Mode Shape for Imperfection Type e	349
Fig. 9.50. Deformed Shape at Failure, Imperfection Type b	351
Fig. 9.51. Inelastic Buckling Strength, Imperfection Type b	352
Fig. 9.52. Inelastic Buckling Strength, Imperfection Type a.....	352

Fig. 9.53. Variation of Inelastic Buckling Strength.....	353
Fig. 9.54. Inelastic Buckling Strength, Geometric Imperfection Type c	355
Fig. 9.55. Ultimate Strength of Straight Flange versus Width-to-Thickness Ratio	359
Fig. 9.56. Ultimate Strength of Curved Flange versus Width-to-Thickness Ratio	361
Fig. 9.57. Cross Section for Negative Moment Design.....	364
Fig. 9.58. Longitudinal Stiffener Arrangement, AASHTO Design.....	365
Fig. 9.59. Longitudinal Stiffener Arrangement, Proposed Design	365
Fig. 3.A.1. Simplified model for web and top flange subjected to a concentrated load	402
Fig. 9.E.1. Incremental Ultimate Strength.....	457

EXECUTIVE SUMMARY

Horizontally curved continuous steel girder bridges have become increasingly popular in modern highway systems including urban interchanges due to efficient dissemination of congested traffic, economic considerations, and aesthetic desirability. Composite box girders render an attractive alternative to the open I-shaped girder due to the superb torsional rigidity from a closed section and advantages in maintenance.

AASHTO Guide Specifications for Horizontally Curved Steel Girder Highway Bridges with Design Examples for I-Girder and Box-Girder Bridges (AASHTO 2003) significantly alleviate the difficulties associated with the original form of the *AASHTO Guide Specifications* (1993). However, the provisions in the current *AASHTO Guide Specifications* (2003) are primarily based upon research performed as part of the CURT (Consortium of University Research Teams) project in the early 1970's. Currently, the bridge engineering community focuses on a consorted effort of consolidating various forms of bridge design specifications into a single LRFD (Load and Resistance Factor Design) form. *AASHTO LRFD Bridge Design Specifications* (2004) do not include provisions on horizontally curved steel girders.

Steel box girders are at their critical stage during construction because the noncomposite steel section must support both the fresh concrete and the entire construction loads. A lateral bracing system is usually installed at the top flange level in the open-top box girder to form a quasi-closed box, thereby increasing the torsional

stiffness. Single diagonal and crossed diagonal bracing systems are typically considered for lateral bracing systems. Internal transverse bracing (also known as internal cross-frames) are provided in the box and usually spaced every one or two lateral bracing panels to retain the original box cross shape, thereby controlling the magnitude of the distortional warping stress level within a prescribed range. External bracing between the interior and exterior box girders may be necessary in the case of very sharply curved bridges in order to control the deflections and rotations of the girders, thereby facilitating the placement of the concrete roadway deck. In composite girders, according to basic structural mechanics, the stresses (whether they are bending stresses and/or shearing stresses) are additive; however, superposition is not valid for the bending moments and the twisting moments because of different cross-sectional properties at each stage of construction.

Horizontally curved bridge girders are subjected to combined bending and torsion. The ultimate positive bending strength almost always approaches the plastic bending moment of a composite box girder when the girder is properly proportioned. The ultimate torsion strength of a composite box girder in the positive bending zone is limited by the relatively low diagonal tension strength of the deck concrete due to torsion. The concurrent compressive stress in the concrete deck improves the shear behavior of concrete, resulting in increased torsional resistance of a box girder. Nevertheless, the ultimate torsional strength of a composite box girder is sensitively affected by the diagonal tensile stress in the concrete deck resulting from torsional moments. Hence, it is necessary to establish an ultimate strength interaction equation for steel/concrete composite box girders subjected to the combined action of bending and torsion.

It is one of the main issues concerning horizontally curved box girder bridges to investigate design procedures of compression flanges in the negative moment zones of continuous spans at interior piers. Although a great deal of research has been devoted to developing design methods and equations, there appears to be not sufficient information available concerning the adequate design of stiffened compression flanges applicable to the horizontally curved box girder system. Elastic buckling behaviors as well as the inelastic ultimate behavior of longitudinally stiffened flanges were not sufficiently characterized and there was not a simple yet rationally conservative equation for the design of longitudinal stiffeners. It has also been found that the current AASHTO provisions for the determination of the ultimate strengths of the stiffened panels in the inelastic buckling range can be unconservative.

Recently, elastomeric bearings are widely used through the world as bridge-support systems because they are very effective for horizontally curved bridges as well as straight bridges. While having high compressive stiffness, elastomeric bearings are flexible enough in shear to accommodate longitudinal movement of girders, thus, mitigate horizontal reactions at internal piers or abutments.

The present research addresses many issues about the horizontally curved steel box girder bridges including: (1) Top lateral bracing systems with different arrangements; (2) Internal transverse bracing; (3) Coupled behaviors of lateral and internal bracing; (4) Intermediate external bracing between box girders; (5) Elastomeric bearings under horizontally curve bridges; (6) Ultimate strength interaction between bending and torsion; (7) Design requirements for longitudinal stiffeners for box girder flanges. Analytical and numerical investigations have been conducted on a number of hypothetical box girder

bridges. Findings from these studies have been incorporated into design equations amenable to the AASHTO LRFD format. The validity and reliability of these newly developed equations have been verified by three-dimensional finite element analyses.

CHAPTER 1

INTRODUCTION

Before the advent of major highway and interstate programs, bridges typically spanned perpendicular to the roads and rivers they crossed. Thus, bridge orientation dictated the roadway alignment and the difficulties associated with complicated bridge geometries and support conditions were essentially avoided. However, modern high speed highway systems have created complex roadway alignments which control the bridge geometry and have thus resulted in bridges with skewed supports and curved alignments. To meet the demand of increasing highway complexity, horizontally curved steel bridges now represent one-third of all new steel bridges built in the United States (Simpson 2000). Horizontally curved steel box girder bridges have become increasingly popular in modern highway systems including interchanges due to economic considerations, aesthetic desirability, and the superb torsional rigidity from a closed section.

In simple terms, the steel box girder may be defined as a longitudinal structural member with four steel plates, two webs and two flanges, arranged to form a closed box section as shown in Fig. 1.1(a). However, in modern highway structures, a more common arrangement is the box girder with open top which is usually referred to as the *tub girder*. In this case, two steel webs with narrow top flanges similar to those of the

plate girders are joined at their bottoms by a full-width bottom flange as shown in Fig. 1.1(b). At fabrication and erection stages, the section may be completely open at the top or it may be braced by a top lateral bracing system. To close the top opening and complete the box, a reinforced concrete deck slab is added which acts compositely with the steel section by a means of shear connectors attached to the top flanges. This box girder system is referred to as a steel/concrete composite box girder. Composite box girder bridge systems may take the form of single box, multi-box, or multi-cellular box as shown in Fig. 1.2.

In steel/concrete composite box girder bridge construction, the steel girder with lateral and transverse bracing is erected first and the deck concrete is cast later. The steel tub girder section is an open section and, during the construction phase, is subjected to full construction loads. The construction loads may include wind, the concrete finishing machine (screed), formwork, and the weight of the fresh concrete. Some difficulties have been encountered in box girder construction, and case histories are available about the change of geometry or excessive rotation of girder before and during the placement of the deck concrete (United States Steel Corporation 1978). The girder characteristics before

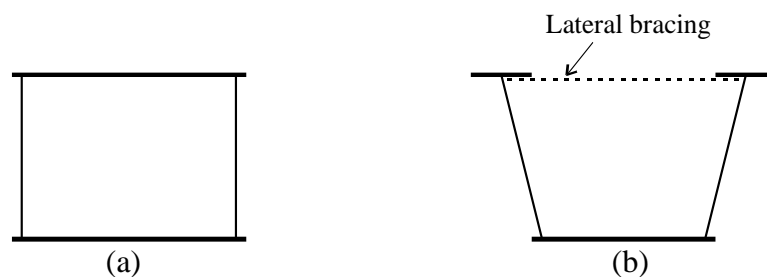


Fig. 1.1. Steel box girders: (a) Enclosed box girder; (b) Tub girder with lateral bracing (quasi-closed box girder)

the deck concrete is hardened are different from those of the completed structures, and special measures have to be taken to ensure strength and stability of the girder during the construction.

Lateral bracing systems are provided at the top flange level to increase the torsional stiffness, and internal cross-frames are used to control distortion of the box cross section due to applied torque. The tub girder with the lateral bracing at top flange level is often referred to as a quasi-closed box girder (Fig. 1.1(b)). In the case of multi-box girder bridge systems with very sharp curvature, intermediate external cross-frames are provided between box girders in order to control the deflection and rotation of each box girder during construction.

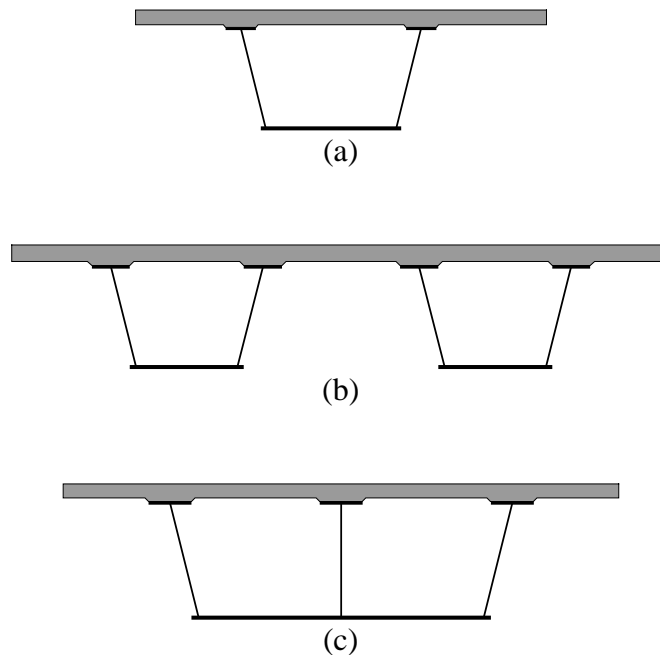


Fig. 1.2. Steel/concrete composite box girders: (a) Single box; (b) Multi-box (twin-box); (c) Multi-cellular box

Although fragmented research results are available in the literature, a comprehensive design guide is not in existence for addressing the strength requirement for bracing members. Examination of current design specifications and codes throughout the world reveals that there are little or no guidelines available for the design of top lateral bracing systems, internal transverse bracing in the box, and external bracing systems between box girders. This general lack of guidance led engineers to develop either overly conservative or, in some instances, inadequate bracing designs, thus resulting in unnecessary cost increase or unexpected failures of bracing members during bridge erection (Chen 2002).

Although the new growth of the steel box girder bridge began following the Second World War (Godfrey 1974), there were a series of disastrous accidents that motivated advances in research on box girders. After the Second World War, hundreds of steel box girder bridges were successfully built in Europe until 1969, when the fourth Danube Bridge in Vienna, Austria, collapsed during construction. This mishap was followed by three major disasters during 2 years in which more than fifty people lost their lives. These failures led bridge engineers to reexamine the design rules and methods of analysis used for steel box girder bridges. A number of researchers concluded that experience of the behavior and design of plate girders could not be extrapolated to cover all the problems encountered in box girder design because of three main differences between the two structural systems. Major differences between a plate girder and a box girder are listed as follows (Dowling 1975):

- (1) Unlike the compression flange of a plate girder, which is concentrated in relatively thick sections over a narrow width, that of a box girder is made of wide thin plate sections, stiffened by an orthogonal grid of stiffeners. Consequently the problems of shear lag and out-of-plane buckling of the flange elements must be considered in the design of box girder flanges.
- (2) Differences in the flanges affect the web behavior. The edge restraints against in-plane normal and tangential movement of the web panels are less in the case of a web bounded by a thin flange plate on one side of the web only than in the case of a web bounded by a thick flange plate symmetrically disposed about the web mid-plane. Thus, tension field theories developed in the context of plate girder webs cannot readily be extrapolated to box girder webs.
- (3) Reactions are transmitted to the supports by load-bearing stiffeners acting as struts in the case of plate girders. In box girders, the reactions are transmitted through plate diaphragms. These diaphragms, which are subjected to a complex system of stresses, must be designed to preclude the possibility of failure by instability.

Design considerations are different in the curved box girder design compared with the curved plate girder design. The plate girder is an open section and is characterized by very low torsional resistance. The twisting of the plate girder results in significant normal stresses on the flanges. Diaphragms and cross-frames between plate girders are an absolute necessity in restraining these stresses to acceptable levels and must be

carefully designed with respect to both the strength and spacing. The single plate girder is inherently unstable and, for a typical bridge girder length, is very flexible and susceptible to a large deformation. Although a box girder is much stronger than a plate girder with regard to torsion due to its superb torsional resistance, care must be taken during fabrication and erection.

There are imperfections caused from fabrication that influence the strengths of box girders. They are generally of two types, i.e., residual stresses and geometric imperfections. Apart from the stresses induced in plates and stiffeners during the mill production, residual stresses are also caused by welding due to uneven cooling. The residual stress distribution is dependent upon the sequence of fabrication and the method of support by jigs during welding. Geometric imperfections are also caused during fabrication. The effect of uneven cooling induces not only the residual stresses but also unavoidable warping. In order to control the out-of-flatness induced by welding, Bridge Welding Code (2002) stipulates dimensional tolerances. It has been pointed out that it is only the magnitude of the initially deflected shape which is sensitive to the buckling mode and strength of the plate panel (Dowling 1975). In ultimate strength analysis using finite element programs, the effect of these two imperfections, residual stresses and initial imperfection, can be accurately reflected in order to preclude unconservative or overly conservative results.

The development of the curved beam theory by Saint-Venant (1843) along with the thin-walled beam theory by Vlasov (1961) marked the birth of all research efforts published to date on the analysis and design of straight and curved box-girder bridges.

Since then, numerous technical papers, reports, and books have been published in the literature concerning various applications of the two theories. In the U.K., Maisel (1970) undertook a comprehensive literature review of analytical and experimental studies on box girder bridges. In the United States, the Subcommittee of Box Girder Bridges was formed under the ASCE-AASHO Committee on Flexural Members in 1963 and charged with the task of assessing the technical adequacy of the design procedures and investigating the economies of box girders. In its report on trends in the design of steel box girder bridges (ASCE-AASHO 1967), the subcommittee listed fifteen areas of research on steel box bridges that were further needed at that time. Eleven years later, the Task Committee on Curved Box Girder of the ASCE-AASHTO Committee on Flexural Members (ASCE-AASHTO 1978b) presented a state-of-the-art report with one hundred and six references dealing primarily with horizontally curved box girder bridges. The Task Committee also presented (ASCE-AASHTO 1978a) results of a survey pertaining to the geometry, design, detailing, construction, and performance of box girder bridges constructed in the United States, Canada, Europe, and Japan. Nakai and Yoo (1988) published a unique reference book on *Analysis and Design of Curved Steel Bridges*. In order to meet the needs of reliable design and construction guide on horizontally curved steel girder highway bridges, the Federal Highway Administration and participating State Departments of Transportation sponsored a research project (FH-11-7389), referred to as CURT in 1969. This comprehensive and systematic research effort was performed between 1969 and 1976 and produced an extensive body of knowledge on the static and dynamic behavior of curved girders. The findings of the CURT project were synthesized

and summarized into the development of the *Tentative Design Specifications for Horizontally Curved Highway Bridges* (CURT 1975). It was adopted by AASHTO as the first *Guide Specifications for Horizontally Curved Highway Bridges* (AASHTO 1980). Although this document has undergone several editorial revisions until its final version in 1993 (AASHTO 1993), the original contents remained essentially intact. Hall and Yoo (1999a, 1999b) completed two design examples for horizontally curved steel I-girder and box girder bridges along with Recommended Specifications for Horizontally Curved Steel Girder Highway Bridges under NCHRP Project 12-38 (1999). AASHTO adopted these works as *Guide Specifications for Horizontally Curved Steel Girder Highway Bridges with Design Examples for I-Girder and Box-Girder Bridges* (AASHTO 2003), which supersede the old Guide Specifications.

1.1 Objectives and Scope

The objectives of this research are enumerated as follows:

- (1) To conduct a comprehensive literature search pertinent to research carried out on steel box girders.
- (2) To study the behavior of quasi-closed box girders, and develop analytical equations for estimating member forces induced in a lateral bracing system due to bending and torsion reflecting different types of lateral bracing systems.
- (3) To investigate the distortional behavior of box cross sections, and develop analytical equations for estimating member forces induced in cross-frames.

- (4) To investigate coupling action of lateral bracing and cross-frames (the coupling action takes place in the case when a girder has a single diagonal type bracing system with cross-frames installed at one-panel spacing), and develop matrix equations for member forces induced in members of lateral bracing and cross-frames.
- (5) To determine the differential deflection and rotation of multiple horizontally curved box girders under the weight of the fresh concrete, and develop equations predicting transverse camber requirements of horizontally curved box girder bridges under various deck casting sequences. These equations include a means of predicting forces induced in external cross-frame members (when they are installed) under various deck casting sequences.
- (6) To review design procedures for elastomeric bearings and hyperelastic material stress-strain relationship for numerical modeling, and investigate the performance of elastomeric bearings through typical horizontally curved bridges.
- (7) To investigate failure behaviors of concrete deck due to diagonal tension and torsion, develop an ultimate strength interaction equation between bending and torsion for steel/concrete composite box girder subjected to combined action of positive bending and torsion.
- (8) To investigate analytically buckling of stiffened compression plates for a variety of parameters, establish the minimum required rigidity based on the

elastic buckling approach and develop a design rule for straight and horizontally curved stiffened flanges for the ultimate loading state.

Each task listed above has basically been conducted as an independent investigation with the results from each presented as follows:

Chapter 2. Literature Review

Chapter 3. Lateral Bracing Systems

Chapter 4. Cross-Frames in Steel Box Girders

Chapter 5. Coupling Action of Lateral Bracing and Cross-Frames

Chapter 6. External Cross-Frames

Chapter 7. Elastomeric Bearings

Chapter 8. Ultimate Strength Interaction of Composite Box Girders

Chapter 9. Requirements for Longitudinal Stiffeners

Chapter 10. Summary and Conclusions

Chapter 2 provides an annotated summary of relevant references. A thorough and comprehensive literature search has been conducted to collect accessible information regarding research on box girders. References are broadly categorized in Chapter 2 to include thin-walled beam theory, quasi-box theory, ultimate responses of box girders, and numerical analysis techniques. Chapter 3 presents an analytical formulation of equations to predict member forces induced in the lateral bracing system in a box girder subjected to vertical and torsional loads. Different responses between a single diagonal type and a crossed diagonal type are investigated. Chapter 4 describes an analytical study on the distortional behavior of box cross sections and equations developed for estimating forces

induced in the diagonal members of cross-frames. Distortional force components are decomposed from applied torsional loads. Both K-shaped and X-shaped internal cross-frames are considered. Chapter 5 presents the effect of the spacing of internal cross-frames on lateral bracing members and internal cross-frames. Interactions between lateral bracing systems and internal cross-frames are investigated and transfer matrix equations are constructed to express forces induced in lateral and internal bracing members. Chapter 6 describes an investigation of the effectiveness of intermediate external bracing between box girders. A number of hypothetical curved box girder bridges were analyzed using three-dimensional finite element models, and the collected data were synthesized and characterized by a means of regression analyses into a design guide. In Chapter 7, design procedures for elastomeric bearings are presented and theoretical and numerical approaches for hyperelastic material modeling are conducted. In Chapter 8, an ultimate strength interaction equation is proposed for steel/concrete composite box girders subjected to the combined action of positive bending and torsion in the positive bending zone. Chapter 9, design equations are established for the minimum required rigidity of longitudinal stiffeners based on the elastic buckling approach and ultimate loading state. Chapter 10 summarizes all the studies done and presents conclusions.

1.2 Methodology

The investigative tools used in this research are basically analytical as opposed to experimental. Whenever practical the development of predictor equations for induced

forces and deformations are based on sound theoretical principles. All predictor equations formulated based on theoretical models have been thoroughly verified to ensure their adherence to fundamental principles of structural mechanics by examining the equilibrium and compatibility requirements. As it is necessary to occasionally introduce a few simplifying assumptions in the theoretical models adopted, all analytically formulated equations have been compared with numerical solutions from three-dimensional finite element analyses and conservative correlations confirmed. MAPLE (2002), a computer program capable of symbolic calculations, and SPSS (1998), a computer program for statistical operations, were of great help in the analytical formulation process of the predictor equations. Analytical formulation based on these theoretical models has been verified using more rigorous and detailed analysis techniques such as the finite element method.

A three-dimensional finite element analysis has been carried out to analyze hypothetical box girder bridges using both ABAQUS (2003) and/or MSC/NASTRAN (1998). Results from these two general purpose finite element codes were compared to those from the analytical formulation. In practically all cases compared, the differences were within the bounds of acceptable precision errors, thus ensuring the rigor of the structural modeling.

CHAPTER 10

SUMMARY AND CONCLUSIONS

Investigated in this research are a number of crucial areas needed to improve the understanding of the issues associated with the design and construction of horizontally curved composite box girder bridges. Unlike comparable straight bridges, the curved girder bridge system must be analyzed as an integral structure, even under gravity loading alone. The top lateral bracing, internal cross-frames, and diaphragms that serve primarily to prevent premature lateral buckling from occurring in straight bridges become major load carrying components for curved bridges and serve to resist induced torsion, restrain the distortion of the cross sections, and to distribute loads between girders. Furthermore, it becomes necessary in horizontally curved composite box girder bridges with sharp curvature to install an external bracing system to control excessive differential deflections and rotations between the inside and outside girders during deck casting. An investigation into the system behavior of the curved box girder system was conducted, and a number of predictor and design equations developed. These equations were compared with existing equations of similar purpose where possible. If there were no existing equations available for comparison, the derived equations were compared with

three-dimensional finite element analyses, and the applicability and accuracy of the proposed equations demonstrated.

Trapezoidal steel box girders are at their critical stage during construction because the noncomposite steel section must support the fresh concrete and the entire construction load. Typical lateral bracing types investigated are a single diagonal (SD type) truss and a crossed diagonal (XD type) truss. Equations from previous studies estimate brace forces for box girders with XD type lateral bracing systems with good accuracy. In some horizontally curved box girders, however, it has been found that substantial axial forces, possibly up to 35% of the total forces, are developed in struts due to induced torsion and distortion. New equations were analytically formulated to compute brace forces developed in bracing members. For box girders with SD type bracing, brace forces can be much better estimated by these new equations than any other existing approximate procedures. Bracing member forces due to bending and torsion computed from these new equations are compared with those evaluated by three-dimensional finite element analyses. Excellent correlation exists between these two values.

The top lateral bracing system in composite tub girders is only required for the construction load. Once the concrete roadway deck is completely hardened, the composite concrete deck takes over the structural function provided by the lateral bracing system. Because of this temporary nature of the bracing system, there is a tendency to take a short-cut on the part of the designers and contractors, thereby resulting in occasional embarrassing experience. Equations have been analytically derived to determine forces in bracing members accurately. These temporary yet important

primary load carrying bracing members, particularly in horizontally curved box girders, can now be designed economically according to sound engineering principles.

In a horizontally curved girder, the bending moment and torsional moment are always coupled due to the curvature of the girder axis. The applied torsional moment is primarily resisted by St. Venant torsion in a girder with a closed cross section. Therefore, stresses (both normal stress and shearing stress) induced due to warping torsion are negligibly small and are not separately considered in the design of the box girder. However, the distortional stresses may become fairly large if adequate distortional stiffnesses are not provided, as the stiffness of a box section against distortion is relatively weak compared with the bending stiffness or torsional stiffness. If cross-frames are provided at a proper spacing, the distortional effects can be controlled in a horizontally curved girder. Torsional moments can be decomposed into a pair of couples inducing a net shear flow and distortion of the cross section. Distortion of box girders is caused by the distortional components. The magnitude and distribution of the distortional components on box girders are a function of the applied torsional loads as well as the cross-sectional geometry of the boxes. Equations to decompose the torsional moment into the force couples causing pure torsional shear flows and distortion of the cross section are given. Data collected from three-dimensional finite element analyses of hundreds of hypothetical horizontally curved box girders show that the ratio of distortional warping stress to bending stress, an important measure of controlling cross-sectional distortion, is affected by a combination of the type of lateral bracing, the spacing of cross-frames, and the aspect ratio of box cross sections. Equations to predict

member forces of cross-frames in trapezoidal box girders have been derived herein.

Member forces computed by the proposed predictor equations have been compared with those obtained from three-dimensional finite element analyses and reasonable correlations have been observed.

Equations to estimate forces in lateral bracing members and cross-frames of tub girders have been suggested in recent years. Comparative examinations of bracing forces computed from the available equations with those from finite element analyses on a selected number of box girder examples reveal that there is a room for improvement in the derived predictor equations. Forces in both struts and diagonals in an SD type bracing are affected by the longitudinal displacements and lateral deflections of the top flanges. Longitudinal displacements are primarily due to vertical bending, while lateral deflections are caused by vertical bending, lateral force components due to inclined webs, torsion, and distortion. It has been observed that member forces in an SD type bracing system are affected by the spacing of cross-frames, i.e., one-panel spacing or two-panel spacing. Box girders with an SD lateral bracing system under vertical bending exhibit significantly different responses whether cross-frames are provided at one-panel spacing or two-panel spacing. The forces are developed in the diagonals primarily due to distortional components that are separated from torsional loads. However, forces are also caused in part in diagonals of cross-frames due to bending. The strut forces in an XD type lateral bracing system due to torsion are small compared with those developed in an SD type lateral bracing system because of the self-equilibrating nature of the crossed-diagonals within a panel in an XD type lateral bracing. Fairly extensive comparisons

given in Figs. 5.13 - 5.23 confirm the validity of the proposed equation for bracing forces. It is hoped that practicing engineers can now take advantage of being able to more accurately compute bracing forces in box girders with the improved predictor equations.

External cross-frames are used to prevent excessive rotations of individual box girders, thus control relative deflection between box girders during deck casting. The K-shaped frame is the preferred type for intermediate external bracing due to its cost advantage associated with fabrication and erection. Differential deflections have been investigated on horizontally curved twin-box girder bridges with intermediate external K-bracing considering different span types. Effects of the number of external cross-frames on the differential deflections are not significantly improved beyond using one cross-frame per span. Differential deflections and forces in external cross frame members are not affected greatly by the strength of external cross-frame member. Maximum forces are developed in two diagonals of K-shaped external cross-frames. Regression analyses have been performed on data collected from finite element analyses of over two hundred hypothetical bridge models and equations have been extracted to predict maximum bracing forces and differential deflections. Comparative studies reveal a high degree of correlation between the differential deflections and member forces in external cross-frames computed from predictor equations and those obtained from finite element analyses. There are no published design guides associated with deck casting sequences, expected differential deflections, and the size and number of external cross-frames for curved steel box girder bridges. It is recommended whenever possible to employ a half-

width deck casting (inner or concave side first) rather than full-width deck casting for horizontally curved bridges to provide a better differential deflection control. Regardless of deck casting sequences, rotation of the entire bridge cross section occurs due to curvature. Predictor equations, Eqs. (6.4) and (6.6), for relative deflections should find their applicability in camber design.

Elastomeric bearings are very effective for horizontally curved bridges. While having high compressive stiffness, elastomeric bearings are flexible enough in shear to accommodate longitudinal movement of girders, thus, mitigate horizontal reactions at internal piers or abutments to the any directions. In Chapter 7, design procedures for elastomeric bearings were briefly reviewed and design examples were introduced following AASHTO LRFD (2004). Theoretical modeling for hyperelastic material is reviewed. Numerical modeling for elastomeric is carried out using a commercial finite element analysis program, ABAQUS (ABAQUS Inc. 2003). It has been observed from the hypothetical bridges that the number of elastomeric layers in the range of 3 to 13 and possible thickness of each layer is between 0.5 in. and 1.8 in. It is also conformed from three-dimensional finite element analysis that shape factors and shear stiffness affect sensitively the compressive stress-strain relationship of elastomeric bearings.

In Chapter 8, ultimate strength interaction relationships between bending and torsion for steel/concrete composite box girder were investigated by both numerical and analytical means. In the numerical investigation, ultimate strength analyses were carried out taking advantage of the incremental nonlinear finite element analysis technique afforded in ABAQUS (2002) reflecting both material and geometric nonlinearities. A

spectrum of ultimate strength interaction data, positive vertical bending moment and concurrent torsional moment, were collected from these numerical analyses and normalized the ultimate bending strength and torsional strength, respectively. The developed ultimate strength interaction values were independently verified by an analytical means. An interaction design equation has been formulated based on the ultimate strength interaction data developed from the numerical and analytical investigation for steel/concrete composite box girders. The design equation was intentionally made conservative in order to reflect the brittle nature of the concrete deck failure due to diagonal tensile stress induced by torsional moments. The proposed ultimate strength interaction equation is simple to apply and is representative for a lower bound of the ultimate strength envelope.

A number of crucial areas needed for the proper design of straight and horizontally curved steel box girder compression flanges have been investigated in Chapter 9. As a consequence of this renewed examination of the design of steel box girders, the development of “new” design approaches based on the ultimate load capacity was emphasized. The effect of initial imperfections on the ultimate strength also came under intense scrutiny at that time and is now being considered in modern design specifications throughout the world. A simple yet remarkably accurate and versatile regression equation, Eq. (9.27), was successfully extracted that encompass all of the theoretically identified parameters. Remarkably Eq. (9.27) can be applied with equal accuracy and validity to both straight stiffened compression flanges and horizontally curved stiffened compression flanges of steel box girders.

CHAPTER 2

LITERATURE REVIEW

A thorough and comprehensive literature search regarding research on box girders has been performed to evaluate available information. Where appropriate, fundamental research publications that are not directly related to the behavior of horizontally curved box girders were also reviewed.

The earliest theoretical work on curved beam theory properly recognizing the coupling action of bending and torsion is credited to St. Venant (1843) over 150 years ago. However, the thin-walled beam theory by Vlasov (1961) that bridges the gap between the Euler-Bernoulli theory of classical solid beams and the theory of shells is regarded as the cornerstone of all research on the analysis and design of straight and horizontally curved thin-walled steel box girder bridges. The advancement of Vlasov's theory permitted for the first time a complete solution of thin-walled members subjected to the combined action of bending and torsion properly accounting for the development of normal stresses due to distortion (warping). Early researchers who recognized the development of distortional stresses in the horizontally curved box girder with lateral and transverse bracing include Oleinik and Heins (1975), Heins and Oleinik (1976), Nakai and Heins (1977), and Heins and Sheu (1982). Wright et al. (1968) used the beam-on-elastic-foundation analogy to describe the distortional behavior of a single-cell box

girder. Hsu et al. (1995) presented an improved approach for the distortional analysis of steel box girder bridges introducing an equivalent-beam-on-elastic-foundation method that accounts for the deformation of the cross section as a function of the rigidity of interior diaphragms and the girder continuity over the supports. Earlier investigators (Bazant and El-Nimeiri 1974; Mikkola and Paavola 1980; Zhang and Lyons 1984; Boswell and Zhang 1984; Fu and Hsu 1995) have combined the thin-walled beam theory of Vlasov (1961) and the finite-element technique to develop a thin-walled box beam element for the elastic analysis of straight and curved cellular bridges. The effect of transverse distortion, longitudinal torsional warping, and shear lag can be accounted for in this element. Because of the rapid advancement of modern-day computer hardware and the development of efficient coding of algorithms, such a beam element appears to be primarily of historical interest.

For a quasi-closed box girder, the torsional analysis may be performed using the equivalent plate method in which the top lateral bracing system is transformed into a fictitious plate with a uniform thickness. Kollbrunner and Basler (1969) developed equations for the fictitious plate thickness of several types of bracing configurations by evaluating the strain energy stored in the system. Dabrowski (1968) presented similar equations to determine the same based on the consistent deformation theory. Two of the major steel companies published instructive manuals concerning the fundamental behavior and the fabrication and construction of steel box girders with lateral and transverse bracing (United States Steel Corporation 1978; Heins and Hall 1981). Recently, Fan and Helwig (1999) made a significant contribution by presenting a means

to estimate the forces induced in top lateral bracing systems for box girders subjected to vertical bending. However, their proposed equations for the single diagonal type bracing system in horizontally curved box girders exhibit fairly large discrepancies although those for the crossed diagonal type bracing system yield forces that are in good agreement with finite element analysis results. Kim and Yoo (2004) suggested improved equations for estimating forces induced in members in the single diagonal bracing system accounting for the effect of each force component separately. Force components considered include those resulting from a decomposition of externally applied torsion into pure torsion and distortion, and those from longitudinal and lateral components due to bending. Fan and Helwig (2002) also studied the distortional behavior of trapezoidal box girders and proposed equations to predict forces in cross-frames as a function of the cross-frame spacing, properties of the box, and applied loads. Their study, however, is limited to K-shaped cross-frames. Topkaya and Williamson (2003) developed a computer program for curved girders under construction loads based on nine-node flat shell elements modeling the concrete deck. A novel feature of this shell element is the inclusion of three shear stresses associated with a basically plane-stress constitutive equation.

Culver and Nasir (1970) and Culver and Mozer (1970; 1971) studied the elastic and inelastic buckling behavior of an unstiffened flange of a curved box girder. Abdel-Sayed (1973) examined the problem of linear elastic responses and the bifurcation type critical limit for loading on webs of curved plate and box girders under combined actions of shear and normal stresses. Corrado and Yen (1973) tested to failure two slender-web

steel box girder models under different combinations of bending, shear, and torsional loads to investigate the postbuckling behavior of such members. A series of experimental and analytical studies on ultimate strength of steel box girders were carried out at Kansai University in Osaka, Japan. Yonezawa et al. (1978) and Dogaki et al. (1979) examined experimentally the ultimate behavior of two horizontally curved steel single-cell box girder bridge models with a longitudinally stiffened steel deck plate. The models were tested under two concentrated loads and the top flange failed due to inelastic buckling. Yonezawa et al. (1985) presented an analytical method to predict the elastic buckling of orthogonally stiffened sector plates under longitudinal compression uniformly distributed at the straight edges. Mikami et al. (1985) evaluated, using a finite difference technique, deflections and stresses in the bottom flange of tapered box girders with cylindrical web plates subjected to an in-plane load in the circumferential direction of the cylindrical web panel. Later, Mikami et al. (1987) tested to failure three straight steel box models subjected to bending. The top flanges in these models were stiffened longitudinally. The overall behavior of box girders after local buckling of one component (i.e., either web plate or flange) was carefully observed until failure of the girder. The test results showed the undesirable sudden collapse of the box girder after inception of local buckling of only one component. Mikami and Niwa (1993) extended this experimental study by testing to collapse three welded steel box girder models with unsymmetrical cross sections subjected to pure bending; combined bending and shear; and combined bending, shear, and torsion, respectively. In the negative moment regions over the interior piers of continuous box-girder bridges, the bottom flanges are subjected to high compressive

forces and buckling of the steel flange plates is frequently a governing factor for design. Yen et al. (1986) strengthened these compression flange plates by a concrete slab acting compositely with them with or without shear studs welded to the flanges. Korol et al. (1988) tested a single-cell steel model to failure to investigate the effect of geometric imperfection on the strength of steel box girders. Thimmhardy (1991) performed a geometrically and materially nonlinear analysis to predict the elastic buckling load and ultimate strength of stiffened compression plates in continuous box-girder bridges. Yoo et al. (2001) analytically developed an equation for a minimum required moment of inertia of longitudinal stiffeners on box girder compression flanges that is applicable to both elastic and inelastic buckling ranges. Analytical data were reduced using nonlinear regression analysis to a simplified design equation suitable for practicing engineers. Choi and Yoo (2004) verified that the equation developed for the minimum required longitudinal stiffener rigidity for straight box flanges can be applied to that for horizontally curved box flanges. Uy (2001) investigated elastic buckling and postbuckling of fabricated steel and concrete-filled composite cross sections experimentally. The test results illustrated the potential increase in both the initial buckling load and ultimate load that can be derived from the inclusion of the concrete infill. Nakai et al. (1990; 1992) performed experimental research on the ultimate strength of thin-walled steel box girder models with and without longitudinal stiffeners subjected to bending and torsion. Interaction curves between bending and torsion at ultimate states were presented.

During the past two decades, the finite element analysis has become a very popular technique for the computer solution of complex problems in engineering. Chapman et al. (1971) conducted a finite element analysis on steel and concrete box-girder bridges to investigate the effect of intermediate diaphragms on the warping and distortional stresses. Lim et al. (1971) developed an element that has a beam-like in-plane displacement field. The element is trapezoidal in shape, and hence, can be used to analyze right, skewed, or curved box-girder bridges with constant depth and width. Earlier the curvilinear boundaries of curved box girder bridges were modeled by a series of straight boundaries using parallelogram elements (Sisodiya et al. 1970). This approximation would require a large number of elements to achieve a satisfactory solution. Such an approach is impractical, especially for highly curved box bridges. Chu and Pinjarkar (1971) developed a modeling technique for curved box girder bridges. Their model consisted of horizontal sector plates and vertical cylindrical shell elements. The model can only be applied to simply supported bridges without intermediate diaphragms. Turkstra and Fam (1978) demonstrated the importance of evaluating warping and distortional normal stresses in a single-cell curved bridge in relation to the bending normal stresses obtained from a classical curved beam theory (as opposed to Vlasov's thin-walled beam theory). Galuta and Cheung (1995) developed a hybrid analytical solution that combines the boundary element method with the finite element method to analyze box-girder bridges. The finite element method was used to model the webs and the bottom flange of the bridge, while the boundary element method was employed to model the top slab. Jeon et al. (1995) presented a procedure for static and

dynamic analysis of composite box girders incorporating a large displacement theory.

The finite element equations of motion for beams undergoing arbitrary large displacements and rotations but small strains (geometric nonlinearity) were obtained from Hamilton's principle. Fafitis and Rong (1995) presented a substructure analysis method for thin-walled box girders. Sennah and Kennedy (2001; 2002) summarized highlights of references pertaining to straight and curved box girder bridges.

Annotated literature summarized herein is intended only as a brief overview of literature accessible on the general subject of analytical, numerical, and experimental investigations of straight and horizontally curved box girders. References that are pertinent to the current study to be presented subsequently will be cited and discussed in detail wherever appropriate.

CHAPTER 3

LATERAL BRACING SYSTEMS

3.1 Introduction

Steel box girder systems have been preferred superstructure types for both horizontally curved and straight bridges because of their structural and aesthetic advantages. A closed box girder in completed bridges has a superb torsional stiffness that may be 100 to more than 1,000 times that of a comparable plate girder (Heins and Hall 1981). The large torsional stiffness makes box girders well suited for horizontally curved box girder bridges in which the bridge geometry may induce large torsional moments in the girders. Due to the health and safety concerns, most box girder bridges in the United States have been built with open tops, and are therefore called *tub girders*. A typical box girder bridge system consists of one or more tub girders that act compositely with a cast-in-place concrete roadway deck. A schematic of a typical twin-girder bridge cross section is shown in Fig. 3.1.

Although the composite box section has a superb torsional rigidity, the noncomposite steel section is critical when subjected to large torsional loading during the early stages of bridge construction prior to hardening of the concrete deck. The noncomposite dead load stress may account for up to 60-70% of the total stress for a typical box girder bridge (Topkaya and Williamson 2003). A lateral bracing system, sometimes referred to as a horizontal top truss, is usually installed at the top flange level

to form a quasi-closed section and thereby increase the torsional stiffness during transport, erection, and construction. Single diagonal (SD type) and crossed diagonal (XD type) bracing systems which are shown in Fig. 3.2 are the most preferred examples for a lateral bracing system. SD type lateral bracing systems have a distinct feature that is not present in XD type lateral bracing systems: top flanges of box girders with SD type truss are subjected to lateral bending, similar to that of continuous beams with intermittent supports, due to the interaction between top flanges and lateral bracing members. Although the horizontal components resulting from sloping webs cause lateral bending in both SD type and XD type lateral bracing systems, most of the lateral bending in a girder with an SD type truss results from the large strut forces induced from vertical bending of the box girder. Since there are two diagonals at both ends of a strut in the XD type truss, the strut forces do not cause lateral bending in the flanges as these force are self-equilibrated within the bracing system. Although rudimentary research results were reported previously (Heins and Hall 1981; AASHTO 1993), Fan and Helwig (1999;

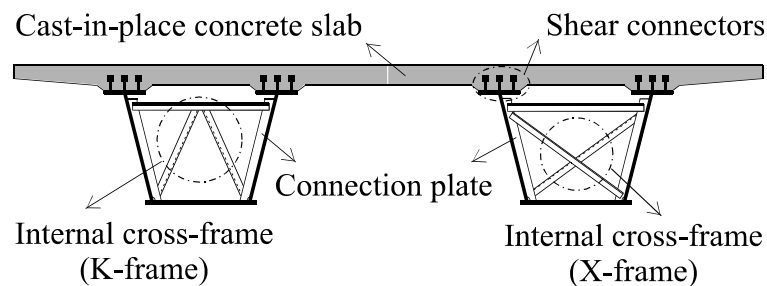


Fig. 3.1. Superstructure of box girder bridge

2002) are believed to be the first who made a significant contribution to the understanding of the lateral bracing system and cross-frames. They successfully presented analytical methods to estimate brace forces for both SD type and XD type lateral bracing systems of the box girders subjected to vertical loads and/or applied torque. According to the equations by Fan and Helwig (1999), strut forces are assumed to be induced only by bending of a box girder and lateral components induced by the sloping webs regardless SD type or XD type lateral bracing systems. It is reasonable to assume that strut forces are induced only by bending of a box girder and lateral load components in an XD type lateral bracing system. In the case of a SD type lateral bracing system, however, a considerable portion of the strut force developed is induced

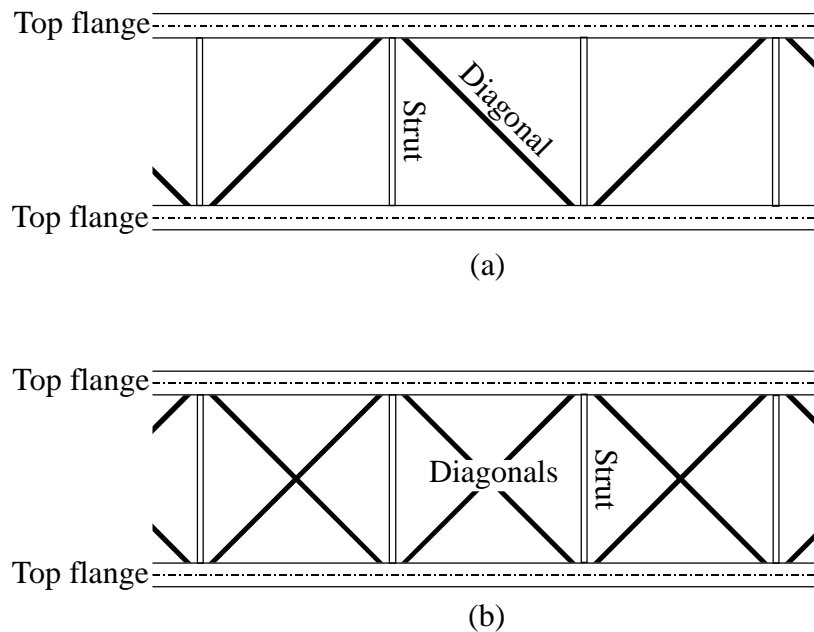


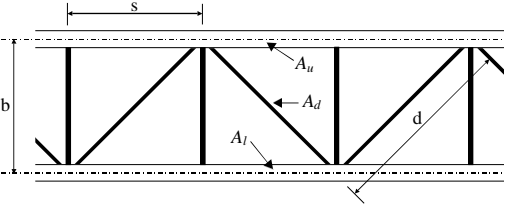
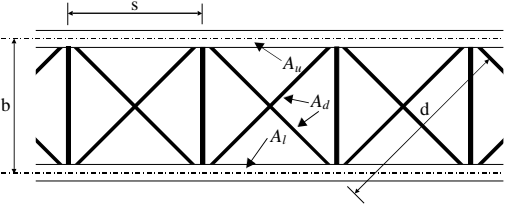
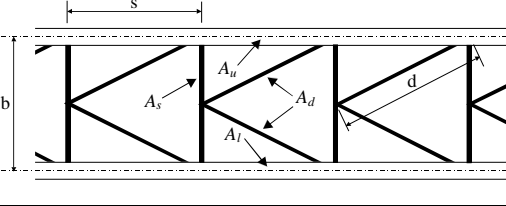
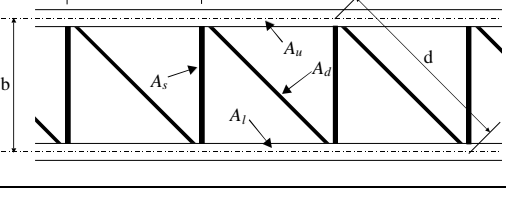
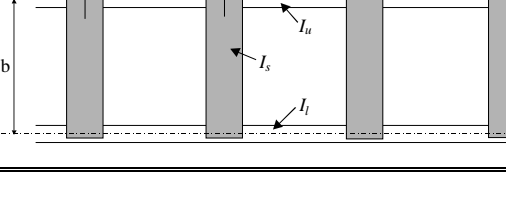
Fig. 3.2. Lateral bracing systems: (a) Single diagonal type (SD type); (b) Crossed diagonal type (XD type)

by the torsional moment. In addition to the torsional effect, brace forces in a SD type system subjected to vertical bending can more exactly be evaluated by considering a proper redistribution of lateral force components (the bending effect). Detailed procedures for this redistribution of lateral forces will be given later in Section 3.5. Equations to predict brace forces in SD type systems are formulated analytically. Brace forces in a SD type system computed by these analytical equations are compared with those obtained from three-dimensional finite element analyses (FEA). An excellent correlation exists.

3.2 Background

For a quasi-closed box girder, the torsional analysis can be performed using the equivalent plate method (EPM) in which the truss system is transformed into a fictitious plate with a uniform thickness. Kollbrunner and Basler (1969) developed equations for the equivalent thickness of several types of bracing systems by evaluating strain energy stored in the system. Table 3.1 summarizes configurations of bracing systems and corresponding equations for equivalent thickness. Dabrowski (1968) presented similar equations for X-shaped and K-shaped bracing systems to determine the fictitious plate thickness based on the consistent deformation theory. The quasi-closed box theory or EPM allows the torsional properties of the box girder to be approximated. The value of the equivalent plate thickness is dependent on the bracing configuration and cross-sectional areas of bracing members. The resulting shear flow in a closed section, q , is equal to $T / (2A_0)$ where T and A_0 are the torsional moment and the enclosed area of the

Table 3.1 Equivalent thickness of top lateral bracing systems (adopted from Kollbrunner and Basler 1969)

Arrangement of top lateral bracing	Equivalent thickness
	$t_{eq} = \frac{E}{G} \frac{sb}{\frac{d^3}{A_d} + \frac{s^3}{3} \left(\frac{1}{A_u} + \frac{1}{A_l} \right)}$
	$t_{eq} = \frac{E}{G} \frac{sb}{\frac{2d^3}{A_d} + \frac{b^3}{4A_s} + \frac{s^3}{12} \left(\frac{1}{A_u} + \frac{1}{A_l} \right)}$
	$t_{eq} = \frac{E}{G} \frac{sb}{\frac{d^3}{2A_d} + \frac{s^3}{12} \left(\frac{1}{A_u} + \frac{1}{A_l} \right)}$
	$t_{eq} = \frac{E}{G} \frac{sb}{\frac{d^3}{A_d} + \frac{b^3}{A_s} + \frac{s^3}{12} \left(\frac{1}{A_u} + \frac{1}{A_l} \right)}$
	$t_{eq} = \frac{E}{G} \frac{I}{\frac{sb^2}{12I_s} + \frac{bs^2}{48} \left(\frac{1}{I_u} + \frac{1}{I_l} \right)}$

box. The shear flow acting on the fictitious plate is then transformed to axial forces of diagonal members in the lateral bracing system as:

$$D_{tor,SD} = \pm \frac{qb}{\sin \alpha} = \pm \frac{b}{2A_0 \sin \alpha} T \quad (3.1)$$

$$D_{tor,XD} = \pm \frac{qb}{2 \sin \alpha} = \pm \frac{b}{4A_0 \sin \alpha} T \quad (3.2)$$

where $D_{tor,SD}$, $D_{tor,XD}$ = forces in SD type and XD type diagonals due to applied torque, respectively; b = top flange width between webs; α = angle between the diagonal and the top flange. Fan and Helwig (1999) confirmed the validity of values determined by Eqs. (3.1) and (3.2) through a series of three-dimensional finite element analyses.

It should be noted, however, that both torsion and vertical bending induce forces in the lateral bracing members. Diagonals in the lateral bracing systems are subjected to the same total longitudinal deformation as the top flanges as shown in Fig. 3.3(a). In addition, the lateral force component resulting from the sloping webs also affects member forces in the lateral bracing system. The magnitude of lateral force component is evaluated from the equivalent moment induced by the applied load on the top flange as shown in Fig. 3.3(b). Fan and Helwig (1999) developed equations to predict brace forces in SD types and XD types and proposed the following expressions for design purposes:

$$S_{Tot} = S_{bend} + S_{lat} \quad (3.3)$$

$$D_{Tot} = D_{EPM} + D_{bend} + D_{lat} \quad (3.4)$$

where S_{Tot} and D_{Tot} = total force in the strut and diagonal, respectively; S_{bend} and D_{bend} = force in the strut and diagonal due to bending of box girder, respectively; S_{lat} and D_{lat} = force in the strut and diagonal due to lateral force components, respectively; D_{EPM} =

diagonal force from the torsional moment determined using the EPM suggested by Eqs. (3.1) and (3.2). For simplicity, Fan and Helwig (1999) recommended designing the strut to carry the entire lateral load component, i.e., $S_{lat} = s$ times w_{lat} and $D_{lat} = 0$ where $s =$ spacing between struts; $w_{lat} =$ lateral load component. This is essentially tantamount to stating that the entire lateral force components are carried by the struts only. It has been observed that there exist up to 30% discrepancies between the values predicted by Eqs. (3) and (4) in some example box girder bridges. This is the impetus of undertaking the effort to derive improved predictor equations that yield a better correlation.

Consider three types of lateral bracing systems shown in Fig. 3.4. The example box girder has a length of 160 ft and 16 panels. Cross-frames are installed under every

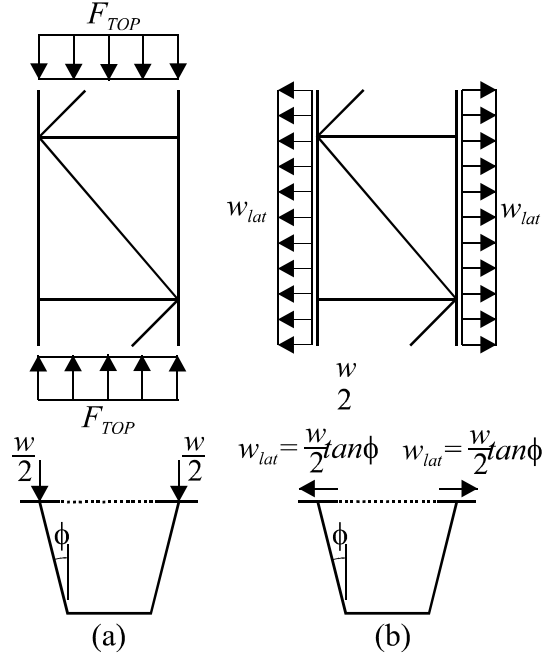


Fig. 3.3. Forces affecting bracing members: (a) Longitudinal deformation; (b) Lateral force components due to inclined webs

other strut location. Two different arrangements (A and B) are considered for SD type top trusses. Fig. 3.4 shows lateral bracing systems (SD types A in Fig. 3.4(a) and B in Fig. 3.4(b), and XD type in Fig. 3.4(c)), box girder dimensions, and bracing members in Fig. 3.4(d). Applied torque and vertical loads are illustrated in Fig. 3.4(e) and Fig. 3.4(f), respectively.

Under the torsional loading, forces developed in diagonals of all three types are in good agreement with the results from Eqs. (3.1) and (3.2) as expected. For strut forces, however, a discernible difference is detected. Contrary to the suggestion by Fan and Helwig (1999) in Eq. (3.3), considerable strut forces are induced under torsional loads in SD type trusses as shown in Fig. 3.5. Strut forces are induced in a SD type truss due to interactions between top flanges and bracing members. A detailed investigation of the box girder braced by SD type top trusses has been carried out. Resulting data are incorporated into predictor equations for the determination of brace forces under a general loading.

3.3 Finite Element Modeling

A general purpose finite element program, ABAQUS (2002), was used in the numerical analyses. The cross sections of the box girders were built up with three-dimensional shell elements (S4R of ABAQUS). The S4R elements are four-node, doubly curved, general-purpose shell elements characterized by reduced integration with hourglass control. The solid diaphragms, also modeled with S4R elements, were placed at both supports for simply supported box girders and additionally at interior piers for

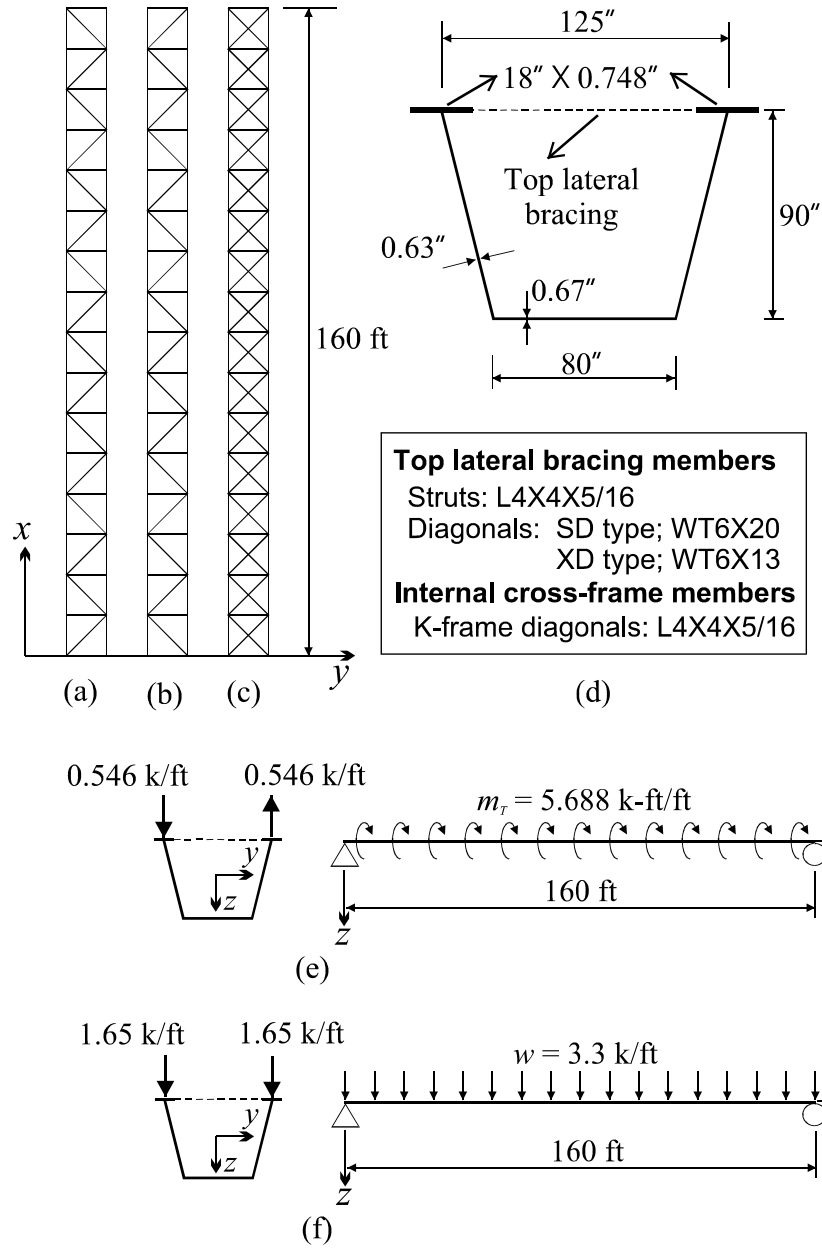


Fig. 3.4. Lateral bracing systems: (a) SD type A; (b) SD type B; (c) XD type; (d) Cross-sectional properties; (e) Applied torque; (f) Applied vertical load

three-span continuous curved girders. Diagonals of the lateral bracing system and cross-frames were modeled with three-dimensional two-node truss elements (T3D2 of ABAQUS). At least eight SR4 elements and at least ten SR4 elements were used to model each top flange and web, respectively. Experience has shown that such grid refinement yields excellent accuracy in all finite element numerical analyses of this type (Yoo et al. 2001; Choi and Yoo 2004). Both K- and X-shaped cross-frames were examined. Cross-frames were placed at every other strut location. In the case of K-frames, the struts of the lateral bracing system also act as top transverse members of the internal K-frame. However, the strut force was computed from the lateral bracing system at this stage of evaluation because the additional force component induced as part of the cross-frame would be added at a later stage. Space beam elements (B31 of ABAQUS) were used for the struts to simply avoid computational instability, i.e., an unstable situation occurs at the K-joint where two legs meet if four truss elements were used to model a K-frame. The rotational degree of freedom of the box was suppressed at the supports. Linear-elastic finite element analyses were performed on noncomposite steel structures using values for modulus of elasticity and Poisson's ratio of the construction steel of 29,000 ksi and 0.3, respectively.

3.4 Bracing Member Forces due to Torsional Loads

Fan and Helwig (2002) studied distortion of trapezoidal box girders and separated the pure torsional components and distortional components from applied torque as shown in Fig. 3.6. The same example box girders as shown in Fig. 3.4 are analyzed. Member

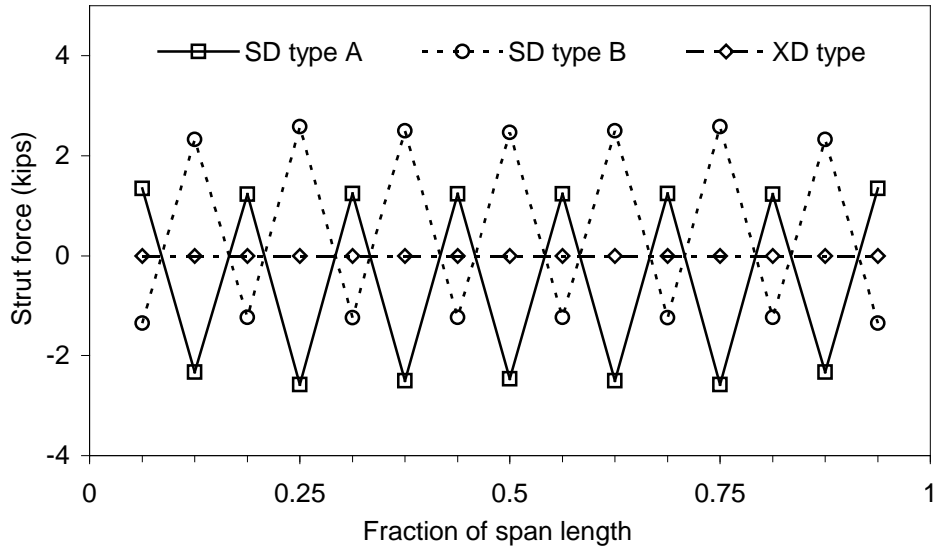


Fig. 3.5. Strut forces in simple span girder due to torsion

$$q_{H,tor} = \frac{1}{4h} \left(\frac{M}{R} + \frac{a}{b} ew \right) \quad q_{H,dist} = \frac{1}{4h} \left(\frac{M}{R} - \frac{a}{b} ew \right)$$

$$q_{V,tor} = \frac{1}{2(a+b)} \left(\frac{M}{R} + \frac{a}{b} ew \right) \quad q_{V,dist} = \frac{1}{2(a+b)} \left(\frac{M}{R} - \frac{a}{b} ew \right)$$

Fig. 3.6. Torsion and distortion components (adopted from Fan and Helwig 2002)

forces in lateral bracing members are affected by longitudinal deformations of top flanges and differential lateral displacements between top flanges. Lateral displacements of top flanges are a major cause of the development of top truss member forces in box girders subjected to torsional loads as longitudinal deformations of the box flanges are comparatively small. Fig. 3.7 shows differential lateral displacements between two top flanges. Lateral force components shown in Fig. 3.8, D_H , which are identified from a vector sum of two adjacent diagonal forces at diagonal-strut junctions, are expressed as:

$$D_H = (D^- + D^+) \sin \alpha \quad (3.5)$$

where D^- , D^+ = torsion induced axial forces in two consecutive diagonals. It should be noted that D^- and D^+ are functions of the torsional moment along the box girder and in opposite signs in two adjacent bays in the case of a SD type top truss. It is seen from Fig. 3.7 that the maximum differential lateral displacements occur at both ends of the box girder. This phenomenon is attributable to the fact that there is no adjacent diagonal as shown in Fig. 3.8. For simplicity, consider top flanges and struts as a separate two-dimensional structure in the horizontal plane as illustrated in Fig. 3.9(a). Parallel top flanges may be considered as beams connected to each other with struts along the span and solid diaphragms at ends. The net lateral load induced from top diagonals acting on this simplified structure may be divided into two sets of force components as shown in Fig. 3.9(b) and Fig. 3.9(c). The forces shown in Fig. 3.9(b) are carried entirely by two top flanges. Forces shown in Fig. 3.9(c) are carried in parts by two top flanges and struts. Net forces applied in the adjacent repeating panels and corresponding deformation configurations are illustrated in Fig 3.9(d). Although D_H is a function of torsional

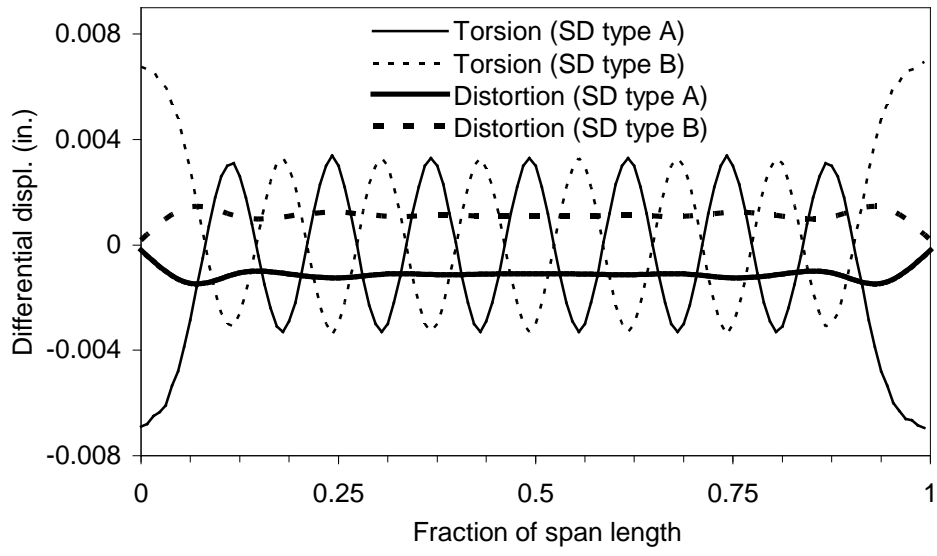


Fig. 3.7. Differential lateral displacements of top flanges due to torsion and distortion

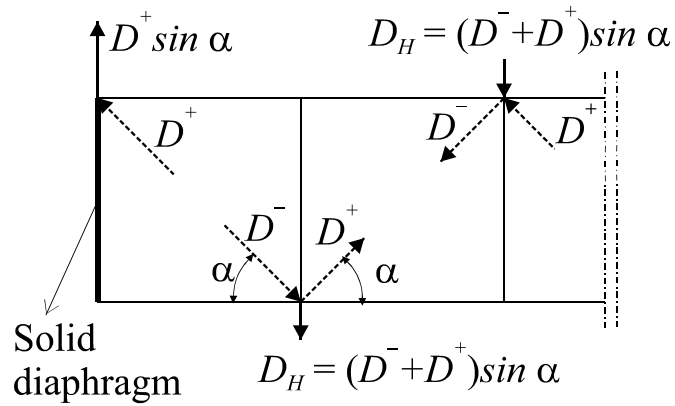


Fig. 3.8. Lateral force resultants balanced from diagonal forces

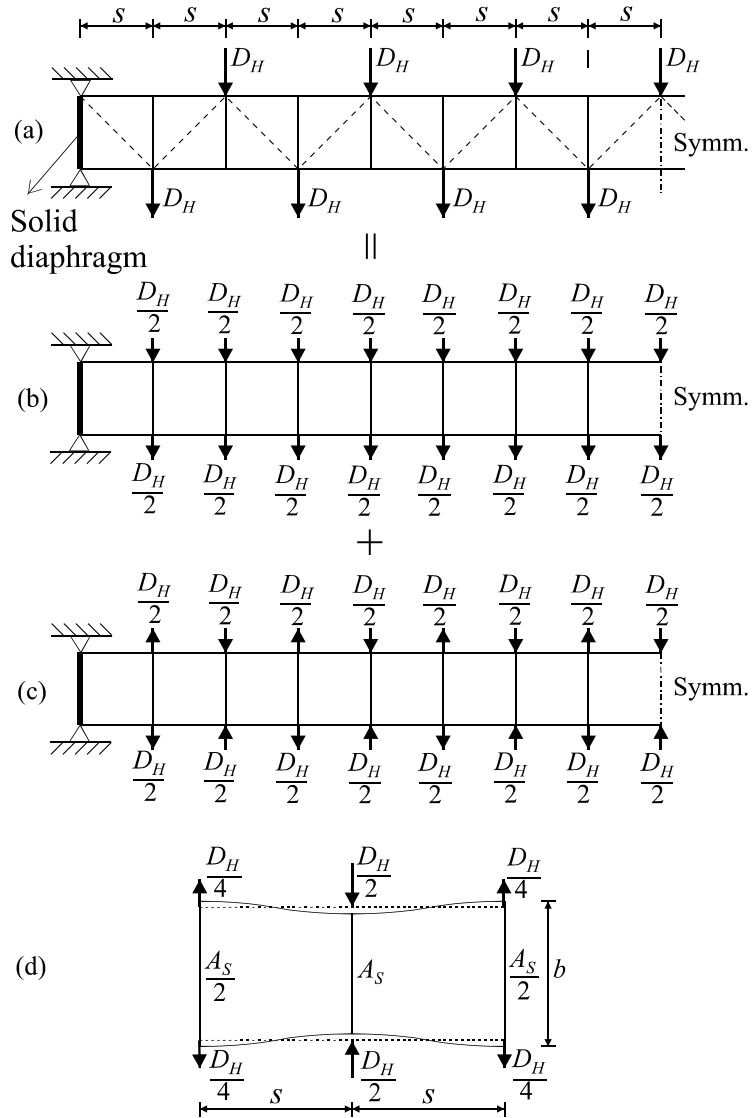


Fig. 3.9. Lateral forces from diagonals: (a) Lateral forces; (b) Lateral force affecting lateral bending; (c) Lateral force affecting struts; (d) Deformation of two repeating adjacent panels

moment that varies along the girder length, strut forces are approximated from lateral forces that are assumed to be the same in magnitude within two adjacent panels, a reasonable approximation as any difference will be small.

$$S_{tor} = \frac{\frac{(2s)^3}{192I_f}}{\left(\frac{b}{2A_s} + \frac{(2s)^3}{192I_f}\right)} D_H \quad (3.6)$$

where S_{tor} = strut force due to pure torsional component; I_f = second moment of inertia of one top flange with respect to the vertical centroidal axis; A_s = cross-sectional area of a strut; and s = spacing between struts.

Axial forces are also developed in struts due to distortional components as illustrated in Fig. 3.7. Diagonal members of cross-frames resist distortional deformations of the box cross section and consequently the resulting member forces are transferred to the top horizontal truss as illustrated in Fig. 3.10(a). The magnitude of horizontal force components, K_H , is determined using the force component associated with distortion proposed by Fan and Helwig (2002). Horizontal force component, K_H , acting on the top truss can be evaluated approximately by multiplying the horizontal force from distortional components denoted as $q_{H,dist}$ in Fig. 3.6 by the cross-frame spacing, $2s$, which yields:

$$K_H = 2sq_{H,dist} = \frac{s}{a+b} \left(\frac{M}{R} - \frac{a}{b} ew \right) \quad (3.7)$$

Duplicating the procedure used in the development of forces in struts due to pure torsional components in Fig. 3.9, net forces applied in the adjacent repeating panels and

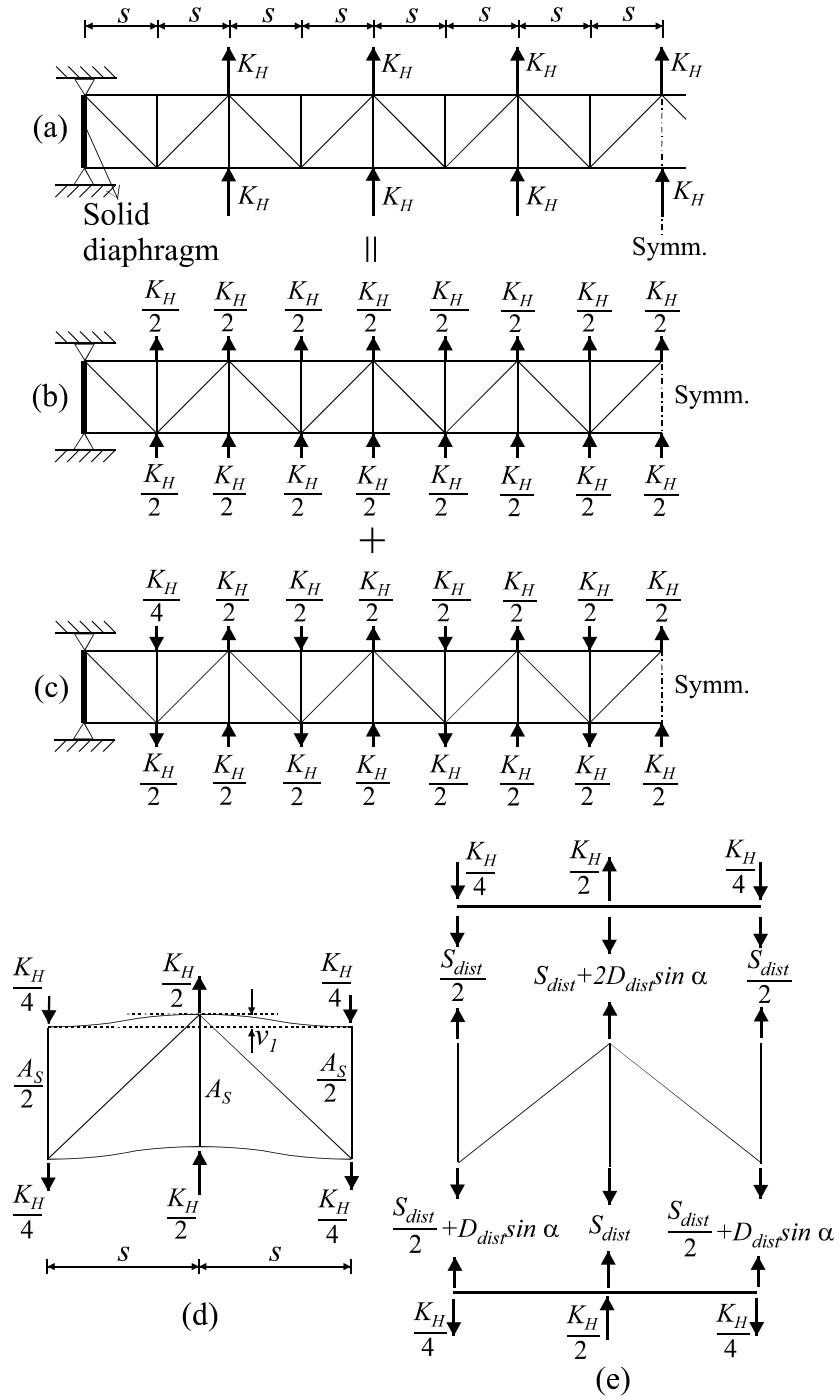


Fig. 3.10. Lateral forces from cross-frames: (a) Lateral forces; (b) Lateral force affecting lateral bending; (c) Lateral force affecting bracing members; (d) Deformation of two repeating adjacent panels; (e) Interface forces

corresponding deformation configurations are illustrated in Fig 3.10(d). Although K_H is a function of bending and torsional moment that varies along the girder length, bracing member forces can also be approximated from lateral forces that are assumed to be the same in magnitude within two adjacent panels. Since the lateral stiffness of the web is negligible, individual top flange should be in lateral equilibrium (Fig. 3.10 (e)), which yields:

$$S_{dist} = -D_{dist} \sin \alpha \quad (3.8)$$

where S_{dist} , D_{dist} = forces in struts and diagonals due to distortion, respectively. Forces in lateral diagonal members can be determined by their elongations and force-deformation relationships represented by Hooke's law. The elongation of the lateral diagonal, δ_D , as shown in Fig. 3.11 is given by

$$\delta_D = (v_1 + v_2) \sin \alpha \quad (3.9)$$

where v_1 = relative displacement of the strut as shown in Fig. 3.10(d) in the lateral

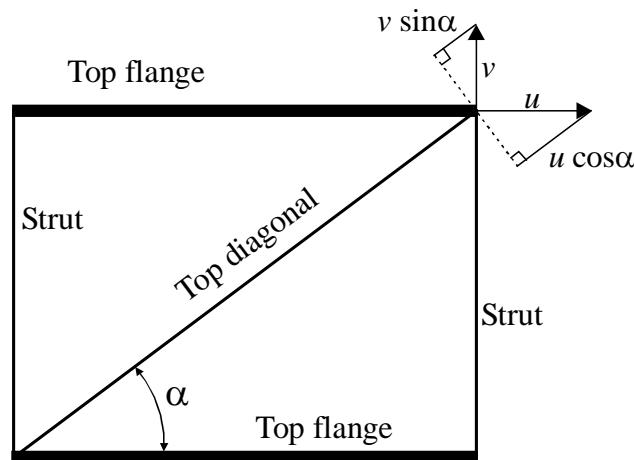


Fig. 3.11. Elongation components of a diagonal member

direction; v_2 = axial elongation of the strut. Each top flange is assumed to bend like a continuous beam between two adjacent strut locations, as shown in Fig. 3.10(d).

Interactive forces between the interface of the top flange and bracing assemblies are shown in Fig. 3.10(e). The relative lateral deflection between two adjacent panel points, v_I , is computed to be

$$v_I = \frac{(2s)^3}{192EI_f} \left(\frac{K_H}{2} + S_{dist} \right) \quad (3.10)$$

Similarly, elongations of the strut, v_2 , and the diagonal, δ_D , are given by

$$v_2 = \frac{bS_{dist}}{EA_s} \quad (3.11)$$

$$\delta_D = \frac{L_D D_{dist}}{EA_D} \quad (3.12)$$

where A_s , A_D = cross-sectional areas of strut and diagonal, respectively; L_D = length of diagonal. Substituting Eqs. (3.10) ~ (3.12) into Eq. (3.9) and solving Eqs. (3.8) and (3.9) simultaneously for D_{dist} , yields

$$D_{dist} = \frac{A_D A_s s^3 \sin \alpha}{48 A_s L_D I_f + 2 A_s A_D s^3 \sin^2 \alpha + 48 A_D b I_f \sin^2 \alpha} K_H \quad (3.13)$$

Eq. (3.13) has been derived to compute the lateral diagonal member force in a simple span box girder. Eq. (3.13) can also be extended to continuous beams. However, care must be exercised near interior supports where solid diaphragms are installed. It is recommended that forces in the lateral diagonal due to distortion be neglected at the panels immediately adjacent to interior solid diaphragms in order to avoid the disturbing effect caused by the solid diaphragm.

3.5 Bracing Member Forces due to Vertical Bending

Equations for forces in SD type lateral bracing members due to vertical bending in a tub girder may be derived based on the following assumptions:

- (1) Cross-frames are assumed installed at every other strut location (the case of installing cross-frames at every strut location will be treated in Chapter 5 as a very complex interaction takes place between the strut and the cross-frame when cross-frames are provided at every strut location).
- (2) Vertical bending affects the longitudinal deformation and lateral bulging of the flanges due to inclined webs as shown in Figs. 3.3(a) and 3.3(b).
- (3) The webs have negligible lateral resistance against lateral bending of the top flanges. This assumption has been verified by analyzing a number of examples of hypothetical box girders (the web contributes approximately 2% of the top flange bending resistance).

The first assumption has an important implication for the behavior of box girders with SD type lateral bracing systems. If cross-frames are installed at every strut location, the lateral bracing system and cross-frames interact substantially differently from those described heretofore and this complex interaction will be examined in Chapter 5.

Concerning the second assumption, Fan and Helwig (1999) successfully derived equations to predict brace forces induced by longitudinal stresses of the top flanges as shown in Fig. 3.3(a). Although Fan and Helwig (1999) recommended that, for simplicity,

the strut be assumed to carry the entire lateral load, a logical redistribution of lateral force components to struts and diagonals leads to a better estimation of brace forces.

Consider an SD type lateral bracing system subjected to lateral loads, w_{lat} , as shown in Fig. 3.3(b). The interactive forces between top flanges and lateral bracing members are shown in Fig. 3.12. Interactive forces, Q_A and Q_B , are determined from the simple equilibrium considerations:

$$Q_A + Q_B = 2sw_{lat} \quad (3.14)$$

$$Q_A = 2D_{lat} \sin \alpha + S_{lat} \quad (3.15)$$

$$Q_B = S_{lat} \quad (3.16)$$

where s = spacing between struts; D_{lat} , S_{lat} = forces in diagonal and strut, respectively.

Substituting Eqs. (15) and (16) into Eq. (14) and rearranging yields

$$S_{lat} = sw_{lat} - D_{lat} \sin \alpha \quad (3.17)$$

The induced lateral load component due to inclined webs causes the top flange to bend in a manner similar to a continuous beam between panel points. As shown in Fig. 3.13, the relative lateral deflection between two adjacent panel points, v_I , is determined from the superposition of deflections due to distributed lateral load, w_{lat} , and concentrated load, Q_A .

$$v_I = \frac{w_{lat} (2s)^4}{384EI_f} - \frac{Q_A (2s)^3}{192EI_f} \quad (3.18)$$

The elongations of the strut, v_2 , and diagonal, δ_D , are

$$v_2 = \frac{S_{lat} b}{EA_s} \quad (3.19)$$

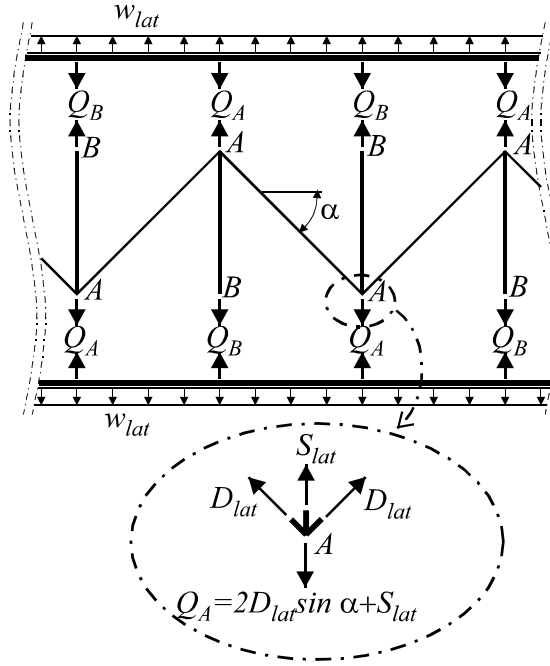


Fig. 3.12. Interface forces between the top flange and lateral bracing members due to lateral force components (w_{lat})

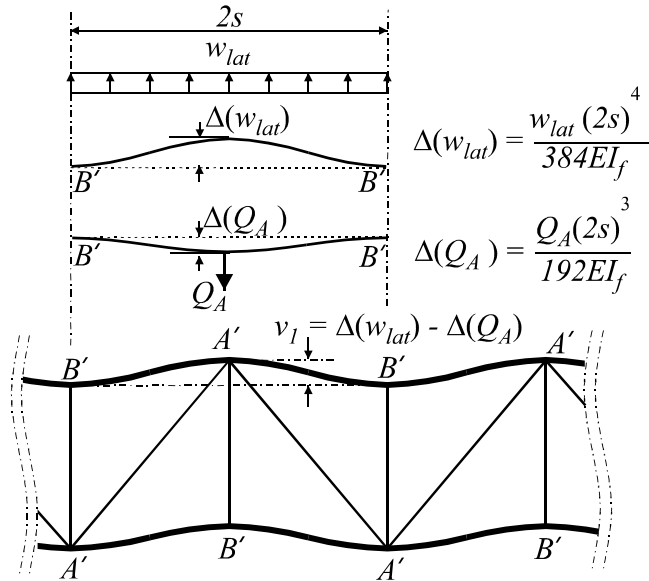


Fig. 3.13. Lateral displacements of top flanges due to lateral force components (w_{lat})

$$\delta_D = \frac{D_{lat} L_D}{EA_D} \quad (3.20)$$

Substituting Eqs. (3.18) ~ (3.20) into Eq. (3.9) and solving for D_{lat} yields the following expression for the diagonal member force induced by lateral loading:

$$D_{lat} = \frac{24A_D b s I_f \sin \alpha}{24A_S L_D I_f + A_D \sin^2 \alpha (A_S s^3 + 24b I_f)} w_{lat} \quad (3.21)$$

3.6 Equations for Brace Forces

Forces in diagonals, D , and struts, S , in the SD type lateral bracing system due to vertical bending and torsional loading are summarized as followings:

$$D = D_{bend} + D_{lat} + D_{tor} + D_{dist} \quad (3.22)$$

$$S = S_{bend} + S_{lat} + S_{tor} + S_{dist} \quad (3.23)$$

where subscripts *bend*, *lat*, *tor*, and *dist* denote brace forces induced by vertical bending, lateral load, pure torsion, and distortion, respectively. They are

$$D_{bend} = \frac{f_{xTop} s \cos \alpha}{\frac{L_D}{A_D} + \frac{b}{A_S} \sin^2 \alpha + \frac{s^3}{24I_f}} \quad (3.24)$$

where f_{xTop} = longitudinal stress at the middle of top flange.

$$D_{lat} = \frac{24A_D b s I_f \sin \alpha}{24A_S L_D I_f + A_D (A_S s^3 + 24b I_f) \sin^2 \alpha} w_{lat} \quad (3.25)$$

$$D_{tor} = \pm \frac{b}{2A_0 \sin \alpha} T \quad (3.26)$$

$$D_{dist} = \frac{A_D A_S s^3 \sin \alpha}{48A_S L_D I_f + 2A_S A_D s^3 \sin^2 \alpha + 48A_D b I_f \sin^2 \alpha} K_H \quad (3.27)$$

$$S_{bend} = -D_{bend} \sin \alpha \quad (3.28)$$

$$S_{lat} = sw_{lat} - D_{lat} \sin \alpha \quad (3.29)$$

$$S_{tor} = \frac{\frac{(2s)^3}{192I_f}}{\left(\frac{b}{2A_s} + \frac{(2s)^3}{192I_f} \right)} D_H \quad (3.30)$$

and

$$S_{dist} = -D_{dist} \sin \alpha \quad (3.31)$$

Eqs. (3.24), (3.26), and (3.28) were adopted from Fan and Helwig (1999). It should be noted that all force components are functions of bending and torsional moments. It is acceptable for diagonal forces to be computed by superimposing only D_{bend} and D_{tor} because the magnitudes of D_{lat} and D_{dist} are relatively small. For strut forces, however, at least three components, S_{bend} , S_{lat} , and S_{tor} are needed. In the case of nonprismatic flanges, the average of the flange moment of inertia with respect to the centroidal vertical axis should be used.

3.7 Comparison of Lateral Bracing Forces

The lateral bracing forces computed from Eqs. (3.22) and (3.23) were compared with the results from finite element analyses of simply supported straight box girders. Box girder properties and vertical and torsional loading are given in Fig. 3.4. Fig. 3.14 compares forces in lateral diagonals determined by Eq. (3.22) with those from the finite element analysis. Strut forces computed from Eq. (3.23) are compared with those obtained from the finite element analysis in Fig. 3.15. Excellent agreement is evident.

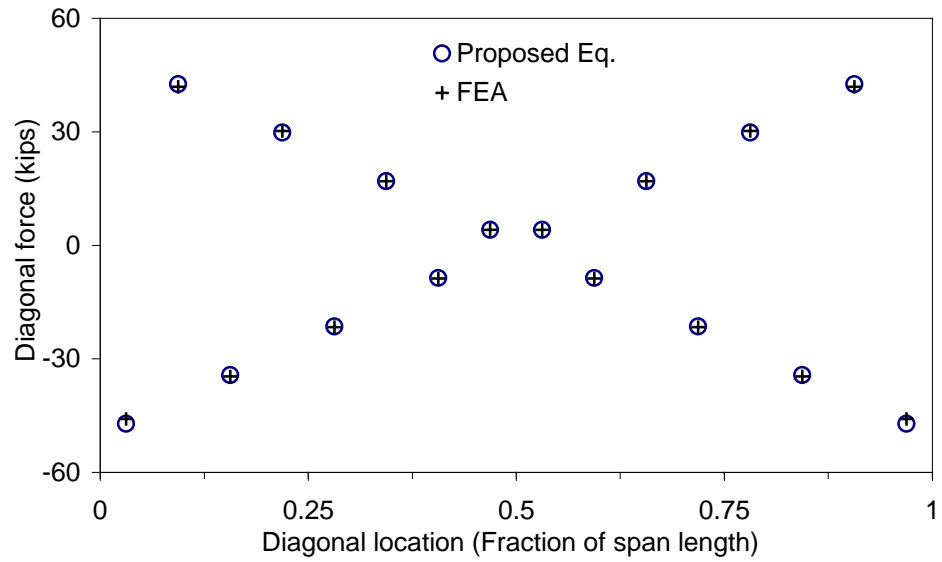


Fig. 3.14. Comparison of diagonal forces in straight girder due to torsion

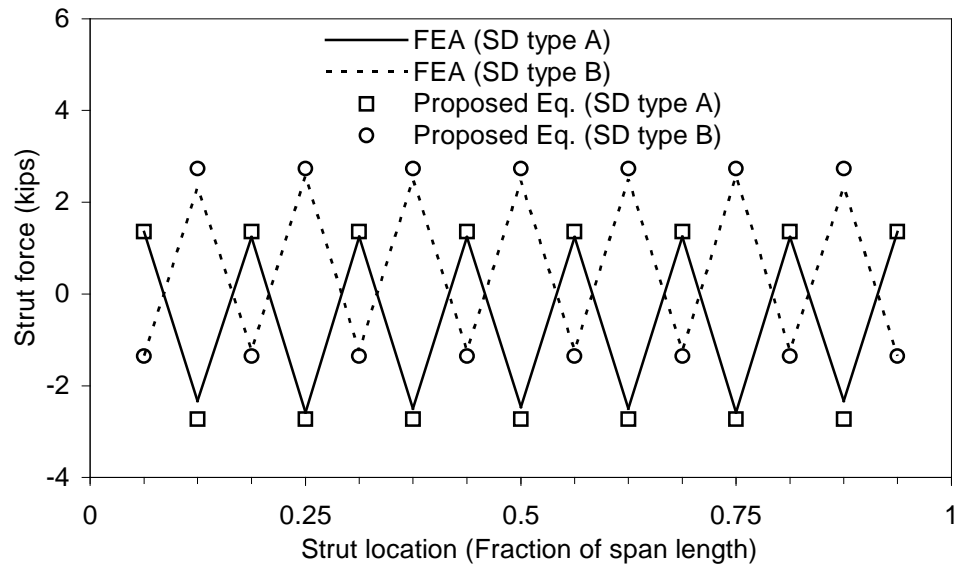


Fig. 3.15. Comparison of strut forces in straight girder due to torsion

Axial forces in SD type lateral bracing members of straight box girders shown in Fig. 3.4 subjected to vertical bending are comparatively shown in Fig. 3.16. It is noted that forces determined from Eqs. (3.22) and (3.23) are only 6% greater than those obtained from finite element analyses while values computed from Fan and Helwig (1999) estimate brace forces 14% greater than those from finite element analyses at the midspan. This improvement is believed to be due to a logical redistribution of lateral force components due to vertical bending to struts and diagonals.

The validity of the proposed formulation was checked also for the three-span curved girder. Pertinent information on the dimensions and loadings are given in Fig. 3.17. The box girder consists of three different types of cross sections with different plate thickness but same heights and widths. X-shaped cross-frames are assumed

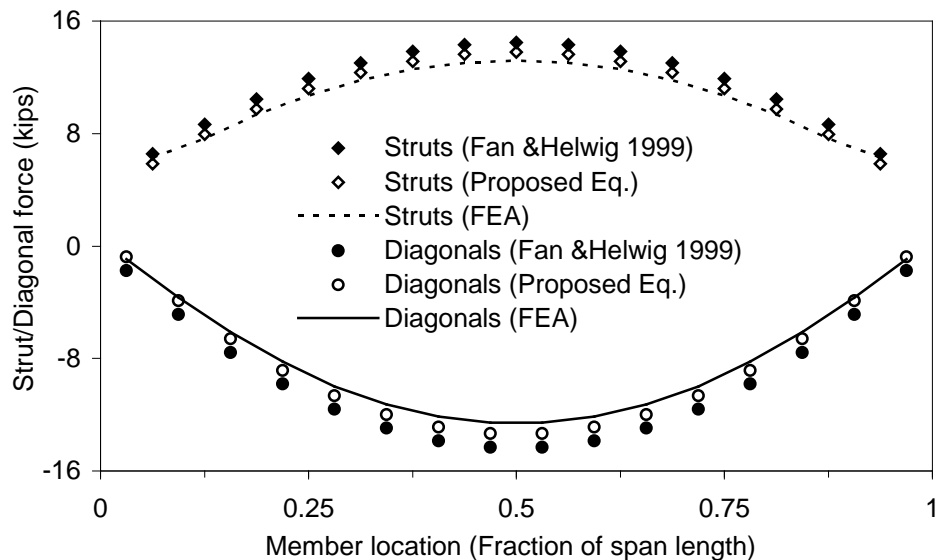


Fig. 3.16. Forces in bracing members in straight girder due to vertical bending

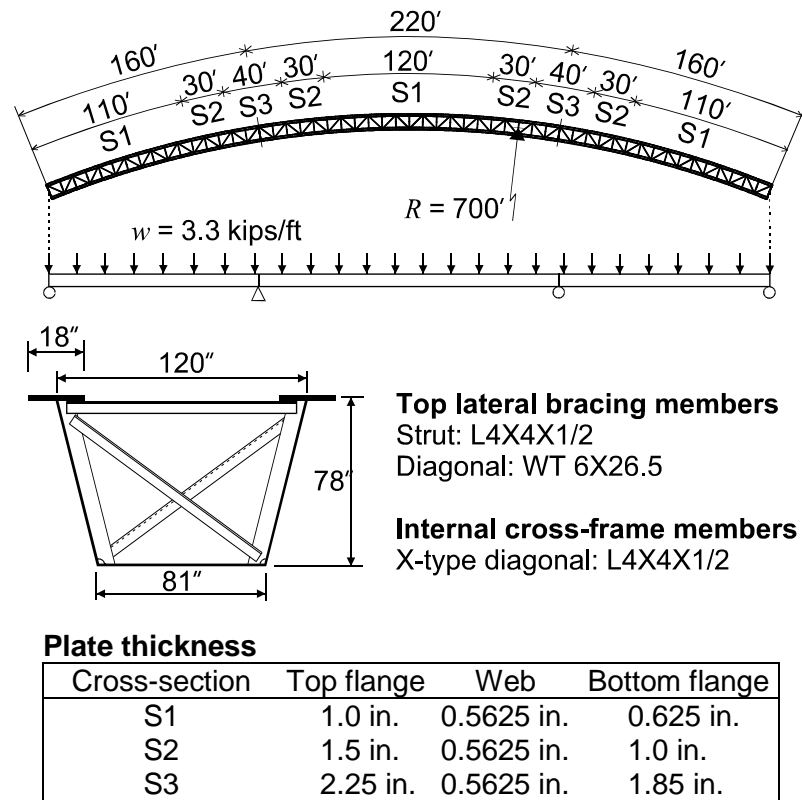


Fig. 3.17. Three-span continuous horizontally curved tub girder

installed at every other strut location. The lateral bracing system has a total of 54 panels (16+22+16). Fig. 3.18 shows bending and torsional moment diagrams. Tables 3.1 and 3.2 comparatively show forces in diagonals and struts in the lateral bracing system for the model shown in Fig. 3.17. As can be seen from Table 3.2, diagonal forces computed from Eq. (3.22) are in fairly good agreement with those from the finite element analysis. It is noted that the greatest discrepancy occurs in diagonals subjected to the lowest forces. As it is likely that the same member will be used for all diagonals in a bracing system, this large discrepancy in diagonals subjected to the lowest forces appears to be inconsequential. Strut forces determined from Eq. (3.23) shown in Table 3.3 compare very well with those from the finite element analysis. Similarly, the greatest discrepancy between these two values occurs in struts subjected to the lowest forces. This discrepancy again appears to be inconsequential. Forces in diagonals and struts of the lateral bracing system of the model given in Fig. 3.17 computed analytically from Eqs. (3.22) and (3.23) and equations presented by Fan and Helwig (1999) are comparatively shown in Figs. 3.19 and 3.20 with those from the finite element analyses. As diagonal forces due to lateral bending and distortion, which were neglected in Fan and Helwig (1999), are relatively small, significant differences between the two analytically determined values are not expected. Fig. 3.19 confirms this expectation. In the case of strut forces, however, significant discrepancies are evident in Fig. 3.20 between the two analytically determined values. Fan and Helwig (1999) underestimate the maximum strut forces (38% at the interior pier and 22% at the maximum positive bending moment location). Unlike the case of diagonals, this discrepancy is considered critical as the

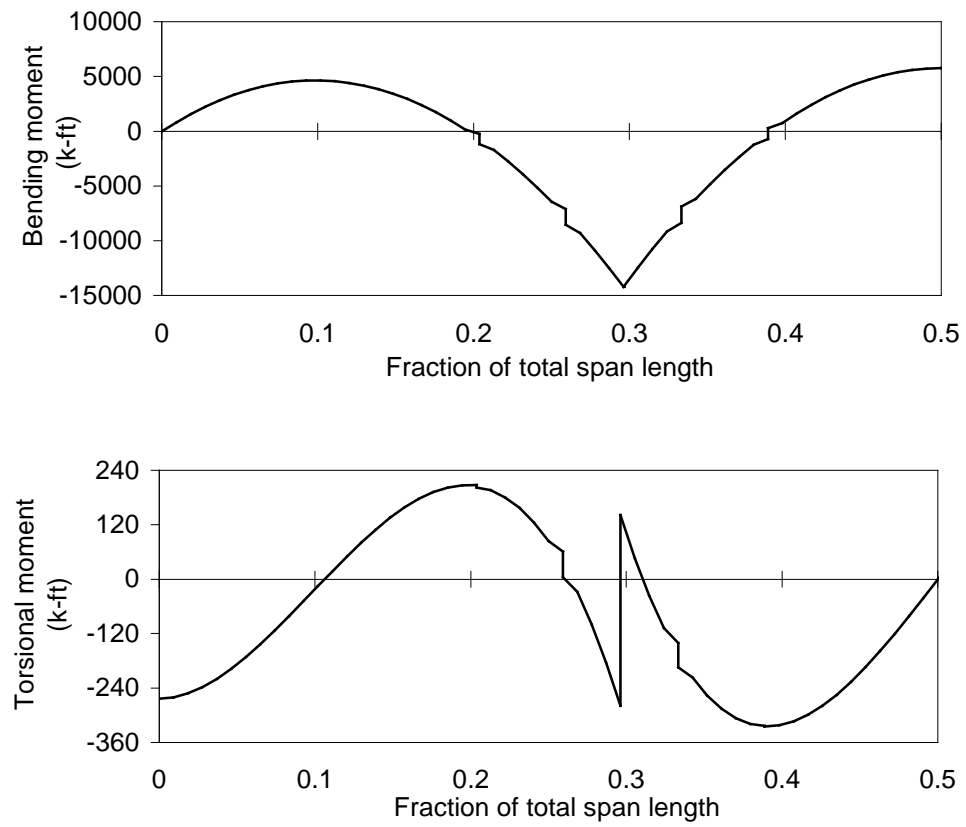


Fig. 3.18. Bending and torsional moment diagrams of three-span continuous horizontally curved girder

Table 3.2. Diagonal forces, three-span continuous horizontally curved girder (kips)

Panel Number	Proposed Equations (kips)					FEA (kips)	Diff. (%)
	D_{bend}	D_{lat}	D_{tor}	D_{dist}	Sum		
1	-1.78	0.83	-33.82	-0.32	-35.09	-33.36	5.2
2	-4.90	0.83	30.91	-0.88	25.97	24.93	4.2
3	-7.29	0.83	-25.66	-1.31	-33.42	-31.93	4.7
4	-8.96	0.83	18.68	-1.60	8.96	8.29	8.1
5	-9.90	0.83	-10.60	-1.77	-21.44	-19.62	9.3
6	-10.13	0.83	2.01	-1.81	-9.09	-10.11	-10.1
7	-9.63	0.83	6.45	-1.72	-4.07	-2.17	87.3
8	-8.40	0.83	-14.18	-1.51	-23.26	-24.37	-4.6
9	-6.46	0.83	20.58	-1.16	13.80	15.47	-10.8
10	-3.79	0.83	-25.01	-0.68	-28.64	-29.78	-3.8
11	-0.40	0.83	26.86	-0.07	27.22	28.69	-5.1
12	3.51	1.07	-25.54	0.57	-20.39	-22.38	-8.9
13	8.08	1.07	20.41	1.31	30.86	33.20	-7.0
14	13.33	1.07	-10.87	2.16	5.69	3.77	50.9
15	16.97	1.32	-3.68	2.57	17.17	18.26	-6.0
16	22.79	1.32	23.87	-	47.98	45.25	6.0
Diaphragm	-----	-----	-----	-----	-----	-----	-----
17	22.70	1.32	5.97	-	29.99	28.69	4.5
18	16.69	1.32	14.02	2.52	34.55	34.15	1.2
19	12.80	1.07	-28.19	2.07	-12.25	-13.94	-12.1
20	7.33	1.07	37.15	1.19	46.74	47.59	-1.8
21	2.55	1.07	-41.50	0.41	-37.47	-37.99	-1.4
22	-1.64	0.83	41.88	-0.29	40.78	40.74	0.1
23	-5.26	0.83	-38.87	-0.94	-44.24	-43.87	0.8
24	-8.15	0.83	33.10	-1.46	24.32	24.57	-1.0
25	-10.32	0.83	-25.18	-1.85	-36.52	-36.11	1.1
26	-11.77	0.83	15.72	-2.11	2.67	3.15	-15.0
27	-12.49	0.83	-5.34	-2.24	-19.24	-18.77	2.5
Symm.	-----	-----	-----	-----	-----	-----	-----

Table 3.3. Strut forces, three-span continuous horizontally curved girder (kips)

Strut Number	Proposed Equations (kips)					FEA (kips)	Diff. (%)
	S_{bend}	S_{lat}	S_{tor}	S_{dist}	Sum		
1	2.36	3.54	0.93	0.35	7.17	7.72	-7.1
2	4.31	3.54	-1.68	0.63	6.80	6.81	-0.1
3	5.74	3.54	2.22	0.85	12.35	12.06	2.4
4	6.67	3.54	-2.58	0.98	8.61	9.01	-4.5
5	7.08	3.54	2.74	1.04	14.40	14.02	2.7
6	6.98	3.54	-2.70	1.03	8.85	9.42	-6.0
7	6.37	3.54	2.47	0.94	13.32	12.96	2.7
8	5.25	3.54	-2.04	0.77	7.52	7.89	-4.6
9	3.62	3.54	1.41	0.53	9.11	8.87	2.6
10	1.48	3.54	-0.59	0.22	4.65	4.46	4.3
11	-1.10	3.45	-0.42	-0.14	1.79	2.01	-11.1
12	-4.10	3.37	1.56	-0.55	0.29	-0.56	-48.3
13	-7.57	3.37	-2.90	-1.01	-8.11	-7.47	8.6
14	-10.71	3.28	4.43	-1.37	-4.38	-5.78	-24.3
15	-14.06	3.19	-5.74	-0.75	-17.35	-16.06	8.1
Diaphragm	-----	-----	-----	-----	-----	-----	-----
16	-13.93	3.19	-5.69	-0.73	-17.15	-15.85	8.2
17	-10.43	3.28	4.03	-1.34	-4.45	-5.55	-19.8
18	-7.12	3.37	-2.73	-0.95	-7.42	-6.80	9.2
19	-3.49	3.37	1.32	-0.47	0.73	-0.39	88.6
20	-0.32	3.45	-0.12	-0.03	2.98	3.19	-6.5
21	2.44	3.54	-0.96	0.36	5.38	5.36	0.3
22	4.74	3.54	1.84	0.70	10.82	10.54	2.6
23	6.53	3.54	-2.53	0.96	8.50	9.05	-6.1
24	7.81	3.54	3.02	1.15	15.51	15.10	2.7
25	8.58	3.54	-3.31	1.26	10.07	10.88	-7.5
26(Symm.)	8.83	3.54	3.41	1.30	17.08	16.62	2.8

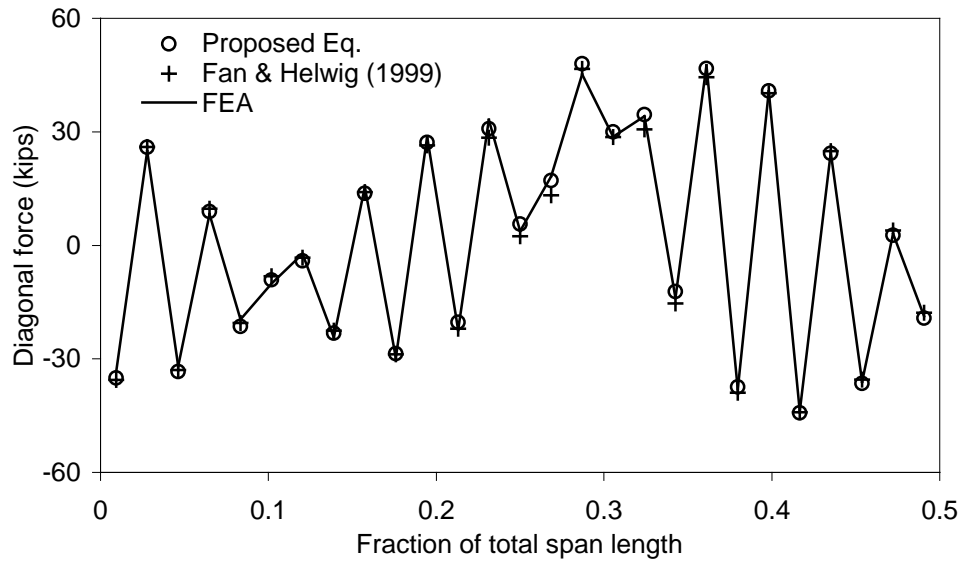


Fig. 3.19. Diagonal forces in lateral bracing system of three-span continuous horizontally curved girder

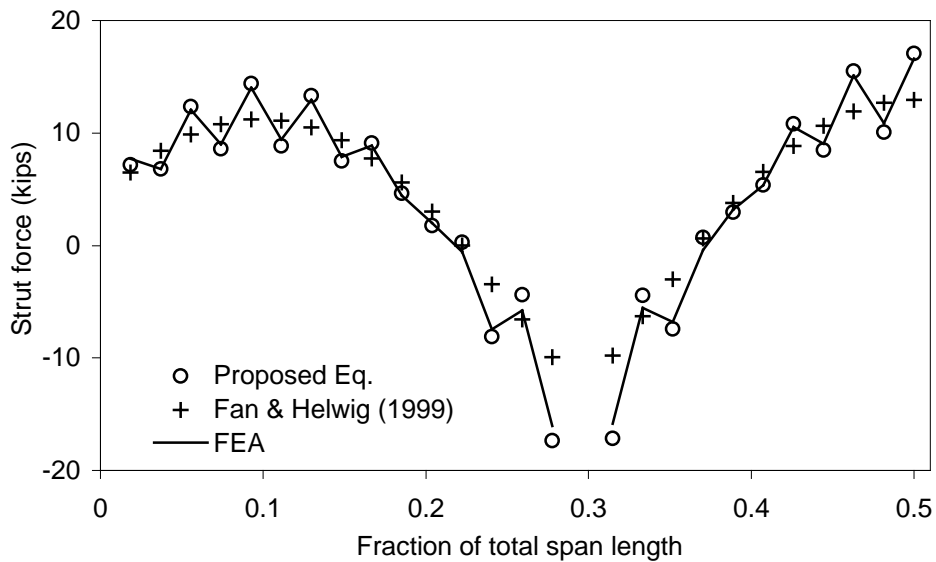


Fig. 3.20. Strut forces in lateral bracing system of three-span continuous horizontally curved girder

approximate strut forces predicted by Fan and Helwig (1999) are unconservative. This may be attributable to the fact that Fan and Helwig (1999) neglected force components due to torsion and distortion in the determination of strut forces.

3.8 Summary and Concluding Remarks

Trapezoidal steel box girders are at their critical stage during construction because the noncomposite steel section must support the fresh concrete and the entire construction load. A lateral bracing system is usually installed at the top flange level to form a quasi-closed box and thereby increase the torsional stiffness during construction. Typical lateral bracing includes a single diagonal (SD type) bracing system and a crossed diagonal (XD type) bracing system. Equations from previous studies estimate brace forces for box girders with XD type lateral bracing systems with good accuracy. In some horizontally curved box girders, however, it has been found that substantial axial forces are developed in struts due to induced torsion and distortion. New equations were analytically formulated to compute brace forces developed in bracing members. For box girders with SD type bracing, brace forces can be much better estimated with these new equations than any other existing approximate procedures. Member forces due to bending and torsion computed from these new equations are compared with those evaluated by three-dimensional finite element analyses. Excellent correlation exists between the new equations and the finite element analysis.

Equations to estimate forces in diagonals and struts in a lateral bracing system of tub girders have been presented in recent years (Fan and Helwig 1999). It has been observed, however, that there are significant discrepancies between member forces

computed from these equations and those from finite element analyses in box girders with a SD type lateral bracing system. Forces in both struts and diagonals in SD type bracing are affected by longitudinal deformations and lateral displacements of top flanges. Longitudinal deformations are primarily caused due to vertical bending. Lateral displacements, however, are caused by vertical bending, lateral force components due to sloping webs, torsion, and distortion. Forces in diagonals are induced primarily due to torsion. The magnitude of forces in a strut in a XD type bracing system is low because of the self-equilibrating nature of the double diagonals in a panel. On the other hand, forces in struts in a SD type bracing are comparatively high. Although the major portion of the strut forces are caused by vertical bending and lateral displacements, torsion and distortion may contribute up to 35% of the strut force in a typical horizontally curved continuous tub girder. The lateral bracing system in composite tub girders is only required for the construction load. Once the concrete roadway deck is completely hardened, the composite concrete deck takes over the structural function provided by the lateral bracing system. Because of the temporary nature of the bracing system, there is a tendency to take a short-cut on the part of the designers and contractors, thereby experiencing occasional embarrassing experiences. Equations have been analytically derived to determine forces in bracing members accurately. These temporary yet important primary load carrying bracing members, particularly in horizontally curved box girders, can now be designed economically using sound engineering principles.

CHAPTER 4

CROSS-FRAMES IN STEEL BOX GIRDERS

4.1 Introduction

Box girders need to be stiffened internally to resist distortional loads and maintain their cross-sectional shapes. Box sections distort primarily due to torsional moments caused by eccentrically applied loads. Torsional moments can be decomposed into equivalent force couples to rotate the girder about its longitudinal axis and distort the cross-sectional shape. Detailed decomposition process and characteristics of each pair of couples will be illustrated later in Section 4.4.

Cross-sectional distortion may alter the profile geometry of the girder flanges. Distortion can be controlled by the installation of cross-frames that are spaced along the girder. Examples of preferred types of internal bracing in the box section are K-shaped frames (hereinafter referred to as K-frame) and X-shaped frames (hereinafter referred to as X-frame) as illustrated in Fig. 4.1. Although customary design practices (rule-of-thumb) are stipulated in current design guides (*AASHTO Guide Specifications* 2003; *Highway Structures Design Handbook* 1986) for the minimum stiffness and spacing requirements, no guidelines are available for the design of cross-frames as a function of induced forces and the spacing. Only limited research results (United States Steel 1978; Heins 1978) have been available concerning distortion of box girders. Fan and Helwig

(2002) are believed to be the first to propose equations to predict brace forces in the cross-frames as a function of the cross-frame spacing, box geometry, and applied loads.

Externally applied torsional moments are resisted internally by a combination of St. Venant torsion and warping torsion depending upon the relative torsional stiffnesses. Since the St. Venant torsional stiffness is dominant over the warping torsional stiffness in a box section, torsional warping stresses, whether they are normal stresses or shearing stresses, are usually relatively small (Kollbrunner and Basler 1969) and are not considered in the design of box girders. However, depending on the magnitude of the applied torsional moments, the cross section of a box girder may distort from its original shape. Warping stresses that develop as a result of distortion of the cross section are referred to as distortional warping stresses. While torsional warping stresses in box girders may be relatively small, distortional warping stresses can be quite significant; thus, proper internal bracing is required to prevent excessive distortion of the box girder.

Cross-sectional distortion in a box girder is induced by the components of the applied torsional moments that do not result in a uniform St. Venant shear flow in the

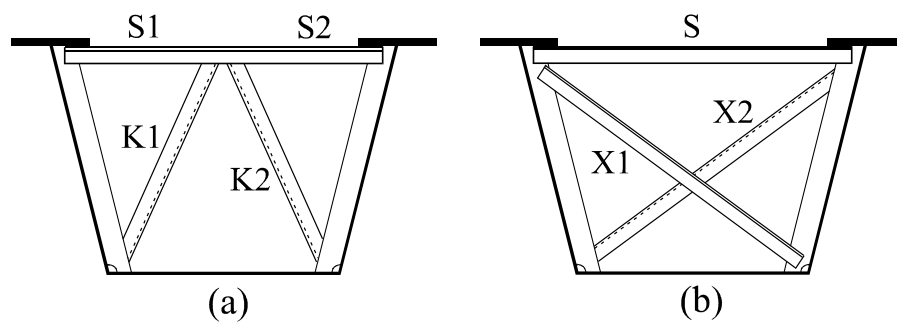


Fig. 4.1. Internal cross-frames for box girders: (a) Internal K-frame; (b) Internal X-frame

cross-section. Applied torsional moments generally include both pure torsional components and distortional components. Although the distortional components of the applied load yield zero net torque on the cross section, these components can lead to large cross-sectional stresses if proper bracing is not provided. It is essential to separate the distortional components from the applied torsional moments in order to investigate the distortional behavior of box cross sections.

In this chapter, the behavior of box girders subjected to torsional moments is briefly reviewed along with pure torsional components and distortional components. Based on the distortional components extracted from applied torsional moments, predictor equations are formulated for the forces induced in the diagonal members of X-shaped cross-frames. The forces computed by predictor equations are compared with the results obtained from a three-dimensional finite element analysis.

4.2 Background

Distortion in a box cross section occurs when part or all of the torsional moments are not resisted by a means of internal St. Venant shear flow. Depending on the source of torsion, the decomposed force couple on a box girder can be modeled by either two vertical forces equal in magnitude but opposite in direction or two horizontal forces equal in magnitude but opposite in direction as shown in Figs. 4.2(a) and 4.2(b), respectively. A force couple consisting of two opposing vertical forces usually results from gravity loads that are applied eccentrically to the centerline of the box girder. A force couple consisting of two horizontal forces acting on the top and bottom plates of the box results

from the effect of horizontal curvature of the girder; this force couple consists of horizontal force components resulting from the non-collinearity of the resultant forces in the top and bottom flange due to vertical bending.

Consider a differential flange element of a horizontally curved girder of radius R subjected to the resultant force due to vertical bending, dp , as shown in Fig. 4.3. Since the force dp is non-collinear due to curvature, lateral force components, dq , in the radial direction is required for equilibrium (V-load equation, Richardson 1963). The fictitious lateral force components, dq , are represented by a simple hoop tension (in a pressure vessel) versus internal compressive pressure relationship ($dq = dp/R$). As lateral force components are required for equilibrium of the non-collinear resultant forces due to vertical bending, lateral force components in the top flange and the bottom flange form a couple that constitutes a torsional moment acting on the horizontally curved girder (Dabrowski 1968; Heins and Hall 1981; Nakai and Yoo 1988; Fan and Helwig 2002).

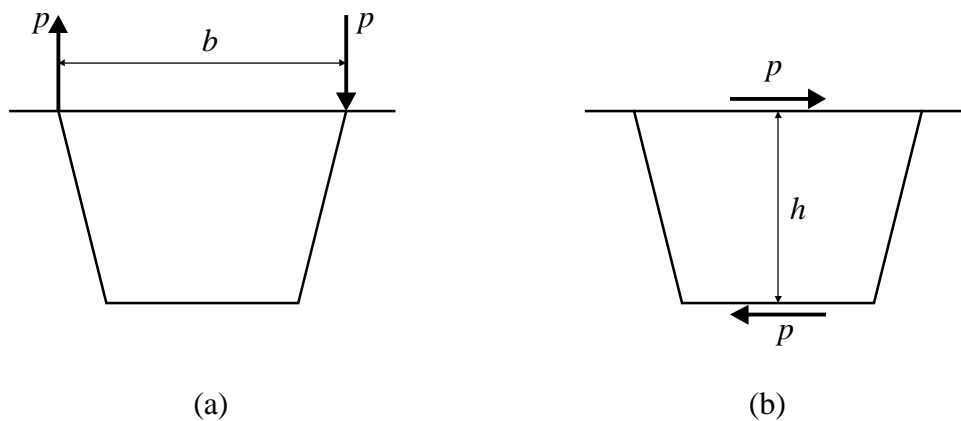


Fig. 4.2. External torsional loads on box girder: (a) Opposing two vertical loads; (b) Opposing two horizontal loads

The distortion of a box girder can be defined as the cross-sectional deformation due to two pairs of coupled internal forces acting on a cross section. The differential equation for the angular distortion, γ , of a curved box girder was given by Dabrowski (1968) as

$$\gamma^{iv} + 4\lambda^4 \gamma = \frac{1}{EI_{Dw}} \left(\rho \frac{M_x}{R} + \frac{m_z}{2} \right) \quad (4.1)$$

where $\lambda = \sqrt[4]{K_{Dw} / 4EI_{Dw}}$ (length⁻¹ unit); K_{Dw} = stiffness of the box section against distortion (force/angle unit); EI_{Dw} = distortional warping rigidity (force \times length⁴ unit); I_{Dw} = distortional warping constant = $\int_A \omega_D^2 dA$ (length⁶ unit); R = radius of curvature; M_x = vertical bending moment; m_z = distributed torque; ω_D = distortional

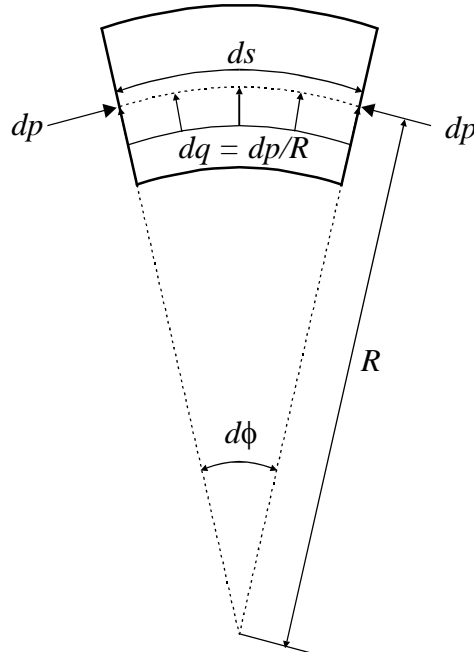


Fig. 4.3. Lateral force component on a horizontally curved flange element

warping function; and ρ = dimensionless parameter consisting of cross-sectional geometric properties (Dabrowski 1968). Eq. (4.1) is analogous to the differential equation for the vertical deflection, γ , of a beam on an elastic foundation (BEF) (Wright et al. 1968), with flexural rigidity, EI_{Dw} , spring constant, K_{Dw} , uniformly distributed load, $m_z/2$, and additional distributed load, $\rho M_x/R$. Since cross-frames are considered analogous to intermediate flexible supports of the BEF and resist the distortional couple on a box girder that causes distortion, placing adequate cross-frames greatly increases the stiffness of the box girder against distortion.

4.3. Limitation on Distortional Stresses

The current design guides (*Highway Structures Design Handbook* 1986; *AASHTO Guide Specifications* 2003) provide guidelines for the minimum stiffness and spacing requirements for the cross-frames to limit the distortional stresses. Since placing a number of cross-frames along the girder can control the magnitude of distortional stresses, the design guides are expressed in terms of the size and spacing of cross-frames. Although there is no explicit provision in *AASHTO Standard Specification for Highway Bridges* (2002) and *AASHTO LRFD Bridge Design Specifications* (2004), Article 10.2.2.3 of the *AASHTO Guide Specifications* (2003) stipulates that the spacing of internal bracing (cross-frames) shall be such that the longitudinal distortion stress in the box does not exceed 10 percent of the longitudinal stress due to vertical bending. Therefore, the normal stress gradient of the box girder flange should be less than 0.1 across the cross section. Article 10.2.2.3 of the *AASHTO Guide Specifications* (2003)

further limits the maximum spacing of cross-frames, which is not to exceed 30 ft. Based on a study of Heins and Olenik (1976), Heins (1978) proposed formulas for the spacing of cross-frames and for the required cross-sectional area of diagonals of cross-frames based on the 10 percent limitation of the distortion stress. Heins (1978) further recommended that cross-frame spacing, s , should not exceed

$$s = L \sqrt{\frac{R}{200L - 7,500}} \leq 25 \text{ (ft)} \quad (4.2)$$

and the cross-sectional area, A_b , of the diagonal should be at least

$$A_b = 75 \frac{sb}{h^2} \frac{t_w^3}{h + b} \quad (4.3)$$

where A_b = area of one diagonal brace (in.²); s = intermediate cross-frame spacing, in.; h = depth of box (in.); b = width of box (in.); t_w = web thickness (in.). *Highway Structures Design Handbook* (1986) adopted those results without any modifications. Fan and Helwig (2002) derived expressions for the determination of forces in the cross-frame members. The cross-frames are provided in a horizontally curved box girder usually at one- or two-panel spacing. *AASHTO Guide Specifications* (2003) stipulate that transverse bracing members are required at both the bottom and the top part of the box section to retain the original cross-sectional shape. It is suggested that the bottom transverse bracing members should be attached to the flange by welding in cases where no longitudinal stiffeners are present or to the longitudinal stiffener(s) of the flange by bolts.

4.4 Pure Torsional and Distortional Loads

The distortional behavior of a box girder is dependent upon the manner in which the external torque is applied to the girder. Forces induced in cross-frames may be evaluated considering equilibrium of the internal bracing system if the distortional force components can possibly be separated from applied torsional moments. However, distortional loads are generally not explicit, but are embedded in the applied torsional moments. The pure torsional components of the applied torsional moments do not cause cross sectional distortion. A distortional load consists of four sets of couples applied to four corners that do not result in net torsion to cause the cross section to rotate with respect to its centroidal axis as illustrated in Fig. 4.4. The direction and magnitude of the distortional loads depend on the shape and dimensions of the girder cross sections, as well as the manner in which the external torsional loads are applied. Fan and Helwig (2002) examined the distortional behavior of rectangular and trapezoidal box cross sections, and proposed a scheme to separate pure torsional and distortional components as shown in Fig 4.4(a) and 4.4(b). The resulting total pure torsional components and distortional components, as denoted by $q_{V,tor}$, $q_{H,tor}$, and $q_{V,dist}$, $q_{H,dist}$ in Fig. 4.4(c) can be computed by the principle of superposition, which yields the following expression (Fan and Helwig 2002):

$$q_{V,tor} = \frac{I}{2(a+b)} \left(\frac{M}{R} + \frac{a}{b} ew \right) \quad (4.4)$$

$$q_{H,tor} = \frac{I}{4h} \left(\frac{M}{R} + \frac{a}{b} ew \right) \quad (4.5)$$

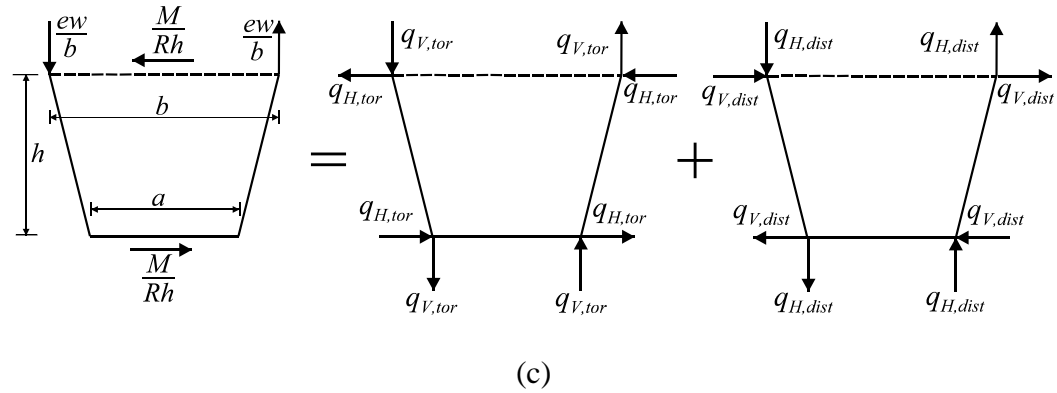
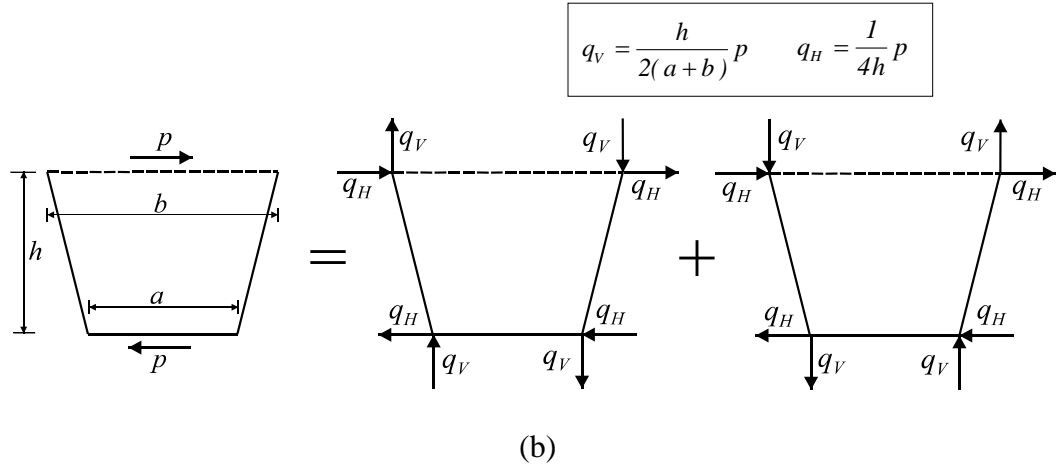
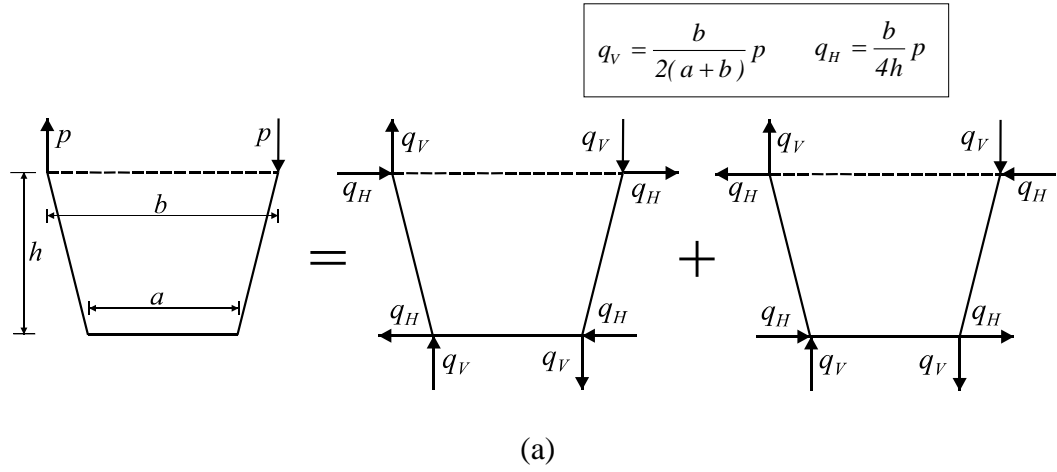


Fig. 4.4. Torsional and distortional components: (a) Due to opposing vertical loads; (b) Due to opposing horizontal loads; (c) Combined from opposing vertical and horizontal loads

$$q_{V,dist} = \frac{I}{2(a+b)} \left(\frac{M}{R} - \frac{a}{b} ew \right) \quad (4.6)$$

$$q_{H,dist} = \frac{I}{4h} \left(\frac{M}{R} - \frac{a}{b} ew \right) \quad (4.7)$$

where M = bending moment; R = radius of curvature; a and b = web spacing at bottom and top flange levels, respectively; e = eccentricity of load relative to box girder centroid; w = uniformly distributed vertical load. Eqs. (4.4) ~ (4.7) are based on the assumption that the torsional loads induced by curvature are in the same direction as the torsional loads induced by eccentric loads. Eccentricity, e , is taken positive if a vertical load is located outside (convex side) the girder centerline.

4.5 Brace Forces in Cross-Frames

Equations to predict forces induced in the cross-frames are derived based on following assumptions:

- (1) Rigidities against angular deformations between the web and flange during box cross-sectional distortion are conservatively assumed to be negligible. Only cross-frames are assumed effective to resist the distortional force components that are separated from applied torque.
- (2) Distortional forces are determined by multiplying the distributed distortional force components and the distance between adjacent cross-frames.

4.5.1 X-Frames

Brace forces in X-frame members can be readily determined from force equilibrium at each corner of the box cross section if distortional force components acting at joints of box cross section are identified. Fig. 4.5 shows an X-frame subjected to concentrated distortional loads represented by the forces H and V at four corners. No net torsional moment results from the components of the distortional loads. From equilibrium, the following equations for member forces (tension and compression) in the diagonals are manifest:

$$X = \pm (H \cos \gamma + V \sin \gamma) \quad (4.8)$$

where H and V are distortional force components in the horizontal and vertical direction, respectively; γ denotes the angle between the diagonal and the strut. Two crossed

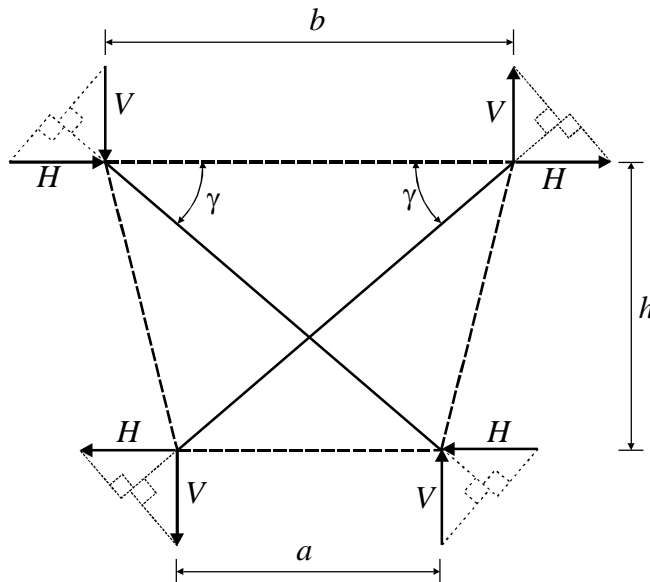


Fig. 4.5. Internal X-frame under distortional load components

diagonals of an X-frame have member forces that are same in magnitude and opposite in direction. Following expressions are evident from the geometry of the box cross-section:

$$\cos \gamma = \frac{a+b}{2L_X} \text{ and } \sin \gamma = \frac{h}{L_X} \quad (4.9)$$

where L_X = length of diagonal member of the X-frame. A simplification can be made by considering the fact that most torsional loads are distributed along the girder length. An approximate solution for the brace forces can be obtained from the product of the X-frame spacing and the intensity of the distortional loads formulated in the previous section. The distortional loads, denoted H and V in Fig. 4.5, can be determined using the above approximation. For an X-frame spaced at s_X , the distortional force components in horizontal and vertical direction at each joint of a box cross section can be approximated by multiplying $q_{H,dist}$ and $q_{V,dist}$ given in Eqs. 4.6 and 4.7 by s_X , which yields:

$$V = \frac{s_X}{2(a+b)} \left(\frac{M}{R} - \frac{a}{b} ew \right) \quad (4.10)$$

$$H = \frac{s_X}{4h} \left(\frac{M}{R} - \frac{a}{b} ew \right) \quad (4.11)$$

Substituting Eqs. (4.9) ~ (4.11) into Eq. (4.8) results in the following equations for X-frame forces:

$$X = \pm \frac{s_X}{8L_X} \left(\frac{a+b}{h} + \frac{4h}{a+b} \right) \left(\frac{a}{b} ew - \frac{M}{R} \right) \quad (4.12)$$

4.5.2 K-Frames

Similarly, Fan and Helwig (2002) derived expressions for the brace forces in the internal K-frame considering applied torque and box girder curvature as following:

$$K = \pm \frac{s_K L_K}{2A_0} \left(\frac{M}{R} - \frac{a}{b} ew \right) \quad (4.13)$$

$$S_K = \pm \frac{s_K a}{4A_0} \left(\frac{a}{b} ew - \frac{M}{R} \right) \quad (4.14)$$

where K and S_K = axial forces of K-frame diagonals and strut, respectively; L_K = length of diagonal of K-frame; M = box girder bending moment; R = radius of curvature of box girder; a and b = web spacing of box girder at the bottom and the top flange level, respectively; e = eccentricity of vertical load with respect to the box girder centroidal axis; w = uniformly distributed vertical load.

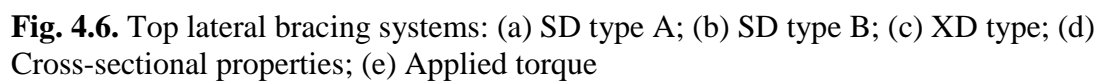
4.6 Finite Element Modeling

The three-dimensional finite element program ABAQUS (2002) was used to verify the expressions developed in the previous section for brace forces in cross-frames. Internal X-frames or K-frames were provided at two-panel spacing in the box. Members of lateral bracing systems and cross-frames were modeled using simple truss elements (T3D2 of ABAQUS) that were fastened to the girder at the junctions between the top flange and web or the bottom flange and web. Single diagonal (SD) type or crossed diagonal (XD) type lateral bracing systems were provided at the top flange level. The rotational degree of freedom for the box was suppressed at the supports. A horizontally curved three-span continuous box girder and simple span straight/curved box girders were modeled and analyzed. Linear elastic finite element analyses were carried out on noncomposite steel box girders using values for the modulus of elasticity and Poisson's ratio for the construction steel of 29,000 ksi and 0.3, respectively.

4.7. Comparison of Results from Equations and Finite Element Analysis

Three-dimensional finite element analyses were carried out on straight box girders to verify Eq. (4.12) that was formulated for internal X-frames. Fig. 4.6 shows simple span quasi-closed box girders with different top lateral bracing systems. For single diagonal lateral bracing systems, two different arrangements are considered (SD type A and SD type B) as shown in Figs. 4.6(a) and 4.6(b), respectively. Internal X-frames are assumed provided at two-panel spacing. Cross-sectional properties are given in Fig. 4.6(d), and vertically opposing distributed loads are applied on the top flanges as shown in Fig. 4.6(e). The moment term in Eq. 4.12 is equal to zero as the loading shown in Fig. 4.6(e) does not result in vertical bending.

Fig. 4.7 shows comparatively forces induced in diagonals of the internal X-frame. Values computed from Eq. (4.12) compare very well with the results of finite element analyses for the cases of XD type lateral bracing system. However, the predicted values differ from those obtained from finite element analyses with a maximum deviation up to 15% for the cases of SD type lateral bracing systems. The reason for this deviation is attributed to the localized effects. The box girders undergo rotations and lateral and vertical displacements due to applied torque or vertical bending. Because of the unsymmetrical arrangements of the diagonals in SD lateral bracing system A and B, the direction of rotations and displacements differ in the case of box girders with the lateral bracing system of type A and type B. This different direction of deformation (that results in a different amount of elongation and contraction) causes the development of unequal diagonal forces in the crossed diagonal and is referred to as the local effects



herein. As the differences in diagonal forces between type A and B are not significant, the proposed equation appears to be applicable for both cases. A box girder braced by XD type lateral bracing system maintains the symmetry after deformations, thus, forces induced in diagonal members of internal X-frames remain the same in magnitude and opposite in direction as shown in Fig. 4.7. It is noted that brace forces induced are small in the members near both ends of the box girder due to the influences of solid diaphragms installed.

Simple span box girders with internal K-frames were analyzed to verify Eqs. (4.13) and (4.14) proposed by Fan and Helwig (2002). Girder length, number of panels, and other box cross-sectional properties remain the same as those used in the previous example illustrated in Fig. 4.6 except X-frames are replaced with K-frames. The effect of the spacing of cross-frames is examined based on the distortional warping stress gradient in the bottom flange and the member forces developed in the cross-frames. Three different spacing's of internal K-frames are considered: $L/2$, $L/4$, and $L/8$, where L represents the span length of the simple box girder. A distributed torque is applied as shown in Fig. 4.6(e).

As stated in Section 4.3, distortional warping stresses can be controlled by the distances between cross-frames provided along the girder length. Fig. 4.8 confirms this. It is evident from Fig. 4.8 that distortional warping stresses are sensitively affected by the values of cross-frame spacing. Figs. 4.9 and 4.10 show the forces induced in diagonals and struts of internal K-frames. For both diagonals and struts, good agreements are evident from Figs. 4.9 and 4.10 between the values computed from proposed equations

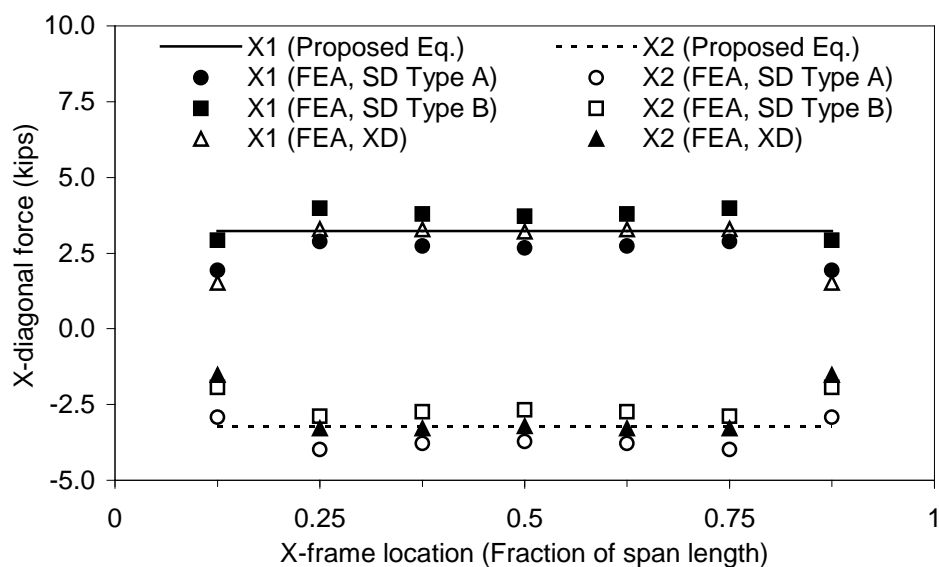


Fig. 4.7. Member forces in X-frame diagonal due to torsion (straight box girder)

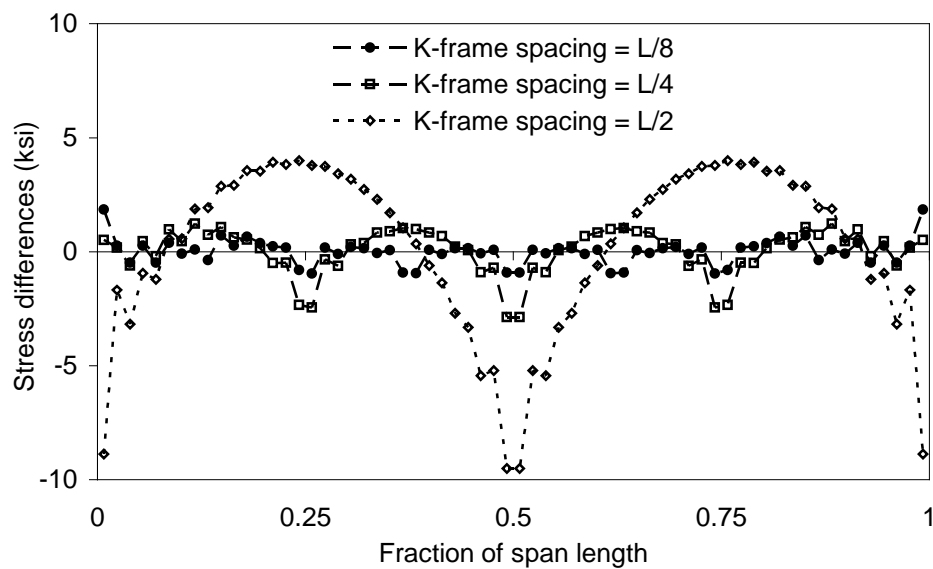


Fig. 4.8. Distortional warping stress gradients along the girder length

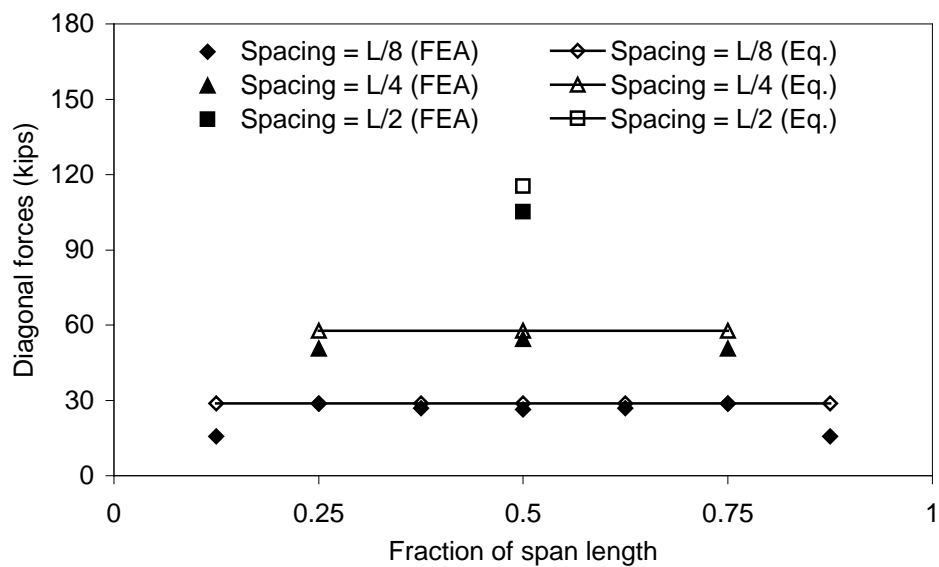


Fig. 4.9. Forces induced in diagonal members of internal K-frames

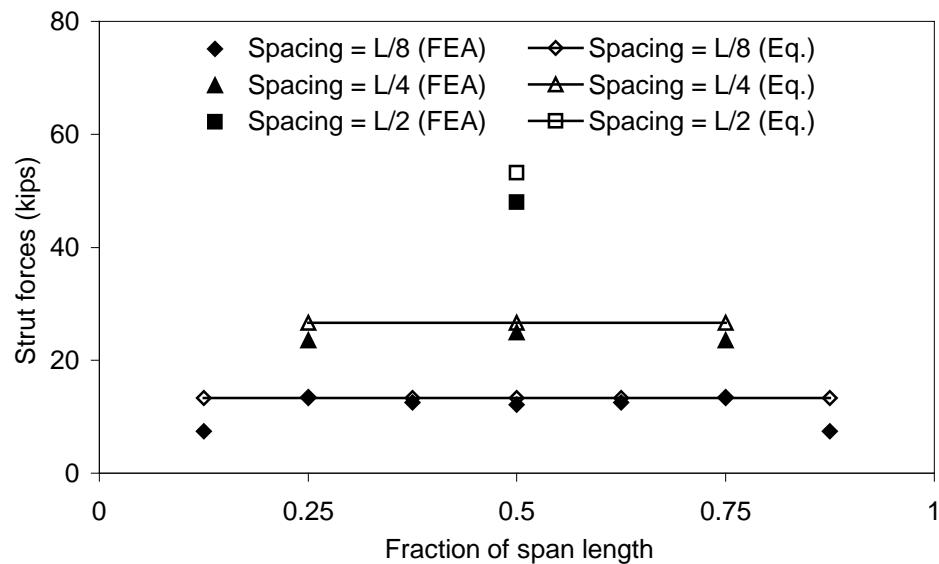


Fig. 4.10. Forces induced in strut members of internal K-frames

and those from finite element analyses. Similarly to the case of X-frames, brace forces are small in the members near both ends of the box girder due to the high distortional stiffness provided by solid diaphragms. Brace forces induced in the K-frames at the midspan of the girder are comparatively plotted in Fig. 4.11 versus the number of cross-frames. In the derivation of the proposed equations, stiffness associated with angular deformations between the web and flange during box cross-sectional distortion are conservatively neglected. In the case of box girders with cross-frames sparsely placed, errors (the conservative approximation) from neglecting the rigidities of angular deformations may be accumulated. This fact may explain that the results from finite element analyses yielded a slightly smaller value than those from the proposed equations in the case of only one cross-frame at the midspan. However, as shown in Fig. 4.11,

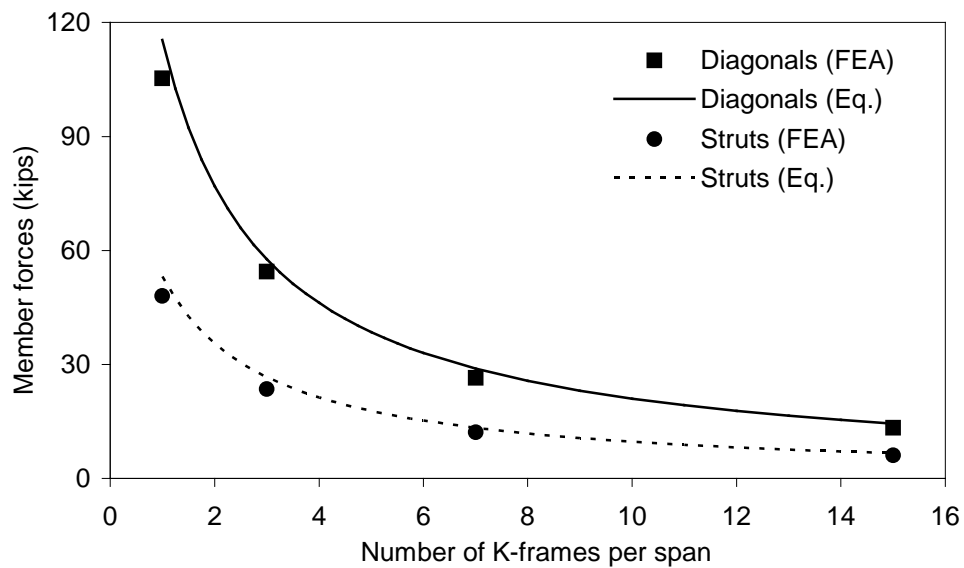


Fig. 4.11. Member forces in internal K-frames versus number of K-frames per span

member forces in the K-frame are proportional to the inverse of the number of K-frames in the span; K-frame member forces are proportional to the distance between K-frames as expected from Eqs. (4.13) and (4.14).

A horizontally curved three-span continuous box girder with SD type lateral bracing and internal X-frames is analyzed. The validity of the proposed formulation is checked for this hypothetical three-span curved girder. Pertinent information on the dimensions and loading are given in Figs. 4.12 and 4.13. The box girder consists of three different types of cross-sections having different plate thicknesses. The dimensions of these three sections remain the same. Cross-sectional properties and loading are also given in Fig. 4.12. X-frames are assumed installed at two-panel spacing. The lateral bracing system has a total of 54 panels (16+22+16). The term representing eccentricity in Eq. (4.6) is ignored as it is assumed here that the vertical load is applied without eccentricity. Fig. 4.14 comparatively shows the forces in diagonal members of X-frames. As can be seen from Fig. 4.14, the differences in diagonal forces between SD type A and type B are not as high as those observed in the case of straight box girders subjected to a pure torsional load. Although the difference in the diagonal forces can be up to 15% between those computed by the predictor equation and by finite element analyses, box girders subjected to pure torsional loading are rare in practice. As most box girders are likely subjected to combined bending and torsion, the proposed equation for diagonal forces in internal X-frames can be safely applied.

Horizontally curved simple span girders are also analyzed in order to compare the member force in K-frames and X-frames. As in the case of straight box girders, three

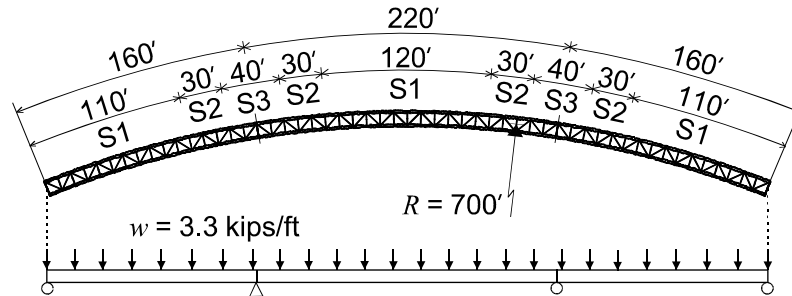


Fig. 4.12. Planar dimensions of three-span continuous horizontally curved girder and vertical loading

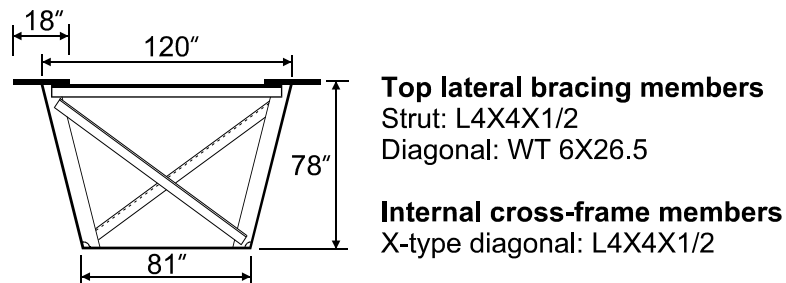


Plate thickness

Cross-section	Top flange	Web	Bottom flange
S1	1.0 in.	0.5625 in.	0.625 in.
S2	1.5 in.	0.5625 in.	1.0 in.
S3	2.25 in.	0.5625 in.	1.85 in.

Fig. 4.13. Dimensions of three cross sections and bracing members

hypothetical box girders with different top lateral bracing systems are selected as shown in Fig. 4.15. Both K-frames and X-frames are placed at two-panel spacing for all three models. A uniformly distributed vertical load of 3.3 kips/ft is applied on the top flanges (1.65 kips/ft per each flange). Forces induced in diagonal members of cross-frames are plotted along the girder length in Figs. 4.16 and 4.17 for the cases of K-frames and X-frames, respectively. It is of interest to note that the diagonal forces in K-frames are hardly affected by the lateral bracing systems and the predictor equation yields very accurate values for the diagonal forces as compared with those obtained from finite element analyses as manifest in Fig. 4.16. However, forces developed in diagonals of X-frames are affected slightly by different lateral bracing systems. Nevertheless, the proposed equation yields diagonal forces in X-frames with a maximum difference of only 3.2%.

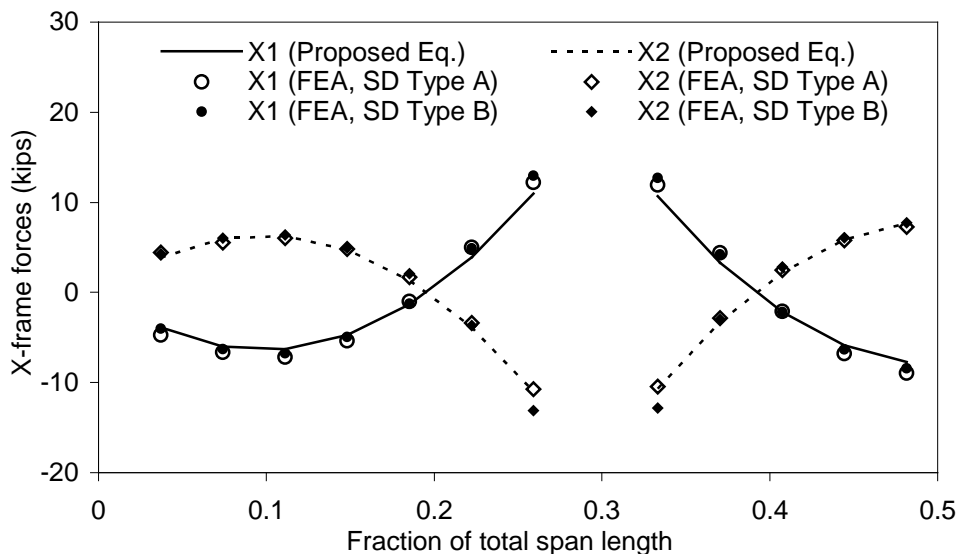


Fig. 4.14. Diagonal forces of X-frames in three-span curved girder

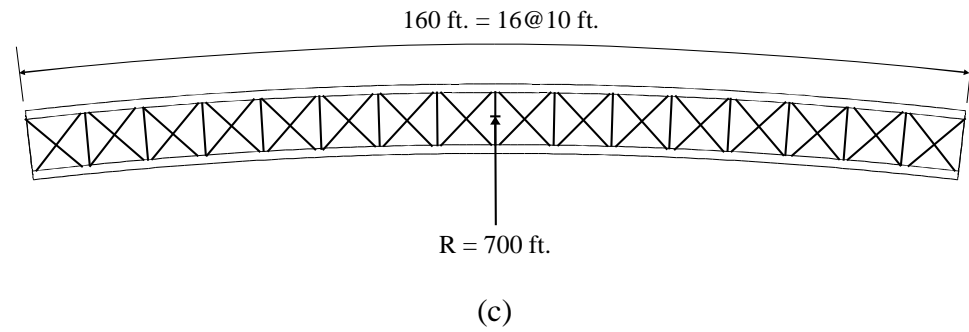
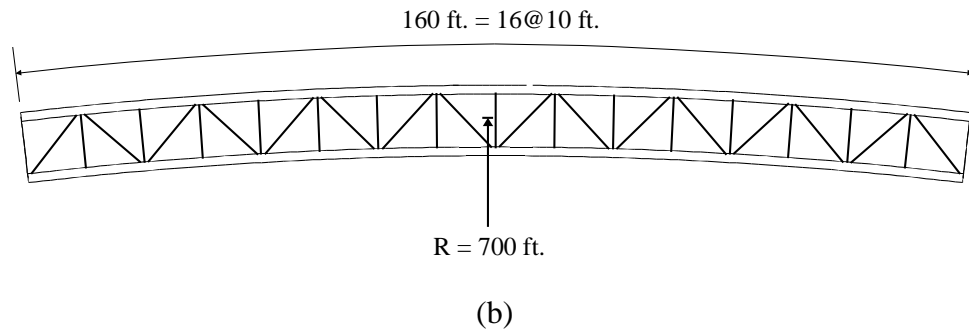
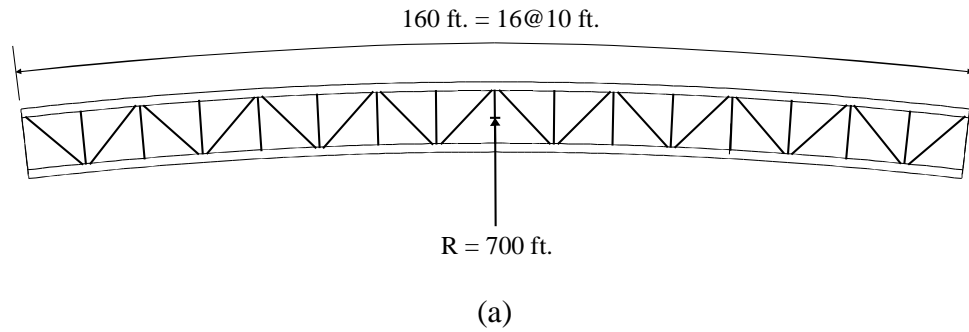


Fig. 4.15. Plan view of the simply supported curved box girders with different arrangements of top lateral bracing systems: (a) SD type A; (b) SD type B; (c) XD type

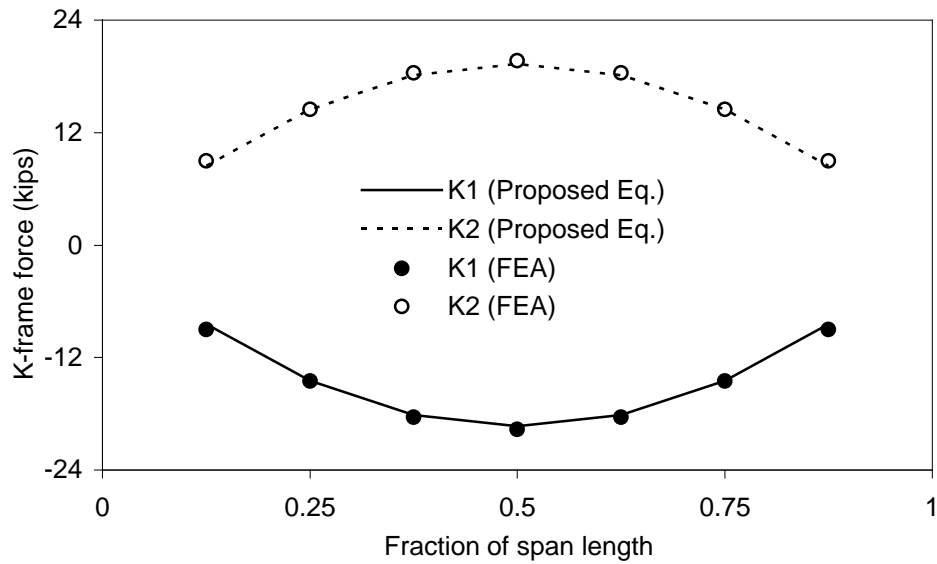


Fig. 4.16. Internal K-frame diagonal member forces of simply supported curved girders subjected to uniformly distributed vertical loads

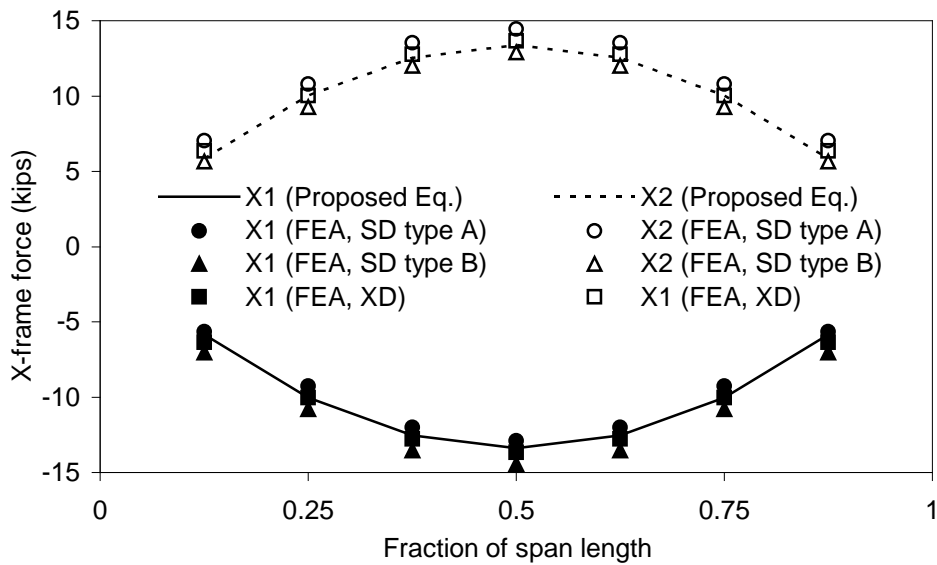


Fig. 4.17. Internal X-frame diagonal member forces of simply supported curved girders subjected to uniformly distributed vertical loads

4.8. Effect of Number of Cross-Frames on Distortion and Cross-Frame Forces

In order to control distortion in box girders, the cross-frames are provided at one- or two-panel spacing. Regardless of whether K-frames or X-frames are used, forces induced in cross-frames are dependent upon the cross-frame spacing and cross-sectional geometry as implied by Eqs. (4.12) ~ (4.14). Bending of a straight box girder causes only insignificant forces in the diagonal members of cross-frames. For box girders braced by XD type lateral bracing systems, forces are induced in cross-frame members depending upon the distance between cross-frames provided in the box girder whether cross-frames are installed at one-panel spacing or two-panel spacing. However, for box girders with SD type lateral bracing, forces induced in cross-frame members are also affected by bending of the box girder in the case of cross-frames installed at one-panel spacing; box girders with cross-frames provided at two-panel spacing are not affected significantly by bending of the girder. The mechanics of box girders with SD type lateral bracing and cross-frames provided at two-panel spacing were investigated in Chapter 3. Horizontally curved simple span girders with cross-frames provided at one-panel spacing and at two-panel spacing are examined in this section in order to examine the effect of the number of cross-frames. The effects of the cross-frame spacing on the forces induced in cross-frame members and the induced normal stress gradients due to distortion are also examined. Figs. 4.18(a) and 4.19(b) show horizontally curved box girders with SD type lateral bracing and internal K-frames that are provided at one-panel and two-panel spacing, respectively. The girder span, L , is 160 ft, and radius of curvature, R , is 700 ft. A uniformly distributed vertical load of 3.3 kips/ft is applied symmetrically on the top

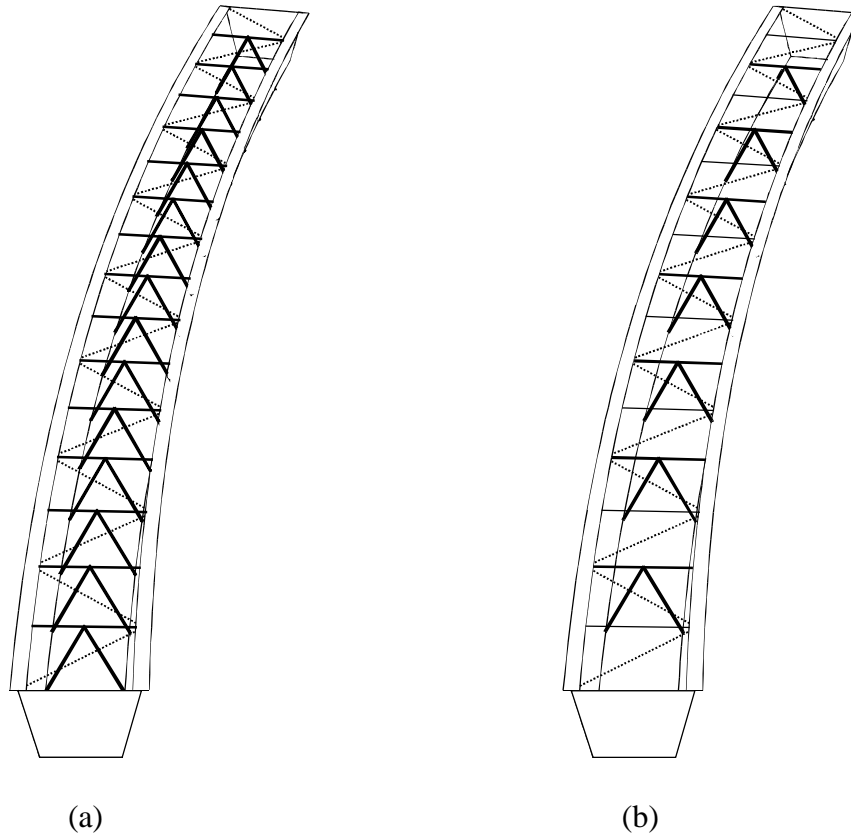


Fig. 4.18. Horizontally curved box girders with SD type lateral bracings and internal K-frames: (a) One-panel spacing; (b) Two-panel spacing

flanges (1.65 kips/ft on each flange). In order to examine the effects of the aspect ratio of the box cross section and the cross-frame spacing on the distortion of the box and consequently the normal stress gradient and member forces in cross-frames, box girders of two different cross sections (shallow and deep) having cross-frames (both X-frames and K-frames) provided at one-panel and two-panel spacing (at a panel spacing of 120 in. and 160 in, respectively) are analyzed. As the lateral bracing system is also varied in every case considered, a total of 32 box girders were analyzed. Figs. 4.19 and 4.20 show two different cross sections (shallow and deep) with K-frames and X-frames, respectively.

Tables 4.1 and 4.2 summarize the ratios of distortional warping stress to the vertical bending stress, σ_w/σ_b , (normal stress gradient) at the bottom flange at the midpoint of the span for the cases of internal K-frame and X-frame, respectively. It is expected that the ratio of distortional warping stress to the vertical bending stress is higher in the case of cross-frames provided at two-panel spacing simply because of the wider spacing between the adjacent cross-frames. Tables 4.1 and 4.2 verify this expectation except for the case of the shallow box section. As shown in Tables 4.1 and 4.2, σ_w/σ_b ratios in the SD type lateral bracing are higher than those in the XD type lateral bracing because member forces in cross-frames associated with SD type lateral bracing were affected more sensitively by bending of the box girder than those in XD type lateral bracing for the case of cross-frames provided at one-panel spacing. Tables 4.1 and 4.2 reveal that, in box girders of shallow sections with SD type lateral bracing, σ_w/σ_b ratios in the case of cross-frames at one-panel spacing are much higher than those in the case of

Table 4.1. Ratio of distortional warping stress to bending stress (σ_w/σ_b) at bottom flange (internal K-frames)

Strut spacing	K-frame spacing	Single diagonal (SD) lateral bracing		Crossed diagonal (XD) lateral bracing	
		Shallow section	Deep section	Shallow section	Deep section
120 in. (one panel)	120 in. (one panel)	4.3 %	2.5 %	1.0 %	1.1 %
	240 in. (two panels)	3.3 %	5.0 %	2.8 %	4.8 %
160 in. (one panel)	160 in. (one panel)	8.4 %	5.2 %	1.5 %	2.4 %
	320 in. (two panels)	5.6 %	8.5 %	4.3 %	7.9 %

((For both box cross sections)

Top Flange: 16 in. \times 1.0 in.

Web Thickness: 0.5625 in.

Bottom Flange Thickness: 0.625 in.

Struts and Internal X-Frame Diagonals : L4 \times 4 \times 1/2 ($A = 3.75 \text{ in.}^2$)

Top Lateral Bracing - SD Type : WT6 \times 26.5 ($A = 7.78 \text{ in.}^2$)

- XD Type : WT6 \times 15 ($A = 4.40 \text{ in.}^2$)

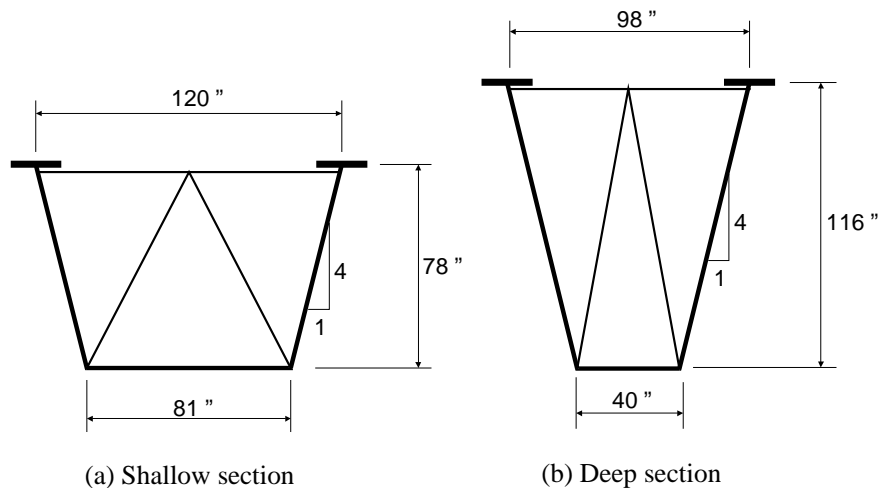


Fig. 4.19. Two different cross sections of box girders with internal K-frames

Table 4.2. Ratio of warping stress to bending stress (σ_w/σ_b) at bottom flange at midspan (internal X-frames)

Strut spacing	X-frame spacing	Single diagonal (SD) lateral bracing		Crossed diagonal (XD) Lateral bracing	
		Shallow section	Deep section	Shallow section	Deep section
120 in. (one panel)	120 in. (one panel)	4.8 %	3.6 %	0.8 %	0.8 %
	240 in. (two panels)	3.0 %	4.4 %	2.5 %	4.2 %
160 in. (one panel)	160 in. (one panel)	9.2 %	5.3 %	1.2 %	2.0 %
	320 in. (two panels)	5.2 %	8.0 %	4.1 %	7.4 %

(For both box cross sections)

Top Flange: 16 in. \times 1.0 in.

Web Thickness: 0.5625 in.

Bottom Flange Thickness: 0.625 in.

Struts and Internal X-Frame Diagonals

Top Lateral Bracing - SD Type

- XD Type

: L4 \times 4 \times 1/2 ($A = 3.75 \text{ in.}^2$)

: WT6 \times 26.5 ($A = 7.78 \text{ in.}^2$)

: WT6 \times 15 ($A = 4.40 \text{ in.}^2$)

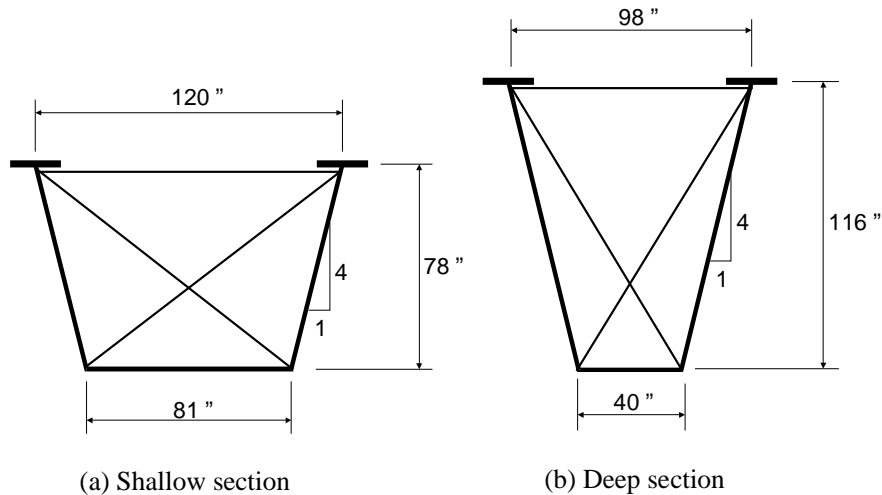


Fig. 4.20. Two different cross sections of box girders with internal X-frames

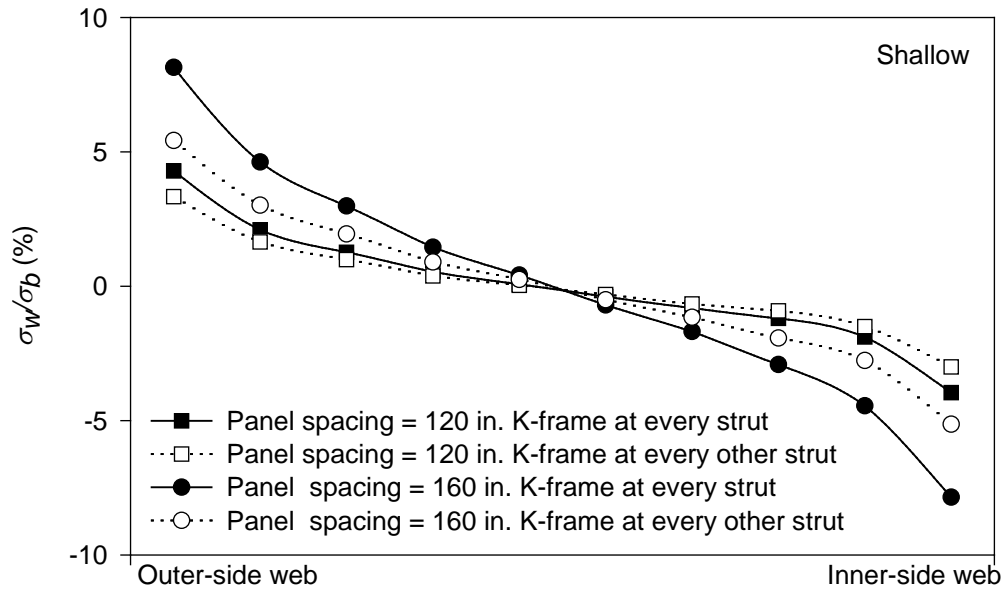


Fig. 4.21. Distortional warping stress distribution in girders of shallow cross section with K-frames ($L=160$ ft, $R=700$ ft)

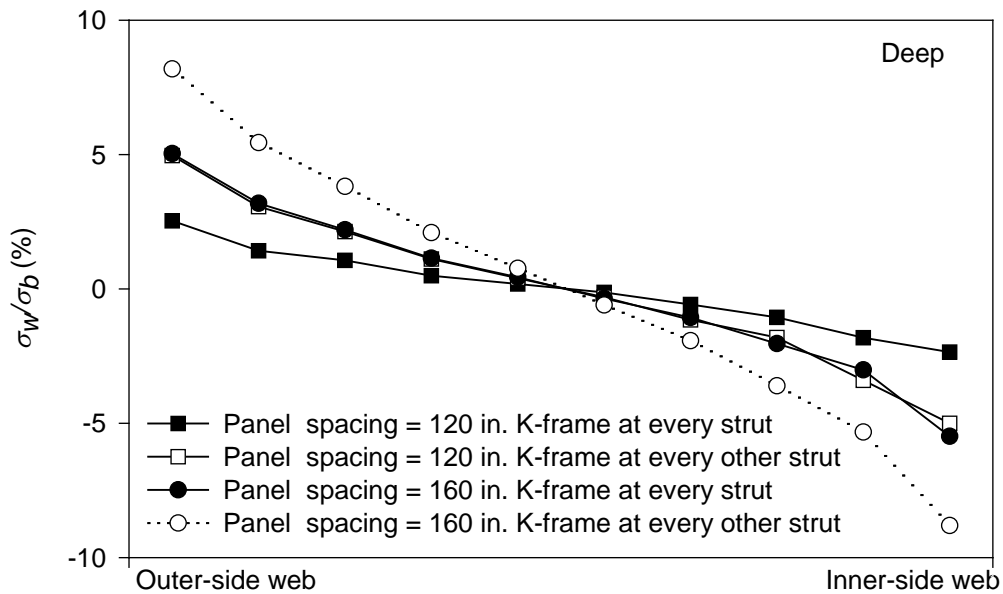


Fig. 4.22. Distortional warping stress distribution in girders of deep cross section with K-frames ($L=160$ ft, $R=700$ ft)

cross-frames at two-panel spacing despite the shorter cross-frame spacing. Figs. 4.21 and 4.22 show typical distribution of distortional warping stresses on the bottom flanges at midspan of shallow and deep box cross sections, respectively. Tables 4.1 and 4.2 clearly indicate that σ_w/σ_b ratios are greatly affected by aspect ratios of box cross sections (shallow and deep). In order to investigate further the effect of aspect ratio of the box cross-section (h/b where h = depth of the section and b = width of the section at the top flange level) on σ_w/σ_b ratios, box depths were varied from 60 in. to 200 in. while keeping the width of the box section constant at the top flange level. Thicknesses of the web and bottom flange, two top flanges, and members of cross-frames are unchanged. Results for 32 box girders with XD type lateral bracing with K-frames and X-frames analyzed are given in Figs. 4.23 and 4.24, respectively. Percentage values of σ_w/σ_b ratios in girders having XD type lateral bracing with cross-frame installed at one-panel spacing are always less than those in the girder with cross-frame installed at two-panel spacing as shown in Figs. 4.23 and 24. In girders having SD type lateral bracing, percentage values of σ_w/σ_b ratios are generally smaller in the case with cross-frame installed at one-panel spacing than those in the case with cross-frames installed at two-panel spacing. However, when the aspect ratio of the cross section (h/b) decreases (for very shallow sections), this trend reverses as shown in Figs. 4.25 and 4.26. A total of 128 model girders were analyzed to generate Figs. 4.23 ~ 4.26.

Although there are a few exceptions in the case of shallow sections, providing cross-frames at one-panel spacing is effective regardless of the lateral bracing system used. However, in case of cross-frames provided at one-panel spacing, generally higher

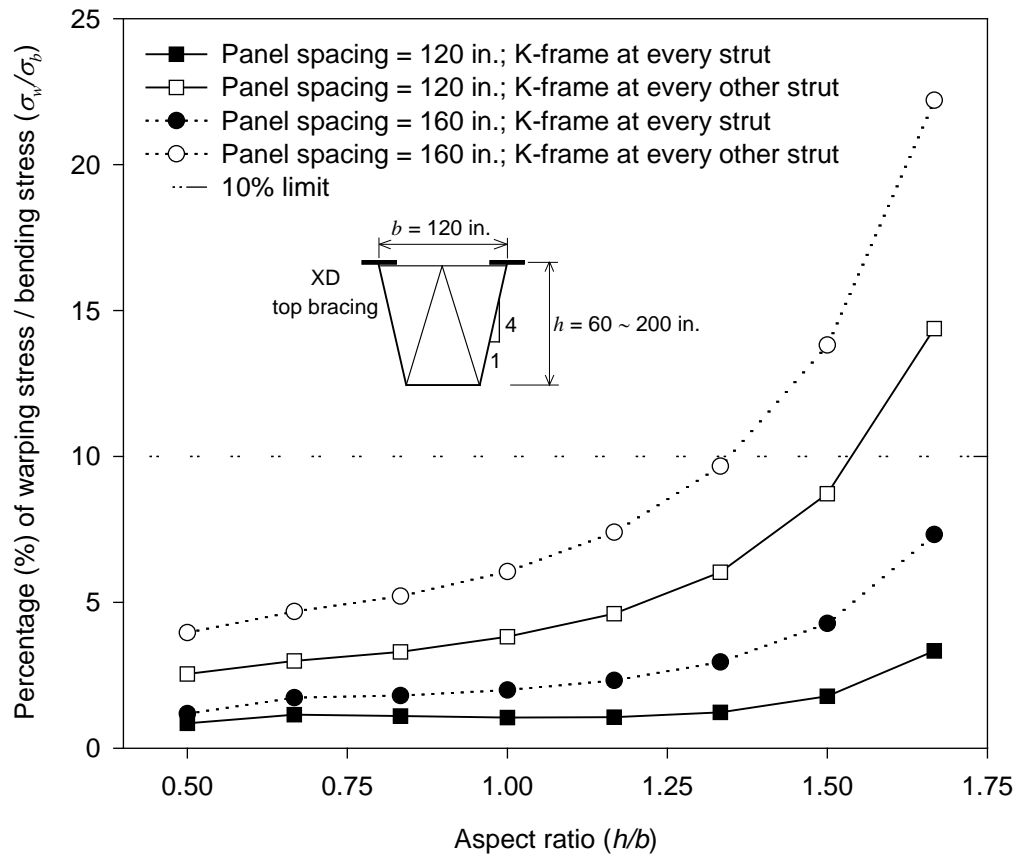


Fig. 4.23. Effect of aspect ratio of horizontally curved trapezoidal box girder with internal K-frames and XD type lateral bracing

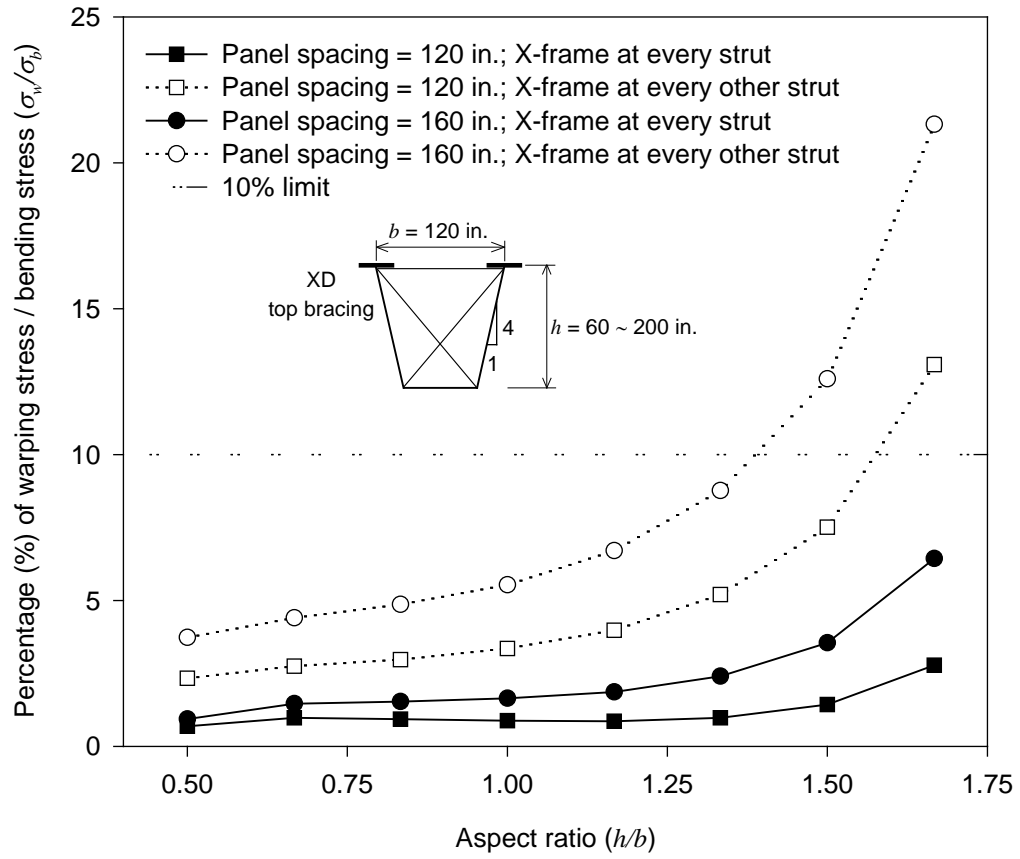


Fig. 4.24. Effect of aspect ratio of horizontally curved trapezoidal box girder with internal X-frames and XD type lateral bracing

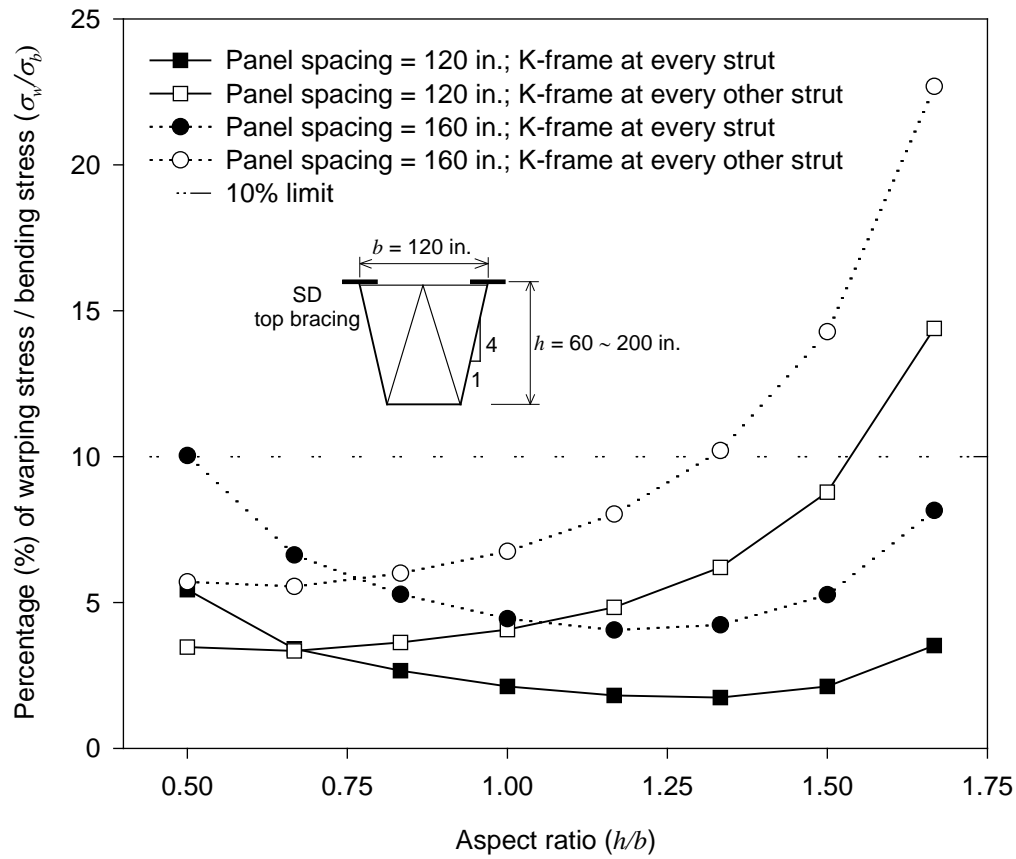


Fig. 4.25. Effect of aspect ratio of horizontally curved trapezoidal box girder with internal K-frames and SD type lateral bracing

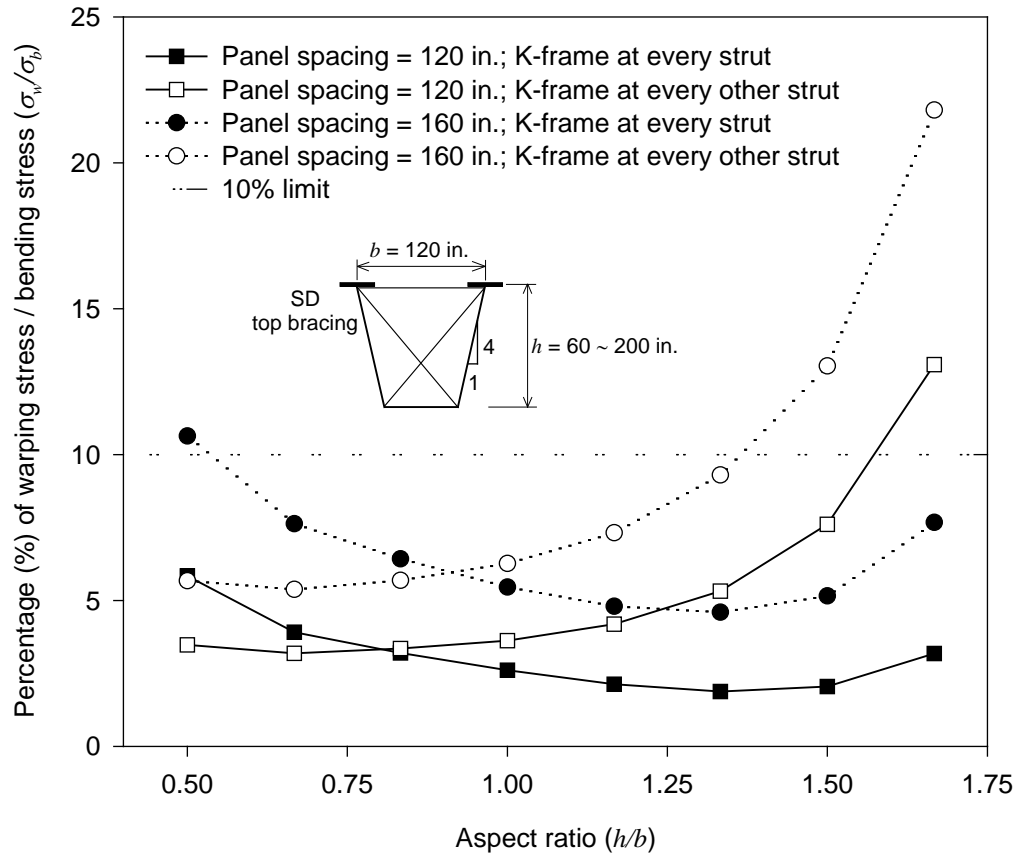


Fig. 4.26. Effect of aspect ratio of horizontally curved trapezoidal box girder with internal X-frames and SD type lateral bracing

forces are induced in diagonal members of cross-frames due to bending, which will be detailed in Chapter 5. Figs. 4.27 and 4.28 show member forces of the K-frame at midspan, and Figs. 4.29 and 4.30 show member forces of the X-frame at midspan for two different cross sections shown in Figs. 4.19 and 4.20.

4.9 Summary and Concluding Remarks

In a horizontally curved girder, the bending moment and torsional moment are always coupled due to the curvature of the girder axis. The applied torsional moment is primarily resisted by St. Venant torsion in a girder with a closed cross section. Therefore, stresses (both normal stress and shearing stress) induced due to warping torsion are negligibly small and are not separately considered in the design of the box girder. Since the stiffness of a box section against distortion is relatively weak compared with the bending stiffness or torsional stiffness, the distortional stresses may become fairly large if adequate distortional stiffnesses are not provided. If cross-frames are provided at a proper spacing, the distortional effects can be controlled in a horizontally curved girder. Torsional moments can be decomposed into a pair of couples inducing a net shear flow and distortion of the cross section. Distortion of box girders is caused by the distortional components. The magnitude and distribution of the distortional components on box girders are a function of the applied torsional loads as well as the cross-sectional geometry of the boxes. Torsional moments on horizontally curved girders are caused by eccentricities of vertical loads and offset of the vertical loads due to the horizontal curvature. Equations to decompose the force couples causing pure torsional shear flows

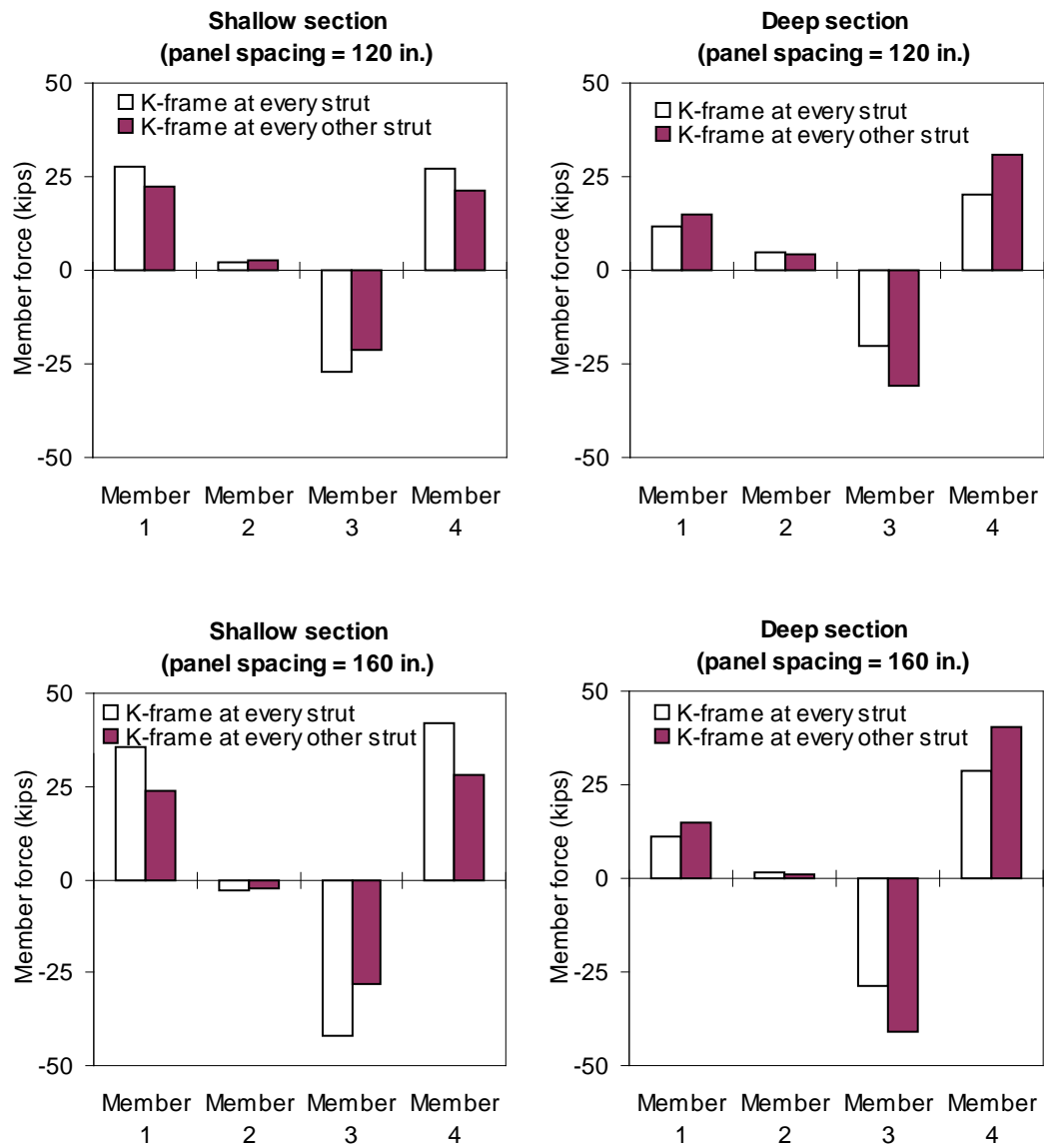
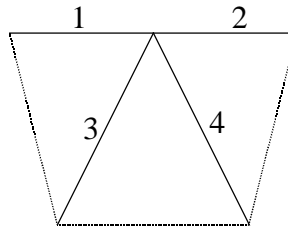


Fig. 4.27. Effect of spacing on cross-frame member forces (K-frame with SD type A)

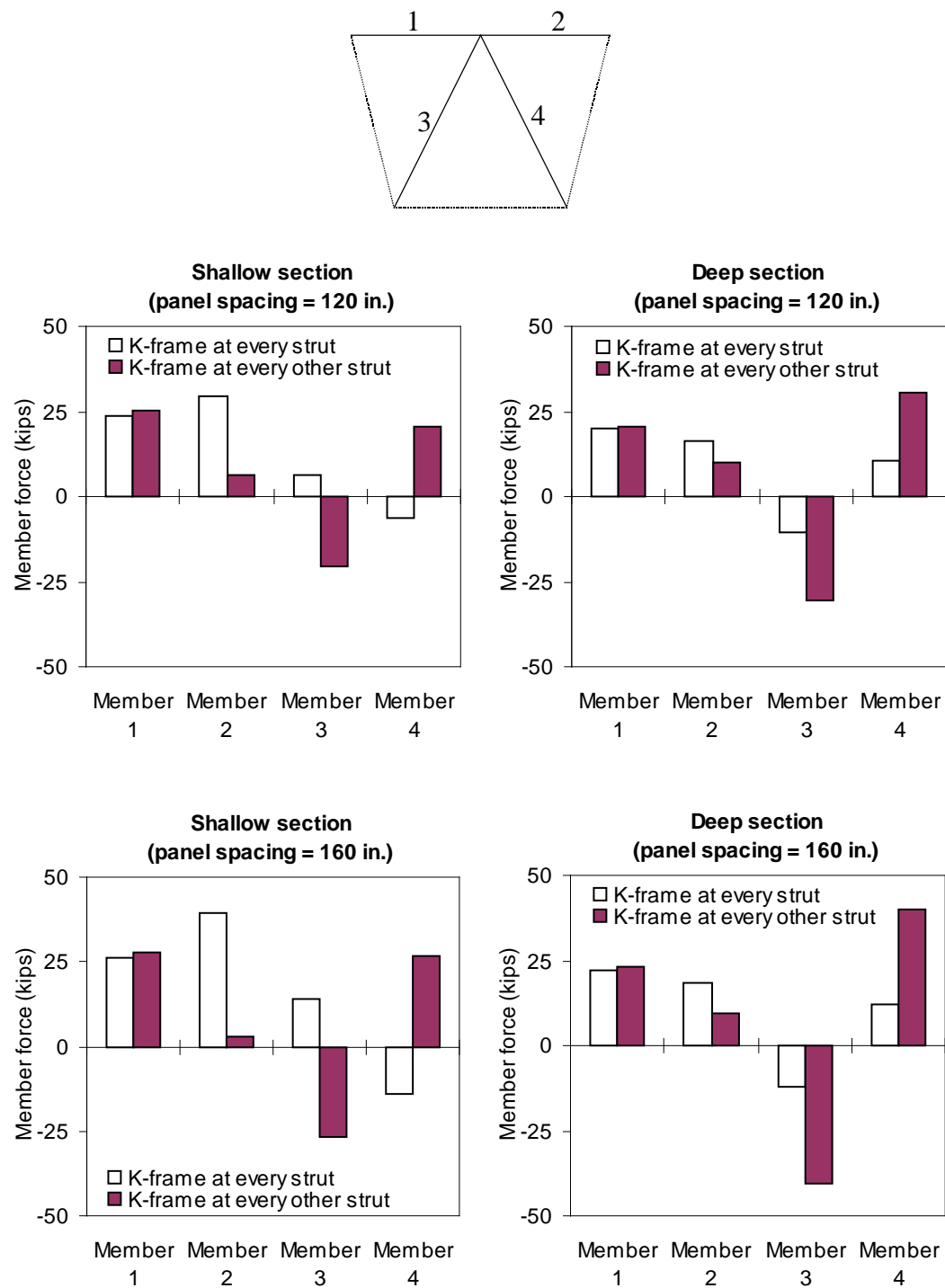


Fig. 4.28. Effect of spacing on cross-frame member forces (K-frame with SD type B)

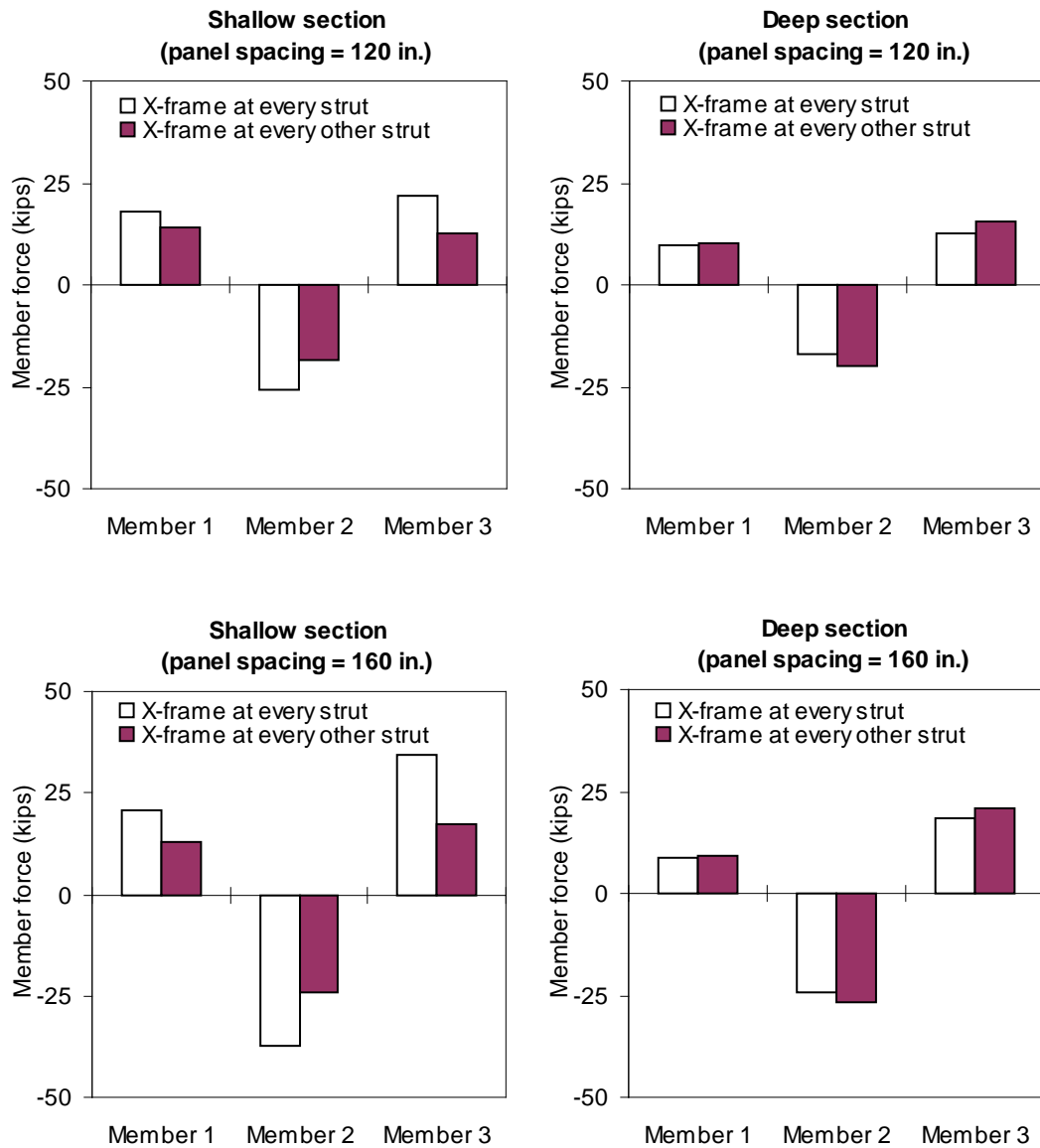
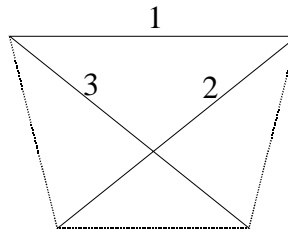


Fig. 4.29. Effect of spacing on cross-frame member forces (X-frame with SD type A)

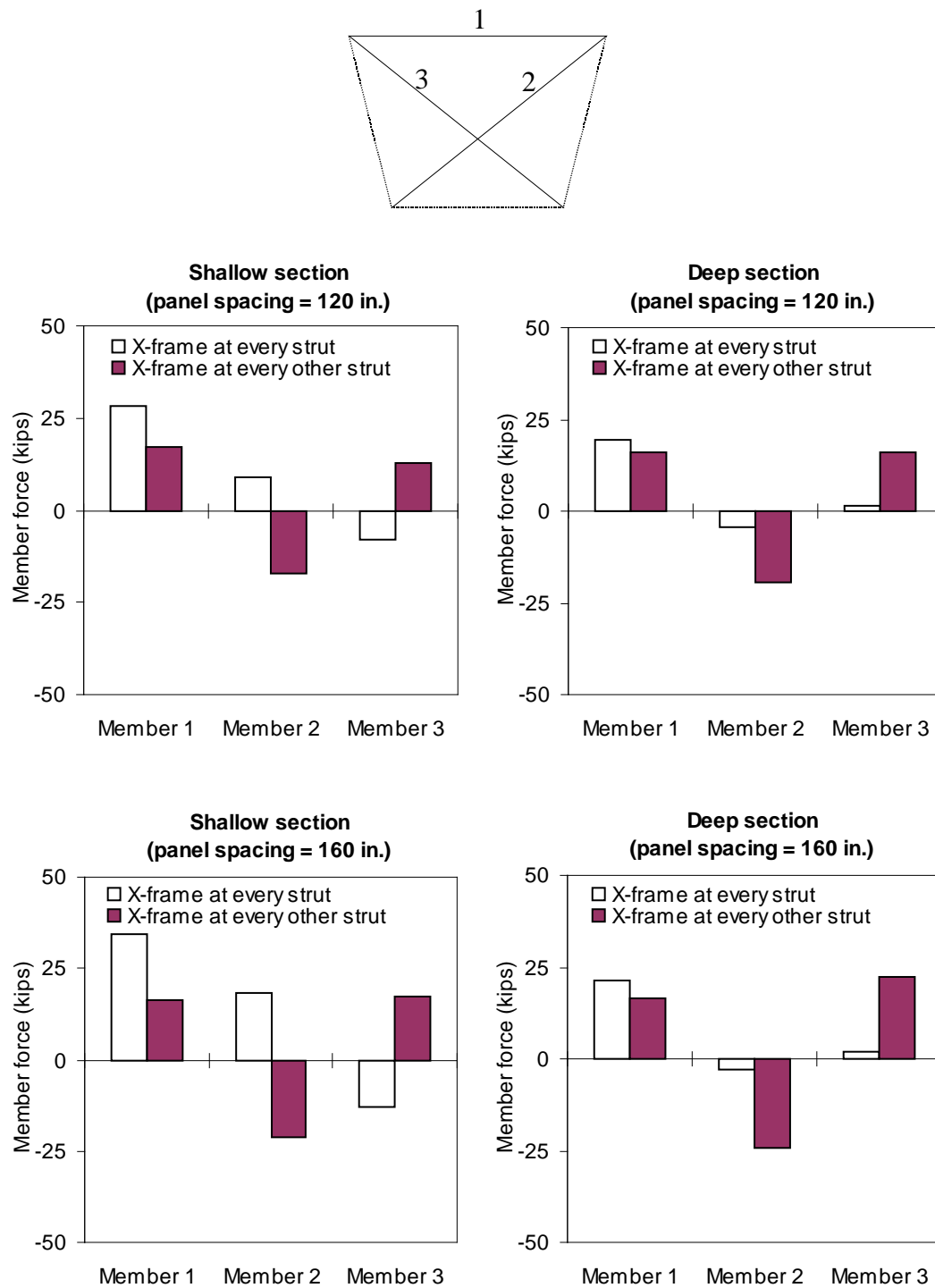


Fig. 4.30. Effect of spacing on cross-frame member forces (X-frame with SD type B)

and distortion of the cross section are given. Equations to predict member forces in cross-frames in trapezoidal box girders have been derived. Member forces computed by the proposed predictor equations have been compared with those obtained from three-dimensional finite element analyses and reasonable correlations have been observed. Data collected from three-dimensional analyses of a total of 128 horizontally curved box girders show that the ratio of distortional warping stress to bending stress, an important measure of controlling cross-sectional distortion, is affected by a combination of the type of lateral bracing, the spacing of cross-frames, and the aspect ratio of box cross sections.

CHAPTER 5

COUPLING ACTION OF LATERAL BRACING AND CROSS-FRAMES

5.1 Introduction

An open top steel tub girder with lateral bracing and cross-frames is a very attractive structural form for horizontally curved girder bridges as well as straight girder bridges because of its superb torsional rigidity and favorable long-term maintenance costs. Composite steel box girders are at their critical stage during construction because the noncomposite steel section must support the fresh concrete and the entire construction load. A top lateral bracing system is installed at the top flange level to form a quasi-closed section, thereby increasing the torsional rigidity during construction. Single diagonal (SD) and occasionally crossed diagonal (XD) bracing systems are typically considered for lateral bracing systems as introduced in Chapter 3. Forces in lateral bracing members are induced by bending and torsion of the girder. Typically 20 ~ 30 percent of forces that develop in the lateral bracing members are induced by longitudinal deformations of top flanges due to vertical bending in horizontally curved girders with moderate to fairly sharp curvature. Fan and Helwig (1999) derived equations for estimating forces in lateral bracing systems induced by vertical bending and applied torque on box girders. Significantly different responses take place in box girders braced with a SD type lateral bracing system and those with an XD type lateral bracing system

with regard to brace forces developed in lateral bracing systems. Kim and Yoo (2004) investigated mechanics of box girders with a SD type lateral bracing system and developed predictor equations for forces in lateral bracing members under general loading.

Due to distortional force components of applied torque, the cross section of a box girder may distort from its original shape. This distortion is resisted by cross-frames that are spaced along the length of the girder. K-frames or X-frames are the most preferred examples of cross-frames in box girders as introduced in Chapter 4. Spacing between adjacent cross-frames controls the distortional warping stresses in box girders. AASHTO Guide Specifications (2003) stipulate that spacing of intermediate internal bracing (cross-frames) shall be such that the longitudinal warping stress in the box does not exceed 10 percent of the longitudinal stress due to vertical bending at the strength limit state. As stated in Chapter 4, cross-frames are provided at one or two-panel spacing along the box girder. In order to meet the requirement of limiting the distortional warping stress to 10 percent of the bending stress, it may be necessary to provide cross-frames at a very close interval in horizontally curved box girders with sharp curvature. As examined in Section 4.8, spacing of cross-frames is a dominant parameter to control the distortional warping stress. However, box girders with SD type lateral bracing systems show significantly different responses if cross-frames are provided at one-panel spacing or two-panel spacing depending whether the girder cross section is shallow or deep. It has been found for girders subjected to only vertical load that member forces induced in the SD type lateral bracing system with cross-frames at one-panel spacing are much larger (up to 25

percent) than those at two-panel spacing. In addition, considerable forces are induced even in cross-frames of the box girder with one-panel spacing due to bending. Although the distortional warping stress (the torsion effect) is proportional to the spacing between adjacent cross-frames (the shorter the better), member forces in lateral bracing and cross-frames are inversely affected by the arrangement of cross-frames, i.e., at one-panel spacing or two-panel spacing.

Member forces in lateral bracing and cross-frames can be evaluated by superimposition of forces developed due to vertical bending and torque of the girder. In this chapter, box girders with SD type lateral bracing and cross-frames provided at one-panel spacing are investigated. Equations are formulated for member forces in lateral bracing and cross-frames due to bending of the girder only. Both K-frames and X-frames are considered. Member forces in SD type bracing and cross-frames computed using the matrix equations are compared with those obtained from three-dimensional finite element analyses (FEA), and good agreement between the two solutions is evident.

5.2 Background

Kim and Yoo (2004) suggested the following equations for forces in SD type lateral bracing members under general loading on the box girders:

$$D = D_{bend} + D_{lat} + D_{tor} + D_{dist} \quad (5.1)$$

$$S = S_{bend} + S_{lat} + S_{tor} + S_{dist} \quad (5.2)$$

where D, S = total diagonal and strut force, respectively; D_{bend}, S_{bend} = diagonal and strut force, respectively, due to vertical bending; D_{lat}, S_{lat} = diagonal and strut force,

respectively, due to lateral force components induced by inclined webs; D_{tor} , S_{tor} = diagonal and strut force, respectively due to torsion; D_{dist} , S_{dist} = diagonal and strut force, respectively, due to distortion. D_{bend} , S_{bend} , D_{lat} , and S_{lat} are force terms evaluated from vertical loads while D_{tor} , S_{tor} , D_{dist} , and S_{dist} are forces terms from torsional loads. Cross-frames were assumed provided at two-panel spacing in the derivation of Eqs. (5.1) and (5.2). Different spacing types of cross-frames (one-panel spacing or two-panel spacing) significantly affect the force terms D_{bend} , S_{bend} . They do not influence other force terms.

Consider two simply supported box girders with SD type and XD type lateral bracing systems, respectively, that are subjected to vertical loads as shown in Fig. 5.1. Each girder in the example has a span length of 160 ft and is made up of 16 lateral bracing panels. Two different spacing types, one-panel spacing and two-panel spacing, are considered along with K-frames. Figs. 5.2 and 5.3 show effects of spacing between adjacent cross-frames on diagonal and strut forces in K-frames, respectively. Notation for bracing members is shown in Fig. 5.1(e). Figs. 5.2 and 5.3 show that forces in diagonals and struts in SD type bracing systems are significantly affected by the spacing types while those in XD type bracing systems are not affected at all. Differences in member forces in SD type bracing systems with cross-frames provided at one-panel spacing and two-panel spacing are up to 29 percent in diagonals and 23 percent in struts.

Fig. 5.4 shows induced forces in diagonal members of internal K-frames provided at one-panel spacing. The difference between $S1$ and $S2$ (strut forces in K-frames) as shown in Fig. 5.3 was balanced by horizontal components of diagonal forces in K-frames. Member forces in lateral bracing are affected by longitudinal and lateral displacements of

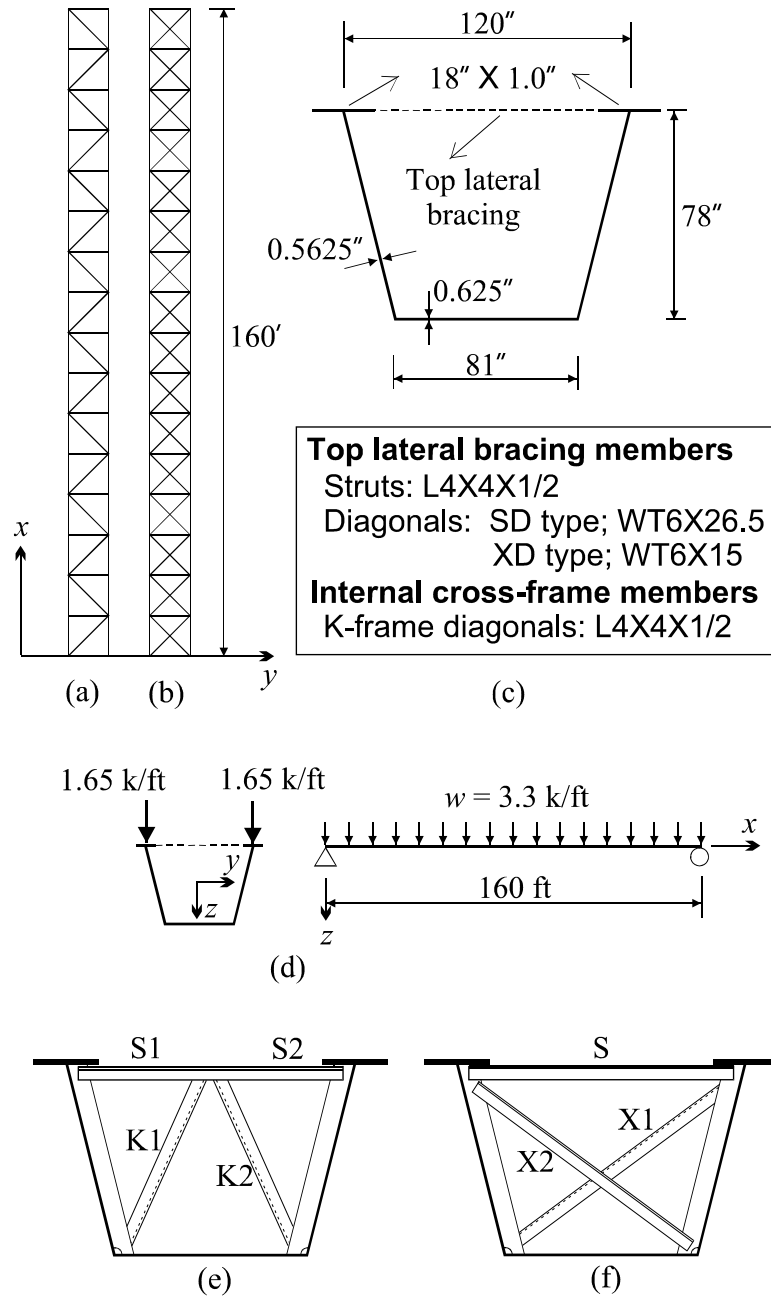


Fig. 5.1. Simple span box girders: (a) SD type; (b) XD type; (c) Cross-sectional properties; (d) Applied vertical load; (e) Notation for K-frame members; (f) Notation for X-frame members

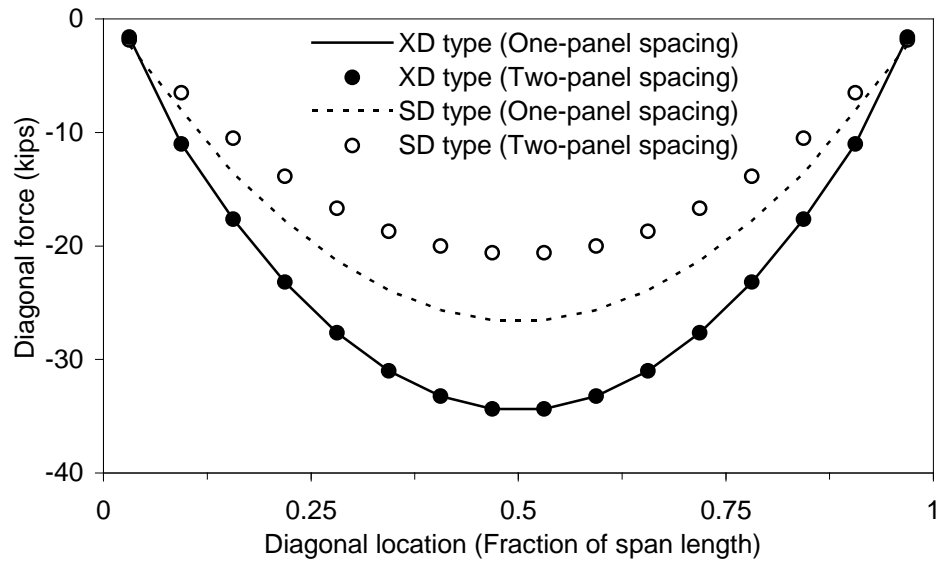


Fig. 5.2. Effects of internal cross-frame spacing on diagonal forces in lateral bracing

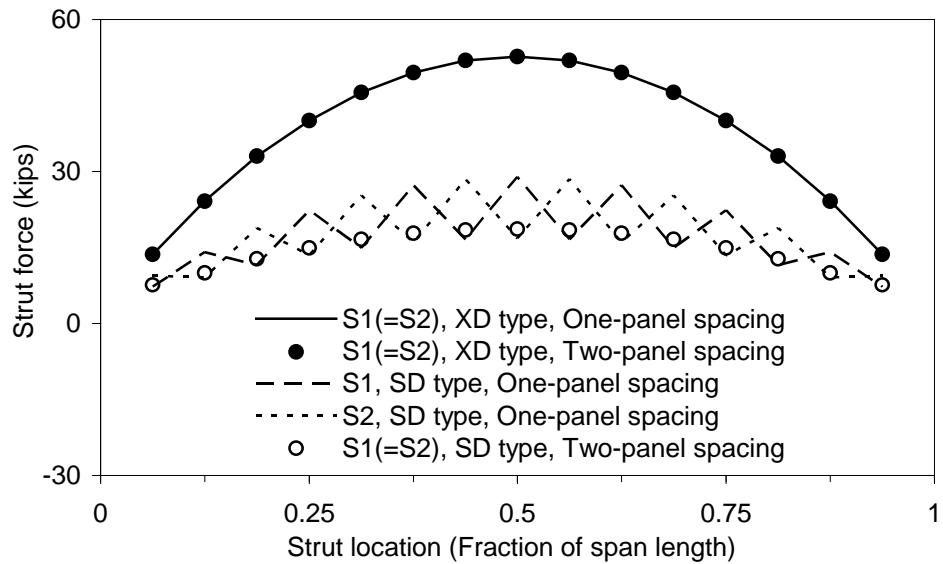


Fig. 5.3 Effects of internal cross-frame spacing on strut forces in lateral bracing

top flanges. Lateral displacements of top flanges are considered to be a major parameter to cause these differences of forces in bracing members because longitudinal deformations are expected to remain practically the same under the two different spacing types. Fig. 5.5 shows lateral displacements of individual top flanges with cross-frames provided at one-panel and two-panel spacing. Fig. 5.6 shows that differential lateral displacements between two top flanges in the box girder top flanges with cross-frames provided at one-panel spacing are larger than those at two-panel spacing. Lateral displacements of the bottom flange of the girder with cross-frames provided at one-panel spacing are entirely different from those at two-panel spacing. Fig. 5.7 shows average lateral displacements of the bottom flange along the girder. These differences in lateral displacements of the bottom flange of the girder with cross-frames provided at one-panel

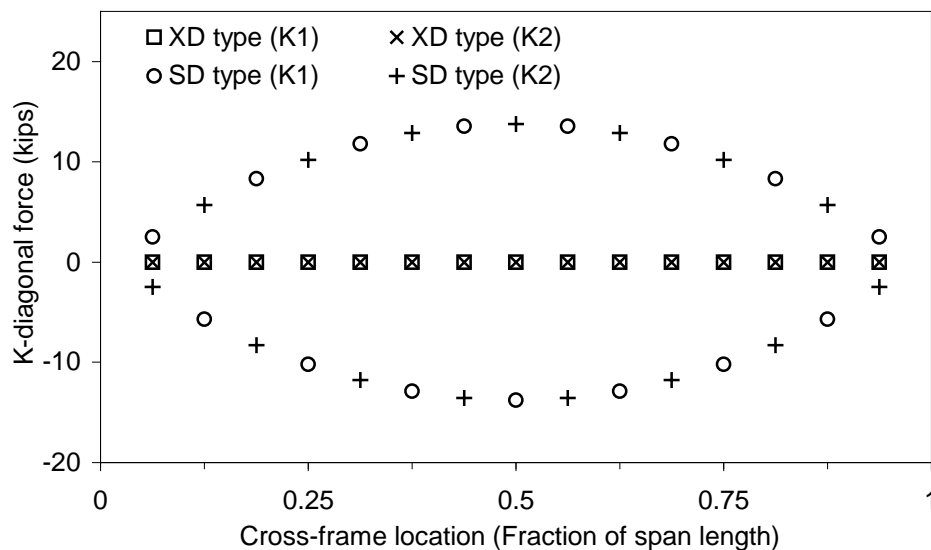


Fig. 5.4. Diagonal forces in K-frames provided at one-panel spacing

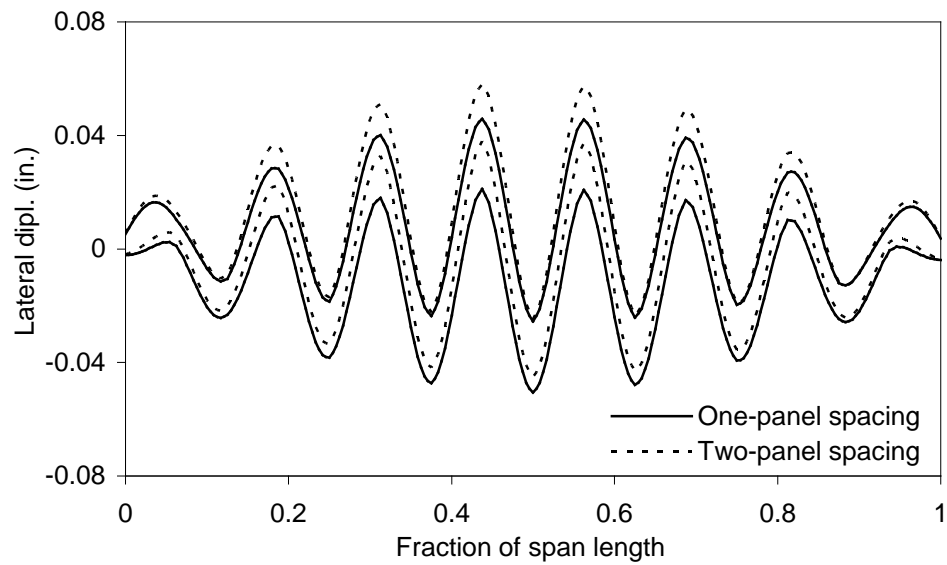


Fig. 5.5. Lateral displacement of top flanges due to vertical bending

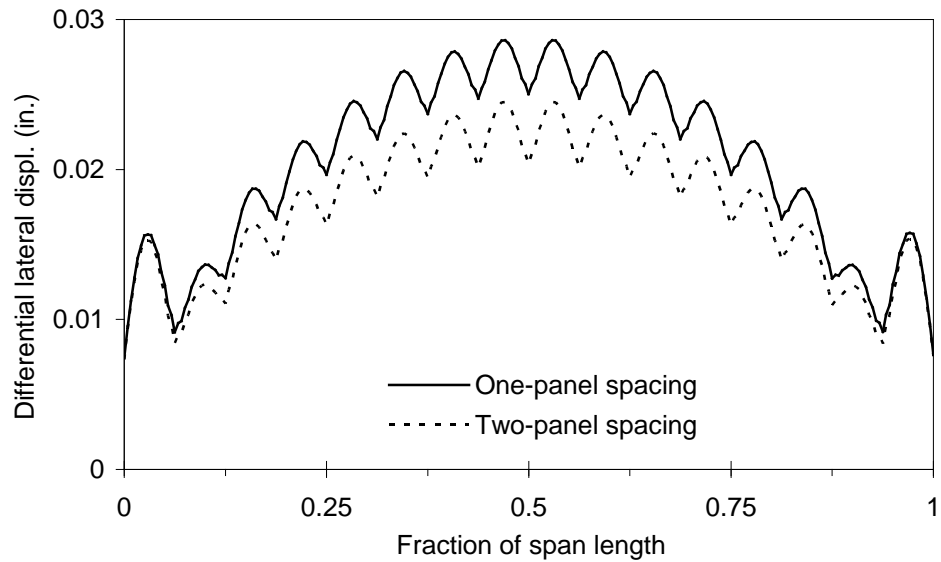


Fig. 5.6. Differential lateral displacement between top flanges due to vertical bending

spacing are believed to be the result of an interaction between SD bracing and K-frames. As a result of the interaction, considerable diagonal forces are believed to be induced in cross-frames. A detailed investigation of a box girder braced by SD type lateral bracing systems and cross-frames that are placed at one-panel spacing has been carried out, and the resulting data have been incorporated into predictor equations for the determination of brace forces. Equations were derived for both K-frames and X-frames. The strut forces in an XD type bracing induced by torsional loads are very small compared with those developed in SD type bracing because of the self-equilibrating nature of the crossed diagonals within a panel.

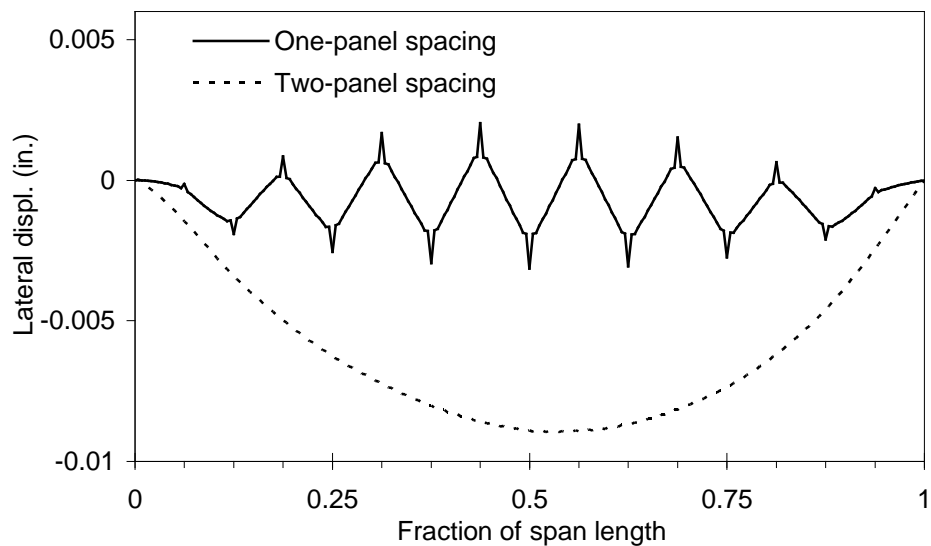


Fig. 5.7. Average lateral displacement at the bottom flange

5.3 Brace Forces in Box Girders with K-Frames

Equations for estimating brace forces are formulated for box girders braced with K-frames subjected to vertical bending only. The following assumptions are made:

- (1) A single diagonal bracing system is installed at the top flange level, and K-frames are provided at one-panel spacing.
- (2) Vertical bending affects the longitudinal deformation and lateral bulging of the top flanges due to inclined webs. Brace forces due to longitudinal deformation and lateral bulging are superimposed for the bending effect.
- (3) The webs have negligible lateral resistance against lateral bending of the top flanges. Verification for this assumption is shown in Appendix I.
- (4) No solid diaphragms are provided in the box girder other than above supports.
Additional forces due to the solid diaphragm for the bracing members immediately adjacent to the internal supports are evaluated separately and added later.

The box girder examined herein has an SD type lateral bracing system that consists of diagonals and horizontal struts and K-frames that consist of horizontal struts and K-diagonals; struts are part of lateral bracing as well as K-frames. Fig. 5.8 shows the interaction between lateral bracing members and the top flanges. At joint *A*, a strut and two lateral diagonals are connected to the top flange while only a strut is connected to the top flange at joint *B*. K-frame diagonals are connected to horizontal struts at joint *C*. The

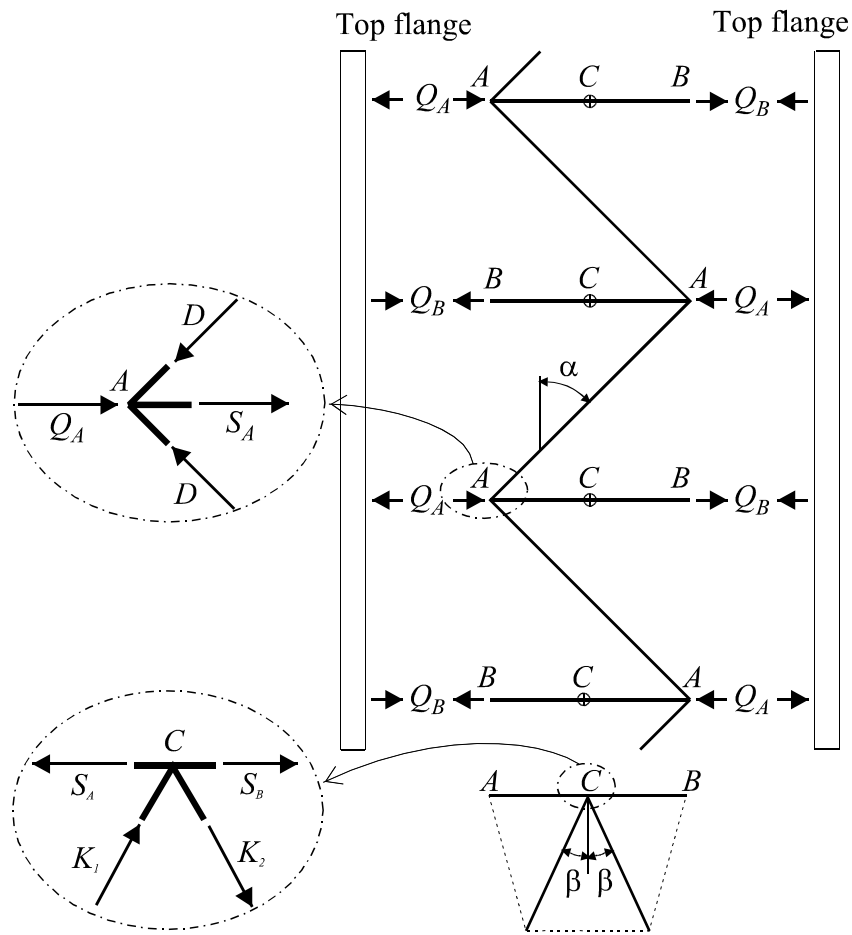


Fig. 5.8. Interactive forces between top flanges and lateral bracing members (internal K-frames)

two different strut forces are designated as S_A and S_B . The member forces in lateral diagonals are designated as D . Although the member forces in two lateral diagonals (D) at a joint are not necessarily identical, they differ by only a small amount (finite element analyses confirm this), and the assumption of equal force greatly simplifies the derivation. The two diagonal forces, K_1 and K_2 , in K-frames must be equal in magnitude and opposite in sign from a simple equilibrium consideration. Static equilibrium at joint A in the horizontal plane and at joint C in the vertical plane must be maintained as shown in Fig. 5.8. The magnitudes of interactive forces between lateral bracing and the top flange, Q_A and Q_B , must be the same due to equilibrium of the isolated flange as shown in Fig. 5.8. Horizontal equilibrium of joints A and B give respectively:

$$Q_A = -2D \sin \alpha - S_A \quad (5.3)$$

$$Q_B = S_B \quad (5.4)$$

where α = angle between lateral diagonal and flange. The diagonal force, D , is in compression, and strut forces, S_A and S_B , are in tension in the positive bending zone.

Lateral equilibrium of the isolated flange in Fig. 5.8 yields:

$$-2D \sin \alpha - S_A = S_B \quad (5.5)$$

Similarly, equilibrium at joint C in the vertical plane of the transverse K-frame leads to

$$S_A - S_B = 2K \sin \beta \quad (5.6)$$

where the angle β is defined in Fig. 5.8. Assumed lateral deformation of top flanges and lateral bracing members is shown in Fig. 5.9(a). Lateral deformation of top flanges is idealized to bend as shown in Fig. 5.9(b), and assumed deformation of a K-frame at joint C is idealized as shown in Fig. 5.9(c). Joints, A , B , and C are assumed to move to A' , B' ,

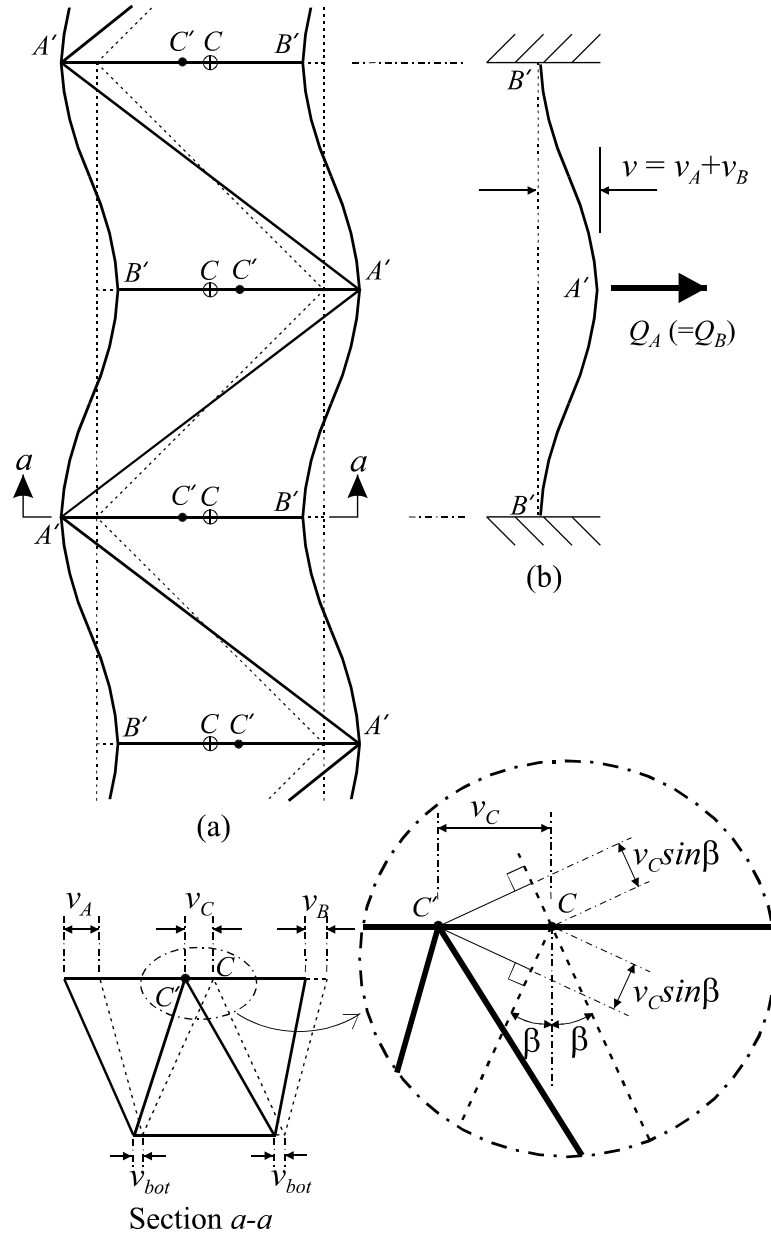


Fig. 5.9. Assumed lateral displacements (internal K-frames): (a) Top flanges and lateral bracing members; (b) Lateral deflection of top flange

and C' . Lateral displacements of joints, A , B , and C are denoted as v_A , v_B , and v_C , respectively. Lateral displacement of the bottom flange is denoted as v_{bot} . The force-deformation relationship of each strut member yields

$$v_A - v_C = \frac{b}{2EA_s} S_A \quad (5.7)$$

$$v_C - v_B = \frac{b}{2EA_s} S_B \quad (5.8)$$

where b = distance between centers of the two top flanges; A_s = the cross sectional area of strut members; and E = modulus of elasticity. The portion of the top flange between two panels is assumed to deform as shown in Fig. 5.9(b). The relative lateral deflection between two adjacent panel points, shown in Fig. 5.9(b), is evaluated by an equation for the deflection at the center of a both-end-fixed beam subjected to a concentrated load at the midspan as

$$v_A + v_B = \frac{S_B (2s)^3}{192EI_{tf}} = \frac{s^3}{24EI_{tf}} S_B \quad (5.9)$$

where I_{tf} = moment of inertia of the top flange with respect to the vertical axis passing through the centroid of the flange. The stiffness of the inclined web plate against the lateral displacement computed in Eq. (5.9) is ignored. It has been verified that the stiffness of the web against the above lateral displacement is negligibly small (on the order of 2% of that of the top flange). Detailed verification is presented in Appendix I. Similarly, lateral displacement of the bottom flange is obtained by:

$$2v_{bot} = C_{bot} \frac{P_{bot} (2s)^3}{192EI_{bf}} \quad (5.10)$$

where C_{bot} = parameter for lateral displacement of bottom flange set to be 2.0; I_{bf} = second moment of inertia of the bottom flange with respect to the vertical centroidal axis. P_{bot} = vertical force component transferred to bottom flange through both webs and diagonals in K-frames, which is computed to be

$$P_{bot} = 2(S_B + K \sin \beta) \quad (5.11)$$

Forces in diagonals of K-frames must be equal in magnitude and opposite in sign. The elongation (positive value) or shortening (negative value) of K-frame diagonals, δ_K , can be expressed in terms of lateral displacements at joint C and bottom flange as

$$\delta_K = (v_C - v_{bot}) \sin \beta \quad (5.12)$$

Substituting Eq. (5.9) in Eq. (5.7) and invoking the force-deformation relationship of K-frame diagonal yields

$$v_C - \frac{s^3 (S_B + K \sin \beta)}{12EI_{bf}} = \frac{L_K}{EA_K \sin \beta} K \quad (5.13)$$

where L_K and A_K = length and cross-sectional area of K-frame diagonal members, respectively. The axial elongation (or shortening), δ_D , of a diagonal member in the horizontal plane is expressed as

$$\delta_D = \frac{L_D D}{EA_D} \quad (5.14)$$

where L_D and A_D = length and cross-sectional area of top diagonal member, and D is axial force in the lateral diagonal. From the geometry of the horizontal plane at the level of top flanges as shown in the Fig. 3.11, δ_D can be expressed based on small displacement theory as

$$\delta_D = u \cos \alpha + v \sin \alpha \quad (5.15)$$

where u and v = relative displacements of lateral diagonal in the longitudinal and lateral directions, respectively. From the force-deformation relationship and the lateral displacement at the panel point A, the relative displacements of the lateral diagonal in the longitudinal and lateral direction, respectively, are expressed as

$$u = \frac{\sigma_x s}{E} = \frac{s y_t}{EI_{bot}} M \quad (5.16)$$

$$v = 2v_A \quad (5.17)$$

where σ_x = longitudinal stress at the centroid of top flange cross section; s = panel length between two adjacent K-frames; I_{box} = moment of inertia of box cross section with respect to horizontal centroidal axis; y_t = vertical distance of the top flange from the neutral axis of the box cross section; E = modulus of elasticity; M = vertical bending moment. Substituting Eqs. (5.14), (5.16), and (5.17) into Eq. (5.15) yields the following expression:

$$\frac{L_D}{EA_D} D = \frac{s y_t \cos \alpha}{EI_{box}} M + 2v_A \sin \alpha \quad (5.18)$$

A number of simultaneous equations, Eqs. (5.5) ~ (5.9), (5.13), and (5.18), may be rewritten in a matrix form:

$$\left[\begin{array}{c|c} K_{11} & K_{12} \\ \hline K_{21} & K_{22} \end{array} \right] \left\{ \begin{array}{c} P_{bend} \\ V_{bend} \end{array} \right\} = \left\{ \begin{array}{c} Y_P \\ Y_V \end{array} \right\} \quad (5.19)$$

where,

$$\left[\begin{array}{c|c} K_{11} & K_{12} \\ \hline K_{21} & K_{22} \end{array} \right] = \left[\begin{array}{cccc|ccc} \frac{L_D}{EA_D} & 0 & 0 & 0 & -2 \sin \alpha & 0 & 0 \\ 2 \sin \alpha & 1 & 1 & 0 & 0 & 0 & 0 \\ 0 & 0 & \frac{s^3}{24EI_{tf}} & 0 & -1 & -1 & 0 \\ 0 & -1 & 1 & 2 \sin \beta & 0 & 0 & 0 \\ \hline 0 & -\frac{b}{2EA_S} & 0 & 0 & 1 & 0 & -1 \\ 0 & 0 & \frac{b}{2EA_S} & 0 & 0 & 1 & -1 \\ 0 & 0 & \frac{s^3}{12EI_{bf}} & \frac{L_K}{EA_K \sin \beta} + \frac{s^3 \sin \alpha}{12EI_{bf}} & 0 & 0 & -1 \end{array} \right],$$

$$\left\{ \begin{array}{c} P_{bend} \\ \hline V_{bend} \end{array} \right\} = \left\{ \begin{array}{c} D_{bend} \\ S_{A,bend} \\ S_{B,bend} \\ \hline K_{bend} \\ v_A \\ v_B \\ v_C \end{array} \right\}, \text{ and } \left\{ \begin{array}{c} Y_P \\ \hline Y_V \end{array} \right\} = \left\{ \begin{array}{c} \frac{sy_t M \cos \alpha}{EI_{box}} \\ 0 \\ 0 \\ 0 \\ \hline 0 \\ 0 \\ 0 \end{array} \right\}$$

By a matrix operation of static condensation (Bathe 1996; Cook et al. 1989), the member force vector $\{P_{bend}\}$ and lateral displacement vector $\{V_{bend}\}$ are obtained in the following simplified forms:

$$\{P_{bend}\} = [C_P]^{-1} \{Y_P\} \quad (5.20)$$

$$\{V_{bend}\} = [C_V] \{P_{bend}\} \quad (5.21)$$

where,

$$[C_P] = \left[\begin{array}{c|c|c|c} \frac{L_D}{EA_D} & -\frac{b \sin \alpha}{EA_S} & \frac{s^3 \sin \alpha}{6EI_{bf}} & -\frac{2L_K}{EA_K} - \frac{s^3 \sin^2 \beta}{6EI_{bf}} \\ 2 \sin \alpha & 1 & 1 & 0 \\ 0 & -\frac{b}{2EA_S} & \frac{b}{2EA_S} + \frac{s^3}{6E} \left(\frac{1}{4I_{tf}} - \frac{1}{I_{bf}} \right) & -\frac{2L_K}{EA_K \sin \beta} - \frac{s^3 \sin \beta}{6EI_{bf}} \\ 0 & -1 & -1 & 2 \sin \beta \end{array} \right], \text{ and}$$

$$[C_V] = \left[\begin{array}{c|c|c|c} 0 & \frac{b}{2EA_S} & \frac{s^3}{12EI_{bf}} & \frac{L_K}{EA_K \sin \beta} + \frac{s^3 \sin \beta}{12EI_{bf}} \\ 0 & 0 & \frac{s^3}{12EI_{bf}} - \frac{b}{2EA_S} & \frac{L_K}{EA_K \sin \beta} + \frac{s^3 \sin \beta}{12EI_{bf}} \\ 0 & 0 & \frac{s^3}{12EI_{bf}} & \frac{L_K}{EA_K \sin \beta} + \frac{s^3 \sin \beta}{12EI_{bf}} \end{array} \right]$$

5.4 Brace Forces in Box Girder with Internal X-Frames

In a manner similar to that used for the case of box girders with K-frames discussed in the previous section, equations are formulated to estimate forces in lateral bracing and X-frames of box girders subjected to vertical loads only. Assumptions are unchanged from those employed in the previous section except K-frames are replaced with X-frames. Fig. 5.10 shows interactive forces between top flanges and lateral bracing members. The following expressions are readily extracted from equilibrium at joints A and B:

$$Q_A = -2D \sin \alpha - S - X_A \cos \gamma \quad (5.22)$$

$$Q_B = S + X_B \cos \gamma \quad (5.23)$$

where D, S = diagonal and strut forces in lateral bracing, respectively; X_A, X_B = forces in X-frame diagonal members connected to joints A and B, respectively; α = angle between

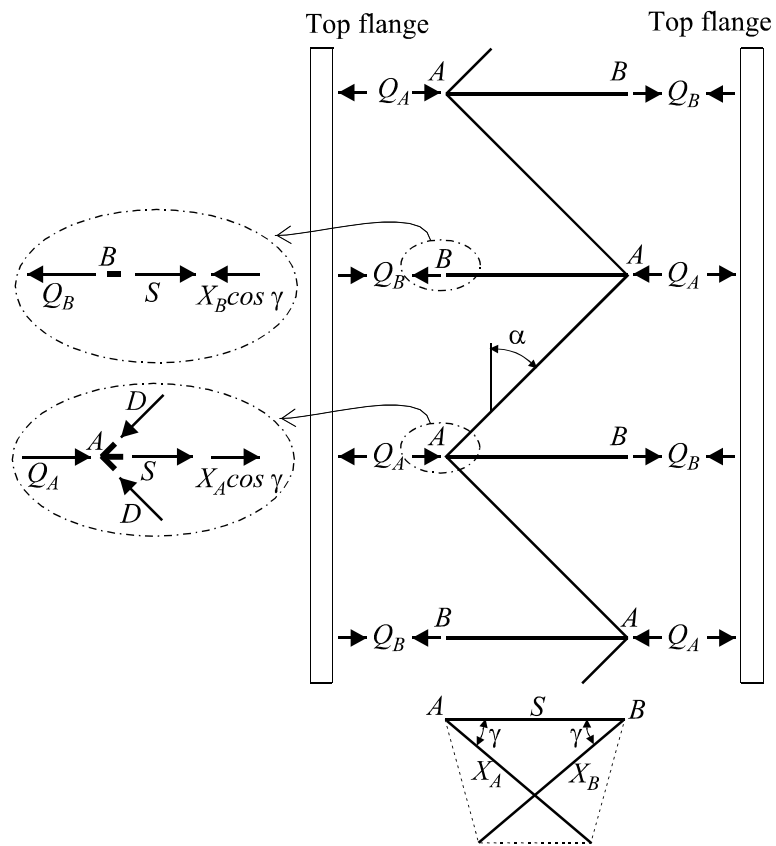


Fig. 5.10. Interactive forces between top flanges and lateral bracing (internal X-frames)

lateral diagonal and top flange; γ = angle between X-frame diagonal and strut. The magnitude of interaction forces, Q_A and Q_B , must be the same.

$$2D \sin \alpha + 2S + (X_A + X_B) \cos \gamma = 0 \quad (5.24)$$

Assumed deformation of top flanges and lateral bracing members in the horizontal plane is shown in Fig. 5.11(a). Relative lateral deflection between two adjacent panel points is analogous to that of the fixed-end beam with the length of two panels shown in Fig. 5.11(b). Similar to the case of K-frames, the relative lateral deflection between two adjacent panel points, denoted as $v_A + v_B$ in Fig. 5.11(b), can be evaluated as

$$v_A + v_B = \frac{(S + X_B \cos \gamma)(2s)^3}{192EI_{tf}} \quad (5.25)$$

Assumed deformation of the box cross section with X-frame diagonals is shown in Fig. 5.11(c). The force-deformation relationship for strut members yields

$$v_A - v_B = \frac{b}{EA_s} S \quad (5.26)$$

The primary source of lateral displacements of the bottom flange at both edges (Fig. 5.11(c)) is assumed to be the longitudinal stress (due to Poisson's effect). Consequently, the sum of lateral displacements is evaluated from a two-dimensional Hooke's law as

$$v_{A,bot} + v_{B,bot} = \frac{av_y M}{EI_{box}} \quad (5.27)$$

where a = width of bottom flange; y_b = distance between the neutral axis of the box cross section and the bottom flange; v = Poisson's ratio. The portion of the top flange between two panels is assumed to deform as shown in Fig. 5.11(b). The relative lateral deflection between two adjacent panel points, shown in Fig. 5.11(b), is evaluated by an equation for

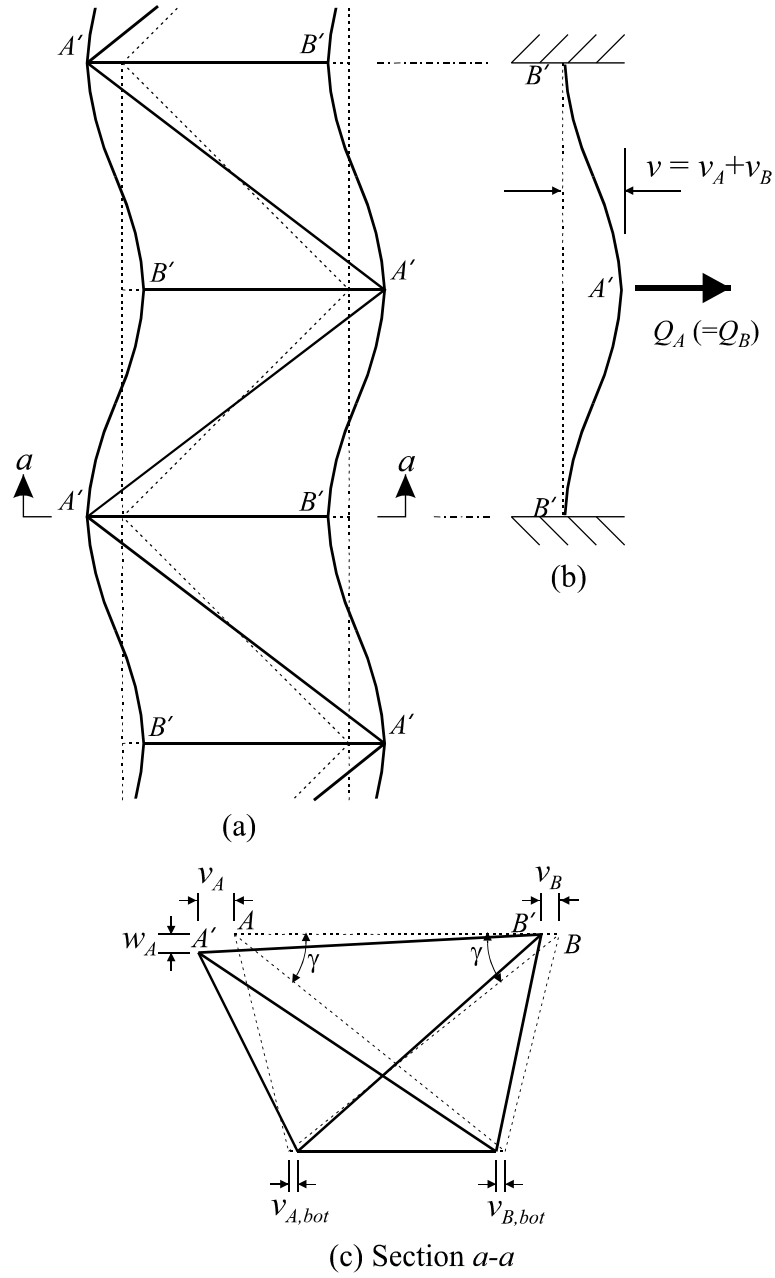


Fig. 5.11. Assumed lateral displacements (internal X-frames): (a) Top flanges and lateral bracing members; (b) Lateral deflection of top flange; (c) Cross section with X-frame

the deflection at the center of a both-end-fixed beam subjected to a concentrated load at the midspan as

$$-v_{A,bot} + v_{B,bot} = C_{bot} \frac{(2S)(2s)^3}{192EI_{bf}} \quad (5.28)$$

where C_{bot} is taken as 2.0 as in the case of K-frame. Based on the assumed deformation configuration of the box cross section with an X-frame shown in Fig. 5.11(c), the force in each diagonal of the X-frame is computed as

$$X_A = (v_A - v_{B,bot} - w_A) \frac{EA_x \cos \gamma}{L_x} \quad (5.29)$$

$$X_B = -(v_B + v_{A,bot}) \frac{EA_x \cos \gamma}{L_x} \quad (5.30)$$

As stated earlier in Chapter 3, forces in lateral bracing members are caused in part by lateral force components resulting from the inclined webs in addition to the longitudinal deformation of top flanges as shown in Fig. 3.3. These lateral force components are resisted by diagonals and struts in lateral bracing and X-frame diagonals. For simplicity, it is assumed that lateral force components are resisted primarily by struts and X-frame diagonals because a relatively small fraction of the total lateral force at joint A shown in Fig. 5.11(a) is resisted by lateral diagonals in the case of an SD lateral bracing and an X-frame combination. Forces induced in the strut and the X-frame diagonal by lateral force components are evaluated by

$$S_{lat} = \frac{A_s L_x s w_{lat}}{A_x b \cos^2 \gamma + A_s L_x} \quad (5.31)$$

$$X_{lat} = \frac{I}{2} \frac{A_x b s w_{lat} \cos \gamma}{A_x b \cos^2 \gamma + A_s L_x} \quad (5.32)$$

where S_{lat} , X_{lat} = strut and X-diagonal forces due to lateral force components, respectively; w_{lat} = lateral force components due to inclined webs. Total forces in struts and X-frame diagonals are the sum of those from the longitudinal deformation of top flanges due to vertical bending and lateral force components. Although the development of forces, X_1 and X_2 , in diagonal members in X-frames is considered separately, the final value of the forces reach same magnitude (in opposite sign) without undergoing these separate steps. At the final stage, X-frame diagonals resist distortion of the box cross section. As distortion of a box section is characterized by the angular deformations only without inducing the stretch or contraction of the box walls, the force in the diagonals of X-frames must be equal in magnitude and opposite in sign, thereby leading to the following:

$$X_A + X_B + 2X_{lat} = 0 \quad (5.33)$$

Substituting Eqs. (5.29), (5.30), and (5.32) into Eq. (5.33) and solving for w_A yields

$$w_A = \frac{L_X b s w_{lat}}{E(A_X b \cos^2 \gamma + A_S L_X)} + v_A - v_B - v_{A,bot} - v_{B,bot} \quad (5.34)$$

And substituting Eq. (5.34) into Eq. (5.29) gives

$$X_A = (v_B + v_{A,bot}) \frac{EA_X \cos \gamma}{L_X} - \frac{A_X L_X b s w_{lat} \cos \gamma}{L_X (A_X b \cos^2 \gamma + A_S L_X)} \quad (5.35)$$

Recalling Eq. (5.18) derived to compute the force in a diagonal of an SD type lateral bracing

$$\frac{L_D}{EA_D} D = \frac{s y_t \cos \alpha}{EI_{box}} M + 2v_A \sin \alpha \quad (5.18)$$

eight simultaneous Eqs. (5.24) ~ (5.28), (5.30), (5.35), and (5.18) are rewritten in a matrix form

$$\left[\begin{array}{c|c} K_{11} & K_{12} \\ \hline K_{21} & K_{22} \end{array} \right] \left\{ \begin{array}{c} P_{bend} \\ V_{bend} \end{array} \right\} = \left\{ \begin{array}{c} Y_P \\ Y_V \end{array} \right\} \quad (5.19)$$

where,

$$\left[\begin{array}{c|c} K_{11} & K_{12} \\ \hline K_{21} & K_{22} \end{array} \right] = \left[\begin{array}{cccc|cccc} \frac{L_D}{EA_D} & 0 & 0 & 0 & -2 \sin \alpha & 0 & 0 & 0 \\ 0 & 0 & 0 & 0 & 0 & 0 & 1 & 1 \\ 0 & 0 & -\frac{1}{\cos \gamma} & 0 & 0 & \frac{EA_X}{L_X} & \frac{EA_X}{L_X} & 0 \\ 2 \sin \alpha & 2 & \cos \gamma & \cos \gamma & 0 & 0 & 0 & 0 \\ \hline 0 & \frac{b}{EA_S} & 0 & 0 & -1 & 1 & 0 & 0 \\ 0 & \frac{s^3}{24EI_{tf}} & 0 & \frac{s^3 \cos \gamma}{24EI_{tf}} & -1 & -1 & 0 & 0 \\ 0 & 0 & 0 & 1 & \frac{EA_X \cos \gamma}{L_X} & 0 & \frac{EA_X \cos \gamma}{L_X} & 0 \\ 0 & \frac{s^3}{6EI_{bf}} & 0 & 0 & 0 & 0 & 1 & -1 \end{array} \right],$$

$$\left\{ \begin{array}{c} P_{bend} \\ V_{bend} \end{array} \right\} = \left\{ \begin{array}{c} D_{bend} \\ S_{bend} \\ X_{A,bend} \\ X_{B,bend} \\ \hline v_A \\ v_B \\ v_{A,bot} \\ v_{B,bot} \end{array} \right\}, \text{ and } \left\{ \begin{array}{c} Y_P \\ Y_V \end{array} \right\} = \left\{ \begin{array}{c} \frac{sy_t \cos \alpha}{EI_{box}} M \\ \frac{sy_b \cos \alpha}{EI_{box}} M \\ \frac{A_X bsw_{lat}}{A_X b \cos^2 \gamma + A_S L_X} \\ \hline 0 \\ 0 \\ 0 \\ 0 \\ 0 \end{array} \right\}$$

By a matrix operation of static condensation, the member force vector $\{P_{bend}\}$ and lateral displacement vector $\{V_{bend}\}$ are expressed in following simplified forms:

$$\{P_{bend}\} = [C_P]^{-1} \{Y_P\} \quad (5.36)$$

$$\{V_{bend}\} = [C_V] \{P_{bend}\} \quad (5.37)$$

where,

$$[C_P] = \begin{bmatrix} \frac{L_D}{EA_D} & -\frac{s^3 \sin \alpha}{24EI_{tf}} - \frac{b \sin \alpha}{EA_S} & 0 & -\frac{s^3 \cos \alpha \cos \gamma}{24EI_{tf}} \\ 0 & \frac{s^3}{6E} \left(\frac{1}{I_{bf}} - \frac{1}{4I_{tf}} \right) - \frac{b}{EA_S} & 0 & -\frac{s^3 \cos \gamma}{24EI_{tf}} - \frac{2L_X}{EA_X \cos \gamma} \\ 0 & -\frac{A_X b}{L_X A_S} & -\frac{1}{\cos \gamma} & -\frac{1}{\cos \gamma} \\ 2 \sin \alpha & \frac{2}{L_X A_S} & \frac{1}{\cos \gamma} & \frac{1}{\cos \gamma} \end{bmatrix}, \text{ and}$$

$$[C_V] = \begin{bmatrix} 0 & \frac{s^3}{48EI_{tf}} + \frac{b}{2EA_S} & 0 & \frac{s^3 \cos \gamma}{48EI_{tf}} \\ 0 & \frac{s^3}{48EI_{tf}} + \frac{b}{2EA_S} & 0 & \frac{s^3 \cos \gamma}{48EI_{tf}} \\ 0 & -\frac{s^3}{48EI_{tf}} - \frac{b}{2EA_S} & 0 & -\frac{s^3 \cos \gamma}{48EI_{tf}} - \frac{L_X}{EA_X \cos \gamma} \\ 0 & \frac{s^3}{2E} \left(\frac{1}{3I_{bf}} - \frac{1}{24I_{tf}} \right) - \frac{b}{2EA_S} & 0 & -\frac{s^3 \cos \gamma}{48EI_{tf}} - \frac{L_X}{EA_X \cos \gamma} \end{bmatrix}$$

The details of the matrix condensation and computation of transfer matrices, $[C_P]$ and $[C_V]$ in both cases of K-frames and X-frames, are given in Appendix II.

5.5 Forces in Bracing Members near Interior Supports

Predictor equations formulated in previous sections have been derived based on K-frames and X-frames. At interior supports, distortion of box sections is not expected

as it is customary to install rigid solid plate diaphragms instead of cross-frames at piers. This alters the fundamental assumptions employed in the derivation of predictor equations for cross-frame forces and as a consequence causes additional forces in lateral bracing members and cross-frames in the panel including a solid diaphragm. Actual and assumed displacements near the interior support are shown in Fig. 5.12. It is noted that longitudinal forces in top flanges and diagonals of lateral bracing are in tension because negative moment zones are developed around interior supports. No lateral displacements are assumed to occur at the interior support. Additional member forces are evaluated by constraints as follows:

For K-frames:

$$D' = (v_A - v_B) \sin \alpha \frac{EA_D}{L_D} \quad (5.38)$$

$$K' = (v_A - v_B) \sin \beta \frac{EA_K}{L_D} \quad (5.39)$$

$$S'_{A,B} = \mp K' \sin \beta \quad (5.40)$$

For X-frames:

$$D' = (v_A - v_B) \sin \alpha \frac{EA_D}{L_D} \quad (5.41)$$

$$X' = (v_A - v_B) \cos \gamma \frac{EA_X}{L_X} \quad (5.42)$$

$$S' = (v_A - v_B) \frac{EA_S}{L_S} \quad (5.43)$$

where v_A, v_B = computed lateral displacements at joints A and B , respectively, at the interior support; symbols with primes are additional forces to be added to member forces in bracing members next to the solid diaphragm, and the symbols without primes are previously defined.

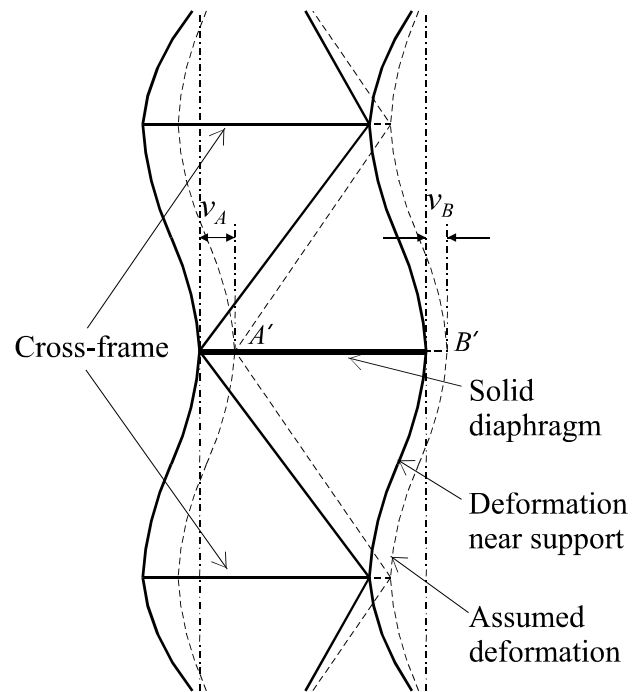


Fig. 5.12. Lateral displacements of top flanges and lateral bracing near interior supports

5.6 Comparison of Bracing Forces

Forces in lateral bracing and K-frames computed from Eq. (5.20) are compared with those from finite element analyses. Comparisons are performed first with the results of finite element analyses of simple span straight box girders and secondly with the results from three-span continuous girders. Likewise, forces in lateral bracing and X-frames computed from Eq. (5.36) are compared with those from finite element analyses. Example box girders are braced with SD type lateral bracing and cross-frames. The girder properties and vertical loads are the same as given in Fig. 5.1. Structural members are identical for K-frames and X-frames. Brace forces in the case of K-frames are comparatively shown in Figs. 5.13 and 5.14 with results from the simple span box girders.

Fig. 5.15 shows dimensions, properties, and loading schemes of three-span continuous straight box girder. Figs. 5.16 and 5.17 show comparatively member forces in lateral diagonals and struts, respectively. Forces in K-frame diagonals are shown comparatively in Fig. 5.18.

Fig. 5.19 compares lateral bracing forces evaluated for the simple span box girder with an SD type lateral bracing and X-frames. Diagonal forces in X-frames are comparatively shown in Fig. 5.20. Figs. 5.21 and 5.22 comparatively show forces in diagonals and struts of a three-span continuous straight box girder with X-frames. Finally, diagonal forces in X-frames of three-span continuous box girder are comparatively shown in Fig. 5.23. Good correlations are evident between the member forces computed from predictor equations and those from finite element analyses

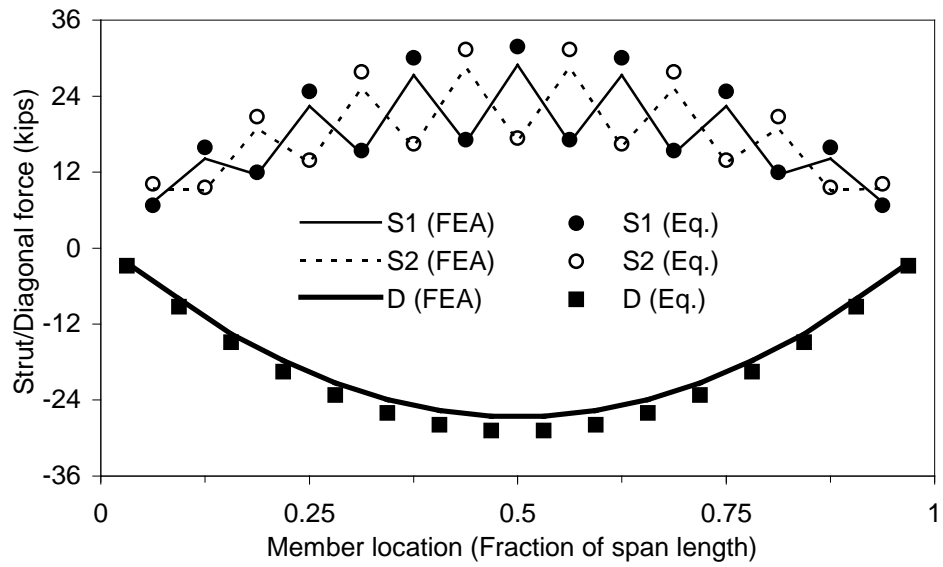


Fig. 5.13. Forces in lateral bracing of simple span box girder with internal K-frames

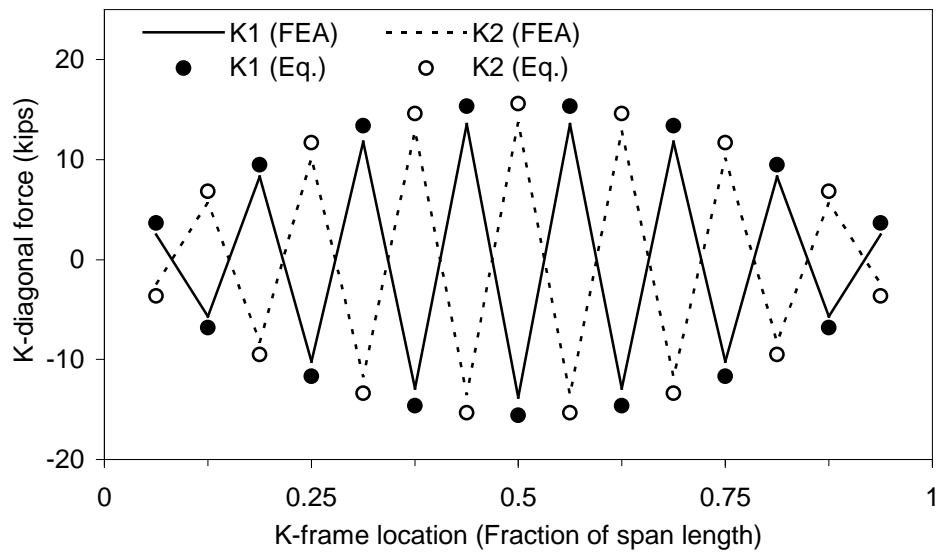


Fig. 5.14. Diagonal forces in internal K-frames of simple span box girder

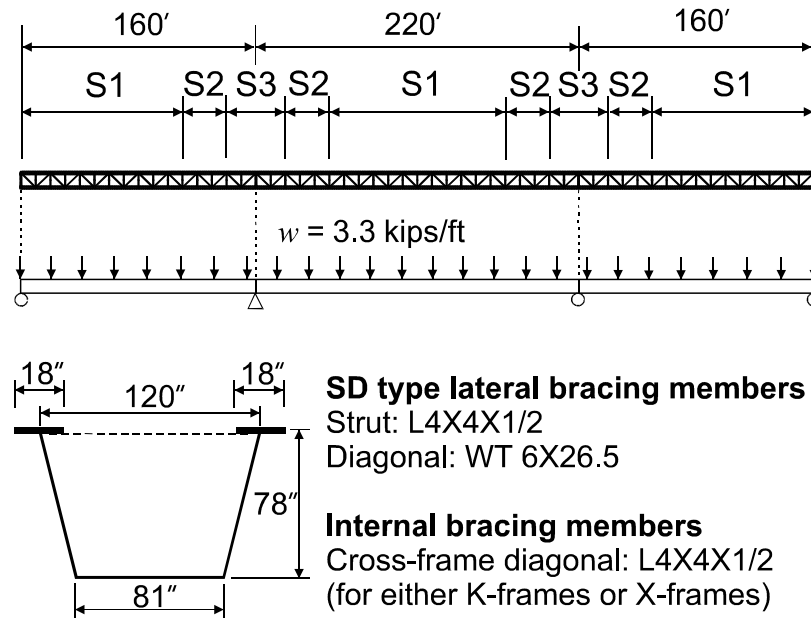


Plate thickness

Cross-section	Top flange	Web	Bottom flange
S1	1.0 in.	0.5625 in.	0.625 in.
S2	1.5 in.	0.5625 in.	1.0 in.
S3	2.25 in.	0.5625 in.	1.85 in.

Fig. 5.15. Three-span continuous straight girder with various cross sections subjected to vertical loads

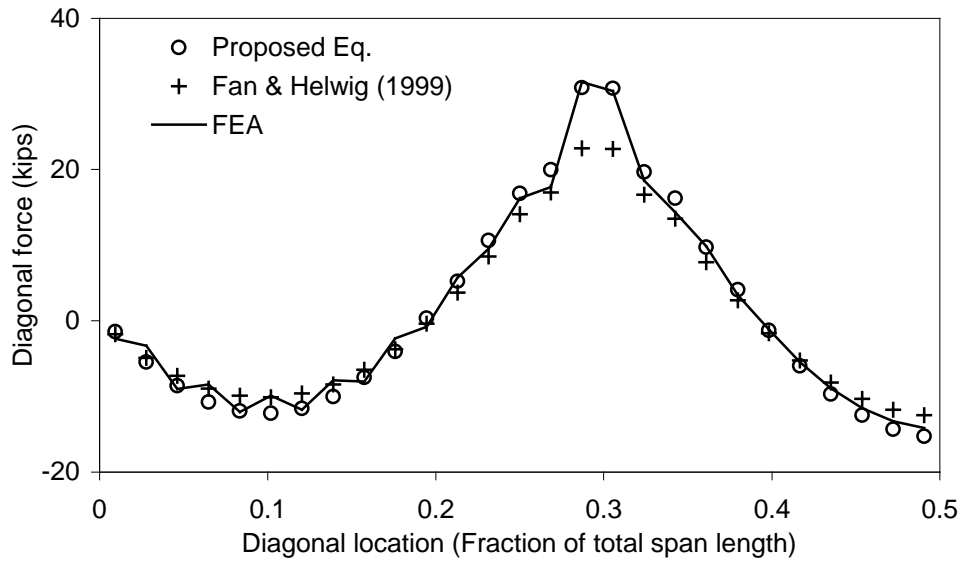


Fig. 5.16. Diagonal forces in lateral bracing of three-span continuous box girder with internal K-frames

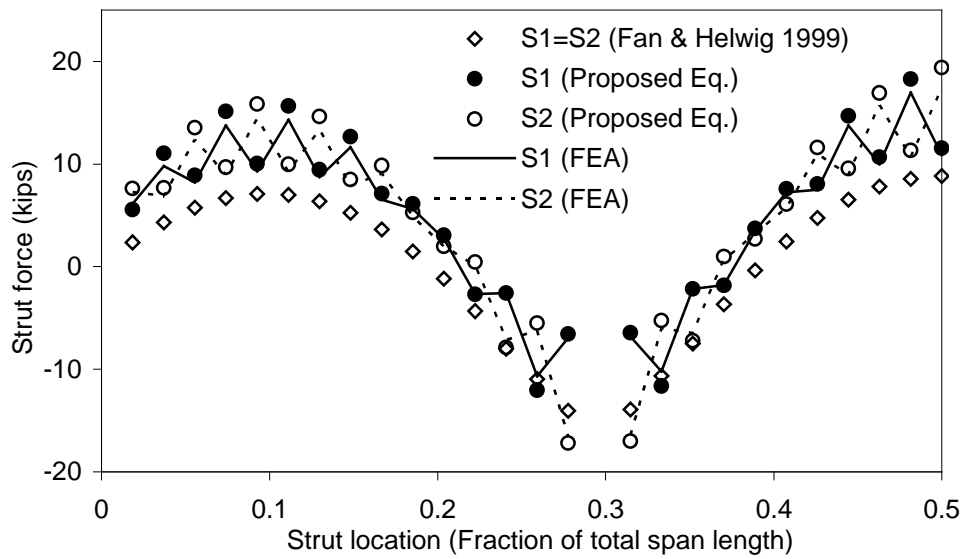


Fig. 5.17. Strut forces in three-span continuous box girder with internal K-frames

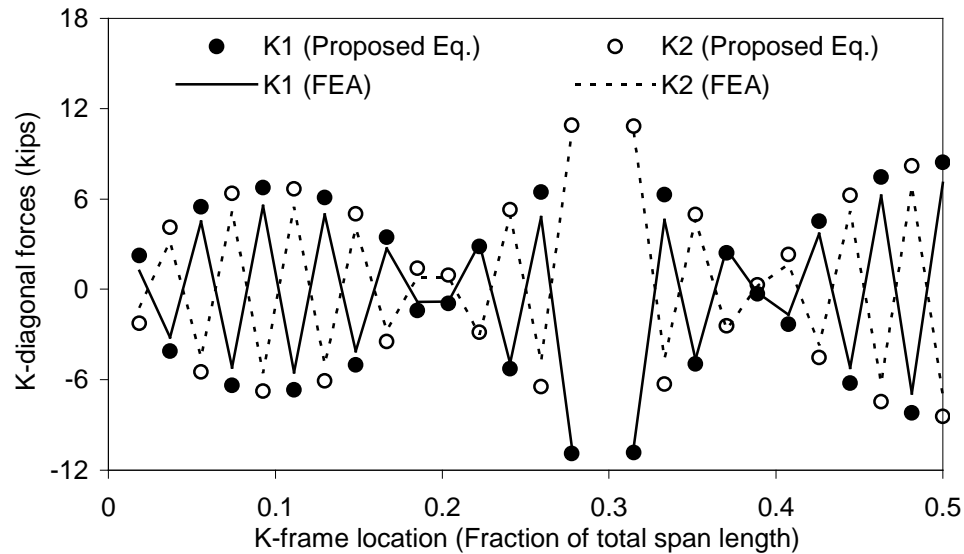


Fig. 5.18. K-diagonal forces three-span continuous box girder

shown in Fig. 5.13 to Fig. 5.23. It is noted that forces computed from proposed equations shown in Figs. 5.13 ~ 5.23 are slightly in the conservative side.

Equations proposed by Fan and Helwig (1999) underestimate strut forces in box girders braced with an SD type lateral bracing system with cross-frames provided at one-panel spacing. The reason for this discrepancy is attributable to the fact that Fan and Helwig (1999) did not consider the interaction between cross-frames and struts in the case of box girders with cross-frames provided at one-panel spacing. It is noted that the assumption of no interaction between cross-frames and lateral bracing systems employed by Fan and Helwig (1999) is valid in the case when the box girders are provided with cross-frames at two-panel spacing under vertical bending as discussed in Chapter 3.

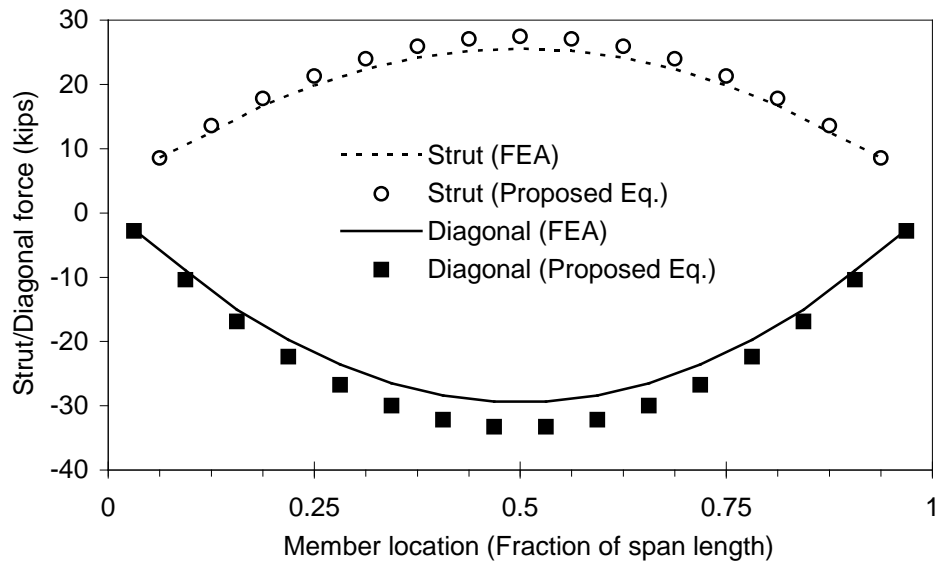


Fig. 5.19. Forces in lateral bracing in simple span box girder with internal X-frames

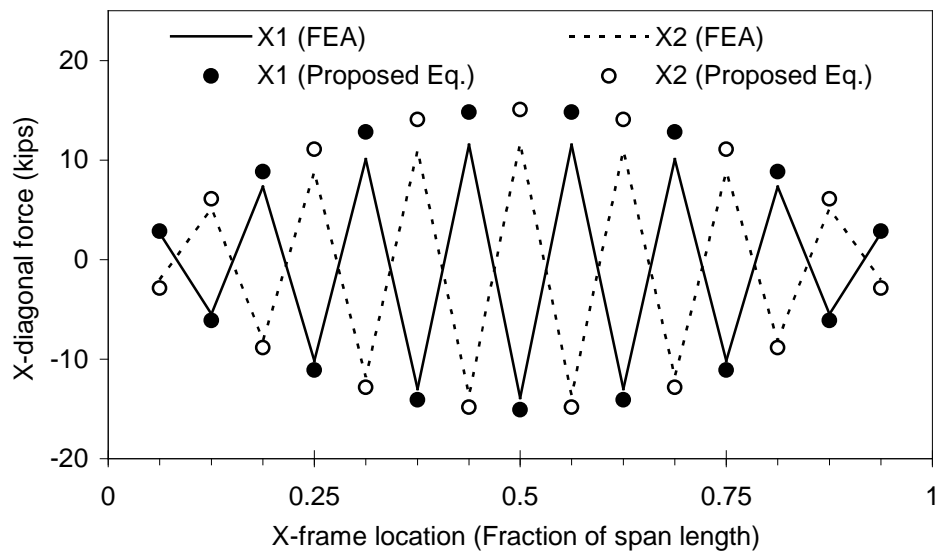


Fig. 5.20. X-diagonal forces in simple span box girder

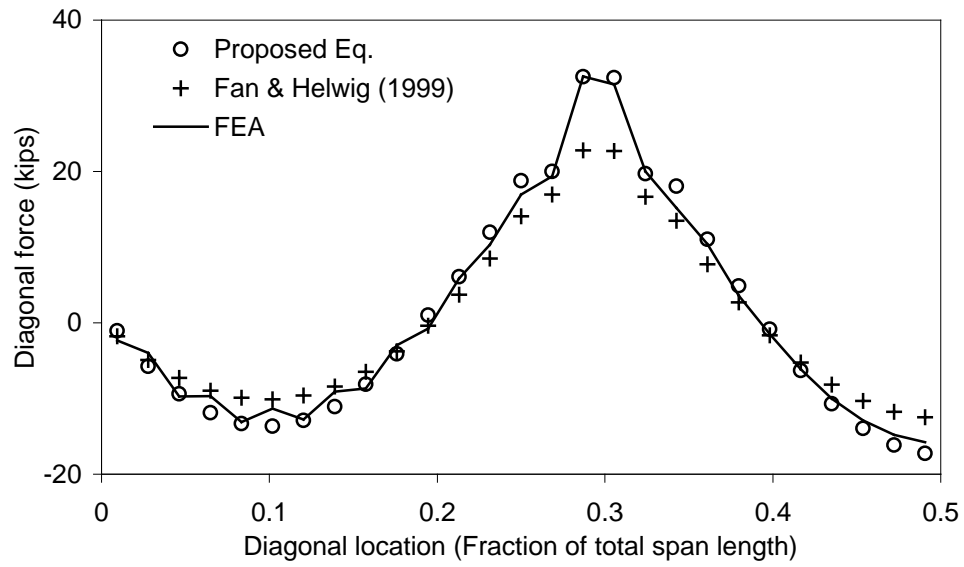


Fig. 5.21. Diagonal forces in lateral bracing of three-span continuous box girder with internal X-frames

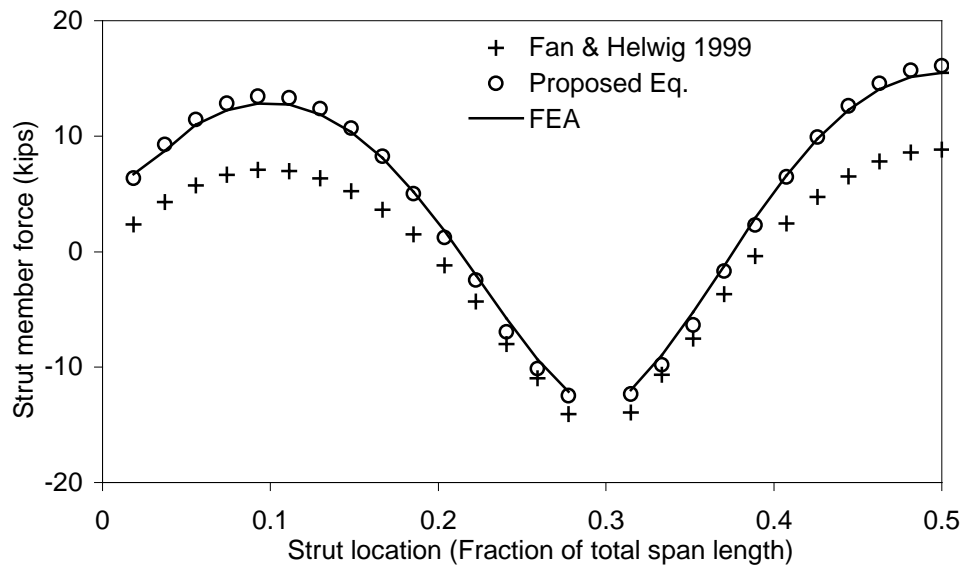


Fig. 5.22. Strut forces in three-span continuous box girder with internal X-frames

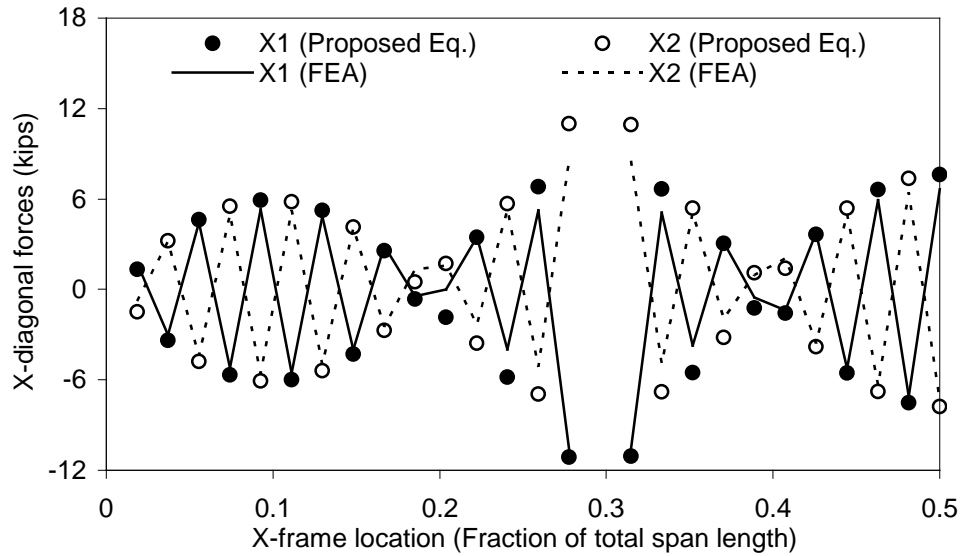


Fig. 5.23. X-diagonal forces in three-span continuous box girder

5.7 Summary and Concluding Remarks

Equations to estimate forces in lateral bracing members and cross-frames of tub girders have been suggested in recent years. Comparative examinations of bracing forces computed from the available equations with those from finite element analyses on a selected number of box girder examples reveal that there is a room for improvement in the existing predictor equations. Forces in both the struts and diagonals in an SD type bracing are affected by the longitudinal displacements and lateral deflections of the top flanges. Longitudinal displacements are primarily due to vertical bending, while lateral deflections are caused by vertical bending, lateral force components due to inclined webs, torsion, and distortion. It has been observed that member forces in an SD type bracing system are affected by spacing of cross-frames, i.e., one-panel spacing or two-panel

spacing. Box girders with an SD lateral bracing system under vertical bending exhibit significantly different responses whether cross-frames are provided at one-panel spacing or two-panel spacing. The forces are developed in the diagonals primarily due to distortional components that are separated from torsional loads. However, forces are also caused in part in the diagonals of cross-frames due to bending. The strut forces in an XD type lateral bracing system due to torsion are small compared with those developed in struts in an SD type bracing system because of the self-equilibrating nature of the crossed-diagonals within a panel in an XD type lateral bracing. Although the major portion of the strut force is caused by vertical bending and lateral force components, torsion and distortion may contribute up to 35% of the strut force in a typical straight tub girder. Fairly extensive comparisons given in Figs. 5.13 ~ 5.14 and 5.15 ~ 5.22 confirm the validity of the proposed equation derived for bracing forces. It is hoped that practicing engineers can now accurately compute bracing forces of box girders by taking advantage of improved predictor equations.

CHAPTER 6

EXTERNAL CROSS-FRAMES

6.1 Introduction

A composite trapezoidal twin-box girder system is frequently utilized for both curved and straight highway bridges due to its advantageous structural characteristics, in particular its superb torsional rigidity, favorable long term maintenance considerations, and aesthetically pleasing appearance. However, due to the coupling action of vertical bending and torsion, horizontally curved box girders are subject to significant rotations. During construction, the noncomposite steel girder must support the wet concrete and steel weight (also known as noncomposite dead loads) in addition to other construction loads such as the dead weight of screed, etc. There have been reports (Dey 2001) of very large differential deflections between box girders, exceeding five inches (127 mm) in some cases. The differential deflection or rotation is defined in this study as the relative deflection or rotation between the exterior box girder (convex side) and the interior box girder (concave side). A large differential deflection and rotation make it difficult to maintain the superelevation specified and to form and key-in the construction joint for the succeeding placements (United States Steel Corporation 1978). In the absence of external cross-frames, the magnitude of the differential deflection depends upon the stiffness of the noncomposite individual box girder(s). Since it is not practical to increase

the girder stiffness simply to minimize the differential deflections and rotations, either external cross-frames or temporary shoring are considered. As external cross-frames are not only expensive but also adversely affect the fatigue characteristics of the steel girder, the number of these cross-frames needs to be kept to an absolute minimum. Furthermore, such external cross-frames must be balanced by internal cross-frames in order to stabilize the web. Fig. 6.1 shows a typical arrangement of external cross-frames and internal

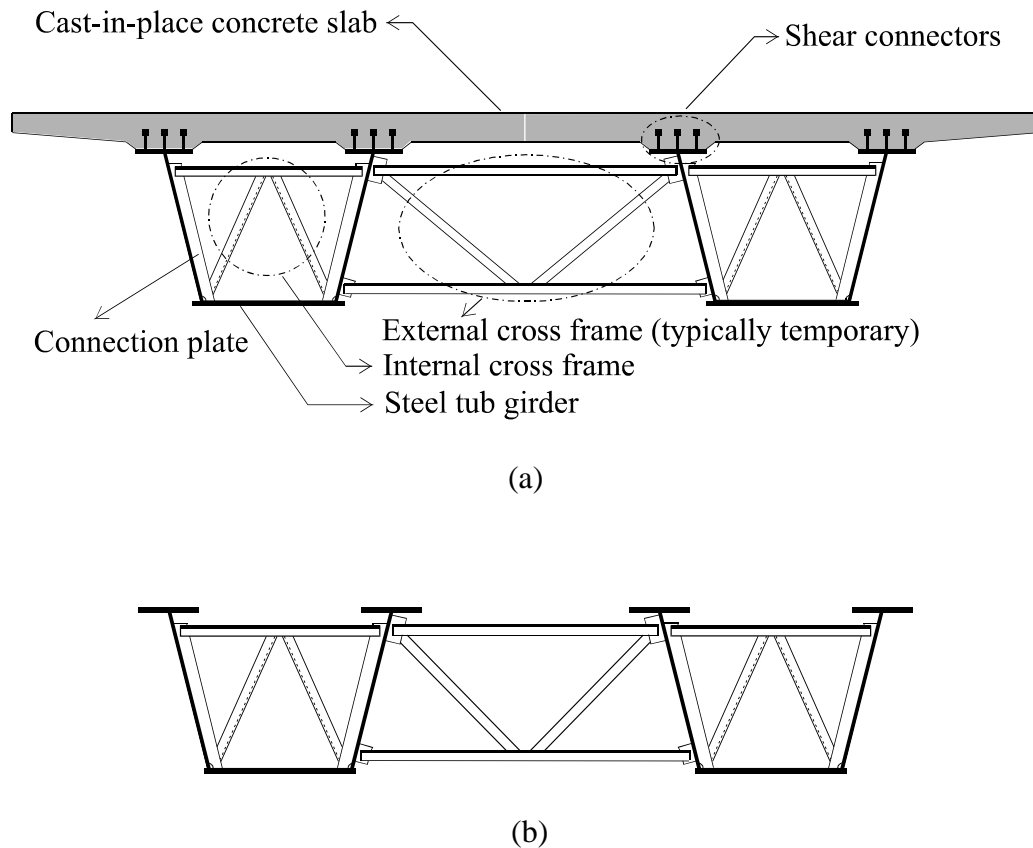


Fig. 6.1. Twin-box girder bridge: (a) Completed stage; (b) Cross-section of steel tub girder during construction

cross-frames in a box girder bridge. At the external cross-frame location, the entire bridge cross section tends to rotate as a unit, and the relative angle of twist between box girders is minimized. Although external cross-frames may be removed after the entire slab is hardened (State of Texas 2000), when a redecking operation at a later time is considered it would be preferable to have a permanent external bracing system in place. However, if they are to remain in place, additional consideration of the fatigue-resistant details and overall structure aesthetics may be required.

The differential deflections between horizontally curved box girders during construction may be controlled by any of the following, either alone or in combination:

- (1) Increasing noncomposite steel girder stiffness based on the deck pouring sequence
- (2) Supporting girders on temporary shoring
- (3) Providing temporary or permanent external cross-frames

Installing temporary shoring or external cross-frames is considered to be a more efficient way of controlling differential deflections than increasing the girder stiffness. Temporary shoring is an effective option in controlling deflections and rotations during construction if the local traffic conditions and terrain permit, although the cost associated with temporary shoring is deceptively expensive. If the construction conditions do not permit temporary shoring, external cross-frames may become the only option. It is, therefore, the impetus of this study to investigate the effects of external cross-frames on differential deflections between box girders. In the case of continuous girder bridges, staged deck pouring sequences should be considered.

Currently, there are no design guides available for intermediate external cross-frames in horizontally curved steel box girder bridges. Article 10.2.3 of The *AASHTO Guide Specifications* (2003) mandates external cross-frames or diaphragms between boxes at abutments and permits them between boxes at interior supports and at intermediate locations between supports if necessary. Memberg (2002) presented a procedure for the design of intermediate external diaphragms, although this appears to be overly conservative as the members are designed to carry forces that are more than ten times higher than those measured experimentally. Zhang (1996) studied the dead load effect in a limited scope.

Except for short span bridges, it is highly unlikely that the entire bridge deck will be cast at once. The *AASHTO Guide Specifications* (2003) stipulate that concrete casts be included in the approved construction plan, but there is no universally accepted deck concrete pouring sequence for continuous box girder bridges. Two deck pouring sequences, the conventional scheme and the Wisconsin DOT scheme, are considered in this study in order to examine their effects on differential deflections and rotations during construction.

6.2 Definition of Deck Unevenness Ratio

In horizontally curved steel box girder bridges, individual box girders undergo deflections and rotations when wet concrete is being poured on the forms for the deck slab, as shown in Figs. 2(a) and 2(b). Due to the induced differential deflections and

rotations between box girders, the reference line of the deck slab becomes uneven, as shown in Fig. 6.6.2(b). Care should be used during deck pouring in order to maintain the

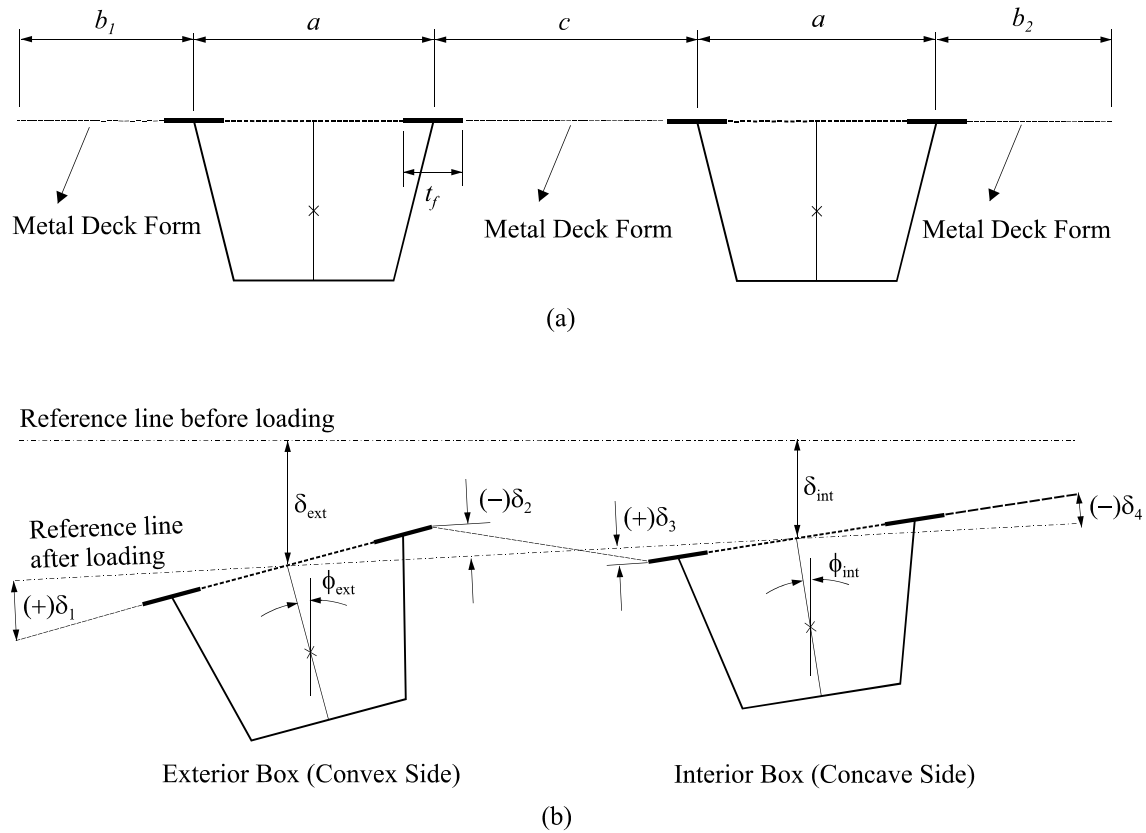


Fig. 6.2. Notation for twin-box girder bridge cross-section: (a) Deck width; (b) Deformed shape

minimum required slab thickness, as the thickness can be varied by the uneven reference line along the deck width caused by the uneven deflections. In addition, unless the uneven reference line is controlled to be within the minimum acceptable amount, it will cause unintended additional dead loads on the noncomposite steel section. In this paper, a parameter for the unevenness ratio of the deck reference line, U_R is defined as:

$$U_R = \frac{I}{t_c} \left[\text{Max}(\delta_1, \delta_2, \delta_3, \delta_4) - \text{Min}(\delta_1, \delta_2, \delta_3, \delta_4) \right] \quad (6.1)$$

where

$$t_c = \text{design deck thickness}$$

$$\delta_1, \delta_2, \delta_3, \delta_4 = \text{relative deflections from reference line after loading at four reference points, as shown in Fig. 6.2}$$

Note that the reference line after loading goes through the mid-points (Points A' and B' in Fig. 6.2(b)) between webs at the top flange level of each box girder. Using the notation given in Fig. 6.2(a), the relative deflections after loading, δ_1 through δ_4 , in Eq. (6.1) are given by the following equations:

$$\delta_1 = \left(\frac{a}{2} + b_1 \right) (\phi_{ext} - \phi_B) \quad (6.2)$$

$$\delta_2 = - \left(\frac{a + w_f}{2} \right) (\phi_{ext} - \phi_B) \quad (6.3)$$

$$\delta_3 = \left(\frac{a + w_f}{2} \right) (\phi_{int} - \phi_B) \quad (6.4)$$

$$\delta_4 = - \left(\frac{a}{2} + b_2 \right) (\phi_{int} - \phi_B) \quad (6.5)$$

where

$$\phi_B = \tan^{-1} \left(\frac{\delta_{ext} - \delta_{int}}{a + c} \right)$$

w_f = top flange width

Deflections below and above the reference line after loading have positive and negative values, respectively.

It is interesting to note that such unevenness ratios could possibly occur even in straight girder bridges depending on the center-to-center distance between flanges of each box, the center-to-center distance between adjacent boxes, and the width of the cantilever overhang portion of the deck slab, as illustrated in Fig. 6.2. The magnitude of the unevenness ratio defined above can be effectively controlled by the use of external cross-frames. In order to investigate the effects of external cross-frames on the unevenness ratio, U_R , a number of hypothetical twin-box girder bridges were analyzed using a general finite element program, ABAQUS (ABAQUS, Inc. 2003).

6.3 Finite Element Modeling

Three-dimensional elastic analyses of hypothetical box girder bridges during each stage of deck pouring were performed by ABAQUS (ABAQUS Inc., 2003). The cross sections of the box girders were built up with three-dimensional shell elements (S4R of ABAQUS). The solid diaphragms, also modeled with S4R elements, were placed at abutments and interior supports. A single diagonal type top lateral bracing system was installed at the level of the top flanges and K-shaped internal cross-frames were provided

at every other strut location. The diagonals of the top lateral bracing system and the internal K-frames were modeled with three-dimensional two-node truss elements (T3D2 of ABAQUS). Space beam elements (B31 of ABAQUS) were used for the struts simply to avoid the numerical instability caused by the lack of constraints against deflection perpendicular to the plane of the K-frame. A minimum of four SR4 elements were used for each top flange and eight SR4 elements were used to model both the bottom flange and webs. Experience (Kim 2004, Kim and Yoo 2005) has shown that such grid refinement yields reasonable accuracy for finite element analyses of typical steel tub girders. Deck slabs were modeled using shell elements of SR4 of ABAQUS. A total of 24 shell elements were used across the bridge deck slab. The shear connectors linking the deck slabs and the top flange of the steel section were modeled using rigid elements. The rotational degree of freedom (DOF) of the box was suppressed at the supports by constraining the vertical DOF of the nodes for the bottom corners of the box cross section near the bearing device. Of these vertically constrained nodes, at least one horizontal DOF was also constrained in order to prevent rigid body motion. As there is a solid diaphragm installed at every support, this boundary condition is believed to be equivalent to suppressing the rotational DOF of the box to the extent of ignoring the elastic deflection of the solid diaphragm itself. Linear elastic finite element analyses were carried out using a modulus of elasticity and Poisson's ratio for the construction steel of 200 GPa (29,000 ksi) and 0.3, respectively.

6.4 Simple-Span Box Girder Bridges

Based on a consideration of the rigid body stability of the superstructure, the subtended angle of a simple-span curved bridge suffers from certain limitations. However, historically there have been few failures of simple-span bridges with relatively sharp curvatures due to highly eccentric dead and/or live loads and an inadequate performance of bearing devices subjected to uplift. As the most severe curvature cases, simply supported horizontally curved bridges with a subtended angle of one radian (57.3°) are investigated in this paper. It is assumed that an adequate bearing design has been performed to resist the potential uplift at the abutments.

The span lengths of the horizontally curved example bridges in this study were 48.77 m (160 ft) and consisted of sixteen panels of lateral bracing spaced at 3.048 m (10 ft). The dimensions of the cross sections of these hypothetical twin-box bridges and the properties of each box cross-sectional are given in Fig. 6.3. A Warren-truss type single diagonal top lateral bracing system was provided at the top flange level and internal K-shaped cross-frames were installed at every other strut location. Internal and external bracing members were assumed to be single angles, $L4 \times 4 \times \frac{1}{2}$, and double angles, $2L5 \times 3 \frac{1}{2} \times \frac{1}{2}$, respectively. Top lateral bracing members were selected to be WT6X26.5. The number of external K-frames was varied to assess their effect. However, it was assumed that the external K-frames were provided at equal spacing (at the midpoint in the case of one frame, and at the quarter points in the case of three). The weight of the wet concrete slab was converted to line loading on the centerline of each top flanges along the box girder. The dead loads of the steel box girders were not applied because the main

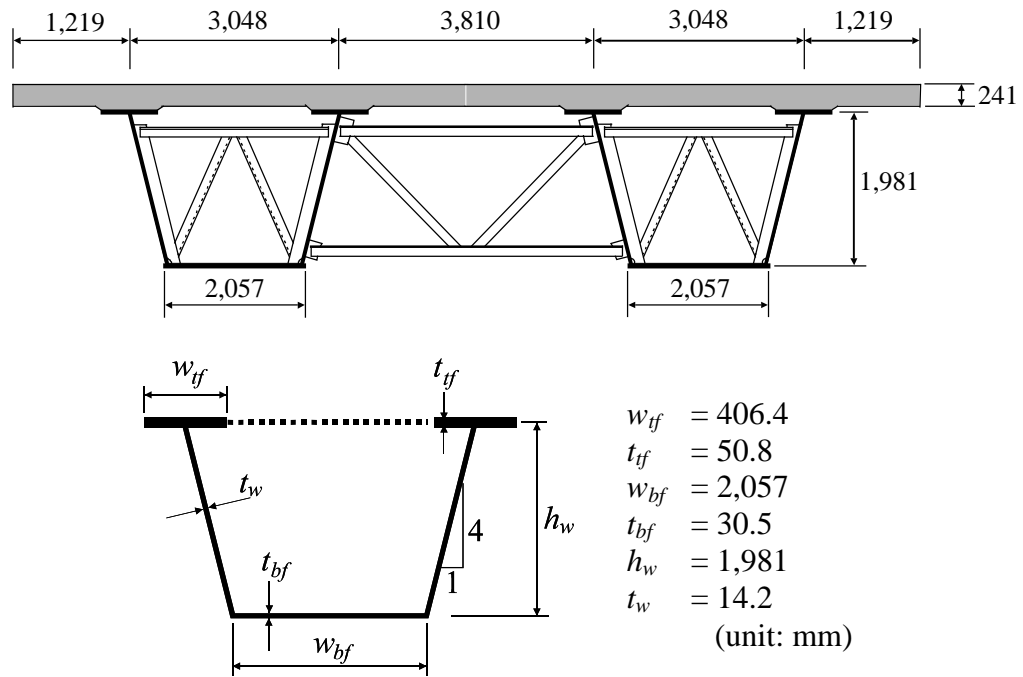


Fig. 6.3. Cross-sectional dimensions of the hypothetical twin-box girder bridge in simple-span

purpose of this study was to investigate unevenness in the deck reference line due to poured deck concrete. The staged deck construction was not considered in the simple-span bridges investigated herein.

Fig. 6.4 shows the unevenness ratios from the three-dimensional finite element modeling and grid analysis for the simple-span example bridge with the one radian subtended angle. The results from both three-dimensional full model and grid analysis methods are in fairly good agreement. As seen in Fig. 6.4, it is evident that providing external cross-frames is effective for controlling the unevenness ratios during deck casting. Although the unevenness ratios are decreased further with the addition of external cross-frames, additional external cross-frames are no effective on the unevenness ratios beyond one.

Error! Not a valid link.

Fig. 6.4. Effect of the number of external cross-frames on the unevenness ratio (subtended angle = 1.0 rad.)

In order to investigate the effect of bracing stiffnesses on the forces and axial stresses induced in the external cross-frames, three different structural members were used in the analyses. Table 6.1 shows the forces and axial stresses induced in the individual structural members used for external K-frames. The member forces in external bracing members are not affected by the member size, although the level of stress is decreased as the size of the member increases.

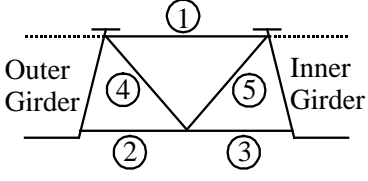
In order to investigate the effect of the stiffness of cross-frame members on the unevenness ratio, three different structural members were tried in the analyses. Fig. 6.5 shows the unevenness ratios at the centerlines of the simple-span bridges from both three-dimensional full model and grid analyses. The three different structural members used in

Error! Not a valid link.

Fig. 6.5. Effect of the stiffness of bracing members on the unevenness ratio (Members, I, II, and III are as given in Table 6.1)

the analyses are given in Table 6.1. It is evident from Fig. 6.5 that the size of the external bracing member does not affect the unevenness ratio significantly. Note that the area of bracing member (III) is almost twice as great as that of member (I).

Table 6.1. Effects of cross-frame stiffness on member forces

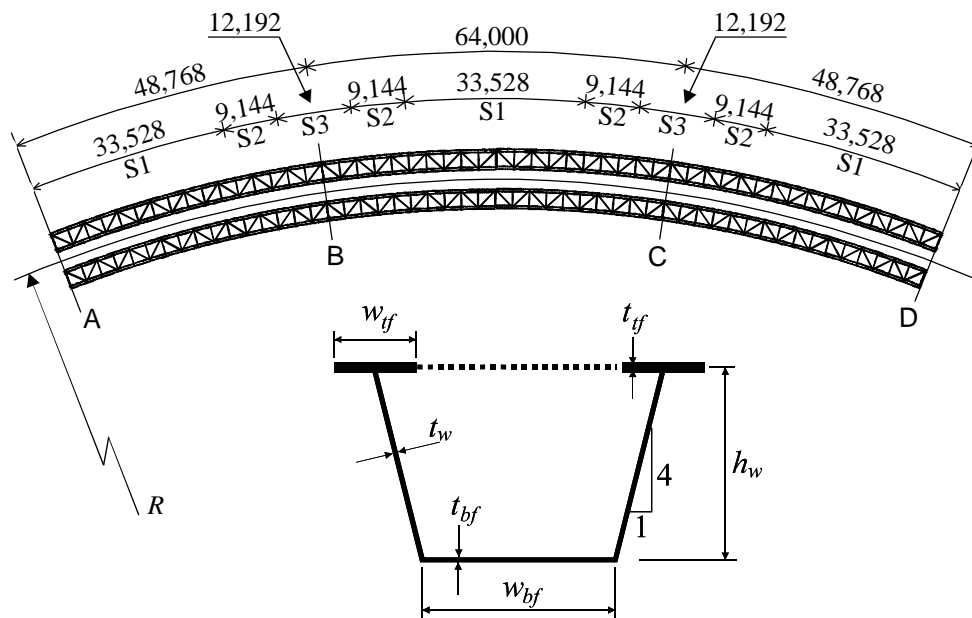
		Bracing Member		
		I*	II**	III***
Cross-sectional area (mm ²)		5,161	7,548	9,935
	①	3.9 (0.8)	3.4 (0.5)	2.7 (0.3)
	②	-83.6 (-16.2)	-84.9 (-11.2)	-85.4 (-8.6)
	③	74.1 (14.3)	75.1 (9.9)	76.0 (7.6)
	④	115.1 (22.3)	117.5 (15.6)	119.1 (12.0)
	⑤	-112.3 (21.8)	-113.3 (15.0)	113.6 (11.4)

- * Double Angle 2L5X3¹/₂X¹/₂ (Cross-sectional area = 5,161 mm²)
 ** Double Angle 2L6X4X⁵/₈ (Cross-sectional area = 7,548 mm²)
 *** Double Angle 2L7X4X³/₄ (Cross-sectional area = 9,935 mm²)

6.5 Three-Span Continuous Box Girder Bridges

The investigation was then extended to three-span continuous composite box girder bridges. The three-span bridges examined all had total lengths of 161.5 m (530 ft), made up of spans of 48.75 m, 64.0 m, and 48.75 m (160 ft - 210 ft - 160 ft), with three different centerline radii of curvature of 45.7 m (150 ft) and 30.5 m (100 ft). Each bridge had a total of 52 bracing panels (16+20+16). Mesh refinements and the finite element modeling of the bridge cross sections were kept the same as those used for the simple-span bridges analyzed. Each box girder consisted of three different cross sections. The thicknesses of the top and bottom flange were varied while keeping all other dimensions unchanged. The dimensions of the hypothetical bridges and three different cross sections are given in Fig. 6.6. Three-dimensional full model analyses were carried out on each.

Except for very short span bridges, it is highly unlikely that the entire three-span continuous girder bridge deck would be cast at once. The *AASHTO Guide Specifications* (2003) stipulate that concrete casts be included in the approved construction plan, but there is no universally accepted deck concrete pouring sequence. Each State establishes its own pouring sequence to meet its perceived needs. Also, the stipulation for construction joints is diverse. For example, the Florida DOT (State of Florida 2005) encourages contractors to install construction joints at a distance of not less than 6 m (20 feet) nor greater than 24 m (80 feet), while the Montana DOT (State of Montana 2002) discourages deck joints. There are two generally agreed upon issues: (1) when the pour volume becomes large, a deck pouring sequence is suggested, where the volume limitation varies from 125 m³ to 230 m³ (165 cu yd to 300 cu yd), and (2) when a deck



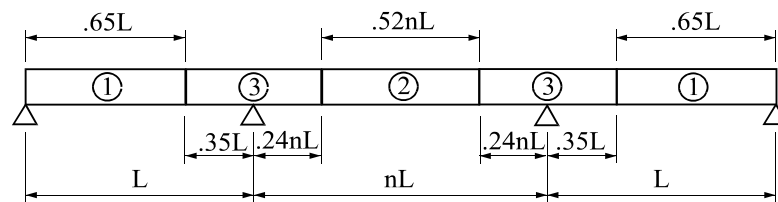
Section	w_{tf}	t_{tf}	w_{bf}	t_{bf}	h_w	t_w
S1	406.4	31.8	2057.4	19.1	1981.2	14.2
S2	406.4	44.5	2057.4	31.8	1981.2	14.2
S3	406.4	82.6	2057.4	44.5	1981.2	14.2

(Unit: mm)

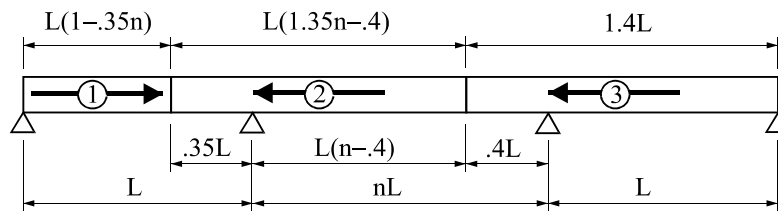
Fig. 6.6. Planar dimensions of a three-span continuous twin-girder and dimensions of three different cross sections

pouring sequence is considered, the objective is to minimize the tensile stresses induced in the previously cast concrete slab. Article 13.3 of the *AASHTO Guide Specifications* (2003) limits the factored tensile stress during deck pouring to be no more than 0.9 times the modulus of rupture. Issa (1999) indicates that deck concrete cracking at early ages is affected by the pouring sequence for multi-span continuous girder bridges.

An effective deck concrete pouring sequence known as the Wisconsin DOT pouring sequence (State of North Carolina 2005), shown in Fig. 6.7(a), was examined here. In addition to the Wisconsin DOT pouring sequence, the conventional deck pouring sequence (United States Steel Corporation 1978; AISC 1996), shown in Fig. 7(b), was also examined for comparison. Figs. 7(a) and 7(b) show the dimensions of



(a) Conventional deck pouring sequence



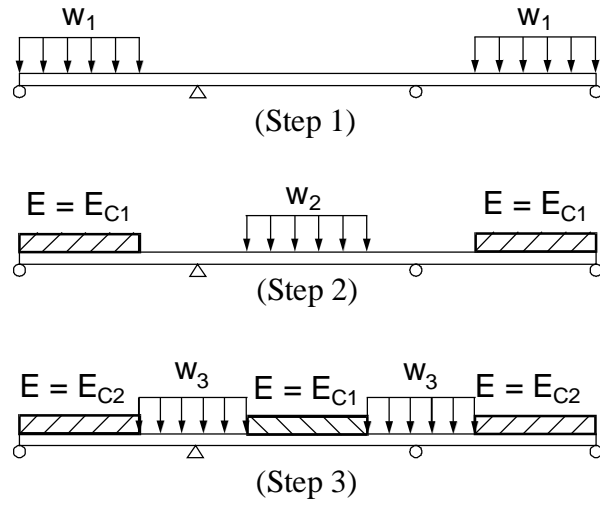
(b) Wisconsin DOT deck pouring sequence

Fig. 6.7. Two different deck pouring sequences considered for three-span continuous bridges

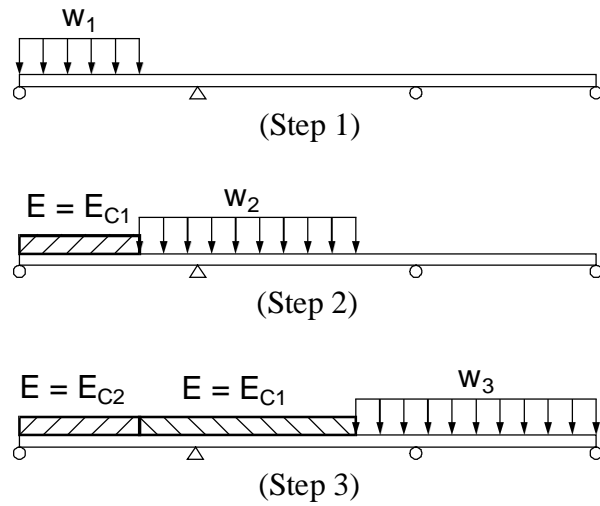
each unit poured for the Wisconsin DOT deck and the conventional pouring sequences, respectively.

In order to investigate the interactions among the external cross-frames, unevenness ratios, and the schemes of deck pouring sequence in the case of a continuous girder bridge, a number of hypothetical horizontally curved bridges were analyzed. The noncomposite dead load analysis procedure may consist of four steps in order to reflect the staged construction: (I) Noncomposite dead load analysis of the steel girder weight; (II) Noncomposite dead load analysis of the wet concrete poured in stage #1; (III) Noncomposite dead load analysis of the wet concrete poured in stage #2, with a modified girder stiffness reflecting the partial composite properties; and (IV) Noncomposite dead load analysis of the wet concrete poured in stage #3, once again with a modified girder stiffness reflecting the partial composite properties. In order to examine the effects of the poured deck concrete on the noncomposite steel girders, step (I) is intentionally omitted in the analysis, as stated in the case of simple-span examples. The analysis steps adopted herein are illustrated in Figs. 8(a) and 8(b) for Wisconsin DOT and the conventional deck pouring sequence, respectively. It is tacitly assumed that the wet concrete is spread evenly to cover the full width of the deck.

As the strength of the concrete is time-dependent, each poured unit will have different material properties for each stage of the sequence. The stiffness of the partially hardened early-aged concrete was considered in the analysis for the units that had been poured previously, according to the sequences. The relative gain in the strength of the concrete was adopted from Mindess et al. (2003) and is shown in Fig. 6.9. The time lag



(a) Conventional deck pouring sequence



(b) Wisconsin DOT deck pouring sequence

Fig. 6.8. Analysis steps for staged deck pouring with partially stiffened deck concrete

for the subsequent pouring was assumed to be 72 hours, as per the Florida DOT specifications (State of Florida 2005). The modulus of elasticity, E_c , of the partially hardened concrete was calculated from Fig. 6.9 by taking the water/cement ratio (w/c) to be 0.6. The 28-day strength of concrete, f'_c , was assumed to be 37.92 MPa (5,500 psi). A total of three different analysis steps, with the corresponding partial stiffness of the affected girder, were considered as shown in Figs. 8(a) and 8(b). When the wet concrete for the second unit was poured, the first unit had a modulus of elasticity, E_{C1} , as shown in Stage 2 of Fig. 6.8. When the concrete for the final unit was poured, the first unit had a different modified modulus of elasticity, E_{C2} , while the second unit had a modulus of elasticity of E_{C1} . The relative strengths and moduli of elasticity, which depended on the aging of the concrete used in the analyses, are given in Table 6.2.

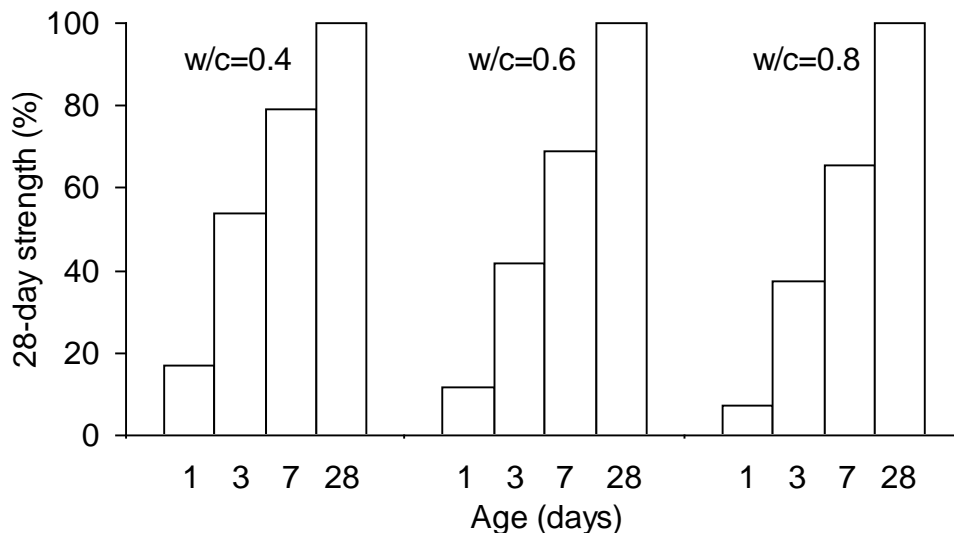


Fig. 6.9. Relative gain in strength with time of concretes with different water/cement (w/c) ratios (adopted from Mindess et al. 2003)

Table 6.2. Strength and stiffness of partially stiffened concrete with aging

Aging (day)	Fraction of 28-day strength, %	Modulus of elasticity, MPa (ksi)
1	12	10,094 (1,464)
2	28	15,417 (2,236)
3	42	18,885 (2,739)
4	51	20,809 (3,018)
5	58	22,195 (3,219)
6	64	23,311 (3,381)

For the purpose of comparison, the structure was analyzed assuming the entire deck was cast at once. Fig. 6.10. shows the effects of external cross-frames and radii of curvature on the unevenness ratio of a three-span continuous bridge for a one-step pouring process. As the external cross-frame installed at the center of each span was satisfactory throughout the range of parameters considered, only the case with one external cross-frame is compared with the case with no external cross-frames. Fig. 6.10 confirms that providing external cross-frames is indeed effective in controlling the unevenness ratios.

The unevenness ratios of an example three-span bridge with $R=100$ ft. during staged deck castings using the conventional and Wisconsin DOT pouring sequences are given Figs. 11 to 13. The unevenness ratios shown in Figs. 6.11 to 13 are the absolute values. The unevenness ratios were examined at each analysis step and the final values for the unevenness ratios were then evaluated by superimposing the analysis results from individual stages.

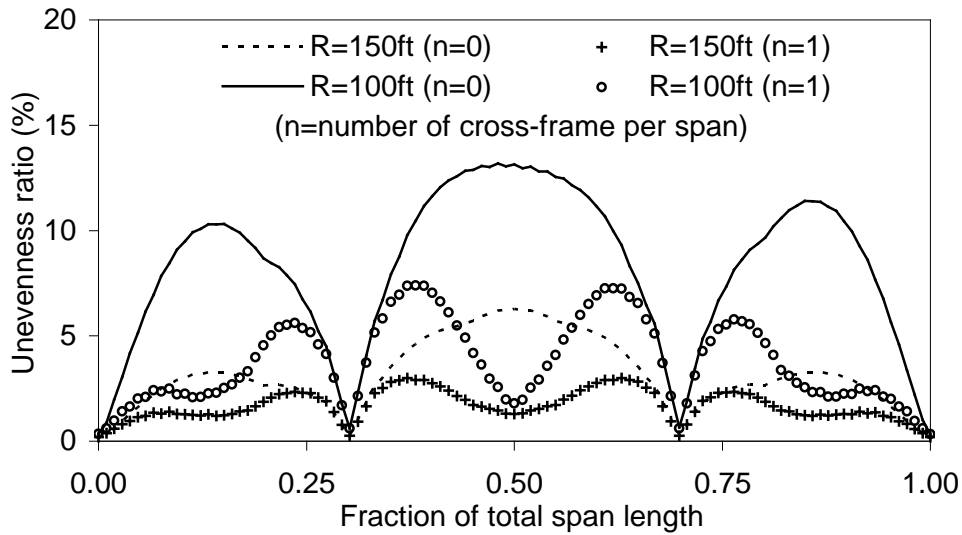


Fig. 6.10. Effect of external cross-frames and radius of curvature on the unevenness ratio of a three-span continuous bridge with one-step pouring

Error! Not a valid link.

Fig. 6.11. Comparison of unevenness ratio during deck pouring sequence after the first stage completed

Error! Not a valid link.

Fig. 6.12. Comparison of unevenness ratio during deck pouring sequence after the second stage completed

Error! Not a valid link.

Fig. 6.13. Comparison of unevenness ratio during deck pouring sequence after the final stage completed

After the first stage was completed, relatively large amounts of unevenness ratios were induced due to the dead loads of the poured deck concrete in every span by both Wisconsin DOT and conventional pouring sequences, as shown in Figs. 6.11 to 6.13. As

would be expected based on the previous analysis of simple-span examples, the effects of the external cross-frames are evident in controlling the unevenness ratios. Once the second pour was complete, the unevenness ratios decreased significantly in both end-spans. At the final stage, when all the concrete has been poured (Fig. 6.13), the unevenness ratios have decreased considerably along the span length, except for relatively small amounts in the right-end-span for the Wisconsin DOT pouring sequence. It should be noted that the radius of curvature of 100 ft. was chosen to represent an unusually severe case in order to better illustrate the trend.

The deck pouring sequence is closely designed with regard to the intensity of the tensile stress developed in previously placed concrete decks that may lead to early cracking of the decks. Although not quantified herein, there was a slight advantage observed in the Wisconsin DOT pouring sequence in reducing the tensile stress intensity on the deck previously poured. However, the intensity of the tensile stress can be controlled by either providing adequate longitudinal reinforcement, as stipulated in Article 6.10.3.2.4 of the *AASHTO LRFD* (2004) or by adjusting the length of each pour, as indicated in Fig. 6.7.

Fig. 6.14 illustrates the effect of the time lag between each deck pouring sequence. As the figure shows, there is no appreciable difference caused by time intervals that vary between one day and three days.

Error! Not a valid link.

(a) Conventional deck pouring sequence

Error! Not a valid link.

(b) Wisconsin DOT deck pouring sequence

Fig. 6.14. Effect of the time lag between the first and second stage on the unevenness ratio (with external cross-frames)

6.6 Concluding Remarks

Differential deflections and rotations caused by the deck concrete pouring were investigated for horizontally curved twin-box girder bridges with and without intermediate external K-frames. For three-span continuous bridges, two different deck pouring sequences were considered. A new parameter, the deck unevenness ratio, was defined to quantify uneven deck reference line in the lateral direction induced by differential deflections and rotations due to deck pouring. The number of external cross-frames did not significantly improve the unevenness ratio beyond that obtainable with only one. The unevenness ratios and forces in the external cross frame members were not greatly affected by the stiffness of the external cross-frame members. With regard to the unevenness ratio, the Wisconsin DOT pouring sequence appeared to offer no clear advantage over the conventional pouring sequence. Although not presented in the paper, the Wisconsin DOT pouring sequence did slightly alleviate the tensile stress intensity for the decks that had previously been poured.

Based only on the effect on the unevenness ratio, the time lag between subsequent pouring of the deck concrete does not influence much whether it is one day or three days duration as shown in Fig. 6.14.

CHAPTER 7

ELASTOMERIC BEARINGS

7.1 Introduction

In bridges, the superstructures experience substantial movements due to various causes such as temperature effects, moving loads, earthquakes, concrete shrinkage and creep. Unless bearings are used to accommodate the effects of these movements, the girders will apply large horizontal forces on the piers or abutments. Bridge bearings fulfill a number of functions that can be summarized as (Lee 1994):

- (1) to transfer forces from one part of the bridge to another, usually from the superstructure to the substructures;
- (2) to allow movement (translation along, and/or rotation about any set of axes) of one part of a bridge in relation to another;
- (3) by allowing free movement in some directions but not in others, to constrain that part of the bridge supported by the bearings to defined positions and/or directions.

Several types of bearing pads have been used to support the girders on the abutments, including sliding devices, rolling devices, rockers, and elastomeric bearings.

Elastomeric bearings are available in two basic forms: bearing pads, which are single unreinforced pads of elastomer (sometimes called plain bearings), and laminated bearings, comprising one or more slabs of elastomer bonded to metal plates in sandwich

form. Translational movement is accommodated by shear in the elastomer, one surface of which moves relative to the other. Rotational movement is accommodated by variations in the compressive strain across the elastomer. The elastomer should have sufficient shearing flexibility to avoid transmitting high horizontal loads and sufficient rotational capacity to avoid the transmission of significant moments to the supports. The vertical stiffness should be such that significant changes in height under changing loads are avoided. The elastomer is normally either natural or synthetic rubber.

One of the first uses of rubber pads was in Australia in 1889 (Lindley 1981). Plain natural rubber pads were used to support a viaduct on top of the piers. The first major application of laminated natural rubber bearings was at the Pelham Bridge in Lincoln, U.K. that was opened to the public in 1958 (Freakley and Payne 1978). In the United States, the first recorded use of neoprene bearing pads was to support prestressed concrete beams in Victoria, Texas in 1957 (Muscarella and Yura 1995). Recently, elastomeric bearings are widely used through the world as bridge-support systems because they

- are effective for horizontally curved bridges as well as straight bridges.

While having high compressive stiffness, they are flexible enough in shear to accommodate longitudinal movement of girders and thus mitigate horizontal reactions at internal piers or abutments. In addition, they immediately start to deform in shear without static friction as in the case of sliding devices;

- distribute the load evenly and absorb vibrations;
- are simple, compact, and easy to install;
- have low initial and installation costs; and

- require little maintenance.

While elastomeric bearings have been used successfully for many years, there have been some instances of less than ideal performance in the past, resulting in bearing slip, delaminating, ozone degradation, and low temperature stiffening.

Two different types of rubber are generally used in elastomeric bearing pads: Natural Rubber (NR) and Synthetic Rubber (SR). The synthetic rubbers most used in bridge bearings are: Neoprene (polychloroprene), Butyl (polyisobutylene), and Nitrile (butadiene-acrylonitrile) (Hamze et al. 1995; 1996). Natural rubber, when slightly stretched, loses most of its resistance to cracking by ozone. Therefore, special waxes are mixed with it, which migrate to the surface and form a protective coating. Neoprene and Butyl, on the other hand, have inherent ozone-resistance. Some countries (e.g. Germany) prohibit completely the use of natural rubber in elastomeric bridge bearings (Schrage 1981).

Stanton and Roeder (1982) conducted a research work on elastomeric bearing practices in the United States and throughout the world for an NCHRP project. Codes from Britain and Europe were analyzed and recommendations for changes to the AASHTO specifications were made. These revisions became part of the specifications with the publication of the interim 1985 AASHTO specifications and remain until in the latest version of *AASHTO LRFD* (2004). Based upon the work by Stanton and Roeder (1982), the second and third phases of the NCHRP project were undertaken by the same authors. These works included an extensive series of laboratory tests on elastomeric bearings of various shapes and sizes, and was reported in NCHRP Reports 298 and 325 (Roeder et al. 1987; 1989). The final results of the test programs were to offer a choice

between two design methods, a simple but restrictive method (known as “Method A”), and another (“Method B”) that was based more on theoretical calculations (Stanton et al. 1990). Method B is reviewed and design examples using it are presented in this study, along with numerical approaches using hyperelastic material modeling. A series of work on elastomeric bearing design was summarized in an ACI journal paper (Roeder and Stanton 1991).

7.2 General Behaviors of Elastomeric Bearing

The performance of the elastomer has a significant impact on the behavior of the elastomeric bearing. Figs. 7.1a through 7.1c show deformed shapes of plain elastomeric bearings under compression, shear force, and applied moment, respectively. In an elastomeric bearing subjected to compression, the elastomer bulges as shown in Fig. 7.1a. The bulging occurs because the elastomer is flexible but maintains nearly constant volume under all types of loading. Horizontal and rotational degrees of freedom are shown in Figs. 7.1b and 7.1c. Figs. 7.2a through 7.2d show the effects of roughness between elastomer and sole plates and reinforced plates inserted in the elastomer. A plain rubber pad compressed between perfectly lubricated surfaces will deform as shown in Figs. 7.2a and 7.2b. Considerable lateral expansion of the rubber occurs, but it is uniform with depth. If the contact surfaces are rough or the rubber is bound to them, the bulging shape shown in Fig. 7.2c results. Because the bulging is the source of compressive deformation, inserting laminated reinforcing shims in the elastomer can significantly increase the compressive stiffness, reducing the magnitude of the bulge, as shown in Fig. 7.2d.

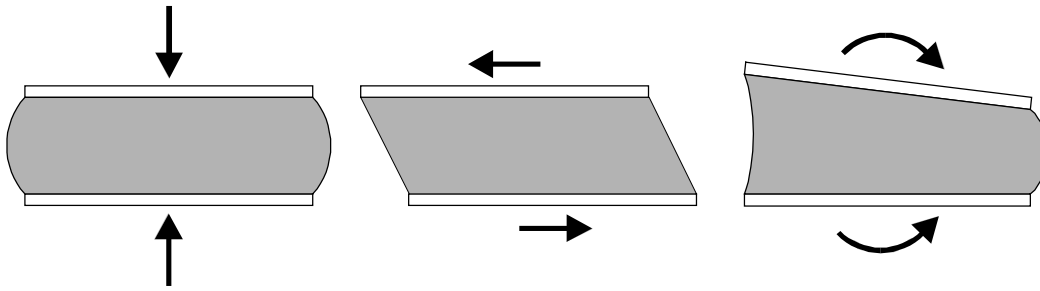


Fig. 7.1. Deformed shapes of plain elastomeric bearings (without reinforcing shims) under applied loads: (a) compression; (b) shear force; and (c) applied moment

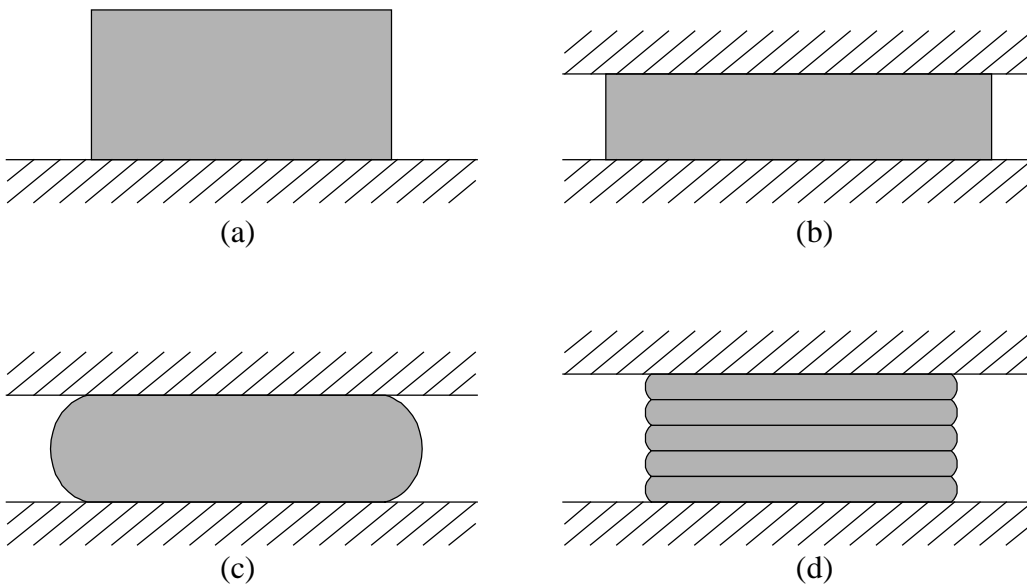


Fig. 7.2. Effects of reinforcing shims and frictions between elastomer and solid plates: (a) Elastomer on the support; (b) deformed shape between solid plates without friction; (c) deformed shape with friction; (d) deformed shape with friction and reinforced shims

The addition of internal reinforcing layers has no appreciable impact on the shear stiffness if the total rubber thickness is unchanged. Thus, the horizontal and vertical stiffness may be controlled independently within wide limits through a suitable choice of reinforcement. The magnitude of the bulge is one of the limiting factors in elastomeric bearing design. The compressive stiffness of an elastomeric bearing depends on the stiffness of the elastomer and the degree of restraint provided by the reinforcement. The shape factor of the elastomer, S , is an approximate indicator of the restraining effect of the reinforcement where

$$S = \frac{\text{Loaded plan area of the bearing}}{\text{Area free to bulge}} \quad (7.1)$$

A bearing layer with a large shape factor and high elastomer stiffness has a larger compressive stiffness than one with a lower elastomer stiffness or small shape factor. The shape factors for most reinforced bridge bearings fall in the range of 4 to 12 (Stanton and Roeder 1982).

Horizontal girder movements at supports due to thermal effects, creep or shrinkage of concrete, and braking or acceleration forces of highway traffic are accommodated by shear deformation of the elastomer, as depicted in Fig. 7.1b. The shear strain in the elastomer is given by the magnitude of the movement, times the shear modulus, G , of the elastomer and its plan area. This force is transmitted to the bridge substructure and superstructure and, as such, can be an important parameter in the design of the bridge and the bearing.

7.3 Review of AASHTO LRFD Design Requirements

Steel reinforced elastomeric bearings may be designed using either of the two methods, commonly referred to as Method A and Method B, suggested by *AASHTO LRFD* (2004). The stress limits associated with Method A usually result in a bearing with a lower capacity than a bearing designed using Method B, in which steel reinforced elastomeric bearing are treated separately. The design requirements for steel reinforcing elastomeric bearings using Method B are briefly reviewed in this section.

7.3.1 Compressive Stress

In any elastomeric bearing layer, the average compressive stress at the service limit state shall satisfy:

- For bearings subjected to shear deformation:

$$\sigma_s \leq 1.66G \cdot S \leq 1.60 \text{ ksi} \quad (7.2)$$

$$\sigma_L \leq 0.66G \cdot S \quad (7.3)$$

- For bearings fixed against shear deformation:

$$\sigma_s \leq 2.00G \cdot S \leq 1.75 \text{ ksi} \quad (7.4)$$

$$\sigma_L \leq 1.00G \cdot S \quad (7.5)$$

where

σ_s = service average compressive stress due to the total load (ksi)

σ_L = service average compressive stress due to the live load (ksi)

G = shear modulus of elastomer (ksi)

S = shape factor of the thickness layer of the bearing

7.3.2 Compressive Deflection

Deflections of elastomeric bearings due to the total load and live load alone are considered separately. Instantaneous deflection is taken as:

$$\delta = \sum \varepsilon_i h_{ri} \quad (7.6)$$

where

ε_i = instantaneous compressive strain in the i^{th} elastomer layer of a laminated bearing

h_{ri} = height of the i^{th} elastomeric layer in a laminated bearing (in.)

A maximum relative deflection across a joint of 0.125 inch is suggested.

7.3.3 Shear Deformation

The maximum shear deformation of the bearing, at the service limit state, D_s , is taken as D_0 , modified to account for the substructure stiffness and construction procedures. If a low friction sliding surface is installed, D_s need not be taken to be larger than the deformation corresponding to the first slip. The bearing is required to satisfy:

$$h_{rt} \geq 2\Delta_s \quad (7.7)$$

where

h_{rt} = total elastomer thickness (in.)

Δ_s = maximum shear deformation of the elastomer at the service limit state (in.)

7.3.4 Combined Compression and Rotation

The provisions of this section apply at the service limit state. Rotations are taken as the maximum sum of the effects of an initial lack of parallelism and subsequent girder end rotation due to imposed loads and movements. Bearings are designed so that uplift does not occur under any combination of loads and corresponding rotations. Rectangular

bearings are taken to satisfy combined compression and rotation requirements if they satisfy:

- For bearings subjected to shear deformation:

$$G \cdot S \left(\frac{\theta_s}{n} \right) \left(\frac{B}{h_{ri}} \right)^2 < \sigma_s < 1.875G \cdot S \left[1 - 0.200 \left(\frac{\theta_s}{n} \right) \left(\frac{B}{h_{ri}} \right)^2 \right] \quad (7.8)$$

- For bearings fixed against shear deformation:

$$G \cdot S \left(\frac{\theta_s}{n} \right) \left(\frac{B}{h_{ri}} \right)^2 < \sigma_s < 2.25G \cdot S \left[1 - 0.167 \left(\frac{\theta_s}{n} \right) \left(\frac{B}{h_{ri}} \right)^2 \right] \quad (7.9)$$

n = number of interior layers of elastomer

h_{ri} = thickness of the i^{th} elastomer layer

B = length of pad if rotation is about its transverse axis or width of pad if

rotation is about its longitudinal axis (in.)

θ_s = maximum service rotation due to the total load (rad)

Circular bearings are taken to satisfy combined compression and rotation requirements if they satisfy:

- For bearings subjected to shear deformation:

$$0.75G \cdot S \left(\frac{\theta_s}{n} \right) \left(\frac{D}{h_{ri}} \right)^2 < \sigma_s < 2.5G \cdot S \left[1 - 0.15 \left(\frac{\theta_s}{n} \right) \left(\frac{D}{h_{ri}} \right)^2 \right] \quad (7.10)$$

- For bearings fixed against shear deformation:

$$0.75G \cdot S \left(\frac{\theta_s}{n} \right) \left(\frac{D}{h_{ri}} \right)^2 < \sigma_s < 3.0G \cdot S \left[1 - 0.125 \left(\frac{\theta_s}{n} \right) \left(\frac{D}{h_{ri}} \right)^2 \right] \quad (7.11)$$

where

θ_s = maximum service rotation due to the total load (rad.)

D = diameter of pad (in.)

7.3.5 Stability of Elastomeric Bearings

Bearings are investigated for instability using the service limit state load combinations specified in Table 3.4.1-1 in *AASHTO LRFD* (2004). Bearings satisfying Eq. (7.12a) are considered stable, and no further investigation of stability is required.

$$2A \leq B \quad (7.12a)$$

in which:

$$A = \frac{1.92 \frac{h_r}{L}}{\sqrt{1 + \frac{2.0L}{W}}} \quad (7.12b)$$

$$B = \frac{2.67}{(S + 2.0) \left(1 + \frac{L}{4.0W} \right)} \quad (7.12c)$$

where

G = shear modulus of the elastomer (ksi)

L = length of a rectangular elastomeric bearing (parallel to longitudinal bridge axis) (in.)

W = width of the bearing in the transverse direction (in.)

For a rectangular bearing where L is greater than W , stability is investigated by interchanging L and W in Eqs. (7.12b) and (7.12c). For circular bearings, stability is investigated by using the equations for a square bearing with $W = L = 0.8D$. For rectangular bearings not satisfying Eq. (7.12a), the stress due to the total load must satisfy either Eq. (7.13) or (7.14):

- If the bridge deck is free to translate horizontally:

$$\sigma_s \leq \frac{G \cdot S}{2A - B} \quad (7.13)$$

- If the bridge deck is fixed against horizontal translation:

$$\sigma_s \leq \frac{G \cdot S}{A - B} \quad (7.14)$$

7.3.6 Reinforcement

The thickness of the steel reinforcement, h_s , is required to satisfy the provisions of Article 14.7.5.3.7 of the AASHTO LRFD Bridge Design Specifications (2004), and following limit states:

- At the service limit state:

$$h_s \geq \frac{3h_{max}\sigma_s}{F_y} \quad (7.15)$$

- At the fatigue limit state:

$$h_s \geq \frac{2h_{max}\sigma_L}{\Delta F_{TH}} \quad (7.16)$$

where

ΔF_{TH} = constant amplitude fatigue threshold for Category A as specified in

Article 6.6 of *AASHTO LRFD* (2004) (ksi)

h_{max} = thickness of thickest elastomeric layer in elastomeric bearing (in.)

σ_L = service average compressive stress due to live load (ksi)

σ_s = service average compressive stress due to total load (ksi)

F_y = yield strength compressive stress due to total load (ksi)

If holes are included in the reinforcement, the minimum thickness is required to be increased by a factor equal to twice the gross width divided by the net width.

AASHTO LRFD (2004) stipulates that the average stress on the elastomer at the service limit state should not exceed 2.9 ksi because average stress on the elastomeric bearing is largely limited by the seal's ability to prevent escape of the elastomer.

7.4 Design Examples

The same example of a three-span continuous bridge used in Chapter 6 is analyzed here to evaluate vertical reactions and horizontal movements at the supports. The cross-sectional dimensions of this sample twin-box girder bridge are given in Fig. 6.4, and the planar dimensions and box cross sections are given in Figs. 6.12 and 6.13, respectively. The detailed description used for the finite element model is given in Section 6.4.

7.4.1. Loading Combinations

AASHTO LRFD (2004) Section 3 is used to determine the acceptable load combinations for strength according to Article 3.1 of the *AASHTO Guide Specifications* (2003). Group I loading is used for the design of most members for the strength limit state. For temperature and wind loadings in combination with vertical loading, Load Groups III, IV, V and VI from Table 3.22.1A of *AASHTO LRFD* (2004) must also be checked. These load groups are defined as follows:

Group I	$1.3[D+5/3(L+I)+CF]$
Group II	$1.3[D+W]$
Group III	$1.3[D+(L+I)+CF+0.3W+WL+LF]$
Group IV	$1.3[D+(L+I)+CF+T]$
Group V	$1.25[W+T]$

$$\text{Group VI} \quad 1.25[D+(L+I)+CF+0.3W+WL+T]$$

Where:

D = Dead load

L = Live load

CF = Centrifugal force

W = Wind

WL = Wind on live load

T = Temperature

LF = Longitudinal force from live load

For horizontally curved bridges, horizontal movements at the supports are caused mainly by the effects of temperature. These thermal movements in curved bridges are complicated by virtue of their geometry. Some engineers orient the bearings along the tangent to the curve of the bridge, while others orient them on the chord from the fixed point of the bridge (Moorthy and Roeder 1992). However, in the case of elastomeric bearings, orientation of the bearings is neglected because horizontal movements over elastomeric bearings are not constrained in any direction. As stated in the previous sections, the magnitudes of vertical reactions and horizontal movements are required in order to follow the design procedures given in AASHTO provisions. Temperature gradients for the concrete and steel superstructure used for temperature loading in the load combinations are shown in Fig. 7.3.

7.4.2 Design of Elastomeric Bearings

Two different types of bearing arrangements are considered in this study:

Type I: one bearing at each support

(midpoint of box bottom under diaphragms)

Type II: two bearings at each support

(near both box bottom corners under diaphragm)

Table 7.1 shows the maximum vertical reactions and horizontal movements and rotations obtained from the finite element analysis results. Rectangular type elastomeric bearings are considered for both Type I and II. The design considerations from AASHTO can thus be examined based on the data given in Table 7.1.

Table 7.1. Maximum vertical reactions and horizontal movements

	Type I	Type II
Vertical reaction due to load group	970 kips (Load Group I)	292 kips (Load Group I)
Vertical reaction due to live load	401 kips	135 kips
Horizontal movement to tangential direction	1.06 in. (Load Group IV)	1.71 in. (Load Group IV)
Horizontal movement to radial direction	0.16 in. (Load Group IV)	0.72 in. (Load Group VI)
Rotation due to total load	0.0031 rad. (Load Group II)	0.0063 rad. (Load Group II)

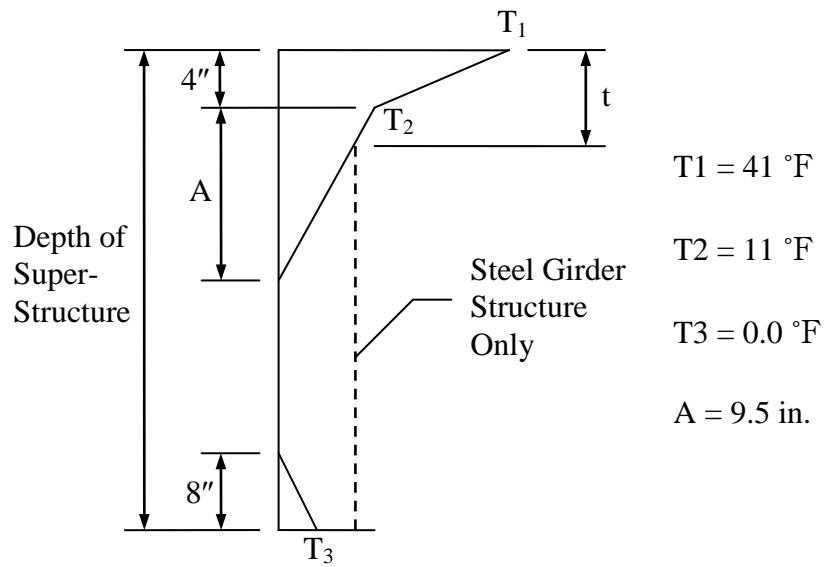


Fig. 7.3. Positive vertical temperature gradient in concrete and steel superstructures.

It is assumed that the two exterior layers at top and bottom have a constant thickness (h_{ro}) and the interior layers also have a constant thickness (h_{ri}). No differences are considered in the material properties between the cover and interior elastomeric layers. The notation used to describe the elastomeric bearings is shown in Fig. 7.4. The possible thickness of the elastomer layer, h_{ro} , along with the number of layers, n , has been determined according to the AASHTO provisions. Planar dimensions ($L \times W$) for Type I and II were assumed to be 24in. \times 28 in. and 16 in. \times 20in., respectively, considering the average pressure exerting on the vertical bearing planes. Two different values, 100 psi and 200 psi, for the shear modulus of the elastomer were considered. Figs. 7.5 through 7.12 show the possible thickness ranges of the elastomer layers, corresponding to the possible number of layers.

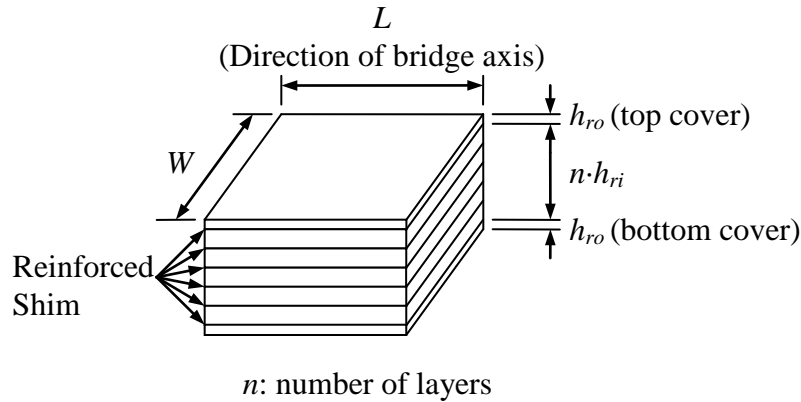


Fig. 7.4. Notation used for rectangular elastomeric bearings

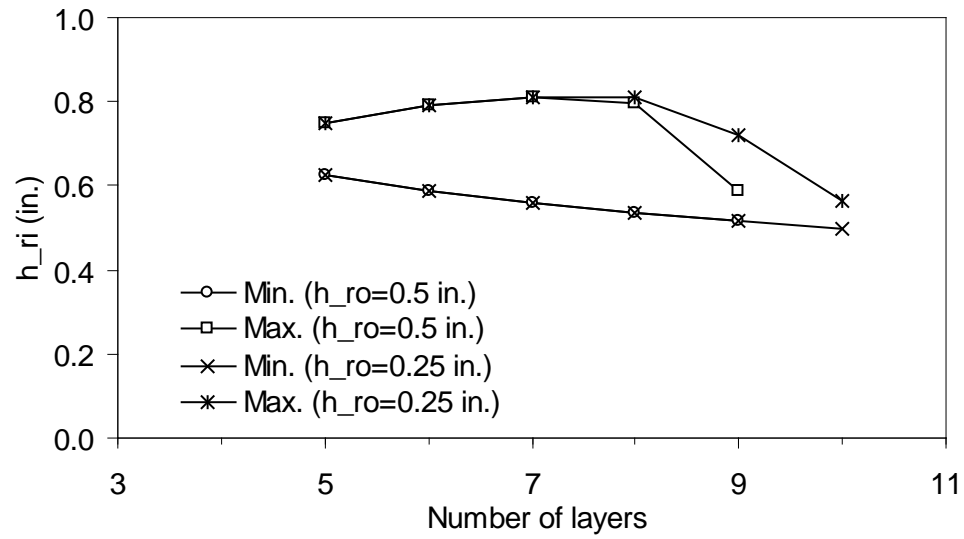


Fig. 7.5. Possible thickness range of interior elastomeric layer versus number of layers (Type I, $G = 100$ psi)

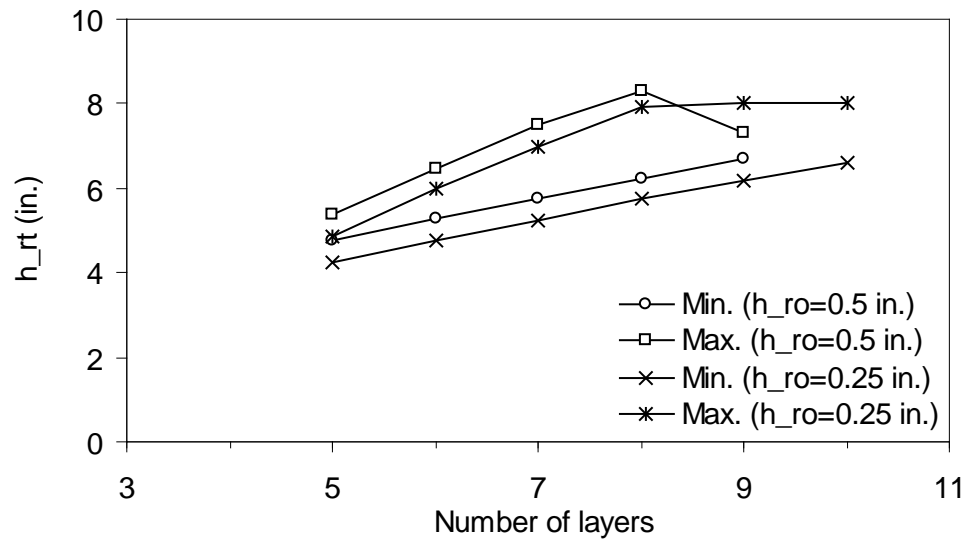


Fig. 7.6. Possible total thickness of elastomeric bearing (Type I, $G = 100$ psi)

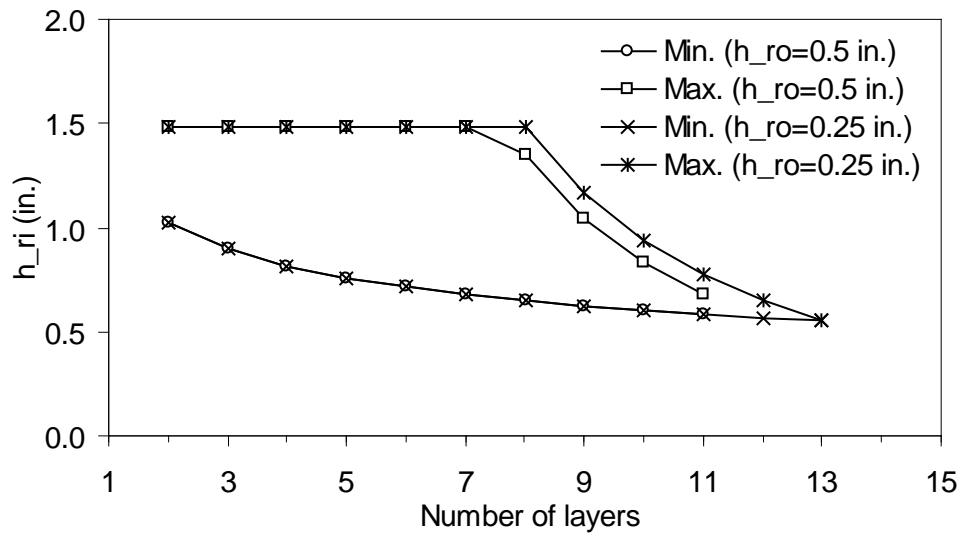


Fig. 7.7. Possible thickness range of interior elastomeric layer versus number of layers (Type I, $G = 200$ psi)

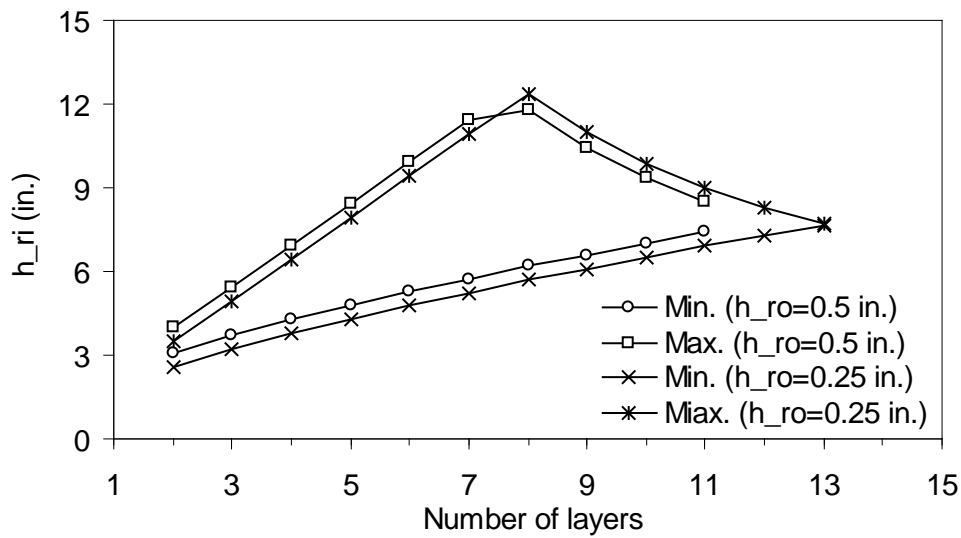


Fig. 7.8. Possible total thickness of elastomeric bearing (Type I, $G = 200$ psi)

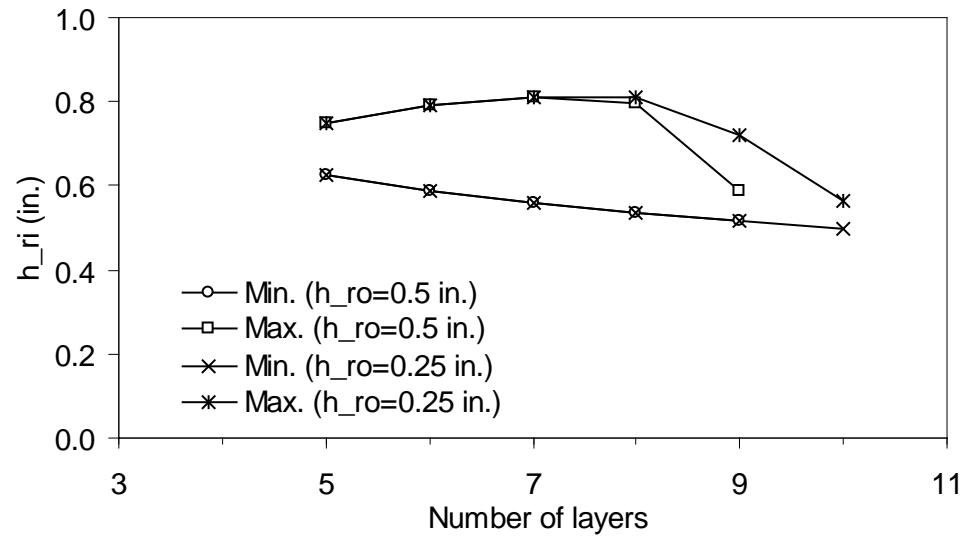


Fig. 7.9. Possible thickness range of interior elastomeric layer versus number of layers (Type II, $G = 100$ psi)

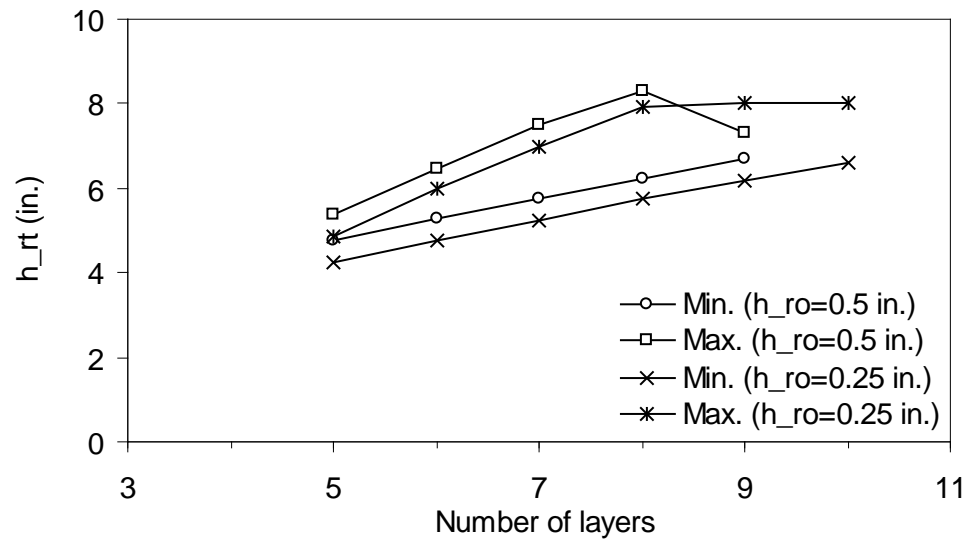


Fig. 7.10. Possible total thickness of elastomeric bearing (Type II, $G = 100$ psi)

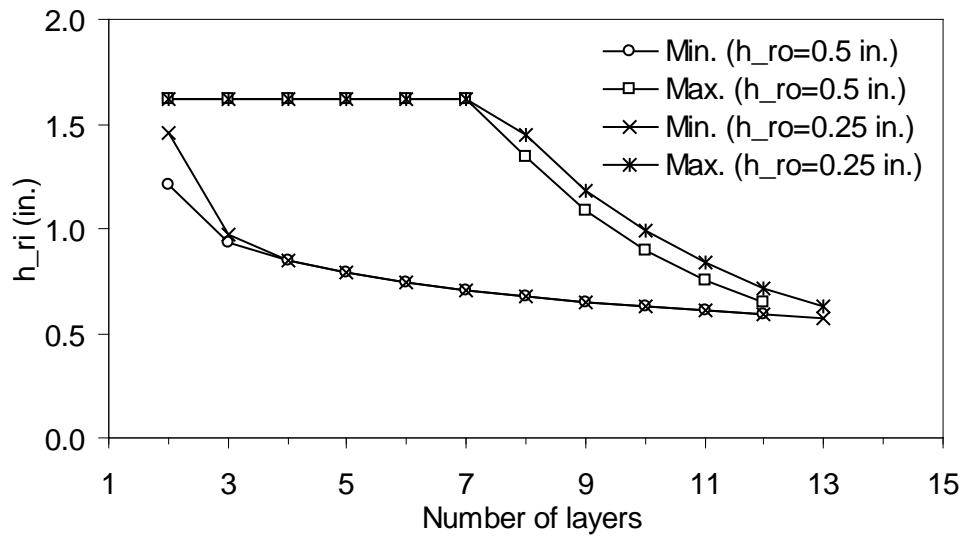


Fig. 7.11. Possible thickness range of interior elastomeric layer versus number of layers (Type II, $G = 200$ psi)

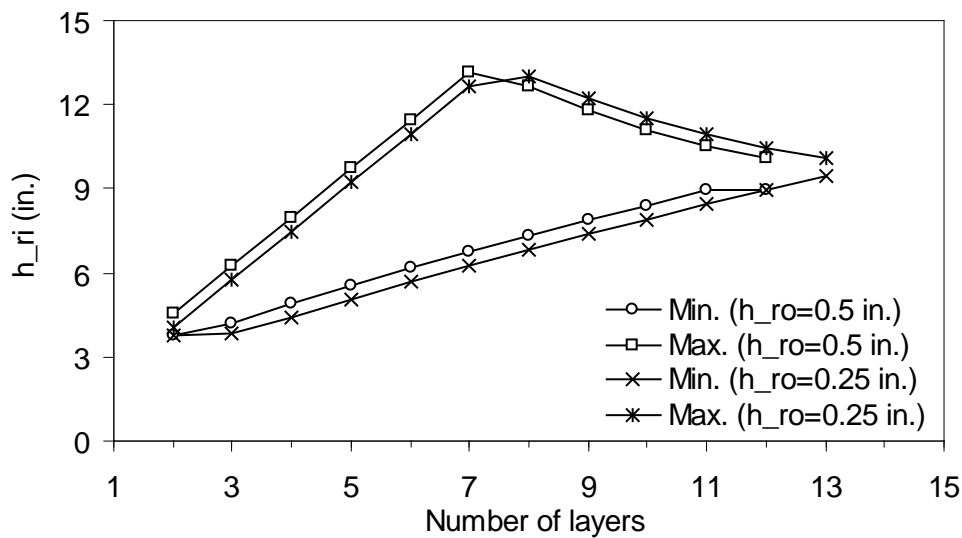


Fig. 7.12. Possible total thickness of elastomeric bearing (Type II, $G = 100$ psi)

7.5 Hyperelastic Material Model

For this study, it is assumed that the rubber is isotropic and its isothermal elastic problems are described in terms of a strain energy function (Rivlin 1956):

$$W = f(I_1, I_2, I_3) \quad (7.17)$$

where W is the strain energy density, and I_1 , I_2 , and I_3 are three invariants of the Green deformation tensor given in terms of the principal extension rates λ_1 , λ_2 , and λ_3 by

$$I_1 = \lambda_1^2 + \lambda_2^2 + \lambda_3^2 \quad (7.18a)$$

$$I_2 = \lambda_1^2 \lambda_2^2 + \lambda_2^2 \lambda_3^2 + \lambda_3^2 \lambda_1^2 \quad (7.18b)$$

$$I_3 = \lambda_1^2 \lambda_2^2 \lambda_3^2 \quad (7.18c)$$

Rivlin (1956) has pointed out that Eq. (7.17) can be approximated by a power series as:

$$W = \sum_{i+j+k=l}^{\infty} C_{ijk} (I_1 - 3)^i (I_2 - 3)^j (I_3 - I)^k \quad (7.19)$$

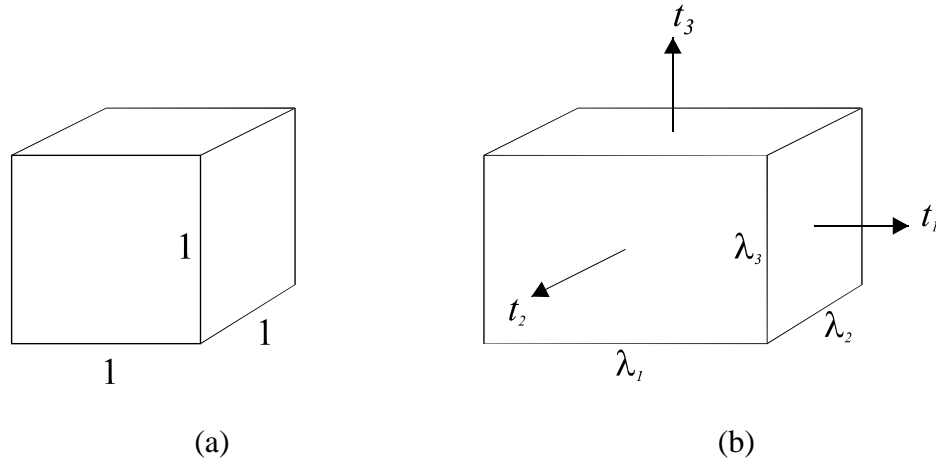


Fig. 7.13. Pure homogeneous deformation diagram: (a) undeformed state; (b) deformed state

For incompressible materials, $I_3 = 1$ and Eq. (7.19) reduces to

$$W = \sum_{i+j=1}^{\infty} C_{ijk} (I_1 - 3)^i (I_2 - 3)^j \quad (7.20)$$

Since rubbers are very nearly incompressible, Eq. (7.20) is usually taken as an adequate approximation. However, the more general form may be introduced. By considering the pure homogeneous deformation of a unit cube of rubber as shown in Fig.

7.13, Rivlin (1956) showed that the Cauchy (true) stresses, t_1 , t_2 , and t_3 are given by

$$t_1 = \frac{2}{\lambda_1 \lambda_2 \lambda_3} \left\{ \lambda_1^2 \frac{\partial W}{\partial I_1} + \lambda_1^2 (\lambda_2^2 + \lambda_3^2) \frac{\partial W}{\partial I_2} + \lambda_1^2 \lambda_2^2 \lambda_3^2 \frac{\partial W}{\partial I_3} \right\} \quad (7.21a)$$

$$t_2 = \frac{2}{\lambda_1 \lambda_2 \lambda_3} \left\{ \lambda_2^2 \frac{\partial W}{\partial I_1} + \lambda_2^2 (\lambda_3^2 + \lambda_1^2) \frac{\partial W}{\partial I_2} + \lambda_1^2 \lambda_2^2 \lambda_3^2 \frac{\partial W}{\partial I_3} \right\} \quad (7.21b)$$

$$t_3 = \frac{2}{\lambda_1 \lambda_2 \lambda_3} \left\{ \lambda_3^2 \frac{\partial W}{\partial I_1} + \lambda_3^2 (\lambda_1^2 + \lambda_2^2) \frac{\partial W}{\partial I_2} + \lambda_1^2 \lambda_2^2 \lambda_3^2 \frac{\partial W}{\partial I_3} \right\} \quad (7.21c)$$

Physically, I_3 can be interpreted as the square of the volume ratio and thus $\partial W / \partial I_3$ is

clearly related to volumetric changes. A convenient way to eliminate $\partial W / \partial I_3$ is to

consider stress differences. Taking differences between stresses and rearranging yields:

$$\frac{t_1 - t_2}{\lambda_1^2 - \lambda_2^2} = \frac{2}{\lambda_1 \lambda_2 \lambda_3} \left(\frac{\partial W}{\partial I_1} + \lambda_3^2 \frac{\partial W}{\partial I_2} \right) \quad (7.22a)$$

$$\frac{t_1 - t_3}{\lambda_1^2 - \lambda_3^2} = \frac{2}{\lambda_1 \lambda_2 \lambda_3} \left(\frac{\partial W}{\partial I_1} + \lambda_2^2 \frac{\partial W}{\partial I_2} \right) \quad (7.22b)$$

$$\frac{t_2 - t_3}{\lambda_2^2 - \lambda_3^2} = \frac{2}{\lambda_1 \lambda_2 \lambda_3} \left(\frac{\partial W}{\partial I_1} + \lambda_1^2 \frac{\partial W}{\partial I_2} \right) \quad (7.22c)$$

Stress-strain relationships for simple deformation modes can be derived from Eqs. (7.22a) through (7.22c). For incompressible materials subjected to uniaxial tension or compression ($\lambda_1\lambda_2\lambda_3 = 1$; $\lambda_2 = \lambda_3$; $\lambda_1\lambda_2^2 = 1$), the following equation can be derived:

$$\frac{\sigma}{\lambda - \lambda^{-2}} = 2 \left(\frac{\partial W}{\partial I_1} + \frac{1}{\lambda} \frac{\partial W}{\partial I_2} \right) \quad (7.23)$$

where σ is the engineering stress that is referred to the undeformed state ($\sigma = t_i/\lambda_i$).

Similarly, the pure shear relationship is given as:

$$\frac{\tau}{\gamma} = 2 \left(\frac{\partial W}{\partial I_1} + \frac{\partial W}{\partial I_2} \right) \quad (7.24)$$

where τ is the shear stress and γ is the shear strain which is related to the invariant I_1 by $\gamma^2 = (I_1 - 3)$. It is noted that the stress-strain behavior is determined by the partial derivatives $\partial W/\partial I_1$ and $\partial W/\partial I_2$. As a result, the task of characterizing the elastic behavior of rubber consists largely of determining the forms of these partial derivatives. The power series in Eq. (7.20) is usually truncated by taking only some of the leading terms.

Some examples are:

Neo-Hookean model (Treloar 1975);

$$W = C_{10} (I_1 - 3) \quad (7.25)$$

Mooney-Rivlin model (Yeoh 1993);

$$W = C_{10} (I_1 - 3) + C_{01} (I_2 - 3) \quad (7.26)$$

Yeoh model (Yeoh 1993);

$$W = C_{10} (I_1 - 3) + C_{20} (I_2 - 3)^2 + C_{30} (I_1 - 3)^3 \quad (7.27)$$

Hamzeh et al. (1995; 1996) added an exponent term in I_1 to Yeoh's cubic polynomials in order to obtain a better representation at small values of strain in a simple shear test:

$$W = \frac{a}{b} \left\{ 1 - e^{-b(I_1 - 3)} \right\} + C_{10} (I_1 - 3) + C_{20} (I_1 - 3)^2 + C_{30} (I_1 - 3)^3 \quad (7.28)$$

Note that C_{10} , C_{01} , C_{20} , C_{30} , a , and b are material constants in Eqs. (7.11) through (7.14).

7.6 Numerical Examples

In order to examine the basic behaviors of elastomeric bearings numerically, three-dimensional finite element modeling was conducted using a commercial program, ABAQUS (ABAQUS Inc. 2003). The hypothetical elastomeric bearing has dimensions of 18 in. (length) by 20 in. (width) with a total of eight elastomer layers and seven reinforcing steel shims. The thickness of the interior layers was varied while that of the exterior layers was fixed at 0.25 in. The elastomer was modeled using 8-node linear brick elements, hybrid with constant pressure (C3D8H of ABAQUS), while the reinforcing steel shims were modeled with 4-node general plate elements (S4 of ABAQUS). Fig. 7.14 shows a typical finite element mesh for elastomeric bearings. The sole and masonry plates were assumed to be rigid plates. Loadings were applied to these rigid plates. The contact between the rigid plates and elastomer was modeled using surface interaction options provided by ABAQUS taking into account friction. The steel reinforcement shims, with a thickness of 12 gauge (0.1046 in.), were assumed to be perfectly elasto-plastic, with elastic modulus, $E = 29,000$ ksi and yielding stress, $f_y = 50$ ksi. Yeoh's model was used to represent the hyperelastic material behavior of the

elastomer, as shown in Eq. (7.27), and the following coefficients were taken from Hamzeh et al. (1995):

	C_{10}	C_{20}	C_{30}
$G = 100$ psi	45.52 psi	3.092 psi	0.1005 psi
$G = 200$ psi	91.03 psi	6.183 psi	0.2010 psi

These values for G represent the mean shear moduli at 50% shear strain (percentage value for horizontal displacement to bearing height). The coefficients were obtained by scaling the material test results of a similar carbon-black-filled rubber reported by Hamzeh et al. (1995).

Fig. 7.15 shows a deformed shape of the hypothetical model due to compressive forces on the sole plate. The sole and masonry plates are not shown in the figure, but the effect of the steel reinforcement is clearly evident. A deformed shape due to applied shearing forces is shown in Fig. 7.16 and a deformed shape due to a combination of applied compressive force and moment is shown in Fig. 7.17.

In order to investigate the effects of the shape factor that is defined in Eq. (7.1), the thickness of the elastomer layers was varied so that the values of the shape factor, S , varied from 3 to 12. The shape factors for most reinforced bridge bearings fall between 4 and 12 (Stanton and Roeder 1982). The compressive stress-strain curves with $G = 100$ psi and $G = 200$ psi are shown in Figs. 7.18 and 7.19, respectively. As stated in Section 7.2, Figs. 7.18 and 7.19 confirm that a bearing layer with a large shape factor and high

elastomer stiffness has a larger compressive stiffness than one with a lower elastomer stiffness or small shape factor.

The effects of frictional coefficients between rigid plates (sole and masonry plates) and elastomer were also investigated. Although among the various factors that affect the friction of rubber against a rigid plate, constant values for the coefficients of friction were assumed in this study, and varied from 0.25 to 0.35. A perfect bond with no slip between the contact layers was also considered. Fig. 7.20 shows the stress-strain curves with different values of frictional coefficients from ABAQUS analyses. As shown in Fig. 7.20, there is no significant difference over the frictional coefficient range of 0.25 to 0.35.

7.7 Summary and Concluding Remarks

Elastomeric bearings are very effective for horizontally curved bridges. While offering high compressive stiffness, elastomeric bearings are flexible enough in shear to accommodate longitudinal movement of girders, thus mitigating horizontal reactions at internal piers or abutments in any direction.

In this chapter, design procedures for elastomeric bearings were briefly reviewed and design examples were introduced following *AASHTO LRFD* (2004). Theoretical modeling for hyperelastic material was also reviewed. Numerical modeling for the elastomeric components was carried out using a commercial finite element analysis program, ABAQUS (ABAQUS Inc. 2003) and Yoeh's model was used to represent the stress-strain relationship for the elastomer. Contacts between the rigid plates and elastomer were considered based on Coulomb-type friction in the finite element analysis. It has been observed for hypothetical bridges that the number of elastomeric layers

should be in the range of 3 to 13, with a possible thickness of each layer of between 0.5 in. and 1.8 in. It was also confirmed from three-dimensional finite element analysis that shape factors and shear stiffness sensitively affect the compressive stress-strain relationship of elastomeric bearings.

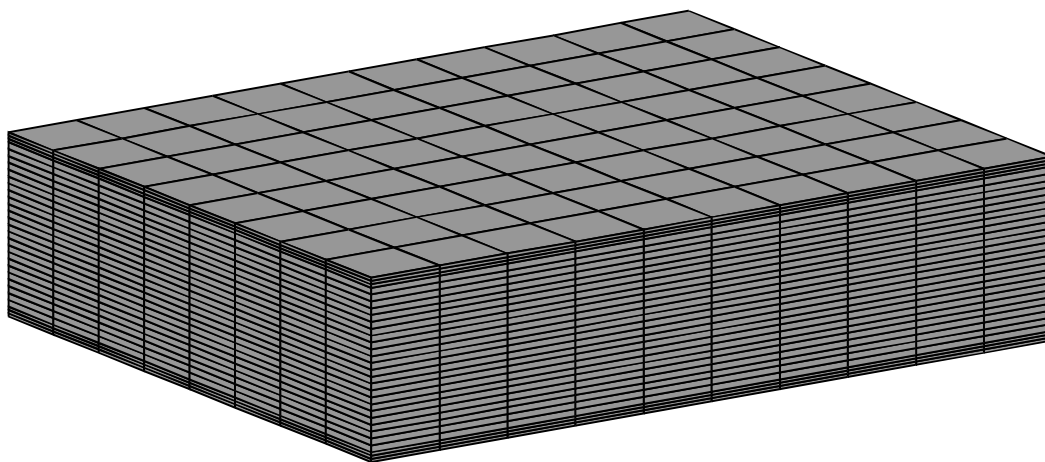


Fig. 7.14. Finite element model for an elastomeric bearing with reinforced shims

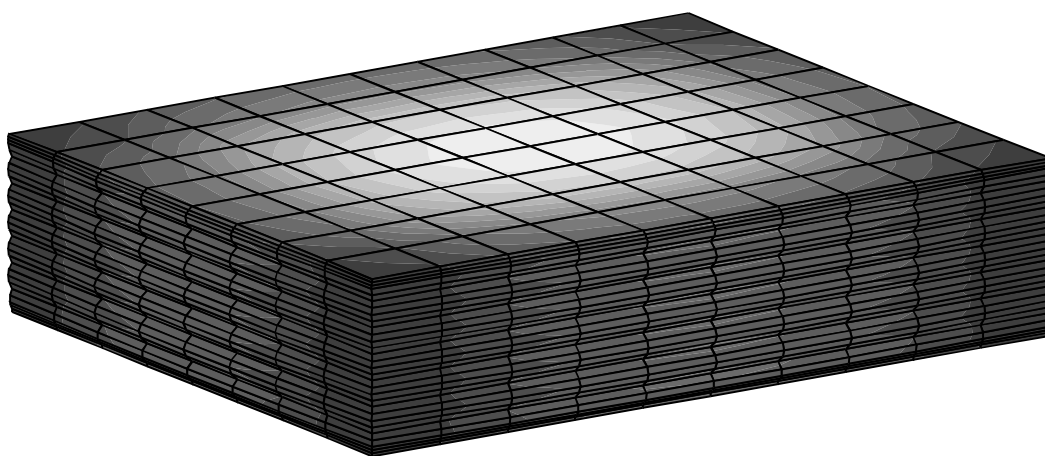


Fig. 7.15. Deformed shape under compressive forces

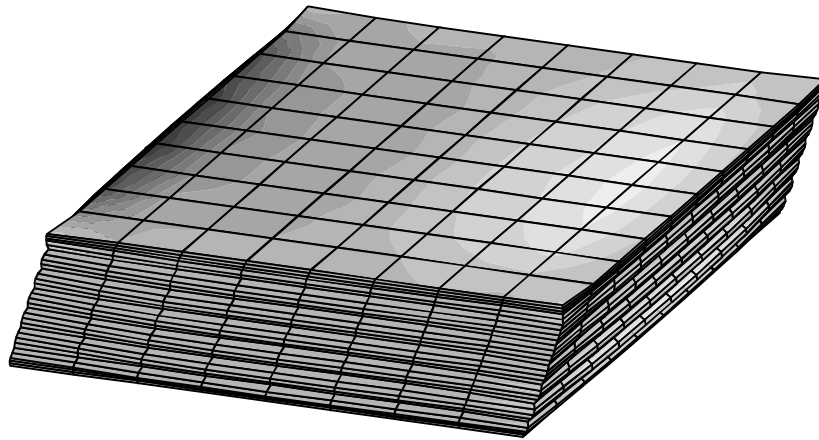


Fig. 7.16. Deformed shape under shearing force

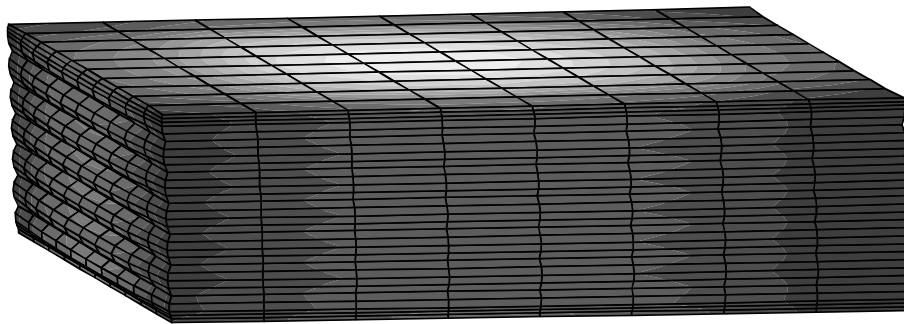


Fig. 7.17. Deformed shape under the combination of compressive force and moment

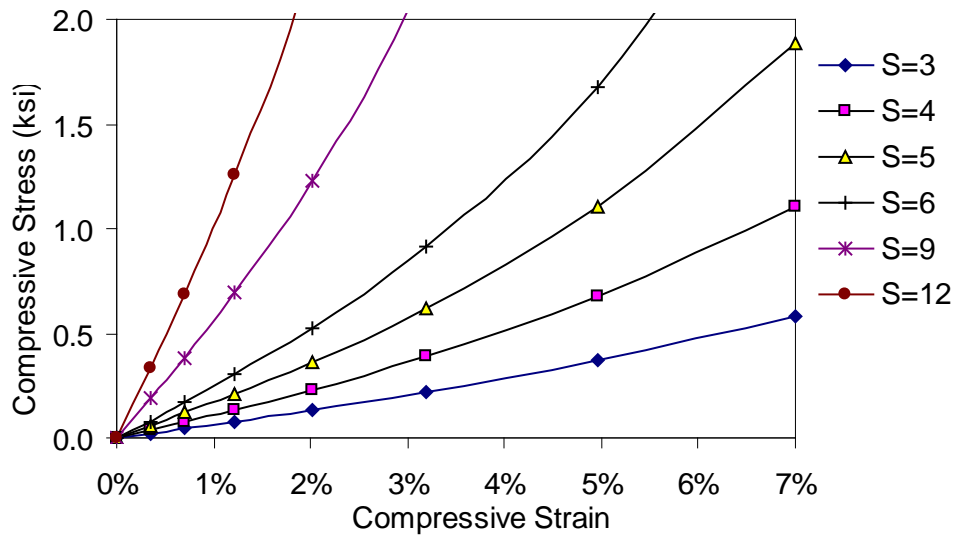


Fig. 7.18. Compressive strain-strain curves with various shape factors ($G = 100$ psi)

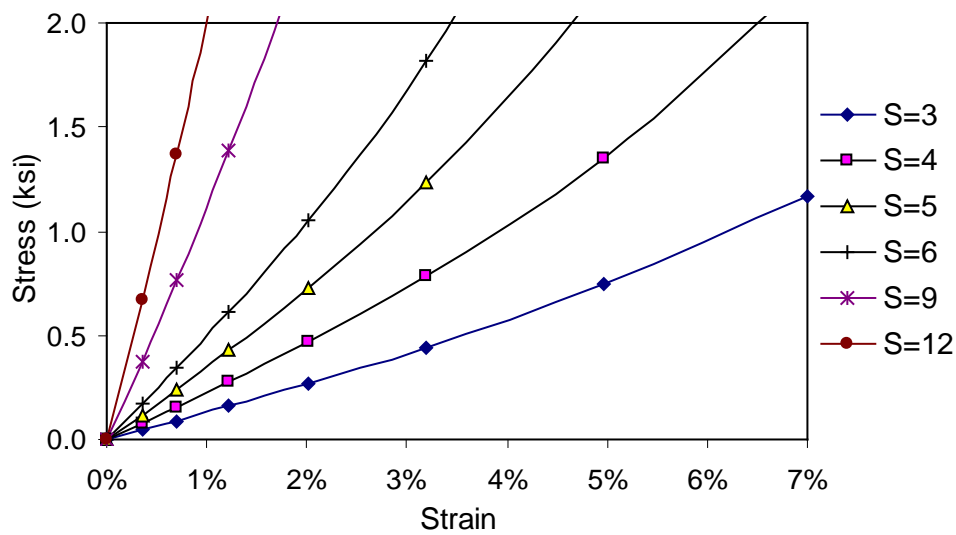


Fig. 7.19. Compressive stress-strain curves with various shape factors ($G = 200$ psi)

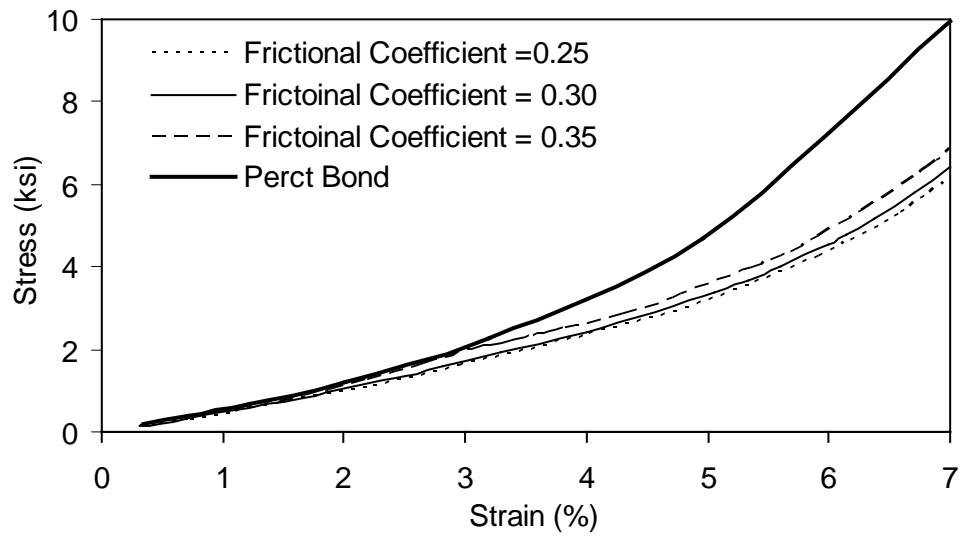


Fig. 7.20. Effect of frictional coefficients between elastomer and rigid plates on compressive stress-strain curve

CHAPTER 8

ULTIMATE STRENGTH INTERACTION OF COMPOSITE BOX GIRDERS

8. 1 Introduction

Composite box girders consisting of open top steel tub sections and concrete roadway slabs are a more common arrangement in modern highway structures in the United States, thereby taking advantage of the strength of both materials. Horizontally curved bridge girders are subjected to combined bending and torsion. The ultimate positive bending strength almost always approaches the plastic bending moment of a composite box girder when the girder is properly proportioned. The ultimate torsion strength of a composite box girder in the positive bending zone is limited by the relatively low diagonal tension strength of the deck concrete due to torsion. The concurrent compressive stress in the concrete deck improves the shear behavior of concrete, resulting in increased torsional resistance of a box girder.

Nevertheless, the ultimate torsional strength of a composite box girder is sensitively affected by the diagonal tensile stress in the concrete deck resulting from torsional moments. Hence, it is necessary to establish a realistic and yet computationally executable constitutive relationship of concrete in tension and compression. The effect of cracking and postcracking has been one of elusive challenges in the numerical investigation of the behavior of reinforced concrete structures. There were, however, a few successful accomplishments. In the 1970s' a numbers of numerical techniques of

modeling concrete material were introduced for finite element applications. Hand et al. (1973) presented a layered nonlinear finite element analysis including the elasto-plastic behavior of steel, bilinear elasto-plastic behavior of concrete, and limiting tension of concrete. Lin and Scordelis (1975) proposed a method for the nonlinear analysis of reinforced concrete shell structures under monotonically increasing loads. Gilbert and Warner (1978) proposed two basically different approaches that should be considered for taking tension stiffening into account in a layered finite element analysis of slabs. Lately, Yamamoto and Vecchio (2001) presented finite element formulations for an improved analysis of reinforced concrete shell structures based on layered isoparametric elements. The major thrust of recent developments in concrete modeling techniques has been incorporated into the finite element analysis programs, which, in turn, made it possible to effectively analyze the postcracking behavior of reinforced concrete.

In this paper, an ultimate strength interaction equation is proposed for steel/concrete composite box girders subjected to the combined action of positive bending and torsion. Although the maximum shear stress due to vertical bending shear is likely to be greater than the maximum shear stress due to torsion in a typical steel/concrete composite box girder section for highway bridges, the maximum vertical bending shearing force and the maximum positive moment are not likely to be developed at the same location along the girder. Therefore, the effect of vertical bending shear stress is not included in the ultimate strength interaction equation proposed. ABAQUS (2002) was used for all incremental nonlinear finite element analyses reflecting latest concrete modeling techniques. A concept of biaxial yield interaction curve was adopted in the

theoretical investigation. Both numerical analysis and theoretical derivation led to essentially the same equation.

In the design of steel/concrete composite box girders, particularly horizontally curved box girders, strength interactions between bending and torsion must be considered. The proposed interaction equation presented in this paper is simple in form yet it does provide a rational lower bound in the design of concrete/steel composite box girders under combined action of bending and torsion. The interaction equation presented is believed to be first for composite box girders, in which both the numerical investigation and the theoretical derivation led to the essentially identical form, thereby enhancing confidence of the methodology adopted in the study.

8.2 Numerical Investigation

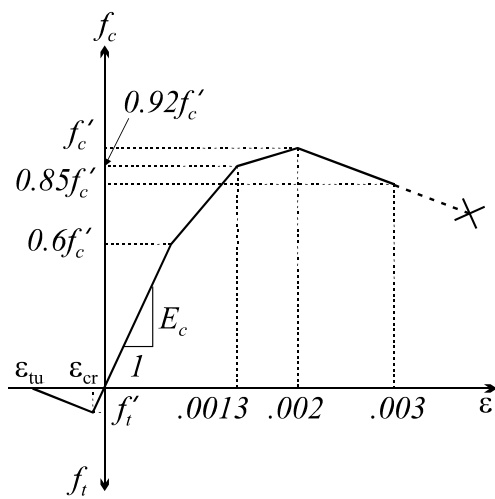
The objective of research is to develop an ultimate strength interaction equation for steel/concrete composite box girder subjected to a combined action of positive vertical bending and torsion. In order to accomplish this research objective by a numerical means, a series of incremental nonlinear finite element analyses were performed. Advanced incremental nonlinear analysis capability afforded by ABAQUS (2003) has been fully utilized: material nonlinearity based on multi-linear stress-strain relationships and geometric nonlinearity based on large displacements represented by the total Lagrangian formulation. Incremental solution strategies were required to trace the proper nonlinear equilibrium path in the analysis. Riks (1979) introduced an incremental approach to the solution of snapping and collapse problems. ABAQUS implemented the modified Riks algorithm (Crisfield 1981) that was recently used for nonlinear

incremental collapse analysis by several researchers including Thevendran et al. (1999) and Pi and Bradford (2001). This algorithm was particularly effective in the analysis of the effect of cracking and postcracking on the behavior of the reinforced concrete deck slab.

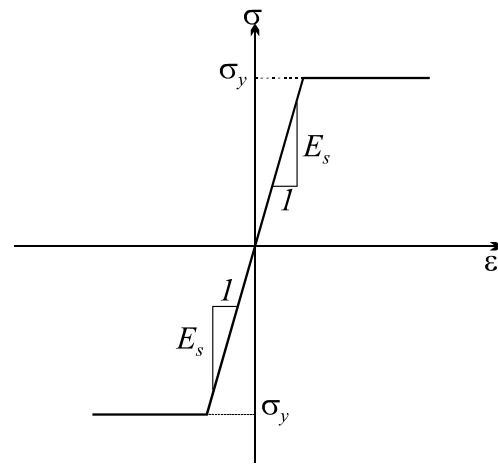
8.2.1 Constitutive Modeling for Concrete and Verification

Whenever concrete members are subjected to tension, cracking is the immediate concern, and hence, a proper and realistic representation of cracking and of postcracking effect is the most important aspect of numerical modeling of such members. The concrete model implemented in ABAQUS is a smeared model in the sense that it does not track individual micro cracks. Constitutive relationships are calculated independently at each integration point of the finite element at each incremental step. The presence of cracks enters into these calculations by way in which the cracks affect the stress and material stiffness associated with the integration point.

In the analysis of cracked reinforced concrete members, the intact concrete between each pair of adjacent tensile cracks is assumed to assist the tensile steel in carrying the internal tensile force. This mechanism, known as *tension stiffening*, therefore, contributes to the overall stiffness of the concrete member (Gilbert and Warner 1978; Yamamoto and Vecchio 2001). The stress-strain diagram affecting the strength of reinforced concrete structures is shown in Fig. 8.1(a). The strain at failure in ordinary concrete structural members is typically in the range of 1.0×10^{-4} in tension and $1.2 \times 10^{-4} \sim 2.0 \times 10^{-4}$ in flexure. MacGregor (1997) suggested that the rising part of stress-strain curve to tensile strength, f_t' , be approximated as a straight line with the same initial slope as in compression, E_c , as shown in Fig. 8.1(a).



(a)



(b)

Fig. 8.1. Idealized uniaxial stress-strain relationship: (a) concrete; and (b) steel.

In order to verify concrete material modeling, an ultimate bending behavior of a flat concrete plate was examined by a means of a sample slab. The slab, sometimes referred to as McNeice's slab, was tested experimentally by McNeice (1967), and has also been analyzed numerically based on finite element programs by a number of researchers, including Hand et al. (1973), Lin and Scordelis (1975), and Gilbert and Warner (1978). Idealized uniaxial stress-strain relationships for concrete and reinforcing steel are shown in Fig. 8.1. Uniaxial compressive and tensile strengths for concrete, f'_c and f'_t , were 5.5 ksi (37.9 MPa) and 0.46 ksi (3.17 MPa), respectively. Moduli of elasticity for concrete and reinforcing steel, E_c and E_s , were 4,150 ksi (28,614 MPa) and 29,000 ksi (200,000 MPa), respectively. Poisson's ratios were 0.15 and 0.3 for concrete and steel, respectively. The flat plate was supported in the transverse direction at its four corners and loaded by a point load at its center. The slab was reinforced in two directions at three-quarter of its depth measured from the top. The reinforcement ratio (volume of steel to volume of concrete) was 8.5×10^{-3} in each direction. Three alternative stress-strain diagrams for concrete in tension as shown in Fig. 8.2 were considered in the analysis of a reinforced concrete flat plate. The geometry of this example is given in Fig. 8.3. In the current nonlinear analysis, only a quarter of the slab was modeled using 8-node shell elements in ABAQUS taking full advantage of symmetry of the geometry and loading. The analysis incorporates three different stress-strain diagrams in tension, as shown in Fig. 8.2. The load versus deflection responses at the center of the slab were compared to those from the experiment, as shown in Fig. 8.4. Ultimate strengths resulting from all three types of tensile constitutive models show no significant difference compared to that determined from the experiment, although a minor deviation exists in

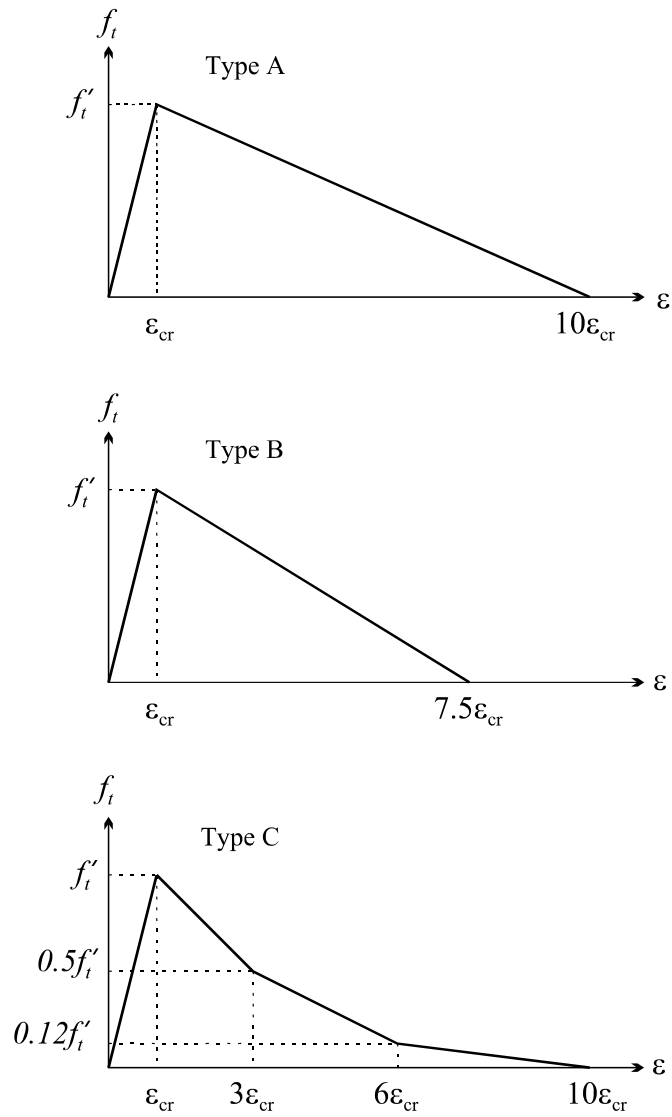


Fig. 8.2. Alternative stress-strain diagrams for concrete in tension.

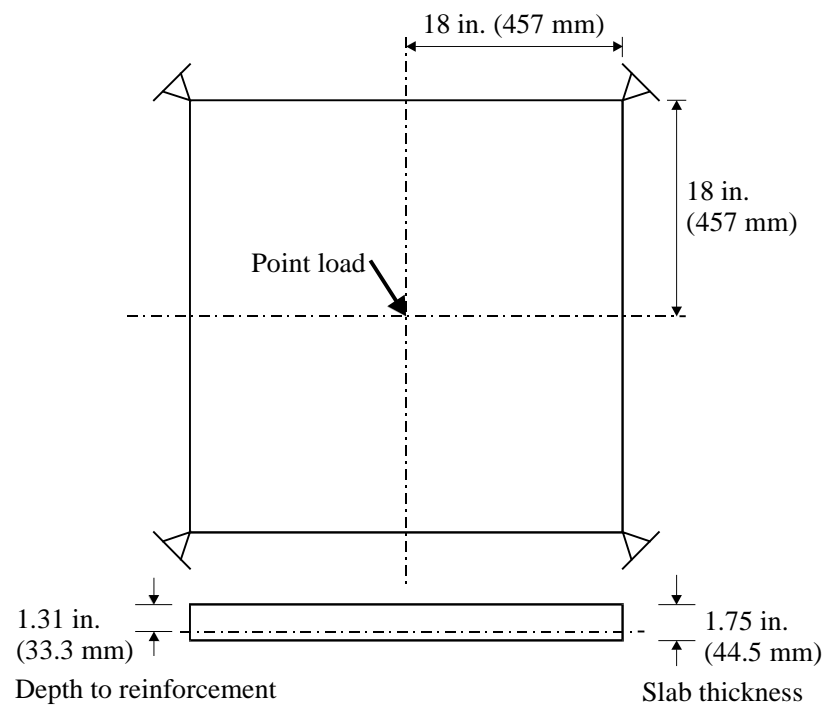


Fig. 8.3. Dimension of corner supported reinforced flat plate.

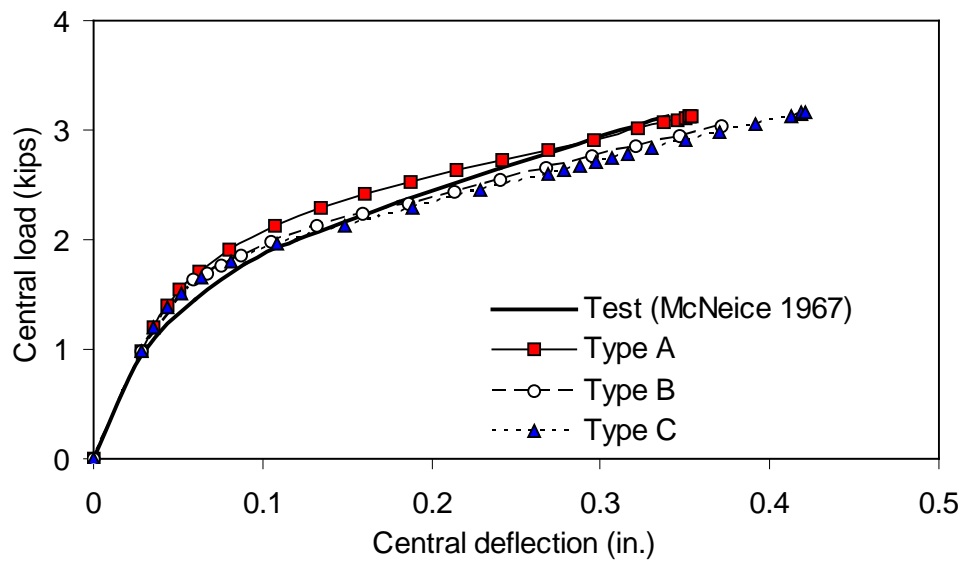


Fig. 8.4. Load-deflection response of the corner supported reinforced flat plate (1 in. =25.3 mm, 1 kips = 4.45 N).

load-deflection paths, particularly in the early stage. Tensile constitutive model of Type A shows the closest correlations in both the load and the deflection of the slab at failure. Type A was used as the tensile constitutive model of concrete for all subsequent analyses, as it is not only simple but yielded numerical results favorably comparable to those determined from the experiment.

8.2.2 Ultimate Strength Interaction of Composite Box Girders

Incremental nonlinear finite element analyses were carried out for composite box girder models under the positive bending (longitudinal compressive stresses in the concrete slab). The 8-node shell elements (S8R of ABAQUS) were used for both steel plates and concrete deck slabs. As the focal point of the numerical analysis is on the concrete deck behavior, the aspect ratio of deck elements was kept close to one. Fig. 8.5 shows an overview of the grid pattern employed in the finite element analysis. The default section points were five for all steel elements, however, a total of 15 section points were specified for the concrete deck slab along the thickness direction to evaluate possible nonlinear stress distribution. Shear studs that connected top flanges and concrete deck were modeled using rigid bars. Cross-sectional properties of two hypothetical single-box girders (Section A and B) are shown in Fig. 8.6. Schematics for loading and boundary conditions are illustrated in Fig. 8.7. This loading scheme allows different combinations of vertical bending and torsion to be examined by simply selecting different values for P and T . Once P and T were selected, the ratio between these two values was kept unchanged up to the final incremental step. Care must be exercised for an initial combination of P and T in order to accomplish the convergence at a minimum number of iteration steps. Although ABAQUS automatically determines an optimum

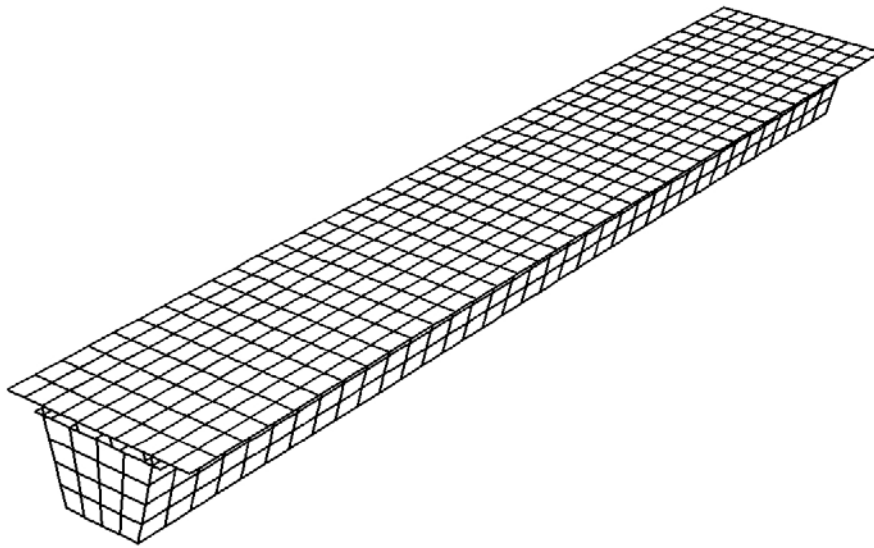
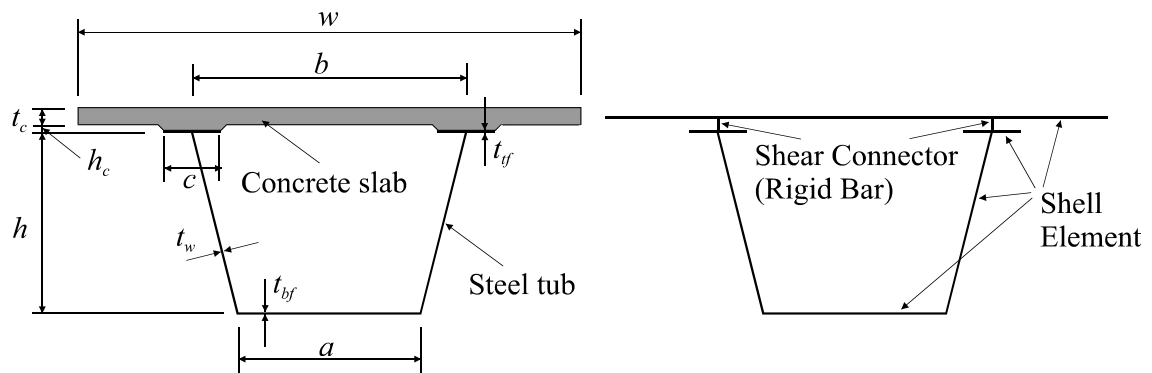


Fig. 8.5. Typical finite element mesh used in incremental nonlinear analysis.



	Section A	Section B
a	80 in. (2,032 mm)	50 in. (1,270 mm)
b	120 in. (3,048 mm)	100 in. (2,540 mm)
c	18 in. (457 mm)	16 in. (406 mm)
w	200 in. (5,080 mm)	200 in. (5,080 mm)
h	80 in. (2,032 mm)	100 in. (2,540 mm)
h_c	4 in. (102 mm)	4 in. (102 mm)
t_c	9.5 in. (241 mm)	8.5 in. (215 mm)
t_{tf}	1.0 in. (25.4 mm)	1.0 in. (25.4 mm)
t_w	0.563 in. (14.3 mm)	0.5 in. (12.7 mm)
t_{bf}	0.625 in. (15.9 mm)	0.625 in. (15.9 mm)

Fig. 8.6. Steel/concrete composite box section: (a) Cross-sectional properties; and (b) Element types used in FEA.

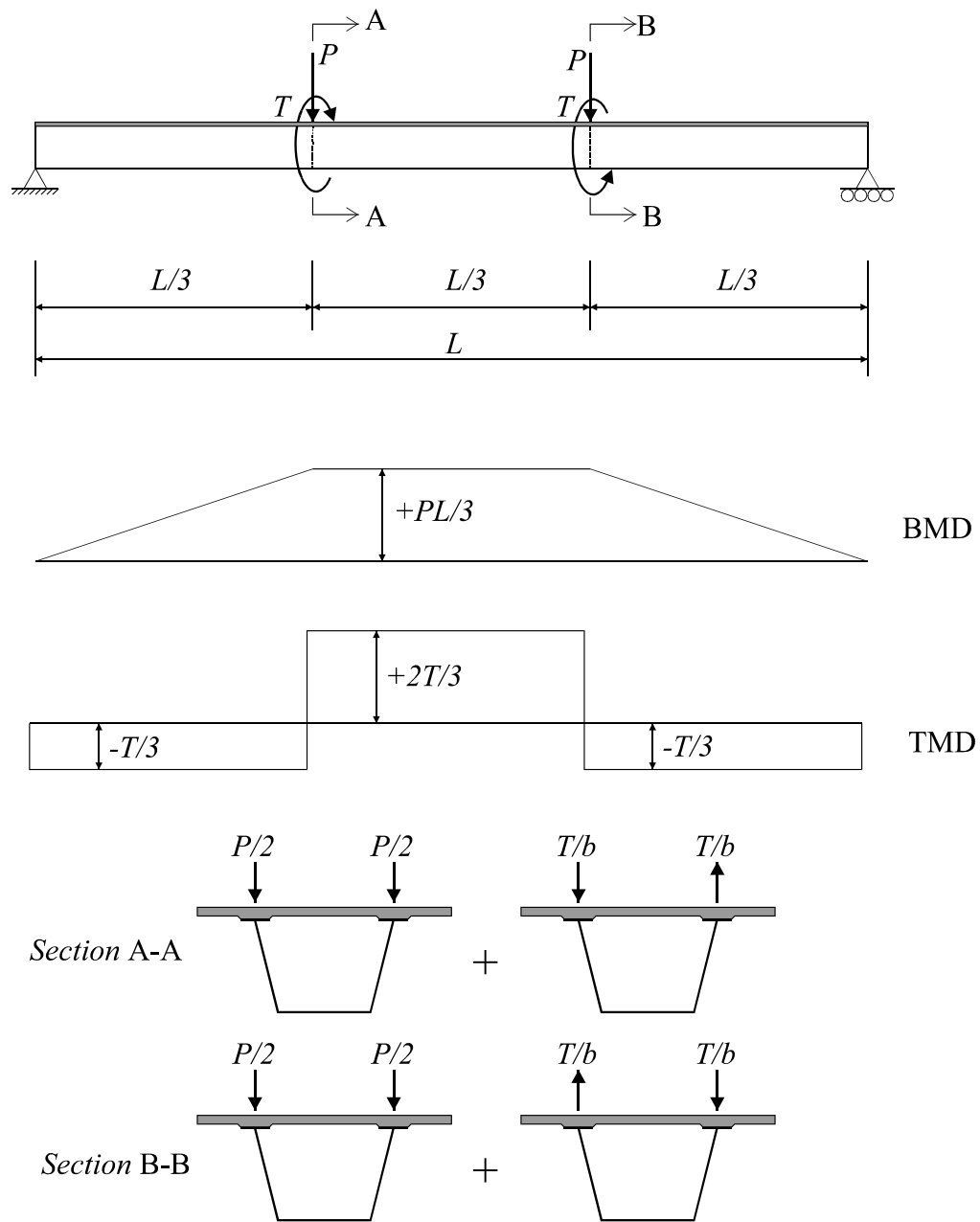


Fig. 8.7. Schematics for analysis of simply supported composite box girder in combined bending and torsion.

iteration interval and numerical tolerances, an initial input of the load size does affect the number of iteration steps. It was not unusual for each pure bending analysis to experience several hundred iteration steps to reach the final ultimate strength. The span length of the model structure of Section A and B is 90 ft (27,432 mm). Concentrated loads are applied at one-third points of the span to create a constant moment zone. Solid diaphragms are provided at load points and at both ends in order not to cause any local stress concentration effects that might be induced by using cross-frames. Steel reinforcements are provided at the top and bottom of deck slabs. The deck reinforcement was assumed to be #5 at 12 in. (#15 at 300 mm) in both transverse and longitudinal directions at the top and bottom, respectively, as per the provisions of empirical design of AASHTO LRFD (2004). The stress-strain relationships of concrete and steel are given in Fig. 8.1. Only Type A stress-strain relationship of concrete in tension was used in the incremental analysis of the deck slab.

In order to determine the ultimate capacity in pure bending and torsion, Section A and B were analyzed by incremental finite element method reflecting again Type A stress-strain relationship of concrete in tension. AASHTO LRFD (2004) provides equations to determine the fully plastic moment, M_p , of the steel/concrete composite cross section in positive bending. Analysis results are given in Table 8.1. As can be seen from Table 8.1, ultimate bending strength obtained from the incremental finite element analysis reaches very close to full plastic moment for both Section A and B (over 98%). Theoretically, the ultimate bending moment evaluated by the incremental finite element analysis cannot be exactly equal to the full plastic bending moment evaluated by simplified formulas such as those given by AASHTO LRFD (2004) as the strain at the

vicinity of the plastic neutral axis must be finite. Plastic neutral axes in section A and B are located in concrete slab at ultimate bending. This ensures that Section A and B are proportioned to meet the ductility requirement of AASHTO LRFD (2004).

Figs. 8 and 9 present normalized data generated during the course of determining the ultimate strengths given in Table 8.1. Fig. 8.8 shows the maximum bending moment and corresponding vertical deflection at the mid-span at selected incremental steps. Fig. 8.8 illustrates the AASHTO LRFD ductility requirement very well. The maximum bending moment is normalized against the ultimate bending moment value, M_u , determined by the incremental finite element analysis shown in Table 8.1. Fig. 8.9 illustrates the normalized applied torsion versus the girder rotation. These values of intermediate bending moment and torsion shown in Figs. 8 and 9 were normalized against the ultimate values given in Table 8.1.

Table 8.1. Ultimate bending and torsional strengths of composite box girders

		Model A (Difference)	Model B (Difference)
Bending	$M_{u,FEA}$	469,440 k-in. (53,027 kN-m, 98.8%*)	483,840 k-in. (54,674 kN-m, 98.5%*)
	M_p (AASHTO 2004)	475,400 k-in. (53,720 kN-m)	491,321 k-in. (55,519 kN-m)
Torsion	$T_{u,FEA}$	70,720 k-in. (8,795 kN-m, 98.9%*)	58,733 k-in. (6,990 kN-m, 100.3%*)
	$T_{u,Theory}$ (Eq. 8.6)	71,530 k-in. (8,937 kN-m)	58,547 k-in. (6,789 kN-m)

* Differences are with respect to M_p or $T_{u,Theory}$.

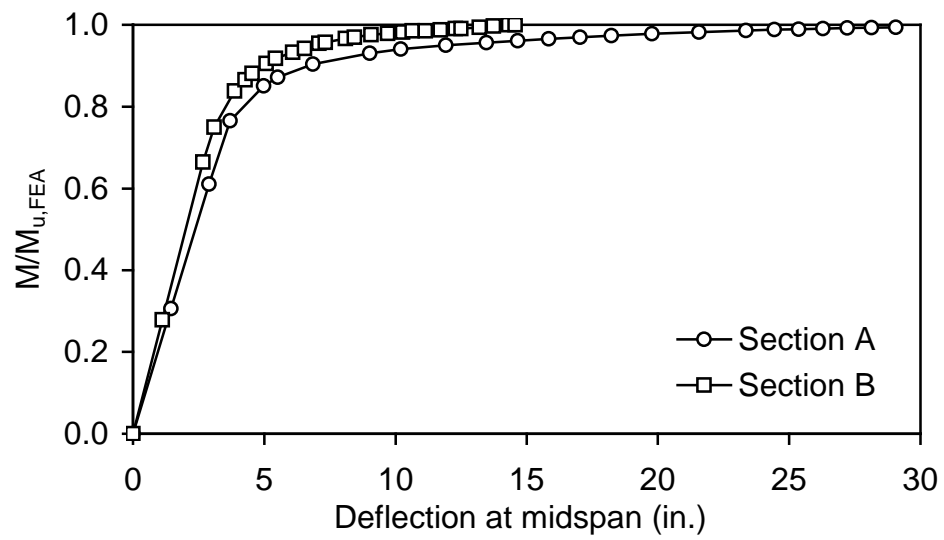


Fig. 8.8. Applied bending moment versus deflection curve for composite box specimen (1 in. = 25.4 mm).

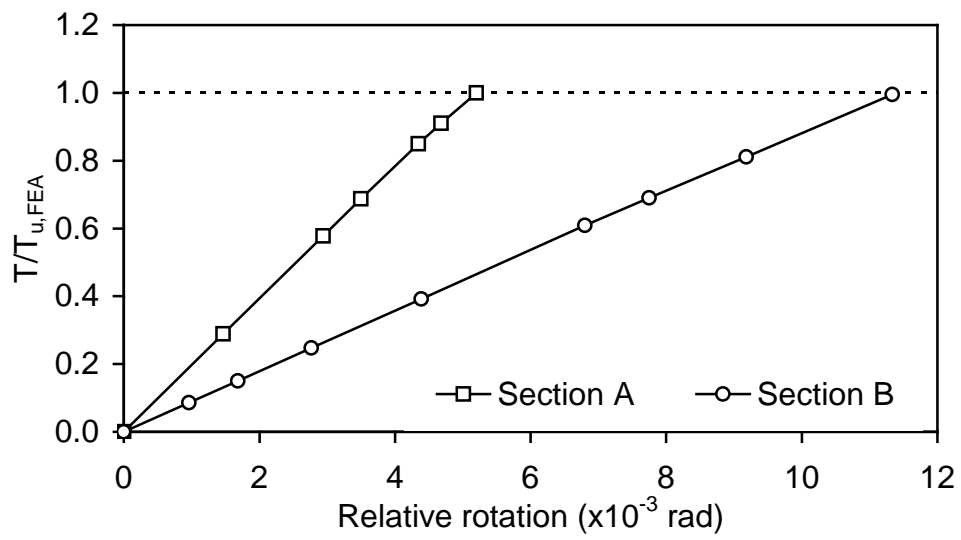


Fig. 8.9. Applied torsional moment versus rotation curve for composite box specimen.

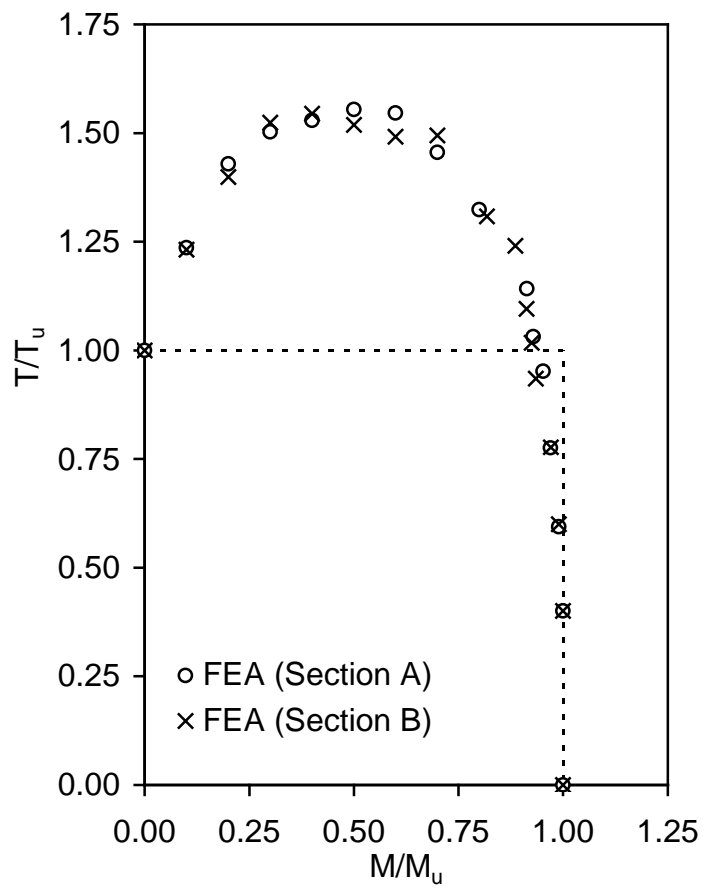


Fig. 8.10. Ultimate strength interaction between bending and torsion of the composite box girder in positive moment region.

It is of interest to note that the torsional moment increases almost linearly up to failure as shown in Fig. 8.9. This is expected as the ultimate torsional strength of a steel/concrete composite box section is limited by the diagonal tensile capacity of the deck concrete that exhibit but a very small ductility as shown in Fig. 8.1(a), which appears justifying the lower value of the strength reduction factor, ϕ , specified for torsional designs in the current ACI code (2002). Clearly, the reinforcement provided as per the AASHTO LRFD empirical design did not affect the ultimate torsional strength, particularly in Section B.

Fig. 8.10 shows the normalized interaction values generated from incremental nonlinear finite element analyses on Section A and B. A number of incremental nonlinear finite element analyses were performed for two different models shown in Fig. 8.6 under various combinations of combined vertical and torsional loads. It is noted that the shear strength of the concrete deck substantially is increased due to the concurrent compression developed from the positive vertical bending moment. This phenomenon can be readily verified by constructing a Mohr's circle. However, as magnitude of bending moment approaches the ultimate value, ultimate shear strength decreases very rapidly. The ultimate bending strength was only marginally affected due to high torsional moment.

8.3 Analytical Investigation

It is intended here to validate the ultimate strength interaction equation for steel/concrete composite girders developed numerically in the previous section by an

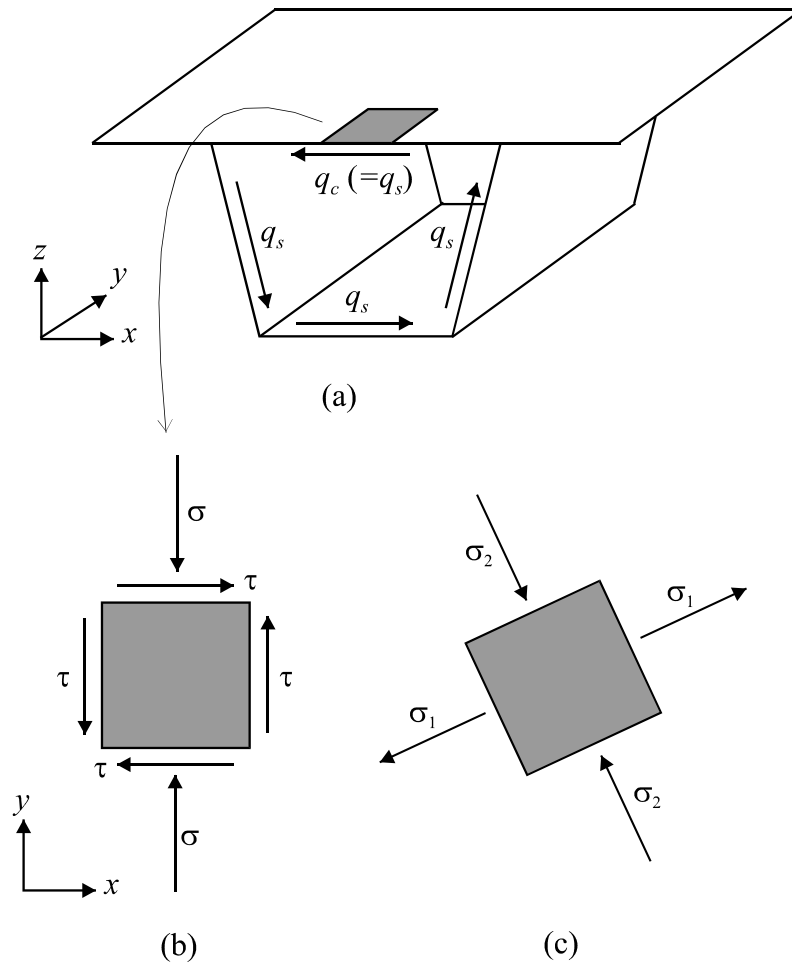


Fig. 8.11. Concrete deck element subjected to shear and normal stresses: (a) Shear flow in composite section; (b) Stress state in positive moment region; and (c) Corresponding principal state.

analytical means. The shear flow, denoted as the product of the average shear stress and the thickness of the box walls, in a steel/concrete composite box section is illustrated in Fig. 8.11(a). Fig. 8.11(b) shows an infinitesimal concrete deck element subjected to the resisting shear stress along with the compressive stress resulting from the positive vertical bending moment. The shear flow in concrete and steel walls is denoted by q_c and q_s , respectively. The magnitude of shear flow is constant in each wall of a box due to Prandtl's analogy (Prandtl 1903). Torsional strength of a steel/concrete composite box section is governed by the shear strength of the concrete slab despite the concrete deck is much thicker than steel walls. This is so because the diagonal tensile stress resulting from the shear stress of the concrete is much less than that of the steel. Strength interaction between bending and torsion of the steel/concrete composite box girder, therefore, may be established by investigating strength interaction between compressive and shear stresses of the concrete slab. Consider an infinitesimal element subjected to compressive stress and shear stress as shown in Fig. 8.11(b). Principal stresses in the infinitesimal element of the concrete deck can be determined readily by a Mohr's circle as shown in Fig. 8.11(c). The induced compressive stress, s , and the shear stress, t , are related to the principal stresses, s_1 and s_2

$$\sigma_{1,2} = \frac{\sigma}{2} \pm \sqrt{\frac{\sigma^2}{4} + \tau^2} \quad (8.1)$$

The concrete deck plate is considered to be at its ultimate torsional strength either when the tensile principal stress, s_1 , reaches its tensile strength or when the compressive principal stress, s_2 , reaches its compressive strength anywhere on the yield curve for biaxial stress in the concrete as shown in Fig. 8.12(a) developed by Kupfer et al. (1969).

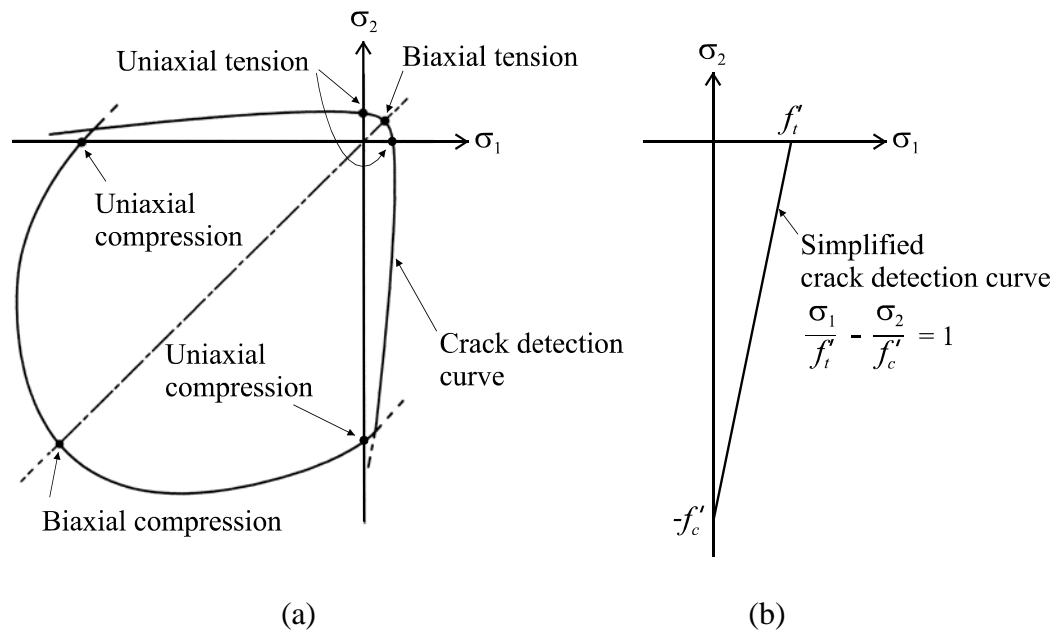


Fig. 8.12. Crack detection curve: (a) Yield surface for stress in concrete; and (b) Simplified crack detection curve in the plane of positive σ_1 and negative σ_2 .

Fig. 8.12(a) is frequently considered as a benchmark interaction curve developed from a series of experimental investigation. Crack detection curves in the biaxial yield interaction curve may be expressed by a simplified linear equation in terms of uniaxial tensile and compressive strength as shown in Fig. 8.12(b). The straight line in Fig. 8.12(b) is expressed by Eq. (8.2).

$$\frac{\sigma_1}{f'_t} - \frac{\sigma_2}{f'_c} = 1 \quad (8.2)$$

where f'_t, f'_c are tensile and compressive strength, respective, of concrete. For the deck concrete that does not reach failure either in tension or in compression, principal stresses lie within the triangular zone bounded by two principal stress axes and the simplified crack detection line such that

$$\frac{\sigma_1}{f'_t} - \frac{\sigma_2}{f'_c} \leq 1 \quad (\sigma_1 > 0, \sigma_2 < 0) \quad (8.3)$$

Substituting Eq. (8.1) into Eqs. (8.7), and rearranging gives:

$$\tau \leq \frac{\sqrt{f'_t f'_c (f'_t - \sigma)(f'_c + \sigma)}}{f'_t + f'_c} \quad (8.4)$$

Fig. 8.13 shows an interaction curve between compressive stresses, σ , and shear stresses, τ , determined from Eq. (8.4) for the concrete having material properties of $f'_c = 5.5$ ksi (37.9 MPa) and $f'_t = 0.46$ ksi (3.17 MPa).

Ultimate strength interaction for a concrete/steel composite box girder may be constructed using Eq. (8.4) if relationship between shear stress and torsional moment along with relationship between longitudinal stress and bending moment are known. As

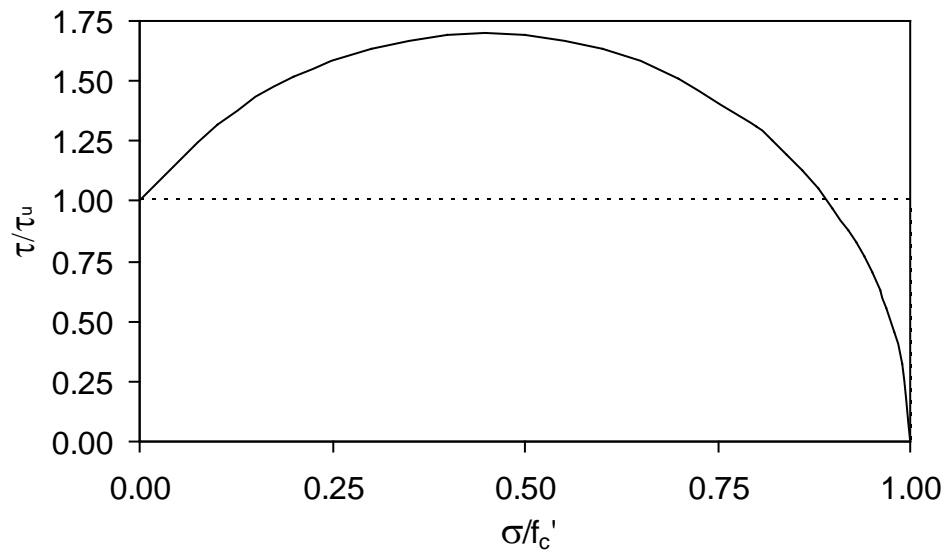


Fig. 8.13. Relationship between τ and σ from Eq. (8.4).

stated, the capacity of shear flow in concrete section is governing, therefore, torsional moment, T , acting on composite section can be evaluated by

$$T = 2\tau t_c A_{box} \quad (8.5)$$

where t_c is thickness of concrete deck; A_{box} is enclosed box area by steel and concrete sections measured along the centerline of each wall. The ultimate torsional strength without bending effect, T_u , can also evaluated by substituting ultimate shear stress of concrete, τ_u , for τ in Eq. (8.5)

$$T_u = 2\tau_u t_c A_{box} \quad (8.6)$$

where τ_u is defined the ultimate shear stress evaluated from Eq. (8.4) by substituting $\sigma = 0$.

The maximum compressive stress at the extreme fiber of the concrete deck is linearly proportional to the positive vertical bending moment in the elastic range. However, it could be easily expected that the relationship between the compressive stress in the concrete deck and corresponding positive vertical moment in the inelastic range would be quite complex as the neutral axis would shift toward the plastic neutral axis as the yielding of the deck concrete propagate and the deck concrete would exhibit a highly nonlinear response. As it is highly unlikely to be able to establish a relationship analytically between the concrete compressive stress evaluated at a point in a cross section and the positive vertical bending moment evaluated for an entire cross section in the inelastic range, Fig. 8.14 was generated empirically relating the compressive stress and the corresponding positive vertical bending moment for the model girders of Section A and B. A series of incremental nonlinear finite element analyses were carried out to develop Fig. 8.14 on the model girders considering vertical bending only. Ultimate

strength interaction curve between bending and torsion can now be constructed by substituting the relationships between the interactive torsion and positive vertical bending moment and corresponding concrete shear stress and compressive stress into Eq. (8.4). The relationship between the interactive torsion, T , and corresponding shear stress, τ , is established by Eq. (8.5) and the relationship between the positive vertical bending moment, M , and corresponding compressive stress, σ , is established by Fig. 8.14. Fig. 8.15 comparatively shows the ultimate strength interaction between positive vertical bending moment and torsion for two typical steel/concrete composite box girders generated from analytical and numerical investigations. Although the process employed in Eq. (8.5) and in Fig. 8.14 lacks certain rigor, fairly good agreement is evident between the two interaction curves developed by analytical and numerical investigations. No such simplifying assumptions were employed, however, during the course of generating numerical data by incremental nonlinear finite element analyses.

8.4 Ultimate Strength Interaction Equation

When a structural member is subjected to two or more major forces, the design of such a member is usually carried out by considering an interaction between the two forces. A simple interaction equation or a curve is highly desirable for practicing engineers. Based on the interaction curves developed from both numerical and theoretical analyses, following interaction equation is proposed for steel/concrete composite box girder in the positive moment region.

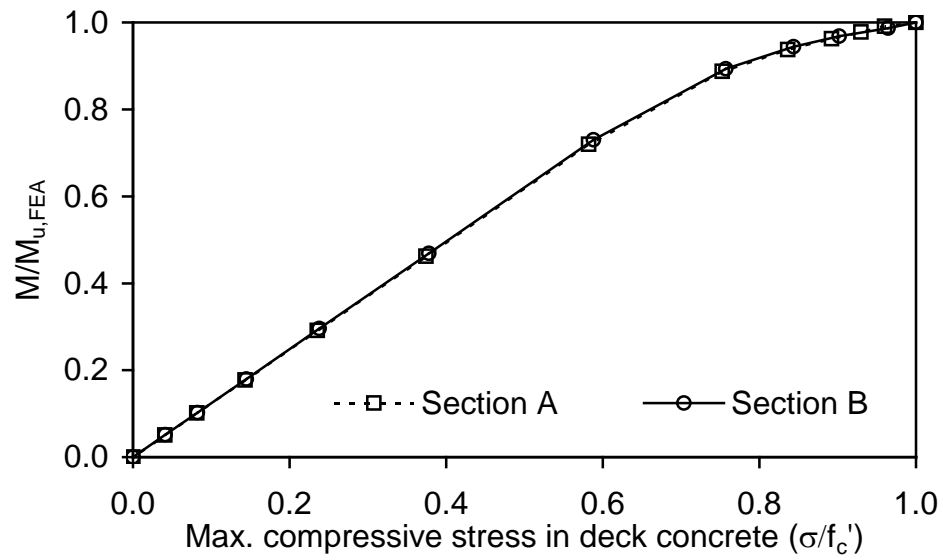


Fig. 8.14. Relationship between composite girder moment and longitudinal stress in deck concrete.

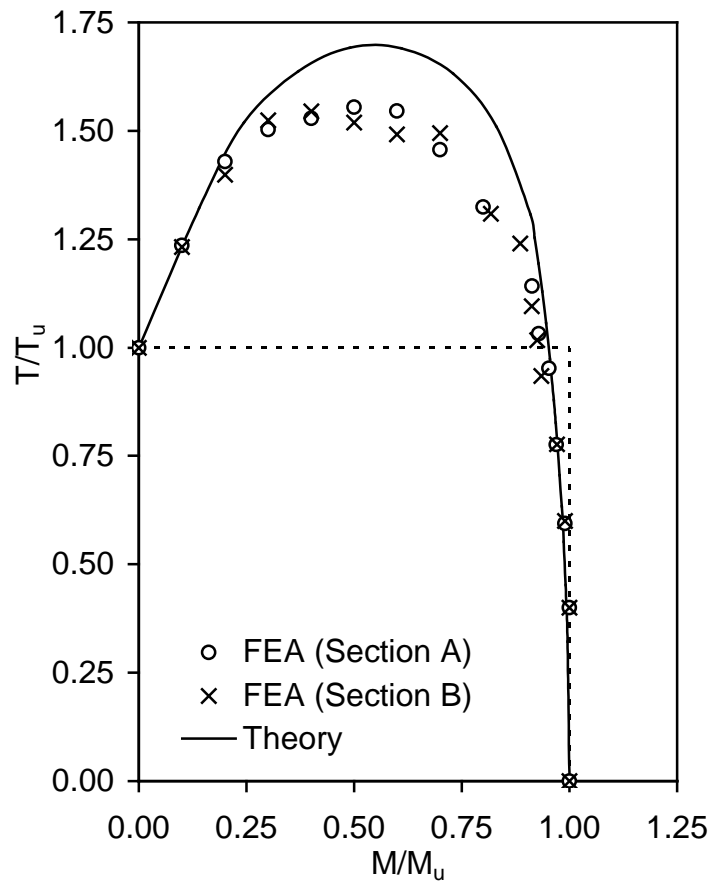


Fig. 8.15. Comparison of ultimate strength interaction curve from EFA and theory for a composite box girder in positive moment zone.

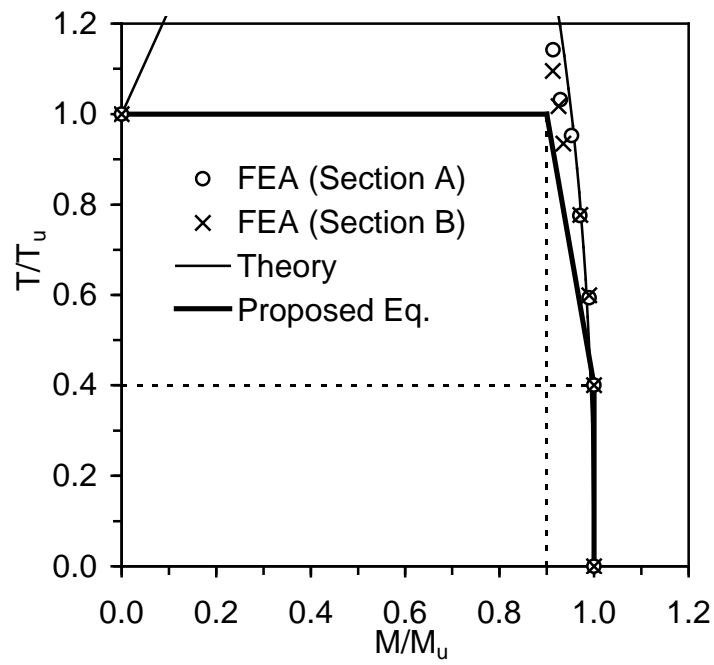


Fig. 8.16. Proposed ultimate strength interaction curve for composite box girders in positive moment zone.

$$6\left(\frac{M}{M_u}\right) + \left(\frac{T}{T_u}\right) \leq 6.4 \quad \left(0 \leq \frac{M}{M_u} \leq 1.0, 0 \leq \frac{T}{T_u} \leq 1.0\right) \quad (8.7)$$

where M_u is the ultimate positive vertical bending moment and T_u is the ultimate torsional moment. In most practical cases of composite box girders, M_u is equal to the plastic moment, M_p , of composite sections specified in Section D6.1 of AASHTO LRFD (2004). Eq. (8.7) is intentionally made conservative in order to reflect the brittle nature of concrete deck failure due to the diagonal tensile stress induced by torsion. Fig. 8.16 illustrates the interaction values computed from the proposed equation along with those determined from finite element analyses and Eq. (8.4).

8.5 Summary and Concluding Remarks

Ultimate strength interaction relationships between bending and torsion for steel/concrete composite box girder were investigated by both numerical and analytical means. In the numerical investigation, ultimate strength analyses were carried out taking advantage of the incremental nonlinear finite element analysis technique afforded in ABAQUS (2002) reflecting both material and geometric nonlinearities. A spectrum of ultimate strength interaction data, positive vertical bending moment and concurrent torsional moment, were collected from these numerical analyses and normalized the ultimate bending strength and torsional strength, respectively. The developed ultimate strength interaction values were independently verified by an analytical means.

The ultimate strength of the steel/concrete composite box girder subjected to torsion is governed by the diagonal tensile stress in the concrete deck induced by the torsional shear flow. An interaction design equation has been formulated based on the

ultimate strength interaction data developed from the numerical and analytical investigation for steel/concrete composite box girders. The design equation was intentionally made conservative in order to reflect the brittle nature of the concrete deck failure due to diagonal tensile stress induced by torsional moments. Ultimate strength interaction equations were constructed based on the results from numerical and analytical investigation and design equation was proposed for steel/concrete composite box girders in the positive moment zones. The proposed ultimate strength interaction equation is simple to apply and is representative for a lower bound of the ultimate strength envelope.

CHAPTER 9

REQUIREMENTS FOR LONGITUDINAL STIFFENERS

9.1. Introduction

Modern highway construction often requires bridges with horizontally curved alignments. According to a recent survey (Task Group 1991), curved bridges represent 20 to 25 percent of the market for new steel bridge construction each year and this trend is likely to increase in the future. Curved girder bridges were once rare. In the past, straight steel or concrete girders were placed on a series of chords of the roadway curve between supports or field splices to approximate the required curvature. The straight girder approach has several disadvantages. Bridges constructed in this manner are not aesthetically pleasing and the advantages of structural continuity are lost (Nakai and Yoo, 1988). Therefore, most modern curved bridge alignments today use continuous horizontally curved girders.

Curved bridges using curved girders are usually characterized by simpler and more uniform construction details, because the girder spacing and the concrete deck overhangs are generally constant along the length of the structure. The curved girder system is aesthetically pleasing with the use of shallower deck on the cantilevered edges of uniform spans as well as its streamlined configuration, particularly in an elevated transit system in an urban area. Curved girders allow for the use of longer spans, which reduces substructure costs and the required number of expansion joints and bearing

details. Deterioration around joints and bearings due to leakage is a significant maintenance problem associated with these details. Because of the reduction of construction cost and time associated with substructures, joints, and bearings, the overall construction cost for the curved girder system could be competitive or less than that for the straight system although it generally costs slightly more to fabricate a curved girder (Nakai and Yoo 1988, Suros and Chu 1991, Schmitt 1966). The construction time is often a very important factor in the selection of a suitable structural system where the construction site needs to be used for other operation during the construction period. Curved girders also more easily satisfy the demand placed on highway structures by predetermined roadway alignments and tight geometric restrictions presented by today's increasing right-of-way restrictions.

Despite all the inherent advantages of curved girders, their behavior is generally much more complex than that of straight girders. Curved girders are subjected to torsion as well as vertical bending. The interaction between adjacent girders is also more important in curved girder bridges than in straight bridges without skew. To assist engineers in dealing with the complexities of curved girders, several practical approximate analysis methods, such as the V-load method for curved I-girder systems and the M/R method for curved box-girder systems, were developed in the 1960s and 1970s. More recently, refined three-dimensional finite element analysis methods and grillage analysis methods have been incorporated into commercially available computer programs for curved bridge analysis and design. It is, therefore, believed that the mathematical complexities have largely been overcome associated with the analysis and design of curved girder bridges.

Construction of horizontally curved steel girder bridges is also generally more complex than construction of straight girder bridges of similar span. Curved girder bridges, once completely constructed, have performed well. Successful completion of a curved bridge, however, often requires that critical phases of construction be engineered so that the final structure has the proper geometry and dead load stresses assumed in the design. Curved girders are often erected based solely on experience, which has sometimes created unanticipated problems, which led to delays, disputes and or cost overruns.

9.1.1 Problem Statement

The earliest horizontally curved girder bridges in the United States were designed by using box sections composed of four plates. One of the first curved girder bridges was built in Springfield, Massachusetts in 1967. It had two simple spans approximately 88 and 130 ft, with a radius of 155 ft, and two boxes in the cross section. The bridge, which was inspected recently, was found to be in excellent condition after almost 30 years of service. The steel weight (approximately 90 lb/ft^2) is considered excessive by today's average weight of approximately 45 lb/ft^2 for a similar span.

Due to recent concerted efforts by the Federal Highway Administration (FHWA) and AASHTO (through National Cooperative Highway Research Program, NCHRP), there has been a significant improvement in the design specifications for horizontally curved steel girder highway bridges (Yoo 1996, Hall et al. 1999b). It seems fair to assess that the design provisions for curved I-girder bridges are reasonably complete. However, there remain a few areas in the design of curved box girders including adequate provisions guiding the proper design of compression flanges of curved box girders. In

general, steel box girders are composed of thin-walled plate components such as webs and flanges. The local buckling strength of the webs and the flanges could have a negative influence on the load carrying capacity of a box girder. More importantly, compression acting on the thin bottom flange causes the buckling action that is the major concern affecting the sizing of the longitudinal stiffeners. It is the impetus of this study to examine the proper design of compression flanges of curved box girders in the negative moment zones of continuous spans at interior piers. To help stiffen these areas, longitudinal stiffeners are placed inside the flange of the steel box girder. The longitudinally stiffened compression plate members render an economical structure by efficiently proportioning the material to resist the induced compressive forces. A longitudinally stiffened plate, therefore, generally yields a lightweight structure. Ultimately, there are two reasons for longitudinal stiffeners in box girder bridges. The first is to increase the buckling strength of the compression flange. The stiffener helps create a nodal line on the bottom compression flange in the buckled mode shape, so that it reduces the width-to-thickness ratio of the rectangular plate panel buckled between the longitudinal stiffeners. This reduction leads to a substantial increase in the buckling strength, since the buckling strength of plate panel is inversely proportional to the square of the width-to-thickness ratio. The second benefit of longitudinal stiffeners is to increase the effective moment of inertia of the cross section, thereby decreasing the bending stress. Although this is not the most effective way of increasing the moment of inertia of the box girder, longitudinal stiffeners do increase the moment of inertia.

9.1.2 Objective

Although a great deal of research has been devoted to developing design methods and equations, there appears to be not sufficient information available concerning the adequate design of stiffened compression flanges applicable to the horizontally curved box girder system. Recently, it was found that an old bridge (curved box girder approach spans to the Fort Duquesne Bridge in Pittsburgh) designed and built before the enactment of an AASHTO provision for the longitudinal stiffeners did not rate for modern day traffic, despite having served for many years.

The goal of this research is, therefore, to investigate analytically the buckling behavior of stiffened compression plates for a variety of parameters, establish the minimum required rigidity based on the elastic buckling approach and develop a design rule for straight and horizontally curved stiffened flanges taking into consideration for the ultimate loading state.

9.1.3 Organization

An extensive review of other research regarding behavior, strength, and design of stiffened plates is presented in Section 9.2. Section 9.3 commences with a detailed theoretical investigation concerning the design requirement of the stiffeners specified in the *AASHTO LRFD Bridge Design Specifications* (1998). This Section concludes with a proposal for a theoretical formulation for the minimum required stiffener rigidity.

An analytical investigation was conducted and is reported in Section 9.4. Extensive parametric studies were conducted concerning the buckling behaviors of stiffened compression plates by using a commercially available three-dimensional finite element solution MSC/NASTRAN (1992, 1994a, 1994b, 1997, 1998). Through the

parametric study, a definite concept of the minimum required rigidity of longitudinal stiffeners under a uniform compression force was established.

In Section 9.5, the induced static behaviors and stresses in horizontally curved box girders subjected to design loadings are discussed based on theoretically and analytically investigated results. In Section 9.6, stability characteristics of horizontally curved stiffened flange are investigated by using the analytical method.

In Section 9.7, the minimum required rigidity of longitudinal stiffeners for horizontally curved box girders is established.

In Section 9.8, geometric and material nonlinear analyses are used to investigate the design rules for longitudinal stiffeners under an inelastic buckling strength. The influence of the stiffener rigidity on the ultimate strength of a stiffened flange, along with the effect of any initial imperfections, is intensively investigated. Conclusions and recommendations are presented in Section 9.9.

9.2. Literature Review

9.2.1 Stiffened Flanges and Webs

Since webs and flanges are fabricated from thin-walled plate elements in modern box girders, the stability of these elements has a significant influence on the overall girder strength. Thus, the design method of stiffeners and the evaluation technique of the ultimate strength of the stiffened components of a box girder under compression have been and are being developed in various design specifications for steel girder bridges.

9.2.1.1 Elastic Buckling Method

Up until the 1960's, there were little specific design rules for steel box girders available since the box type girder was a relatively recent girder type and was not widely used. At the time, rules and procedures for the design of a plate girder web were also adopted in the design of a compression flange (SSRC, 1998).

Until the end of the 1960's, the general approach for the design of a plate girder was based strictly on the classical theory of linear elastic stability developed by Timoshenko (Timoshenko and Gere, 1961), Bleich (1952), and others (Bryan, 1891; Stowell et al., 1952; Gerard and Becker, 1957; Gerard, 1962).

An example of this trend can be found in the 1952 edition of German specification *DIN 4114*, where the general approach is based strictly on the classical theory of linear elastic stability. In this edition of the specification, the design of a flange follows the design rules for the web of a plate girder. The formulas for the required stiffener rigidity and for a buckling coefficient, k , developed for plate girder webs were also adopted for the flange. The inelastic strength of compact members under stresses close to the yield stress was considered by applying a transition curve based on the reduced modulus of elasticity, which was called "Engesser's buckling modulus" (Engesser, 1889).

In the early developmental stages, numerous studies on the instability of longitudinally stiffened flanges were conducted based on the linear elastic buckling theory. This theory adopted the concept of the instantaneous bifurcation of the load-deflection curve at the point of the critical buckling load, similar to the Euler load in the case of column buckling. Based on the elastic buckling theory, the stiffeners were mainly classified as either rigid stiffeners or flexible stiffeners. The rigid stiffeners were those

with “sufficient” rigidity to form a nodal line in a buckled mode shape, while the flexible stiffeners had a smaller rigidity and bent together with the embedded plate. In studies based on the classical buckling theory, it was commonly agreed that along with the stiffener stiffness, the strength of a stiffened plate converges to a non-stiffened plate strength corresponding to the same width-to-thickness ratio (Timoshenko and Gere, 1961).

Bryan (1891) presented an analysis of the elastic critical stress for a rectangular plate simply supported along all four edges and subjected to a uniform longitudinal compressive stress. In his study, the elastic critical stress of a long plate segment is determined by the plate width-to-thickness ratio and the restraint conditions along the longitudinal boundaries.

The important problem of the stability of rectangular plates supported on all four edges and reinforced with stiffeners was treated theoretically by Timoshenko (1921). According to Bleich (1952), Timoshenko was the first to consider the problem of the minimum rigidity required for the rigid stiffeners, and he established the theoretical relationship between the cross-sectional dimension of stiffeners and the critical value of compressive stresses by using his energy method as presented later (Timoshenko and Gere, 1961). Due to highly complex mathematical expressions used, the relationship could only be represented by numerical tables for a rather small range of factors, and was limited to the cases of one or two longitudinal stiffeners. These tables are neither simple to apply, nor sufficiently detailed to be used for a wide range of practical designs, and cannot readily be extended to investigate the buckling behavior of compression flanges stiffened with multiple longitudinal stiffeners.

Bleich (1952) derived an expression for the required moment of inertia of the longitudinal stiffener by combining the solution of a differential equation describing an overall buckled shape and the Bryan's elastic critical stress equation for simply supported plates. However, his results are limited to simply supported plates having one or two equally spaced stiffeners, and the procedures are much too complex to be suitable for a practical use.

At the beginning, most studies that evaluate the buckling strength and establish the relationship between the stiffener rigidity and the buckling stress were limited to compression flanges stiffened by one or two longitudinal stiffeners. These studies formed a basis for the design rules for a stiffened flange. However, similar research has never extended to the buckling behavior of compression flanges stiffened by multiple longitudinal stiffeners. To alleviate this limitation, the *Commentary on Criteria for Design of Steel-Concrete Composite Box Girder Highway Bridges* (unpublished committee report) was prepared by Mattock et al. in August 1967. These criteria were intended to supplement the provisions of *Division I, Design, of the 9th Edition of the Standard Specifications for Highway Bridges* (1965) of the American Association of State Highway Officials, Inc.

The equation for the required minimum stiffness for longitudinal stiffeners is given by Eq. (10-76) of the *16th Edition of the AASHTO Standard Specifications* (1996). Exactly the same requirement, Eq. (6.11.3.2.1-2), is stipulated in *the AASHTO LRFD Bridge Design Specifications* (1996). The required minimum stiffness for longitudinal stiffeners is

$$I_s = \Phi t_f^3 w \quad (9.1)$$

where $\Phi = 0.125 k^3$ for a value of $n = 1$ and $\Phi = 0.07 k^3 n^4$ for values of n greater than 1; t_f = thickness of the flange; w = width of the flange between longitudinal stiffeners or the distance from the web to the nearest longitudinal stiffener; n = number of longitudinal stiffeners; and k = bend-buckling coefficient, which shall not exceed 4. Although the equation may give a reasonable required value when the number of longitudinal stiffeners is less than or equal to two, the equation requires unreasonably large values when the number of longitudinal stiffeners becomes large.

Despite the practicing engineers' intuitive realization of the unreasonableness of the equation, it is still in force. Recently, it was found that an old bridge (curved box girder approach span to the Fort Duquesne Bridge in Pittsburgh) designed and built before the enactment of the criterion given by Eq. (9.1) did not rate for modern day traffic, despite having served for many years. The designer is compelled to use unnecessarily large stiffeners that are required by the existing criteria. The reasons for this were investigated in detail and are presented in Section 9.3. It was discovered that an erroneous process was adopted during the derivation of the equation by Mattock et al. in the interpretation of the overall buckling strength derived by Timoshenko and Gere.

Design rules proposed in Article 3.2.4 of the *Japanese Specifications for Highway Bridges* (1984) for the minimum moment of inertia of a longitudinal stiffener have a similar form to that of Bleich's equations. The flexural rigidity of the longitudinal stiffener is given by a ratio to that of the compression flange and the maximum value is limited as to ensure the local buckling (plate action) of the stiffened plate between its longitudinal stiffeners based on Giencke's study (1964).

9.2.1.2 Ultimate Strength Method - Strut Approach vs. Plate Approach

Three major collapses that occurred during the erection of box girder bridges, at Milford Haven (1970) in Wales, West Gate (1970) in Australia, and Koblenz (1971) in Germany, caused the entire basis of the design of box girders to be reviewed in Europe (H.M. Stationary Office, 1973; ICE, 1973) and in the United States (Wolchuk and Mayrbaur, 1980).

As a consequence of this renewed examination of the design of steel box girders, the development of “new” design approaches based on the ultimate load capacity was emphasized. The effects of initial imperfections on the ultimate strength also came under intense scrutiny at that time and are now being considered in modern design specifications throughout the world. The literature related to the effect of the geometric initial imperfection of stiffened flange plates will be treated in more detail in Section 9.8.

A strut (column action) approach that became widely used to evaluate the ultimate strength of a stiffened flange was simply based on an ultimate limit state in which the compression flange was believed to behave essentially as a column. The basis of this approach is to treat a compression plate stiffened by several equally spaced longitudinal stiffeners as a series of unconnected compression members or struts, each of which consists of a stiffener acting together with an associated width of the plate that represents the plate between stiffeners (Ostapenko and Vojta, 1967; Dwight and Little, 1976; Dowling and Chatterjee, 1977). The calculation of the inelastic buckling strength of the strut was obtained from a column formula. However, the strut approach cannot consider detailed interactions between the boundary conditions and the tension field membrane action.

The application of a strut approach for the design of a stiffened flange under an ultimate load was initiated in the U.K. The investigative committee looking into the box girder bridge collapses was chaired by A. W. Merrison. Hence, guidelines and rules resulted from the work of the committee for the design and construction of steel box girder bridges are usually referred to "Merrison Rules". The committee proposed *Interim Design and Workmanship rules (IDWR)*, a final draft for new design provisions otherwise known as the "Merrison Rules" method (H.M. Stationary Office, 1973a, 1973b, 1974). Several variations of the "column behavior" theory include the Merrison Rules, the "effective width" method (Horne and Narayana, 1975, 1976b; Chatterjee and Dowling, 1975, 1976), the "effective yield" method (Dwight et al., 1973, 1975; Dwight and Little, 1974, 1976; Little, 1976) and the "interaction diagram" method (Wolchuk and Mayrbaurl, 1980). All of the above cited research present extremely complex procedures to calculate the effective stiffener length to be incorporated in the column strength formula.

During the course of formulating the *IDWR* design rules, the effect of the geometric initial imperfection (Falconer and Chapman, 1953) was also considered. Falconer and Chapman discovered that the shape of a geometric initial imperfection had a critical influence on the strength of the plate and the most unfavorable shape was a sinusoidal imperfection with a half-wave length equal to the theoretical length of the buckled mode. In the investigation of the ultimate strength of the strut, the concept of tangent stiffness and the effect of residual stresses were also included. The limit state was considered to be reached either when the maximum stress on the surface of the plate reached its yield stress, or the maximum stress on the top of the stiffener reached the torsional buckling stress. The fabrication tolerances were specified for the required

flatness of the plate panels and the straightness of the stiffeners, although these were criticized by fabricators because they were quite elaborate and impractically small limit values. According to Wolchuk and Mayrbaur (1980), the *IDWR* design rules had never been incorporated in the interim draft of the British bridge specification mainly because of the huge volume of the provisions and the mathematical complexities.

In the strut approach presented in the U.K., the concept of effective width was developed to reflect the reduction of the ultimate strength caused by local buckling and shear lag, etc. Moffatt and Dowling (1972, 1975) studied the effective width of a box girder incorporating the shear lag phenomenon at an early stage. Subsequently, the reduced effective width of the plate due to local buckling was presented by Horne and Narayana (1976c). However, Lamas and Dowling (1980) later concluded from the numerical studies that shear lag could be ignored in calculating the ultimate compression strength of stiffened flanges (*SSRC*, 1998).

The design rules for the stiffened compression flange of box girders presented in the *BS 5400* (1982) are the final draft of the British specification. In this specification, several simplifications, such as a simple effective width approach, were introduced. The effective width used in *BS 5400* was derived from a series of parametric studies, which took into account for the practicality of the provisions by simplifying the effects of the initial imperfections and residual stresses.

After the Koblenz bridge disaster, the concept of the effective width was incorporated into the German specification. Design rules based on this approach were published in the *Interim DIN 4114* (1973), which mandated an ultimate strength analysis

for columns and included fabrication tolerances and erection imperfections, especially for the stiffeners.

Wolchuk and Mayrbaur (1980) proposed design criteria for stiffened flanges based on the strut approach using an interaction diagram method. The interaction diagram was set up based on theoretical works by Little (1976). Little (1976) conducted an inelastic column buckling analysis of the strut panel model using an improved iterative numerical method for the moment-curvature relationship. An initial out-of-straightness of $L/500$ for longitudinal stiffeners and the effect of residual stresses were considered where L being the column length. From this analytical study, various strength curves for stiffened panels were drawn including the effect of various parameters. Taking an average of these various strength curves, a representative strength curve was constructed.

Dwight and Little (1974) are credited to be the first who developed an expression for the plate strength curve of a stiffened flange panel taking into account the residual stress and the out-of-flatness of the flange panel between stiffeners. The strength curve was reflected in the interaction diagram developed by Wolchuk and Mayrbaur (1980), but their work was not adopted by AASHTO although a commentary referring the work has been included in AASHTO LRFD Bridge Design Specifications (1996).

9.2.1.3 Ultimate Strength Method Based on Elastic Buckling with a Factor of Safety

After the 1970s, an ultimate strength limit state was widely considered for the design of box girder bridges as mentioned earlier. However, shortly thereafter, it became clear that the design methods based on the ultimate strength were unlikely to be sufficiently developed for immediate practical use and could not be verified

comprehensively (Scheer and Nölke, 1976; ECCS, 1976). It appeared at that time that it would take a long while to develop completely reliable design method based on an ultimate strength limit state.

In order to alleviate the time constraint associated with the development of the design rules based on the ultimate strength in a stiffened flange, several design specifications, including the German specification, tried an interim design method by applying a factor of safety to the buckling strength of the component being designed, whereas the British specification adhered to the strut approach.

Scheer and Nölke (1976) stated that in Germany “confidence in the methods of bridge design based on the linear theory had not been diminished” and they also insisted that the *DIN 4114* (1952) Specifications were not directly responsible for the construction failures. The design philosophy based on the linear elastic theory was reflected in the new provisions contained in *DAST Richtlinie* (1978) (Wolchuk and Mayrbaurl, 1980). And the probable discrepancy between the actual load capacity and the buckling critical load was supposed to be reduced by the suggested factors of safety.

In *DAST Richtlinie* (1978), the strength of the stiffened plate was determined from the interaction diagram of the plate strength curve and the European column curve, which reflect the local plate buckling and the overall column buckling of the stiffened plate, respectively. The provisions included the tolerance limits for structural imperfection, which were essentially similar to those used in the British specification, *BS 5400*. The tolerance limits were given as 1/250 of the shorter dimension of the unstiffened panel for the maximum deviation from flatness and 1/500 of the stiffener length for the out-of-straightness of stiffeners.

The European Convention for Constructional Steelwork (1976) also proposed in their design recommendation manual, *Manual on the Stability of Steel Structures* an original design method to reflect the ultimate strength state of a wide, stiffened flange based on an elastic buckling theory. A “correction coefficient” approach was introduced as a convenient way to account for the discrepancy between the ultimate strength and the elastic critical buckling strength for the stiffened flange plate.

However, the process of selecting a valid correction coefficient was too simple as to be practical, because it did not reflect a variety of influential parameters that must be considered. The rules included a table of fabrication tolerances, which were actually the same as that in German specifications.

9.2.1.4 Modern Ultimate Strength Analysis

When the currently available design rules were derived, a comprehensive ultimate strength analysis capability was not fully developed. There were no simple, and comprehensive, practical, and reliable design rules available for a stiffened flange based on the ultimate strength state.

The finite element method can be used for general nonlinear analyses, which include an ultimate strength analysis or large deflection analysis, a variety of nonlinear stress-strain relations, and geometric nonlinear formulations such as Total Lagrangian or Updated Lagrangian techniques.

Nowadays, advanced general-purpose finite element analysis packages such as NASTRAN, ADINA, ABAQUS, ANSYS, and other proprietary codes have extensive structural modeling capabilities that include elastic buckling analysis and geometric and

material nonlinear analysis. Numerical data generated in this study are primarily based on a number of NASTRAN runs.

9.2.2 Stress Evaluation in Horizontally Curved Box Girders

Few studies have been performed so far and sufficient useful information has not been available for the development of comprehensive design rules for a horizontally curved stiffened flange. Vertical bending and torsional actions are always coupled in a horizontally curved beam under a simple vertical loading. This is the primary source of the mathematical complexity in the analysis of the curved girder.

The externally applied torsion to a bridge girder is resisted internally by a combination of St. Venant torsion and warping torsion. Warping torsion is the dominant resisting torsion in a girder with an open section and St. Venant torsion resists the externally applied torsion in a girder with a closed cross section. The stress distribution in a stiffened flange of a horizontally curved box under a vertical loading, such as that experienced by a bridge due to the passage of vehicles and its own dead weight, results in a combination of flexural stresses, St. Venant torsional shear stress, distortional normal stress, and perhaps warping torsional normal stress of a lesser degree.

The load deformation response of curved girders with an open section, which considers the combination of bending, torsion and warping deformations, was established by Vlasov (1961). Dabrowski (1964) later modified Vlasov's equations to obtain the correct displacement in the plane of curvature and he (1965) further presented the fundamental equations for the torsional warping of a curved box girder. As a result of the rapid advances in digital computers and numerical techniques, difficulties in the practical

application of curved girder theories due to their mathematical complexity have been alleviated.

It is believed that the torsional warping was included in a matrix formulation of a horizontally curved beam element by Yoo (1979) for the first time. Kang (1992) and Kang and Yoo (1994a, 1994b) extended Yoo's work further in a finite curved beam element including the warping in order to apply it to the bifurcation buckling and large displacement analyses, as well as the linear static analysis.

As a consequence of classical beam theories adopted in these formulations, these elements can only be used to predict the behavior of a rigid box girder section when the box sections are assumed to retain their original shape during the load-deformations history by assuming a liberal placement of internal cross-frames. However, the placement of internal cross-frames is a very costly item in bridge building and hence, the cross-frames are usually placed at an interval balancing the cost-benefit consideration. Therefore, it becomes quite important to correctly understand the fundamental distortional behavior in the design and analysis of curved box girder bridges.

Since complex refined analytical methods are difficult to apply in a practical design process, Wright et al. (1968) developed a method to analyze the box girder distortion based on beams on elastic foundations (BEF Analogy) analogy. They were subsequently able to approximately evaluate the induced distortional stresses and suggested graphical presentations of the effects of design parameters (Heins and Hall, 1981).

Dabrowski (1968) is credited as being the first to develop a differential equation to predict the distortion in a curved box girder. The cross-sectional angular deformation

due to the distortion was included in the governing differential equation. The induced normal and shear stresses due to the cross-sectional angular deformation were determined from the solution of the differential equation. Based on the study, he suggested a method for the spacing of the cross-frames to limit the level of the induced stresses.

Since a distortional deformation and the induced distortional stresses can produce detrimental effects that are difficult to include in a design process, most recommended specifications require that the distortional stresses be controlled, by the proper placement of internal cross-frames, to be within a specified ratio of the vertical bending stress (Japanese Road Association, 1980, AASHTO Guide Spec, 1993, Hall and Yoo, 1998).

Oleinik and Heins (1975) conducted a series of parametric studies to investigate the required spacing of the internal cross-frames. In a later paper, Heins (1978) proposed a simplified design equation for the diaphragm spacing and the required stiffness. Nakai and Miki (1980) tried to improve the accuracy in calculating the induced stresses due to distortion in a curved box girder section by applying the transfer matrix method to the fundamental differential equation. Sakai and Nagai (1977) developed a series of equations for the diaphragm spacing, l_D , for straight box-girder bridges and also proposed an equation for the required rigidity of the diaphragm. Nakai and Murayama (1981) proposed an equation for the determination of the diaphragm spacing for the curved box-girder bridges based on an extension of Sakai and Nagai's study.

Yabuki and Arizumi (1989) examined a series of parametric studies on the distortional warping response of the curved box girders using the BEF analogy and suggested a simple method for the spacing of internal diaphragms. The parametric studies were conducted using the section properties of several bridges with curved box-

girders actually constructed in Japan. Hsu et al. (1995) developed a modified approach called the EBEF, equivalent beam on elastic foundations, to overcome the limitations of the BEF analogy. In the equivalent beams on elastic foundation analogy, the procedural difficulty associated with non-prismatic beams and continuous spans can be treated readily.

Although there have been many studies of the distortion of a box girder, sufficiently detailed information for a practical application is still lacking to determine the induced stresses in a flange, especially in a curved box girder flange. Additionally, there still exist considerable discrepancies among the currently available methods. As a rapid development in digital computer technologies continues, a variety of advanced numerical techniques including the finite element method can be an attractive tools to advance analytical investigations on many aspects of the behavior of horizontally curved girders as was done by Davidson et al. (1996, 1999a, 1999b, 1999c, 1999d) and Lee and Yoo (1999). The induced stress analysis presented in this study in Section 9.5 is conducted through an extensive use of NASTRAN runs.

9.3. Theory on Stiffened Plates

9.3.1 Introduction

As briefly introduced in Chapter 2, the current AASHTO Eq. (10-138) was originated from a study by Timoshenko and Gere (1961). However, as mentioned in Chapter 2, the reasonableness of the equation was questioned. In this chapter, the validity of the equation is closely examined and the reasons why the equation does not provide a reasonable design are traced in detail. The theory (Timoshenko and

Gere, 1961) of stiffened plates is examined using this new perspective and a modified theoretical equation is formulated.

9.3.2 Timoshenko and Gere's Theory

Timoshenko and Gere (1961) conducted a series of theoretical investigation on stability of simply supported rectangular plates stiffened with longitudinal stiffeners. A typical plan view of the simply supported rectangular plate, which was considered in their study, is represented in Fig. 9.1. For this case, they described the deflection surface of the buckled plate in the form of a double trigonometric series as

$$v = \sum_{m=1}^{m=\infty} \sum_{n=1}^{n=\infty} a_{mn} \sin \frac{m\pi x}{a} \sin \frac{n\pi y}{b} \quad (9.2)$$

where, a = length of compression flange and b = whole width of flange.

The corresponding strain energy of bending of the plate is

$$\Delta U = \frac{\pi^4 D}{2} \frac{ab}{4} \sum_{m=1}^{m=\infty} \sum_{n=1}^{n=\infty} a_{mn}^2 \left(\frac{m^2}{a^2} + \frac{n^2}{b^2} \right) \quad (9.3)$$

where, $D = \frac{Et_f^3}{12(1-\nu^2)}$ and it is called the flexural rigidity of the plate; t_f =

compression flange thickness; E = modulus of elasticity; ν = Poisson's ratio (0.3 for steel). Assuming a general case of several longitudinal stiffeners and denoting by EI_i the flexural rigidity of i^{th} stiffener at the distance c_i from the edge, $y = 0$, the strain energy of bending of each stiffener, when buckled together with the plate, is given by Eq. (9.4).

$$\Delta U_i = \frac{EI_i}{2} \int_0^a \left(\frac{\partial^2 v}{\partial x^2} \right)^2_{y=c_i} dx$$

$$= \frac{\pi^4 EI_i}{4a^3} \sum_{m=1}^{m=\infty} m^4 \left(a_{m1} \sin \frac{\pi c_i}{b} + a_{m2} \sin \frac{2\pi c_i}{b} + \dots \right)^2 \quad (9.4)$$

where, I_i = moment of inertia of each stiffener and c_i = distance between the i^{th} stiffener and an edge of the plate. The work done during buckling by the compressive forces N_x acting on the plate becomes

$$\Delta T = \frac{N_x}{2} \frac{ab}{4} \sum_{m=1}^{m=\infty} \sum_{n=1}^{n=\infty} \frac{m^2 \pi^2}{a^2} a_{mn}^2 \quad (9.5)$$

The work done during buckling by the compressive force P_i acting on a stiffener is

$$\Delta T_i = \frac{P_i}{2} \int_0^a \left(\frac{dw}{dx} \right)^2_{y=c_i} dx \quad (9.6)$$

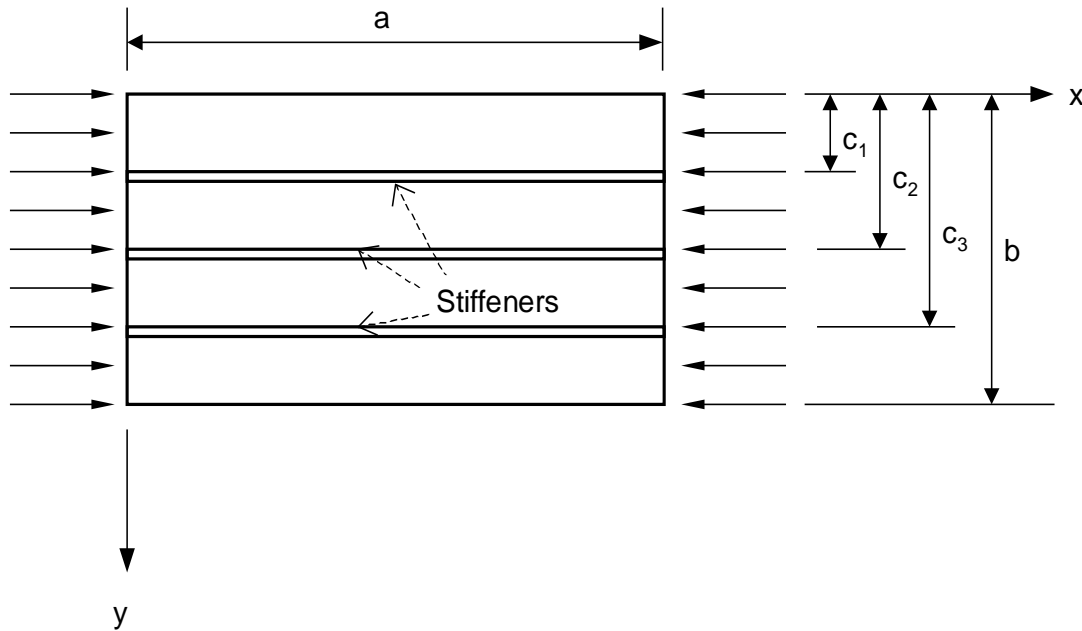


Fig. 9.1. Longitudinally Stiffened Plate

The general equation for calculating the critical stress is expressed as

$$\Delta U + \Delta \sum_i U_i = \Delta T + \Delta \sum_i T_i \quad (9.7)$$

Using the notations,

$$\frac{a}{b} = \beta \quad (9.8)$$

$$\frac{E I_i}{bD} = \gamma_i \quad (9.9)$$

$$\frac{P_i}{bN_x} = \frac{A_i}{bt_f} = \delta_i \quad (9.10)$$

where β is the aspect ratio for the entire width of the bottom flange, bt_f is the cross-sectional area of the plate and A_i is that of one stiffener. Equating to zero the derivatives of Eq. (9.7) with respect to coefficients, a_{mn} , a system of homogeneous linear equations of the following type can be obtained.

$$\begin{aligned} & \frac{\pi^2 D}{b^2 h} \left[a_{mn} (m^2 + n^2 \beta^2)^2 + 2 \sum_i \gamma_i \sin \frac{n \pi c_i}{b} m^4 \sum_{p=1}^{p=\infty} a_{mp} \sin \frac{p \pi c_i}{b} \right] \\ & - \beta^2 \sigma_{cr} \left(m^2 a_{mn} + 2 \sum_i \delta_i \sin \frac{n \pi c_i}{b} m^2 \sum_{p=1}^{p=\infty} a_{mp} \sin \frac{p \pi c_i}{b} \right) = 0 \end{aligned} \quad (9.11)$$

where m and n represent the number of terms in the assumed deflection shape expressed by a double sinusoidal series. By assuming the value of m is equal to one and then equating to zero the determinant of this system of equations, two types of equations for the critical stress are obtained. One type of the equations corresponds to the case when value of n is equal to a multiple of the number of longitudinal stiffeners used plus one. The critical stress from this type of equations represents the buckling stress of the plate panels between the longitudinal stiffeners in an anti-

symmetric mode (plate action) where longitudinal stiffeners remain straight. It can be shown that the lowest critical stress obtained is given by Eq. (9.12).

$$F_{cr} = \frac{\pi^2 D}{b^2 t_f} \frac{(1 + (n' + 1)^2 \beta^2)^2}{\beta^2} = \frac{\pi^2 D}{w^2 t_f} \frac{(1 + \alpha^2)^2}{\alpha^2}$$

$$= \frac{p^2 D}{w^2 t_f} \frac{1}{\alpha^2} + \frac{4}{3} \frac{p^2 D}{w^2 t_f} \quad (9.12)$$

where, n' = number of longitudinal stiffeners; α = aspect ratio of a plate panel between longitudinal stiffeners; F_{cr} = critical compressive stress. From Eq. (9.12), it becomes evident that the most critical stress is given by Eq. (9.13) corresponding to an aspect ratio equal to one.

$$F_{cr} = \frac{4}{3} \frac{p^2 D}{w^2 t_f} \quad (9.13)$$

Eq. (9.13) is identical to the classical plate critical stress equation presented by Bryan (1891). The other type of equations is associated with the symmetric buckling shape (strut action) in which the stiffeners buckle along with the plate. Taking only the first term associated with a_{11} from the system of equations, Eq. (9.11), it can be shown that an approximate equation for F_{cr} can be written as

$$F_{cr} = \frac{\pi^2 D}{b^2 t_f} \frac{(1 + \beta^2)^2 + 2 \sum_i \gamma \sin^2 \frac{\pi c_i}{b}}{\beta^2 \left(1 + 2 \sum_i \delta \sin^2 \frac{\pi c_i}{b} \right)} \quad (9.14)$$

Timoshenko and Gere concluded that the approximation given by Eq. (9.14) is fairly accurate for longer plates, say for $\beta > 2$ and for shorter plates, a larger number of terms from Eq. (9.11) must be considered.

9.3.3 Mattock's Work

Mattock et al. proposed Eq. (9.1) for the minimum required moment of inertia of longitudinal stiffeners, which was first adopted in 1965 by AASHTO (1965).

According to the unpublished committee report (Grubb, 1999), *The Commentary on Criteria for Design of Steel-Concrete Composite Box Girder Highway Bridge* (1967), the basis for Eq. (9.1) appears to be Eq. (9.14). In Mattock's work, the terms of Eq. (9.14) for n longitudinal stiffeners spaced equally were expressed in a different way as follows:

$$2 \sum_i \gamma \sin^2 \frac{\pi c_i}{b} = (n+1)\gamma \quad (9.15)$$

and

$$2 \sum_i \delta \sin^2 \frac{\pi c_i}{b} = (n+1)\delta \quad (9.16)$$

By taking the derivative of Eq. (9.14) with respect to β^2 , and setting it equal to zero, the critical value for β was determined to be:

$$\beta_{cr} = \sqrt[4]{1 + (n+1)\gamma} \quad (9.17)$$

The plate buckling coefficient in Eq. (9.14), k_{min} , was obtained by substituting Eqs.

(9.15) to (9.17) into Eq. (9.14) as below:

$$k_{min} = \frac{2 \cdot \left[\sqrt{1 + (n+1)\gamma} + 1 \right]}{(n+1)^2 [1 + (n+1)\delta]} \quad (9.18)$$

A value of γ corresponding to k_{min} was determined for a given stiffened plate, which led to a corresponding minimum value of the moment of inertia of longitudinal stiffeners, I_s .

Table 9.1. Buckling Coefficient, k , according to the AASHTO Design Equation

Number of Stiffeners	Assumed value of " k "	Φ $= .07k^3n^4$	Value of " k " Calculated by Elastic Theory for $I_s = \Phi t^3 w$
2	1	1.1	0.91
2	2	8.9	1.91
2	3	30.3	3.03
2	4	71.8	4.15
3	1	5.7	0.90
3	2	45.5	1.98
3	3	153.0	3.05
3	4	362.0	4.12
4	1	17.9	0.89
4	2	143.0	1.92
4	3	482.0	2.89
4	4	1140.0	3.75
5	1	43.8	0.87
5	2	350.0	1.82
5	3	1180.0	2.65
5	4	2800.0	3.63

In Table 9.1, values of the plate buckling coefficient, k , that were yielded from Eq. (9.18) by inserting the stiffener stiffness calculated from Eq. (9.1) are compared with the initially assumed k to compute the coefficient, Φ . It can be seen from Table 9.1 that the k values calculated from Eq. (9.1) are very close to the initially assumed values. Thus, Table 9.1 was presented as evidence supporting the validity of Eq. (9.1)

9.3.4 Current AASHTO Provision

Although Eq. (9.1) appears to be verified through Table 9.1, it is known that Eq. (9.1) requires an unreasonably high stiffness for longitudinal stiffeners. The reasons for this unreasonableness of Eq. (9.1) are examined below.

9.3.4.1 Errors in Mattock's Work

The influence of the aspect ratio a/w (α) of the plate panel between longitudinal stiffeners is not included in Eq. (9.1). Despite this parameter is obviously associated with the notation β , it was removed during the derivation process of Eq. (9.1) for the critical aspect ratio for the entire width of the flange, β_{cr} , by Mattock et al. as they erroneously assumed that the consideration of β_{cr} only was sufficient to include every conceivable case of plate configurations. The β_{cr} was determined inexplicably too high. Using a trial and error process based on data for I_s determined from a series of Eqs. (9.9), (9.17), and (9.18), they extracted Eq. (9.1) without incorporating the parameter relating the plate aspect ratio. As a result, Eq. (9.1) provides an equal stiffener stiffness for plates of different aspect ratio if n and k are not varied, regardless of the actual aspect ratio of a stiffened plate. According to a series of parametric studies presented in Section 9.4,

however, it is shown that the aspect ratio, α , is an important influential parameter for the required stiffener stiffness.

From Eqs. (9.9), (9.17), (9.1), and (9.19), the proper expression for β_{cr} can be derived as follows:

$$\gamma = \frac{EI_s}{bD} = \frac{EI_s}{(n+1)w} \left[\frac{12(1-\mu^2)}{Et_f^3} \right] \quad (9.9)$$

Substituting 0.3 for the Poisson's ratio for the steel into Eq. (9.9), gives

$$\gamma = \frac{10.92 I_s}{(n+1)wt_f^3} \quad (9.19)$$

Substituting Eqs. (9.1) and (9.19) into (9.17), yields

$$\beta_{cr} = \sqrt[4]{1 + (n+1)\gamma} = \sqrt[4]{1 + \frac{10.92 I_s}{wt_f^3}} = \sqrt[4]{1 + 10.92 \Phi} = \sqrt[4]{1 + 10.92 (0.07 k^3 n^4)},$$

which reduces to

$$\beta_{cr} = \sqrt[4]{1 + (0.7049 k^3 n^4)} \quad (9.20)$$

Since $\beta = \frac{a}{b} = \frac{\alpha w}{(n+1)w} = \frac{\alpha}{(n+1)}$, the critical aspect ratio becomes:

$$\alpha_{cr} = (n+1)\beta_{cr} \quad (9.21)$$

As can be seen in Eq. (9.21), the critical value is determined only by n and k .

The relationships between α_{cr} and n and k are presented in Table 9.2. It can be observed from Table 9.2 that the value of α_{cr} is greatly influenced by n or k . Since it was assumed by Mattock et al. that the plate strip could be infinitely long, the critical aspect ratio α_{cr} must have been considered in the derivation process of Eq.

(9.1). Since the parameter α was excluded in the process, however, the huge difference in the required moment of inertia of longitudinal stiffeners appears inherent. It was found from a series of the parametric studies that the influence of the number of longitudinal stiffeners n on the required stiffener stiffness did not reach very much to the level shown in Eq. (9.1).

Table 9.2. Variation of α_{cr} with n and k

Number of Stiffeners	Assumed value of "k "	Value of "k " Calculated for $I_s = \Phi t^3 w$	α_{cr}
2	1	1.87	5.62
2	2	3.09	9.27
2	3	4.18	12.54
2	4	5.19	15.56
3	1	2.76	11.04
3	2	4.63	18.50
3	3	6.27	25.07
3	4	7.78	31.10
4	1	3.67	18.35
4	2	6.17	30.83
4	3	8.36	41.78
4	4	10.37	51.83
5	1	4.58	27.50
5	2	7.71	46.23
5	3	10.44	62.66
5	4	12.96	77.75

In most practical structures, longitudinal stiffeners are braced by transverse stiffeners. These members help to control the transverse bending stress due to bend buckling and the additional longitudinal stress due to distortions of the cross sections. Therefore, the requirement for the transverse stiffeners is not unduly demanding.

9.3.4.2 Limitation in Available Timoshenko and Gere's Equation

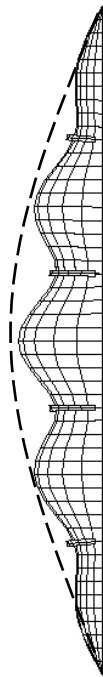
Timoshenko and Gere (1961) stated that Eq. (9.14) provides an acceptable critical stress for sufficiently long stiffened plates. It was found from a series of the finite element analyses that Eq. (9.14) considerably overestimates the elastic stability of stiffened plates when β has a value under 2, particularly less than 1. This discrepancy is attributed to the inadequacy of the assumed deflection shape of buckled stiffened plates. Though the deflection shape of the buckled plate was taken to follow the form of a double trigonometric series by Timoshenko and Gere (1961), it was assumed in the derivation process of Eq. (9.14) that the stiffened plate buckles into a sinusoidal shape, and only the first term in the double trigonometric series was used to derive the simplified form of this Eq. (9.14). However, for some cases, this simplified deflection shape might be considerably different from the most critical mode shape, particularly for a plate of small aspect ratio, say $\beta < 1$. The comparison of the bucking mode shape and the critical stresses are given in Fig. 9.2 and Table 9.3.

Therefore, to extract a design equation from Eq. (9.14) could cause an incorrect design for the range of β values less than 1 due to the assumption of the incompatible deflection shape. Although this limitation does not greatly affect the required minimum moment of inertia for the longitudinal stiffener, nevertheless, it does affect the reasonableness of I_s .

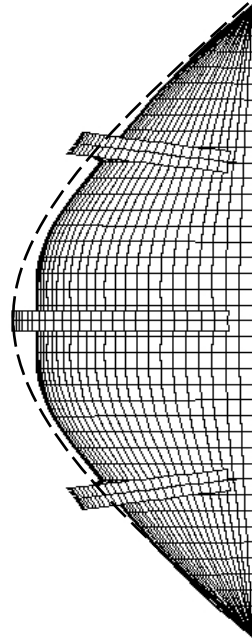
Table 9.3. Comparison of F_{cr} (ksi) from FEM Analysis and Eq. (9.14)

β	n	α	w (in.)	t_f (in.)	w/t	I_s , Used	F_{cr} , Eq. (9.14)	F_{cr} , F.E.M	Diff. (%)
0.2	4	1	80	1	80.0	23.3	16.928	14.565	16.22
1.25	3	5	60	1	60.0	527.2	18.030	17.081	5.56
1.25	3	5	60	1	60.0	626.5	29.758	27.649	7.63
2.5	1	5	80	1.25	64.0	1086.3	27.988	26.650	5.02

----- Assumed Deflection Shape in Eq. (9.14)



$\beta=0.2$, n=4.



$\beta=1.25$, n=3.

Fig. 9.2. Buckling Mode Shapes from F.E.M Analysis

9.3.5 Theoretical Formulation of Design Equation

Timoshenko and Gere's series equations obtained from the determinant of the system equations of Eq. (9.11) can be made available for the stiffened plates of a finite length. According to Timoshenko and Gere's (1961) theory, a stiffened plate buckles in one of the two types of modes. Eq. (9.13) gives the critical strength of stiffened plates buckled in an anti-symmetric mode shape (plate action). Eq. (9.14) represents the symmetric mode buckling (strut action). Eq. (9.14) has a linear relationship with γ which is a function of I_s . Depending upon the value of I_s , the critical stress given by Eq. (9.14) can be high or low.

The equation for the minimum required moment-of-inertia of longitudinal stiffeners can be derived by setting Eq. (9.13) equal to Eq. (9.14) as follows:

$$\frac{\pi^2 D}{b^2 t_f} \frac{(1 + \beta^2)^2 + (n+1)\gamma}{\beta^2(1 + (n+1)\delta)} = \frac{4\pi^2 D}{w^2 t_f} \quad (9.22)$$

Eq. (9.22) is further simplified to

$$\frac{(1 + \beta^2)^2 + (n+1)\gamma}{\alpha^2(1 + (n+1)\delta)} = 4 \quad (9.23)$$

Therefore,

$$\gamma = \frac{4\alpha^2(1 + (n+1)\delta) - (1 + \beta^2)^2}{(n+1)} \quad (9.24)$$

Substituting Eq. (9.9) into Eq. (9.24) and rearranging, yields,

$$I_s = \frac{w t_f^3}{12(1 - \mu^2)} \left[4\alpha^2(1 + (n+1)\delta) - (1 + \beta^2)^2 \right]$$

$$\begin{aligned}
&= \frac{4\alpha^2 w t_f^3}{12(1-\mu^2)} \left[1 + (n+1)\delta - \frac{(1+\beta^2)^2}{4\alpha^2} \right] \\
&= \frac{\alpha^2 w t_f^3}{3(1-\mu^2)} \left[1 + \frac{A_s}{w t_f} - \frac{I}{4\alpha^2} \left(1 + \left(\frac{\alpha}{n+1} \right)^2 \right)^2 \right] \tag{9.25}
\end{aligned}$$

Eq. (9.25) gives the required moment-of-inertia for longitudinal stiffeners to ensure that the plate buckling stress given by Eq. (9.13) is attained regardless of the type of buckling mode shape. The terms within the square bracket do not affect the value of I_s given by Eq. (9.25) significantly. It is, therefore, evident that the expression of Eq. (9.25) excluding the square bracket terms contains every major parameters included in the regression equation obtained from a series of finite element analyses presented in Section 9.4.

9.4. Buckling of Straight Stiffened Plates

9.4.1 Introduction

The validity of Eq. (10-138) of the 16th Edition of the AASHTO Standard specifications (1996) has been thoroughly examined in Section 9.3 including the range of its applicability and the potential sources of discrepancies that might have been hidden from the simplifying process adopted. It was concluded that the equation does not provide a rational design guide, particularly for flanges stiffened by multiple longitudinal stiffeners. Through extensive literature review and theoretical studies, it was found that none of the existing studies could lead to formulate a simple yet reasonable design guide for longitudinally stiffened flanges of box girder. In order to provide a reliable design

guide to this very important area in the steel box girder design, a multi-year comprehensive research project has been initiated at Auburn University.

The objective of the study presented in this Section is thus to identify significant design parameters and to formulate criteria for use in the practical design of longitudinally stiffened flanges. The elastic buckling analysis was performed on a number of hypothetical stiffened plate models by using the finite element commercial software package, MSC/NASTRAN. An extensive parametric study was conducted on the collected data. In the parametric study, an attempt was made to retain the parameters identified in Eq. (9.25). The detailed procedure for the derivation of the regression equation for the minimum required moment-of-inertia was given by Ford (2000) and the highlight of the regression equation and its application to actual problems was published (Yoo et al., 2001). Therefore, only the relevant portions of the procedure will be illustrated in this chapter just to maintain the continuity of the flow of logic.

9.4.2 Exploratory Modeling

The reason for implementing finite element analysis to numerically extract data in this research was to have a method that was not as complex as using analytical solutions. Since the stiffeners are located only on one side (interior of the box girder bottom flange) of the plate and the compressive stress developed in the flange is due to vertical bending of the box girder, the stiffeners are considered to be loaded eccentrically. Analytical solutions for structures loaded in such a manner become rather involved and much more time consuming. Therefore, the finite element numerical analysis was executed, and as a result, allowed many different parameters to be analyzed in the development of a regression formula.

From the data produced in the finite element numerical analysis, it became obvious that narrow rectangular sections could not be used. The width-to-thickness ratio of the longitudinal stiffener limited to avoid the premature local buckling failure following the current AASHTO (1996) provision (Eq. (10-88)). The limiting width-to-thickness ratio of the unstiffened element of the flange stiffener is given by Eq. (9.26).

$$\frac{b'}{t'} = \frac{2600}{\sqrt{F_y}} \quad (9.26)$$

where b' = width of outstanding stiffener element; t' = thickness of outstanding stiffener element, and F_y = yield stress of outstanding stiffener element (psi). This is graphically shown in Fig. 9.3.

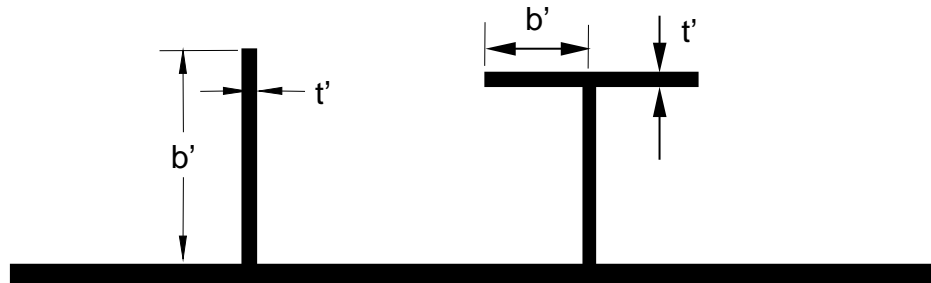


Fig. 9.3. Compression Flange Showing Rectangular and T-section Stiffeners

Over 360 finite element models were run using the rectangular shaped stiffener. The thickness and width of the stiffener were varied from 0.5" to 1.0" and from 5.0" to 12.0", respectively. The aspect ratio, a/w , of the subpanels of the

compression flange was varied from 1 to 5. Upon examination of the results from these model analyses, it became evident that this stiffener shape was not optimal. The torsional rigidity of rectangular stiffeners is much less than that of structural tees (WT). The bending rigidity of tee-shape stiffeners of the same total cross-sectional area is also larger than that of rectangular stiffeners. In fact, Kerensky (1973) discourages the use of flat-plate stiffeners for compression members, due to decreased torsional rigidity and bending stiffness.

After realizing the efficiency of tee-shape stiffeners, more than 540 hypothetical models were analyzed, varying the thickness of the compression flange from .75 to 2.5 inches. The size of tee-shape stiffeners was also varied following the thickness of the compression flange. The largest WT being a WT20x87, and the smallest being a WT2x6.5, which were selected from the AISC LRFD (2001). The thicknesses of the tee-shape stem and the top flange were varied from .375 to 2.5 inches and from 0.375 to 5.0 inches, respectively. The aspect ratio of the subpanel of the compression flange ranged from 1 to 5. In most cases, the thickness of the stiffener for the rectangular shape and the stem on the tee-shape stiffeners was held to be less than or equal to the compression flange thickness. In a few trial cases, this value was increased up to twice the thickness of the compression flange.

9.4.3 Modeling of Compression Flange

The three-dimensional finite element model used to represent the compression flange was represented as a single plate. Fig. 9.4 shows a typical compression flange with one tee-shaped stiffener. In this example, the aspect ratio of the subpanel, a/w , is

equal to two. Fig. 9.5 shows the buckled shape of the model. In order to simulate the connection between the web plates and the compression flange as simply supported one, the following constraints were imposed: The plate was restrained at the outside edge parallel to the longitudinal direction from moving in the x direction. On the loaded edge, a constraint was imposed to prevent the transverse movement (y-direction) of the plate at the midpoint of the plate edge. All other edge nodes were restrained in the z-direction to prevent out-of-plane displacements. The orientations of the coordinates are given in Figs. 9.4 and 9.5. These constraints allowed the compression flange to “pull-in” and rotate. A concentrated load was applied at each node on the loaded edges and at each end node of the stiffener simulating the stress distribution induced by the vertical bending. It has been reported by Ford (2000) and Yoo et al. (2001) that this simplified flat plate model can represent the actual boundary condition at the juncture between the web and the flange up to 96 percent accuracy.

After a series of exploratory runs to examine the convergence characteristics, it was decided that a 4-node plate/shell element, NASTRAN/CQUAD4, was deemed adequate to represent the plate and stiffeners for the model where at least ten subdivisions were employed per each side of the subpanel. The stress-strain relationship was assumed to be linear and isotropic in these analyses.

Additional cases were also analyzed using a bilinear stress-strain relationship to examine the inelastic strength of the stiffened compression flanges. The inelastic strength investigation is presented in detail in Section 9.8.

9.4.4 Minimum Required Stiffener Rigidity

Examination of the data collected from the analyses revealed that that the critical stresses and the buckling mode shape of a stiffened plate are sensitively influenced by the moment of inertia of longitudinal stiffeners. When the bending rigidity of the longitudinal stiffener is small, the longitudinal stiffener does bend along the entire buckled surface of the panel, which has a symmetric mode shape about the centerline of the whole width. The critical stress of the stiffened panels varies almost linearly with respect to the bending rigidity of the longitudinal stiffener up to the threshold value for an anti-symmetric buckling as shown in Fig. 9.6. This type of buckling action is referred to as the column behavior in the U.K and the buckling mode shape was sometimes called the symmetric buckling.

When the bending rigidity of the longitudinal stiffener is increased beyond a certain limiting value, the plate subpanels buckle between the longitudinal stiffeners. In this type of buckling mode shape, clearly discernible nodal lines form along the longitudinal stiffener and the longitudinal stiffener remains straight. Once this type of buckling action is attained, there is no more appreciable increase in the buckling stress corresponding to the increase of the bending rigidity of the stiffeners. This action is referred to as the plate behavior and is sometimes called the anti-symmetric buckling. The symmetric (strut action) and/or anti-symmetric buckling (plate action) used herein is

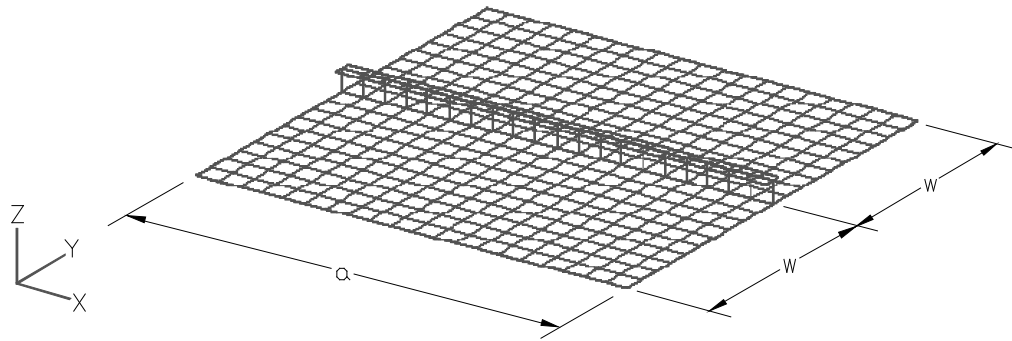


Fig. 9.4. Undeformed Shape of Typical Compression Flange

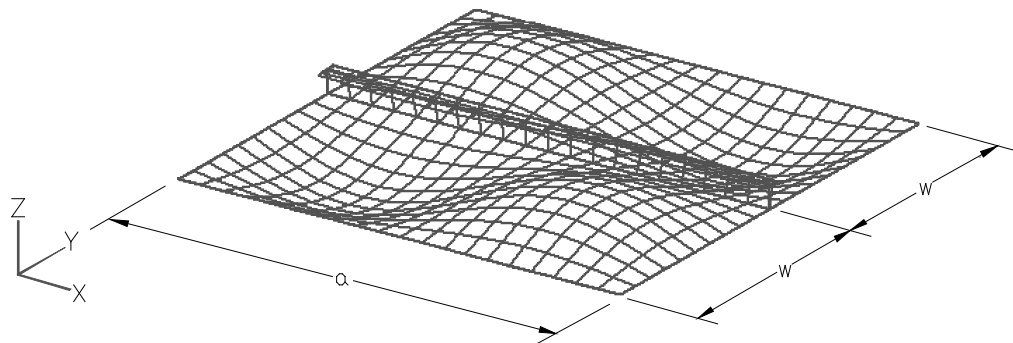


Fig. 9.5. Deformed Shape of Typical Compression Flange

simply a remnant of old terminology adopted by Bleich (1952) and Timoshenko and Gere (1961) just to distinguish whether the buckling mode is symmetrical or anti-symmetrical with respect to a longitudinal stiffener placed at the centerline of the compression flange. Thus, it is meaningless to increase the bending rigidity than this limiting value and this limiting value corresponds to the maximum strength that can be effectively achieved by the plate subpanel for the stiffener arrangement. Therefore, this limiting value is defined in this study as the minimum required moment of inertia for the longitudinal stiffener. There can be a number of design combinations to attain a critical strength of a longitudinally stiffened plate, i.e., plate thickness, stiffener arrangement and stiffener rigidity. Since little increase is expected in the critical stress of a stiffened plate by increasing the size of the longitudinal stiffeners if it is already larger than the minimum required value for an anti-symmetric buckling, increasing the stiffener size leads to waste. If a plate is stiffened by smaller size stiffeners than the required minimum, a large number of stiffeners or a thicker flange plate should be required to attain a critical strength of the plate stiffened by longitudinal stiffeners of the minimum required stiffness. As the major cost item is likely to be the welding in most stiffened plate fabrication, increasing the number of stiffeners is certainly not an attractive solution. Likewise increasing the thickness of the compression flange at the expense of using a smaller size stiffener is not a viable solution either. Consequently, for wide plate flanges requiring a stiffened system, an optimum design can be achieved by using the stiffeners of the minimum required moment of inertia.

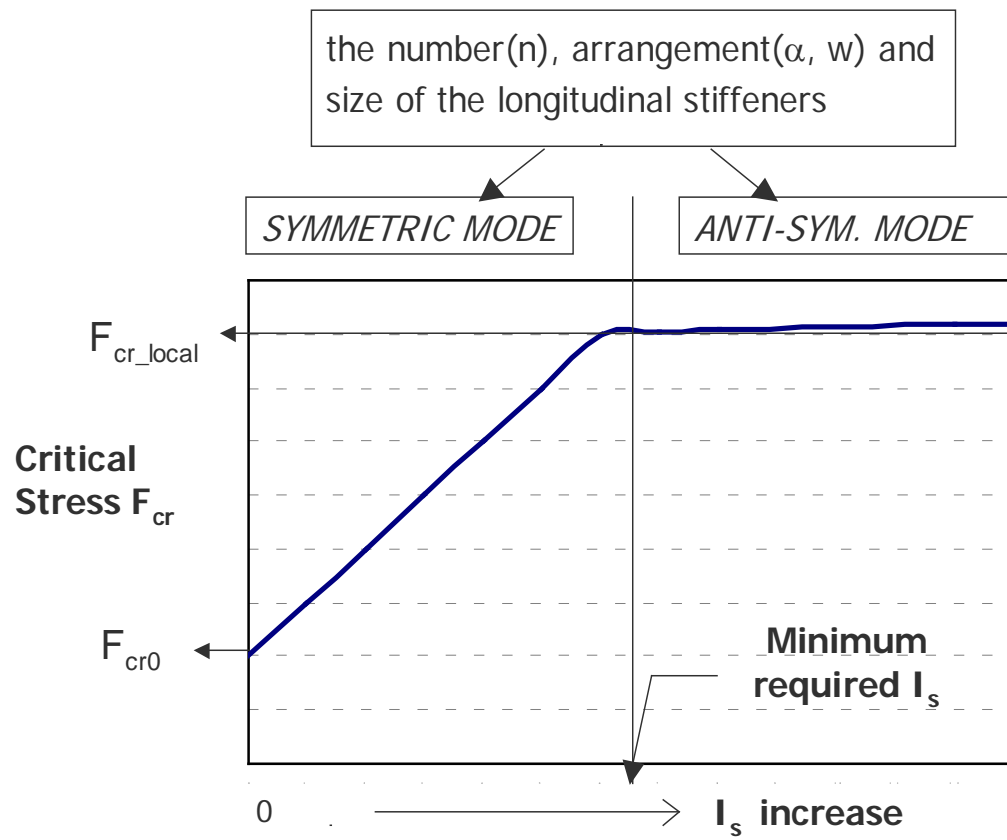


Fig. 9.6. Critical Stress versus Moment of Inertia of Longitudinal Stiffeners

An added advantage in using the minimum required moment of inertia is ease of evaluating the elastic critical stress afforded by a classical formula given by Eq. (3.12) a corresponding rectangular unstiffened plate having the same dimensions as the subpanel. Therefore, parametric studies were conducted with respect to the minimum required moment of inertia for longitudinally stiffeners that would ensure an anti-symmetric buckling.

9.4.5 Parametric Study

A series of parametric studies were conducted to characterize and quantify the effects of each parameter on the minimum required moment of inertia for longitudinal stiffeners. Major parameters were identified in Eq. (3.24), which were the number of stiffeners, the aspect ratio of the subpanel, the stiffener spacing, the compression flange thickness, the cross-sectional area and the torsional rigidity of the stiffeners.

9.4.5.1 Number of Longitudinal Stiffeners

Fig. 9.7 illustrates the effect of the number of longitudinal stiffeners, n , on the minimum required moment of inertia. Although the effect of the number of stiffeners, n , on the required moment of inertia of the longitudinal stiffener is reflected by the 4th power form in the current AASHTO (1996), the parametric study reveals that the effect of the number of longitudinal stiffeners can be expressed approximately as 1/2nd power form.

9.4.5.2 Aspect Ratio

Fig. 9.8 illustrates the effect of the aspect ratio, a/w , of the subpanel on the minimum required moment of inertia. These data represent models for a compression flange that have two longitudinal stiffeners the thickness, t_f , of 1.0 inch and the width

between stiffeners, w , of 80 inches. Through a series of analyses varying the aspect ratio of stiffened plates while holding the stiffener size and number of stiffeners constant, it was discovered that the aspect ratio significantly influences the minimum required moment of inertia. As can be seen from Fig. 9.8, the effect of the aspect ratio on the required moment of inertia is represented by a square form. It is of interest to note that the current AASHTO requirement, Eq. (9.1) does not include this obviously important parameter.

9.4.5.3 Flange Thickness

Fig. 9.9 illustrates the effect of the flange plate thickness on the minimum required moment of inertia of longitudinal stiffeners. The models which yield data presented in Fig. 9.9 has a subpanel width, w , of 160 inches, three longitudinal stiffeners and an aspect ratio, These data represent a series of compression flanges that has the width between stiffeners, of 160 inches, three longitudinal stiffeners, the aspect ratio, a/w , of subpanels of 5. The thickness, t_f , of the compression flange was varied from 1 to 2.5 inches. It can be noted from Fig. 9.9 that the plate thickness has a significant effect on the minimum required moment of inertia, which can be represented by the 3rd power form.

9.4.5.4 Flange Width Between Stiffeners

Fig. 9.10 illustrates the effect of the width between longitudinal stiffeners on the minimum required moment of inertia. The data presented in Fig. 9.10 data were generated from a series of model analyses. The thickness, t_f , of the compression flange was set equal to 1.0 inch. The number of longitudinal stiffeners, n , was set equal to three and the length of the plate was adjusted to yield the aspect ratio of the subpanels to be

equal to 5. The widths between longitudinal stiffeners, w , are varied from 60 inches to 200 inches.

It can be noted from Fig. 9.10 that the width, w , of the subpanel has a linear relationship on the minimum required moment of inertia.

9.4.5.5 Torsional Rigidity of Stiffeners

Fig. 9.11 illustrates the effect of the torsional rigidity of the longitudinal stiffeners on the minimum required moment of inertia. The models which yield data presented in Fig. 9.11 has a subpanel width, w , of 80 inches, three longitudinal stiffeners. These data represent a series of compression flanges that has the aspect ratio, a/w , of subpanels of 5. The thickness, t_f , of the compression flange has 1.0 inch. From Fig. 9.11, it is evident that the torsional rigidity of a stiffener has little influence on the minimum required moment of inertia.

9.4.5.6 Area of Stiffeners

Fig. 9.12 shows the effect of the cross-sectional area on the minimum required moment of inertia of longitudinal stiffeners. The thickness of the compression flange, t_f , and the width of the subpanels are 1 and 80 inches, respectively. Three longitudinal stiffeners are used. The aspect ratio of subpanels, a/w , is equal to 5. It should be noted that a high profile slender tee shape is preferred to a shallow and thick shape to the extent that the width-to-thickness ratio given by Eq. (9.26) is satisfied. Generally, the stiffener area-to-flange area ratio falls between 0.1 and 0.2 in most practical designs. As can be seen from Fig. 9.12, the area ratio parameter considered does not have significant influence on the required minimum moment of inertia.

9.4.6 Regression Analysis

One hundred twenty data points were collected corresponding hypothetical stiffened compression flange models that yield an anti-symmetric buckling (Ford, 2000). Nonlinear regression analysis based on the theoretical and analytical parametric studies yielded Eq. (9.27) for the limiting value of the moment of inertia I_s , which is required to ensure an anti-symmetric buckling (Ford, 2000, Yoo et al., 2001). The coefficient of correlation, R , was greater than 0.95.

$$I_s = 0.3\alpha^2 \sqrt{nw} t_f^3 \quad (9.27)$$

Verification of Eq. (9.27) is provided in Table 4.1 prepared on a selected number of case studies conducted. From Table 4.1, it is evident that the I_s used and I_s are very close. The theoretical critical stress and the corresponding stress determined by the finite element analysis compare well also.

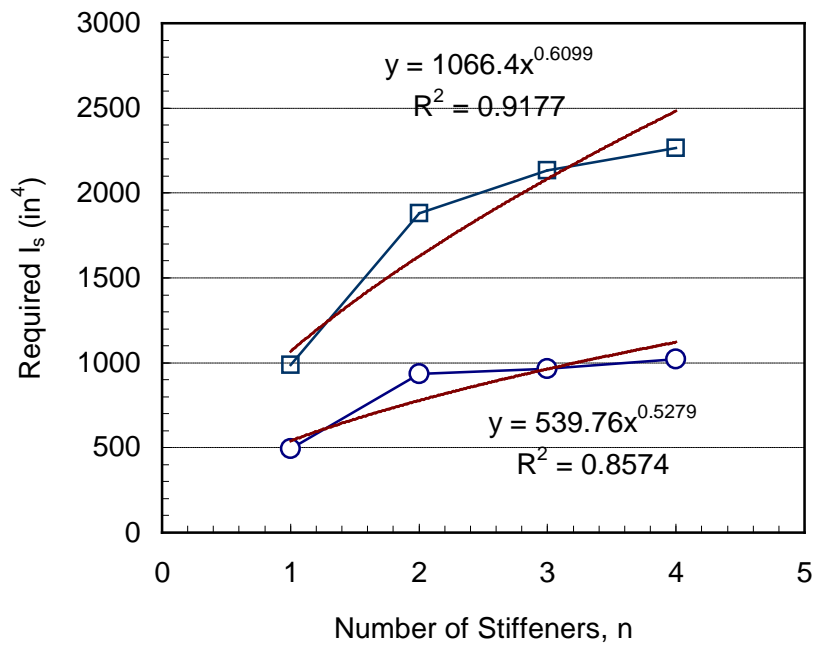


Fig. 9.7. Required I_s versus Number of Stiffeners

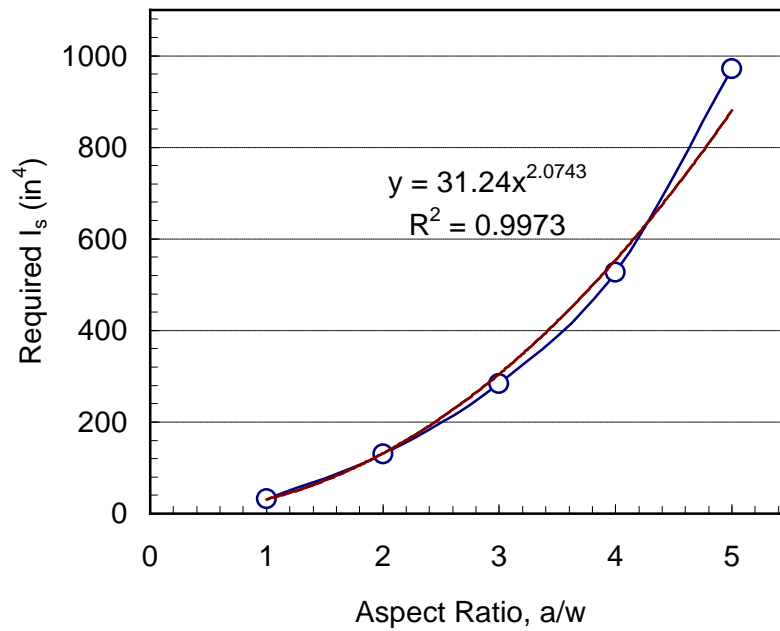


Fig. 9.8. Required I_s versus Aspect Ratio, a/w

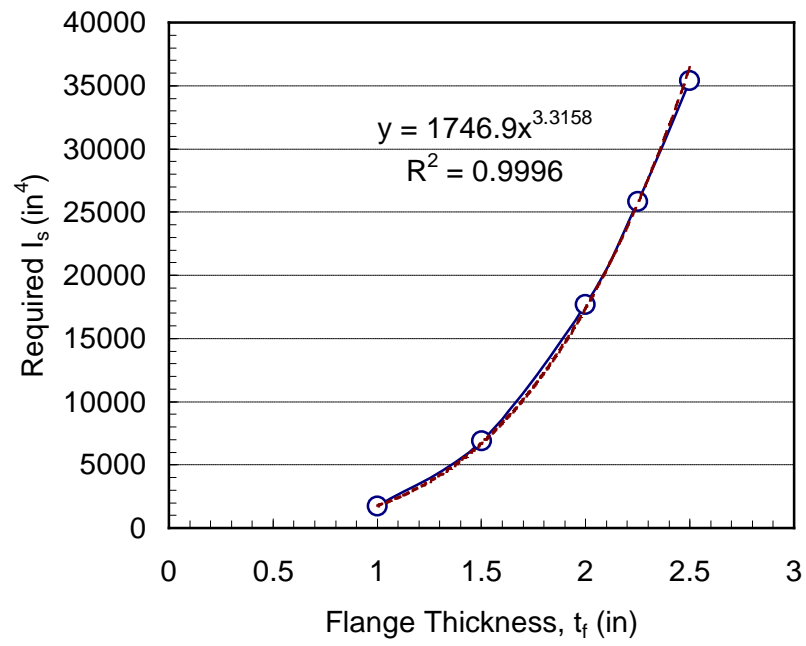


Fig. 9.9. Required I_s versus Flange Thickness

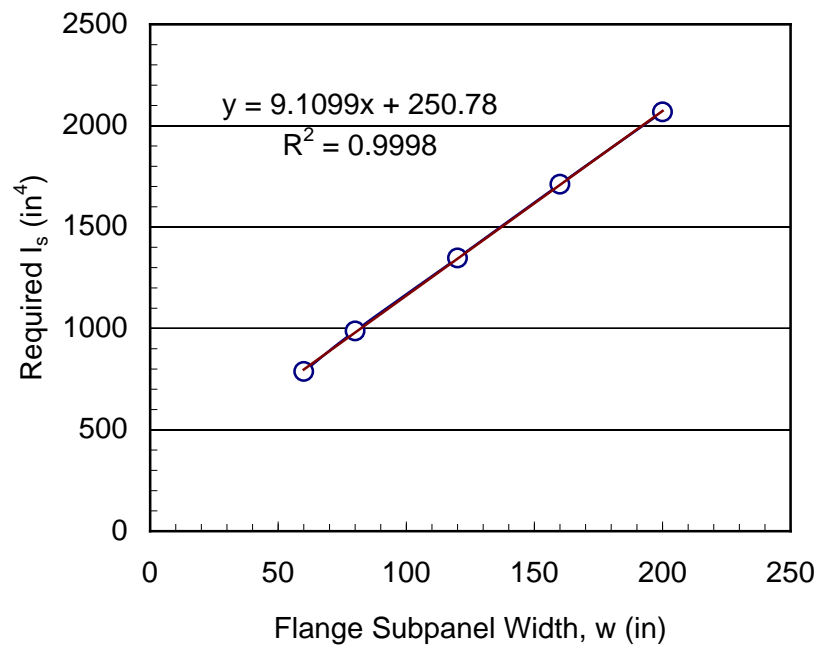


Fig. 9.10. Required I_s versus Flange Subpanel Width

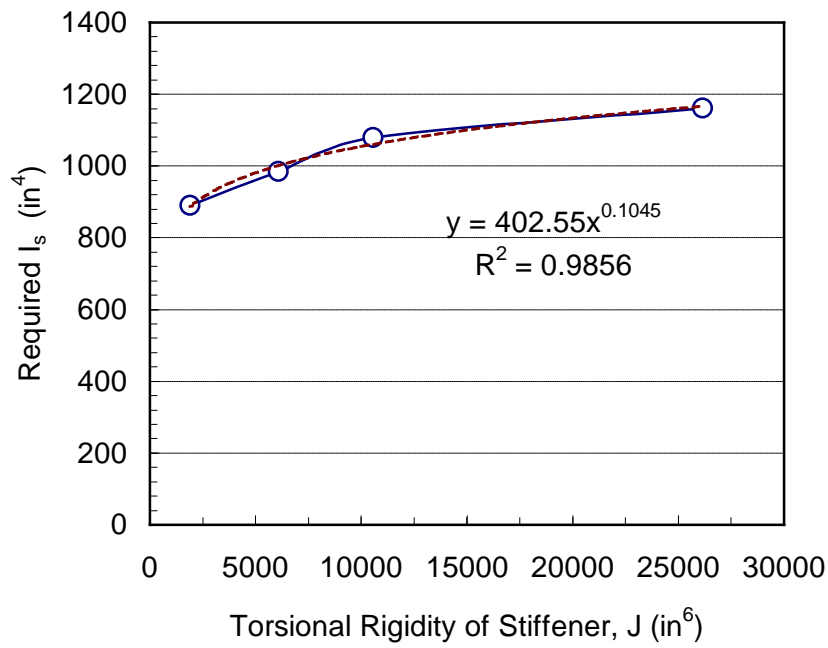


Fig. 9.11. Required I_s versus Torsional Rigidity of Stiffener

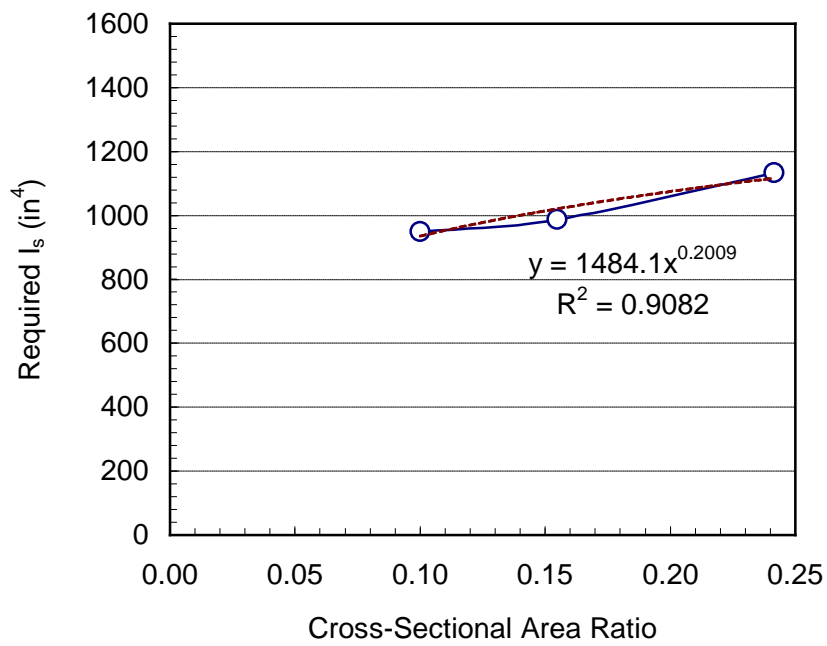


Fig. 9.12. Required I_s versus Cross-Sectional Area Ratio, A_s/A_f

Table 9.4. Minimum Required Moment of Inertia (in⁴)

α	n	w (in.)	t_f (in.)	I_s <i>Eq.(9.27)</i>	I_s (<i>Used</i>)	$F_{cr, theory}$ (ksi)	$F_{cr, FEM}$ (ksi)
1	1	80	0.75	10.13	13.07	9.21	9.43
5	1	80	0.75	253.13	197.07	9.21	9.51
1	3	80	0.75	17.54	12.44	9.21	9.27
5	3	80	0.75	438.43	404.41	9.21	10.17
1	1	80	1.00	24.00	30.29	16.38	16.47
3	1	80	1.00	216.00	385.98	16.38	17.00
5	1	80	1.00	600.00	492.50	16.38	16.62
1	3	80	1.00	41.57	29.50	16.38	16.33
3	3	80	1.00	374.12	385.98	16.38	17.40
5	3	80	1.00	1039.23	966.49	16.38	17.04
1	1	80	1.25	46.88	68.52	25.60	26.39
3	1	80	1.25	421.87	694.23	25.60	27.33
1	3	80	1.25	81.19	68.52	25.60	26.58
5	1	80	1.25	1171.86	986.68	25.60	26.58
3	3	80	1.25	730.71	783.84	25.60	28.50
5	3	80	1.25	2029.75	2134.32	25.60	26.60
5	3	100	0.75	548.03	450.42	5.90	6.08
5	3	160	1.50	7014.81	6734.91	9.21	9.99

9.5 Induced Stresses in Horizontally Curved Box Girder Flanges

9.5.1 Introduction

The stress distribution in a horizontally curved box girder flange is quite complicated due to the inherent coupling of vertical bending and torsion plus stresses induced by box distortion. As the pre-buckling static analysis is a prerequisite for all elastic buckling analysis of a complex structural system, a detailed examination of stresses induced in a horizontally curved box girder flange is presented in this Section. The resulting normal stresses that developed in the flange are used in subsequent eigenvalue analyses.

9.5.2 Static Behaviors of a Horizontally Curved Box Girder

In a horizontally curved girder, the bending moment and torsional moment are always coupled with each other due to the curvature of the girder axis. As a result, an externally applied vertical force is resisted internally by a combination of a bending component, a torsional component, and a distortional component. The internal bending component includes longitudinal normal stresses (abbreviated as longitudinal stresses) and flexural shear stresses in a cross section of the box girder. The torsional component includes St.Venant torsion (pure torsion) and non-uniform torsion (warping torsion). The St.Venant torsion induces torsional shear stresses and the warping torsion induces longitudinal normal stresses and shear stresses (secondary) in a cross section of the box girder, which are referred to as torsional warping stresses. The distortional component induces distortional stresses that consist of longitudinal normal stress and shear stress (secondary).

Thus, the longitudinal stress in a box girder is composed of bending, distortional, and torsional warping stresses. It is well known that the distortion and the torsional warping induce a non-uniform normal stress distribution in the flanges as shown in Fig. 9.13. The torsional shear stress due to St.Venant torsion in a box girder is the main resisting mechanism against the applied torsion. Stresses induced by warping torsion are small compared to the St. Venant torsional shear stress. Therefore, stresses induced by warping torsion are not considered in the design of girders with closed box type cross-sections. Since the stiffness of the box section against distortion is relatively weak compared with the bending stiffness or torsional stiffness, the distortional stresses may become fairly large if adequate distortional stiffnesses are not provided to the box girder. Therefore, the distortional stresses must be examined closely in box girders that are subjected to torsional moment.

9.5.3 Distortional Stresses

The distortion of a box girder can be defined as the cross sectional deformation due to two pairs of coupled internal forces acting on the cross section which are equilibrated with each other. The distortional force acting on the cross-section, consisting of the two pairs of coupled forces, is shown in Fig. 9.14(b).

When an eccentric loading is applied to a box girder of a symmetric cross-section, the applied force can be resolved into a vertical bending force, P , and a torsional force, $Pb/2$, as shown in Fig. 9.14(a). The torsional force is then divided into pure torsion and distortion as shown in Fig. 9.14(b). As can be noted from Fig. 9.14(b), the distortional force occurs in a box girder when a torsional force

represented by a pair of coupled forces is not completely balanced with the St.Venant shear flow.

The distortional force can also occur in horizontally curved box girders under a horizontal couple as shown in Fig. 9.16. Consider a differential element of a horizontally curved girder flange of width, db , length, ds , thickness, t , and radius, R , under bending normal stress σ_f as shown in Fig. 9.15(a).

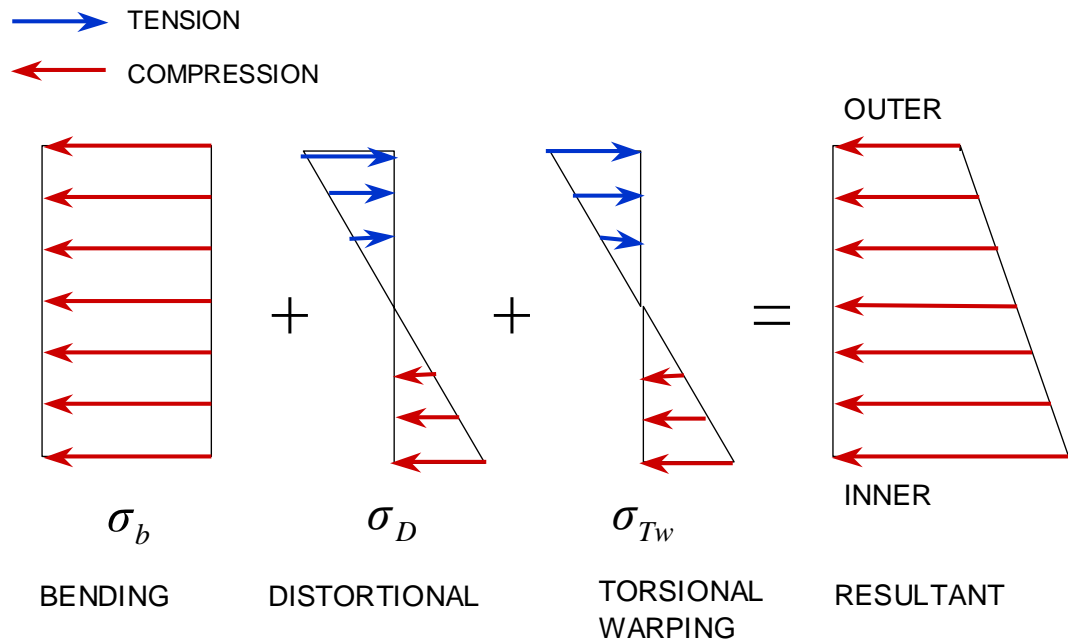


Fig. 9.13. Normal Stress Components in Bottom Flange

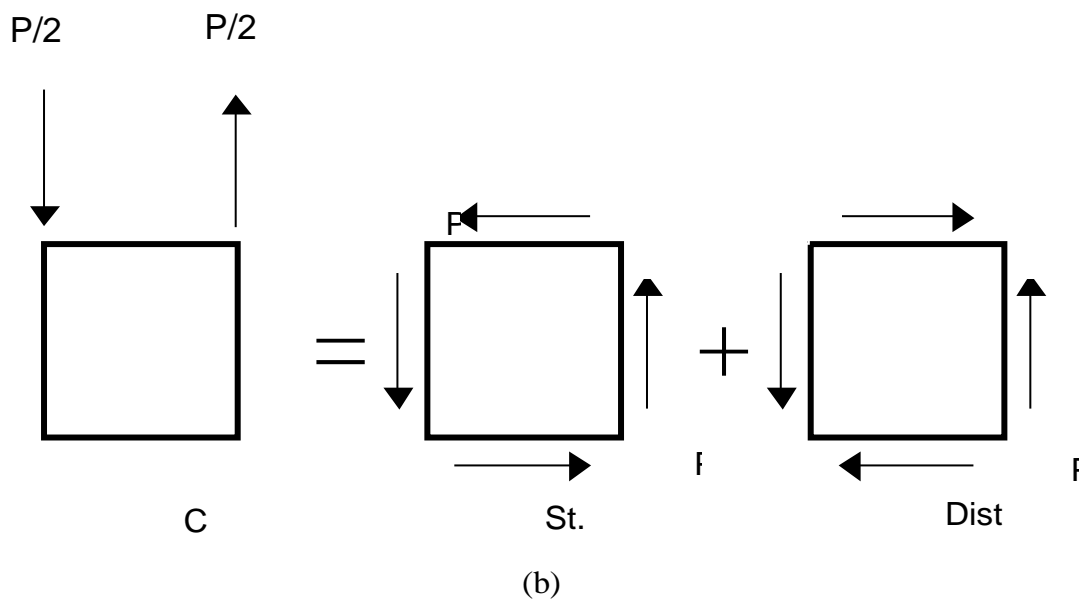
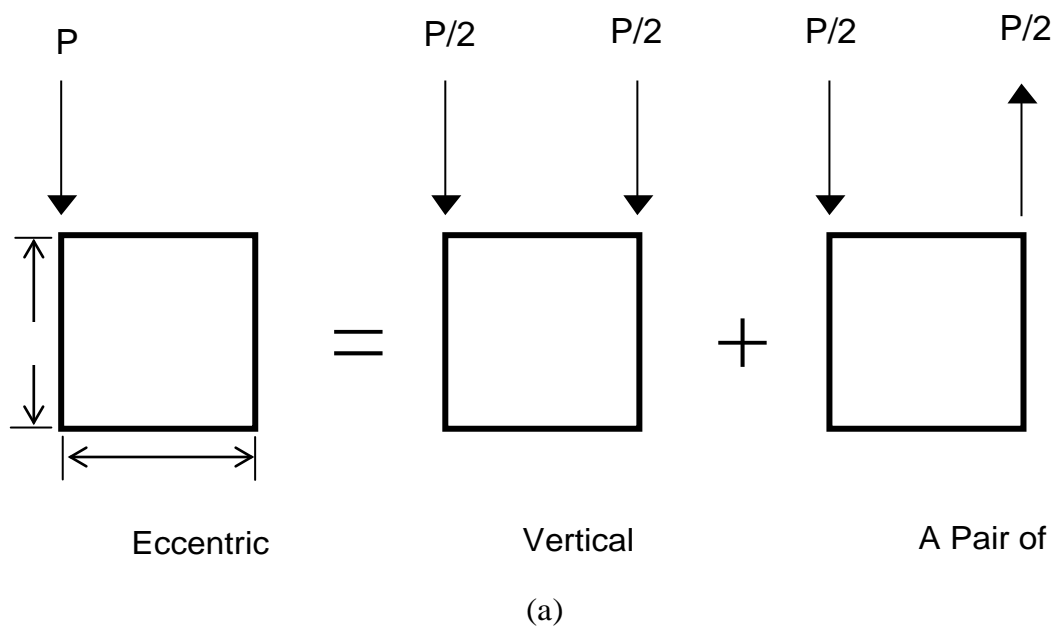
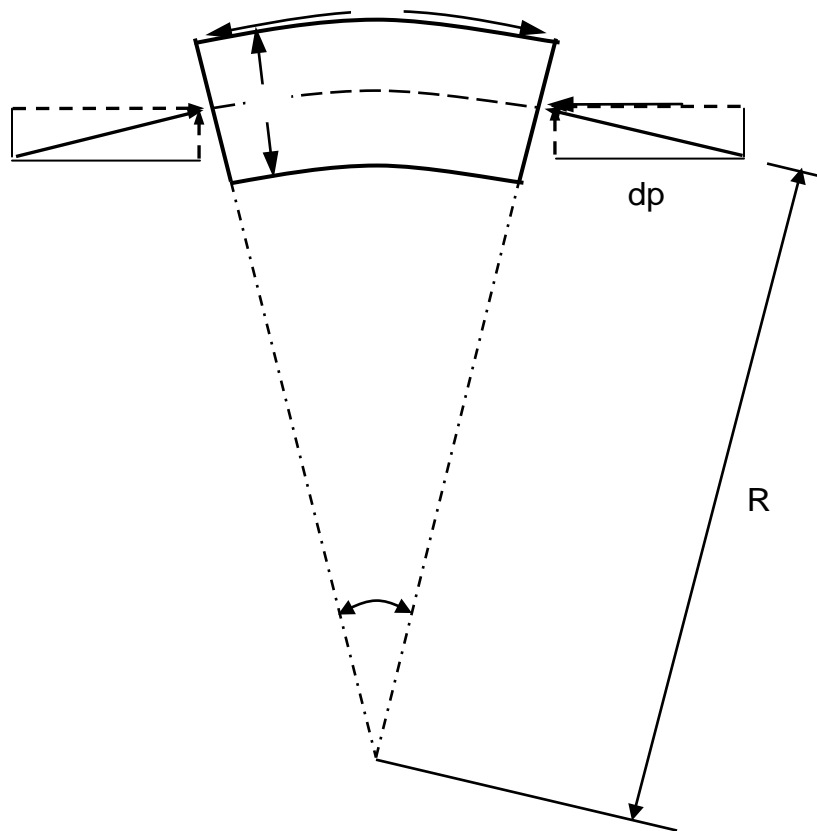
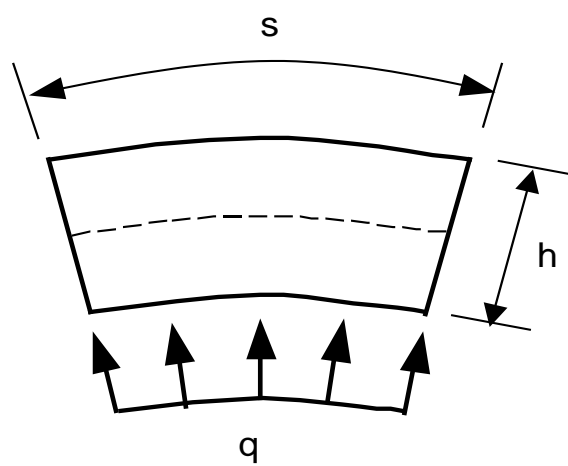


Fig. 9.14. Distortional Force on a Box Girder



(a) Resultant Lateral Force Component



(b) Lateral Force Distribution

Fig. 9.15. Lateral Force Component on a Horizontally Curved Flange

Since the resultant force of the bending stress, $dp (= \sigma_f t db)$, is non-collinear due to the curvature, the lateral force component dq_f is required for equilibrium. This lateral force acts in the radial direction of the girder and it is distributed over the girder flange. The distributed lateral force component dq_f and the resultant force q_f are expressed as (U.S. Steel Corp., 1984)

$$dq_f = \frac{dp}{R} = \frac{\sigma_f t db}{R} \quad (9.28)$$

$$q_f = \int_0^b \frac{dp}{R} = \int_0^b (\sigma_f t db) \frac{1}{R} = \frac{\sigma_f t b}{R} \quad (9.29)$$

The lateral force is induced in the webs as well as in the flanges of the box girder. As can be seen from Eq. (9.28), the lateral force components are linearly proportional to the bending normal stresses. The distribution of the lateral force component in the webs is shown in Fig. 9.16(a). Since the resultant forces due to vertical bending in the top and bottom flanges are identical in magnitude and opposite in sign, the resultant lateral forces in the top and bottom flanges form a pair of couple on a box girder section as shown in Fig. 9.16(b). Thus, the distortional force is induced by the force couple in the horizontally curved box girder, as shown in Fig. 9.16(b). Although it is not a major part of the total torsion, vehicles traveling in the outer lane (convex side) on a horizontally curved bridge may cause a distortional force shown in Fig. 9.17(a) due to the torsional moment created by the eccentricity and the centrifugal force. The distortional force due to the curvature has the same sign as that created by the vehicles under a negative bending moment as shown in Fig. 9.17(b). In the positive bending zone, it can be noted that the

distortional force induced on a curved box girder has an opposite sign as shown in Fig. 9.15(c).

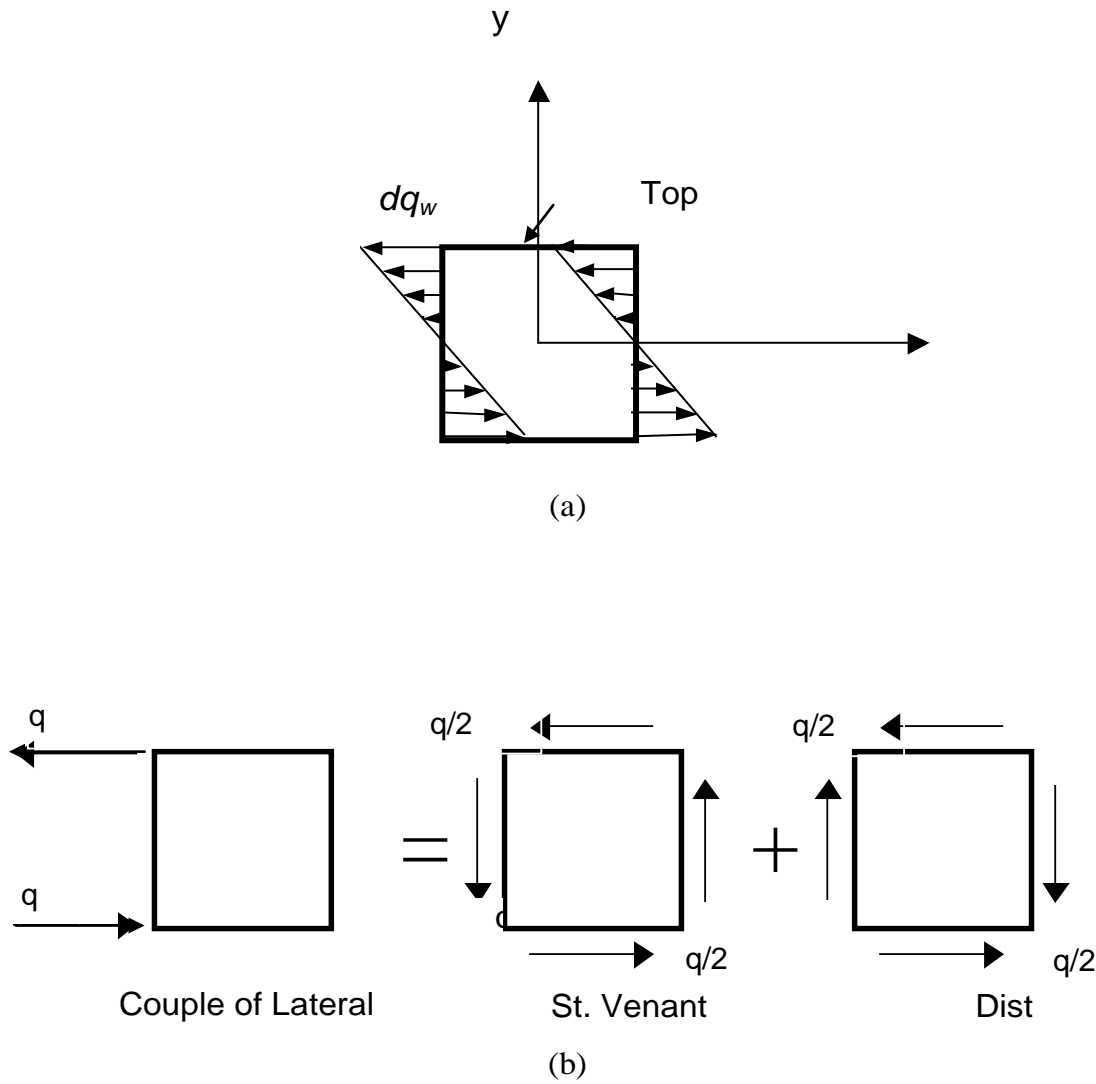
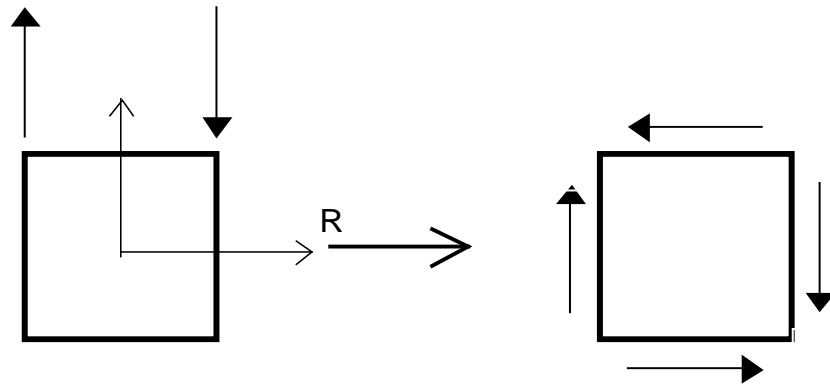
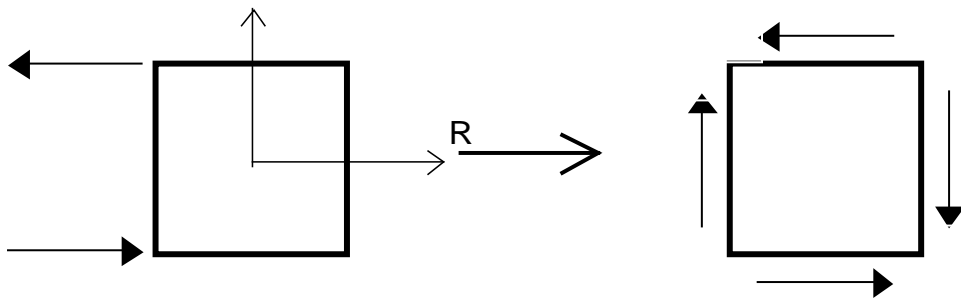


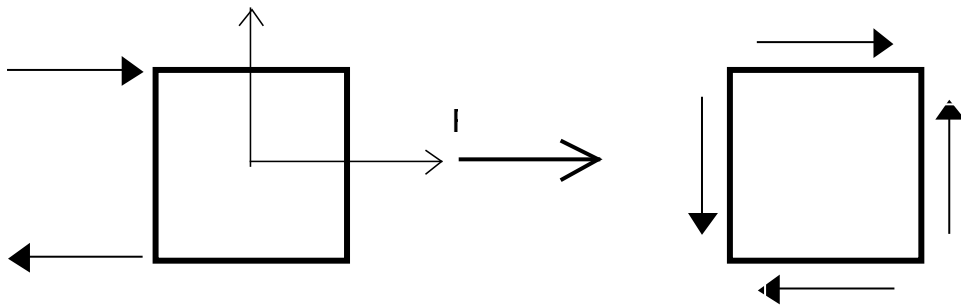
Fig. 9.16. Distortional Force in the Horizontally Curved Box Girder



(a) Distortional Force Direction due to Eccentric Load



(b) Distortional Force Direction due to Curvature in Negative Moment Zone



(c) Distortional Force Direction due to Curvature in Positive Moment Zone

Fig. 9.17. Distortional Force Direction in Horizontally Curved Girder

The distortion of the box girder is expressed as the angular change of the cross section, as shown in Fig. 9.18. The rectangular coordinate axes (x, y, z) are taken at the distortional center, D and the curvilinear coordinate axis, s , is adopted along the perimeter of the cross-section as shown in Fig. 9.18. The angular change, γ , is defined as

$$\gamma = \frac{v_l - v_u}{h} + \frac{w_i - w_o}{b} \quad (9.30)$$

where v, w = the displacements in the direction of the x and y coordinate directions, respectively. They have their origin at the distortional center, D . The differential equation for distortion of the horizontally curved box girder was given initially by Dabrowsky (1968) as

$$\gamma^{iv} + 4\lambda^4 \gamma = \frac{1}{EI_{Dw}} \left(\rho \frac{M_x}{R} + \frac{m_z}{2} \right) \quad (9.31)$$

where $\lambda = \sqrt[4]{K_{Dw} / 4EI_{Dw}}$ (length⁻¹ unit); K_{Dw} = stiffness of the box section against distortion (force / angle unit); EI_{Dw} = distortional warping rigidity (force x length⁴ unit); I_{Dw} = distortional warping constant = $\int_A \omega_D^2 dA$ (length⁶ unit); R = radius of curvature; M_x = bending moment; m_z = distortional force (= qh for the case shown in Fig. 9.16(b)); ρ = dimensionless parameter consisting of cross-sectional geometric properties (Dabrowski, 1968). The distortional warping function, ω_D , is expressed as

$$\omega_D(s) = - \int_0^s r(s) ds + C_1 \quad (9.32)$$

where C_1 is an integration constant and $r(s)$ represents the vertical distance parallel to the y axis along the perimeter of cross section, s . It is noted that the unit of w_D is

length square. The derivative of the angular distortion, γ' , yields the displacement, u , in the direction of the longitudinal z -axis as given by Eq. (9.33). The displacement, u , develops if the shearing strain associated with distortion is assumed to be infinitesimal.

$$u = \frac{\int g}{\int z} w_D(s) \quad (9.33)$$

For the case where the displacement, u , is restrained, normal and shearing stresses develop in the box section. The distortional normal stress is then given by Hooke's law as

$$s_{Dw} = Ee = E \frac{\int u}{\int z} = E g'' w_D \quad (9.34)$$

where E = Young's modulus. Since the distortion does not produce any additional axial force, N_z , bending moments, M_x , and M_y , the following equations must be satisfied:

$$N_z = \int_A \sigma_{Dw} dA = 0 \quad (9.35a)$$

$$M_x = \int_A \sigma_{Dw} y dA = 0 \quad (9.35b)$$

$$M_y = \int_A \sigma_{Dw} x dA = 0 \quad (9.35c)$$

Substitution of equations (9.32) and (9.34) into (9.35) determines the distribution of the distortional function, w_D , in a cross-section of a box girder as shown in Fig. 9.19.

The distortional normal stresses are distributed in proportion to the distortional function, as given by Eq. (9.34). Fig. 9.19 illustrates the distribution pattern of the distortional normal stresses.

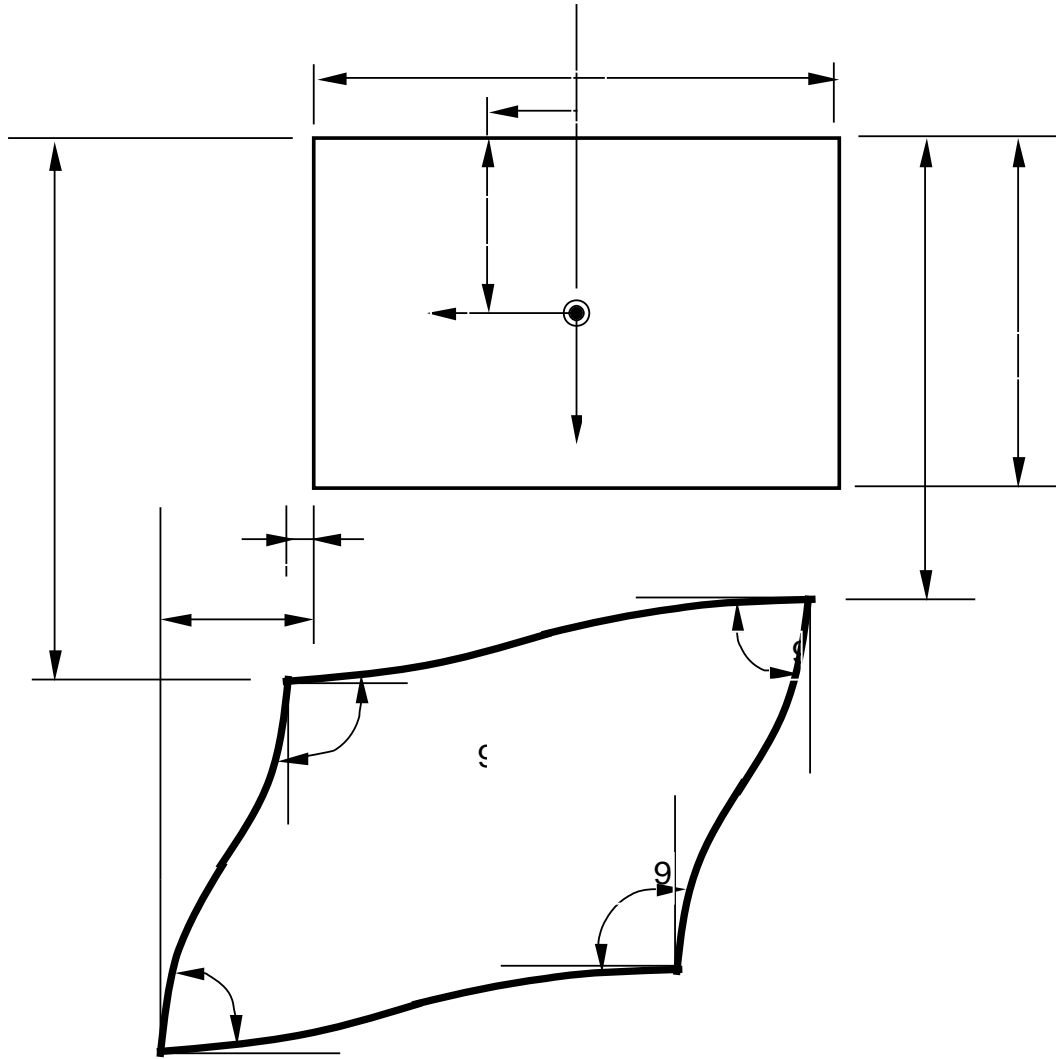


Fig. 9.18. Angular Change, γ , in a Box Girder due to Distortion

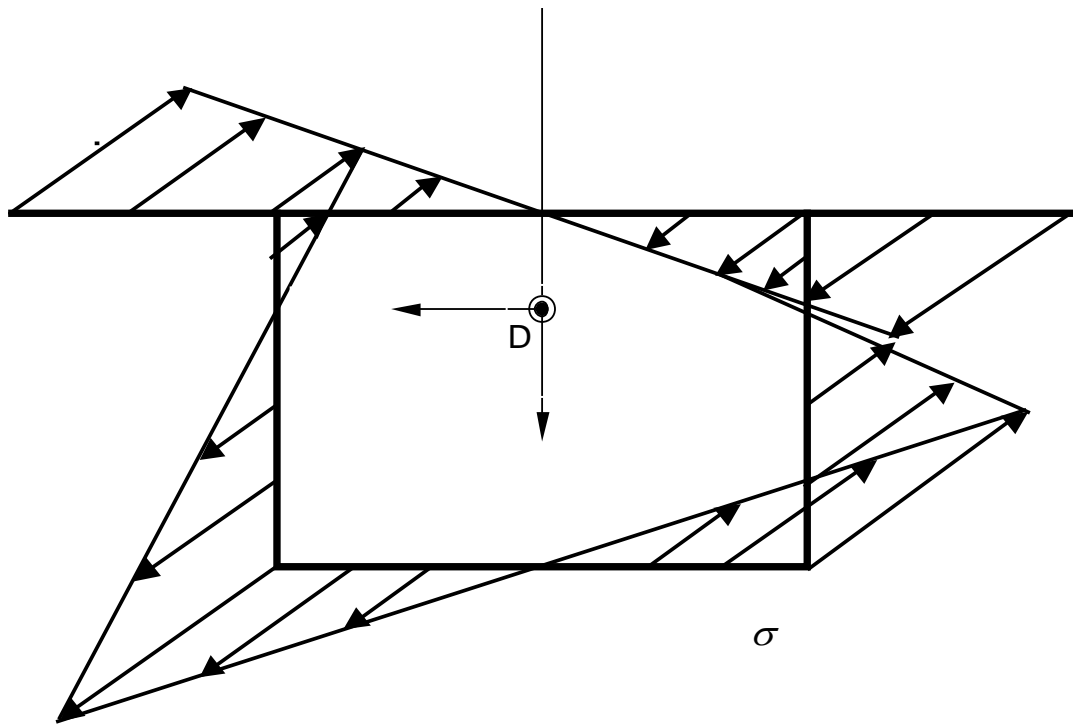
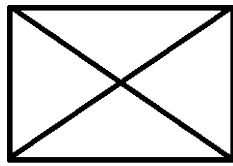


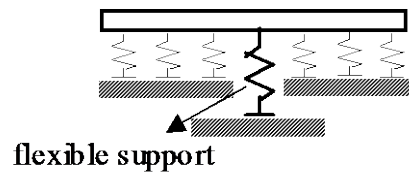
Fig. 9.19. Distortional Normal Stress Distribution on a Box Girder

9.5.4 Effects of Internal Diaphragm on Distortional Stress

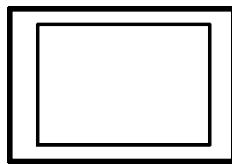
Since internal diaphragms resist the coupled forces on a box girder that cause an internal distortional force, placing adequate internal diaphragms to a box girder greatly increases the stiffness against distortion and facilitates to retain the original shape of the cross-section. The differential equation for distortion of a curved box girder, Eq. (9.31), is similar to the equation for the deflection, γ , of a beam on an elastic foundation, with flexural rigidity, EI_{Dw} , spring constant, K_{Dw} , uniformly distributed load, $m_T/2$ and additional distributed load, $\rho M_x/R$, thus, using the beam on elastic foundation (BEF) analogy, the effect of the internal diaphragms on the distortional normal stress can be represented. Consider a hypothetical girder on an elastic foundation as shown in Fig. 9.21. The hypothetical girder is subjected to a uniformly distributed load, $m_T/2$ and an additional distributed load, $\rho M_x/R$ as shown in Figs. 9.21(a) and 9.21(b), respectively. The girder is elastically supported by not only the elastic foundation of stiffness, K_{Dw} , but also the internal diaphragms of stiffness, K_D . Typical internal diaphragms are shown in Fig. 9.20 with an associated boundary condition to be used in the BEF system. As can be seen from Fig. 9.20(a), the internal cross-frame in a box girder corresponds to a flexible intermediate support for the BEF system. Thus, the approximate moment diagram of the BEF system, represented in Fig. 9.21(c), is same as the moment diagram of a continuous beam with intermediate flexible supports. In Fig. 9.21(c), the spacing of the intermediate supports is represented by L_D and the span length by L .



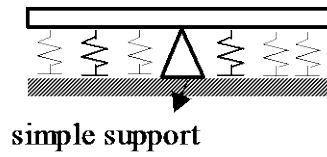
Truss X type



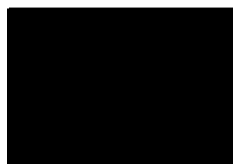
(a)



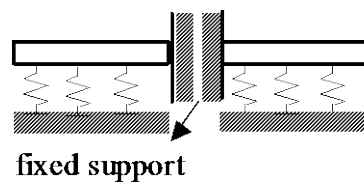
Frame or thin-plate type



(b)

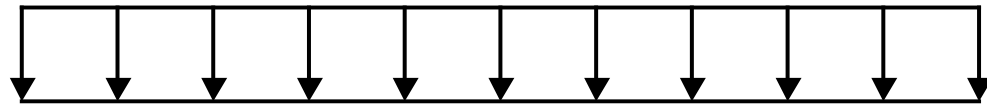


Solid-plate type

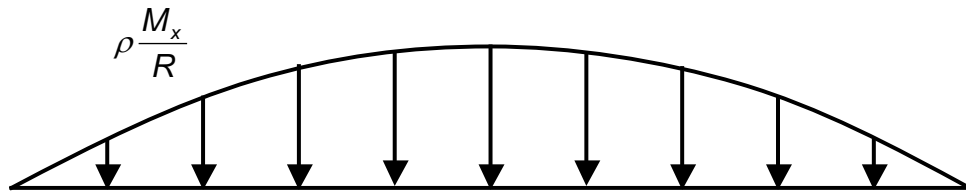


(c)

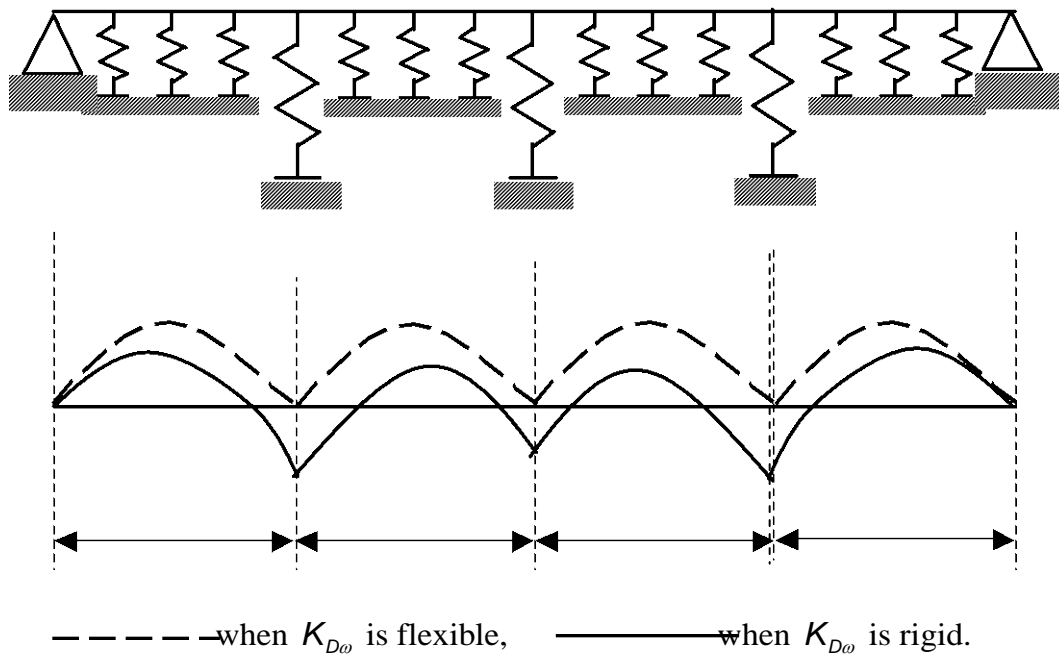
Fig. 9.20. Internal Diaphragms and Corresponding Support Type in BEF Analogy



(a) Distorsional Force, $m_T/2$



(b) Distorsional Force Due to Curvature



(c) BEF with Elastic Supports and Moment Diagrams along the Stiffness of Elastic Supports

Fig. 9.21. BEF Analogy for Horizontally Curved Box Girder

The square of the cross-frame spacing, L_D^2 , is proportional to the maximum moment of the BEF system in Fig. 9.21(c) and the stiffness of the flexible supports, K_D , is inversely proportional to the maximum moment. The moment, M , of the BEF system is given by $E I_{Dw} \gamma''$ which is analogous to the distortional bimoment M_{Dw} of the box girder. It is noted that the unit of M_{Dw} is force times length square. The distortional normal stress is evaluated by Eq. (9.36).

$$\sigma_{Dw} = \frac{M_{Dw}}{I_{Dw}} \omega_D \quad (9.36)$$

Thus, the moment diagram of the BEF system actually represents the variation of the distortional normal stress of a box girder along the span. Therefore, there exists an analogy between the effects of the spacing and the stiffness of the cross-frames on the bimoment and corresponding distortional stresses of the box girder and the effects of the spacing and the stiffness of the intermediate flexible supports on the vertical bending moment and corresponding bending stresses of the BEF system. Thus, it can be said that the distortional normal stresses in a box girder can be controlled by adequate number of internal cross-frames. Nakai and Yoo (1988) present detailed background information given here in Eqs. (9.30) through (9.38).

9.5.5 Design Requirements for Distortional Stresses

As illustrated above, uncontrolled development of the distortional normal stress has a significant detrimental effect on the strength of a box girder. Therefore, modern specifications stipulate the maximum allowable distortional normal stresses. Since the distortional stresses can be controlled by placing adequate cross-frames, the design requirements are mainly concerned with the spacing and the stiffness of the

internal cross-frames. Although there is no explicit provision in AASHTO (1996) and AASHTO LRFD (1996), AASHTO Guide Specifications (1993) adopted in Article 1.29 that *Spacing of internal bracing shall be such that the longitudinal distortion stress in the box shall not exceed 10 percent of the longitudinal stress due to vertical bending*. Oleinik and Heins (1975) are believed to be the first who suggested the 10 percent rule in the U.S. Hall and Yoo (1998) adopted the same requirement in their recommended specifications. If the designer adheres to the above stipulation, the normal stress gradient across the flanges of box girders should be less than 0.1. Hall and Yoo (1998) propose that *spacing of intermediate internal bracing shall not exceed 30 feet in all curved box girders*.

Japanese researchers have also examined the requirements imposed on the distortional stresses and the spacing of intermediate diaphragms. It was recommended by the Japanese researchers (Nakai and Murayama, 1981; Yabuki and Arizumi, 1989) that the distortional stress, σ_{Dw} , should be less than 5 percent of the vertical bending stress. This recommendation has been adopted by Japanese *Specifications for Highway Bridges* (1990) and the design guidelines established by the Hanshin Expressway Public Corporation (1988).

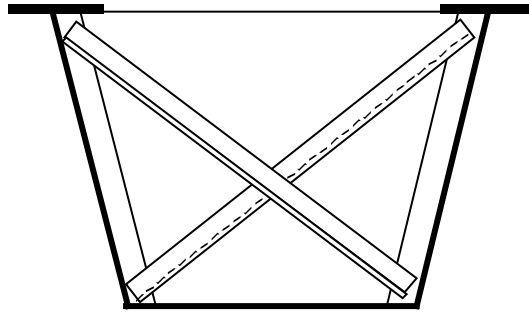
9.5.6 Analytical Studies

Though studies have been conducted to examine analytically the longitudinal stresses on the bottom flange of a box girder with a horizontally curved geometry, the existing studies do not provide sufficiently detailed predictor equations to guide a simple determination of the design parameters, i.e., the expected intensity of distortional stress and the required diaphragm spacing for a curved box girder.

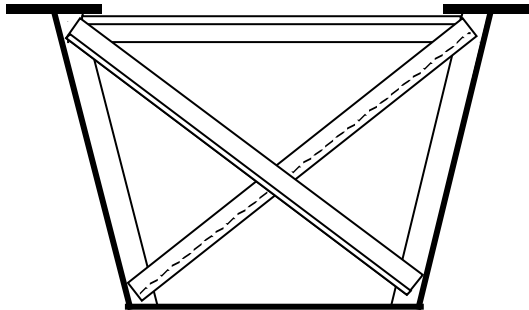
Therefore, as a part of this study, analytical studies were conducted by using the finite element method to examine the induced pre-buckling stresses in a trapezoidal composite box girder with a horizontally curved geometry, along with the spacing of the cross-frames. Through a series of hypothetical bridge analyses, the relationship between the induced distortional stress and corresponding diaphragm spacing is established.

9.5.6.1 Model Description

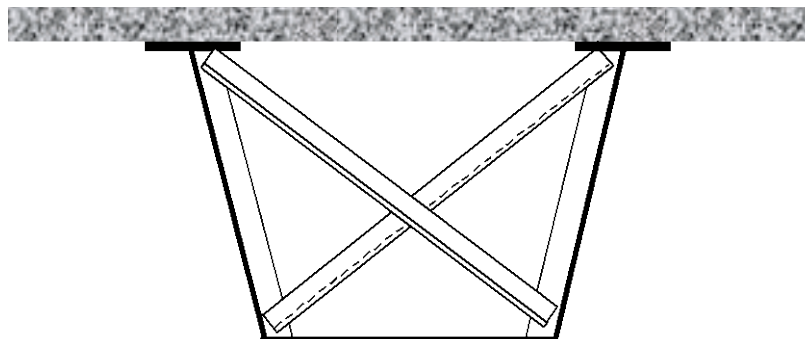
A typical curved box girder bridge currently constructed in the U.S was selected for the analytical study (U.S. Steel Corp, 1978). A one span hypothetical girder with a span length of 150 feet was modeled with simple supports in order to effectively conduct various comparative studies. It should be noted that the loading is applied to induce compression at the bottom flange. The radius for the horizontal curvature of the bridge is 300 feet at the center of the roadway. Thus, the subtended angle of the entire span is 28.65 degrees. The edge-to-edge deck width is 20 feet. There is one 14-foot traffic lane. Supports are arranged in radial directions. The modeled box girder has one tub girder with a trapezoidal shaped cross-section. Fig. 9.22 shows the steel-concrete composite section. The actual vertical girder depth is 72 inches and the slope of the webs is one-on-four. Structural steel having a specified minimum yield stress of 50 ksi is used throughout. The deck is conventional cast-in-place concrete with a 28-day compressive strength of 3,600 psi.



(a) Non-composite section with fictitious flange

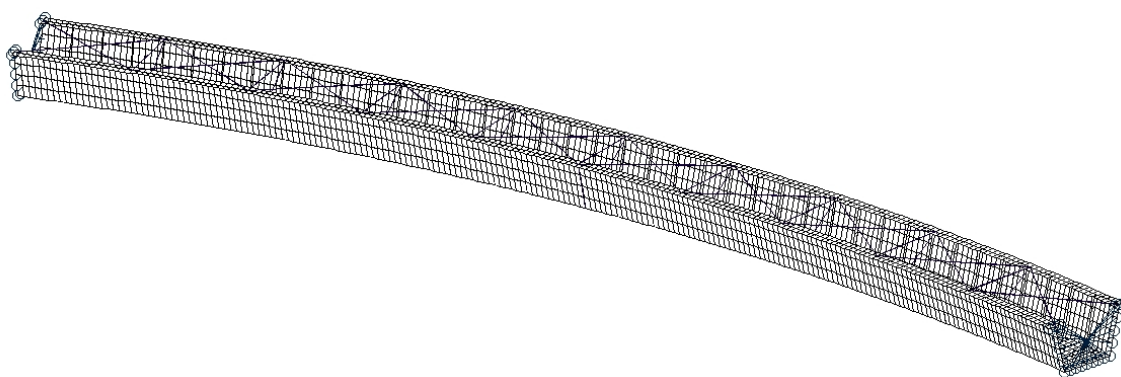


(b) Non-composite section with top bracing

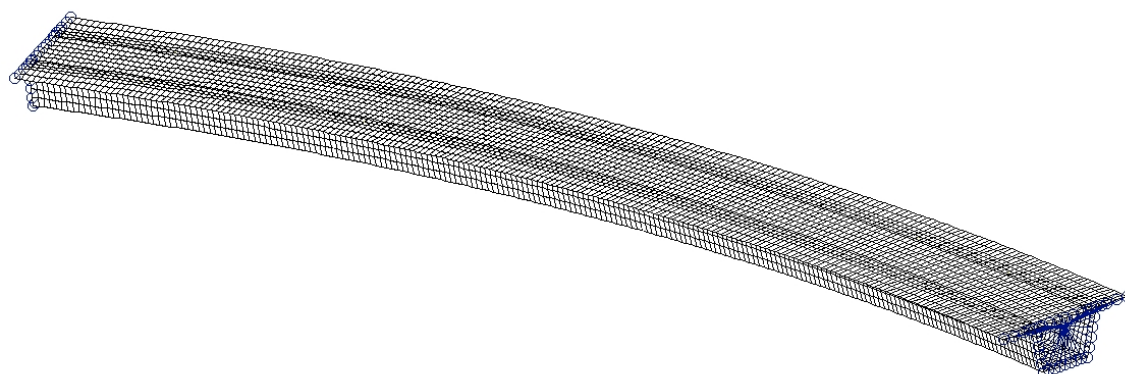


(c) Steel-Concrete composite section

Fig. 9.22. Cross-sections of Curved Box Girder Model



(a) Non-Composite Section Girder



(b) Composite Section Girder

Fig. 9.23. Finite Element Model Description

9.5.6.2 Loading Combination

A design load combination is determined from Article 3.22 of AASHTO (1996). This article provides various combinations of loads to which a structure may be subjected. The loading combinations for *Service Load Design* and *Load Factor Design* are represented as *Group (N)* and they are reproduced in Eq. (9.37).

$$\begin{aligned} Group(N) = & \gamma [\beta_D D + \beta_L (L + I) + \beta_C CF + \beta_E E + \beta_B B + \beta_S SF + \beta_W W \\ & + \beta_{LF} LF + \beta_R (R + S + T) + \beta_{EQ} EQ + \beta_{ICE} ICE] \end{aligned} \quad (9.37)$$

where N = group number; γ = load factor pertaining to design method; β = load factor pertaining to different load category; D = dead load; L = live load; I = live load impact; E = earth pressure; B = buoyancy; W = wind load on structure; WL = wind load on live load-100 pounds per linear foot; LF = longitudinal force from live load; CF = centrifugal force; R = rib shortening; S = shrinkage; T = temperature; EQ = earthquake; SF = stream flow pressure; ICE = ice pressure. The information for load factors and coefficients is contained in Table 3.22.1A of AASHTO (1996). Among the load combination groups, *Group (1)* was selected as a representative case for this analytical study. For the horizontally curved girder, *Group (1)* loading is expressed as follows.

$$Group(1) = 1.3 \left[1.0 D + \frac{5}{3} (L + I) + 1.0 CF \right] \quad (9.38)$$

The *Group (1)* includes the dead load, the live load with the impact effect, and the centrifugal load. Lane load, HS25, was adopted for the live load following the AASHTO (1996). Since it is specified in the specifications that equivalent lane load shall not be used in the computation of centrifugal forces, centrifugal forces are not

included for this analytical study. The Impact factor I is determined by the formula (3-1) of AASHTO (1996) as presented in Eq. (9.39).

$$I = \frac{50}{L+125} \leq 0.3 \quad (9.39)$$

where, L is defined as the length in feet of the portion of the span that is loaded to produce the maximum stress in the member, 150 feet for this analytical model case.

The dead load consists of the steel weight and deck weight and the superimposed dead load. The steel weight is assumed to be placed at one time. Since an unshored construction scheme is adopted, dead loads are separated as the loads on a non-composite cross-section and the load on a completed composite cross-section. The dead loads that are loaded on a non-composite section are the steel frame weight and the concrete deck weight and they are referred to as DL1. Unlike the dead load, DL1, the superimposed dead loads are applied on a composite cross-section and they are represented by DL2. The DL2 consists of the weight of parapets and the future wearing surface. The vehicle live load (LL) on a bridge girder is always associated with the impact factor I . The live load including the impact factor is represented by $LL+I$ in the study. DL1, the load on the non-composite section, DL2, and $LL+I$, both of which act on the composite section, were separately loaded and analyzed for this study.

9.5.7 Modeling for Finite Element Analysis

Article 4.1 of the recommended specification (Hall and Yoo, 1998) for the curved girder bridge requires that the analysis be performed using a rational method that accounts for the interactions of the entire superstructure. Therefore, analyses for

this study were performed using a three-dimensional finite element method. The commercial finite element software, MSC/NASTRAN v2001, was used for the finite element analysis. Girder webs and flanges were modeled using a 4-node plate-shell element, CQUAD4, because of its simple yet numerically stable performance. In a series of previous numerical studies (Davidson and Yoo, 1996; Lee and Yoo, 1999), it had been shown that a minimum of four, square QUAD4 elements for each flange and web was adequate to model the built-up thin-walled members. Each hypothetical plate panel in this study was modeled by using ten subdivisions between the adjacent longitudinal stiffeners or the webs. Full-depth solid diaphragms are provided at supports.

A cylindrical coordinate system is ideally suited for modeling of the curved girder bridge. Steel weight is introduced into the model by the use of inertial body forces. DL2 and LL+I loadings are applied as a distributed loading.

9.5.7.1 Internal Cross Frames

The box girders are internally braced at intermediate locations by X shape cross-frames. The spacing of cross-frames are varied from 150 feet, the same as the entire span length L , to 6 feet, corresponding to $L/25$ so as to investigate the effect of cross-frame spacing on the distortional stress of the curved box girder. A pair of structural angles is used for the cross-frame member. The cross-sectional shape of the combined angles corresponds to a T-section shape structural member. Thus, a WT section was selected to model the internal cross-frames. The size of the cross-frames was determined through a trial and error process to stabilize the induced

distortional stress. The cross-frames of a WT section were modeled by a one-dimensional beam element, CBAR of NASTRAN.

9.5.7.2 Bracing of Tub Flanges

The cross section of a composite steel-concrete box girder is closed by the deck slab in its final configuration. However, prior to placing of the slab, the girder has an open section that is subjected to lateral torsional instability. An effective way to increase the torsional stiffness of the open section is to place a horizontal lateral bracing system (diagonal members) connecting the top flanges. When the bracing system is introduced into a tub girder, this type of cross-section is sometimes referred to as the “quasi-closed” section. Tests had shown that the bracing system could provide a required torsional stiffness for the quasi-closed section, although not as effective as a solid plate of the same thickness used in the bottom flange (U.S. Steel Corp, 1978). Thus, the top flanges of the tub girder model are braced with diagonal bracings placed at the same level between the tub flanges. The top flange bracing members are modeled by a one dimensional beam element, CBAR.

9.5.8 Analysis Results

Normal stresses in the bottom flange are obtained from the FEM analysis. Figs. 9.24 to 9.27 shows the normal stress distribution along the width of the bottom flange under a DL1 loading, a DL2 loading, an LL+I loading and the load combination Group (I), respectively. It can be seen from the figures that the normal stresses in the bottom flange are almost linearly distributed and decrease in the outer radial direction.

9.5.8.1 Effect of Top Flange Lateral Bracing

A quasi-closed section is established by the addition of a lateral bracing system to the top flanges of a non-composite open tub section. The analysis revealed that the stiffness of the top flange bracing has an influence on the warping stresses of a non-composite girder section and the warping-to-bending normal stress ratio of the bottom flange. The variation of the warping stress ratio is presented in Fig. 9.28 along with the cross-sectional area of the top flange bracing. It is found from Fig. 9.28 that as the stiffness of the top bracing increases, the warping-to-bending stress ratio in the bottom flange of the quasi-closed section converges to that of the fully closed box. As the top bracing member becomes more flexible, smaller warping stresses are induced in the girder section. The smaller warping stresses in the quasi-closed tub girder imply an occurrence of a larger cross-sectional deformation, which implies that the diagonal bracing is not sufficient enough to ensure the quasi-closed section response. There exists a minimum size of diagonal stiffeners to make a quasi-closed section that is almost equivalent to a complete closed section with a solid plate element. The effectiveness of the diagonal bracing will not increase corresponding to the member size beyond this limiting minimum value.

9.5.8.2 Effect of Stiffness of Cross-Frames on Distortional Stress

There is no detailed design specification for the determination of the internal cross-frame size. Therefore, a parametric study was conducted to examine which size of structural member would be appropriate for the internal cross-frame. The parametric study revealed that the cross-sectional area of internal cross-frames affect the distortional stresses of a closed composite girder section. The variation of the

distortional stress ratio is presented, along with the stiffness of the cross-frame in Fig. 9.29. After a certain point, there is no more variation in the ratio as the area continues to increase. Therefore, an optimum size for the cross-frame can be determined at this point. For this model bridge, the structural tee section, WT 7X24, was selected for the cross-frame member after a few trials.

9.5.8.3 Effect of Spacing of Cross-Frames on Distortional Stress

It is evident from Figs. 9.24 to 9.27 that the distortional stress is linearly distributed across the cross-section of the bottom flange of horizontally curved box girders and the maximum value is greatly influenced by the spacing of cross-frames. The maximum distortional stress is inversely proportional to the spacing of the cross-frames. When the cross-frame spacing was reduced from 30 feet to 15 feet, the maximum ratio of the distortional stress to vertical bending stress ratio reduced from 10% to 4.8%. When the cross-frame spacing was reduced by half again, i.e., from 15 feet to 7.5 feet, the maximum stress ratio reduced only from 4.8% to 3.5%. There is no substantial decrease in the stress ratio corresponding to further reduction in the cross-frame spacing.

The maximum distortional stress ratio versus the cross-frame spacing is plotted in Fig. 9.30. Fig. 9.30 shows the variation of the maximum distortional stress vs. the cross frame spacing. As the cross-frame spacing reduces, the maximum distortional stress decreases rapidly down to a certain value around 10% of the vertical bending stress. The maximum distortional stress, however, reduces very

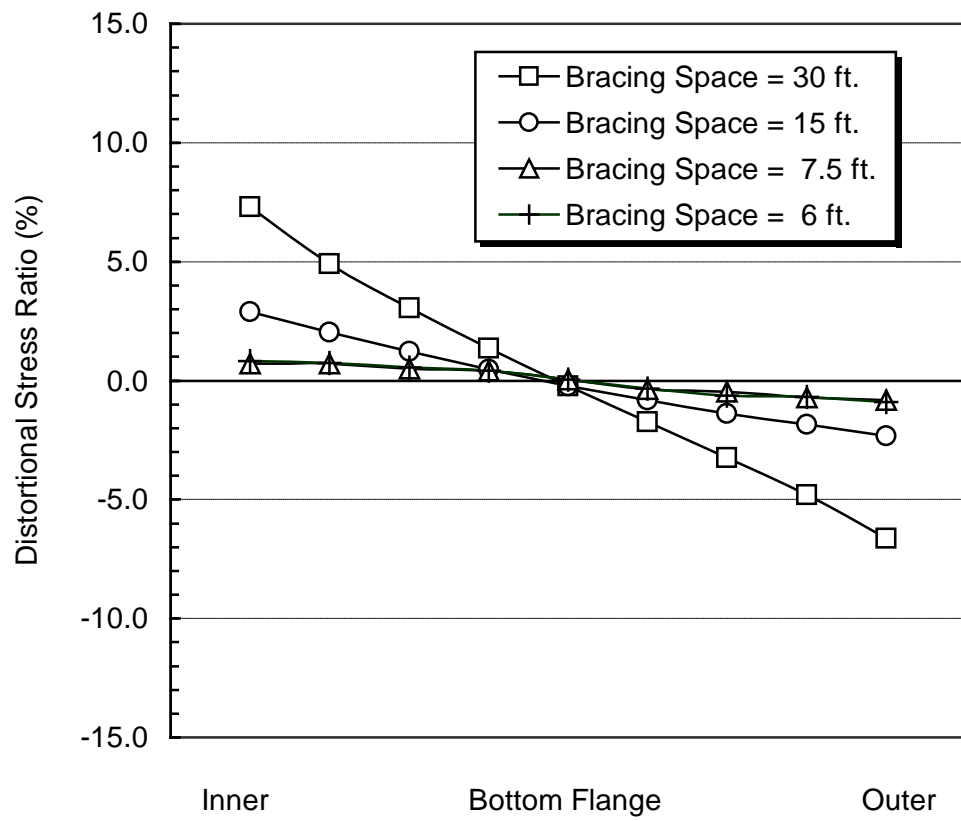


Fig. 9.24. Non-Uniform Normal Stress Distribution in the Bottom Flange (Under DL1)

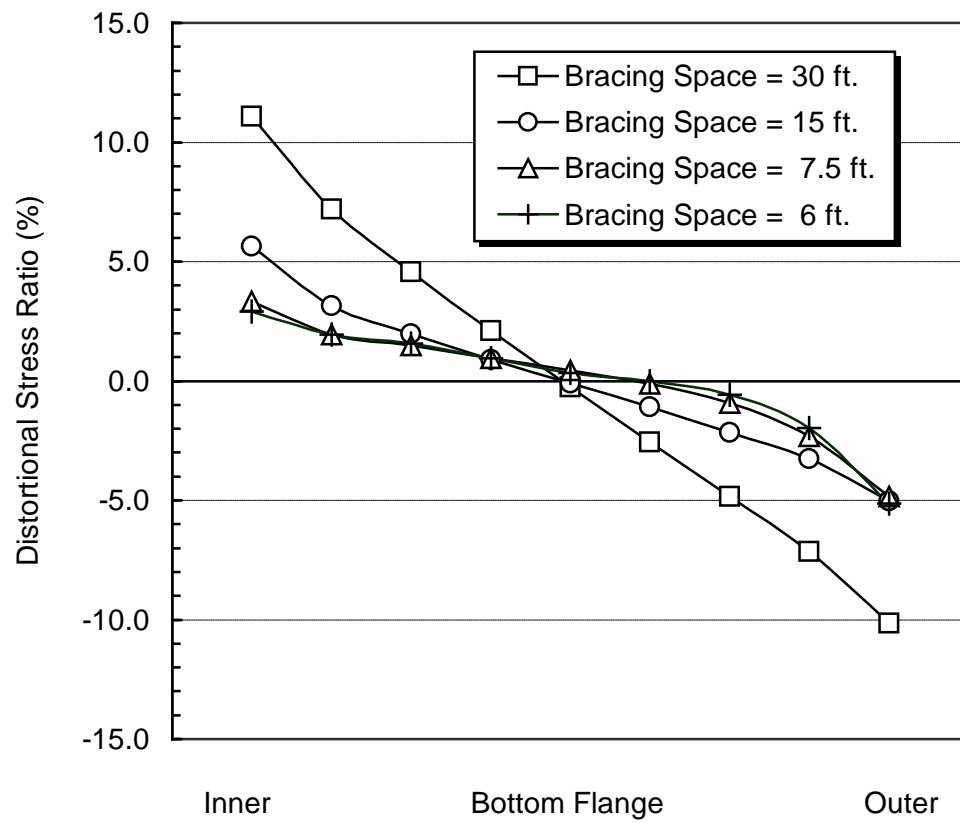


Fig. 9.25. Non-Uniform Normal Stress Distribution in the Bottom Flange (Under DL2)

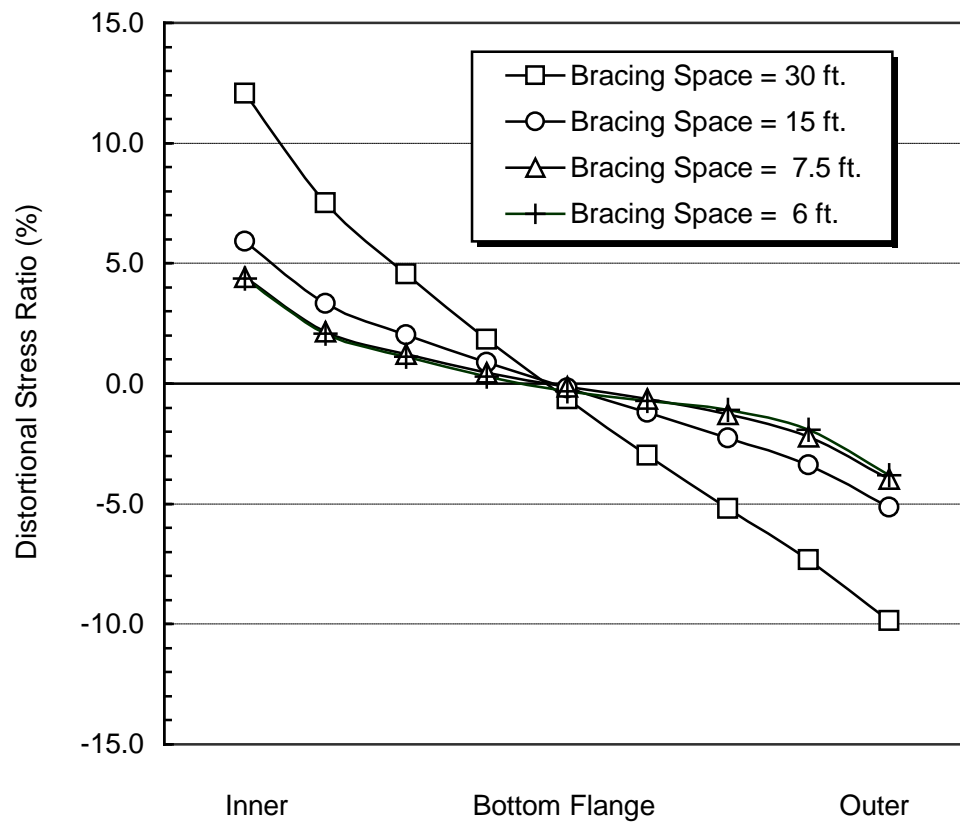


Fig. 9.26. Non-Uniform Normal Stress Distribution in the Bottom Flange (Under LL+I)

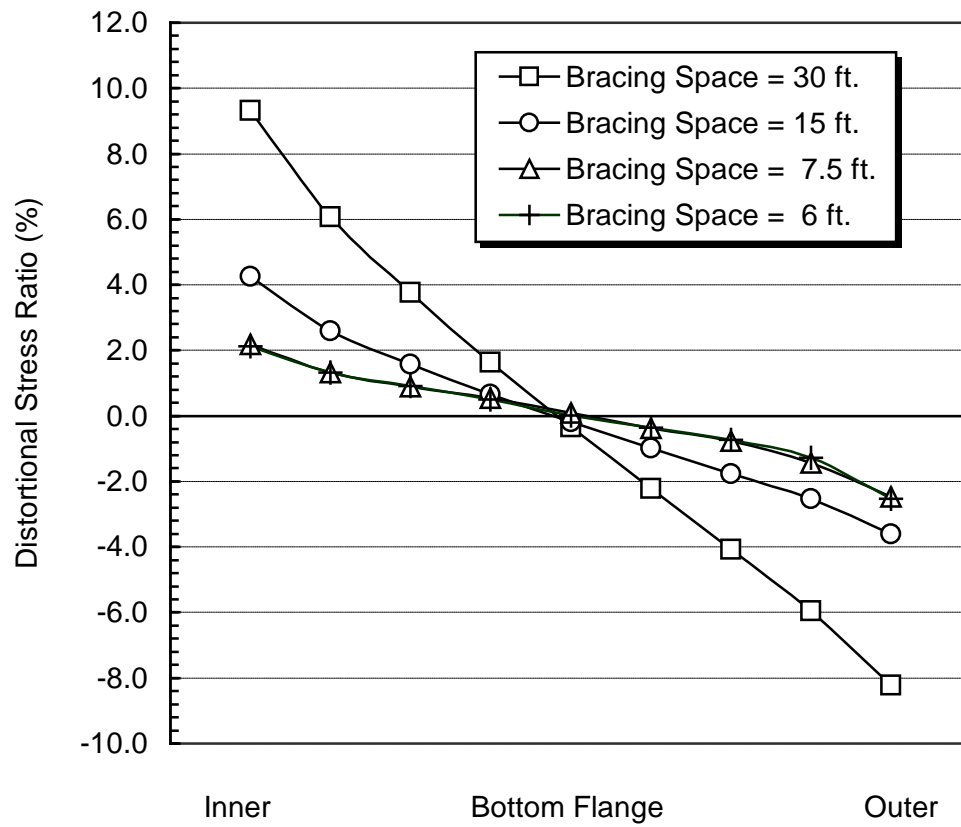


Fig. 9.27. Non-Uniform Normal Stress Distribution in the Bottom Flange (Under the Load Combination Group (I))

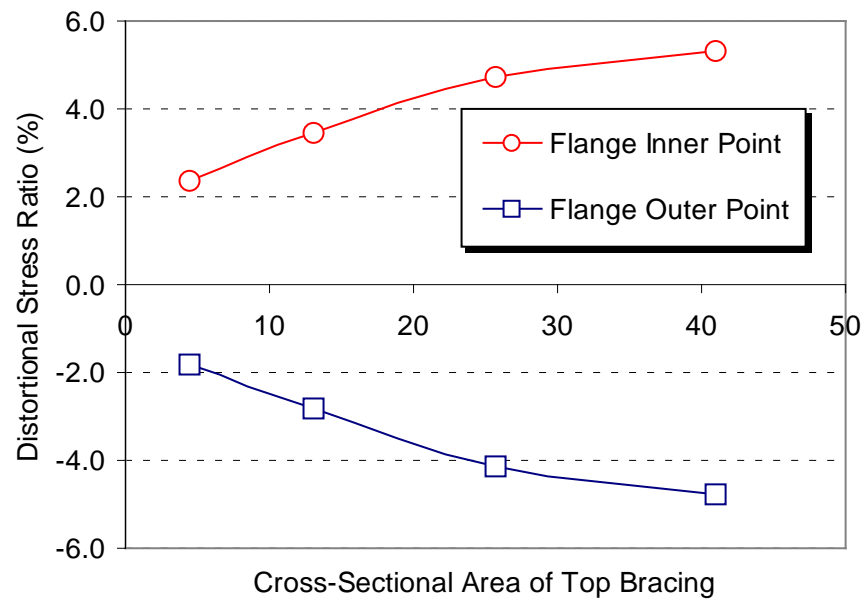


Fig. 9.28. Effect of Top Flange Bracing on Distortional Stress

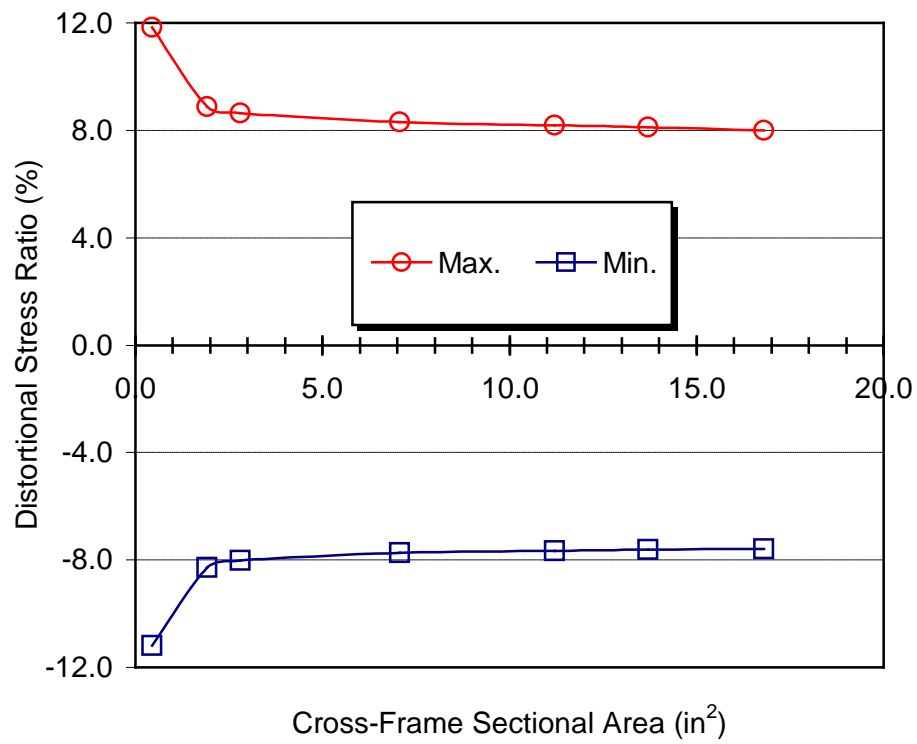


Fig. 9.29. Effect of Sectional Area of Cross-Frames on Distortional Stress

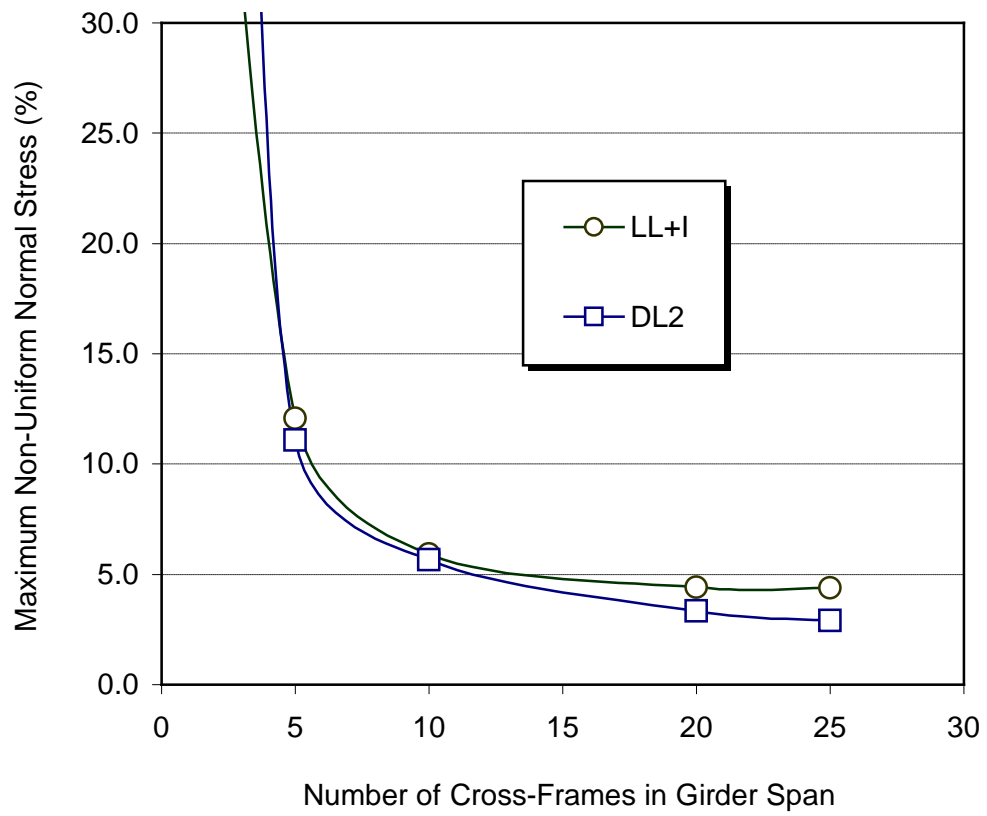


Fig. 9.30. Variation of Maximum Distortional Stress Ratio vs. Number of Cross-Frames

slowly in the range below 10 percent of the vertical bending stress although a larger number of cross-frames are placed in this hypothetical bridge examined.

9.5.9 Stress Distribution in a Well-Designed Box Flange

Fig. 9.30 indicates that the number of cross-frames needs to be six. The cross-frame spacing is determined to be 21 feet (span length of 150 feet divided by 7 intervals) in this example. Thus, an analytical model with a cross-frames spacing of 15 feet was selected to demonstrate a typical stress distribution in the bottom flange of horizontally curved box girders. The normal stresses were almost uniformly distributed in the bottom flange. The maximum non-uniform normal stress was 5.23 percent of the vertical bending stress, which occurred in the midpoint between adjacent cross-frames. The minimum gradient of the normal stress distribution was found around the cross-frames. It is noted that the pattern of the developed the distortional bimoment resembles the moment diagram of a continuous beam with a series of very flexible supports such that the negative moments at the interior supports are smaller than those at the midpoints between these supports.

9.5.10 Longitudinal Stiffeners for the Flanges of a Horizontally Curved Box Girder

In the typical cross-frame as shown in Fig. 9.31, transverse bracing members are required in the bottom and top of the box section to retain the original cross-sectional shape. Hall and Yoo suggest (1998) that the transverse bracing members shall be attached to the box flange by welding or to the longitudinal stiffeners by bolting. If the transverse bracings are bolted with the longitudinal stiffeners, it is

expected that they should act as a support restraining the vertical displacement of the longitudinal stiffeners at the connected point.

The cross-frame spacing of 21 feet amounts to one seventh of the span length, which is assumed to be smaller than the length of the negative moment zone in most continuous curved box girder bridges. Thus, the longitudinal stiffeners should be designed for the spacing between the adjacent cross-frames. The aspect ratio, α , of the subpanel of the stiffened flange, thus, is determined as

$$\alpha = \frac{l_b}{w}$$

where $l_b = L/(N_{cb} + 1)$ = cross-frame spacing; $w = b/(n + 1)$ = subpanel width; L = span length; N_{cb} = the number of cross-bracings. In the box girder model, the subtended angle between the adjacent cross-frames is calculated as

$$\phi_b = \frac{1}{(N_{cb} + 1)} \cdot \frac{L}{R} = \frac{l_b}{R} = \frac{21 \text{ ft.}}{300 \text{ ft.}} = 0.07 \text{ radian} = 4.01^\circ.$$

A typical connection detail for the cross-frame and longitudinal stiffener is shown in Fig. 9.31.

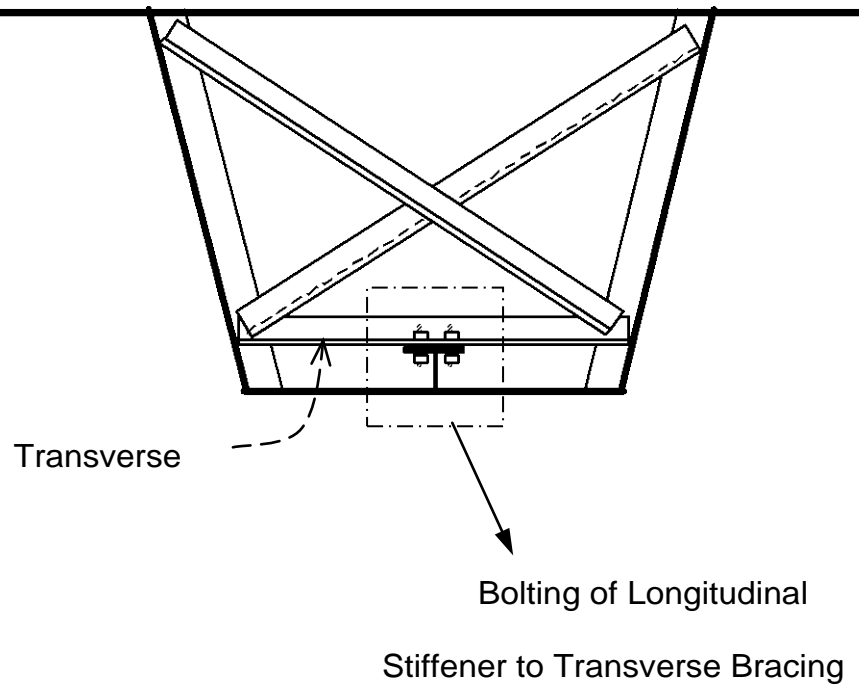


Fig. 9.31. Typical Connection of Transverse Bracing of Cross-Frames and Longitudinal Stiffener in Box Girder

9.6 Stability of Horizontally Curved Stiffened Flanges

9.6.1 Introduction

Longitudinal stiffeners are attached to a flat plate member in compression in order to enhance its stability and increase its strength. The influence of longitudinal stiffeners on the stability of the flange of a horizontally curved box girder was investigated as a major part of this study. For the stability analysis, a series of elastic buckling analyses were conducted on computer models of horizontally curved stiffened flanges using MSC/NASTRAN.

During an exploratory analysis on a selected number of example cases, it was found that there exists a definite range of geometrical properties of a horizontally curved stiffened flange to yield optimum design. Only the design of longitudinal stiffeners needs to be considered in order to achieve an optimum design of the bottom flange of a horizontally curved box girder. In order to reflect a realistic design condition in the numerical models analyzed, the curved stiffened flange panels were selected to be within the distortion stress limits established in Section 9.5. The longitudinal stiffener has the same length as the spacing of the adjacent cross-frames and the pre-buckling stresses were set to have same proportions as the induced stresses in a realistic box girder flange.

Although it would be much simpler to adopt an isolated flange model for a curved stiffened flange as was done the case of straight flanges Section 9.4, an isolated curved flange model cannot possibly accommodate a non-uniform stress distribution across the flange width. Therefore, a complete box girder model including two webs and a top flange (rectangular section) was used. The stresses considered in the model include all possible stresses that develop in a horizontally curved box girder flange.

9.6.2 Model Description

The analytical model is a simple span horizontally curved box girder. The end boundary condition simulates a pin-roller condition for vertical bending and a torsionally simple end. A set of bearings at either end prevents the girder from flipping over due to torsion.

The test girder has three parts, as shown in Fig. 9.32. The compression flange test region for the investigation is located in the central part of the girder. The other two parts are located on each side of the test region.

In order to simulate a nearly uniform compression state at the bottom flange, a pair of upward concentrated loads was applied symmetrically near the one-fifth points of the span, thereby, creating a uniform moment region in the middle test region as shown in Fig. 9.32. From the loading condition, nearly uniform compressive stress is induced in the flange. Cross-frames are placed at one-fifth points such that the normal stress gradient is less than 0.1 across the bottom flange. The test region was isolated from the concentrated load points to minimize the potential stress concentration effects.

It has been shown by Yoo et al. (2001) that the effective boundary condition at the juncture of an inclined web and the bottom flange of a box girder is rather close to a simple connection. Therefore, Article 10.51.5.4 of AASHTO (1996) appears justified. It requires that the longitudinal stiffeners be placed with an even spacing across the bottom flange neglecting any reserve strength of the plate strip adjacent to the web afforded by a clamping effect at the boundary.

The longitudinal stiffeners are attached to the bottom flange across the entire span just for the ease of automatic modeling. The initial trial value for the moment of inertia

of the stiffeners is calculated using the equation formulated for the stiffeners of the straight panel.

A 4-node plate/shell element, CQUAD4, in MSC/NASTRAN was used to represent both the plate and stiffeners. The finite element mesh of the model is presented in Fig. 9.33. The stress-strain relationship was assumed to be linear and isotropic in these elastic analyses.

9.6.3 Analysis Results

9.6.3.1 Linear Static Analysis

It is intended here that the box girder model being considered is adequate to create the pre-buckling stress distribution in the bottom flange of a curved box girder. Fig. 9.34 shows the longitudinal stress distribution in the bottom flange from the static analysis of the model being considered. The horizontal axis represents the distortion stress divided by the vertical bending stress and the vertical axis stands for positions across the flange width. It can be seen from Fig. 9.34 that the longitudinal stress distribution across the flange width varies linearly. At the center of the test region (the middle one- fifth span), the distortional stress at the inner edge is additive to the vertical bending stress, thereby implying a flange bending moment (or distortional bimoment) is being developed due to the distortional action. It should be noted that the distortional stress at the one-quarter point of the test region is more than one-half of the maximum value at the center of the test region. This is a further testimony that the effect of the cross-frames is considered very flexible (rather than immovable support conditions) as discussed in Section 9.5 (Fig. 9.21). Fig. 9.35 shows the effect of the subtended angle, a/R , between the adjacent cross-frames on the distortional stress distribution in the bottom flange. In Fig 9.35, the y-axis

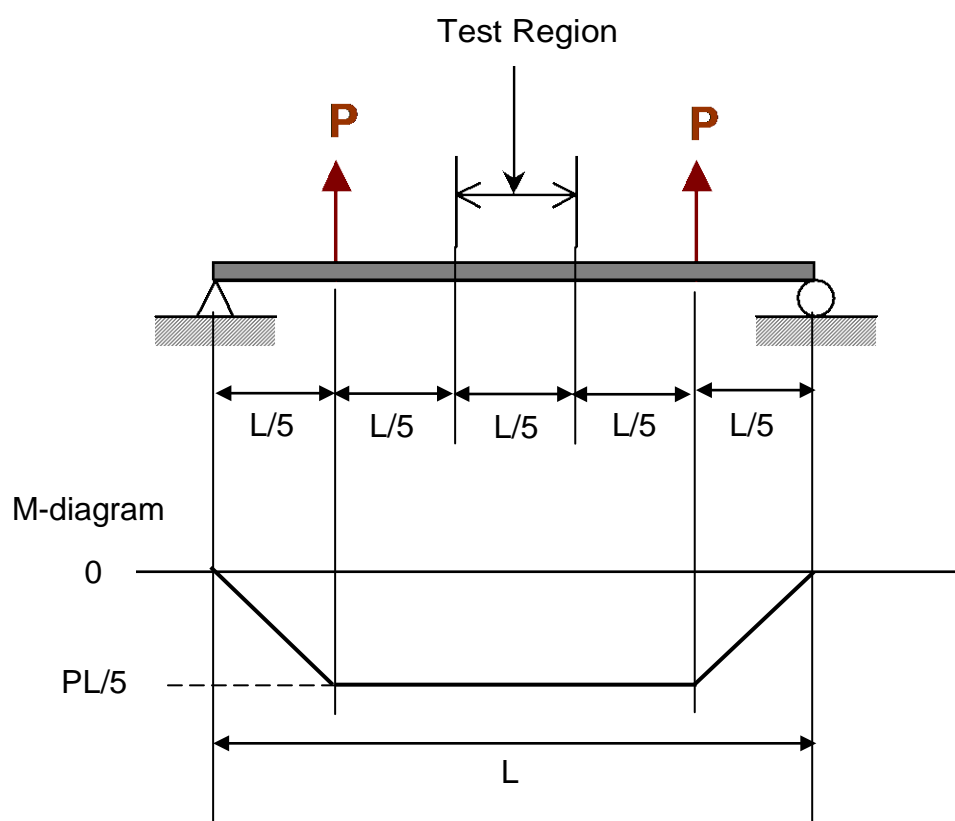


Fig. 9.32. Loading Scheme and Approximate Moment Diagram

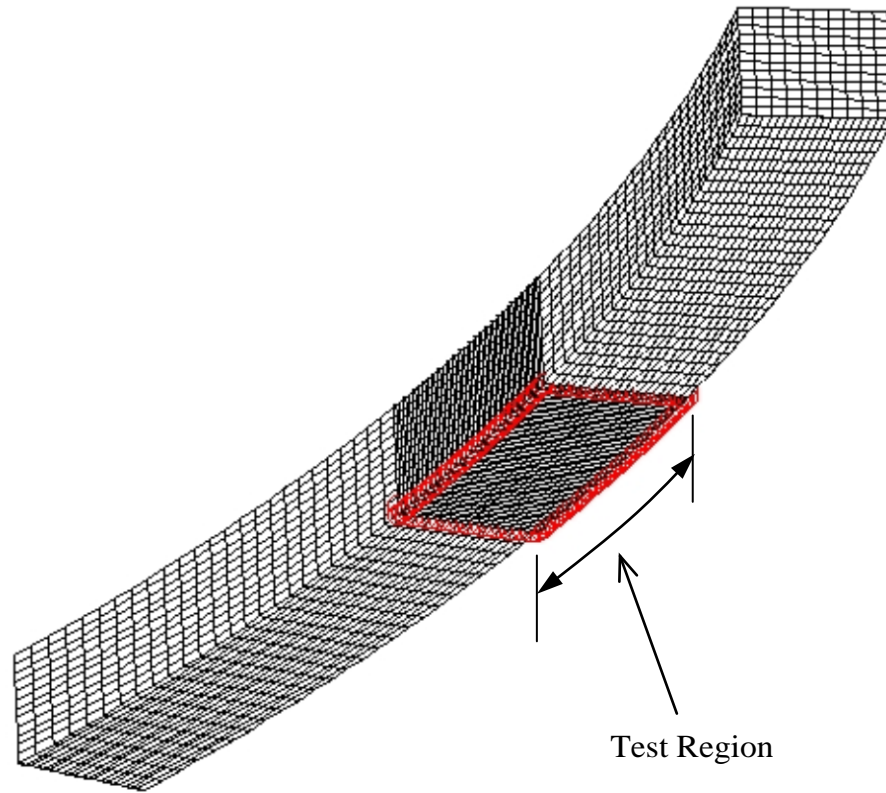


Fig. 9.33. Finite Element Mesh of Box Girder Model

stands for the maximum ratio of the distortional stress to the vertical bending stress and the x-axis indicates the subtended angles, a/R . It can be seen from Fig. 9.35 that the maximum distortional stress is almost linearly proportional to the subtended angle of the bottom flange.

9.6.3.2 Elastic Buckling Analysis

The lateral forces developed due to the curvature effect are proportional to the subtended angle between the adjacent transverse stiffeners (Davidson, 1996; Culver and Mozer, 1972). Since the usual subtended angles between the adjacent transverse stiffeners are very small (less than 5°), it is expected that the effect of the lateral force is not substantial. This expectation was indeed verified from the elastic buckling analysis of the model that the effect of the lateral force on the buckling mode shape and the elastic buckling strength of the horizontally curved stiffened flange were not influenced as to be a practical concern. It was found from the elastic buckling analysis that the bending rigidity of the longitudinal stiffener affected the elastic buckling stress and corresponding buckling mode shape. It was found that the buckling mode shapes of the curved stiffened flanges have basically the same as those of straight flanges.

When the rigidity of the longitudinal stiffener is small, the longitudinally stiffened compression flange buckles in the symmetric mode and the stiffeners buckle along with the embedded panel as shown in Fig. 9.36(a). However, when the rigidity of the longitudinal stiffeners is increased beyond a certain limiting value, the panel buckles into the anti-symmetric mode. In the anti-symmetric buckling mode shape, the longitudinal stiffeners remain straight along the nodal line, although they are twisted as shown in Fig.

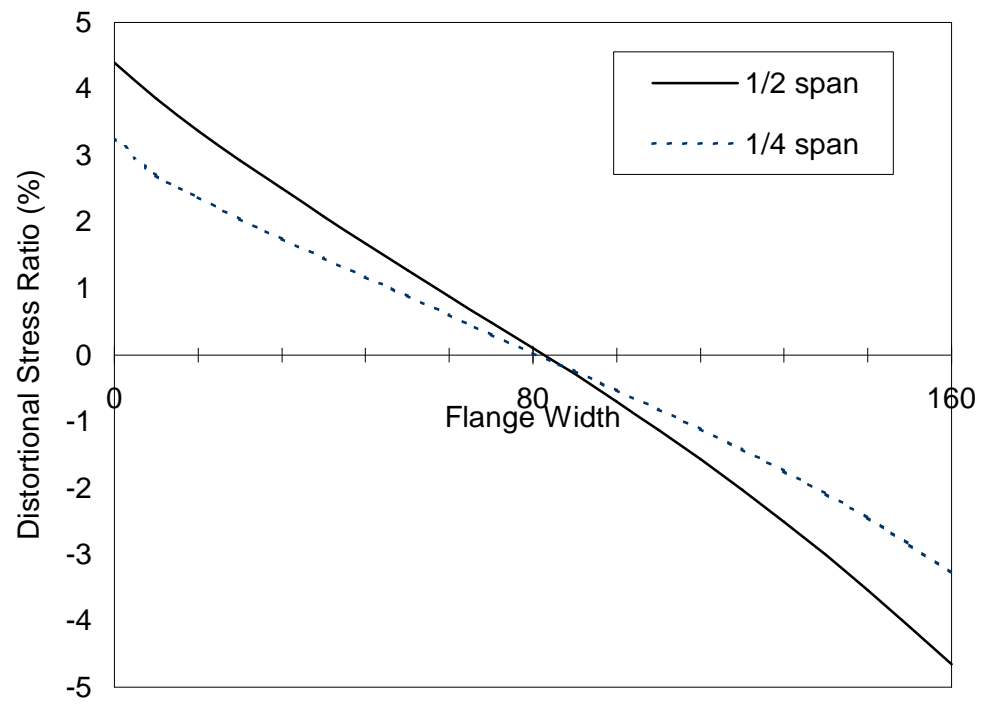


Fig. 9.34. Distortional Normal Stress Variation in Curved Bottom Flange Model ($n=1$, $\alpha=5$, $w=80$ in., $t_f=1.0$ in., $R=800$ ft.)

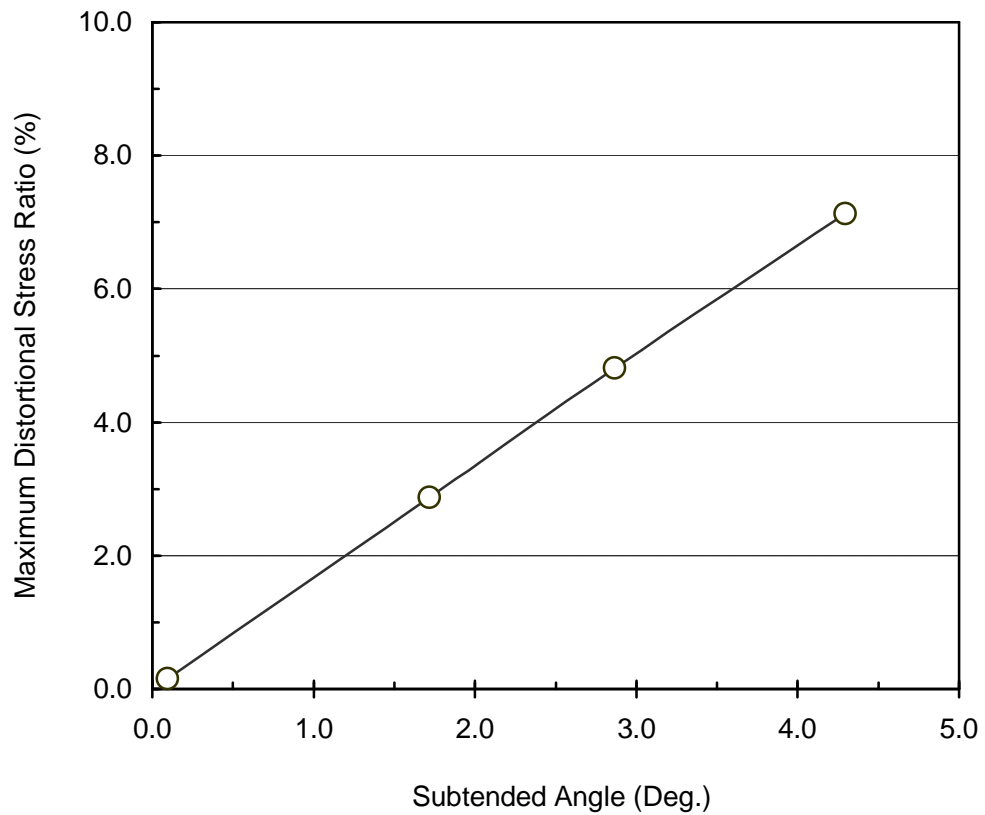


Fig. 9.35. Maximum Distortional Stress versus Subtended Angle ($n=1$, $\alpha=3$, $w=60$ in., $t_f = 1.0$ in.)

9.36(b). Fig. 9.37 illustrates the anti-symmetric buckling mode shape in the bottom flange of the box girder model. Fig. 9.36(b) is a simplified view of Fig. 9.37 highlighting the anti-symmetric buckling mod shape of the test region. Fig. 9.38 illustrates that the elastic buckling strength of the symmetric buckling (strut action) is almost linearly proportional to the bending rigidity of the longitudinal stiffeners.

The increase in the moment of inertia of the longitudinal stiffeners beyond the limiting value does not accompany corresponding increment in the elastic buckling strength of the stiffened panels as shown in Fig. 9.38. Thus, it is only wasteful to specify longitudinal stiffeners with higher moment of inertia than this limiting value. Therefore, this limiting value of the moment of inertia was considered as the minimum required rigidity of the longitudinal stiffener. Fig. 9.38 is essentially the same as Fig. 9.6. An anti-symmetric buckling is essentially a local buckling. Therefore, the strength of a longitudinally stiffened panel is essentially dependent on the plate properties when the bending rigidity of the stiffener is above the minimum value. It is well known that the minimum buckling coefficient, k , of a panel becomes four when the panel shape is a square.

In the anti-symmetric buckling mode, the subtended angle corresponding to one half sinusoidal wave shape (refer to Fig. 9.36(b)) becomes equal to the subtended angle between the adjacent cross-frames, a/R , divided by the aspect ratio, α . The subtended angle corresponding to one sinusoidal buckling shape, ϕ_s , can be expressed by Eq. (9.40).

$$f_s = \frac{f_b}{a} = \frac{1}{a} \times \frac{1}{N_{cb} + 1} \times \frac{L}{R} \quad (9.40)$$

where N_{cb} is the number of cross-frames in a girder span. It can be seen from Eq. (9.40) that the subtended angle, ϕ_s , can be much smaller than the subtended angle of an entire girder, L/R .

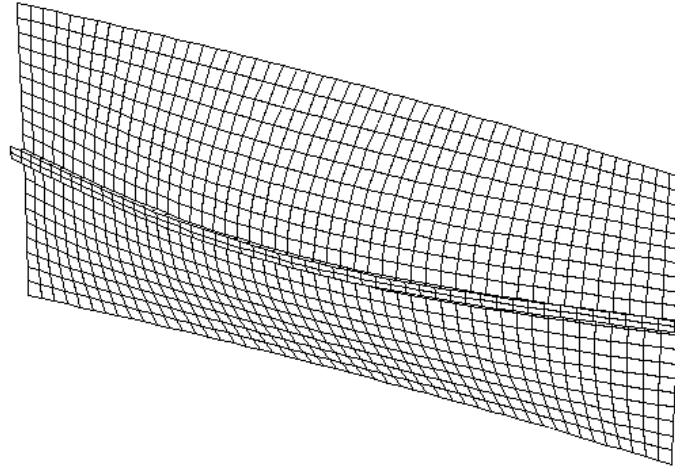
As explained in the Chapter 2, Bryan (1891) presented an analysis of the elastic critical strength for a rectangular plate that were simply supported along all edges and subjected to a uniform longitudinal compressive loading, and proposed Eq. (9.13) for the elastic critical strength of a long plate. The elastic critical strength of the rectangular plate is determined by the plate width-to-thickness ratio, t/w .

$$F_{cr} = \frac{k \rho^2 E}{12 (1 - \mu^2)} \left(\frac{a}{w} \right)^2 \quad (9.13)$$

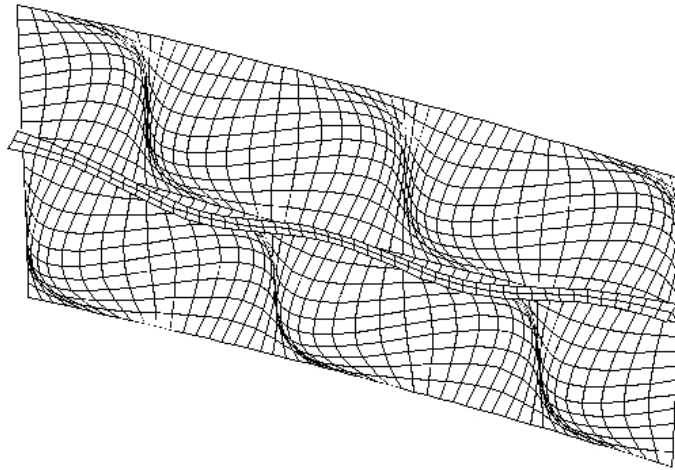
where k = the bend-buckling coefficient; E = modulus of elasticity; and μ = Poisson's ratio.

Table 9.5 shows the elastic buckling analysis results for the curved stiffened flange models. The critical stress values from the selected cases are compared with those from Eq. (9.13) in Table 9.5. The “ $F_{cr} Diff$ ” column in Table 9.5 implies the percentage differences between the analysis results and those from Eq. (9.13). It can be seen from Table 9.5 that the anti-symmetric buckling strength of the curved stiffened flanges shows a good correlation with Eq. (9.13).

Since slender plate members can often sustain additional loads in the post-buckling range, the ultimate failure strength of a slender stiffened flange might be higher than the elastic buckling stress. However, current AASHTO (1996) design philosophy for steel bridge structures does not include the post-buckling strength in vertical bending



(a) Symmetric Buckling Mode Shape



(b) Anti-symmetric Buckling Mode Shape

Fig. 9.36. Typical Buckling Mode Shapes of Curved Stiffened Flanges ($n=1$, $\alpha=5$)

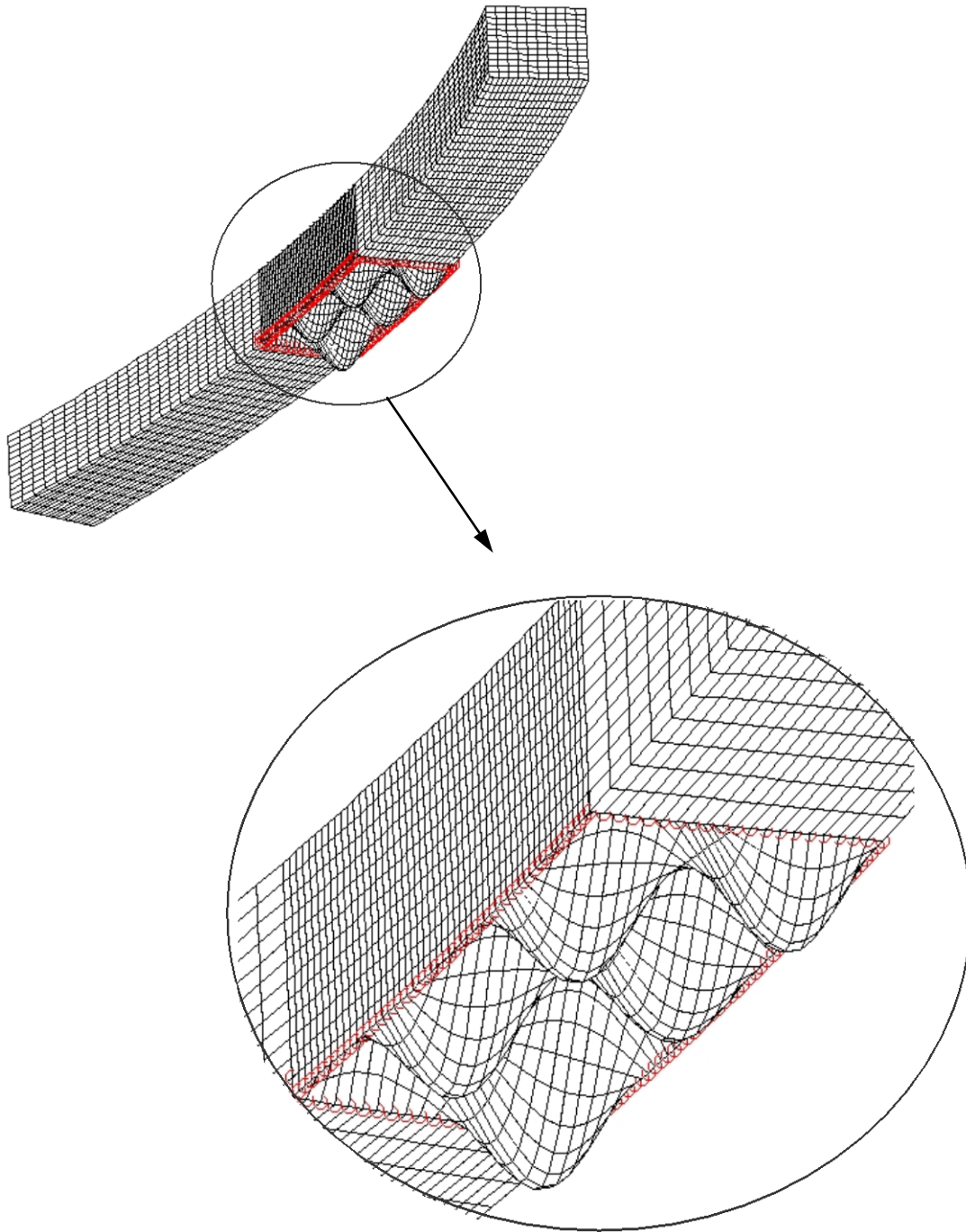


Fig. 9.37. Buckling Mode Shape in a Hypothetical Box Girder Model

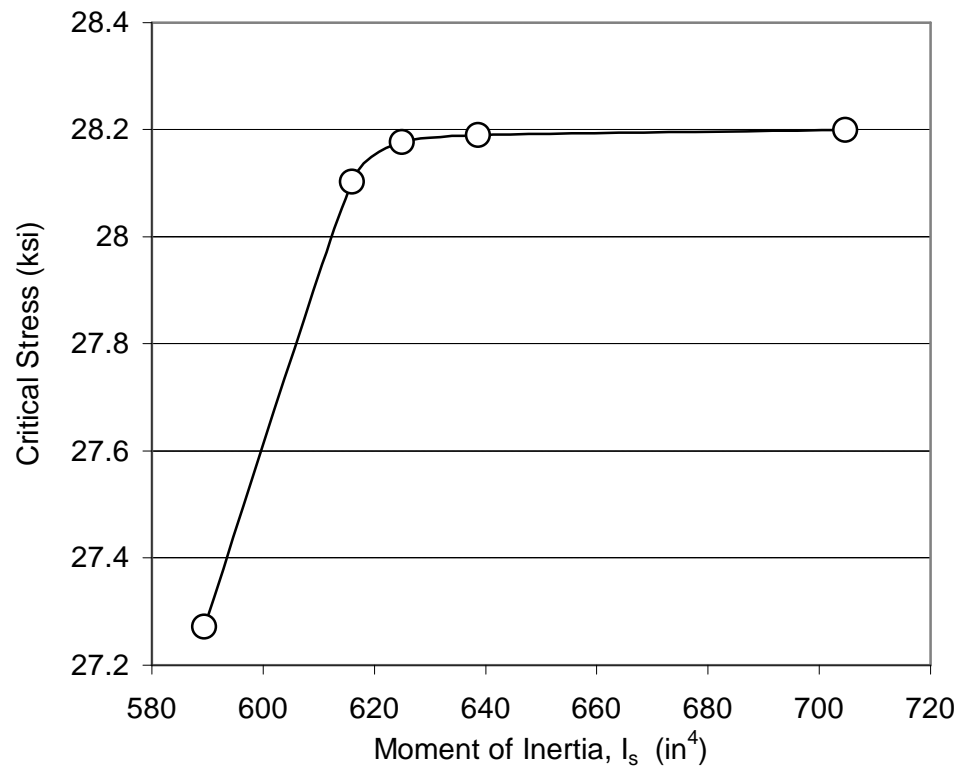


Fig. 9.38. Elastic Critical Stresses of Curved Stiffened Flange ($n=2$, $\alpha=5$, $w=60$ in., $t_f=1.0$ in., $R=300$ ft)

as the post-buckling phenomenon in flexure requires excessive deflections of the compression flange.

Table 9.5. Elastic Buckling Stress of Curved Stiffened Flanges

n	α	w (in.)	t (in.)	R (ft.)	I_s , Eq. (9.42) (in ⁴)	I_s , used (in ⁴)	F_{cr} , Eq. (9.13) (ksi.)	F_{cr} , <i>FEM</i> (ksi.)	F_{cr} , <i>DIFF.</i> (%)
1	3	60	1	300	185.7	162.0	29.12	29.11	-0.04
1	3	120	1.5	500	1151.1	1093.5	16.38	16.26	-0.77
1	5	60	1	200	452.1	450.0	29.12	29.32	0.67
1	7	30	0.438	300	33.6	36.9	22.30	23.10	3.61
2	5	60	1	300	638.7	636.4	29.12	30.09	3.33
3	3	120	1	700	564.0	561.2	7.28	7.47	2.66
3	3	120	1.5	800	1771.0	1894.0	16.38	16.57	1.17
3	5	60	1	600	779.4	779.4	29.12	30.69	5.38
Note: 1 in. = 25.4 mm; 1 ksi = 6.985 MN/m ²									

9.7 Moment of Inertia of Longitudinal Stiffeners Attached to Curved Box Girder Flanges

9.7.1 Introduction

The minimum required rigidity of the longitudinal stiffeners used in curved box girder flanges is determined based on the elastic buckling analyses of the horizontally curved box girder models. The analysis results were collected from 142 hypothetical models varying the key parameters for a wide range of practical proportions. A numerical equation is formulated based on a series of regression analyses on the data collected for the determination of the minimum required moment of inertia of the longitudinal stiffener attached on the horizontally curved box girder flange.

9.7.2 Parameters for Data Collection

A series of exploratory elastic buckling analyses of the hypothetical models for the horizontally curved box girder flange revealed that the elastic buckling behavior of the stiffened flanges of horizontally curved box girders has fundamentally similar characteristics to those of straight stiffened flanges. This is somewhat expected phenomenon considering the subtended angles between the adjacent cross-frames being very small as examined in Section 9.6, which implies that the portion of the stiffened subpanel of the box girder compression flange is essentially straight. Therefore, the key parameters used in Section 9.4.5 for the determination of the minimum required rigidity of the longitudinal stiffeners attached on the straight box flanges are considered adequate.

The parameters are the number of stiffeners, n , the aspect ratio, a , the thickness of the compression flange, t_f , the distance between stiffeners or the distance from the

stiffener to the nearest web plate, w , and the subtended angle, ϕ_b , of the adjacent cross-frames, which was added to reflect the effect of the curved geometry.

A simple and direct method that can be used to determine the minimum required rigidity of the longitudinal stiffeners does not exist. The limiting value can be recognized readily in a plot similar to the one given in Fig. 9.38. Thus, an iterative process must be used to obtain the threshold value as the minimum required rigidity. In order to extract a data point, the hypothetical model of the curved stiffened flange shown in Fig. 9.32 was analyzed several times by varying the moment of inertia, I_s .

As pointed out by Kerensky (1973) and discussed in Section 9.4.2, if a simple flat plate is used as the longitudinal stiffener, it must have an impracticably large thickness to attain the threshold value for the moment of inertia. The threshold value of the rigidity can be achieved by using ordinary structural tee shape available in AISC *LRFD* (2001). 142 model cases were analyzed. Selected analysis results of the model cases are listed in Table 9.5. In Table 9.5, values in the column designated by " I_s used" are the minimum required moment of inertia of the longitudinal stiffener determined through the iterative process.

9.7.3 Regression Analysis

A simple form of $I_s = C n^w \alpha^{\bar{\phi}} t_f^3 w$ has been selected for a regression equation for the determination of the minimum required moment of inertia of the straight longitudinal stiffener. A factor $f(\phi_b)$ is added to the simple form so as to consider the curvature effect. Thus, the regression equation is expected to have a form as

$$I_s = C n^{\beta} \alpha^{\bar{\phi}} t_f^{\zeta} w^w f(\phi_b)$$

where C , β , α , ψ , ζ , and η are constants to be determined by the regression analysis.

Generally, the straight flange can be considered as a special horizontally curved flange having a subtended angle equal to the null value. Thus, the following relationship is assumed between the minimum required moment of inertia of the straight longitudinal stiffener and that of the curved longitudinal stiffener:

$$I_{s \text{ (curved)}} = f(\phi_b) I_{s \text{ (straight)}}$$

which is rearranged to give,

$$f(\phi_b) = \frac{I_{s \text{ (curved)}}}{I_{s \text{ (straight)}}} \quad (9.41)$$

Note that $f(\phi_b) = 1$ for $\phi_b = 0$.

The regression equation for the minimum required moment of inertia of the straight longitudinal stiffener has already been given by Eq. (9.27).

$$I_{s \text{ (straight)}} = 0.3 n^{0.5} \alpha^2 t_f^3 w \quad (9.27)$$

Therefore, it is expected that

$$I_{s \text{ (curved)}} = f(\phi_b) (0.3 n^{0.5} \alpha^2 t_f^3 w) \quad (9.42)$$

In order to complete Eq. (9.42), $f(\phi_b)$ needs to be determined. A typical variation of the required minimum moment of inertia of curved longitudinal stiffeners is shown in Fig. 9.39. In Fig. 9.39, the x-axis represents the subtended angle between adjacent cross-frames of the curved stiffened flange and the y-axis is for the minimum required moment of inertia of the curved longitudinal stiffener divided by that of the straight longitudinal stiffener of the subpanel with exactly the same key parameters.

Examination of Fig. 9.39 reveals that the function $f(\phi_b)$ does not vary as to alter the minimum moment of inertia of the straight longitudinal stiffener in all ranges of practical design parameters. Therefore, the function of the subtended angle, $f(\phi_b)$, is determined to be equal to one and the minimum required moment of inertia for curved longitudinal stiffener is identical to that of the straight longitudinal stiffener when other key parameters, n , α , w , t_f remain the same.

Eq. (9.27) contains parameters representing the length of the panel between two adjacent transverse stiffeners. Because a longitudinal stiffener subjected to compression acts in a similar way to a column, the inclusion of a parameter representing the length of the member appears logical, although it is not included in the current AASHTO (1996) equations. Note that the required moment of inertia of the longitudinal stiffener used for compression flanges stiffened longitudinally and transversely is given in the AASHTO (1996) as

$$I_s = 8t_f^3 w \quad (9.43)$$

Comparison of Eq. (9.27) with Eq. (9.43) reveals that Eq. (9.43) generally gives an unconservative value for the required moment of inertia for most cases in practical designs. Therefore, it is proposed that Eq. (9.27) replace the AASHTO (1996) equations for both straight and curved box girders.

Substituting relevant values ($k=4$ and $\mu=0.3$) into Eq. (9.25) reveals that the coefficient for the required minimum moment of inertia, I_s , of the straight longitudinal stiffener becomes a little smaller than 0.3 as determined by the regression process.

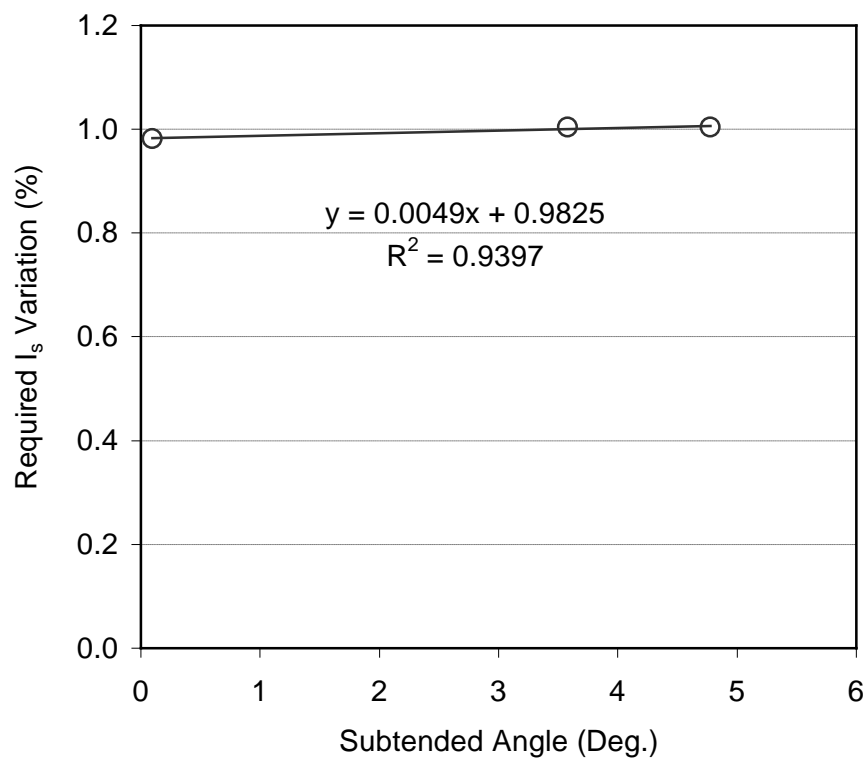


Fig. 9.39. Required Stiffener Rigidity along with Subtended Angle ($n = 2$, $\alpha = 5$, $w = 60$ in., $t_f = 1.0$ in.)

Therefore, it is considered to be prudent to use the coefficient of 0.3 conservatively in Eq. (9.27) for all required minimum moment of inertia for the straight longitudinal stiffener.

9.7.4 Conservatisms of the Proposed Design Equation

9.7.4.1 Effect of Boundary Condition

The simply supported boundary condition has been assumed on all sides of the test flange model of the hypothetical curved box girder in order to simulate the boundary conditions compatible to the model that yielded the elastic plate buckling Eq. (9.13).

Unlike a simply supported boundary condition, the bottom flange of a real box girder is continuous in the longitudinal direction of the girder on both ends of the test flange, and also the flange is connected to the web on both edges parallel to the longitudinal direction. Thus, there are certainly differences between the boundary conditions of flanges in real box girder and those of flanges in the hypothetical box girder analyzed in this study.

The longitudinal stiffeners are attached continuously between the transverse bracing and they may have a nearly rigid connection to the transverse bracing. Thus, the end boundary condition must be closer to the fixed boundary condition or an intermediate boundary condition between the hinged and fixed boundary condition.

A selected number of stiffened curved flange models with boundary conditions as close to the real structure as allowed by MSC/NASTRAN were analyzed in order to assess the differences in the elastic buckling strength. As for the effect of the web connection to the bottom flange, Ford (2000) and Yoo et al. (2001) have reported that the simply supported conditions were acceptable for boundary conditions between the web plates and compression flange through numerical tests for a hypothetical straight box

girder as discussed in Section 9.4.3. Since the effect of the web connection to the elastic stability must be fundamentally the same regardless of the curvature, the effect of the simple web connection to the flange was considered deemed adequate for curved box girder flanges.

9.7.4.2 Effect of Continuous Boundary on Flange Edges

The bottom flange of a box girder is subjected to compressive force in the negative moment zone between the interior pier and the inflection point, or the low moment zone. A solid interior diaphragm is generally used at the pier, and a transverse stiffener is likely to be placed at the other end of the compression flange panel, as per Article 10.51.5.4.4 of AASHTO (1996). The transverse stiffeners must have a size equal to that of a longitudinal stiffener. Although the translation degree of freedom in the out-of-plane direction is not complete restrained as assumed in the hypothetical plate model at the load application points, the presence of the transverse stiffener is considered adequate to restrain these degrees of freedom effectively. Since the bottom flange is continuous at the interior diaphragm or transverse stiffener location, it is readily recognized that the rotational degrees of freedom is essentially restrained at both ends of the bottom flange as opposed to the assumption employed in the simple boundary condition used in the hypothetical models.

To determine the amount of differences between the simply supported boundary condition used in the models and the more realistic boundary condition in box girder flanges at the edges perpendicular to the line of loading, a selected number of plate models with continuous boundaries were analyzed.

A typical buckling mode shape for these models is shown in Fig. 9.40. As can be

seen from Table 9.6, the critical stresses with continuous boundaries are consistently higher than the theoretical critical stresses evaluated from Eq. (9.13). This is as expected because the buckling strength of the flange panels with the continuous boundaries will increase due to the restraining effect of rotation with respect to an axis perpendicular to the line of force along the loaded boundary. Thus, it can be concluded that the realistic boundary condition at the load point increases the buckling strength of the bottom flange and this acts as an added factor of conservatism for the proposed equation for the minimum required moment of inertia of the curved longitudinal stiffener.

9.7.4.3 Effect of Stiffener Edge Boundary Condition

Overall buckling of the longitudinal stiffener is fundamentally identical to the Euler column buckling. The critical load for a column is given by the Euler formula as

$$P_{cr} = \frac{\pi^2 EI}{\lambda^2} \quad (9.44)$$

where E = modulus of elasticity; and I = moment of inertia of the column. Eq. (9.44) gives the critical load for any column, regardless of the boundary conditions, provided the effective length of the member, λ , is determined that is the length of one half sine wave.

In order to demonstrate the effect of the stiffener boundary condition on the computed buckling strength of the stiffened curved bottom flange, analytical studies were conducted on a selected number of models. Examination of the analysis results shown in Table 9.7, it becomes evident that the end boundary conditions of the curved longitudinal stiffener significantly affect the required minimum moment of inertia of the longitudinal stiffener.

Table 9.6. Critical Stress, F_{cr} (ksi) for Test Flange with Continuous Boundaries

n	α	w (in.)	t (in.)	R (ft.)	I_s , Eq. (9.27)	I_s , used	F_{cr} , Eq. (9.13) (ksi)	F_{cr} , FEM (ksi)	Differ. (%)
1	7	30	0.44	300	36.9	37.2	22.30	24.38	9.34
1	3	60	1	200	162.0	162.1	29.12	30.77	5.67
2	5	60	1	400	636.4	638.7	29.12	30.94	6.25
3	3	120	1.5	800	1894.0	1902.2	16.38	17.13	4.58

Note: 1 in. = 25.4 mm; 1 ksi = 6.985 MN/m²

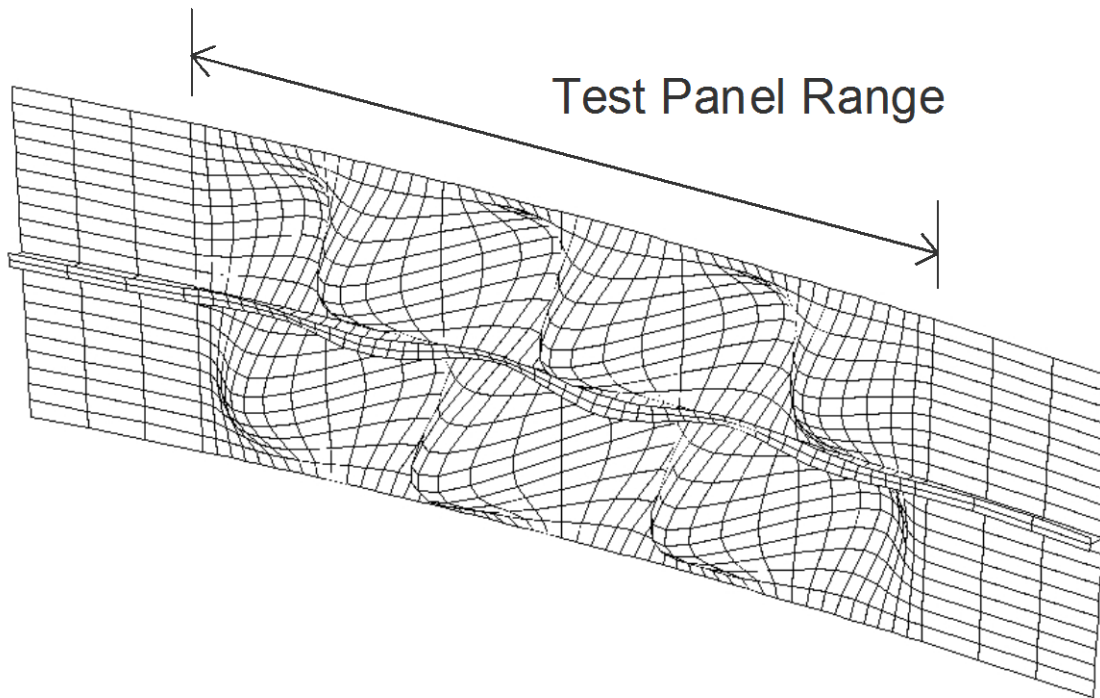


Fig. 9.40. Typical Buckling Mode Shape of Test Flange with Continuous Boundary

Table 9.7. Effect of Different Stiffener Edge Boundary Conditions

Stiffener End Boundary	Required I_s , used (in. ⁴)	I_s , Eq. (9.29) (in. ⁴)	$\frac{I_s (used)}{I_s^*}$	$\frac{I^2}{L^2}$	F_{cr} , FEM (ksi)	F_{cr} , Eq. (9.13) (ksi)
Hinged-Hinged	527.1	543.1	0.97	1	17.081	16.382
Fixed-Fixed	139.4	543.1	0.26	0.25	16.799	16.382
Fixed-Hinged	274.0	543.1	0.50	0.49	16.513	16.382

Note: $n=2$, $\alpha=4$, $w=80$ in., and $t_f=1.0$ in.

9.7.4.4 Effect of Moment Gradient

The box girder bottom flange is subjected to a very sharp vertical bending moment gradient between the interior pier and the point of contra-flexure. To assess the effect of the moment gradient on the critical buckling stress of the compression flange, a selected number of panel models were analyzed. As shown in Fig. 9.41, the moment gradient was conservatively assumed to be linear. Thus, the models were loaded with point loads simulating a linear variation of the moment. A typical buckling mode shape for these models is shown in Fig. 9.42. As can be seen from Table 9.8, the critical stresses for the compression flanges subjected to a linear moment gradient show significantly higher values than those computed from the Eq. (9.13). Note that the difference in the critical stresses decreases gradually for the plate panels with higher aspect ratios.

Table 9.8. Critical Stress, F_{cr} (ksi) for Test Flange under Linear Moment Gradient

n	α	w (in.)	t_f (in.)	R (ft.)	I_s , Eq.(9.27) (in. ⁴)	I_s , used (in. ⁴)	F_{cr} , Eq. (9.13) (ksi.)	F_{cr} , FEM (ksi.)	Differ. (%)
1	5	60	1	800	450.0	451.5	29.12	31.64	8.65
1	4	60	1	700	288.0	293.0	29.12	32.78	12.56
1	3	60	1	600	162.0	174.7	29.12	34.13	17.20
1	2	60	1	400	72.0	73.8	29.12	35.83	23.04
1	1	60	1	250	18.0	18.5	29.12	39.54	35.75
Note: 1 in. = 25.4 mm; 1 ksi = 6.985 MN/m ²									

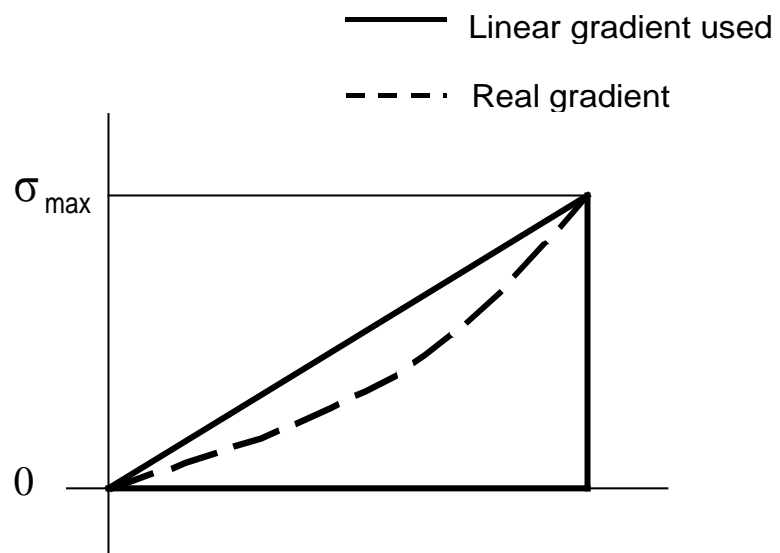


Fig. 9.41. Bending Moment Gradient and Applied Compressive Stress Gradient

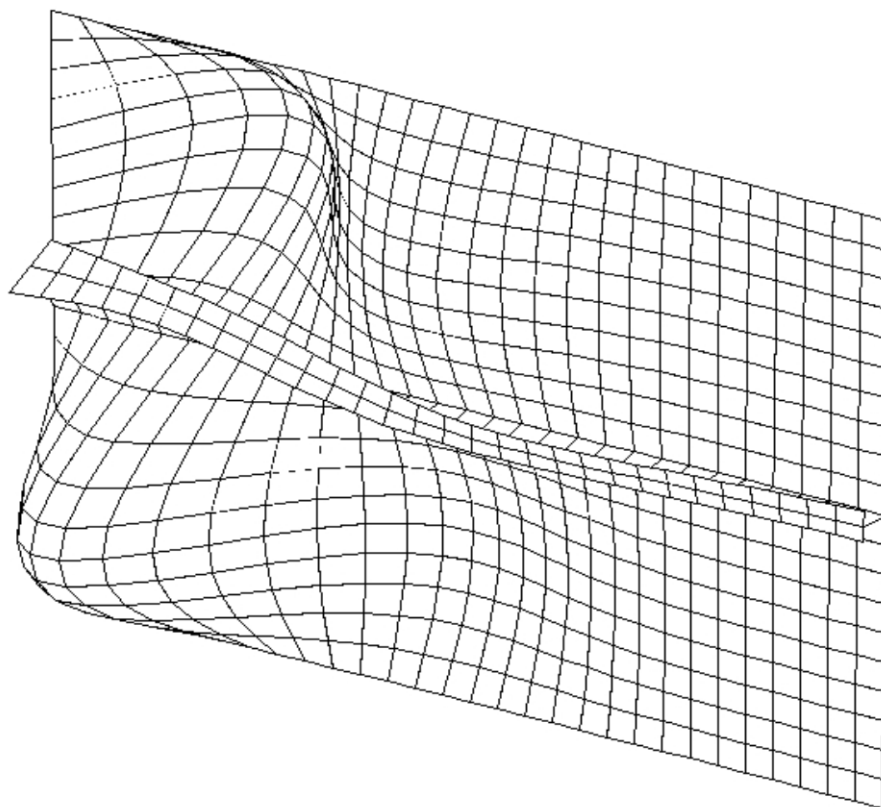


Fig. 9.42. Typical Buckling Mode Shape of Test Flange under Linear Moment Gradient.

9.8 Inelastic Buckling Strength

9.8.1 Introduction

The equations for the minimum required rigidity of the longitudinal stiffeners were derived in Sections 9.4 and 9.7 for straight and curved flanges. The proposed equations are formulated based on the elastic buckling analysis. However, an optimum design is usually accomplished by utilizing a compressive stress in the inelastic buckling range. The slope drawn on the critical stress curve is the steepest in the inelastic buckling range between the stocky (compact) region and the slender region that corresponds to an optimality criterion. Therefore, the strength of the stiffened flange of the steel box girder in the inelastic buckling range is investigated in this section.

9.8.2 Background

9.8.2.1 Inelastic Buckling Strength of Stiffened Flanges

Obviously the critical stress cannot be larger than the material yield stress when the plate slenderness ratio (width-to-thickness ratio) becomes small. This is the reason why it has been the topic of research for many years after Euler presented his critical stress concept for a pin-ended column in 1757. Simply because of the inability to provide a valid critical stress for the inelastic buckling range, the Euler critical stress concept was buried for almost 150 years until von Kármán first presented an inelastic transition curve in 1910 in his dissertation study. In the meantime, approximately 2000 column test data were generated throughout the world, particularly in the inelastic buckling range.

There were a series of attempts to provide valid transition curves (SSRC, 1998). For steel columns, various transition curves had been proposed for the range between the Euler curve and the yield stress plateau, which was referred to as “transition zone”

(Batterman and Johnston, 1967; Bjorhovde, 1972). Since a stiffened plate was simply assumed by an equivalent strut column (Ostapenko and Vojta, 1967; Dwight and Little, 1976; Dowling and Chatterjee, 1977), transition curves were applied to define the ultimate strength of the stiffened plate in a similar transition zone. The inelastic buckling occurs in the structural plate that has a width-to-thickness ratio corresponding to the non-compact or compact sections criterion, where the linear Hooke's law is no longer valid.

Modern finite element method incorporates both total Lagrangian and updated Lagrangian formulations for linearized iteration analyses of nonlinear problems. The inelastic buckling strength of stiffened plates is investigated using a procedure in NASTRAN based on the updated Lagrangian formulation.

9.8.2.2 AASHTO Inelastic Transition Curve

The strength of a longitudinally stiffened flange is given in Article 10.51.5.4.1 to 10.51.5.4.3 of AASHTO (1996), as follows. Article 10.51.5.4.1 states that for a longitudinally stiffened flange designed for the yield stress, F_y , the ratio w/t shall not exceed the value given by the following formula:

$$\frac{w}{t} = \frac{3,070 \sqrt{k}}{\sqrt{F_y}} \quad (9.45)$$

where w = the width between stiffeners; and t = flange thickness.

Article 10.51.5.4.2 states that for greater values of w/t given as

$$\frac{3,070 \sqrt{k}}{\sqrt{F_y}} < \frac{w}{t} < \frac{6,650 \sqrt{k}}{\sqrt{F_y}} \quad (9.46)$$

the buckling stress of the flange, including stiffeners, is given as follows:

$$F_{cr} = 0.592 F_y \left(1 + 0.687 \sin \frac{c\pi}{2} \right) \quad (9.47)$$

where c shall be taken as

$$c = \frac{6,650 \sqrt{k} - \frac{w}{t} \sqrt{F_y}}{3,580 \sqrt{k}} \quad (9.48)$$

Article 10.51.5.4.3 states that for the value of w/t in the range determined by Eq. (9.49), the buckling stress of the flange, including stiffeners, is given by the formula describing the plate elastic buckling strength, Eq. (9.13), where k is the buckling coefficient of a flange panel and has the value of 4 in this study.

$$\frac{w}{t} > \frac{6,650 \sqrt{k}}{\sqrt{F_y}} \quad (9.49)$$

According to Eqs. (9.45) and (9.46), for a stiffened plate having a yield strength of 50 ksi, the yield stress is to be used for the critical stress for a w/t value up to 27.46 and the inelastic buckling stress given by Eq. (9.47) is to be used for a w/t value up to 59.48.

9.8.2.3 Plate Inelastic Buckling Strength Prediction

A parabolic transition curve was developed by Johnson et al. (1899) to predict the centrally loaded column buckling strength in the inelastic buckling zone based on a curve-fitting. Gerard and Becker (1957) proposed a method for predicting the buckling failure of stiffened panels by using a parabola connecting the yield stress at the upper limit of the lower slenderness ratio to the Euler stress corresponding to the minimum elastic slenderness ratio. They regarded the stiffened plate as a combined column member with an effective width of plate that acts in conjunction with the stiffeners. The column buckling curve was then applied directly to evaluate the stiffened plate strength.

Unlike Gerard and Becker's application of the column strength curve, a parabolic transition curve will be proposed to present the inelastic buckling strength of the stiffened flange panel following exactly the same procedure used in the development of the column curve by SSRC in this section. This transition curve connects smoothly the fully plastic strength and the Bryan's elastic critical stress, Eq. (9.13).

The parabolic curve can be expressed as a following square function:

$$f(x) = ax^2 + bx + c \quad (9.50)$$

where x represents the width-to-thickness ratio, w/t . Thus, the three parameters, a , b , and c , require the same number of condition equations to determine the parabola given in Eq. (9.50) uniquely. The three conditions are

1. $f(0) = F_y$, the yield stress of material. Since $f(0) = c$, therefore, $c = F_y$.
2. The slope of the parabola at C_c should be identical to that of the elastic buckling curve. So, $f'(C_c) = F'_{cr}(C_c)$.
3. The stress value must be the same at C_c from both equations. Thus, $f(C_c) = F_{cr}(C_c)$.

By applying the three conditions to Eq. (9.50), gives

$$a = -\frac{\pi^2 E}{(1 - \mu^2)} \frac{I}{C_c^4} + \frac{F_y}{C_c^2} \quad (9.51)$$

$$b = -\frac{4}{3} \frac{\pi^2 E}{(1 - \mu^2)} \frac{I}{C_c^3} + \frac{2F_y}{C_c} \quad (9.52)$$

$$f\left(\frac{w}{t}\right) = \left[-\frac{\pi^2 E}{(1 - \mu^2)} \frac{I}{C_c^4} + \frac{F_y}{C_c^2} \right] \left(\frac{w}{t}\right)^2 + \left[-\frac{4}{3} \frac{\pi^2 E}{(1 - \mu^2)} \frac{I}{C_c^3} + \frac{2F_y}{C_c} \right] \left(\frac{w}{t}\right) + F_y \quad (9.53)$$

When $f(C_c)$ is assumed to be $F_y/2$, the transition curve is given as

$$f\left(\frac{w}{t}\right) = F_y - \frac{F_y}{2} \frac{I}{C_c^2} \left(\frac{w}{t}\right)^2 \quad (9.54)$$

9.8.3 Initial Geometric Imperfections

The inelastic buckling response of the stiffened plate is calculated by using an incremental analysis based on a nonlinear formulation on a hypothetical model with an initial imperfection. It is well known that the representative initial imperfections in the steel box girder bridge are the geometric imperfection and residual stresses.

Since the induced residual stresses should be self-equilibrated in the stiffened flange where a uni-axial compression force dominates, their effect on the ultimate strength of the stiffened plate is not expected to be substantial. Thus, only initial geometric imperfections are considered for the examination of the inelastic buckling strength of the stiffened flange.

Unintended geometric imperfections are inevitably created in the stiffened flanges of a box girder during fabrication and construction. The maximum deviation and the shape of the initial geometric imperfection influences significantly the inelastic buckling strength of the stiffened flanges having the width-to-thickness ratio in-between zero and C_c (Wolchuk and Mayrbaur, 1980; SSRC, 1998). Therefore, it is very important to properly represent the maximum magnitude and the shape of the geometric imperfections in the analytical model in order to effectively evaluate the minimum required bending rigidity for the stiffened flanges. For this reason, the literature was reviewed to find an appropriate means that describe the maximum magnitude and shape of the initial geometric imperfections.

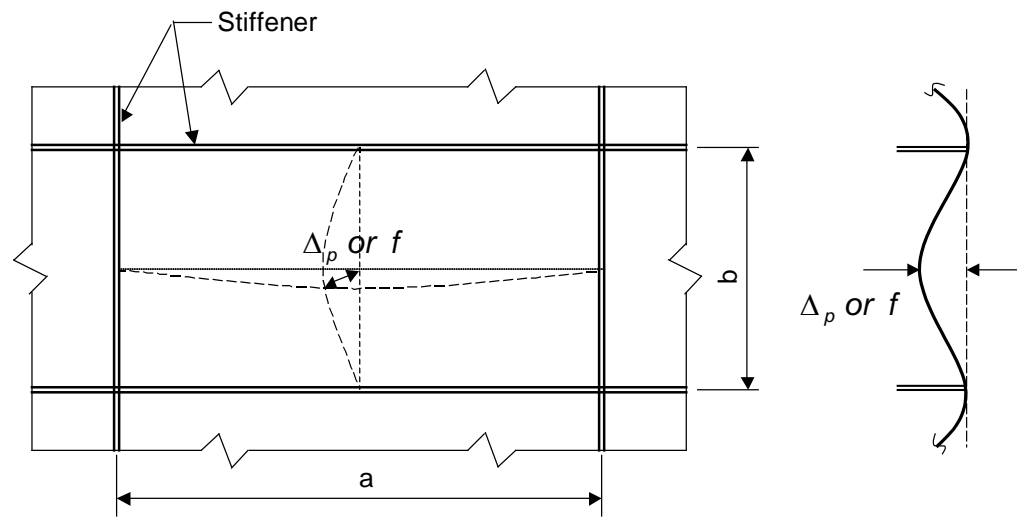
Design specifications generally stipulate that the dimension of any structural members shall be within the specified tolerance limits. Deviations in the stiffened flanges are the flatness of the panel and the straightness of the stiffener. The flatness of the panels and the straightness of the stiffeners are graphically depicted in Fig. 9.43. The term “subpanel” is used in this study to mean a clear area of steel plate surface bounded by stiffeners, webs or plate edges and not further subdivided by any such member elements, following the definition used in the current AASHTO (1996).

The tolerance limits have been established in many countries in a variety of ways. Article 2.10.48B(1) of AASHTO (1973) recommended for the first time that the maximum deviation from the detailed flatness of the panel should not exceed the greater of 3/16 inch or $D / (144\sqrt{T})$ for the bottom flange panels of a box girder, where D is the shorter dimension of the panel and T is the thickness of the panel, which is superseded by *Bridge Welding Code* (2002). Many Europe countries have used the following limit for the maximum deviation of the flatness:

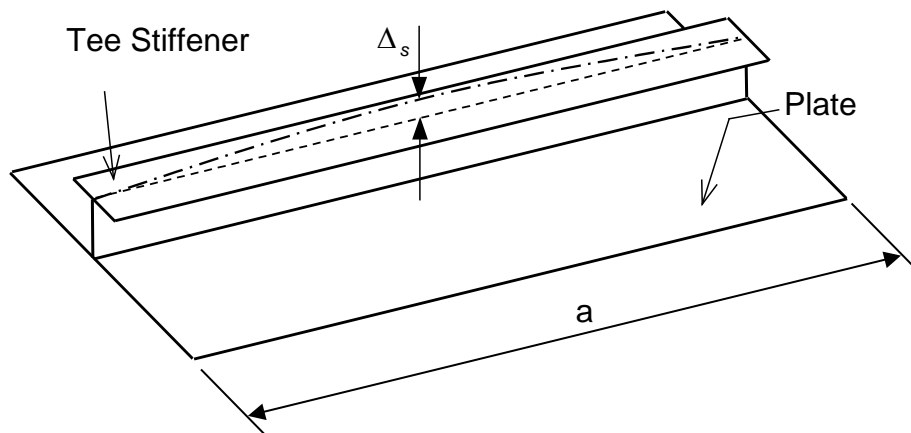
$$|f / b| \leq 1 / 250 \quad (9.55)$$

where f is the out-of-plane deviation and b is the plate width. However, it was reported by Massonnet (1980) that this specified limit was commonly exceeded in bridges in those countries. For an example case, he revealed that the 95% of surveyed imperfection value presented from f/b is 1/127 for bottom flanges and 1/106 for webs in West Germany.

Korol et al. (1984) investigated the magnitudes of geometric imperfections induced from the fabrication of welded steel box girders constructed in Canada. For plate panel thickness less than 30 mm, the 95% of the surveyed value of f/b was found to be 1/124, with 1/117 for bottom flanges and 1/135 for webs. This was



(a) Out-of-Flatness of Flange Panel



(b) Out-of-Straightness of Stiffener

Fig. 9.43. Out-of-Plane Deviations

determined from 7900 measurements of webs and bottom flanges of the bridges included in their study. They also discovered from the measured data that the out-of-plane deviation could be expressed as a function of the plate panel thickness, because there was the general tendency found that the out-of-plane deviations reduce as the plate panel thickness increases. In 1988, they published another paper reporting the following equations representing the variation of non-dimensional parameters, Δ_p / t , by b/t , using linear regression analysis:

$$\text{For } b/t > 40, \text{ Flanges: } \frac{\Delta_p}{t} = \frac{1}{147} \frac{t}{b} - \frac{1}{40}, \text{ Webs: } \frac{\Delta_p}{t} = \frac{1}{132} \frac{t}{b} - \frac{1}{20}.$$

$$\text{For } 60 > b/t > 30, \text{ Flanges: } \frac{\Delta_p}{t} = \frac{1}{155} \frac{t}{b}, \text{ Webs: } \frac{\Delta_p}{t} = \frac{1}{150} \frac{t}{b}.$$

The maximum deviation from flatness of a panel due to welding has been specified most recently as $D/120$ in Articles 3.5 and 9.19 of the *Bridge Welding Code* (1996). Although Article 11.4.13.2, Division II of the current AASHTO (2002) retains the same flatness requirement as that adopted in AASHO (1973), there seems to be a general tendency of relaxing the tight tolerance limit.

Therefore, in this study, a slightly more conservative value of $w/100$ than that specified in Bridge Welding Code (2002) is taken for the maximum deviation of the flatness in the model for calculation of the inelastic ultimate strength.

As to the tolerance limit for the straightness of stiffeners, Article 2.10.48B(1) of the AASHO (1973) recommended that the maximum deviation from detailed straightness, Δ_s , shall be less than $L/480$ for longitudinal stiffeners of box girder bottom flanges, in which L is the length of the stiffener or rib between cross members, webs or flanges. The tolerance limit for the straightness of the longitudinal and/or transverse

stiffeners, Δ_s / a , was proposed as 1/500 by Massonnet (1980) and Dowling et al. (1977). Thimmhardy and Korol (1988) reported based on 2200 measurements gathered on nine steel box girder bridges that a practical tolerance level for the out-of-straightness of stiffeners, which the steel industry could achieve, was $a/500$. They also reported that most of the bridges investigated in Canada would generally comply with a limit of $a/500$ for stiffeners.

Article 11.4.13.3 of the current AASHTO (2002) suggests for the orthotropic plates that for the straightness of longitudinal stiffeners, the maximum deviation from detailed straightness in any direction perpendicular to its length shall not exceed $L/480$, where L = the length of the stiffener or rib between cross members, webs, or flanges. Thus, the maximum deviation value for the straightness of longitudinal stiffeners is selected to be in-between $a/480$ and $a/500$ for the analytical studies of stiffened flanges in the inelastic transition. It is noted that there is no appreciable differences in the computed inelastic buckling strengths whether an initial imperfection value used is $a/480$ or $a/500$.

As discussed earlier, the shapes of geometric initial imperfections also have a substantial influence on the inelastic ultimate strength of stiffened flange plates. Several deformed shapes were included for this analytical study to be considered as geometric initial imperfections in the stiffened flanges of the box girder.

The longitudinal stiffeners act as supports to restrain the vertical displacement due to the bending. Thus, the cross-sectional shape of the deformed stiffened flanges after the welding process becomes similar to the deflected shape of a continuous beam under flexural loading. Since the transverse stiffeners and cross-frames have a restraining effect reducing the deformation of the flange panels, a half wave shape, which has a

maximum value around the central part, should be assumed for the deformed shape along the longitudinal direction due to the welding. Korol and Thimmhardy (1984) reported from a series of the measurements for the bridge girder that for the typical deformed shape of flange panels, the maximum out-of-flatness deviation generally was found at the panel's center and it tended to be drawn inward, as described in Fig. 9.43(a).

Carlsen and Czujko (1978) reported from measurements of 196 plates that the deformed shape of welded stiffened plates used in ship structures could be expressed by a double trigonometric series. They also found that the most critical shape was obtained when only one term of the series was used with an n_p value of the same number as the aspect ratio, which is expressed in the following equation:

$$w_p(x, y) = w_0 \sin(n_p \pi x / L) \sin(\pi y / B) \quad (9.56)$$

where $n_p = \alpha$ (aspect ratio); L = length of plate; and B = width of plate.

The anti-symmetric mode can be the critical one when the moment of inertia of the longitudinal stiffener is higher than that used for the symmetrical buckling strength analysis, the anti-symmetric mode shape scaled by the maximum flatness deviation needs to be considered for the evaluation of the inelastic buckling strength corresponding to the anti-symmetric buckling.

Due to shrinkage caused by welding to the flange, the longitudinal stiffeners tend to deviate from the straightness. Such a deviation can induce a geometric imperfection shape corresponding to the symmetric buckling mode shape. Since the symmetric buckling mode can be the critical one when the moment of inertia of the longitudinal stiffener is low, the symmetric buckling mode shape scaled by the tolerance limit for the maximum straightness deviation is considered for the geometric initial imperfection in

the determination of the inelastic critical stresses.

Therefore, the following five types of geometric initial imperfection shapes are included in this analytical study for the evaluation of the inelastic ultimate strength of the stiffened flanges:

- a) the symmetric mode shape scaled with the tolerance limit for the straightness of the longitudinal stiffener
- b) the anti-symmetric mode shape scaled with the tolerance limit for the flatness of the flange panel
- c) the panel welding deflection shape scaled with the tolerance limit for the flatness of the flange panel illustrated in Fig. 9.44(c)
- d) the combined shape of a) and b)
- e) the combined shape of a) and c)

The five selected geometric imperfection shapes are shown in Fig. 9.44.

Subsequently, a series of inelastic nonlinear analyses was performed on selected models taking into account these five types of initial imperfection modes in order to perform a comparative study regarding the effect of initial imperfections on the inelastic buckling strength of stiffened flanges.

9.8.4 Effects of Various Geometric Imperfections on Ultimate Strengths

The inelastic buckling strengths were determined from incremental nonlinear analysis taking into account the material nonlinearity available in MSC/NASTRAN. The material nonlinear analysis was based on a bilinear stress-strain curve (linearly elastic and perfectly plastic) and the von Mises yield criterion was adopted to determine the inelastic buckling strength.

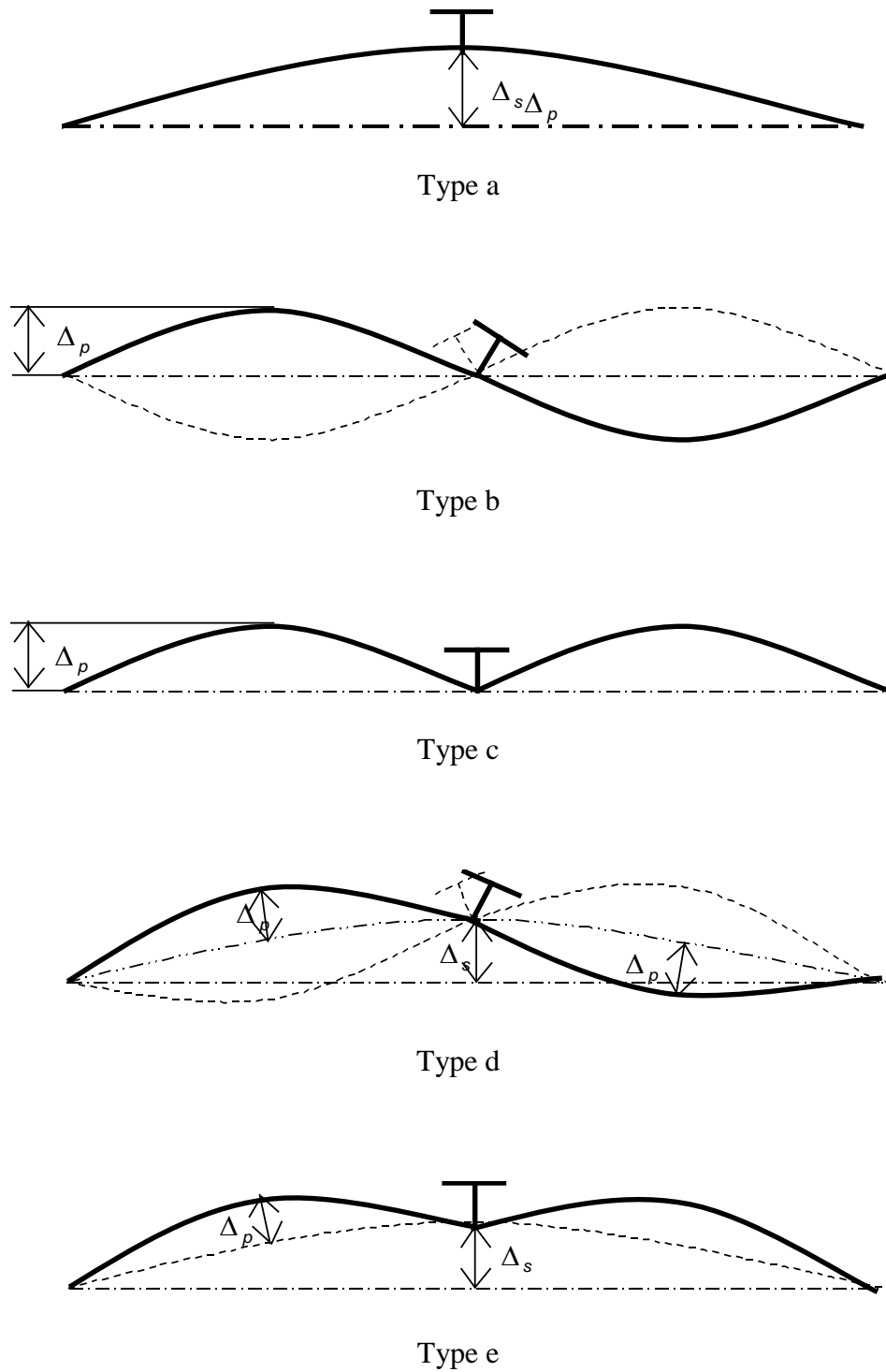


Fig. 9.44. Cross-Sectional Shapes of Geometric Imperfections

As shown in Table 9.9, the inelastic buckling strength of panels having a with-to-thickness ratio in-between C_c and zero is substantially influenced by the initial shape of their geometric imperfections as well as their maximum value.

From this comparison of the strength results, it should be noted that there is a negligible difference, say less than 3%, between the geometric imperfection types b and d or between the types c and e. This result shows that there is little combined effect of the out-of-straightness of the stiffener and the out-of-flatness of the subpanel on the reduction of the ultimate strength of a stiffened flange. Thus, it can be concluded that the geometric imperfections can be considered separately for the ultimate strength evaluation. Only an imperfection shape associated with the most critical mode has a dominant effect on the inelastic ultimate strength of the stiffened flange. Grondin et al. (1998) also reported a similar result to the results stated above, i.e., initial imperfections in the plate were found to have a negligible effect on the capacity of plate failure by overall stiffener buckling.

The moment of inertia of longitudinal stiffeners was calculated from the proposed Eq. (9.27). For the stiffener rigidity by Eq. (9.27), the model incorporating the imperfection type b produced the minimum strength compared to those obtained from models incorporating the three different types a, b, and c. This implies that when Eq. (9.27) is applied for the design of longitudinal stiffeners, the geometric imperfection shape associated with the anti-symmetric buckling mode should determine the inelastic buckling strength of a flange panel. It was shown in Table 9.9 that imperfection types a and c always lead to a similar ultimate strength result.

When compared with the AASHTO (2002) inelastic transition strength given by Eq. (9.47), the strengths of the flange subpanels associated with imperfection types a and

c show a good correlation for a relatively wide range of width-to-thickness ratios that falls within two extreme values of zero and C_c . Therefore, it can be concluded that the inelastic transition curve given by AASHTO is valid for the non-compact stiffened flanges of box girders if the shape of the geometric imperfection is of type a or c. However, the ultimate strength for the geometric imperfection of type c shows a much lower value compared with that given by Eq. (9.47). It was shown that as the width-to-thickness ratio, w/t , approaches to zero or to C_c , the ultimate strength values from different models incorporating different types were not affected much.

It is noted that different types of initial imperfections do affect the inelastic buckling strengths, however, only the inelastic buckling strengths corresponding to mode shapes illustrated in Figs. 9.46 and 9.48 are pertinent to the minimum values sought.

9.8.5 Minimum Required Rigidity for Subpanels in Inelastic Buckling Range

A typical stiffened plate model in the inelastic buckling range was analyzed by 3D finite element analysis using MSC/NASTRAN. For the stiffened plate model, the number of stiffeners, n , is 4, the aspect ratio, $\alpha (=a/w)$, is 2, the width between stiffeners, w , is 50 inches and the thickness of flange plate, t_f , is 1 inch, making the width-to-thickness ratio equal to 50.

The incremental nonlinear analysis was implemented by considering type b out-of-flatness of the subpanel and the out-of-straightness of the longitudinal stiffeners. Several different models having different values of moment of inertia of the longitudinal

Table 9.9. Critical Stresses versus Initial Imperfection Types

w/t	<i>Critical Stresses, F_{cr} (ksi)</i>						<i>Difference (%)</i>			
	AASHTO	type a	type b	type c	type d	type e	col. (6) & (4)	col. (6) & (2)	col. (7) & (5)	col. (7) & (2)
25.6	50.00	46.98	46.07	47.50	46.00	45.77	-0.15	-8.00	-3.64	-8.46
40	46.02	47.25	39.20	47.90	38.41	45.44	-2.03	-16.54	-5.14	-1.27

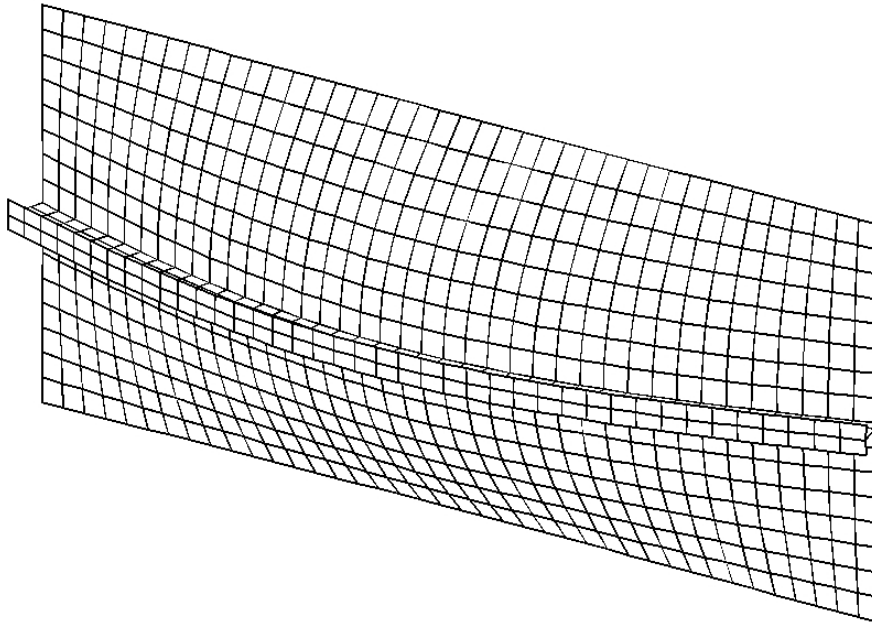


Fig. 9.45. Failure Mode Shape for Imperfection Type a

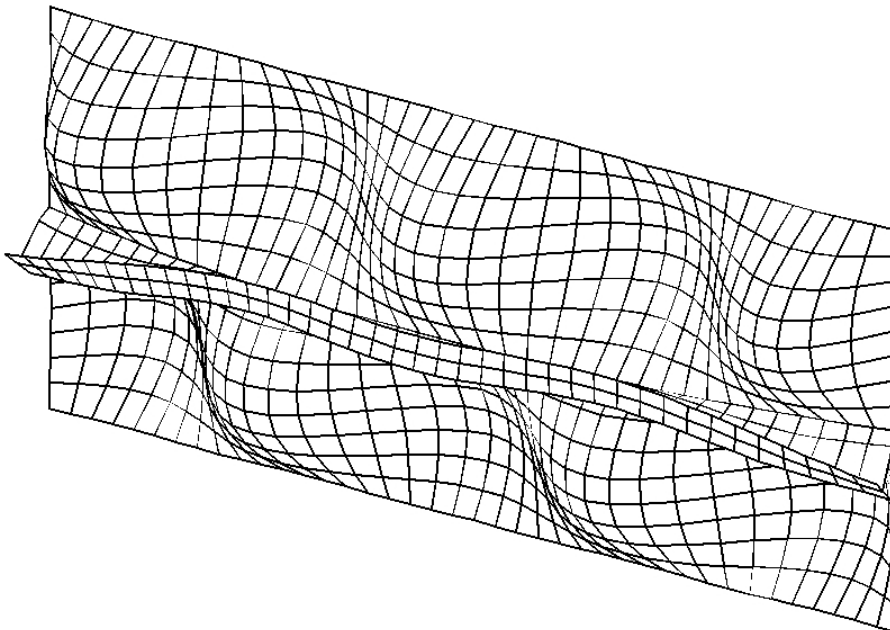


Fig. 9.46. Failure Mode Shape for Imperfection Type b

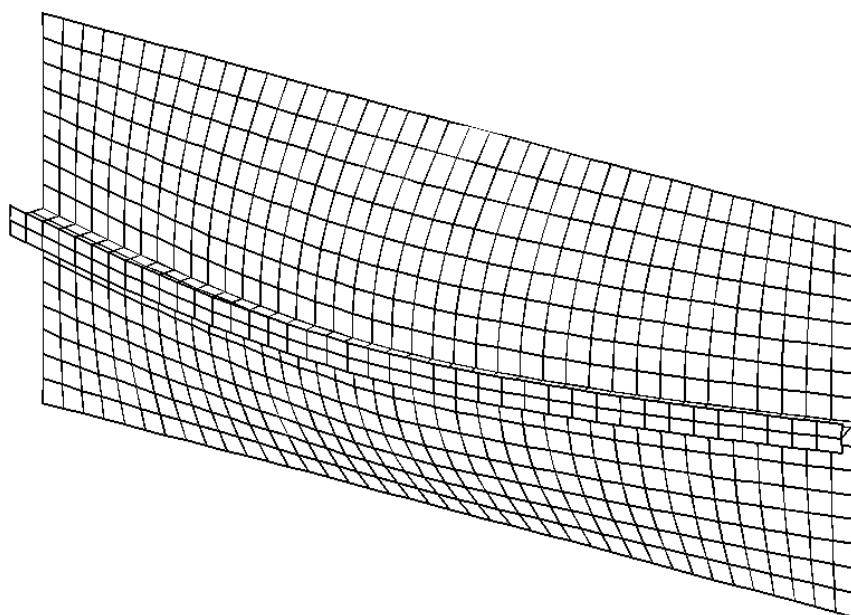


Fig. 9.47. Failure Mode Shape for Imperfection Type c

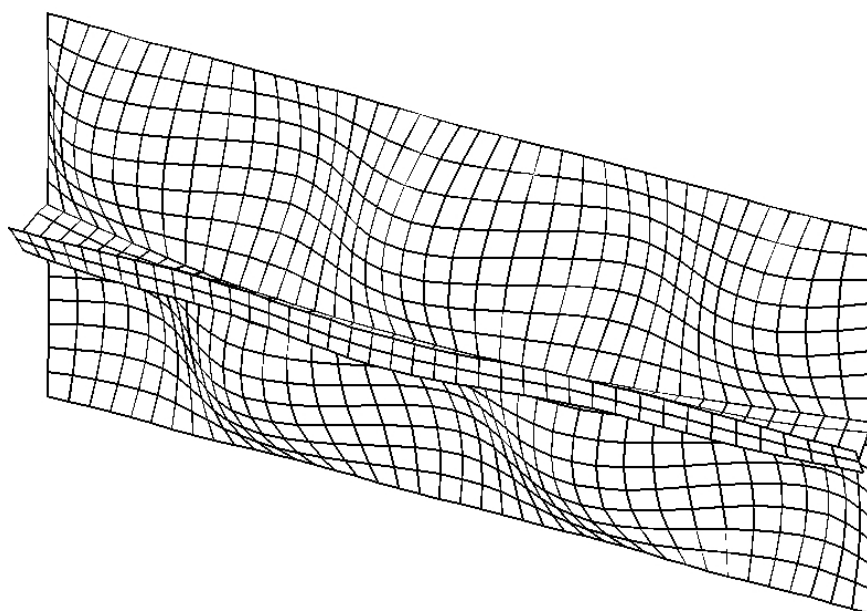


Fig. 9.48. Failure Mode Shape for Imperfection Type d

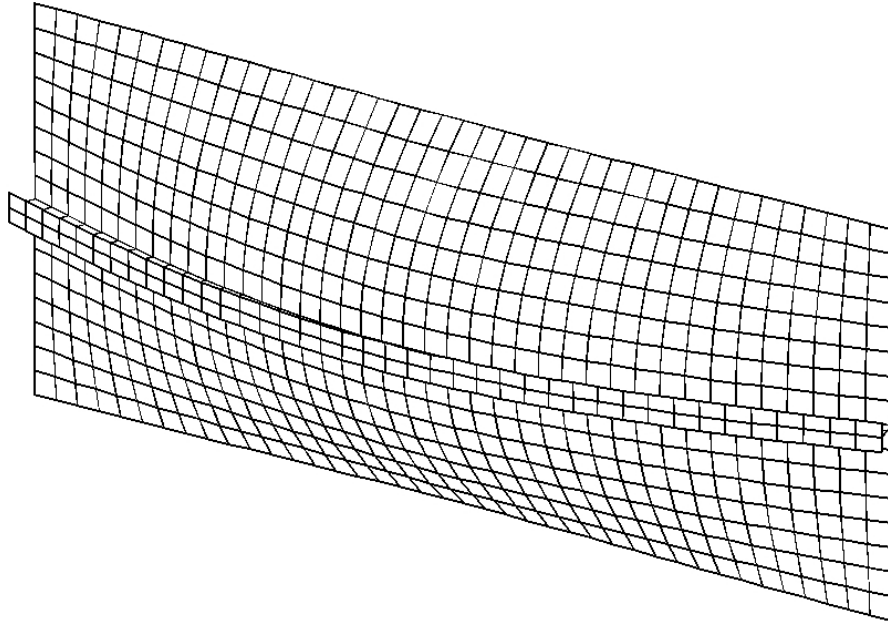


Fig. 9.49. Failure Mode Shape for Imperfection Type e

stiffener were analyzed to examine the effect of the stiffener rigidity on the inelastic buckling strength. The analysis results associated with the out-of-straightness of the stiffeners are plotted in Fig. 9.52, which shows a steady and rapid increase in the inelastic buckling strength as the moment of inertia of the longitudinal stiffener increases. As the geometric imperfection was type a (symmetric mode), the inelastic buckling strength shown in Fig. 9.52 may not necessarily be the smallest value sought.

The analysis results associated with type b out-of-flatness of the flange panel are plotted in Fig. 51. When the moment of inertia increases from an arbitrarily small value up to the value given by Eq. (9.27), the inelastic buckling strength of the stiffened flange increases a little rapidly. However, when the moment of inertia of the stiffener exceeds the limit value given by Eq. (9.27), the inelastic buckling strength increases only very slowly.

Since the smallest value, among the calculated inelastic buckling strengths under various different types of geometric imperfections, becomes the ultimate stress capacity, the inelastic strength of the stiffened flange can be determined from Fig. 9.53 by taking a lower value. The trend of the ultimate strength variations shown in Fig. 9.53 is similar to those determined from the elastic buckling analysis.

It is noted in Fig. 9.53 that around the point on the x-axis corresponding to the moment of inertia from Eq. (9.27), the inelastic buckling strength associated with the type b geometric imperfection starts to give a lower value that does not vary much.

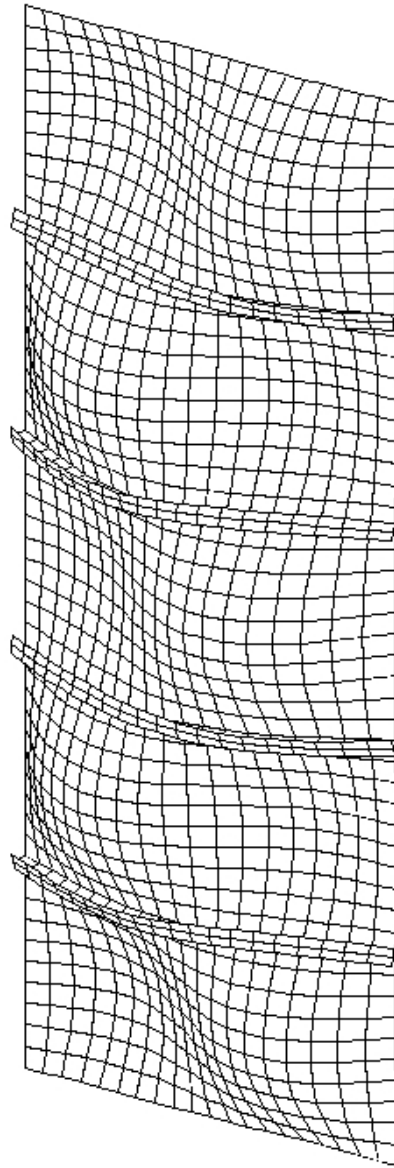


Fig. 9.50. Deformed Shape at Failure, Imperfection Type b

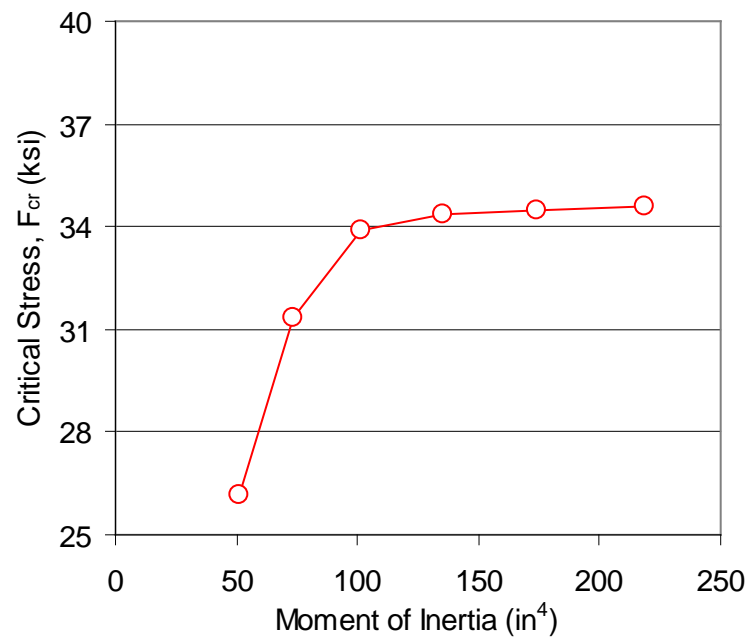


Fig. 9.51. Inelastic Buckling Strength, Imperfection Type b

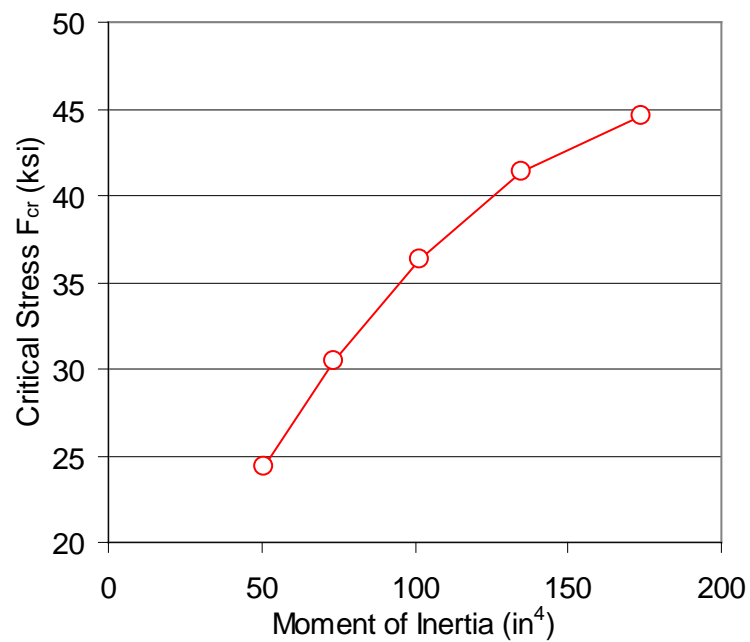


Fig. 9.52. Inelastic Buckling Strength, Imperfection Type a

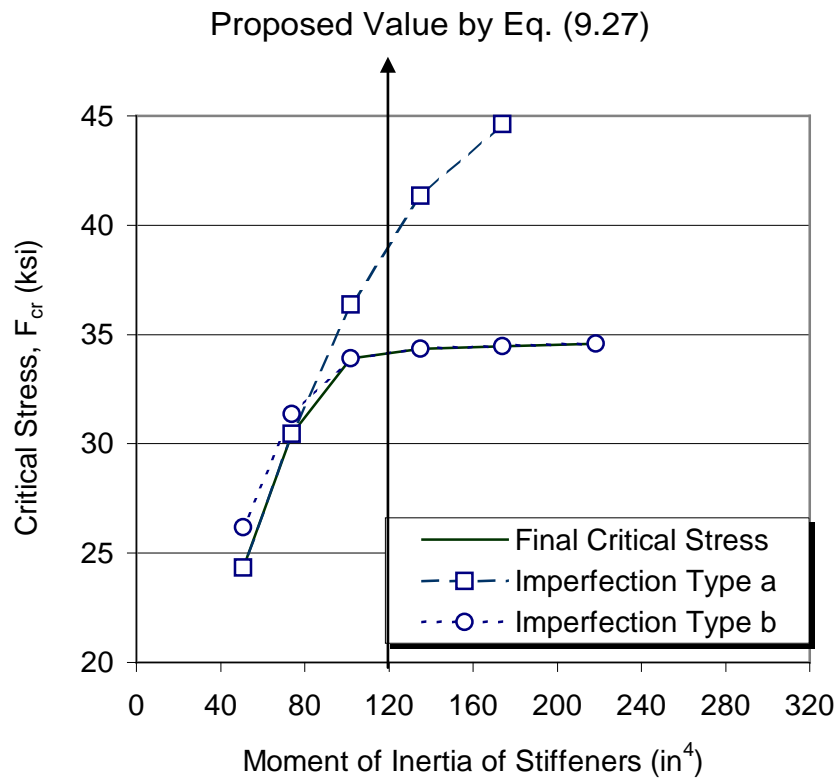


Fig. 9.53. Variation of Inelastic Buckling Strength

Thus, this shows that the inelastic ultimate strength of the stiffened flange will have a limiting value associated with longitudinal stiffeners having the moment of inertia given by Eq. (9.27). Therefore, Eq. (9.27) does provide the minimum required moment of inertia of the longitudinal stiffeners in the inelastic transition zone as well as in the elastic buckling region.

The inelastic buckling strength variation associated with type c geometric imperfection was examined. Fig. 9.54 shows the variation of the resulting ultimate strength versus the moment of inertia of the longitudinal stiffeners. The ultimate strength of the stiffened flange starts to increase slowly after exceeding the moment of inertia given by Eq. (9.27). The strength value that corresponds to the moment of inertia given by Eq. (9.27) reached 95% of the strength produced when the moment of inertia is increased to 2.5 times larger than the value used.

Therefore, it is also verified from Fig. 9.54 that the proposed Eq. (9.27) does provide an adequate moment of inertia of the longitudinal stiffener for a subpanel with type c geometric imperfection.

9.8.6 Further Validation of Eq. (9.27)

In order to further validate the reliability of the regression Eq. (9.27), two sets of six additional examples (four in the inelastic range, one in in-between range and one in the elastic range) were analyzed with the type b geometric imperfection; one set for straight stiffened panels and the other set for curved stiffened panels. These six models had width-to-thickness ratios ranging from a low value of 14 to a high value of 80 such that they would spread reasonably well across the slenderness ratio range likely to be

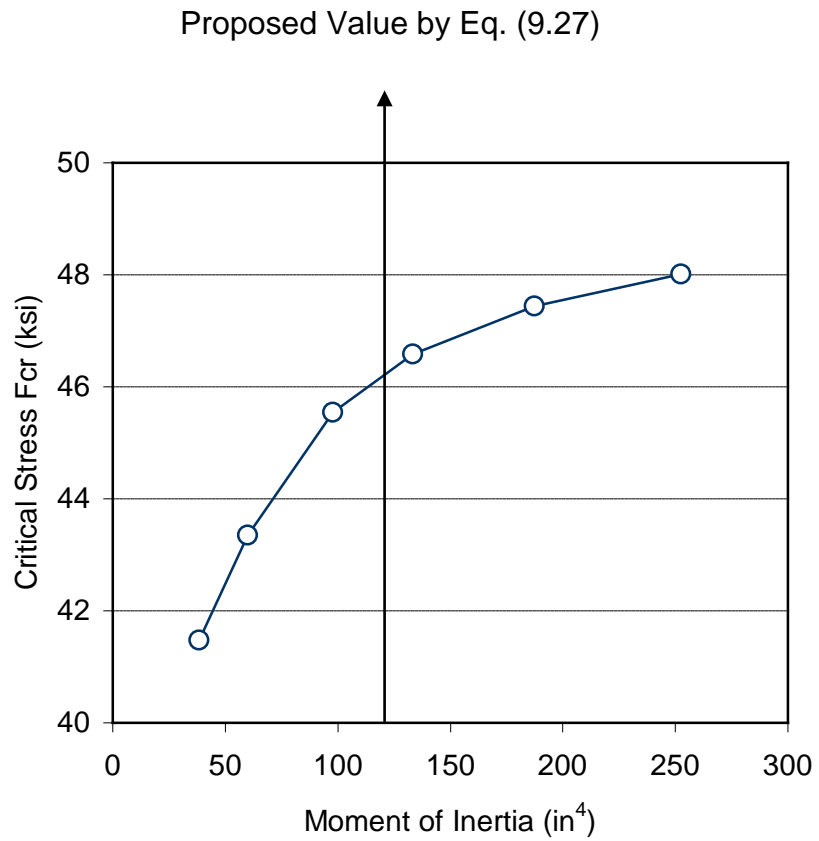


Fig. 9.54. Inelastic Buckling Strength, Geometric Imperfection Type c

used in practical designs. The type b geometric imperfections were scaled with the out-of-flatness value of $w/100$ and $w/1000$. The $w/1000$ was selected to simulate a straight plate panel. Model details such as dimensions, aspect ratio, and the number of longitudinal stiffeners, are presented in Table 9.10 for straight panels and Table 9.11 for curved panels, respectively. The analysis results are compared in these two tables and also illustrated in Figs. 9.55 and 9.56, respectively.

It can be seen from Table 9.10 and Fig. 9.55 for the isolated straight stiffened flange that there is discernible postbuckling strength in the elastic buckling range. The analysis results correlate rather well with the value predicted by the AASHTO (1996) transition curve for straight plate panels represented by models having the geometric imperfection value of $w/1000$. When the maximum geometric imperfection values allowed by the AWS (1996) are considered the analysis results correlate well with a parabolic transition curve, Eq. (9.54), derived following the SSRC procedure used for columns. The inelastic transition curve of the AASHTO, Eq. (5.47), appears to be unconservative for the width-to-thickness ratio values approximately from 10 to 40 when the maximum geometric imperfection values allowed by the AWS are considered.

Based upon the spirit of SSRC Technical Memorandum No. 5, the parabolic curve appears to better represent the behavior of compression elements in the inelastic transition range.

Table 9.11 and Fig. 9.56 represent the analysis results from six examples for the horizontally curved box girder flange. Examination of Table 9.11 and Fig. 9.56 reveals that the comparisons made for the curved stiffened compression flanges show identical trend as that obtained for the straight stiffened flanges. As the minimum required

moment of inertia of the longitudinal stiffener given by Eq. (9.27) is used in all foregoing analyses, this confirms again that the minimum required moment of inertia for the longitudinal stiffener, given by the Eq. (9.27), is valid in both the elastic buckling range and the inelastic buckling range.

9.8.7 Comparative Design

A design example is selected from Clinton et al. (1986) to demonstrate the usage of Eq. (9.27) for the longitudinally stiffened flange of a curved box girder (Choi and Yoo, 2002). Clinton et al. illustrated several design examples following the report by Wolchuk and Mayrbaur (1980). Although this work has never been officially adopted by AASHTO, it is nevertheless mentioned in the Commentary of AASHTO LRFD (1998). Therefore, it is fair to say that the design examples done by Clinton et al. represent the current AASHTO procedure. The bridge is assumed to have spans of 310-400-310 feet with a radius of 1,200 feet measured along the centerline of the bridge. The cross section for the negative moment design is shown in Fig. 9.57. The maximum negative unfactored moments are noncomposite dead load moment (DL1) = -129,200 kip-ft, superimposed dead load moment (DL2) = -27,600 kip-ft, and live load plus impact moment (LL+I) = -31,240 kip-ft.

Fig. 9.58 shows the longitudinal stiffener arrangement for the AASHTO procedure, and Fig. 9.59 shows the longitudinal stiffener arrangement for the proposed procedure. The total number of longitudinal stiffeners is reduced from 10 (WT9x25) to 4 (WT12x27.5). Thus, it can be concluded that the proposed design is better.

Table 9.10. Comparison of Ultimate Strength of Straight Flange, F_{cr} (ksi)

	n	w (in.)	t (in.)	w/t	I_s , Eq.(9.27)	I_s , Used	F_{cr} (AASHTO)	F_{cr} (FEM,w/1000)	F_{cr} (FEM,w/100)
2	4	50	0.625	80.0	29.3	31.4	16.380	22.825	21.220
3	3	80	1.25	64.0	730.7	731.2	25.596	29.956	27.200
2	4	50	1	50.0	120.0	124.0	38.719	41.866	34.338
5	1	20	0.5	40.0	18.8	19.6	46.206	48.594	38.970
3	3	24	0.9375	25.6	92.5	93.0	50.000	49.569	46.075
4	4	14	1	14.0	134.4	141.0	50.000	49.806	48.100

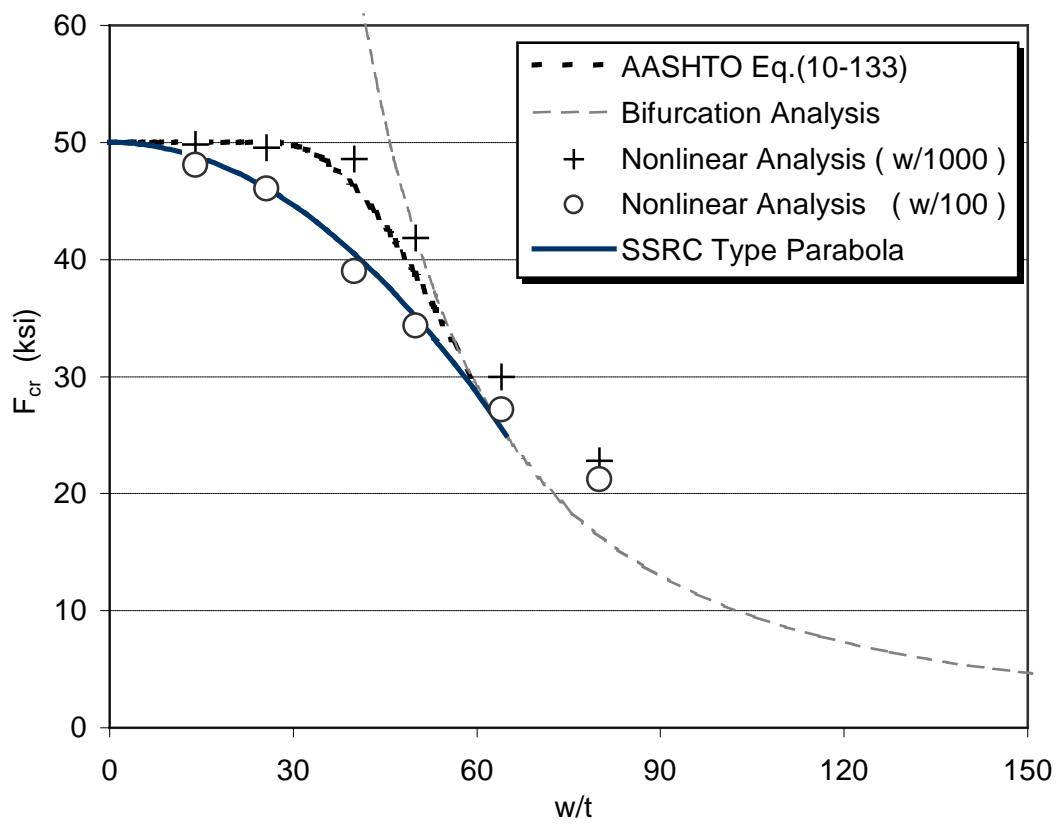


Fig. 9.55. Ultimate Strength of Straight Flange versus Width-to-Thickness Ratio

Table 9.11. Comparison of Ultimate Strength of Curved Flange, F_{cr} (ksi)

α	n	w (in.)	t (in.)	w/t	R (ft.)	I_s , Eq.(9.27)	I_s , Used	F_{cr} (AASHTO)	F_{cr} (FEM, $w/1000$)	F_{cr} (FEM, $w/100$)
3	3	120	1.5	80.0	800	1894.0	1902.3	16.380	23.649	19.060
3	2	60	0.9375	64.0	200	188.8	188.9	25.596	29.990	27.290
3	1	60	1.125	53.3	200	230.7	232.5	35.639	37.303	31.843
5	3	30	0.75	40.0	200	164.4	164.8	46.207	46.662	38.395
5	1	30	1.25	24.0	300	439.5	441.6	50.000	49.972	45.573
5	1	30	1.875	16.0	200	1483.2	1509.8	50.000	50.000	49.811

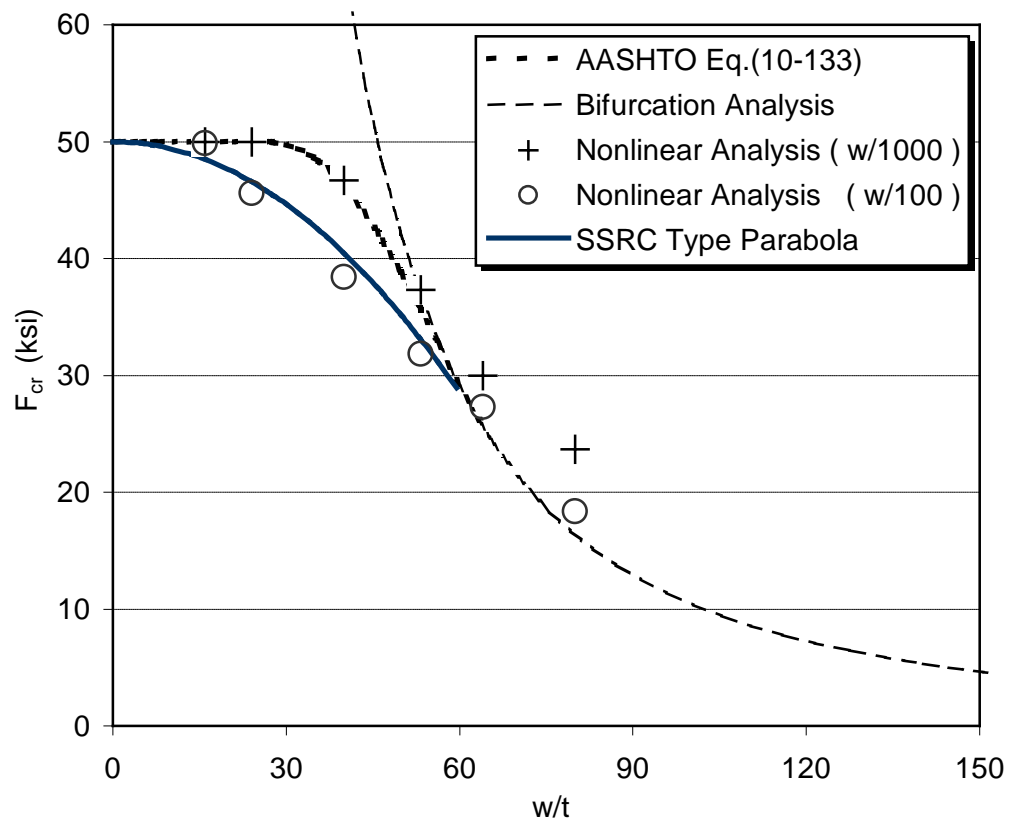


Fig. 9.56. Ultimate Strength of Curved Flange versus Width-to-Thickness Ratio

Section properties based on Figs. 9.58 and 9.59 are given in Table 9.12. The maximum stress results are given in Table 9.13. It is assumed that the transverse stiffener spacing is 16 ft (wider than 10 ft spacing used in Clinton et al. example) at the maximum negative moment region, which gives $\alpha = 16/4 = 4$. For $n = 2$, $w = 48$ in., and $t = 1.25$ in., and the minimum required moment of inertia, I_s , is computed from Eq. (9.27) to be 636.4 in^4 .

The provided moment of inertia of the longitudinal stiffener, WT 12x27.5, is

$$I_s = 117 + 8.1(11.785 - 3.50)^2 = 673.0 \text{ in}^4$$

The width-to-thickness ratio at the exterior box is $9 \times 12 / 2 / 1.25 = 43.2$. From AASHTO 10.51.5.4.2,

$$\frac{3,070\sqrt{k}}{\sqrt{F_y}} = \frac{3,070 \times 2}{\sqrt{50,000}} = 27.46 < 43.2 < \frac{6,650\sqrt{k}}{\sqrt{F_y}} = \frac{6,650 \times 2}{\sqrt{50,000}} = 59.5 \quad (\text{AASHTO 10-139})$$

$$c = \frac{6,650\sqrt{k} - \frac{w}{t}\sqrt{F_y}}{3,580\sqrt{k}} = \frac{6,650 \times 2 - 43.2\sqrt{50,000}}{3,580 \times 2} = 0.5084 \quad (\text{AASHTO 10-140})$$

From AASHTO Eq. (10-134)

$$\begin{aligned} F_{cr} &= 0.592 F_y \left(1 + 0.687 \sin \frac{c\pi}{2} \right) = 0.592 \times 50 \left(1 + 0.687 \sin \frac{0.5084\pi}{2} \right) \\ &= 44.17 \text{ ksi} > 43.01 \text{ ksi } O.K \end{aligned}$$

(See Table 9.13)

AASHTO inelastic transition curve was adopted in above example design process for a consistent comparison between two different designs for the longitudinal stiffener arrangement. However, it is noted herein that the use of AASHTO inelastic transition curve can be unconservative if the maximum geometric imperfection allowed by the AWS is considered.

Table 9.12. Section Properties

Application	Case	I (in. ⁴)	y_T (in.)	y_B (in.)
Noncomposite	AASHTO	5,174,800	81.15	66.85
	Proposed	5,145,279	79.56	68.42
Composite	AASHTO	5,597,400	77.15	70.85
	Proposed	5,552,434	75.56	72.42

Table 9.13. Stress Results (ksi)

Point	Case	Noncomp DL	SuperIm DL	LL + Impact	Total
Top Flange	AASHTO	31.60	5.90	11.20	48.70
	Proposed	31.17	5.86	11.06	48.09
Bottom flange	AASHTO	26.00	5.40	11.30	41.70
	Proposed	26.80	5.62	10.59	43.01

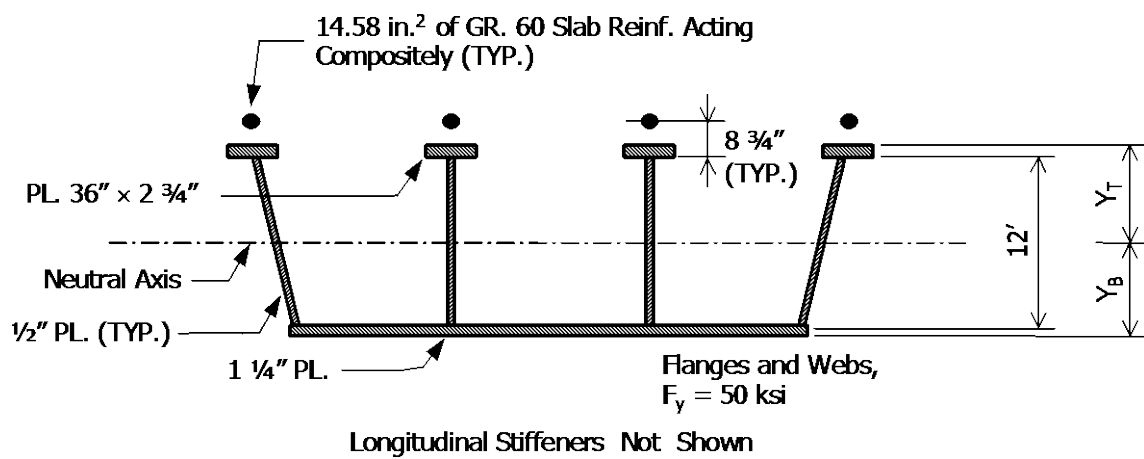


Fig. 9.57. Cross Section for Negative Moment Design

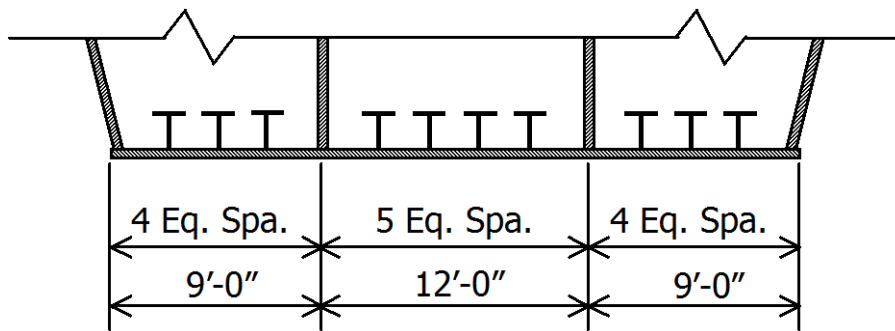


Fig. 9.58. Longitudinal Stiffener Arrangement, AASHTO Design

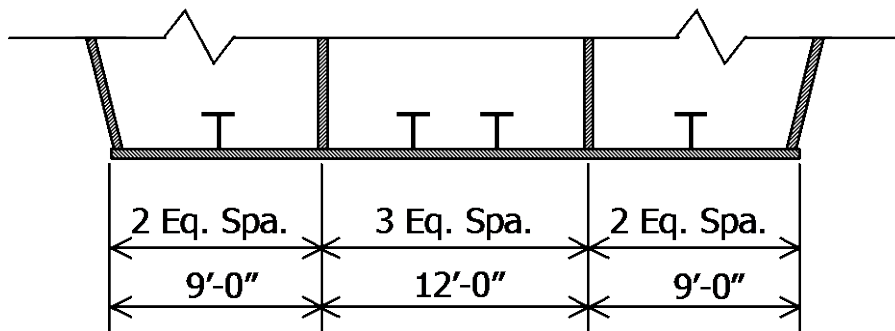


Fig. 9.59. Longitudinal Stiffener Arrangement, Proposed Design

9.9 Summary and Concluding Remarks

A number of crucial areas needed for the proper design of straight and horizontally curved steel box girder compression flanges have been investigated in this chapter. The application of steel box girders in the highway bridge construction is relatively recent practice. Three major collapses that occurred during the erection of box girder bridges, at Milford Haven (1970) in Wales, West Gate (1970) in Australia, and Koblenz (1971) in Germany, caused the entire basis of the design of box girders to be reviewed in Europe (H.M. Stationary Office, 1973a, 1973b) and in the United States (Wolchuk and Mayrbaur, 1980).

As a consequence of this renewed examination of the design of steel box girders, the development of “new” design approaches based on the ultimate load capacity was emphasized. The effect of initial imperfections on the ultimate strength also came under intense scrutiny at that time and are now being considered in modern design specifications throughout the world.

A strut (column action) approach and a plate buckling (plate action) approach have been tried in various regions of the world and the resulting design rules have been adopted in different design specifications. However, there has been a fairly wide difference of determining the ultimate strength of stiffened plates and the proper design of longitudinal stiffeners. Although a great deal of research has been devoted to developing design methods and equations, there appears to be not sufficient information available concerning the adequate design of stiffened compression flanges applicable to the horizontally curved box girder system. Recently, it was found that an old bridge (curved box girder approach spans to the Fort Duquesne Bridge in Pittsburgh) designed

and built before the enactment of an AASHTO provision for the longitudinal stiffeners did not rate for modern day traffic, despite having served for many years.

Taking advantage of superb numerical analysis capabilities afforded by the modern day finite element method, a number of hypothetical straight stiffened compression flange models and horizontally curved stiffened compression flange of box girder models were analyzed. These models were designed to have a variety of parameters including the thickness, width, and length of compression flanges, the number of longitudinal stiffeners, the aspect ratio of subpanels, the geometric imperfection, and residual stress distribution. These models were analyzed to determine the ultimate compressive strength by examining the bifurcation behavior in the elastic range and incremental nonlinear responses in the inelastic range.

In order to characterize and quantify the large volume of collected data for the ultimate strength of the stiffened compression flanges, a regression analysis was conducted for the determination of the minimum required moment of inertia of longitudinal stiffeners. Before commencing the regression analysis, extensive theoretical studies were performed to identify dominant parameters that need to be incorporated in the regression equation.

A simple yet remarkably accurate and versatile regression equation, Eq. (9.27), was successfully extracted that encompass all of the theoretically identified parameters. Remarkably, Eq. (9.27) can be applied with equal accuracy and validity to both straight stiffened compression flanges and horizontally curved stiffened compression flanges of steel box girders.

It has been found that the geometric imperfections caused by a number of sources including fabrication tolerances, mill practices, shipping and handling, and construction practices have significant influences on the ultimate strengths of these stiffened panels. It has also been found that the current AASHTO provisions for the determination of the ultimate strengths of the stiffened panels in the inelastic buckling range can be unconservative. This is the case for subpanels having width-to-thickness ratios fall in-between two extreme values, i.e., zero and the threshold value separating the elastic buckling range and the inelastic buckling range when the maximum geometric imperfection allowed by the AWS is incorporated.

In order to alleviate this potential unconservative design, a parabolic transition curve has been derived following the procedure adopted by SSRC for the strength of centrally loaded columns in the inelastic range. It has been demonstrated that the numerically determined ultimate strengths correlate very well with the proposed parabolic predictor equation.

Finally, an actual design example studied by Clinton et al. to substantiate the proposal made by Wolchuk and Mayrbaurl has been revisited to demonstrate the superb features of the proposed procedure. By this comparative illustration of the proposed design being superior over the one created by the current AASHTO provisions, the validity and versatility of the successful research results are established.

With the successful demonstration of the applicability of the proposed Eq. (9.27) that is valid for both the elastic buckling range and the inelastic range along with the proposed parabolic transition equation for the determination of the ultimate strength of the stiffened panels, unnecessary conservatism in the design of longitudinal stiffeners in

both straight and curved panels is no longer needed. The awkward controversy associated with the rating of an old highway bridge can now be avoided the optimal number and shape of stiffeners can now be calculated with confidence.

But of course there is much work yet to be performed. Experimental verification of the proposed procedure is crucial. The envisioned experimental program can be intimidating. The minimum scale of the specimens is pragmatic. The number of the minimum required specimens encompassing the variety of parameters can be huge. It appears to be extremely beneficial to conduct an experimental verification on a selected number of cases just to spot check the proposed equations.

REFERENCES

- AASHO (1965). *Standard Specifications for Highway Bridges, 9th Edition*, American Association of State Highway Officials, Inc., Washington, D.C.
- AASHO (1973). *Standard Specifications for Highway Bridges, 11th Edition*, American Association of State Highway Officials, Inc., Washington, D.C.
- AASHTO (1980). *Guide Specifications for Horizontally Curved Highway Bridges*, American Association of State Highway Officials, Inc., Washington, D.C.
- AASHTO (1993). *Guide Specifications for horizontally curved Highway Bridges*, American Association of State Highway Officials, Inc., Washington, D.C.
- AASHTO (1996). *Standard Specifications for Highway Bridges, 16th Edition*, American Association of State Highway Officials, Inc., Washington, D.C.
- AASHTO (1998). *LRFD Bridge Design Specifications, 2nd Edition*, American Association of State Highway Officials, Inc., Washington, D.C.
- AASHTO (2002). *Standard Specifications for Highway Bridges, 17th Edition*, American Association of State Highway Officials, Inc., Washington, D.C.
- AASHTO (2003). *Guide Specifications for Horizontally Curved Steel Girder Highway Bridges with Design Examples for I-Girder and Box-Girder Bridges*. Washington, D.C.
- AASHTO (2004). *LRFD Bridge Design Specifications, 3rd Edition*, American Association of State Highway Officials, Inc., Washington, D.C.
- AASHTO/NSBA Steel Bridge Collaboration (2004). *Steel Bridge Bearing Design and Detailing Guidelines*. AASHTO Document No: SBB-1.
- ABAQUS (2003). *Analysis User's Manual*, ABAQUS Inc., Pawtucket, RI.
- ABAQUS User's Manual*. (2002). Habbitt, Karlsson and Sorensen, Inc., Pawtucket, RI.
- ABAQUS Theory Manual*. (2002). Habbitt, Karlsson and Sorensen, Inc., Pawtucket, RI.

- Abdel-Sayed, G. (1973). "Curved webs under combined shear and normal stresses." *Journal of the Structural Division*, ASCE, Vol. 99, No. ST3, pp. 511–525.
- ACI Committee 318 (2002), "Building Code Requirements for Structural Concrete (ACI 318M-02) and Commentary," American Concrete Institute, Farmington Hills, MI.
- AISC LRFD (2001), 3rd Edition, American Institute of Steel Construction, Inc., Chicago, IL.
- American Iron and Steel Institute (AISI). (1996). *Four LRFD Design Examples of Steel Highway Bridges*, Vol. II, Chap. 1A, Highway Structures Design Handbook, Chicago, IL.
- ASCE-AASHTO Subcommittee on Box Girder Bridges of the Committee on Flexural members. (1967). "Trend in the design of steel box girder bridges." *Journal of the Structural Division*, ASCE, Vol. 93, No. ST3, pp. 165–180.
- ASCE-AASHTO Task Committee on Curved Box Girders of the Committee on Flexural Members of the Committee on Metals of the ASCE. (1978a). "Curved steel box-girder bridges: a survey." *Journal of the Structural Division*, ASCE, Vol. 104, No. ST11, pp. 1697–1718.
- ASCE-AASHTO Task Committee on Curved Box Girders of the Committee on Flexural Members of the Committee on Metals of the ASCE. (1978b). "Curved steel box-girder bridges: state-of-the-art." *Journal of the Structural Division*, ASCE, Vol. 104, No. ST1, pp. 1719–1740.
- Bathe, K. (1996). *Finite Element Procedures*. Prentice Hall, Upper Saddle River, NJ.
- Batterman, R. H., and Johnston, B. G. (1967), "Behavior and maximum strength of metal columns," *Journal of the Structural Division*, ASCE, Vol. 93, No. ST2, pp. 205–230.
- Bazant, Z. P., and El-Nimeiri, M. (1974). "Stiffness method for curved box girders at initial stress." *Journal of the Structural Division*, ASCE, Vol. 100, No. ST10, pp. 2071–2090.
- Bjorhovde, R. (1972), "Deterministic and Probabilistic Approaches to the Strength of Steel Columns," Ph.D. dissertation, Lehigh University, Bethlehem, PA.
- Bleich, F. (1952). *Buckling Strength of Metal Structures*, McGraw-Hill Book Co., Inc. New York, NY.

- Boswell, L. F., and Zhang, S. H. (1984). "The Effect of Distortion in Thin-Walled Box Spine Beams." *International Journal of Solids and Structures*, Vol. 20(9/10), 845–862.
- Bridge Welding Code*. (1996). ANSI/AASHTO/AWS D1.5-96, A Joint Publication of American Association of State Highway and Transportation Officials, Washington, D.C. and American Welding Society, Miami, FL.
- Bridge Welding Code*. (2002). ANSI/AASHTO/AWS D1.5:2002, A joint publication of American Association of State Highway and Transportation Officials, Washington, D.C. and American Welding Society, Miami, FL.
- British Standard Institution (1982). "Steel, Concrete and Composite Bridges, BS 5400, Part 3," Code of Practice for Design of Steel Bridges, BSI, London.
- Bryan, G. H. (1891). "On the Stability of a Plane Plate under Thrusts in Its Own Plane, with Applications to the 'Buckling' of the Sides of a Ship," *Proceeding of London Mathematics Society*, Vol. 22
- Carlsen, C. A. and Czujko, J. (1978). "The Specification of post-welding distortion tolerances for stiffened plates in compression," *The Structural Engineer*, Vol. 56, No. 5, pp. 133-141.
- Chapman, J. C., Dowling, P. J., Lim, P. T. K., and Billington, C. J. (1971). "The structural behavior of steel and concrete box girder bridges." *The Structural Engineering*, Vol. 49, No. 3, pp. 111–120.
- Chatterjee, S., and Dowling, P. (1975). *Proposed Design Rules for Longitudinal Stiffeners in Compression Flanges of Box Girders*, Civ. Eng. Dept., Imperial College, London, CESLIUC Report BG40, May.
- Chatterjee, S., and Dowling, P. (1976). "The design of box girder compression flanges," Paper 8, in *Proc. I.C.S.P.S.*, pp. 196-228.
- Chen, B. S. (2002). *Top-lateral bracing systems for trapezoidal steel box-girder bridges*. Ph.D. Thesis, University of Texas, Austin, TX.
- Choi, B. H., and Yoo, C. H. (2002). "Design of longitudinal stiffeners on curved box girder flanges," *South Eastern Conference on Theoretical and Applied Mechanics XXI*, May 19-21, Orlando, Florida.
- Choi, B. H. and Yoo, C. H. (2004). "Strength of stiffened flanges in horizontally curved box girder," *Journal of Engineering Mechanics*, ASCE, Vol. 131, No. EM2, pp. 167-176.

- Clinton, H., Joehnk, G., and Petzold III, E. (1986). *Design examples for steel box girders*, Report No. FHWA-TS-86-209, Federal Highway Administration, Washington, D.C.
- Chu, K. J., and Pinjarkar, S. G. (1971). "Analysis of horizontally curved box girder bridges." *Journal of the Structural Division*, ASCE, Vol. 97, No. ST10, 2481–2501.
- Cook, R. D., Malkus, D. S., and Plesha, M. E. (1989). *Concepts and applications of finite element analysis*. John Wiley & Sons, Inc.
- Corrado, J. A., and Yen, B. T. (1973). "Failure tests of rectangular model steel box girders." *Journal of the Structural Division*, ASCE, Vol. 99, No. ST7, pp. 1439–1455.
- Crisfield, M. A. (1981), "A Fast Incremental/Iteration Solution Procedure that Handles 'Snap-Through'," *Computers and Structures*, 13(1-3), pp. 55-62.
- Culver, C. G., and Nasir, G. (1970). *Buckling of unstiffened curve plates*. Report No. 68-32, Pennsylvania DOT, Bureau of Public Roads, Carnegie Mellon University, Pittsburgh, PA.
- Culver, C. G., and Mozer, J. D. (1970). *Stability of curved box girder*. Report No. B1, Consortium of University Research Teams, Carnegie-Mellon University, Pittsburgh, PA.
- Culver, C. G., and Mozer, J. D. (1971). *Stability of curved box girder*. Report No. B2, Consortium of University Research Teams, Carnegie-Mellon University, Pittsburgh, PA.
- CURT (1975). *Tentative Design Specifications for Horizontally Curved Highway Bridges*. Prepared for U. S. Department of Transportation by Consortium of University Research Teams, Washington, DC.
- Dabrowski, R. (1964). "The analysis of curved thin-walled girders of open section," *Der Stahlbau*, Vol. 33, No. 12, pp. 364-372.
- Dabrowski, R. (1965). "Warping torsion of curved box girders of non-deformable cross-section," *Der Stahlbau*, Vol. 34, No. 5, pp. 135-141.
- Dabrowski, R. (1968). *Curved thin-walled girders: Theory and analysis*. Translated from the German Original, Cement and Concrete Association, U.K.

- DA Stahlbau (1978). "Beulsicherheitsnachweise für platten," DASt-Richtlinie 12, Deutscher Ausschuss für Stahlbau, Cologne, Germany.
- Davidson, J.S. (1996). *Nominal bending and shear strength of horizontally curved steel I-girder bridges*, Ph. D. dissertation, Auburn University, Auburn, Alabama.
- Davidson, J.S., and Yoo, C.H. (1996). "Local buckling of curved I-girder flanges," *Journal of Structural Engineering*, ASCE, Vol. 122, No. 8, pp. 936-947.
- Davidson, J.S., Ballance, S.R., and Yoo, C.H. (1999a). "Behavior of curved I-girder webs subjected to combined bending and shear," *Journal of Bridge Engineering*, ASCE, Vol. 5, No. 2, pp. 165-170.
- Davidson, J.S., Ballance, S.R., and Yoo, C.H. (1999b). "Effects of longitudinal stiffeners on curved I-girder webs," *Journal of Bridge Engineering*, ASCE, Vol. 5, No. 2, pp. 171-178.
- Davidson, J.S., Ballance, S.R., and Yoo, C.H. (1999c). "Finite displacement behavior of curved I-girder webs subjected to bending," *Journal of Bridge Engineering*, ASCE, Vol. 4, No. 3, pp. 213-220.
- Davidson, J.S., Ballance, S.R., and Yoo, C.H. (1999d). "Analytical model of curved I-girder web panels subjected to bending," *Journal of Bridge Engineering*, ASCE, Vol. 4, No. 3, pp. 204-212.
- Dey, G. (2001). "Bridging the curve: Design and fabrication issues affecting economy and constructability," *Bridgeline*, Vol. 11, No. 1, HDR Engineering, Omaha, NE.
- DIN 4114 (1952). "Stabilitätsfälle: Berechnungsgrundlagen Vorschriften," Blatt 1, Beuth Vertrieb, Berlin, Germany. DIN 4114 (1973). "Ergänzungsbestimmungen zur DIN 4114," Der Bundesminister für Verkehr, Bonn, Germany.
- Dogaki, M., Mikami, I., Yonezawa, H., and Ozawa, K. (1979). *Further test of the curved girder with orthotropic steel plate deck*. Technical Report No. 20, Kansai University, Osaka, Japan (in Japanese).
- Dowling, P. J. (1975). "Strength of steel box-girder bridges," *Journal of the Structural Division*, ASCE, Vol. 101, No. ST9, pp. 1929-1946.
- Dowling, P. J., and Chatterjee, S. (1977). "Design of box girder compression flanges," 2nd Int. Colloq. Stab., European Convention for Constructional Steelwork, Brussels, Belgium, pp. 153.

- Dwight, J. B., and Little, G. H. (1976). "Stiffened steel compression flanges, a simpler approach," *Structural Engineering*, Vol. 54, No. 12, pp. 501-509.
- Dwight, J. B., and Ratcliffe, A. T. (1968). "The strength of thin plates in compression," *Thin Walled Steel Structures*, Crosby Lockwood, London.
- Dwight, J., and Little, G. (1974). *Stiffened steel compression panels-A design approach*, University of Cambridge, Dept. of Engineering, Tecn. Report CUED (C-Struct), TR. 38.
- Dwight, J., et al. (1975). "A possible design procedure for stiffened compression panels," *Steel Construction*, Vol. 9, No. 3, Australian Institute of Steel Construction
- Dwight, J., Little, G., and Rogers, N. (1973). *An approach to stiffened steel compression Panels*, University of Cambridge, Dept. of Engineering, Tecn. Report CUED (C-Struct) TR. 32.
- Engesser, F. (1889). "Zeitschrift fur Architektur und Ingenieurwesen," Ver. Hannover, Vol. 35, pp. 455.
- ECCS, European Convention for Constructional Steelwork (1976). *Manual on the stability of steel structures*, An Introductory Report, 2nd ed., S.I.C.S. - ECCS, Tokyo.
- Fafitis, A., and Rong, A. Y. (1995). "Analysis of thin-walled box girders by parallel processing." *Thin-Walled Structures*, Vol. 21, No. 3, pp. 233-240.
- Falconer, B. H., and Chapman, J. C. (1953). "Compressive buckling of stiffened plates," *The Engineer*, pp. 789-791 & 822-825.
- Fan, Z., and Helwig, T. A. (1999). "Behavior of steel box girders with top flange bracing." *Journal of Structural Engineering*, ASCE, Vol. 125, No. 8, pp. 829-837.
- Fan, Z., and Helwig, T. A. (2002). "Distortional loads and brace forces in steel box girders." *Journal of Structural Engineering*, ASCE, Vol. 128, No. 6, pp. 710-718.
- Ford, E. M. (2000). *Stiffness requirements for longitudinally stiffened compression flanges*, Master thesis, Auburn University, Auburn, Alabama.
- Freakley, P. K. and Payne, A. R. (1978). *Theory and practice of engineering with rubber*, Applied Science Publishers Ltd., London, UK.

- Fu, C. C., and Hsu, Y. T. (1995). "Development of an improved curvilinear thin-walled Vlasov element." *Computers and Structures*, Vol. 54, No. 1, pp. 147–159.
- Galuta, E. M., and Cheung, M. S. (1995). "Combined boundary element and finite element analysis of composite box girder bridges." *Computers and Structures*, Vol. 57, No. 3, pp. 427–437.
- Gerard, G. (1962). *Introduction to structural stability theory*, McGraw-Hill Book Company, Inc.
- Gerard, G., and Becker, H. (1957), *Handbook of structural stability, I: Buckling of flat plates*, NACA Tech. Notes Nos. 3781.
- Giencke, E. (1964). "Über die Berechnung regelmässiger Konstruktion aus Kontinuum," *Der Stahlbau*, Heft 33, s. 39-48 (in German).
- Gilbert, R. I. and R. F. Warner. (1978), "Tension Stiffening in Reinforced Concrete Slabs," *Journal of the Structural Division*, ASCE, 104, No. ST12, pp. 1885-1900.
- Godfrey, G. B. (1974). "The evolution and international development of box girder bridges." *Proceedings*, Canadian Structural Engineering Conference, Canada.
- Grondin, G. Y., Chen, Q., Elwi, A. E., and Cheng, J. J. (1998). "Stiffened steel plates under compression and bending," *Journal of Constructional Steel Research*, Vol. 45, No. 2, pp. 125-148.
- Grubb, M. A. (1999). "Box-girder longitudinal stiffener study," Letter to the author, July.
- H.M. Stationary Office (1973a). "Inquiry into the basis of design and method of erection of steel box girder bridges," Report of the Committee - Appendix I, Interim Design and Workmanship Rules, Part III: Basis for the Design Rules and for the Design of Special Structures Not Within the Scope of Part I: Loading and General Design Requirements, Part II: Design Rules, London.
- H.M. Stationary Office (1973b). "Inquiry into the basis of design and method of erection of steel box girder bridges," Report of the Committee - Appendix I, Interim Design and Workmanship Rules, Part IV: Materials and Workmanship, London.
- H.M. Stationary Office (1974). "Inquiry into the basis of design and method of erection of steel box girder bridges," Report of the Committee - Appendix I, Interim Design and Workmanship Rules, Part III: Basis for the Design Rules and for the Design of Special Structures Not Within the Scope of Part II, London.

- Hamzeh, O. N., Tassoulas, J. L., and Becker, E. B. (1995). *Analysis of elastomeric bridge bearings*, Research Report No. 1304-5, Center for Transportation Research, University of Texas, Austin, TX.
- Hamzeh, O. N., Tassoulas, J. L., and Becker, E. B. (1996). "Behavior of Elastomeric Bridge Bearings: Computational Results," *Journal of Bridge Engineering*, ASCE, Vol. 3, No. 3, pp. 140-146.
- Hand, F. D., D. A. Pecknold, and W. C. Schnobrich. (1973), "Nonlinear analysis of reinforced concrete plates and shells," *Journal of the Structural Division*, ASCE, 99, No. ST7, pp. 1491-1505.
- Hall, D. H. (1997). "Proposed curved girder provisions for AASHTO," Building to Last Structures Congress - Proceedings, Vol. 1, ASCE, New York, NY, USA, pp. 151-154.
- Hall, D. H., Grubb, M. A., and Yoo, C. H. (1999). *Improved design Specifications for horizontally curved steel girder highway bridges*, NCHRP Report 424, National Cooperative Highway Research Program, Transportation Research Board, National Research Council, Washington, D.C., pp. 1-130.
- Hall, D. H. and Yoo, C. H. (1998). *Recommended Specifications for Steel Curved-Girder Bridges*. Interim Report, NCHRP Project 12-38, submitted to National Cooperative Highway Research Program, Washington, D.C.
- Hall, D. H., and Yoo, C. H. (1999a). *Design example horizontally curved steel I girder bridge*. Report for NCHRP Project 12-38.
- Hall, D. H., and Yoo, C. H. (1999b). *Design example horizontally curved steel box girder bridge*. Report for NCHRP Project 12-38.
- Hanshin Express Public Corporation and Steel Structure Study Committee (1988). *Guidelines for the design of horizontally curved girder bridges (Draft)*, Hanshin Expressway Public Corporation, October.
- Heins, C. P. (1978). "Box girder bridge design – State of the art." *Engineering Journal*, American Institute of Steel Construction, Vol. 15, No. 4 pp. 126-142.
- Heins, C. P., and Hall, D. H. (1981). *Designer's guide to steel box girder bridges*. Bethlehem Steel Corporation, Bethlehem, PA.
- Heins, C. P., and Oleinik, J. C. (1976). "Curved box beam bridge analysis." *Computers and Structures*, Vol. 6, No. 2, pp. 65-73.

- Heins, C. P., and Sheu, F. H. (1982). "Design/analysis of curved box girder bridges." *Computers and Structures*, Vol. 15, No. 3, pp. 241–258.
- Highway Structures Design Handbook*. (1986). AISC Marketing, Inc.
- Horne, M. R., and Narayana, R. (1975). "An approximate method for the design of stiffened steel compression panels," *Proc. Institution of Civil Engineers*, Part 2, September, pp. 501-514.
- Horne, M. R., and Narayana, R. (1976a). *Further tests on the ultimate load capacity of longitudinally stiffened panels*, Simon Engineering Laboratories, University of Manchester, July.
- Horne, M. R., and Narayana, R. (1976b). "Ultimate strength of stiffened panels under uniaxial compression," Paper 1, In *Proc. I.C.S.P.S.*, pp. 1-23.
- Hsu, Y. T., Fu, C. C., and Schelling, D. R. (1995). "EBEF method for distortional analysis of steel box girder bridges." *Journal of Structural Engineering*, ASCE, Vol. 121, No. 3, pp. 557–566.
- Issa, M. A. (1999). "Investigation of cracking in concrete bridge decks at early ages." *Journal of Bridge Engineering*, ASCE, Vol. 4, No. 2, pp. 116–124.
- Japan Road Association (1980). *Specification for Highway Bridges, Part II: Steel Bridges*, February, Japan.
- Japan Road Association (1990). *Specifications for highway bridges*, February, Japan.
- Jeon, S. M., Cho, M. H., and Lee, I. (1995). "Static and dynamic analysis of composite box beams using large deflection theory." *Computers and Structures*, Vol. 57, No. 4, pp. 635–642.
- Johnson, J. B., Bryan, C. W., and Turneaure, F., E. (1899), *Theory and practice of modern framed structures*, 7th ed., John Wiley and Sons.
- Kang, Y. J. (1992). *Nonlinear theory of thin-walled curved beams and finite element formulation*, Ph.D. dissertation, Auburn University, Auburn, Alabama.
- Kang, Y. J., and Yoo, C. H. (1994a). "Thin-walled curved beams. II: Analytical solutions for buckling of arches," *Journal of Engineering Mechanics*, ASCE, Vol. 120, No. 10, October, pp. 2102-2125.
- Kang, Y. J., and Yoo, C. H. (1994b). "Thin-walled curved beams. I: Formulation of nonlinear equations," *Journal of Engineering Mechanics*, ASCE, Vol. 120, No. 10, October, pp. 2072-2101.

- Kármán, T. (1910). “Untersuchungen über knickfestigkeit,” Mitteilungen über Forschungsarbeiten auf dem Gebiete des Ingenieurwesens, No. 81, Berlin.
- Kerensky, O. A. (1973). “Conception,” Proceedings of the International Conference of Steel Box Girder Bridges, Institution of Civil Engineers, London, England, pp. 7-10.
- Kim, K. (2004). Research on horizontally curved steel box girders, Ph.D. Dissertation, Auburn University, Auburn, AL.
- Kim, K., and Yoo, C. H. (2005). “Brace forces in steel box girders with single diagonal lateral bracing systems.” *Journal of Structural Engineering*, ASCE, in print.
- Kollbrunner, C. F. and Basler, K. (1969). *Torsion in structures*, Springer-Verlag, Berlin/Heidelberg/New York.
- Korol, R. M., Thimmhardy, E. G., and Cheung, M. S. (1984). “Field investigation of out-of-plane deviations for steel box girder bridges,” *Canadian Journal of Civil Engineering*, Vol. 11, pp. 377-386.
- Korol, R. M., Thimmhardy, E. G., and Cheung, M. S. (1988). “An experimental investigation of the effects of imperfections on the strength of steel box girders.” *Canadian Journal of Civil Engineering*, Vol. 15, No. 3, pp. 443–449.
- Kupfer, H., Hilsdorf, H. K., and Rusch, H. (1969). “Behavior of concrete under biaxial stresses.” *Journal of the American Concrete Institute*, Vol. 66, No. 8, pp. 656–666.
- Lamas, A. R. G., and Dowling, P. J. (1980), “Effect of shear lag on the inelastic buckling behavior of thin-walled structures,” in *Thin-Walled Structures* (ed. J. Rhodes and A.C. Walker), Granada, London, pp. 100.
- Lee, D. J. (1994). *Bridge Bearings and Expansion Joints*, 2nd ed., E & FN Spon, London, UK.
- Lee, S. C., and Yoo, C. H. (1999). “Strength of curved I-girder web panels under pure shear,” *Journal of Structural Engineering*, ASCE, Vol. 125, No. 8, pp. 847-853.
- Lim, P. T., Kilford, J. T., and Moffatt, K. R. (1971). *Finite element analysis of curved box girder bridges*. Devel Bridge Design and Construction, U.K.

- Lin, C. S. and Scordelis, A. C. (1975), "Nonlinear Analysis of Reinforced Concrete Shells of General Form," *Journal of the Structural Division*, ASCE, 101(ST3), pp. 523-238.
- Lindley, P. (1981). "Natural rubber structural bearings," *Joint Sealing and Bearing Systems for Concrete Structures*, SP-70, pp. 353-378, ACI, Detroit, MI.
- Little, G. (1976). "Stiffened steel compression panels-theoretical failure analysis," *The Structural Engineer*, Vol. 54, No. 12, December, pp. 489-500.
- MacGregor, J. G. (1997), *Reinforced concrete: mechanics and design*. 3rd edition, Prentice Hall, Upper Saddle River, NJ.
- McNeice, A. M. (1967), "Elastic-Plastic Bending of Plates and Slabs by the Finite Element Method," Ph.D. Thesis, London University, London, U.K.
- Maisel, B. I. (1970). *Review of literature related to the analysis of thin-walled beams*. Technical Report No. 42440, Cement and Concrete Association, London, U.K.
- MAPLE (2002). *Introduction to MAPLE 8.00*. Waterloo Maple Inc.,
- Massonnet, C. (1980). "Tolerances in steel plated structures," International Association of Bridge and Structural Engineering, Surveys S-14/80, Zurich, Switzerland, pp. 49-76.
- Mattock, A. H., et al. (1967). *Commentary on criteria for design of steel-concrete composite box girder highway bridges*, Report of the Committee (unpublished).
- Memberg, M. A. (2002). *A design procedure for intermediate external diaphragms on curved steel trapezoidal box girder bridges*. MS Thesis, University of Texas, Austin, TX.
- Mikkola, M., and Paavola, J. (1980). "Finite element analysis of box girders." *Journal of the Structural Division*, ASCE, Vol. 106, No. 6, pp. 1343–1357
- Mikami, I., Morisawa, Y., Yomashina, J., and Tanaka, K. (1985). *Linear analysis of discretely stiffened cylindrical panels under circumferential in-plane load*. Technical Report No. 26, Kansai University, Osaka, Japan (in Japanese).
- Mikami, I., Morisawa, Y., Fukuzumi, T., Yoshizawa, A., and Nakamura, T. (1987). *Ultimate strength tests on steel box girders under bending*. Technol. Rep. No. 29, Kansai University, Osaka, Japan (in Japanese).

- Mikami, I., and Niwa, K. (1993). *Ultimate strength test of steel box girders with unsymmetrical cross section*. Technical Report No. 35, Kansai University, Osaka, Japan (in Japanese).
- Mindess, S., Young, J. F., and Darwin, D. (2003). *Concrete*. Prentice Hall, Upper Saddle River, NJ.
- Moffatt, K. R., and Dowling, P. J. (1975). "Shear lag in steel box girder bridges," *The Structural Engineer*, London, October, pp. 439-447.
- Moffatt, K. R., and Dowling, P. J. (1972). *Parametric study on the shear lag phenomenon in steel box girder bridges*, CESLIC Report BG17, Engineering Structures Laboratories, Imperial College, London.
- Moorty, S. and Roeder, C. H. (1992). "Temperature-Dependent Bridge Movements." *Journal of Structural Engineering*, American Society of Civil Engineers, Vol. 118, No. 4, pp. 1090-1105.
- MSC/NASTRAN (1992). *Handbook for nonlinear analysis*, Version 67, The MacNeal-Schwendler Corporation, Los Angeles, California.
- MSC/NASTRAN (1994a). *Reference manual*, Version 68, Volume I, II, III, The MacNeal-Schwendler Corporation, Los Angeles, California.
- MSC/NASTRAN (1994b). *Linear static analysis*, Version 68, The MacNeal-Schwendler Corporation, Los Angeles, California.
- MSC/NASTRAN (1997). *Common questions and answers*, 3rd Edition, The MacNeal-Schwendler Corporation, Los Angeles, California.
- MSC/NASTRAN (1998). *Quick reference guide*, Version 70.5, The MacNeal-Schwendler Corporation, Los Angeles, California.
- MSC/PATRAN (1988). *User's guide*, Version 8, Volume I, II, III, IV, The MacNeal-Schwendler Corporation, Los Angeles, California.
- Muscarella, J. V. and Yura, J. A. (1995). *An experimental study of elastomeric bridge bearings with design recommendations*, Research Report No. 1304-3, Center for transportation Research, University of Texas, Austin, TX.
- Nakai, H., and Heins, C. P. (1977). "Analysis criteria for curved bridges." *Journal of the Structural Division*, ASCE, Vol. 103, No. 7, pp. 1419-1427.

- Nakai, H., and Miki, T. (1980). "Theoretical and experimental research on distortion of thin-walled horizontally curved box bridges," *Journal of Civil Engineering Design*, Vol. 2, No. 1, pp. 63-101.
- Nakai, H., and Murayama, T. (1981). "Distortional stress analysis and design aid for horizontally curved box girder bridges with diaphragms," *Proceedings of the Japanese Society of Civil Engineers*, No. 309, May, pp. 25-39 (in Japanese).
- Nakai, H., Murayama, Y., Kitada, T., and Takada, Y. (1990). "An experimental study on ultimate strength of thin-walled box beams subjected to bending and torsion," *Journal of Structural Engineering*, Japanese Society of Civil Engineers, Vol. 36A, pp. 64–70 (in Japanese).
- Nakai, H., Murayama, Y., and Kitada, T., (1992). "An experimental study on ultimate strength of thin-walled box beams with longitudinal stiffeners subjected to bending and torsion," *Journal of Structural Engineering*, Japanese Society of Civil Engineers, Vol. 38A, pp. 155–165 (in Japanese).
- Nakai, H. and Yoo, C. H. (1988). *Analysis and design of curved steel bridges*. McGraw-Hill Book Company, New York, NY.
- Ostapenko, A., and Vojta, J. F. (1967), *Ultimate strength design of longitudinally stiffened plate panels with large b/t*, Fritz Eng. Lab. Rep. No. 248.18, Lehigh University, Bethlehem, PA.
- Oleinik, J. C., and Heins, C. P. (1975). "Diaphragms for curved box beam bridges." *Journal of the Structural Division*, ASCE, Vol. 101, No. ST10, pp. 2161–2178.
- Pi, Y., Bradford, M. A. (2001), "Strength design of steel I-section beams curved in plan," *Journal of Structural Engineering*, ASCE, 127(ST6), pp. 639-646.
- Prandtl, L. (1903), "Zur Torsion von prismatischen Stäben," *Physik Zeit.*, Vol. 4, pp. 758.
- Richardson, Gordon and Associates (1963). *Analysis and design of horizontally curved steel bridge girders*. United States Steel Structural Rep. ADUCO 91063.
- Riks, E. (1979). "An incremental approach to the solution of snapping and buckling problems," *International Journal of Solids and Structures*, 15(7-B), pp. 529-551.
- Ritz, W. (1909). "Rayleigh-Ritz Method," *Crelle's Journal* (presently known as *Journal für die reine und angewandte Mathematik*), Vol. 85, Genthiner Strasse 13, D-10785 Berlin/Germany.

- Rivlin, R. S. (1956). "Large Elastic Deformations," In F. R. Eirich, editor, *Rheology: Theory and Applications*, Vol. 1. Academic Press, New York
- Roeder, C. W., Stanton, J. F. and Feller, T. (1989). *Low temperature behavior and acceptance criteria for elastomeric bridge bearings*, NCHRP 325, TRB, Washington, DC.
- Roeder, C. W., Stanton, J. F. and Taylor, A. W. (1987). *Performance of elastomeric bearings*, NCHRP 298, TRB, Washington, DC.
- Saint-Venant, B. (1843). "Memoire sur le calcul de la resistance et de la flexion des pieces solides a simple ou a double courbure, en prenant simultanement en consideration les divers efforts auxquels elles peuvent entre soumises dans tous les sens." *Compts-Rendus*, Vol. 27, l'Academic des sciences de Paris, Paris, pp. 1020–1031 (in French).
- Sakai, F., and Nagai, M. (1977). "A Recommendation on the design of intermediate diaphragms in steel box girder bridges," *Proceedings of Japanese Society of Civil Engineers*, No. 261, August, pp. 21-34 (in Japanese).
- Schrage, I. (1981). "Anchoring of bearing by friction," *Joint Searing and Bearing Systems for Concrete Structures*, SP-70, pp. 197-213, ACI, Detroit, MI.
- Scheer, J., and Nölke, H. (1976). "The background to the future german plate buckling design rules," Paper 21, in Proceeding of I.C.S.P.S, pp. 503-523.
- Schmitt, W. (1966). "Interchange utilizes arcwelded horizontally curved span," unpublished paper submitted to Lincoln Arc Welding Foundation.
- Sennah, K. M., and Kennedy, J. B. (2001). "State-of-the-art in design of curved box-girder bridges." *Journal of Bridge Engineering*, ASCE, Vol. 6, No. 3, pp. 159–167.
- Sennah, K. M., and Kennedy, J. B. (2002). "Literature review in analysis of box-girder bridges." *Journal of Bridge Engineering*, ASCE, Vol. 7, No. 2, pp. 134–143.
- Simpson, M. D. (2000). "Analytical investigation of curved steel girder behaviour." Ph.D. Thesis, University of Toronto, Toronto, Canada.
- Sisodiya, R. G., Cheung, Y. K., and Ghali, A. (1970). "Finite element analysis of skew, curved box girder bridges." *International Association of Bridges and Structural Engineering (IABSE)*, Vol. 30, No. II, pp. 191–199.
- SPSS (1998). *Base 8.0, Application Guide/SPSS*. SPSS, Inc., Chicago, IL.

- SSRC (1998). *Structural stability research council guide to stability design criteria for metal structures*, 5th ed., edited by T. V. Galambos, John Wiley and Sons, Inc., New York, NY.
- Stanton, J. F. and Roeder, C. W. (1982). *Elastomeric bearings design, construction, and materials*, NCHRP 248, TRB, Washington, DC.
- State of Florida, 2005. *Structures detailing manual*. on-line version at <http://www.dot.state.fl.us/Structures/StructuresManual/CurrentRelease/FDOTBridgeManual.htm>, Department of Transportation, Florida. [cited 2 May 2005]
- State of Montana, 2002. *Montana structures manual*. Vol. II, Chap. 15. on-line version at http://www.mdt.state.mt.us/bridge/net/external/structures-manual/part_II/chp-15-final.pdf, Department of Transportation, Montana. [cited 4 May 2005]
- State of North Carolina, 2005. *Structure design – Metric design manual*. on-line version at <http://www.doh.dot.state.nc.us/preconstruc/highway/structur/MetricDesignManual/metric/toc.htm>, Department of Transportation, NC. [cited 22 March 2005]
- State of Texas, 2000. *Preferred practices for steel bridge design, fabrication, and erection*. Texas Steel Quality Council, Department of Transportation, Texas
- Roeder, C. H., and Stanton, J. F. (1991). “State-of-the-Art Elastomeric Bridge Bearing Design.” *ACI Structural Journal*, Vol. 88, No. 1, pp. 31-41.
- Stanton, J. F., Scroggins, G., Taylor, A. W., and Roeder, C. H. (1990). “Stability of Laminated Elastomeric Bearings.” *Journal of Engineering Mechanics*, American Society of Civil Engineers, Vol.116, No. 6, pp. 1351-1371.
- Stowell, E. Z., Heimerl, G. J., Libove, C., and Lundquist, E. E. (1952), “Buckling stresses for flat plates and sections,” *Trans. Am. Soc. Civ. Eng.*, Vol. 117, pp. 545-578.
- Suros, O., and Chu, H. Y. (1991). “Reducing Airport Congestion,” *Modern Steel Construction*, June, pp. 21-25.
- Task Group 1c. (1991). *A look to the future*, Report of Workshop on Horizontally Curved Girders, Structural Stability Research Council, Chicago, IL, April 14-15, pp. 1-8.
- Thevendran, V., Chen, S., Shanmugam, and N. E., Liew, J. Y. (1999). “Nonlinear analysis of steel-concrete composite beams curved in plan,” *Finite Elements in Analysis and Design*, 32(1999), Elsevier Science, pp. 125-139.
- Thimmhardy, E. G. (1991). “Nonlinear analysis of buckling behavior of steel box-girder components.” *Computers and Structures*, Vol. 40, No. 2, pp. 469–474.

- Timoshenko, S. P. (1921). "Über die Stabilität versteifter Platten," *Der Eisenbau*, pp. 147.
- Timoshenko, S. P., and Gere, J. M. (1961). *Theory of elastic stability*, 2nd ed., McGraw-Hill Book Company, Inc., New York, New York.
- Topkaya, C., and Williamson, E. B. (2003). "Development of computational software for analysis of curved girders under construction loads," *Computers and Structures*, Vol. 81, No. 2003, pp. 2087–2098.
- Treloar, L. R. G. (1975). *The physics of rubber elasticity*. 3rd ed. Oxford University Press, London, UK.
- Trukstra, C. J., and Fam, A. R. (1978). "Behaviour study of curved box bridges." *Journal of the Structural Division*, ASCE, Vol. 104, No. ST3, pp. 453–462.
- United States Steel Corporation (1978). *Steel/concrete composite box-girder bridges: A construction manual*, Pittsburgh, PA.
- United States Steel Corporation (1984). *V-Load Analysis*, ADUSS 88-8535-01, available from AISC Marketing, Inc., Chicago, IL., pp. 1-56.
- Uy, B. (2001). "Local and postlocal buckling of fabricated steel and composite cross sections." *Journal of Structural Engineering*, ASCE, Vol. 127, No. 6, pp. 666–677.
- Vlasov, V. Z. (1961). *Thin-walled elastic beams*. OTS61–11400, National Science Foundation, Washington, D.C.
- Wolchuk, R., and Mayrbaur, R. M. (1980). *Proposed design Specifications for steel box girder bridges*, Report No. FHWA-TS-80-205, Contract No. DOT-FH-11-9259, Federal Highway Administration, Office of Research & Development, Washington, D. C.
- Wright, R. N., Abdel-Samad, S. R., and Robinson, A. R. (1968). "BEF analogy for analysis of box girder." *Journal of the Structural Division*, ASCE, Vol. 94, No. 7, pp. 1719–1743.
- Yabuki, T., and Arizumi, Y. (1989). "A provision on intermediate diaphragm spacing in curved steel-plated box-bridge-girders," *Structural Eng./Earthquake Eng.*, JSCE, Vol. 6., No. 2, October, pp. 207s-216s.

- Yamamoto, T. and Vecchio F. J. (2001). "Analysis of reinforced concrete shells for transverse shear and torsion," *ACI Structural Journal*, 98(2), pp. 191-200.
- Yen, B. T., Huang, T., Wang, D., Chuang, C. K., and Daniels, J. H. (1986). "Steel box girders with composite bottom flanges." *Proceedings of Third Annual International Bridge Conference*, ASCE, Reston, VA., pp. 79–86.
- Yeoh, O. H. (1993). "Some Forms of the Strain Energy Function for Rubber." *Rubber Chemistry and Technology*, Vol. 66, No. 5, pp. 754-771.
- Yonezawa, H., Mikami, I., Akamatsu, Y., and Dogaki, M. (1978). *Test of a curved girder with orthotropic steel plate deck*. Technical Report No. 19, Kansai University, Osaka, Japan (in Japanese).
- Yonezawa, H., Dogaki, M., and Adachi, H. (1985). *Elastic buckling of orthogonally stiffened sector plates under circumferential compression*. Tech. Rep. No. 26, Kansai University, Osaka, Japan (in Japanese).
- Yoo, C. H. (1979). "Matrix formulation of curved girders," *Journal of the Engineering Mechanics Division*, ASCE, Vol. 105, No. ST6, pp. 971-988.
- Yoo, C. H. (1996). *Progress Report on FHWA-CSBRP-Task D*, FHWA Contract No. DTFH61-92-C-00136, Auburn University, Department of Civil Engineering Interim Report submitted to HDR Engineering, Inc., Pittsburgh Office, Pittsburgh, PA, August.
- Yoo, C. H., Choi, B. H., and Ford, E. M. (2001). "Stiffness requirements for longitudinally stiffened box-girder flanges." *Journal of Structural Engineering*, ASCE, Vol. 127, No. 6, pp. 705–711.
- Zhang, Jianan (1996). *Parametric studies of horizontally curved box girders under dead loads (Effects of external and internal bracing)*. MS Thesis, Auburn University, Auburn, AL.
- Zhang, S. H., and Lyons, L. P. R. (1984). "Thin-walled box beam finite element for curved bridge analysis." *Computers and Structures*, Vol. 8, No. 6, pp. 1035–1046.

APPENDICES

APPENDIX 3.A

LATERL STIFFNESS CONTRIBUTION OF WEBS TO TOP FLANGES

The top flanges of the box girder bend as in a manner similar to a continuous beam between every two panel points in the lateral direction due to interaction between top flanges and lateral bracing members, i.e., diagonals and struts as shown in Figs. 3.10(d) and 4.10(a). Forces from lateral bracing members are balanced by lateral bending stiffness of the top flange and the web plate. Fig. 3.A.1. shows a simplified model with a top flange and a web plate resisting a force from lateral bracing members. From static equilibrium and geometric compatibility, followings are given:

$$P = P_{tf} + P_{web} \quad (3.A.1)$$

$$\delta_{tf} = \delta_{web} \quad (3.A.2)$$

where P = force from bracing members; P_{tf} = force balanced by top flange; P_{web} = force balanced by web; δ_{tf} = deformation due to P_{tf} ; δ_{web} = deformation due to P_{web} . Resisting forces P_{tf} and P_{web} may be conservatively evaluated using the Ritz method, a energy method based on the principle of minimum potential energy (Ritz 1908). A segment of two consecutive panels of the web plate and top flange may be modeled with appropriate boundary conditions. The assumed boundary conditions, one free edge and three fixed edges shown in Fig. 3.A.1, are conservative compared to actual conditions of the web plate. Assuming deflection curves along x -axis and y -axis to be those of a fixed-ended beam and a cantilever, respectively, the deflection of the plate in the z -direction, w_z , is expressed as a function of x and y coordinates, which yields:

$$w_z = \delta_{web} \left(\frac{x}{s} \right)^2 \left(3 - 2 \frac{x}{s} \right) \left[1 - \frac{3}{2} \left(\frac{y}{h} \right) + \frac{1}{2} \left(\frac{y}{h} \right)^2 \right] \quad (0 \leq x \leq s, 0 \leq y \leq h) \quad (3.A.3)$$

where w_0 = deflection at the point P_{web} is applied.

The total potential energy of a structural system, Π , consists of its strain energy, U , plus the potential of the work done by the external forces, V , which are written as:

$$\Pi = U + V \quad (3.A.4)$$

$$U = \frac{D_P}{2} \int_0^h \int_0^{2s} \left(\frac{\partial^2 w_z}{\partial x^2} + \frac{\partial^2 w_z}{\partial y^2} \right) dx dy \quad (3.A.5)$$

$$V = -P_{web} w_0 \quad (3.A.6)$$

where D_P = flexural rigidity of plate defined by:

$$D_P = \frac{Et_{web}^3}{12(1-\nu^2)}$$

where E = Elastic modulus; ν = Poisson's ratio; t_{web} = thickness of web plate. The unknown constant, w_0 , is determined from the minimum potential energy principle; thus

$$\frac{\partial \Pi}{\partial w_0} = \frac{\partial (U + V)}{\partial w_0} = 0 \quad (3.A.7)$$

Substituting Eqs. (3.A.5) and (3.A.6) into (3.A.7) and solving for δ_{web} yield:

$$\delta_{web} = \frac{35P_{web}h^3s^3}{6D_P(33h^4 + 13s^4)} \quad (3.A.8)$$

Similarly, deflection of top flange due to P_{tf} , δ_{tf} , is written as:

$$\delta_{tf} = \frac{P_{tf}(2s)^3}{192EI_f} \quad (3.A.9)$$

where I_f is second moment of inertia of top flange in the lateral direction. Substituting Eqs. (3.A.8) and (3.A.9) into Eq. (3.A.2) and solving Eqs. (3.A.1) and (3.A.2) simultaneously for P_{tf} and P_{web} gives following expression for portions of forces resisted by the top flange and the web plate, respectively.

$$\frac{P_{tf}}{P} = \frac{140h^3 EI_f}{140h^3 EI_f + D_p(33h^4 + 13s^4)} \quad (3.A.10)$$

$$\frac{P_{web}}{P} = \frac{D_r(33h^4 + 13s^4)}{140h^3 EI_f + D_p(33h^4 + 13s^4)} \quad (3.A.11)$$

Evaluation for Eqs. (3.A.8) and (3.A.9) for typical values of cross-frame spacing and box depth with different plate thickness ratio of top flange to web are shown in Tables 3.A.1 and 3.A.2. The width of the top flange was taken 18 in. and 16 in. for the results in Table 3.A.1 and 3.A.2, respectively. As shown in Table 3.A.1 and 3.A.2, the effect of the stiffness of the web plate can be neglected in interaction between bracing members and box-girder plates.

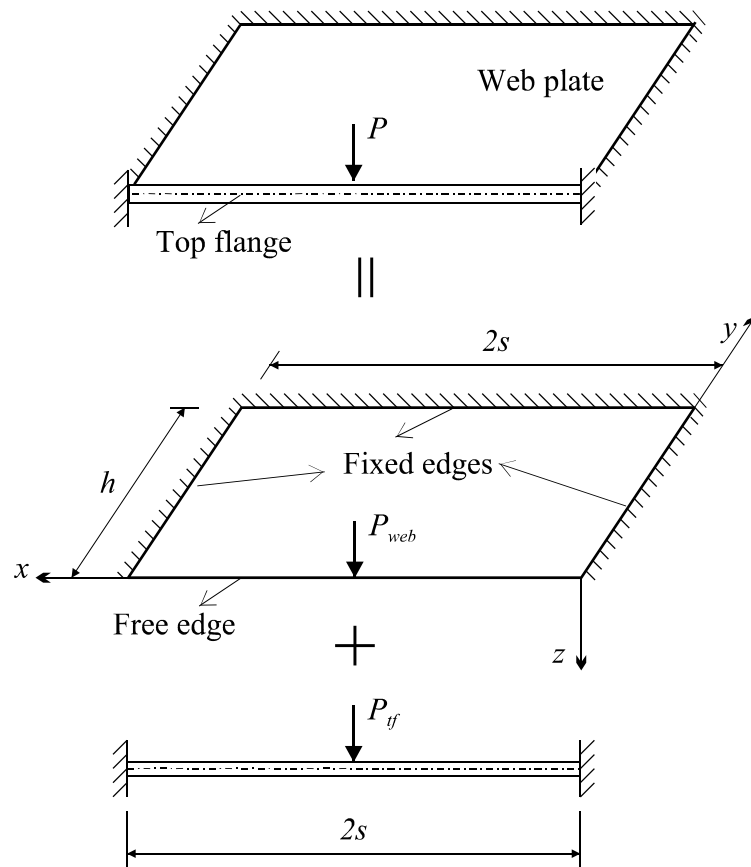


Fig. 3.A.1. Simplified model for web and top flange subjected to a concentrated load

Table 3.A.1. Lateral stiffness contribution of top flange and web (top flange width = 18 in.)

Panel Spacing (in.)	Box Depth (in.)	Thickness ratio t_{tf}/t_{web}	Top flange (%)	Web (%)
100	60	1.0	99.66	0.34
		2.5	99.86	0.14
		4.0	99.91	0.09
	90	1.0	99.80	0.20
		2.5	99.91	0.08
		4.0	99.95	0.05
	120	1.0	99.80	0.20
		2.5	99.91	0.08
		4.0	99.95	0.05
140	60	1.0	97.94	1.06
		2.5	99.57	0.43
		4.0	99.73	0.27
	90	1.0	99.71	0.42
		2.5	99.88	0.17
		4.0	99.93	0.10
	120	1.0	99.71	0.29
		2.5	99.88	0.12
		4.0	99.93	0.07
180	60	1.0	97.30	2.70
		2.5	98.90	1.10
		4.0	99.31	0.69
	90	1.0	99.08	0.92
		2.5	99.63	0.37
		4.0	99.77	0.23
	120	1.0	99.50	0.50
		2.5	99.80	0.20
		4.0	99.87	0.13

Table 3.A.2. Lateral stiffness contribution of top flange and web (top flange width = 16 in.)

Panel Spacing (in.)	Box Depth (in.)	Thickness ratio t_{tf}/t_{web}	Top flange (%)	Web (%)
100	60	1.0	99.52	0.48
		2.5	99.81	0.19
		4.0	99.88	0.12
	90	1.0	99.71	0.29
		2.5	99.88	0.12
		4.0	99.93	0.07
	120	1.0	99.72	0.28
		2.5	99.89	0.11
		4.0	99.93	0.07
140	60	1.0	98.50	1.50
		2.5	99.39	0.61
		4.0	99.62	0.38
	90	1.0	99.41	0.59
		2.5	99.76	0.24
		4.0	99.85	0.15
	120	1.0	99.59	0.41
		2.5	99.83	0.17
		4.0	99.90	0.10
180	60	1.0	96.20	3.80
		2.5	98.44	1.56
		4.0	99.02	0.98
	90	1.0	98.70	1.30
		2.5	99.48	0.52
		4.0	99.66	0.33
	120	1.0	99.29	0.71
		2.5	99.71	0.29
		4.0	99.82	0.18

APPENDIX 4.A

CONDENSATION AND VERIFICATION OF TRANSFER MATRICES

Condensation, also known as static condensation, is the process of reducing the number of degree of freedom (DOF) by substitution, for example, by starting a Gauss elimination solution of equations for unknowns but stopping before the transfer matrix has been fully reduces. Condensation is a strict manipulation of matrices and introduces no approximation (Cook, Malkus, and Plesha 1986). Consider following matrix equation with partitioned DOFs that were established in Chapter 4:

$$\left[\begin{array}{c|c} K_{11} & K_{12} \\ \hline K_{21} & K_{22} \end{array} \right] \left\{ \begin{array}{c} P_{bend} \\ V_{bend} \end{array} \right\} = \left\{ \begin{array}{c} Y_P \\ Y_V \end{array} \right\} \quad (4.A.1)$$

Expanding Eq. (A2.1) yields:

$$[K_{11}]\{P_{bend}\} + [K_{12}]\{V_{bend}\} = \{Y_P\} \quad (4.A.2)$$

$$[K_{21}]\{P_{bend}\} + [K_{22}]\{V_{bend}\} = \{Y_V\} \quad (4.A.3)$$

The lower partition is solved for $\{V_{bend}\}$:

$$\{V_{bend}\} = -[K_{22}]^{-1} ([K_{21}]\{P_{bend}\} - \{Y_V\}) \quad (4.A.4)$$

Next, $\{V_{bend}\}$ is substituted into Eq. (A2.2). Thus

$$([K_{11}] - [K_{12}][K_{22}]^{-1}[K_{21}])\{P_{bend}\} = \{Y_P\} - [K_{12}][K_{22}]^{-1}\{Y_V\} \quad (4.A.5)$$

Since $\{Y_V\}$ has all zero elements as in usual static condensation, Eqs. (4.A.5) and (4.A.4)

are rewritten as following simplified forms:

$$\{P_{bend}\} = [C_P]^{-1} \{Y_P\} \quad (4.A.6)$$

$$\{V_{bend}\} = [C_V]\{P_{bend}\} \quad (4.A.7)$$

where $[C_P]$ and $[C_V]$ are transfer matrices for the brace force vector, $\{P_{bend}\}$, and lateral displacement vector, $\{V_{bend}\}$, defined by

$$[C_P] = [K_{11}] - [K_{12}][K_{22}]^{-1}[K_{21}] \quad (4.A.8)$$

$$[C_V] = -[K_{22}]^{-1}[K_{21}] \quad (4.A.9)$$

Static condensation used for brace force vector $\{P_{bend}\}$ and lateral displacement vector $\{V_{bend}\}$ in Chapter 3 is verified using MAPLE 8. Transfer matrices, $[C_P]$ and $[C_V]$, are evaluated and $\{P_{bend}\}$ and $\{V_{bend}\}$ are computed for the examples, simply supported box girders with internal K-frame and internal X-frame adopted in Chapter 3. Followings are the results of MAPLE 8 runs.

Brace forces in the box girder with internal K-frames

```
> restart:
> with(linalg):
> K11:=matrix ([[L[SD]/E/A[SD],0,0,0],[2*sin(alpha),1,1,0],[0,0,
(2*s)^3/192/E/I[tf],0],[0,-1,1,2*sin(beta)]]);
```

$$K11 := \begin{bmatrix} \frac{L_{SD}}{EA_{SD}} & 0 & 0 & 0 \\ 2 \sin(\alpha) & 1 & 1 & 0 \\ 0 & 0 & \frac{1}{24} \frac{s^3}{EI_{tf}} & 0 \\ 0 & -1 & 1 & 2 \sin(\beta) \end{bmatrix}$$

```
> K12:=matrix ([[(-2*sin(alpha)),0,0],[0,0,0],[-1,-1,0],[0,0,0]]);
```

$$K12 := \begin{bmatrix} -2 \sin(\alpha) & 0 & 0 \\ 0 & 0 & 0 \\ -1 & -1 & 0 \\ 0 & 0 & 0 \end{bmatrix}$$

```
> K21:=matrix ([[0,-b/2/E/A[S],0,0],[0,0,b/2/E/A[S],0],[0,0,
s^3/24/E/I[bf],L[KD]/E/A[KD]/sin(beta)+s^3*sin(beta)/24/E/I[bf]]]);
```

$$K21 := \begin{bmatrix} 0 & -\frac{1}{2} \frac{b}{EA_S} & 0 & 0 \\ 0 & 0 & \frac{1}{2} \frac{b}{EA_S} & 0 \\ 0 & 0 & \frac{1}{24} \frac{s^3}{EI_{bf}} & \frac{L_{KD}}{EA_{KD} \sin(\beta)} + \frac{1}{24} \frac{s^3 \sin(\beta)}{EI_{bf}} \end{bmatrix}$$

```
> K22:=matrix([ [1,0,-1],[0,1,-1],[ -0,0,-1 ] ]);
```


$$K22 := \begin{bmatrix} 1 & 0 & -1 \\ 0 & 1 & -1 \\ 0 & 0 & -1 \end{bmatrix}$$

> C[V]:=evalm(-inverse(K22) &* K21);

$$C_V := \begin{bmatrix} 0 & \frac{1}{2} \frac{b}{EA_S} & \frac{1}{24} \frac{s^3}{EI_{bf}} & \frac{L_{KD}}{EA_{KD} \sin(\beta)} + \frac{1}{24} \frac{s^3 \sin(\beta)}{EI_{bf}} \\ 0 & 0 & -\frac{1}{2} \frac{b}{EA_S} + \frac{1}{24} \frac{s^3}{EI_{bf}} & \frac{L_{KD}}{EA_{KD} \sin(\beta)} + \frac{1}{24} \frac{s^3 \sin(\beta)}{EI_{bf}} \\ 0 & 0 & \frac{1}{24} \frac{s^3}{EI_{bf}} & \frac{L_{KD}}{EA_{KD} \sin(\beta)} + \frac{1}{24} \frac{s^3 \sin(\beta)}{EI_{bf}} \end{bmatrix}$$

> C[P]:=evalm(K11- K12 &* inverse(K22) &* K21);

$$C_P := \begin{bmatrix} \frac{L_{SD}}{EA_{SD}} & -\frac{\sin(\alpha) b}{EA_S} & \frac{1}{12} \frac{\sin(\alpha) s^3}{EI_{bf}} & -2 \sin(\alpha) \left(\frac{L_{KD}}{EA_{KD} \sin(\beta)} + \frac{1}{24} \frac{s^3 \sin(\beta)}{EI_{bf}} \right) \\ 2 \sin(\alpha) & 1 & 1 & 0 \\ 0 & \frac{1}{2} \frac{b}{EA_S} & \frac{1}{24} \frac{s^3}{EI_{bf}} + \frac{1}{2} \frac{b}{EA_S} - \frac{1}{12} \frac{s^3}{EI_{bf}} & -\frac{2 L_{KD}}{EA_{KD} \sin(\beta)} - \frac{1}{12} \frac{s^3 \sin(\beta)}{EI_{bf}} \\ 0 & -1 & 1 & 2 \sin(\beta) \end{bmatrix}$$

> Y[P]:=matrix([[s*y[t]*cos(alpha)/E/I[box]*M],[0],[0],[0]]);

$$Y_P := \begin{bmatrix} \frac{s y_t \cos(\alpha) M}{EI_{box}} \\ 0 \\ 0 \\ 0 \end{bmatrix}$$

> a:=81.: b:=120.: h:=78: s:=120: E:=29000.: A[S]:=3.75: A[KD]:=3.75:
A[SD]:=7.78: bf:=18.: tf:=1.0: tbf:=0.625: alpha:=arctan(b/s):
beta:=arctan(a/2./h): phi:=arctan(1./4.): L[SD]:=sqrt(s^2+b^2):
L[KD]:=sqrt((a/2)^2+h^2): If:=bf^3*tf/12.: Ibf:=eta*a^3*tbf/12:
Af:=bf*tf: w:=0.275: Pl:=w*s*0.25/2.: Sz:=-175782./42.1:
wlat:=0.275/2*0.25: eta:=0.5:

> P[bend]:=evalm(inverse(CP)&*YP);

$$P_{bend} := \begin{bmatrix} -0.000235116091 M \\ 0.000223376199 M \\ 0.000109128165 M \\ 0.000123962942 M \end{bmatrix}$$

> V[bend]:=evalm(CV&*P[bend]);

$$V_{bend} := \begin{bmatrix} 0.370469060310^{-6} M \\ 0.187018376310^{-6} M \\ 0.247227019410^{-6} M \end{bmatrix}$$

Transfer matrices for a box girder with internal X-frames

```
> restart:
> with(linalg):
> K11:=matrix ([[L[D]/E/A[D],0,0,0],[0,0,0,0],[0,0,-1/cos(gamma),0],
[2*sin(alpha),2,cos(gamma),cos(gamma)]]);
```

$$K11 := \begin{bmatrix} \frac{L_D}{EA_D} & 0 & 0 & 0 \\ 0 & 0 & 0 & 0 \\ 0 & 0 & -\frac{1}{\cos(\gamma)} & 0 \\ 2 \sin(\alpha) & 2 & \cos(\gamma) & \cos(\gamma) \end{bmatrix}$$

```
> K12:=matrix([[-2*sin(alpha),0,0,0],[0,0,1,1],[0,E*A[X]/L[X],
E*A[X]/L[X],0],[0,0,0,0]]);
```

$$K12 := \begin{bmatrix} -2 \sin(\alpha) & 0 & 0 & 0 \\ 0 & 0 & 1 & 1 \\ 0 & \frac{EA_X}{L_X} & \frac{EA_X}{L_X} & 0 \\ 0 & 0 & 0 & 0 \end{bmatrix}$$

```
> K21:=matrix([[0,b/E/A[S],0,0],[0,s^3/24/E/I[tf],0,
s^3*cos(gamma)/24/E/I[tf]],[0,0,0,1],[0,s^3/6/E/I[bf],0,0]]);
```

$$K21 := \begin{bmatrix} 0 & \frac{b}{EA_S} & 0 & 0 \\ 0 & \frac{1}{24} \frac{s^3}{EI_{tf}} & 0 & \frac{1}{24} \frac{s^3 \cos(\gamma)}{EI_{tf}} \\ 0 & 0 & 0 & 1 \\ 0 & \frac{1}{6} \frac{s^3}{EI_{bf}} & 0 & 0 \end{bmatrix}$$

```
> K22:=matrix([[-1,1,0,0],[-1,-1,0,0],[E*A[X]*cos(gamma)/L[X],0,
E*A[X]*cos(gamma)/L[X],0],[0,0,1,-1]]);
```

$$K22 := \begin{bmatrix} -1 & 1 & 0 & 0 \\ -1 & -1 & 0 & 0 \\ \frac{EA_X \cos(\gamma)}{L_X} & 0 & \frac{EA_X \cos(\gamma)}{L_X} & 0 \\ 0 & 0 & 1 & -1 \end{bmatrix}$$

```
> C[V]:=evalm(-inverse(K22) &* K21);
```

$$C_V := \begin{bmatrix} 0 & \frac{1}{2} \frac{b}{EA_S} + \frac{1}{48} \frac{s^3}{EI_{tf}} & 0 & \frac{1}{48} \frac{s^3 \cos(\gamma)}{EI_{tf}} \\ 0 & \frac{1}{2} \frac{b}{EA_S} + \frac{1}{48} \frac{s^3}{EI_{tf}} & 0 & \frac{1}{48} \frac{s^3 \cos(\gamma)}{EI_{tf}} \\ 0 & \frac{1}{2} \frac{b}{EA_S} - \frac{1}{48} \frac{s^3}{EI_{tf}} & 0 & \frac{1}{48} \frac{s^3 \cos(\gamma)}{EI_{tf}} - \frac{L_X}{EA_X \cos(\gamma)} \\ 0 & \frac{1}{2} \frac{b}{EA_S} - \frac{1}{48} \frac{s^3}{EI_{tf}} + \frac{1}{6} \frac{s^3}{EI_{bf}} & 0 & \frac{1}{48} \frac{s^3 \cos(\gamma)}{EI_{tf}} - \frac{L_X}{EA_X \cos(\gamma)} \end{bmatrix}$$

> C[P]:=evalm(K11-K12*inverse(K22)*K21);

$$C_P := \begin{bmatrix} \frac{L_D}{EA_D} & -\frac{\sin(\alpha) b}{EA_S} - \frac{1}{24} \frac{\sin(\alpha) s^3}{EI_{tf}} & 0 & \frac{1}{24} \frac{\sin(\alpha) s^3 \cos(\gamma)}{EI_{tf}} \\ 0 & -\frac{b}{EA_S} - \frac{1}{24} \frac{s^3}{EI_{tf}} + \frac{1}{6} \frac{s^3}{EI_{bf}} & 0 & \frac{1}{24} \frac{s^3 \cos(\gamma)}{EI_{tf}} - \frac{2 L_X}{EA_X \cos(\gamma)} \\ 0 & -\frac{A_X b}{L_X A_S} & -\frac{1}{\cos(\gamma)} & -\frac{1}{\cos(\gamma)} \\ 2 \sin(\alpha) & 2 & \cos(\gamma) & \cos(\gamma) \end{bmatrix}$$

> Y[P]:=matrix([[s*y[t]*cos(alpha)/E/I[box]*M],[s*y[t]*cos(alpha)/E/I[box]*M],[A[X]*b*s*w[lat]/(A[X]*b*(cos(gamma))^2+A[S]*L[X])],[0]]);

$$Y_P := \begin{bmatrix} \frac{s y_t \cos(\alpha) M}{EI_{box}} \\ \frac{s y_t \cos(\alpha) M}{EI_{box}} \\ \frac{A_X b s w_{lat}}{A_X b \cos(\gamma)^2 + A_S L_X} \\ 0 \end{bmatrix}$$

> a:=81.: b:=120.: h:=78: s:=120: E:=29000.: AS:=3.75: AX:=3.75:
AD:=7.78: bf:=18.: tf:=1.0: tbf:=0.625: alpha:=arctan(b/s):
beta:=arctan(a/2./h): phi:=arctan(1./4.): LD:=sqrt(s^2+b^2):
LX:=sqrt(((a+b)/2)^2+h^2): Itf:=bf^3*tf/12.: Ibf:=a^3*tbf/12: Af:=bf*tf:
w:=0.275: Pl:=w*s*0.25/2.: Ibox:=175782.: yt:=-42.2: yb:=(h-42.2):
wlat:=0.275/2*0.25: nu:=0.3: gamma:=arctan(2*h/(a+b)):
> P[bend]:=evalm(inverse(CP)*YP);

$$P_{bend} := \begin{bmatrix} -0.0002750704954M + 0.7911569080 \\ 0.0001945042125M + 0.2048146901 \\ 0.0001257454633M - 1.828105692 \\ -0.0001257454633M - 0.1067297100 \end{bmatrix}$$

> V[bend]:=evalm(CV*P[bend]);

$$V_{bend} := \begin{bmatrix} 0.0004207908384 + 0.350395607910^{-6} M \\ 0.0001947884217 + 0.135770269910^{-6} M \\ -0.0000367427595 + 0.50433974510^{-7} M \\ 0.0000367427593 + 0.120220194210^{-6} M \end{bmatrix}$$

APPENDIX 9.A

Compression Straight Flange Geometric Parameters and Data for the Anti-Symmetric Buckling Modes

n	α	w	t_f (in)	t_s (in)	t_t (in)	$2b'$ (in)	s (in)	Eigenvalue (kips/in)	I_s (in ⁴)
4	5	160	1.50	1.500	3.000	15.00	15.750	16.80	11388.94
4	5	160	1.50	1.500	2.000	15.00	15.750	16.44	8132.00
4	5	160	1.50	1.500	1.750	15.00	15.750	16.31	7322.03
4	5	160	1.50	1.375	1.750	15.00	15.750	16.12	7204.61
4	5	160	1.50	1.250	1.750	15.00	15.750	15.90	7087.18
3	5	160	1.50	1.500	2.000	15.00	15.750	16.34	8132.00
3	5	160	1.50	1.500	1.750	15.00	15.750	16.21	7322.03
3	5	160	1.50	1.500	1.625	15.00	15.750	16.14	6917.61
3	5	160	1.50	1.000	1.750	15.00	15.750	15.29	6852.34
3	5	160	1.50	0.875	1.750	15.00	15.750	14.99	6734.91
2	5	160	1.50	1.500	2.000	15.00	15.750	16.14	8132.00
2	5	160	1.50	1.500	1.500	15.00	15.750	15.87	6513.54
2	5	160	1.50	1.250	1.500	15.00	15.750	15.50	6272.40
2	5	160	1.50	1.000	1.500	15.00	15.750	15.05	6031.27
1	5	160	1.50	2.000	2.000	10.00	13.000	15.22	3957.14
1	5	160	1.50	1.000	2.000	10.00	13.000	14.33	3482.53
1	5	160	1.50	1.000	1.750	10.00	13.000	14.24	3121.17
1	5	160	1.50	1.000	1.625	10.00	13.000	14.19	2940.83
4	5	160	2.00	2.000	4.000	15.75	18.250	39.37	21194.82
4	5	160	2.00	2.000	3.500	15.75	18.250	39.07	18941.99
4	5	160	2.00	2.000	3.250	15.75	18.250	38.88	17819.67
4	5	160	2.00	1.875	3.250	15.75	18.250	38.50	17660.72
4	5	160	2.00	1.750	3.250	15.75	18.250	38.08	17501.78
3	5	160	2.00	2.000	4.000	15.75	18.250	39.13	21194.82
3	5	160	2.00	2.000	3.500	15.75	18.250	38.83	18941.99
3	5	160	2.00	2.000	3.250	15.75	18.250	38.67	17819.67
3	5	160	2.00	2.000	3.125	15.75	18.250	38.58	17259.48
3	5	160	2.00	1.875	3.125	15.75	18.250	38.19	17098.62
3	5	160	2.00	1.750	3.125	15.75	18.250	37.78	16937.76
2	5	160	2.00	2.000	4.000	15.75	18.250	38.65	21194.82
2	5	160	2.00	2.000	3.000	15.75	18.250	38.02	16699.92
2	5	160	2.00	2.000	2.750	15.75	18.250	37.82	15582.64
2	5	160	2.00	1.875	2.750	15.75	18.250	37.46	15415.94
2	5	160	2.00	1.750	2.750	15.75	18.250	37.09	15249.24
2	5	160	2.00	1.625	2.750	15.75	18.250	36.68	15082.54
2	5	160	2.00	1.500	2.750	15.75	18.250	36.26	14915.85
1	5	160	2.00	2.000	2.000	15.75	18.250	35.89	12244.40
1	5	160	2.00	1.000	2.000	15.75	18.250	33.37	10814.06
1	5	160	2.00	1.000	1.500	15.75	18.250	33.09	8531.72
1	5	160	2.00	1.000	1.250	15.75	18.250	32.93	7392.49
3	5	160	2.50	2.500	5.000	15.75	21.500	75.34	37116.78
3	5	160	2.50	2.500	4.500	15.75	21.500	74.91	34042.78
3	5	160	2.50	2.375	4.500	15.75	21.500	74.26	33799.78
3	5	160	2.50	2.250	4.500	15.75	21.500	73.57	33556.78
2	5	160	2.50	2.500	5.000	15.75	20.250	74.29	32336.25

n	α	w	t_f (in)	t_s (in)	t_t (in)	$2b'$ (in)	s (in)	Eigenvalue (kips/in)	I_s (in ⁴)
2	5	160	2.50	2.500	4.875	15.75	20.250	74.15	31656.23
2	5	160	2.50	2.500	4.750	15.75	20.250	73.93	30977.14
1	5	160	2.50	2.500	5.000	18.00	16.750	72.74	23640.83
1	5	160	2.50	2.500	4.000	18.00	16.750	71.68	19444.31
1	5	160	2.50	2.500	3.875	18.00	16.750	71.52	18923.64
1	5	160	2.50	2.375	3.875	18.00	16.750	71.06	18819.69
1	5	160	2.50	2.250	3.875	18.00	16.750	70.58	18715.74
1	5	160	2.50	2.125	3.875	18.00	16.750	70.08	18611.80
1	5	160	2.50	2.000	3.875	18.00	16.750	69.55	18507.85
4	5	100	0.75	0.375	0.500	7.00	11.875	4.61	640.93
4	5	100	0.75	0.375	0.375	7.00	11.875	4.59	528.15
4	5	100	0.75	0.375	0.563	6.50	10.469	4.60	490.71
4	5	100	0.75	0.625	1.000	14.75	7.250	5.38	752.37
4	5	100	0.75	0.625	0.875	14.75	7.250	5.35	666.42
4	5	100	0.75	0.500	0.875	14.75	7.250	5.18	655.31
4	5	100	0.75	0.375	0.875	14.75	7.250	4.91	644.19
3	5	100	0.75	0.438	0.688	11.00	9.156	4.86	671.04
3	5	100	0.75	0.438	0.500	11.00	9.156	4.81	514.77
3	5	100	0.75	0.375	0.688	11.00	9.156	4.73	658.53
3	5	100	0.75	0.375	0.500	11.00	9.156	4.70	501.84
3	5	100	0.75	0.375	0.563	6.50	10.469	4.57	490.71
3	5	100	0.75	0.375	0.500	6.50	10.469	4.56	450.42
2	5	100	0.75	0.500	0.813	7.63	9.219	4.79	585.00
2	5	100	0.75	0.500	0.750	7.63	9.219	4.77	548.77
2	5	100	0.75	0.500	0.625	7.63	9.219	4.74	476.37
2	5	100	0.75	0.375	0.625	7.63	9.219	4.60	450.50
2	5	100	0.75	0.375	0.438	6.50	10.531	4.53	416.05
1	5	100	0.75	0.375	0.625	10.00	7.063	4.60	312.11
1	5	100	0.75	0.375	0.500	7.13	8.281	4.56	278.86
1	5	100	0.75	0.375	0.563	7.00	8.219	4.51	296.42
1	5	100	0.75	0.375	0.500	7.00	8.219	4.49	270.15
1	5	100	0.75	0.375	0.438	7.00	8.219	4.48	243.88
4	5	80	0.75	0.500	0.500	6.50	9.875	7.46	425.29
4	5	80	0.75	0.375	0.500	6.50	9.875	7.19	392.31
4	5	80	0.75	0.750	1.500	7.00	7.500	8.34	599.78
4	5	80	0.75	0.750	1.250	7.00	7.500	8.25	513.99
4	5	80	0.75	0.750	1.375	7.00	7.500	8.30	556.83
4	5	80	0.75	0.625	1.250	7.00	7.500	8.03	502.55
4	5	80	0.75	0.500	1.250	7.00	7.500	8.07	491.11
3	5	80	0.75	0.750	1.500	7.00	7.500	8.29	599.78
3	5	80	0.75	0.750	1.000	7.00	7.500	8.07	428.64
3	5	80	0.75	0.625	1.000	7.00	7.500	7.88	416.52
3	5	80	0.75	0.500	1.000	7.00	7.500	7.63	404.41
2	5	80	0.75	0.750	1.500	7.00	7.500	8.19	599.78
2	5	80	0.75	0.750	1.000	7.00	7.500	7.97	428.64
2	5	80	0.75	0.750	0.875	7.00	7.500	7.91	386.10

n	α	w	t_f (in)	t_s (in)	t_t (in)	$2b'$ (in)	s (in)	Eigenvalue (kips/in)	I_s (in ⁴)
2	5	80	0.75	0.625	0.875	7.00	7.500	7.73	373.64
2	5	80	0.75	0.500	0.875	7.00	7.500	7.52	361.18
1	5	80	0.75	0.750	1.500	5.00	6.500	7.62	321.60
1	5	80	0.75	0.750	1.000	5.00	6.500	7.40	232.49
1	5	80	0.75	0.750	0.875	5.00	6.500	7.34	210.40
1	5	80	0.75	0.625	0.875	5.00	6.500	7.24	202.74
1	5	80	0.75	0.500	0.875	5.00	6.500	7.14	195.07
4	5	80	1.00	1.000	1.500	7.00	11.000	19.25	1468.55
4	5	80	1.00	1.000	1.000	7.00	11.000	18.85	1105.67
4	5	80	1.00	0.750	1.000	7.00	11.000	18.01	1022.33
4	5	80	1.00	0.500	1.000	7.00	11.000	17.01	939.00
4	5	80	1.00	0.625	1.000	7.00	11.000	17.53	980.67
3	5	80	1.00	1.000	2.000	9.00	11.250	19.80	2395.08
3	5	80	1.00	1.000	1.500	9.00	11.250	19.62	1895.96
3	5	80	1.00	1.000	1.250	9.00	11.250	19.50	1647.53
3	5	80	1.00	0.750	0.750	9.00	11.250	18.17	1059.56
3	5	80	1.00	0.500	0.750	9.00	11.250	17.04	966.49
2	5	80	1.00	1.000	2.000	7.50	8.500	19.19	1079.33
2	5	80	1.00	1.000	1.750	7.50	8.500	19.00	963.92
2	5	80	1.00	0.750	1.750	7.50	8.500	18.22	933.78
2	5	80	1.00	0.625	1.750	7.50	8.500	17.74	918.70
1	5	80	1.00	0.500	1.000	7.50	8.500	16.69	550.94
1	5	80	1.00	0.500	0.875	7.50	8.500	16.62	492.50
4	5	80	1.25	0.750	0.875	14.00	12.750	34.46	2200.84
4	5	80	1.25	0.625	0.875	14.00	12.750	33.35	2134.32
4	5	80	1.25	0.750	1.500	13.00	11.250	35.12	2445.77
4	5	80	1.25	0.750	1.375	13.00	11.250	35.02	2266.08
3	5	80	1.25	0.625	0.875	14.00	12.750	33.24	2134.32
2	5	80	1.25	0.625	0.875	14.00	12.750	33.06	2134.32
2	5	80	1.25	0.750	0.750	14.00	12.750	33.91	1949.71
2	5	80	1.25	0.625	0.750	14.00	12.750	32.94	1882.12
1	5	80	1.25	0.625	0.750	9.00	11.250	32.03	986.68
4	1	80	0.75	0.500	0.625	5.00	2.500	7.03	15.21
4	1	80	0.75	0.375	0.625	5.00	2.500	6.98	14.96
4	1	80	0.75	0.500	0.500	5.00	2.500	6.96	12.44
4	1	80	0.75	0.375	0.500	5.00	2.500	6.87	12.17
3	1	80	0.75	0.750	0.750	5.00	2.500	7.15	18.45
3	1	80	0.75	0.500	0.500	5.00	2.500	6.95	12.44
2	1	80	0.75	0.750	1.500	4.00	2.125	7.30	19.75
2	1	80	0.75	0.750	1.000	4.00	2.125	7.10	13.07
2	1	80	0.75	0.500	1.000	4.00	2.125	7.01	12.91
1	1	80	0.75	0.750	1.500	4.00	2.125	7.21	19.75
1	1	80	0.75	0.750	1.250	4.00	2.125	7.15	16.32
1	1	80	0.75	0.750	1.000	4.00	2.125	7.07	13.07
4	1	80	1.00	1.000	2.000	4.00	3.125	17.33	59.22
4	1	80	1.00	1.000	1.000	4.00	3.125	16.76	31.09

n	α	w	t_f (in)	t_s (in)	t_t (in)	$2b'$ (in)	s (in)	Eigenvalue (kips/in)	I_s (in ⁴)
4	1	80	1.00	0.875	0.875	4.00	3.125	16.42	27.39
4	1	80	1.00	0.500	1.000	4.00	3.125	16.34	29.50
3	1	80	1.00	1.000	2.000	4.00	3.125	17.28	59.22
3	1	80	1.00	1.000	1.000	4.00	3.125	16.75	31.09
3	1	80	1.00	0.875	0.875	4.00	3.125	16.42	27.39
3	1	80	1.00	0.500	1.000	4.00	3.125	16.33	29.50
2	1	80	1.00	1.000	2.000	4.00	3.125	17.15	59.22
2	1	80	1.00	1.000	1.000	4.00	3.125	16.68	31.09
2	1	80	1.00	0.875	1.000	4.00	3.125	16.60	30.69
2	1	80	1.00	0.750	1.000	4.00	3.125	16.53	30.29
1	1	80	1.00	1.000	1.000	4.00	3.125	16.59	31.09
1	1	80	1.00	0.875	1.000	4.00	3.125	16.53	30.69
1	1	80	1.00	0.750	1.000	4.00	3.125	16.47	30.29
1	1	80	0.75	0.750	0.750	7.00	8.000	7.29	400.75
1	2	80	0.75	0.750	0.750	7.00	8.000	7.49	400.75
1	3	80	0.75	0.750	0.750	7.00	8.000	7.57	400.75
1	4	80	0.75	0.750	0.750	7.00	8.000	7.61	400.75
1	5	80	0.75	0.750	0.750	7.00	8.000	7.63	400.75
1	1	80	1.00	0.750	0.750	7.00	8.000	16.73	385.98
1	2	80	1.00	0.750	0.750	7.00	8.000	16.94	385.98
1	3	80	1.00	0.750	0.750	7.00	8.000	17.00	385.98
1	4	80	1.00	0.750	0.750	7.00	8.000	17.01	385.98
1	1	80	1.25	0.750	0.750	7.00	8.000	32.12	371.55
1	2	80	1.25	0.750	0.750	7.00	8.000	32.26	371.55
2	1	80	0.75	0.750	0.750	7.00	8.000	7.45	400.75
2	2	80	0.75	0.750	0.750	7.00	8.000	7.70	400.75
2	3	80	0.75	0.750	0.750	7.00	8.000	7.80	400.75
2	4	80	0.75	0.750	0.750	7.00	8.000	7.84	400.75
2	5	80	0.75	0.750	0.750	7.00	8.000	7.87	400.75
2	1	80	1.00	0.750	0.750	7.00	8.000	16.93	385.98
2	2	80	1.00	0.750	0.750	7.00	8.000	17.19	385.98
2	3	80	1.00	0.750	0.750	7.00	8.000	17.29	385.98
2	1	80	1.25	0.750	0.750	7.00	8.000	32.33	371.55
2	2	80	1.25	0.750	0.750	7.00	8.000	32.51	371.55
3	1	80	0.75	0.750	0.750	7.00	8.000	7.52	400.75
3	2	80	0.75	0.750	0.750	7.00	8.000	7.79	400.75
3	3	80	0.75	0.750	0.750	7.00	8.000	7.89	400.75
3	4	80	0.75	0.750	0.750	7.00	8.000	7.94	400.75
3	1	80	1.00	0.750	0.750	7.00	8.000	17.01	385.98
3	2	80	1.00	0.750	0.750	7.00	8.000	17.30	385.98
3	3	80	1.00	0.750	0.750	7.00	8.000	17.40	385.98
3	1	80	1.25	0.750	0.750	7.00	8.000	32.40	371.55

n	α	w	t_f (in)	t_s (in)	t_t (in)	$2b'$ (in)	s (in)	Eigenvalue (kips/in)	I_s (in ⁴)
3	2	80	1.25	0.750	0.750	7.00	8.000	32.61	371.55
4	1	80	0.75	0.750	0.750	7.00	8.000	7.56	400.75
4	2	80	0.75	0.750	0.750	7.00	8.000	7.84	400.75
4	3	80	0.75	0.750	0.750	7.00	8.000	7.94	400.75
4	4	80	0.75	0.750	0.750	7.00	8.000	7.99	400.75
4	1	80	1.00	0.750	0.750	7.00	8.000	17.05	385.98
4	2	80	1.00	0.750	0.750	7.00	8.000	17.36	385.98
4	3	80	1.00	0.750	0.750	7.00	8.000	17.47	385.98
4	1	80	1.25	0.750	0.750	7.00	8.000	32.44	371.55
4	2	80	1.25	0.750	0.750	7.00	8.000	32.66	371.55
3	1	80	0.75	0.625	0.625	5.00	2.500	7.10	9.41
3	1	80	0.75	0.500	0.625	5.00	2.500	7.00	9.36
2	1	80	0.75	0.750	1.250	4.00	2.125	7.20	9.62
2	1	80	0.75	0.750	1.125	4.00	2.125	7.20	9.55

APPENDIX 9.B

Horizontally Curved Bottom Flange Parameters and Data for the Anti-Symmetric Buckling Modes

n	α	w (in.)	t (in.)	R (ft.)	I_s (in. ⁴)	I_s , regression (in. ⁴)	F_{cr} , Eq. (9.13) (ksi)	F_{cr} , FEM (ksi)
1	1	120	1.00	300	52.3	36.0	7.28	7.10
1	1	120	1.00	600	52.3	36.0	7.28	7.35
1	3	60	1.00	200	193.9	162.0	29.12	28.94
1	3	60	1.00	300	185.7	162.0	29.12	29.11
1	3	60	1.00	500	177.6	162.0	29.12	29.54
1	3	60	1.00	9000	162.1	162.0	29.12	29.93
1	3	120	1.00	500	324.4	324.0	7.28	7.16
1	3	120	1.00	600	331.9	324.0	7.28	7.24
1	3	120	1.00	900	324.4	324.0	7.28	7.24
1	3	120	1.00	1800	324.4	324.0	7.28	7.26
1	3	120	1.00	3500	324.4	324.0	7.28	7.26
1	3	120	0.75	500	137.3	136.7	4.10	4.11
1	3	120	0.75	900	137.3	136.7	4.10	4.12
1	3	120	0.75	3500	137.3	136.7	4.10	4.12
1	3	120	1.50	500	1151.1	1093.5	16.38	16.26
1	3	120	1.50	650	1097.4	1093.5	16.38	16.01
1	3	120	1.50	900	1097.4	1093.5	16.38	16.52
1	3	120	1.50	3500	1097.4	1093.5	16.38	16.75
1	5	60	1.00	200	452.1	450.0	29.12	29.32
1	5	60	1.00	400	452.1	450.0	29.12	29.39
1	5	60	1.00	600	452.1	450.0	29.12	29.62
1	5	60	1.00	1200	452.1	450.0	29.12	30.11
1	5	60	1.00	2400	452.1	450.0	29.12	30.32
2	3	60	1.00	350	229.4	229.1	29.12	28.87
2	3	60	1.00	500	229.4	229.1	29.12	29.10
2	3	60	1.00	900	229.4	229.1	29.12	29.43
2	3	60	1.00	3600	229.4	229.1	29.12	29.97
2	3	60	0.75	250	96.8	96.7	16.38	16.24
2	3	60	0.75	500	96.8	96.7	16.38	16.72

n	α	w (in.)	t (in.)	R (ft.)	I_s (in. ⁴)	I_s , regression (in. ⁴)	F_{cr} , Eq. (9.13) (ksi)	F_{cr} , FEM (ksi)
2	3	60	0.75	500	96.8	96.7	16.38	16.72
2	3	60	0.75	3000	96.8	96.7	16.38	17.01
2	3	60	0.75	15000	90.6	96.7	16.38	17.09
2	3	120	1.00	500	421.6	458.2	7.28	7.09
2	3	120	1.00	600	421.6	458.2	7.28	7.15
2	3	120	1.00	900	421.6	458.2	7.28	7.34
2	3	120	1.00	1800	421.6	458.2	7.28	7.48
2	3	120	1.00	3500	421.6	458.2	7.28	7.53
2	3	120	0.75	600	194.4	193.3	4.10	4.04
2	3	120	0.75	900	194.4	193.3	4.10	4.10
2	3	120	0.75	1800	194.4	193.3	4.10	4.13
2	3	120	0.75	3500	194.4	193.3	4.10	4.21
2	5	60	1.00	300	638.7	636.4	29.12	30.09
2	5	60	1.00	600	638.7	636.4	29.12	30.28
2	5	60	1.00	15000	625.0	636.4	29.12	30.65
3	3	120	0.75	700	197.8	236.7	4.10	4.13
3	3	120	0.75	4000	180.6	236.7	4.10	4.24
3	3	120	1.00	700	418.5	561.2	7.28	7.47
3	3	120	1.00	1000	433.5	561.2	7.28	7.56
3	3	120	1.00	4000	476.9	561.2	7.28	7.67
3	3	120	1.50	800	1509.9	1894.0	16.38	16.57
3	3	120	1.50	4000	1509.9	1894.0	16.38	16.80
3	5	60	1.00	300	737.6	779.4	29.12	29.94
3	5	60	1.00	600	737.6	779.4	29.12	30.69
3	5	60	1.00	3000	696.7	779.4	29.12	29.42
3	5	60	1.00	18000	696.7	779.4	29.12	29.73
1	7	30	0.4375	300	33.6	36.9	22.30	23.10
3	9	30	0.3750	500	33.6	66.6	16.38	17.12
2	5	30	0.50	100	47.1	39.8	29.12	30.45
4	3	60	1.00	300	317.0	324.0	29.12	30.21
4	9	30	0.50	100	166.4	182.3	29.12	34.17
4	5	30	0.5000	100	47.1	56.3	29.12	30.47

APPENDIX 9.C

Typical NASTRAN Input Files for Eigenvalue Buckling Analysis of Hypothetical
Horizontally Box Girder Model


```

$*****
$
$
$   TEST MACHINE FOR INVESTIGATING
$   THE CURVATURE EFFECT ON THE REQUIRED MINIMUM
$   STIFFNESS OF THE LONGITUDINAL FLANGE STIFFENERS
$
$   -- SIMPLY SUPPORTED
$   -- AXIALLY COMPRESSED
$   -- HALF MODEL
$
$
$*****
$
ASSIGN OUTPUT2 = 'cs_76_bk.op2', UNIT = 12, STATUS = UNKNOWN
$ Elastic Buckling Analysis, Database
SOL 105
TIME 6000
$ Direct Text Input for Executive Control
CEND
SEALL = ALL
SUPER = ALL
TITLE = MSC/NASTRAN job created on 24-Apr-01 at 07:23:45
ECHO = NONE
MAXLINES = 999999999
$ Direct Text Input for Global Case Control Data
SUBCASE 1
$ Subcase name : buck1
  SUBTITLE=buck1
  SPC = 2
  LOAD = 2
$   SPCFORCES(SORT1,REAL)=ALL
SUBCASE 2
$ Subcase name : buck1
  SUBTITLE=buck1
  SPC = 2
  METHOD = 1
  VECTOR(SORT1,REAL)=ALL
$   SPCFORCES(SORT1,REAL)=ALL
$ Direct Text Input for this Subcase
BEGIN BULK
PARAM      POST      -1
PARAM      PATVER    3.
PARAM      AUTOSPC   YES
PARAM      COUPMASS  -1
PARAM      K6ROT     0.
PARAM      WTMASS    1.
PARAM,NOCOMPS,-1
PARAM      PRTMAXIM   YES
EIGRL , 1, 0., , 1, 0
$
$ Referenced Coordinate Frames
$
CORD2C, 1, 2, 0., 0., 0., 0., 0., 1.,+A

```

```

+A, 100., -6.611051, 10.
CORD2C, 2, , 0., 0., 0., 0., 0., 1.,+B
+B, 0., 1., 1.
$
$*****
$
$      BOTTOM FLANGE - TEST SPECIMEN
$
$
$*****
$
GRID, 110101, 1, 7680.000, 5.288841, 0.0, 1
= , *1, 1, =, *(.088147), ==
=14
GRID, 110201, 1, 7692.000, 5.288841, 0.0, 1
= , *1, 1, =, *(.088147), ==
=14

```

*****Note: Only beginning and ending GRID data are shown*****

```

GRID, 112101, 1, 7920.000, 5.288841, 0.0, 1
= , *1, 1, =, *(.088147), ==
=14
$
$
CQUAD4, 110101, 1101, 110101, 110201, 110202, 110102
= , *1, =, *1, *1, *1, *1
=13

```

*****Note: Only beginning and ending CQUAD4 elements are shown*****

```

CQUAD4, 112001, 1101, 112001, 112101, 112102, 112002
= , *1, =, *1, *1, *1, *1
=13
$
$
$*****
$
$      WEB FLANGE - TEST SPECIMEN
$
$
$*****
$
GRID, 120101, 1, 7680.000, 5.288841, 0.0, 1
= , *1, 1, =, *(.088147), ==
=14
GRID, 120201, 1, 7680.000, 5.288841, 24.00, 1
= , *1, 1, =, *(.088147), ==
=14

```

*****Note: Only beginning and ending GRID data are shown*****

```

GRID, 123001, 1, 7920.000, 5.288841, 216.00, 1
= , *1, 1, =, *(.088147), ==

```

```

=14
$
$
CQUAD4, 120101, 1201, 120101, 120201, 120202, 120102
=      ,      *1,      =,      *1,      *1,      *1,      *1
=13

```

*****Note: Only beginning and ending CQUAD4 elements are shown*****

```

CQUAD4, 123001, 1201, 123001, 131101, 131102, 123002
=      ,      *1,      =,      *1,      *1,      *1,      *1
=13
$
$
$*****
$
$      TOP FLANGE - TEST SPECIMEN
$
$
$*****
$
GRID, 130101, 1, 7680.000, 5.288841, 240.00, 1
=      ,      *1, 1,      =, *(.088147), ==
=14
GRID, 130201, 1, 7704.000, 5.288841, 240.00, 1
=      ,      *1, 1,      =, *(.088147), ==
=14

```

*****Note: Only beginning and ending GRID data are shown*****

```

GRID, 131101, 1, 7920.000, 5.288841, 240.00, 1
=      ,      *1, 1,      =, *(.088147), ==
=14
$
$
CQUAD4, 130101, 1101, 130101, 130201, 130202, 130102
=      ,      *1,      =,      *1,      *1,      *1,      *1
=13

```

*****Note: Only beginning and ending CQUAD4 elements are shown*****

```

CQUAD4, 131001, 1101, 131001, 131101, 131102, 131002
=      ,      *1,      =,      *1,      *1,      *1,      *1
=13
$
$*****
$
$      BOTTOM FLANGE - NON SPECIMEN REGION 1
$
$*****
$
GRID, 210101, 1, 7680.000, 0.0, 0.0, 1
=      ,      *1, 1,      =, *(.352589), ==

```

=14

*****Note: Only beginning and ending GRID Data are shown*****

GRID, 212001, 1, 7908.000, 0.0, 0.0, 1
= , *1, 1, =, *(.352589), ==

=14

GRID, 212101, 1, 7920.000, 0.0, 0.0, 1
= , *1, 1, =, *(.352589), ==

=14

\$

\$

CQUAD4, 210101, 2101, 210101, 210201, 210202, 210102
= , *1, =, *1, *1, *1, *1

=13

CQUAD4, 210201, 2101, 210201, 210301, 210302, 210202
= , *1, =, *1, *1, *1, *1

=13

*****Note: Only beginning and ending CQUAD4 elements are shown*****

CQUAD4, 212001, 2101, 212001, 212101, 212102, 212002
= , *1, =, *1, *1, *1, *1

=13

\$

\$

\$*****

\$

\$ WEB FLANGE - NON SPECIMEN REGION 1

\$

\$

\$*****

GRID, 220201, 1, 7680.000, 0., 24.00, 1
= , *1, 1, =, *(.352589), ==

=14

GRID, 220301, 1, 7680.000, 0., 48.00, 1
= , *1, 1, =, *(.352589), ==

=14

*****Note: Only beginning and ending GRID data are shown*****

GRID, 223001, 1, 7920.000, 0., 216.00, 1
= , *1, 1, =, *(.352589), ==

=14

\$

\$

CQUAD4, 220101, 2201, 210101, 220201, 220202, 210102
= , *1, =, *1, *1, *1, *1

=13

*****Note: Only beginning and ending CQUAD4 elements are shown*****

```

CQUAD4, 223001, 2201, 223001, 231101, 231102, 223002
=      ,      *1,      =,      *1,      *1,      *1,      *1
=13
$
$
$*****
$
$      TOP FLANGE - NON SPECIMEN REGION 1
$
$*****
$
GRID, 230101, 1, 7680.000, 0.0, 240.00, 1
=      ,      *1, 1,      =, *(.352589), ==
=14
GRID, 230201, 1, 7704.000, 0.0, 240.00, 1
=      ,      *1, 1,      =, *(.352589), ==
=14

*****Note: Only beginning and ending GRID data are shown*****

GRID, 231101, 1, 7920.000, 0.0, 240.00, 1
=      ,      *1, 1,      =, *(.352589), ==
=14

$
$
CQUAD4, 230101, 2301, 230101, 230201, 230202, 230102
=      ,      *1,      =,      *1,      *1,      *1,      *1
=13
CQUAD4, 230201, 2301, 230201, 230301, 230302, 230202
=      ,      *1,      =,      *1,      *1,      *1,      *1
=13
CQUAD4, 230301, 2301, 230301, 230401, 230402, 230302
=      ,      *1,      =,      *1,      *1,      *1,      *1
=13
CQUAD4, 230401, 2301, 230401, 230501, 230502, 230402
=      ,      *1,      =,      *1,      *1,      *1,      *1
=13
CQUAD4, 230501, 2301, 230501, 230601, 230602, 230502
=      ,      *1,      =,      *1,      *1,      *1,      *1
=13
CQUAD4, 230601, 2301, 230601, 230701, 230702, 230602
=      ,      *1,      =,      *1,      *1,      *1,      *1
=13
CQUAD4, 230701, 2301, 230701, 230801, 230802, 230702
=      ,      *1,      =,      *1,      *1,      *1,      *1
=13
CQUAD4, 230801, 2301, 230801, 230901, 230902, 230802
=      ,      *1,      =,      *1,      *1,      *1,      *1
=13
CQUAD4, 230901, 2301, 230901, 231001, 231002, 230902
=      ,      *1,      =,      *1,      *1,      *1,      *1
=13
CQUAD4, 231001, 2301, 231001, 231101, 231102, 231002

```

```
=      ,      *1,      =,      *1,      *1,      *1,      *1
=13
```

```
$
$*****
```

```
$
$      DIAPHRAGM 1
$
$*****
```

```
$
GRID, 250201, 1,      7704.000, 0.000,      24.00, 1
=      ,      *100, =,      *24, ==
=7
*****Note: Only beginning and ending GRID data are shown*****
```

```
GRID, 250209, 1,      7704.000, 0.000,      216.00, 1
=      ,      *100, =,      *24, ==
=7
$
```

```
$ 1st & 10th columns
CQUAD4, 250101, 2501, 210101, 220201, 250201, 210301
CQUAD4, 250102,      =, 220201, 220301, 250202, 250201
=      ,      *1,      =,      *100,      *100,      *1,      *1
=6
```

*****Note: Only beginning and ending CQUAD4 elements are shown*****

```
CQUAD4, 250902, 2501, 250901, 250902, 251002, 251001
=      ,      *1,      =,      *1,      *1,      *1,      *1
=6
```

```
$
$
$*****
```

```
$
$      BEARING(LOADING) STIFFENERS : 2701
$
$*****
```

```
$
CBAR, 270101,      2701, 210101, 220201,      100.,      0.,      1000.
CBAR, 270102,      2701, 220201, 220301,      100.,      0.,      1000.
=      ,      *1,      =,      *100,      *100,      ==
=6
```

```
CBAR, 270120,      2701, 221001, 230101,      100.,      0.,      1000.
$
CBAR, 270121,      2701, 212101, 222201,      100.,      0.,      1000.
CBAR, 270122,      2701, 222201, 222301,      100.,      0.,      1000.
=      ,      *1,      =,      *100,      *100,      ==
=6
```

```
CBAR, 270140,      2701, 223001, 231101,      100.,      0.,      1000.
$
```

```
$      LOADING STIFFENERS : 2702
$
CBAR, 270201,      2701, 210108, 220208,      100., 2.468126,      1000.
CBAR, 270202,      2701, 220208, 220308,      100., 2.468126,      1000.
=      ,      *1,      =,      *100,      *100,      ==
```



```

=6
CBAR, 270210, 2701, 221008, 230108, 100., 2.468126, 1000.

CBAR, 270221, 2701, 212108, 222208, 100., 2.468126, 1000.
CBAR, 270222, 2701, 222208, 222308, 100., 2.468126, 1000.
= , *1, =, *100, *100, ==
=6
CBAR, 270230, 2701, 223008, 231108, 100., 2.468126, 1000.
$*****
$
$ FLANGE TRANVERSE STIFFENERS - NON SPECIMEN REGION
$
$*****
$
CBAR, 241701, 2710, 210108, 210208, 100., 2.468126, 1000.
= , *1, =, *100, *100, ==
=18
CBAR, 241721, 2710, 210112, 210212, 100., 3.878484, 1000.
= , *1, =, *100, *100, ==
=18
$
$*****
$
$ WEB TRANSVERSE STIFFENER
$
$*****
$
CBAR, 273001, 2701, 210116, 220216, 100., 5.288841, 1000.

*****Note: Only beginning and ending CBAR elements are shown*****

CBAR, 273030, 2701, 223016, 231116, 100., 5.288841, 1000.
$
$*****
$
$ WEB LONGITUDINAL STIFFENER
$
$*****
$
CBAR, 272001, 2720, 220301, 220302, 1000., 100., 0.
= , *1, =, *1, *1, ==
=13

*****Note: Only beginning and ending CBAR elements are shown*****

CBAR, 272501, 2720, 222901, 222902, 1000., 100., 0.
= , *1, =, *1, *1, ==
=13
CBAR, 172501, 2720, 122901, 122902, 1000., 100., 0.
= , *1, =, *1, *1, ==
=13
$
$*****
$

```

```

$      CROSS BRACINGS
$
$
$*****
$
GRID, 225116, 1,      7800.000,   5.288841,   120.00, 1
$
CBAR, 271001, 2710, 210116, 225116, 1000., 5.288841, 1000.
CBAR, 271101, 2710, 225116, 231116, 1000., 5.288841, 1000.
CBAR, 271201, 2710, 230116, 225116, 1000., 5.288841, 1000.
CBAR, 271301, 2710, 225116, 212116, 1000., 5.288841, 1000.
$
$
GRID, 225108, 1,      7800.000,   2.468126,   120.00, 1
$
CBAR, 271401, 2710, 210108, 225108, 1000., 2.468126, 1000.
CBAR, 271501, 2710, 225108, 231108, 1000., 2.468126, 1000.
CBAR, 271601, 2710, 230108, 225108, 1000., 2.468126, 1000.
CBAR, 271701, 2710, 225108, 212108, 1000., 2.468126, 1000.
$
$*****
$
$      LONGITUDINAL & TRANSVERSE STIFFENER - BOTTOM
$
$*****
$
GRID, 140101, 1,      7796.000,   5.288841,   12.6125, 1
=      ,      *1,      =,      =,*(.088147), ==
=14

*****Note: Only beginning and ending GRID data are shown*****

GRID, 240301, 1,      7804.000,   0.0,   12.6125, 1
=      ,      *1,      =,      =,*(.352589), ==
=14
$
$ STIFFNER FLANGE
$ st1
CQUAD4, 140101, 1401, 140101, 140201, 140202, 140102
=      ,      *1,      =,      *1,      *1,      *1,      *1
=13

*****Note: Only beginning and ending CQUAD4 elements are shown*****

CQUAD4, 240301, 1403, 240201, 211101, 211102, 240202
=      ,      *1,      =,      *1,      *1,      *1,      *1
=13
$
$ TRANSVERSE STIFFENER
$
GRID, 240401, 1,      7680.000, 5.288841, 12.6125, 1
=      ,      *1,      =,      *12,      ==
=19
GRID, 240501, 1,      7680.000, 5.259459, 12.6125, 1

```

```

= , *1, =, *12, ==
=19
GRID, 240601, 1, 7680.000, 5.318224, 12.6125, 1
= , *1, =, *12, ==
=19
$ transverse stiffener web 1
CQUAD4, 240401, 1403, 210116, 240401, 240402, 210216
= , *1, =, *100, *1, *1, *100
=18
$ transverse stiffener flange 1
CQUAD4, 240601, 1401, 240601, 240401, 240402, 240602
= , *1, =, *1, *1, *1, *1
=18
CQUAD4, 240501, 1401, 240401, 240501, 240502, 240402
= , *1, =, *1, *1, *1, *1
=18
$
PSHELL, 1401, 101, .775, 101, , 101
PSHELL, 1403, 101, .500, 101, , 101
$
$*****
$
$ LONGITUDINAL & TRANSVERSE STIFFENER - TOP
$
$*****
$
GRID, 143101, 1, 7796.000, 5.288841, 227.3875, 1
= , *1, =, =,*(.088147), ==
=14

*****Note: Only beginning and ending GRID data are shown*****

GRID, 243301, 1, 7804.000, 0.0, 227.3875, 1
= , *1, =, =,*(.352589), ==
=14
$
$ STIFFNER FLANGE
$ st1
CQUAD4, 143101, 1401, 143101, 143201, 143202, 143102
= , *1, =, *1, *1, *1, *1
=13
CQUAD4, 143201, 1401, 143201, 143301, 143302, 143202
= , *1, =, *1, *1, *1, *1
=13
CQUAD4, 243101, 1401, 243101, 243201, 243202, 243102
= , *1, =, *1, *1, *1, *1
=13
CQUAD4, 243201, 1401, 243201, 243301, 243302, 243202
= , *1, =, *1, *1, *1, *1
=13
$ STIFFNER WEB
CQUAD4, 143301, 1403, 143201, 130601, 130602, 143202
= , *1, =, *1, *1, *1, *1
=13

```

```

CQUAD4, 243301, 1403, 243201, 230601, 230602, 243202
=      ,      *1,      =,      *1,      *1,      *1,      *1
=13
$
$ TRANSVERSE STIFFENER
$
GRID, 241401, 1, 7680.000, 5.288841, 227.3875, 1
=      ,      *1, =,      *24, ==
=9
GRID, 241501, 1, 7680.000, 5.259459, 227.3875, 1
=      ,      *1, =,      *24, ==
=9
GRID, 241601, 1, 7680.000, 5.318224, 227.3875, 1
=      ,      *1, =,      *24, ==
=9
$ transverse stiffener web 1
CQUAD4, 241401, 1403, 230116, 241401, 241402, 230216
=      ,      *1,      =,      *100,      *1,      *1,      *100
=8
$ transverse stiffener flange 1
CQUAD4, 241601, 1401, 241601, 241401, 241402, 241602
=      ,      *1,      =,      *1,      *1,      *1,      *1
=8
CQUAD4, 241501, 1401, 241401, 241501, 241502, 241402
=      ,      *1,      =,      *1,      *1,      *1,      *1
=8
$
$
$*****
$
$      ELEMENT PROPERTIES
$
$*****
PSHELL, 1101, 101, 1.50, 101, , 101
PSHELL, 1201, 101, 1.50, 101, , 101
PSHELL, 1301, 101, 1.50, 101, , 101
PSHELL, 2101, 101, 2.00, 101, , 101
PSHELL, 2201, 101, 2.00, 101, , 101
PSHELL, 2301, 101, 2.00, 101, , 101
PSHELL, 2501, 101, 3.00, 101, , 101
$
$      CROSS BRACINGS WT 10.5 X 41.5
PBARL, 2710, 101, , T , , , , +B11
+B11, 8.355, 10.715, 0.835, 0.515
$
$      CROSS BRACINGS WT 18 X 128
$PBARL, 2710, 101, , T , , , , +B11
$+B11, 12.215, 18.715, 1.730, 0.960
$
$      CROSS BRACINGS WT 9 X 17.5
$PBARL, 2710, 101, , T , , , , +B11
$+B11, 6.000, 8.850, 0.425, 0.30
$
$      CROSS BRACINGS WT 13.5 X 64.5

```

```

$PBARL, 2710, 101, , T , , , , +B11
$+B11, 10.010, 13.815, 1.100, 0.610
$      WEB STIFFENER
PBARL  2720      101      BAR
+C11
+C11    2.5      12.5
$      LOADING STIFFNER
PBARL  2701      101      BAR
+A11
+A11    11.      2.0
$
MAT1, 101, 29000., , .3
$
$*****
$
$
$      LOADING AND BOUNDARY CONDITIONS
$
$
$*****
$
SPCADD, 2, 1, 2, 3, 7
LOAD, 2, 1., 10., 1
$ SYMMETRIC BOUNDARY CONSTRAINTS : SPECIMEN EDGE.
SPC1, 3, 2, 120116, 121116, 130116, 131116
$ TRANSVERSE AND LATERAL CONSTRAINTS
SPC1, 7, 3, 210101, 212101
SPC1, 7, 1, 210101, 212101
SPC1    1      246      110116  110216  110316  110416  110516  110616
+      J

*****Note: Only beginning and ending SPC input are shown*****

+      Y 144216  144316  143116  143216  143316

$
$ NODAL FORCES : UPWARD
FORCE, 1, 230108, 1, 1., 0., 0., 1.
=      ,  =, 231108, ==
$
$
$      VIRTUAL LOADING AT STIFFENERS
$
FORCE, 1, 140101, 1, 0.1, 0., 0.0788, 0.
FORCE, 1, 140201, 1, 0.1, 0., 0.3303, 0
FORCE, 1, 140301, 1, 0.1, 0., 0.079, 0.
FORCE, 1, 111101, 1, 0.1, 0., 0.1853, 0.
$
$
$
$*****
$
$      RIGID BAR ELEMENTS FOR PIN-CONNECTIONS
$

```

```

$*****
$
$ BOTTOM FLANGE TO WEB
RBAR, 270301, 110101, 120101, 123456, , , 12346
= , *1, *1, *1, ==
=13
$ SPECIMEN REGION TO NON-SPECIMEN IN THE WEB

*****Note: Only beginning and ending RIGID elements are shown*****
$
$ SPECIMEN REGION TO NON-SPECIMEN IN BOT. STIFFENER
$
$ stiffener 1
$
RBAR, 270804, 240216, 240411, 123456, , , 123456
$
$
$ LONGITUDINAL STIFF. AND TRANSVERSE STIFFENER
$RBAR, 270807, 240411, 140201, 123456, , , 1
$
ENDDATA

```

APPENDIX 9.D

Typical NASTRAN Input File for Incremental Nonlinear Analysis of Hypothetical
Horizontally Box Girder Model


```

$*****
$
$
$   TEST MACHINE FOR INVESTIGATING
$   THE CURVATURE EFFECT ON THE REQUIRED MINIMUM
$   STIFFNESS OF THE LONGITUDINAL FLANGE STIFFENERS
$
$   -- AXIALLY COMPRESSED
$   -- HALF MODEL
$
$
$*****
$
ASSIGN OUTPUT2 = 'CS_N4_nl.op2', UNIT = 12, STATUS = UNKNOWN
$ Nonlinear Incremental Analysis, Database
SOL 106
TIME 6000
$ Direct Text Input for Executive Control
CEND
SEALL = ALL
SUPER = ALL
TITLE = MSC/NASTRAN job created on 10-Mar-00 at 10:00:01
ECHO = NONE
MAXLINES = 999999999
$ Direct Text Input for Global Case Control Data
SET 5 = 110125, 110225, 110325, 110425, 110525, 110625,
110725, 110825, 110925, 111025, 111125, 111225, 111325, 111425,
111525, 111625, 111725, 111825, 111925, 112025,
112125, 112225, 112325, 112425, 112525, 112625,
112725, 112825, 112925, 113025, 113125, 113225, 113325, 113425,
113525, 113625, 113725, 113825, 113925, 114025
SUBCASE 1
$ Subcase name : step1
  SUBTITLE=step1
  NLPARM = 1
  SPC = 2
  LOAD = 2
  DISPLACEMENT(SORT1,REAL)=ALL
  SPCFORCES(SORT1,REAL)=ALL
  STRESS(CORNER) = 5
$ Direct Text Input for this Subcase
SUBCASE 2
$ Subcase name : step2
  SUBTITLE=step2
  NLPARM = 2
  SPC = 2
  LOAD = 6
  DISPLACEMENT(SORT1,REAL)=ALL
  SPCFORCES(SORT1,REAL)=ALL
  STRESS(CORNER) = 5
$ Direct Text Input for this Subcase
SUBCASE 3
$ Subcase name : step3
  SUBTITLE=step3

```

```

NLPARM = 3
SPC = 2
LOAD = 10
DISPLACEMENT(SORT1,REAL)=ALL
SPCFORCES(SORT1,REAL)=ALL
STRESS(CORNER)= 5
$ Direct Text Input for this Subcase
BEGIN BULK
PARAM      POST      -1
PARAM      PATVER     3.
PARAM      AUTOSPC    NO
PARAM      COUPMASS   -1
PARAM      K6ROT      100.
PARAM      WTMASS      1.
PARAM      LGDISP      2
PARAM,NOCOMPS,-1
PARAM      PRTMAXIM   YES
NLPARM      1          10                AUTO      5          25          PW          YES
*          A
*          A          .001                1.-7
*          B
*          B
NLPARM      2          6                AUTO      5          25          PW          YES
*          C
*          C          .001                1.-7
*          D
*          D
NLPARM      3          12               AUTO      5          25          PW          YES
*          E
*          E          .001                1.-7
*          F
*          F
$
$ Referenced Coordinate Frames
$
CORD2C, 1, 2, 0., 0., 0., 0., 0., 1.,+A
+A, 100., -8.952466, 10.
CORD2C, 2, , 0., 0., 0., 0., 0., 1.,+B
+B, 0., 1., 1.
$
$*****
$
$      BOTTOM FLANGE NODES
$
$*****
$
GRID  110101      1      2340.00      7.16237      0.0012      1
GRID  110102      1      2340.00      7.23401      0.0015      1

*****Note: Only beginning and ending GRID data are shown*****

GRID  114124      1      2460.00      8.80924      0.0013      1
GRID  114125      1      2460.00      8.88086      0.0013      1
GRID  114126      1      2460.00      8.95247      0.0012      1

```

```

$
$*****
$
$      BOTTOM FLANGE - TEST SPECIMEN
$
$
$*****
$
CQUAD4, 110101, 1101, 110101, 110201, 110202, 110102
=      ,      *1,      =,      *1,      *1,      *1,      *1
=23

```

*****Note: Only beginning and ending CQUAD4 elements are shown*****

```

CQUAD4, 113901, 1101, 113901, 114001, 114002, 113902
=      ,      *1,      =,      *1,      *1,      *1,      *1
=23
CQUAD4, 114001, 1101, 114001, 114101, 114102, 114002
=      ,      *1,      =,      *1,      *1,      *1,      *1
=23

```

```

$
$
$*****
$
$      WEB FLANGE - TEST SPECIMEN
$
$
$*****
$
GRID, 120101, 1, 2340.000, 7.161972, 0.0, 1
=      ,      *1, 1,      =, *(.071620), ==
=24
GRID, 120201, 1, 2340.000, 7.161972, 12.00, 1
=      ,      *1, 1,      =, *(.071620), ==
=24

```

*****Note: Only beginning and ending GRID data are shown*****

```

GRID, 122901, 1, 2460.000, 7.161972, 96.00, 1
=      ,      *1, 1,      =, *(.071620), ==
=24
GRID, 123001, 1, 2460.000, 7.161972, 108.00, 1
=      ,      *1, 1,      =, *(.071620), ==
=24
$
$
CQUAD4, 120101, 1201, 120101, 120201, 120202, 120102
=      ,      *1,      =,      *1,      *1,      *1,      *1
=23
CQUAD4, 120201, 1201, 120201, 120301, 120302, 120202
=      ,      *1,      =,      *1,      *1,      *1,      *1
=23

```

*****Note: Only beginning and ending CQUAD4 elements are shown*****

```
CQUAD4, 122901, 1201, 122901, 123001, 123002, 122902
=      ,      *1,      =,      *1,      *1,      *1,      *1
=23
CQUAD4, 123001, 1201, 123001, 132101, 132102, 123002
=      ,      *1,      =,      *1,      *1,      *1,      *1
=23
$
$
$*****
$
$      TOP FLANGE - TEST SPECIMEN
$
$
$*****
$
GRID, 130101, 1, 2340.000, 7.161972, 120.00, 1
=      ,      *1, 1,      =, *(.071620), ==
=24
```

*****Note: Only beginning and ending GRID data are shown*****

```
GRID, 132101, 1, 2460.000, 7.161972, 120.00, 1
=      ,      *1, 1,      =, *(.071620), ==
=24

$
$
CQUAD4, 130101, 1101, 130101, 130201, 130202, 130102
=      ,      *1,      =,      *1,      *1,      *1,      *1
=23
```

*****Note: Only beginning and ending CQUAD4 elements are shown*****

```
CQUAD4, 132001, 1101, 132001, 132101, 132102, 132002
=      ,      *1,      =,      *1,      *1,      *1,      *1
=23

$
$*****
$
$      BOTTOM FLANGE - NON SPECIMEN REGION 1
$
$*****
$
GRID, 210101, 1, 2340.000, 0.0, 0.0, 1
=      ,      *1, 1,      =, *(.358099), ==
=19
```

*****Note: Only beginning and ending GRID data elements are shown*****

```

GRID, 214101, 1, 2460.000, 0.0, 0.0, 1
= , *1, 1, =, *(.358099), ==
=19

```

```

$
$
CQUAD4, 210101, 2101, 210101, 210201, 210202, 210102
= , *1, =, *1, *1, *1, *1
=18

```

*****Note: Only beginning and ending CQUAD4 elements are shown*****

```

CQUAD4, 214001, 2101, 214001, 214101, 214102, 214002
= , *1, =, *1, *1, *1, *1
=18

```

```

$
$
$*****
$
$      WEB FLANGE - NON SPECIMEN REGION 1
$
$
$*****
GRID, 220201, 1, 2340.000, 0., 12.00, 1
= , *1, 1, =, *(.358099), ==
=19

```

*****Note: Only beginning and ending GRID data are shown*****

```

GRID, 223001, 1, 2460.000, 0., 108.00, 1
= , *1, 1, =, *(.358099), ==
=19
$
$
CQUAD4, 220101, 2201, 210101, 220201, 220202, 210102
= , *1, =, *1, *1, *1, *1
=18

```

*****Note: Only beginning and ending CQUAD4 elements are shown*****

```

CQUAD4, 223001, 2201, 223001, 232101, 232102, 223002
= , *1, =, *1, *1, *1, *1
=18
$
$
$*****
$
$      TOP FLANGE - NON SPECIMEN REGION 1
$

```

```

$*****
$
GRID, 230101, 1, 2340.000, 0.0, 120.00, 1
= , *1, 1, =, *(.358099), ==
=19

```

*****Note: Only beginning and ending GRID data are shown*****

```

GRID, 232101, 1, 2460.000, 0.0, 120.00, 1
= , *1, 1, =, *(.358099), ==
=19
$
$
CQUAD4, 230101, 2301, 230101, 230201, 230202, 230102
= , *1, =, *1, *1, *1, *1
=18

```

*****Note: Only beginning and ending CQUAD4 elements are shown*****

```

CQUAD4, 232001, 2301, 232001, 232101, 232102, 232002
= , *1, =, *1, *1, *1, *1
=18

```

```

$
$*****
$
$      DIAPHRAGM 1
$
$*****
$
GRID, 250201, 1, 2346.000, 0.000, 12.00, 1
= , *100, =, *6, ==
=17
GRID, 250202, 1, 2346.000, 0.000, 24.00, 1
= , *100, =, *6, ==
=17

```

*****Note: Only beginning and ending GRID data are shown*****

```

GRID, 250208, 1, 2346.000, 0.000, 96.00, 1
= , *100, =, *6, ==
=17
GRID, 250209, 1, 2346.000, 0.000, 108.00, 1
= , *100, =, *6, ==
=17
$
$ 1st & 20th columns
CQUAD4, 250101, 2501, 210101, 220201, 250201, 210301
CQUAD4, 250102, =, 220201, 220301, 250202, 250201
= , *1, =, *100, *100, *1, *1
=6

```

*****Note: Only beginning and ending CQUAD4 elements are shown*****

```
CQUAD4, 251802, 2501, 251801, 251802, 251902, 251901
=      ,      *1,      =,      *1,      *1,      *1,      *1
=6
CQUAD4, 251902, 2501, 251901, 251902, 252002, 252001
=      ,      *1,      =,      *1,      *1,      *1,      *1
=6
```

```
$
$
$*****
$
$      BEARING(LOADING) STIFFENERS : 2701
$
$*****
$
CBAR, 270101, 2701, 210101, 220201, 100., 0., 1000.
```

*****Note: Only beginning and ending CBAR elements are shown*****

```
CBAR, 270140, 2701, 223001, 232101, 100., 0., 1000.
$
$      LOADING STIFFENERS : 2702
$
CBAR, 270201, 2701, 210111, 220211, 100., 3.580986, 1000.
```

*****Note: Only beginning and ending CBAR elements are shown*****

```
CBAR, 270230, 2701, 223011, 232111, 100., 3.580986, 1000.
$*****
$
$      FLANGE TRANVERSE STIFFENERS - NON SPECIMEN REGION
$
$*****
$
CBAR, 241701, 2710, 210111, 210211, 100., 3.580986, 1000.
=      ,      *1,      =,      *100,      *100,      ==
=38
CBAR, 241741, 2710, 210116, 210216, 100., 5.371479, 1000.
=      ,      *1,      =,      *100,      *100,      ==
=38
$
$*****
$
$      WEB TRANSVERSE STIFFENER
$
$*****
$
CBAR, 273001, 2701, 210121, 220221, 100., 7.161972, 1000.
CBAR, 273002, 2701, 220221, 220321, 100., 7.161972, 1000.
=      ,      *1,      =,      *100,      *100,      ==
=6
CBAR, 273010, 2701, 221021, 230121, 100., 7.161972, 1000.
```

```

CBAR, 273021, 2701, 214121, 222221, 100., 7.161972, 1000.
CBAR, 273022, 2701, 222221, 222321, 100., 7.161972, 1000.
= , *1, =, *100, *100, ==
=6
CBAR, 273030, 2701, 223021, 232121, 100., 7.161972, 1000.
$
$
$
$*****
$
$
$ WEB LONGITUDINAL STIFFENER
$
$*****
$
CBAR, 272001, 2720, 220301, 220302, 1000., 100., 0.
= , *1, =, *1, *1, ==
=18

```

*****Note: Only beginning and ending CBAR elements are shown*****

```

CBAR, 172501, 2720, 122901, 122902, 1000., 100., 0.
= , *1, =, *1, *1, ==
=23
$
$*****
$
$ CROSS BRACINGS
$
$
$*****
$
GRID, 225121, 1, 2400.000, 7.161972, 60.00, 1
$
CBAR, 271001, 2710, 210121, 225121, 1000., 7.161972, 1000.
CBAR, 271101, 2710, 225121, 232121, 1000., 7.161972, 1000.
CBAR, 271201, 2710, 230121, 225121, 1000., 7.161972, 1000.
CBAR, 271301, 2710, 225121, 214121, 1000., 7.161972, 1000.
$
$
GRID, 225111, 1, 2400.000, 3.580986, 60.00, 1
$
CBAR, 271401, 2710, 210111, 225111, 1000., 3.580986, 1000.
CBAR, 271501, 2710, 225111, 232111, 1000., 3.580986, 1000.
CBAR, 271601, 2710, 230111, 225111, 1000., 3.580986, 1000.
CBAR, 271701, 2710, 225111, 214111, 1000., 3.580986, 1000.
$
$*****
$
$ LONGITUDINAL & TRANSVERSE STIFFENER - BOTTOM
$
$*****
$ STIFFENER 1
$
$

```



```

GRID, 240101, 1, 2367.500, 0.0, 7.0925, 1
= , *1, =, =,*(.358099), ==
=19
GRID, 240201, 1, 2370.000, 0.0, 7.0925, 1
= , *1, =, =,*(.358099), ==
=19
GRID, 240301, 1, 2372.500, 0.0, 7.0925, 1
= , *1, =, =,*(.358099), ==
=19
$
$ STIFFNER FLANGE
$ st1
CQUAD4, 140101, 1401, 140101, 140201, 140202, 140102
= , *1, =, *1, *1, *1, *1
=23
CQUAD4, 140201, 1401, 140201, 140301, 140302, 140202
= , *1, =, *1, *1, *1, *1
=23
CQUAD4, 240101, 1401, 240101, 240201, 240202, 240102
= , *1, =, *1, *1, *1, *1
=18
CQUAD4, 240201, 1401, 240201, 240301, 240302, 240202
= , *1, =, *1, *1, *1, *1
=18
$ STIFFNER WEB 1
CQUAD4, 140301, 1403, 140201, 111101, 111102, 140202
= , *1, =, *1, *1, *1, *1
=23
CQUAD4, 240301, 1403, 240201, 211101, 211102, 240202
= , *1, =, *1, *1, *1, *1
=18
$
$ STIFFENER 2
$
GRID, 242101, 1, 2397.500, 0.0, 7.0925, 1
= , *1, =, =,*(.358099), ==
=19
GRID, 242201, 1, 2400.000, 0.0, 7.0925, 1
= , *1, =, =,*(.358099), ==
=19
GRID, 242301, 1, 2402.500, 0.0, 7.0925, 1
= , *1, =, =,*(.358099), ==
=19
$
$ STIFFNER FLANGE
$ st2
CQUAD4, 142101, 1401, 142101, 142201, 142202, 142102
= , *1, =, *1, *1, *1, *1
=23
CQUAD4, 142201, 1401, 142201, 142301, 142302, 142202
= , *1, =, *1, *1, *1, *1
=23
CQUAD4, 242101, 1401, 242101, 242201, 242202, 242102
= , *1, =, *1, *1, *1, *1

```

```

=18
CQUAD4, 242201, 1401, 242201, 242301, 242302, 242202
=      ,      *1,      =,      *1,      *1,      *1,      *1
=18
$ STIFFNER WEB
CQUAD4, 142301, 1403, 142201, 112101, 112102, 142202
=      ,      *1,      =,      *1,      *1,      *1,      *1
=23
CQUAD4, 242301, 1403, 242201, 212101, 212102, 242202
=      ,      *1,      =,      *1,      *1,      *1,      *1
=18
$
$ STIFFENER 3
$
GRID, 243101, 1, 2427.500, 0.0, 7.0925, 1
=      ,      *1,      =,      =,*(.358099), ==
=19
GRID, 243201, 1, 2430.000, 0.0, 7.0925, 1
=      ,      *1,      =,      =,*(.358099), ==
=19
GRID, 243301, 1, 2432.500, 0.0, 7.0925, 1
=      ,      *1,      =,      =,*(.358099), ==
=19
$
$ STIFFNER FLANGE
$ st3
CQUAD4, 143101, 1401, 143101, 143201, 143202, 143102
=      ,      *1,      =,      *1,      *1,      *1,      *1
=23
CQUAD4, 143201, 1401, 143201, 143301, 143302, 143202
=      ,      *1,      =,      *1,      *1,      *1,      *1
=23
CQUAD4, 243101, 1401, 243101, 243201, 243202, 243102
=      ,      *1,      =,      *1,      *1,      *1,      *1
=18
CQUAD4, 243201, 1401, 243201, 243301, 243302, 243202
=      ,      *1,      =,      *1,      *1,      *1,      *1
=18
$ STIFFNER WEB 3
CQUAD4, 143301, 1403, 143201, 113101, 113102, 143202
=      ,      *1,      =,      *1,      *1,      *1,      *1
=23
CQUAD4, 243301, 1403, 243201, 213101, 213102, 243202
=      ,      *1,      =,      *1,      *1,      *1,      *1
=18
$
$ TRANSVERSE STIFFENER
$
GRID, 240401, 1, 2340.000, 7.161972, 7.0925, 1
=      ,      *1,      =,      *3,      ==
=39
GRID, 240501, 1, 2340.000, 7.102289, 7.0925, 1
=      ,      *1,      =,      *3,      ==
=39

```

```

GRID, 240601, 1, 2340.000, 7.221656, 7.0925, 1
= , *1, =, *3, ==
=39
$ transverse stiffener web 1
CQUAD4, 240401, 1403, 210121, 240401, 240402, 210221
= , *1, =, *100, *1, *1, *100
=38
$ transverse stiffener flange 1
CQUAD4, 240601, 1401, 240601, 240401, 240402, 240602
= , *1, =, *1, *1, *1, *1
=38
CQUAD4, 240501, 1401, 240401, 240501, 240502, 240402
= , *1, =, *1, *1, *1, *1
=38
$
PSHELL, 1401, 101, .565, 101, , 101
PSHELL, 1403, 101, .380, 101, , 101
$
$*****
$
$ LONGITUDINAL & TRANSVERSE STIFFENER - TOP
$
$*****
$
$ STIFFENER 1 TOP
$
GRID, 144101, 1, 2367.500, 7.161972, 112.9025, 1
= , *1, =, =,*(.071620), ==
=24

```

*****Note: Only beginning and ending GRID data are shown*****

```

GRID, 244301, 1, 2372.500, 0.0, 112.9025, 1
= , *1, =, =,*(.358099), ==
=19
$
$ STIFFNER FLANGE
$ st1
CQUAD4, 144101, 1401, 144101, 144201, 144202, 144102
= , *1, =, *1, *1, *1, *1
=23
CQUAD4, 144201, 1401, 144201, 144301, 144302, 144202
= , *1, =, *1, *1, *1, *1
=23
CQUAD4, 244101, 1401, 244101, 244201, 244202, 244102
= , *1, =, *1, *1, *1, *1
=18
CQUAD4, 244201, 1401, 244201, 244301, 244302, 244202
= , *1, =, *1, *1, *1, *1
=18
$ STIFFNER WEB
CQUAD4, 144301, 1403, 144201, 130601, 130602, 144202
= , *1, =, *1, *1, *1, *1
=23

```

```

CQUAD4, 244301, 1403, 244201, 230601, 230602, 244202
=      ,      *1,      =,      *1,      *1,      *1,      *1
=18
$
$      STIFFENER 2 TOP
$
GRID, 145101, 1, 2397.500, 7.161972, 112.9025, 1
=      ,      *1,      =,      =,*(.071620), ==
=24

```

*****Note: Only beginning and ending GRIDs are shown*****

```

GRID, 245301, 1, 2402.500, 0.0, 112.9025, 1
=      ,      *1,      =,      =,*(.358099), ==
=19
$
$ STIFFNER FLANGE
$ st2
CQUAD4, 145101, 1401, 145101, 145201, 145202, 145102
=      ,      *1,      =,      *1,      *1,      *1,      *1
=23

```

*****Note: Only beginning and ending CQUAD4 elements are shown*****

```

CQUAD4, 245301, 1403, 245201, 231101, 231102, 245202
=      ,      *1,      =,      *1,      *1,      *1,      *1
=18
$
$
$      STIFFENER 3 TOP
$
GRID, 146101, 1, 2427.500, 7.161972, 112.9025, 1
=      ,      *1,      =,      =,*(.071620), ==
=24

```

*****Note: Only beginning and ending GRIDs are shown*****

```

GRID, 246301, 1, 2432.500, 0.0, 112.9025, 1
=      ,      *1,      =,      =,*(.358099), ==
=19
$
$ stiffener 3
CQUAD4, 146101, 1401, 146101, 146201, 146202, 146102
=      ,      *1,      =,      *1,      *1,      *1,      *1
=23

```

*****Note: Only beginning and ending CQUAD4 elements are shown*****

```

CQUAD4, 246301, 1403, 246201, 231601, 231602, 246202
=      ,      *1,      =,      *1,      *1,      *1,      *1
=18
CQUAD4, 241501, 1401, 241401, 241501, 241502, 241402
=      ,      *1,      =,      *1,      *1,      *1,      *1
=18

```

```

$
$
$*****
$
$      ELEMENT PROPERTIES
$
$*****
PSHELL, 1101, 101, 0.75, 101, , 101
PSHELL, 1201, 101, 0.75, 101, , 101
PSHELL, 1301, 101, 0.75, 101, , 101
PSHELL, 2101, 101, 0.75, 101, , 101
PSHELL, 2201, 101, 0.75, 101, , 101
PSHELL, 2301, 101, 0.75, 101, , 101
PSHELL, 2501, 101, 1.5, 101, , 101
$
$      CROSS BRACINGS
PBARL, 2710, 101, , T , , , , ,+B11
+B11, 12.215, 18.715, 1.730, 0.960
$      WEB STIFFENER
PBARL 2720 101 BAR
+C11
+C11 2.95 14.
$      LOADING STIFFNER
PBARL 2701 101 BAR
+A11
+A11 11. 2.0
$
$
$
MATS1 101 PLASTIC 0. 1 1 50.
MAT1 101 29000. .3
$
$*****
$
$
$      LOADING AND BOUNDARY CONDITIONS
$
$
$*****
$
SPCADD, 2, 1, 2, 7
$ Loads for Load Case : step1
LOAD, 2, 10., 250., 1
$ Loads for Load Case : step2
LOAD, 6, 10., 280., 1
$ Loads for Load Case : step3
LOAD, 10, 10., 320., 1
$ TRANSVERSE AND LATERAL CONSTRAINTS
SPC1, 7, 3, 210101, 214101
SPC1, 7, 1, 210101, 214101
SPC1 1 246 110126 110226 110326 110426 110526
110626 + J

```

*****Note: Only beginning and ending SPC-boundary conditions are shown*****

```

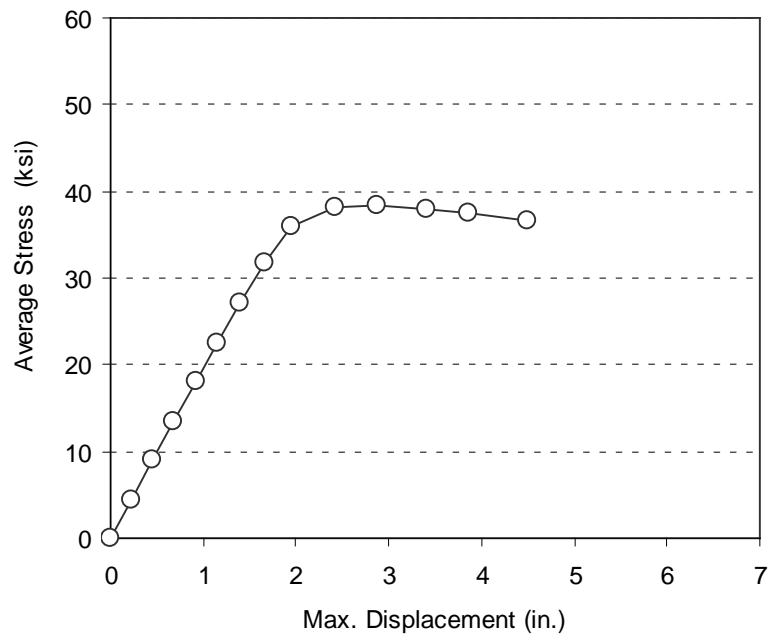
SPC1      1      246      114126  113226  113326  113426  113526
113626 +      AJ
+      AJ 113726  113826  113926  114026  131726  131826  131926
+      AU
+      AU 132026  132126
$
$ NODAL FORCES : UPWARD
FORCE,  1, 230111, 1, 1., 0., 0., 1.
=      ,  =, 232111, ==
$
$
$ VIRTUAL LOADING AT STIFFENERS 1
$
FORCE,  1, 140101, 1, 0.1, 0., 0.1026, 0.
FORCE,  1, 140201, 1, 0.1, 0., 0.4183, 0
FORCE,  1, 140301, 1, 0.1, 0., 0.1026, 0.
FORCE,  1, 111101, 1, 0.1, 0., 0.2307, 0.
$
$
$
$*****
$
$ RIGID BAR ELEMENTS FOR PIN-CONNECTIONS
$
$*****
$
$ BOTTOM FLANGE TO WEB
RBAR, 270301, 110101, 120101, 123456, , , 12346
=      ,      *1,      *1,      *1, ==
=23
*****Note: Only beginning and ending RIGID elements are shown*****

RBAR, 270809, 240431, 143201, 123456, , , 1
$
ENDDATA

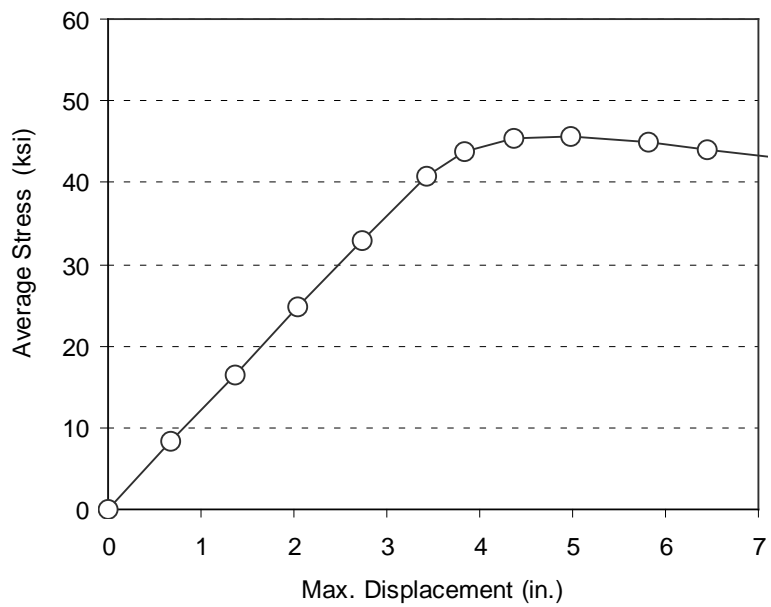
```

APPENDIX 9.E

Ultimate Strength Curves

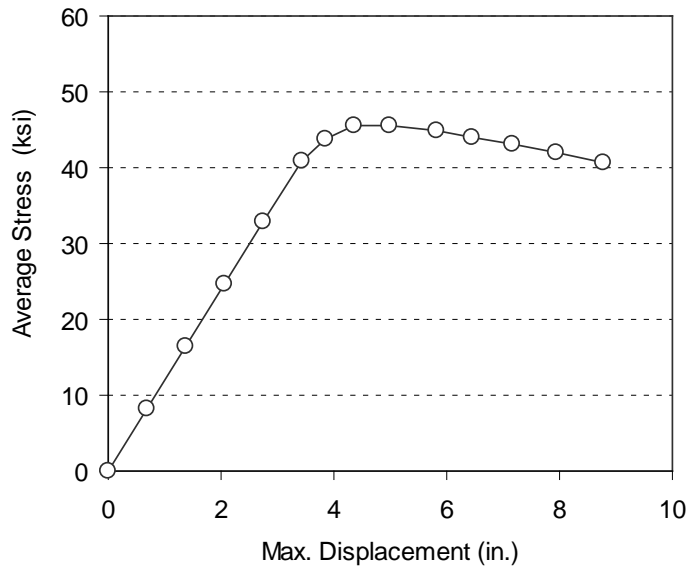


($a=5$, $n=3$, $w=30$ in., $t_f=0.75$ in., $R=200$ ft.)

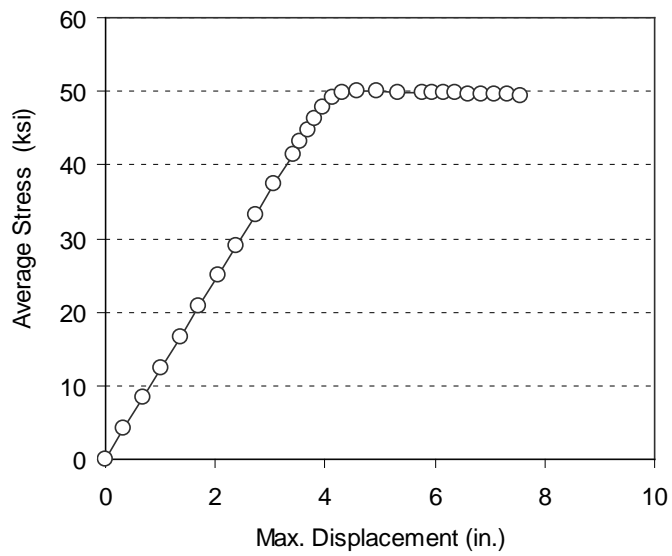


($a=5$, $n=1$, $w=30$ in., $t_f=1.25$ in., $R=300$ ft.)

Fig. 9.E.1. Incremental Ultimate Strength

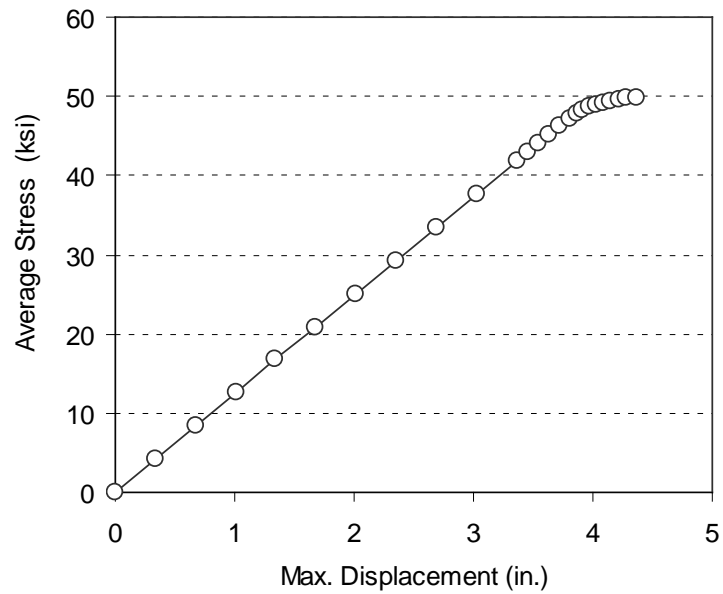


(a) Out-of-Flatness: $w/100$

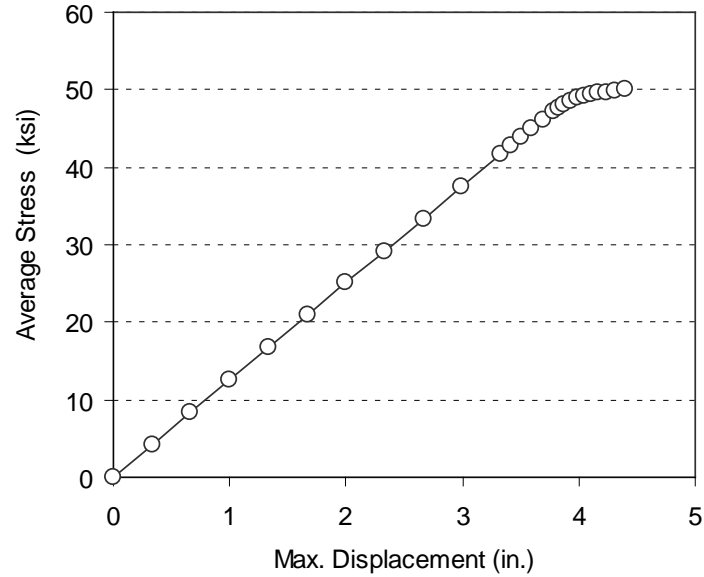


(b) Out-of-Flatness: $w/1000$

Fig. E.2. Incremental Ultimate Strength ($a=5$, $n=1$, $w=30$ in., $t_r=1.25$ in., $R=300$ ft.)

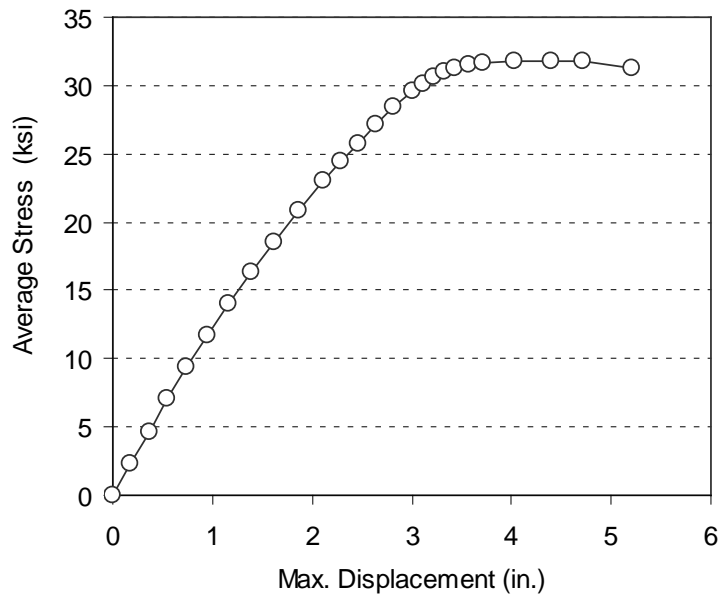


(a) Out-of-Flatness: $w/100$

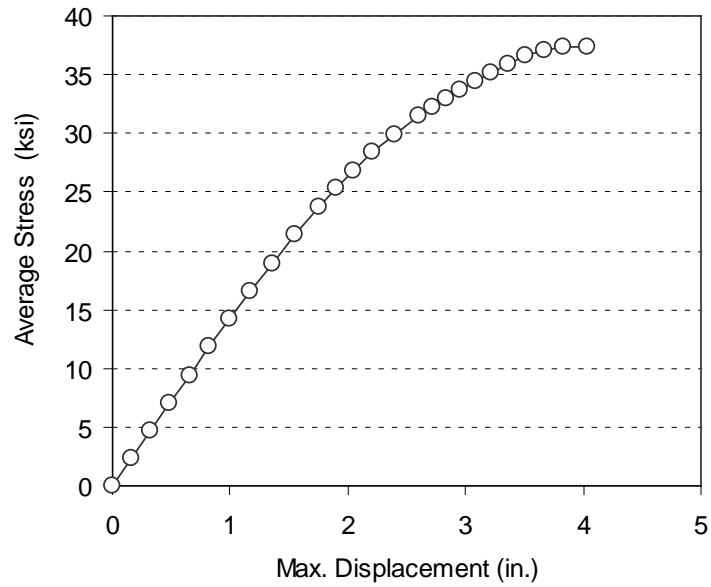


(b) Out-of-Flatness: $w/1000$

Fig. 9.E.3. Incremental Ultimate Strength ($a=5$, $n=1$, $w=30$ in., $t_f=1.875$ in., $R=200$ ft.)



(a) Out-of-Flatness: $w/100$

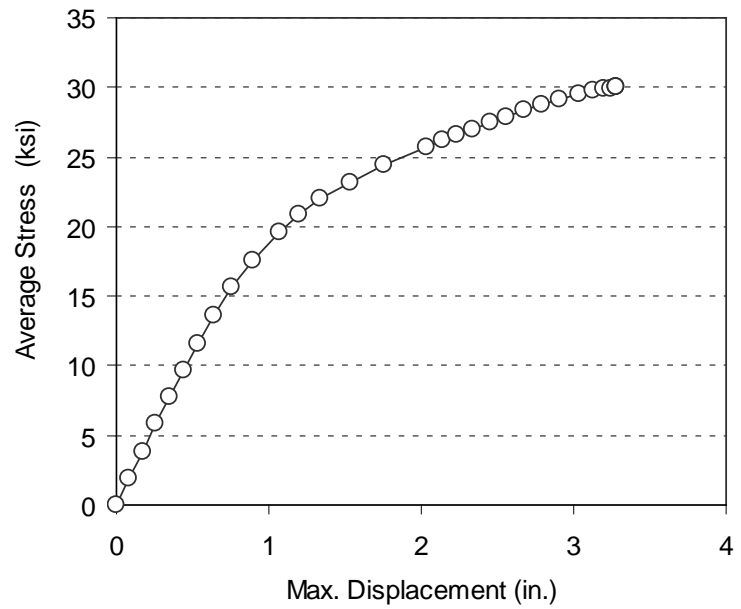


(b) Out-of-Flatness: $w/1000$

Fig. 9.E.4. Incremental Ultimate Strength ($a=3$, $n=1$, $w=60$ in., $t_f=1.125$ in., $R=200$ ft.)



(a) Out-of-Flatness: $w/100$



(b) Out-of-Flatness: $w/1000$

Fig. 9.E.5. Incremental Ultimate Strength ($a=3$, $n=2$, $w=60$ in., $t_f=0.9375$ in., $R=200$ ft.)

APPENDIX 9.F

Regression Analysis Output Sheets

Regression

Variables Entered/Removed^b

Model	Variables Entered	Variables Removed	Method
1	LGANG, LGN, LGW ^a , LGT, LGA	.	Enter

a. All requested variables entered.

b. Dependent Variable: LGIS

Model Summary

Model	R	R Square	Adjusted R Square	Std. Error of the Estimate
1	.998 ^a	.997	.996	2.381E-02

a. Predictors: (Constant), LGANG, LGN, LGW, LGT, LGA

ANOVA^b

Model		Sum of Squares	df	Mean Square	F	Sig.
1	Regression	8.680	5	1.736	3061.841	.000 ^a
	Residual	2.892E-02	51	5.670E-04		
	Total	8.709	56			

a. Predictors: (Constant), LGANG, LGN, LGW, LGT, LGA

b. Dependent Variable: LGIS

Coefficients^a

Model		Unstandardized Coefficients		Standardized Coefficients	t	Sig.
		B	Std. Error	Beta		
1	(Constant)	-.548	.062		-8.832	.000
	LGN	.426	.016	.220	26.854	.000
	LGA	1.989	.037	.640	53.112	.000
	LGW	1.019	.025	.504	40.791	.000
	LGT	3.029	.033	.957	92.918	.000
	LGANG	1.361E-02	.007	.016	1.840	.072

a. Dependent Variable: LGIS

Regression

Variables Entered/Removed^a

Model	Variables Entered	Variables Removed	Method
1	LGT, LGN ^a , LGA, LGW	.	Enter

a. All requested variables entered.

b. Dependent Variable: LGIS

Model Summary

Model	R	R Square	Adjusted R Square	Std. Error of the Estimate
1	.998 ^a	.996	.996	2.435E-02

a. Predictors: (Constant), LGT, LGN, LGA, LGW

ANOVA^a

Model		Sum of Squares	df	Mean Square	F	Sig.
1	Regression	8.678	4	2.169	3658.732	.000 ^a
	Residual	3.083E-02	52	5.930E-04		
	Total	8.709	56			

a. Predictors: (Constant), LGT, LGN, LGA, LGW

b. Dependent Variable: LGIS

Coefficients^a

Model		Unstandardized Coefficients		Standardized Coefficients	t	Sig.
		B	Std. Error	Beta		
1	(Constant)	-.556	.063		-8.772	.000
	LGN	.426	.016	.220	26.233	.000
	LGA	2.002	.038	.645	53.323	.000
	LGW	1.021	.026	.505	39.969	.000
	LGT	3.021	.033	.955	91.404	.000

a. Dependent Variable: LGIS

Regression

Variables Entered/Removed^d

Model	Variables Entered	Variables Removed	Method
1	LGANG, ^a LGN, LGA	.	Enter

a. All requested variables entered.

b. Dependent Variable: LGIS_MOD

Model Summary

Model	R	R Square	Adjusted R Square	Std. Error of the Estimate
1	.996 ^a	.993	.992	2.384E-02

a. Predictors: (Constant), LGANG, LGN, LGA

ANOVA^b

Model		Sum of Squares	df	Mean Square	F	Sig.
1	Regression	4.175	3	1.392	2449.631	.000 ^a
	Residual	3.011E-02	53	5.681E-04		
	Total	4.205	56			

a. Predictors: (Constant), LGANG, LGN, LGA

b. Dependent Variable: LGIS_MOD

Coefficients^a

Model		Unstandardized Coefficients		Standardized Coefficients	t	Sig.
		B	Std. Error	Beta		
1	(Constant)	-.493	.015		-33.860	.000
	LGN	.423	.016	.315	26.915	.000
	LGA	1.954	.027	.905	73.344	.000
	LGANG	1.265E-02	.007	.021	1.723	.091

a. Dependent Variable: LGIS_MOD

Regression

Variables Entered/Removed^b

Model	Variables Entered	Variables Removed	Method
1	LGANG ^a	.	Enter

- a. All requested variables entered.
b. Dependent Variable: LGIS_M1

Model Summary

Model	R	R Square	Adjusted R Square	Std. Error of the Estimate
1	.116 ^a	.014	-.004	2.911E-02

- a. Predictors: (Constant), LGANG

ANOVA^b

Model		Sum of Squares	df	Mean Square	F	Sig.
1	Regression	6.389E-04	1	6.389E-04	.754	.389 ^a
	Residual	4.661E-02	55	8.474E-04		
	Total	4.725E-02	56			

- a. Predictors: (Constant), LGANG
b. Dependent Variable: LGIS_M1

Coefficients^a

Model		Unstandardized Coefficients		Standardized Coefficients	t	Sig.
		B	Std. Error	Beta		
1	(Constant)	-.534	.004		-124.268	.000
	LGANG	7.372E-03	.008	.116	.868	.389

- a. Dependent Variable: LGIS_M1

Regression

Variables Entered/Removed^b

Model	Variables Entered	Variables Removed	Method
1	LGN ^a	.	Enter

- a. All requested variables entered.
b. Dependent Variable: LGIS_M2

Model Summary

Model	R	R Square	Adjusted R Square	Std. Error of the Estimate
1	.963 ^a	.927	.925	2.438E-02

- a. Predictors: (Constant), LGN

ANOVA^b

Model		Sum of Squares	df	Mean Square	F	Sig.
1	Regression	.412	1	.412	693.696	.000 ^a
	Residual	3.268E-02	55	5.941E-04		
	Total	.445	56			

- a. Predictors: (Constant), LGN
b. Dependent Variable: LGIS_M2

Coefficients^a

Model		Unstandardized Coefficients		Standardized Coefficients	t	Sig.
		B	Std. Error	Beta		
1	(Constant)	-.515	.005		-105.945	.000
	LGN	.421	.016	.963	26.338	.000

- a. Dependent Variable: LGIS_M2

Regression

Variables Entered/Removed^b

Model	Variables Entered	Variables Removed	Method
1	LGA ^a	.	Enter

a. All requested variables entered.

b. Dependent Variable: LGIS_M3

Model Summary

Model	R	R Square	Adjusted R Square	Std. Error of the Estimate
1	.993 ^a	.987	.987	2.875E-02

a. Predictors: (Constant), LGA

ANOVA^b

Model		Sum of Squares	df	Mean Square	F	Sig.
1	Regression	3.452	1	3.452	4177.243	.000 ^a
	Residual	4.545E-02	55	8.263E-04		
	Total	3.497	56			

a. Predictors: (Constant), LGA

b. Dependent Variable: LGIS_M3

Coefficients^a

Model		Unstandardized Coefficients		Standardized Coefficients	t	Sig.
		B	Std. Error	Beta		
1	(Constant)	-.508	.017		-29.930	.000
	LGA	1.955	.030	.993	64.632	.000

a. Dependent Variable: LGIS_M3

Regression

Variables Entered/Removed^a

Model	Variables Entered	Variables Removed	Method
1	LGA, LGN ^b	.	Enter

a. All requested variables entered.

b. Dependent Variable: LGIS_MOD

Model Summary

Model	R	R Square	Adjusted R Square	Std. Error of the Estimate
1	.996 ^a	.992	.992	2.427E-02

a. Predictors: (Constant), LGA, LGN

ANOVA^a

Model		Sum of Squares	df	Mean Square	F	Sig.
1	Regression	4.173	2	2.087	3543.833	.000 ^a
	Residual	3.180E-02	54	5.888E-04		
	Total	4.205	56			

a. Predictors: (Constant), LGA, LGN

b. Dependent Variable: LGIS_MOD

Coefficients^a

Model		Unstandardized Coefficients		Standardized Coefficients	t	Sig.
		B	Std. Error	Beta		
1	(Constant)	-.498	.014		-34.363	.000
	LGN	.423	.016	.315	26.436	.000
	LGA	1.969	.026	.912	76.638	.000

a. Dependent Variable: LGIS_MOD

Where, LGA = $\log \alpha$; LGN = $\log n$; LGANG = $\log \phi_b$; LGW = $\log w$; LGT = $\log t_f$; LGIS = $\log I_s$; LGIS_MOD = $\log (I_s/w t_f^3)$.